WHOLE BUILDING HEAT AND MOISTURE ANALYSIS

Fitsum Tariku

A Thesis

in

The Department

of

Building, Civil and Environmental Engineering

Presented in Partial Fulfillment of the Requirements
for the Degree of Doctor of Philosophy at
Concordia University
Montreal, Quebec, Canada

April 2008

Your file Votre référence
ISBN: 978-0-494-37741-3
Our file Notre référence
ISBN: 978-0-494-37741-3

ABSTRACT

Whole Building Heat, Air and Moisture Analysis

Fitsum Tariku, Ph.D.

Concordia University, 2008

The current indoor, building envelope and energy analysis tools are in the form of stand-alone packages, where there is no direct link among them but rather simplifying assumptions are made on the indoor conditions or building envelope when designing for one. For example, indoor models attempt to predict the indoor condition with a simplified approach or no coupling with the building components, which in fact could have a moisture buffering effect. Building envelope models use predefined simple indoor environmental conditions in assessing the hygrothermal performance of a particular building component. Energy models usually ignore the moisture effect on the thermal transport and storage properties of materials. Incorrect prediction of indoor humidity condition and ignoring moisture effect in the energy calculation may lead to over or under sizing of HVAC equipments and the associated effects on building enclosure moisture performance and occupants' comfort and health. In reality, the indoor environmental conditions, more specifically, temperature and relative humidity, are unknown quantities, and have to be determined from the heat and mass balance in the zone considering the heat and mass transfer across the building enclosure, the internal heat and moisture generated by occupants and their activities, and the heat and moisture supply from mechanical systems depending on the mode of operation of the building. In

this research work, a whole building hygrothermal model, which considers the building as a system and deals with the dynamic heat, air and moisture (HAM) interactions among building envelope components, indoor environment and mechanical systems, is developed. The model takes into account the three interrelated and coupled components and evaluates the indoor temperature and relative humidity, building enclosure moisture performance and energy efficiency of the building in an integrated manner on a single platform. The model along with two primary models, namely building envelope and indoor models, are benchmarked against internationally published analytical, numerical and experimental test cases. After successful benchmarking, its usefulness in practical applications are demonstrated through indoor humidity modeling of an existing building, and evaluation of the subsequent retrofit options to attain indoor humidity that is favorable to occupants' comfort and health and at the same time high energy efficiency and durable building. The whole building heat and moisture analysis that are carried out in this research work underlines the importance of an integrated design approach in designing new buildings or retrofitting existing buildings in order to attain an optimized building performance.

ACKNOWLEDGEMENT

It is my great pleasure to express my gratitude and feelings to those who supported me in one way or another, and made possible the accomplishment of this research work.

First, I would like to express my sincere gratitude to my thesis supervisor Prof. Paul Fazio for believing in me participating in the international research project, IEA-Annex 41, and carrying out this research. His encouragement and support throughout the whole course of the work is truly appreciated. I would also like to extend my special thanks to my co-supervisor Dr. Kumar Kumarn, who introduced me to building physics research nine years ago as I started my career at the National Research Council, Institute for Research in Construction (NRC-IRC) and continued his inspiring discussions in my thesis work. His guidance and generosity in sharing his valuable time and knowledge without hesitations, as well as his advise on my personal matters is truly appreciated.

I would also like to acknowledge the support of the Director, Building Envelope and Structures Program at NRC-IRC, Dr. Ralph Paroli, Group leader, Mr. Mike Swinton and NRC as a whole for making me realize my ambition and interest in a convenient and enjoyable manner. I am also grateful to my colleagues at NRC-IRC, Dr. Wahid Maref, Ms. Madeleine Rousseau, Mr. Steve Cornick and Dr. Nadi Said for kindly sharing their experimental and survey data.

My special thanks go to my wife Azmarina Isaac, my son Michael and daughter Belane, who keep me strong all the time with their stimulating love and support. I owe you all the precious time that I have spent without you in pursuit of completing this thesis. I would like to extend my thanks to my parents, my brothers and sisters and my

friends who encouraged me in pursuing my Ph.D. study, and gave me their enthusiastic moral help throughout my work

This thesis is dedicated

to

My children, Michael and Belane, for their unconditional love.

And

My wife, Azmarina Isaac, for her unending love, patience and understanding.

I could not have achieved this goal without her.

TABLE OF CONTENTS

LIST OF FIGURES

LIST OF TABLES

NOMENCLATURE

A_c condensate surface area (m^2)

A_i surface area of surface i (m^2)

A_e evaporative surface area (m^2)

Cv_m specific capacity of solid matrix (J/kg)

Cp_a specific capacity of air (J/kg)

Cp_l specific capacity of water (J/kg)

Cp_v specific capacity of water vapor (J/kg)

D_l liquid conductivity (s)

$\vec{g}$ acceleration due to gravity (m/s^2)

h_i^m mass transfer coefficient of surface i (kg/sm^2Pa)

h_i^h heat transfer coefficient of surface i (W/m^2K)

h_c^m mass transfer coefficient for condensate surface (kg/sm^2Pa)

h_e^m mass transfer coefficient for evaporation surface (kg/sm^2Pa)

h_{fg} latent heat of evaporation/condensation (J/kg)

k_a air flow coefficient (s)

$\dot{m}$ mass flow rate of dry air (kg/s)

M molecular mass of water molecule (0.01806 kg/mol)

$\dot{Q}_s$ heat source (W/m^3)

p zone vapour pressure (Pa)

P_{atm} atmospheric pressure (Pa)

P_s suction pressures (Pa)

P_v vapour pressure (Pa)

$\hat{P}$ saturated vapor pressure (Pa)

p_i^s surface vapor pressure of surface i (Pa)

$\hat{p}_e$ saturated vapor pressure of reservoir e (Pa)

$\hat{p}_c$ saturated vapor pressure of condensate c (Pa)

R universal gas constant (8314 J/Kmol)

T temperature (^oC)

T_e outdoor air temperature (^oC)

T_i^s surface temperature of surface i (^oC)

$\tilde{T}$ set point temperature (^oC)

V air velocity (m/s)

$\tilde{V}$ volume of the zone (m^3)

w moisture content (kg/m^3)

Y_a mass fraction of air (-)

Y_l mass fraction of liquid water (-)

Y_v mass fraction of water vapor (-)

Greek letters

δ_v vapor permeability (s).

Θ sorption capacity (kg/m^3)

λ_{eff} effective thermal conductivity (W/m.K)

μ air dynamic viscosity (kg/(m.s)

ρ_a density of air (kg/m^3)

ρ_w density of water (kg/m^3)

ρ_m density of material (kg/m^3)

ϕ relative humidity (-)

ω humidity ratio (kg/kg air)

ω_e humidity ratio of outdoor air (kg/kg air)

ω_i^s humidity ratio of surface i (kg/kg air)

$\tilde{\omega}$ set point humidity ratio (kg/kg)

1 INTRODUCTION

Buildings are designed to create an isolated space from the surrounding environment and provide desired interior environmental conditions for the occupants. In addition to fulfilling the function of creating a favorable indoor environmental conditions, buildings are expected to be durable and energy efficient. To achieve these goals the designer has to consider two primary hygrothermal loadings on the building. These are the time varying exterior climatic loading which includes: ambient temperature, relative humidity, wind conditions (wind speed and direction), solar radiation and precipitation; and the internal loadings, which are expressed in terms of the amount of indoor heat and moisture generations or removal and are mainly linked to the intended use of the building; for example, a swimming pool produces more internal moisture loading than an office building. Failure to account for these loadings appropriately during building design may result in serious building envelope damage (Figure 1-1) and/or cause health risk for the occupants (Figure 1-2).

Figure 1-1 Moisture damage on the exterior sheathing of the envelope

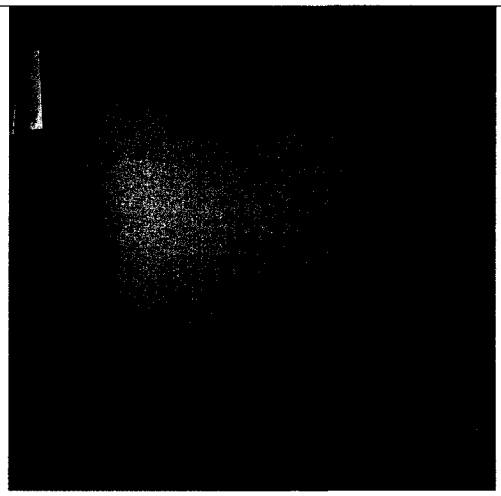

Figure 1-2 Mold growth due to high indoor humidity condition

The desired indoor environmental conditions, energy efficiency and durability of the building should be optimized by considering these design external and internal loadings and by selecting proper materials and mechanical systems for ventilation, heating, cooling, humidification and dehumidification, as necessary. This optimization process is necessary: 1) to provide comfortable indoor environment to occupant since people spend most of their time in indoors and their productivity is dependent on how they perceive their indoor environment (Fang et al., 1998a,b; Fang, 2002), 2) due to the higher level of investment in the construction and maintenance cost of new buildings and repair due to building failures, and 3) due to the high energy consumption of low energy efficient buildings which results in high energy bills to maintain the desired building operating conditions. Dealing with one aspect of the building may lead to problems in the other aspects. For example, in the early 1970's buildings were constructed and retrofitted to be more airtight and insulated (with more insulation) to reduce energy consumption (Hens, 1996). Although the energy efficiency of the buildings was improved, this new strategy created more problems in the durability of the building envelope due to high moisture accumulation in the building structure. The indoor humidity level was also elevated due to the low air exchange, which resulted in low occupant comfort and health problems (Shaw and Kim, 1984; TenWolde, 1988).

The current indoor, building envelope and energy analysis tools are in the form of separate, stand-alone packages, where there is no direct link among them but rather simplifying assumptions are made on the other two when designing for one. For example, the indoor models attempt to predict the indoor conditions with a simplified approach or no coupling with the building components, which could have a moisture buffering effect. The building envelope models, on the other hand, usually use predefined indoor

environmental conditions in assessing the hygrothermal performance of a particular building component. However, in reality the indoor conditions are determined by the heat and mass balance of the external and internal loading as well as the mechanical systems' outputs. Energy models usually ignore the moisture effect on the thermal transport and storage properties of materials (Mednes et al., 2003). However, incorrect prediction of indoor air conditions and ignoring moisture in the energy calculation may lead to incorrect prediction of required ventilation rate for removing excess indoor humidity, energy demand for heating/cooling as well as humidification/ dehumidification needed to maintain the intended building operating conditions. An integrated approach is desirable to deal with these inter-related and coupled effects, and to evaluate and optimize the whole building performance. Recently, the International Energy Agency (IEA) initiated an international research project called Annex 41 "Whole building heat, air, moisture response—MOIST-ENG" (IEA-EXCO Annex 41, 2003) to develop and exchange knowledge in this new research area (holistic-approach). As observed from the common exercises results (Rode et al., 2006), the variations of the results of this relatively new modeling technique are significant and the models needed improvements. This thesis research is part of this on-going international effort to develop and validate a reliable whole building hygrothermal model.

2 BACKGROUND

2.1 Hygrothermal performance assessment of building enclosure

Building enclosures are subjected to a random climatic loading on the exterior surface and relatively stable indoor conditions on the interior. These loadings result in the transport of Heat, Air and Moisture (HAM) across the structure. The direction of flow of these entities depends on the gradient of the driving potential of the respective entity. In addition to the time varying external loading due to time varying weather conditions, the thermal and moisture storage characteristics of the layers, which constitute the enclosure component, make the heat and moisture transport in the building envelope a transient process. The transfer mechanisms can be by convection, diffusion or both. In the case of convection, the heat and moisture are carried by airflow, and this is possible only if there is a pressure gradient across the envelope. The driving potentials for moisture and heat transfer by the second mechanism, diffusion, are vapor pressure and temperature gradients, respectively. Figure 2-1 shows the indoor and outdoor hygrothermal loadings on a typical building envelope component. On the exterior surface, the building envelope component is subjected to the outdoor temperature, relative humidity, wind conditions (wind–direction and speed), solar radiation, long-wave radiation exchange with the surrounding and sky as well as wind-driven rain. These parameters are usually available in the local weather data. The interior surface of the component is subjected to the indoor air temperature and relative humidity. Depending on the boundary conditions, the component may experience wetting or drying. The weather parameters which play an important role in the wetting of the envelope are ambient vapor pressure of the outdoor

weather, which can be calculated from the ambient temperature and relative humidity, and wind-driven rain, which is directional and a function of rainfall intensity, wind speed and wind direction. Although the main mechanism of wetting is due to wind-driven rain deposition on the exterior surface of the cladding and/or penetration into the structure, vapor condensation on cold part of the structure during vapor transport either from interior to exterior or vise verse by diffusion and/or convection (air-leakage) is also important. The local wind speed and direction affect the pressure difference across the envelope, which governs the convection transport of heat and moisture due to air-leakage. As the weather conditions change by hours and seasons the envelope may dry by evaporating moisture through the surfaces. The drying mechanism is facilitated by the increase in ambient temperature, solar gain and/or long wave radiation exchanges with the sky and surrounding. These dynamic wetting and drying processes of the building envelope can be captured using computer models. In various research projects, hygrothermal models are used to assess the performance of a wall system as it is exposed to climatic conditions of different geographical locations, and also to select an appropriate building envelope system for a given geographic locations (Tariku and Kumaran, 1999a,b; Mukhopadhyaya and Tariku, 1999; Djebbar et al., 2002).

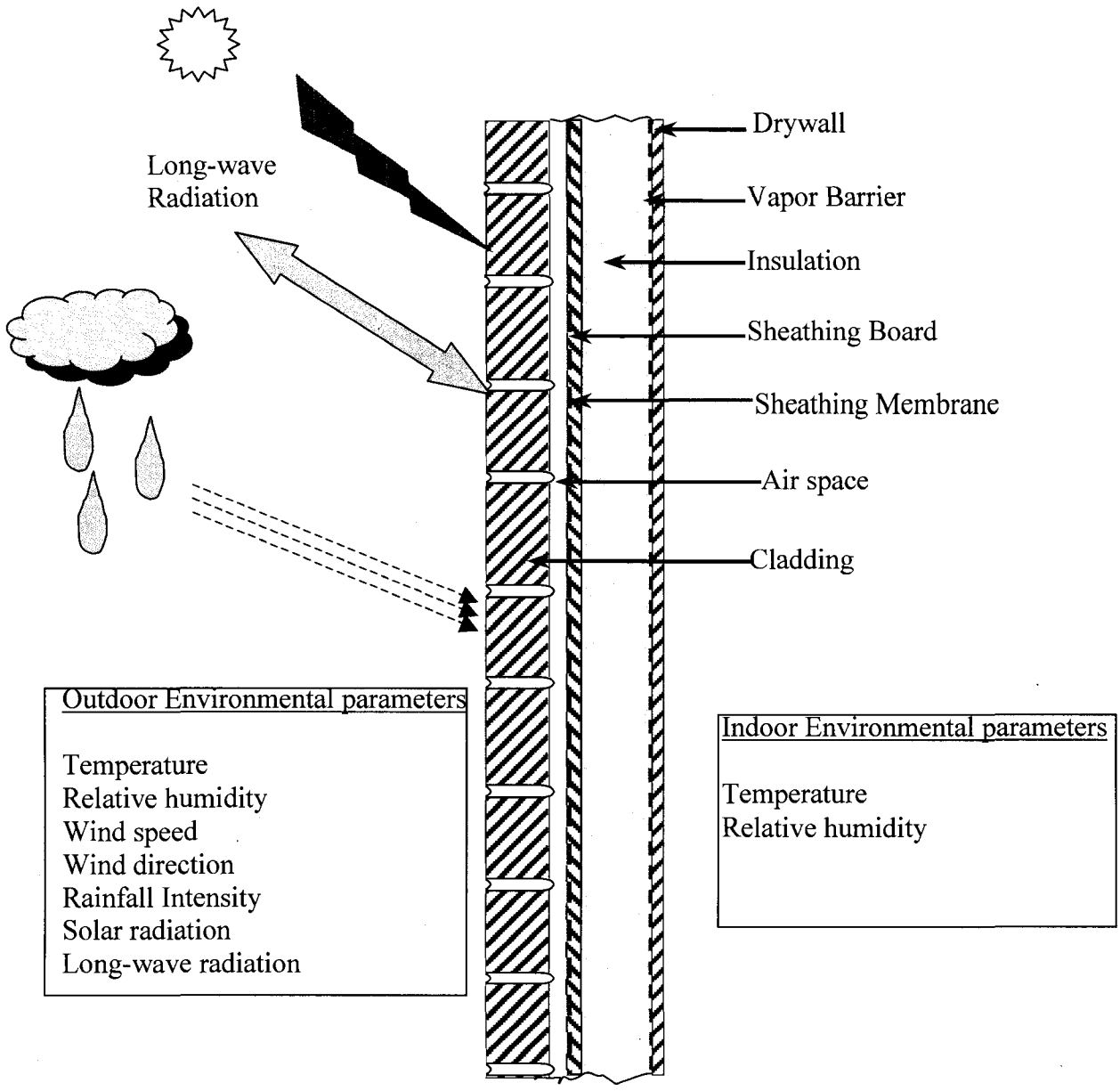

Figure 2-1 Typical building envelope component and hygrothermal loadings

Drying and wetting can occur locally at different parts of the envelope and involves a simultaneous HAM transfer. The heat and moisture transfer are coupled in a way that the temperature (heat transfer) determines the saturated vapor pressure and influences the moisture storage and transport properties of the materials, which are the fundamental parameters in the moisture transport. In building physics analysis, the effect

of temperature in the moisture storage capacity of the material is usually assumed to be negligible (Hagentoft, 1997; Wang, 2003). The heat transfer is dependant on moisture in three ways: 1) the heat release and sink due to phase change (condensation and evaporation), 2) enthalpy transfer due to moisture transport and 3) the change in thermal conductivity and heat capacity of the material due to the presence of moisture. The air that passes through a structure carries heat and moisture (convective heat and mass transfer), which could be a dominant form of HM transport mechanisms. Consequently, analysis of HAM transport through building envelope components requires a simultaneous analysis of the coupled heat, air and moisture transports while taking their interdependency into account.

In the last 20 years, various hygrothermal computer models with various degrees of complexities have been developed to assess the long-term moisture and thermal performances of new or existing building envelope components. The basis for these advanced hygrothermal models' development are the work of Phillip and De Veries (1957) and Luikov (1966), who developed transient models which account for both vapor and liquid flows. IEA Annex 24 (Hens, 1996) carried out a comprehensive review of thirty-seven hygrothermal models and computer codes, and subsequently categorized them into nine groups based on how they handle the following HAM transport modeling issues: 1) steady vs. transient transport of HAM, 2) influence of heat on moisture transfer [saturated vapor pressure as thermal-hygric link], 3) influence of moisture on heat transfer [latent heat as thermal-hygric link], 4) inclusion of convection heat and moisture transport [air-thermal link (enthalpy transfer and stack effect) and air-hygric link], 5) inclusion of liquid transport mechanism and 6) constant vs. variable material properties. The models differ one from the other in the assumptions made in the above HAM

transport phenomena. Some models such as WUFIZ (Kuenzel, 1995), MATCH (Pederson, 1990), MOIST (Burch, 1989) did not consider airflow through the porous media, and therefore the heat and moisture carried by a possible airflow are ignored (Kuenzel, 1995; Pederson, 1990; Burch, 1989), others (TCC2D, 1D-HAM) considered only vapor transport, while disregarding the capillary liquid water transport at high moisture content (Ojanen and Kohonen, 1989; Ojanen et al. 1994; Hagentoft, 1992) which can happen, for example during wind-driven rain events. WALLDRY (Schuyler et al., 1989), which is the model from the Canada Mortgage and Housing Corporation—CMHC, treat airflow and heat transfer as steady state and moisture transfer as a transient problem. The underlying assumption in this model is that the heat and air transport processes are fast when compared to moisture transport, and therefore can be treated as steady state transport processes. The other important distinction is the assumption on the material properties as constant properties or as a set of non-linear properties, which are functions of driving potentials.

The simplest model of all is based on Glaser method (DIN 4108). In this steady state model the heat transfer is by conduction and moisture transport is by vapor diffusion. There is no coupling between thermal and moisture flow, except that the saturated vapor pressure, which is a function of temperature (heat transfer), is used to check condensation. Rivard (1993) implemented this method in a user-friendly software called CONDENSE, which is described in detail recently in Gerbasi (2008). The software will indicate whether there is a chance of condensation occurring, but doesn't indicate the drying potential of the system. The other simple moisture analysis tools, which are similar to Glaser method in all the assumptions but with slight difference in graphical representation, are the dew point method and Kieper diagram (TenWolde, 2001). A

transient analysis, which indicates a net accumulation or drying of moisture, is required to properly assess the performance of a building system. The simplest model of such type is HAMPI (Hens, 1996), which does transient calculation on heat and vapor flow, and the heat and moisture flow are coupled by saturated vapor pressure and latent heat. The next level of transient models include airflow module, and the convection heat and vapor transfer are superimposed on the diffusion transport mechanisms (TCCC2D (Ojanen and Kohonen, 1989; Kumaran, 1992; Ojanen et al. 1994), 1D-HAM (Hagentoft, 1992), FSEC (Gu et al., 1993) and 2DHAV (Janssens, 1998)). The next higher level of models extended the moisture transfer mechanisms to include capillary liquid transport by using both the sorption and suction curves for moisture storage, and the vapor and liquid transport with diffusion and capillary suction. WUFI (Kunezel, 1995; Kuenzel and Kiessl, 1997; Kuenzel, 1998), MATCH (Pedersen, 1990; Pederson, 1992), and MOIST (Burch, (1993); Burch and TenWolde, 1993) are part of these extended models but with no airflow (convection heat and moisture transfer). The MATCH and MOIST models have many similarities (Straube and Burnett, 2001). The relatively more complete hygrotherml models, which include convection heat and moisture transport in addition to diffusion and capillary transport, are TRATMO2 (Salonvaara, 1993), LATENITE (Karagiozis, 1993; Salonvaara and Karagiozis, 1994; Salonvaara and Karagiozis, 1996), DELPHIN.4 (Grunewald et al., 1999), WUFI ORNL/IBP (Karagiozis et al., 2001), MOISTUR-EXPERT (Karagiozis, 2001) and HAM-Tools (2004). The IRC's (Institute for Research in Construction at the National Research Council of Canada) latest version of LATENITE is called hygIRC (Tariku and Kumaran, 2006; Tariku and Kumaran, 2002; Maref et al., 2002). The earlier version of TRATMO2, which is developed by Kohonen

(1984), is called TRATMO. In this model the moisture transport properties are assumed to be constant.

One of the common limitations of all the models described above is in dealing with hysteresis effect, the difference between absorption and desorption curves. Although this is not a problem in exclusively wetting or drying experiments, where the corresponding absorption or desorption curves can be used, the common approach for real scenario cases, where both wetting and drying processes are expected at different time or/and location of the assembly, is to use an average of the absorption and desorption values.

The main distinction among these fully extended models lies on: i) the choice made on moisture driving potentials, ii) the assumption made on the vapor and liquid flux, and iii) the complexity of the airflow modeling approach. i) The driving potentials adopted for vapor and liquid flows in the LATENITE, hygIRC and TRATMO2 models are vapor pressure and moisture content, respectively. HAM-Tools and DELPHINE 4.1 use vapor pressure and suction pressure, whereas WUFI ORNL/IBP and MOISTURE-EXPERT use relative humidity as a driving potential for both vapor and liquid flows. ii) In the earlier models (Phillip and De Veries, 1957; Luikov, 1966) the vapor and liquid flows are lumped and a single driving potential (moisture content) and flow coefficient (moisture diffusivity) are used. But most of the current advanced hygrothermal models split the vapor and liquid flow into two ways: LATENITE, hygIRC and TRATMO2 treat the moisture transport as a two-part process of vapor transport in the hygroscopic region (< 95% relative humidity) and capillary liquid transport in super hygroscopic region (> 95% relative humidity). In these models the moisture transfer coefficients are the measured water vapor permeability and liquid diffusivity, respectively. In the second

category of models, the vapor and liquid transport are treated in parallel in the whole moisture transport range. WUFI ORNL/IBP assumes a constant vapor flow coefficient (dry-cup value), whereas in the HAM-Tools the vapor permeability decreases as the relative humidity increases, which is probably the more realistic case. In these models, the liquid transport coefficient is developed using the standard water-vapor permeability measurement (dry-cup and wet-cup measurements) to include liquid flow in the hygroscopic region. iii) Airflow modeling approach: in DELPHINE 4.1, LATENITE, HAM-Tools and hygIRC models, the airflow in the structure is modeled using Darcy flow equations, whereas TRATMO2, WUFI ORNL/IBP and MOISTURE EXPERT have the capability of using the full Navier-Stockes equation to improve the heat and moisture transfer in air spaces. The application of this computational intensive Navier-Stokes equation is limited to laminar flow.

2.2 Indoor humidity prediction

Accurate prediction of indoor conditions, more specifically indoor temperature and relative humidity, are important for the following four reasons:

1) To better assess the hygrothermal performance of building envelope components (Tsongas et al., 1996). High indoor humidity can result in excess moisture accumulation in the structures and results in the deterioration of components due to mold/decay or corrosion.

2) To maintain the critical relative humidity range which is specific to the building's operation (Trechsel, 2001; Rode, 2003). For example churches, museums and

libraries need to maintain an optimum relative humidity to avoid moisture damage on paintings, artifacts and books.

3) To create an acceptable indoor air quality. Unless controlled, high relative humidity, which is a favorable condition for mold growth, can cause health problems for the occupants and damage to the interior lining of the building (Sterling et al., 1985; Clausen et al., 1999; Oreszczyn and Pretlove, 1999).

4) To create a comfortable environment for occupants as recommended in the ASHRAE Standard 55-1992 and ASHRAE Standard 62-1999. The satisfaction and dissatisfaction of occupants are related to the level of indoor relative humidity and temperature (Toftum et al, 1998; Fang et al., 1998a,b). In the ASHRAE Handbook—Fundamentals (1997), the acceptable levels of operative temperature and humidity for people in typical summer and winter clothing are represented in a comfort zone diagram.

There are two ways to control the indoor relative humidity level. One is the passive approach, which involves introducing moisture-buffering items during construction. The moisture buffering material could modulate the indoor relative humidity by absorbing moisture during high generation periods and releasing at relatively dry periods. Knowledge of the moisture buffering characteristics of the material is a prerequisite for this approach. The second one is an active approach that uses ventilation to carry the moisture out (Tariku et al. 2006). In this approach the incoming air may or may not be conditioned. If mechanical ventilation is employed the ventilation rate has to be optimized for energy consumption, indoor humidity and occupant comfort level. However, before implementing either or both approaches to control the indoor relative humidity, the possible moisture sources to the indoor space must be quantified. The main

sources of moisture to the indoor air are shown in Figure 2-2 below. Generally they can be categorized into three groups:

1) The first one is moisture release from the building envelope components to the indoor air; this is more important during the initial years of the construction when the construction components release their initial moisture content during their first drying process. Christian (1994) estimated a total of 200 liter moisture release by an average house constructed with 19% moisture content lumber; and 90 liters of water release per cubic meter of concrete used during the construction. Based on his analysis, the total moisture input from construction sources can be at an average of 10 L/day for the first year and 5 L/day in the second year. Karagiozis and Salonvaara (2001) showed the effect of the initial construction moisture source on the indoor relative humidity using a computer model (VTT version of LATENITE). Bedner and Dreyer (2006) reported similar effect of initial construction moisture on the indoor air.

2) The second source of moisture is related to the outside weather conditions. In humid climate a significant amount of moisture can be carried into the indoor environment by means of air leakage through cracks and unintentional openings, or intended natural or mechanical ventilation system (Trowbridge et al., 1994; Kuenzel, et al., 2003). The other moisture source, which is related to weather, occurs when wind-driven rain penetrates the building envelope enclosure through defects and deposit liquid water inside the construction. In fact, the ASHRAE Standard Project Committee 160P—*Design Criteria for Moisture Control in Buildings*, recommends an arbitrary moisture load of 1% of wind-driven rain at the exterior surface of the barrier to be considered in the moisture analysis and design of exterior wall systems. In most cases, the building envelope dries out by moisture release to the indoor or outdoor. Moisture migration from

wet soil through foundation walls and floor slabs by capillary force is also a major source of moisture to the indoor environment (Quirouette, 1983; TenWolde, 2007). A noticeable dampness and smell of a basement of a building is usually an indicator of the presence of this type of moisture movement.

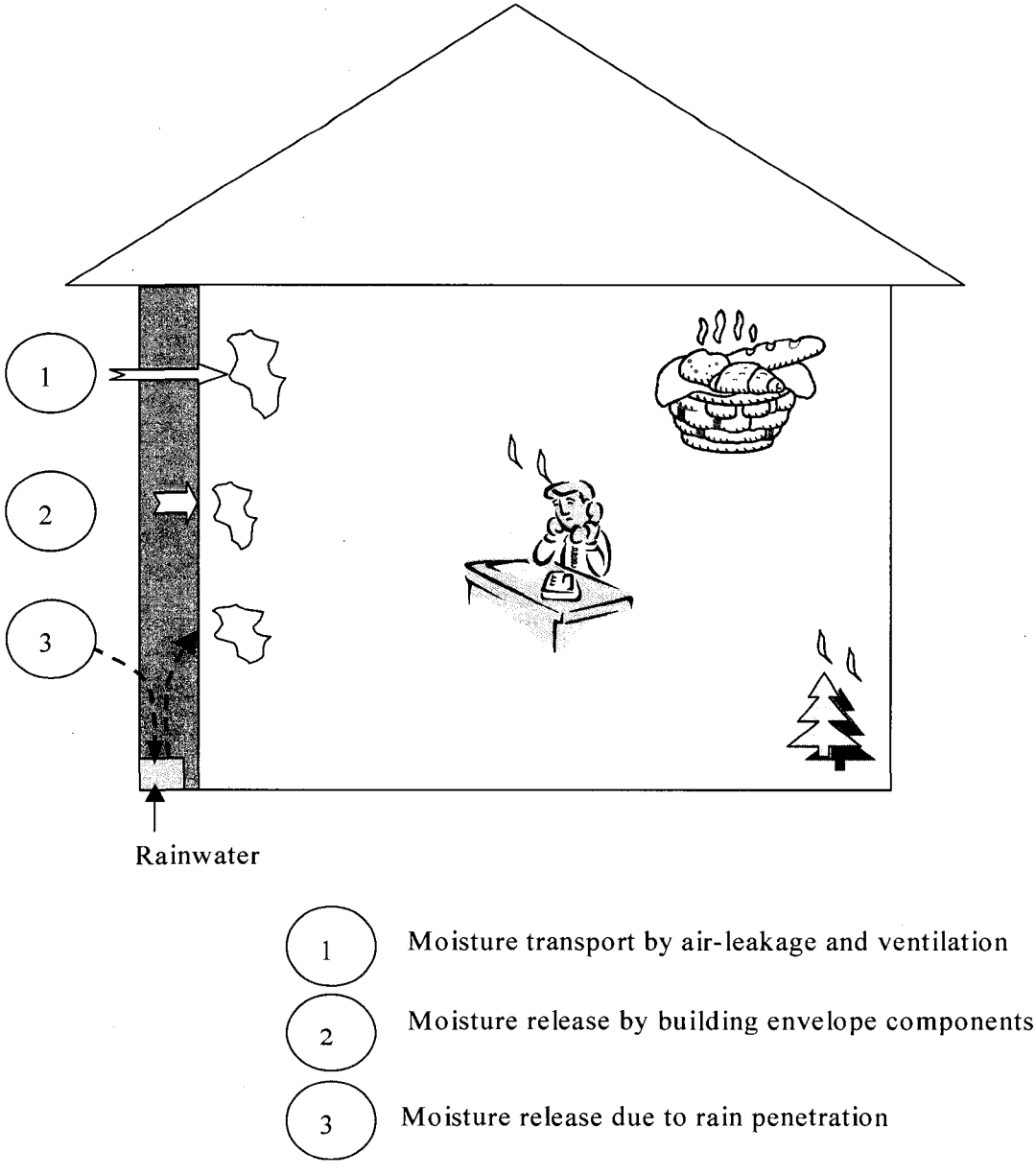

Figure 2-2 Moisture sources to the indoor air

3) The third type of moisture source is generated inside the indoor environment and the main contributors are: humans and plants. Humans release moisture by respiration and perspiration. The amount of releases depends on their activities. For an occupant, Christian (1994) estimated 0.03 to 0.06 liter per hour for light activity, 0.12 to 0.2 liter per hour for medium activity and 0.2 to 0.3 liter per hour for hard work. These estimations of moisture load per person widely vary; for example, ASHRAE Handbook of Equipment (1988) recommends 0.09 liter per hour while the occupant is resting and 0.27 liter per hour while working hard. Quirouette (1983) and Sawers (1983) estimated the amount of moisture release to the indoor air due to various activities such as bathing, showering, cooking, dish washing, and cloth washing and drying to 2.4 liters per day. According to the IEA-Annex 14 (1991) the daily average moisture release of a typical family of four is estimated to be 13.3 kg. Most of the water used for watering of plants will be released to the indoor air. Christian (1994) noted that only 0.2% (at most) of the water used to water plants used for growth, the rest would enter the air. For an average size plant, Quirouette (1983) estimated 0.5 liters of water evaporation per week. In addition to the total quantity of moisture production, knowledge of the rate and frequencies of the moisture production (the transient record of moisture production during sleeping, taking shower, cooking etc) are important in controlling the indoor relative humidity.

Knowledge of the level of indoor relative humidity in the living space is important for the evaluation of building enclosure moisture performance, and control of ventilation rate which may be required to maintain the desired indoor air quality and comfort. Various models have been developed in the past to predict the indoor humidity

level of the indoor environment. These models can be broadly categorized into three groups:

1) The first group consists of empirical models, which are based on large-scale field measurement data of various buildings. In these models the indoor vapor pressure is estimated from the outdoor temperature (Sandberg, 1995) or outdoor vapor pressure (Abranties and Freitas, 1989). The factors that determine the actual indoor humidity level such as internal moisture source, ventilation/air leakage, absorption/desorption effect of building material, and other factors are masked and represented by a single parameter called occupant type. These models at best can be good for a rough estimation of the indoor humidity especially for summer condition when the natural ventilation could be higher. In the work of Abrantie and Freitas (1989) the buildings are categorized into four classes based on vapor pressure difference: Gymnasium (0-250 Pa), Housing and School (250-500 Pa), Textile Industry (500-750 Pa), Swimming (Over 750 Pa). Sandberg (1995), on the other hand, classified the buildings into five classes: very-low, low, medium, high and very high, Figure 2-3. The corresponding representative building types are: storage area, offices, normal family house, kitchen and swimming pool, respectively. For each specific class of building, he developed upper bound limits, which are defined by a linear relationship between the outdoor monthly mean temperature and indoor vapor pressure for conditions in which the outside mean temperature lies between 0-20°C. The vapor pressure difference beyond this range is assumed to be zero for outdoor mean temperature over 20°C and a typical constant winter value for temperature below 0°C.

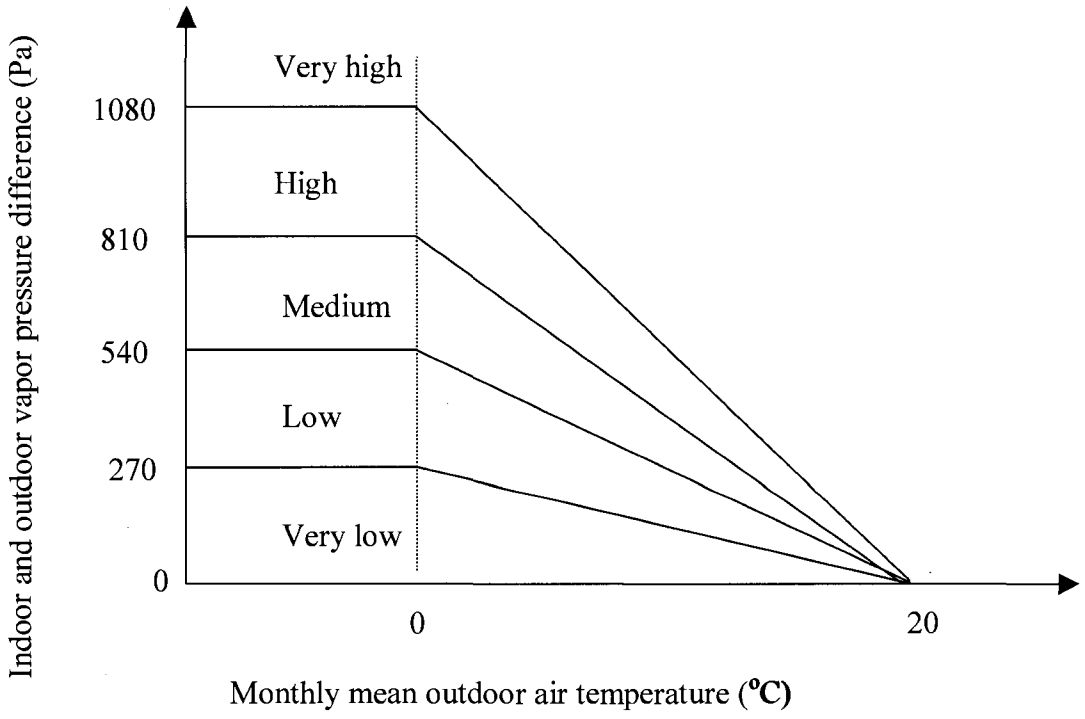

Figure 2-3 Indoor humidity classifications in Class model (Sandberg, 1995).

Similarly, Sanders (1995, 1996) classified the indoor climate into four classes. He based his classification on HAM analysis of building envelope components, more specifically north-facing wall and roof. The border limits of the classes, which are referred to as pivot points, are construction dependent and define the maximum allowable internal vapor pressure before condensation starts and/or net moisture accumulation occurs inside a "benchmark construction".

2) The second group of models is based on steady state analysis of moisture balance. These models are more detailed, and need specific information about the building such as building volume, air-exchange-rate (ACH) and occupant behavior in relation to moisture production/removal. In this category of models the only moisture transport mechanism is by ventilation (Loudon, 1971; Hutcheon and Handegord, 1995;

Tsongas et al., 1996; TenWolde, 2001a). Ventilation rate and moisture generation need to be explicitly defined, but the moisture absorption and release by the interior furnishing and furniture are differed in these models as well. The basic equation of such type of model is:

$$\omega_i = \frac{M_g}{\dot{m}_a} + \omega_o$$

where ω_i (kg/kg air) is the indoor humidity ratio, ω_o is the outdoor air humidity ratio (kg/kg air), M_g moisture generation rate (kg/s) and $\dot{m}_a$ ventilation rate (kg/s).

3) The third group of models is an improvement of the second group, and based on a transient analysis of humidity balance differential equation. In these models the moisture buffering effects of internal furnishing and furniture are accounted for. These materials could absorb as much as one third of the moisture release into the indoor air (El Diasty et al., 1992; Jones, 1995) and thereby modulate the indoor humidity level (Simonson et al., 2004a,b). Isothermal indoor humidity simulation results of TenWolde (1988) and El Diasty et al. (1992) demonstrated the importance of moisture buffering effect in indoor humidity modeling, especially, in cases where ventilation rate is very low. In humidity prediction models, the moisture buffering effects is represented in many ways with various simplifying assumptions. In early 1980's Tsuchiya presented an indoor relative humidity model where the moisture buffering effect of interior surfaces is given by an empirical expression. As it is presented in Kusuda (1983) paper, the moisture exchange between the indoor air and the moisture buffering material is limited to the contact surface only. Moreover, the surface humidity ratio (ω_s) of the surface is

expressed by an empirical relation, which contains constants (41 and 5.46) and is given by the form:

$$\omega_s = \frac{\tilde{\omega}_s}{41}\left(\frac{w_i}{w_o C}T - 5.46\right)$$

In this equation, w_i (moisture content of the material) and $w_o C$ (surface average moisture content of the surface) have to be determined from experiment. $\tilde{\omega}_s$ is the saturated humidity ratio of the indoor air at temperature T. TenWolde (1988) developed a mathematical model called FPLRH1 where the moisture storage effect of hygroscopic materials is treated in a simplified way by the following equation:

$$\dot{Q}^m_{ad} = A \cdot K \cdot \left(\phi_i - \phi_{avg}\right)$$

where $\dot{Q}^m_{ad}$ is the moisture absorption/desorption rate of the material (kg/s), A is the total floor area of the building (m^2), K is a sorption parameter, and ϕ_i and ϕ_{avg} are the instantaneous and time averaged relative humidity of the indoor air, respectively. One of the problems of this model is, the sorption parameter (K) and the time period for back averaging of indoor relative humidity (ϕ_{avg}) are arbitrary values since they depend on the type of construction and interior furnishings. The fundamental assumption of this model is that the moisture buffering material is in equilibrium with three to six weeks average of the indoor relative humidity. The assumption does not make distinction between the bulk (where the change in moisture condition is slow) and the thin surface layer of the material where the change in the moisture condition may actually be fast and in dynamic equilibrium with the indoor humidity with some time lag. Later, TenWolde (1994) upgraded his indoor humidity model FPLRH1 to FPLRH2. In this improved model, the

moisture buffering effect of the interior furnishing materials is related to exponentially weighted back average of indoor relative humidity, which gives more weight for recent humidity conditions, rather than arithmetic average as used in the earlier model. The other variant of this class of indoor model is Jones model (1993, 1995), which considers the indoor moisture generation and ventilation rate as well as the absorption/desorption effect. The absorption/desorption characteristics of the interior furnishing are represented by two empirical coefficients: alpha(α) and beta(β). These coefficients are called moisture admittance factors, and represent the moisture absorption and desorption characteristics of the interior furnishing, respectively.

$$\dot{Q}_{ad}^{m} = \rho V\left(\alpha\omega - \beta\tilde{\omega}_{s}\right)$$

where ρ, V and $\tilde{\omega}_{s}$ are density of air, volume of the room and saturated humidity ratio of the indoor air at temperature T, respectively. In this model the moisture contents of the moisture buffering materials are assumed to be constant. Moreover, the surface and air temperatures are assumed to be the same. On the basis of these assumptions, he suggested that six pair of admittance factors could be enough for indoor air humidity modeling. These empirically determined coefficients would represent the high, medium and low moisture admittance under summer and winter conditions. This implies that for a given building, the coefficients remain the same for a period of a season (winter or summer), and the absorption/desorption of moisture buffering material will be linearly proportional to the indoor humidity and temperature.

As Kumaran (2005) pointed out, the models in this category and identified by Jones (1995) as "current humidity models" are similar to the early work of Tsuchiya, and only vary in the assumption made in representing the terms, particularly the moisture

absorption/desorption by moisture buffering materials. Because of their underlying assumption of constant moisture content, these models may not capture the dynamic responses of the moisture buffering material to a transient or abrupt moisture production/removal in the indoor air. To capture this dynamic process El Diasty et al. (1992, 1993) developed a more advanced humidity model using transient heat transfer analysis analogy. They formulate a linear differential equation, which characterizes the indoor air humidity balance based on the moisture exchange by ventilation, moisture generation, and absorption/desorption of interior surfaces. Then, the transient humidity response of the indoor air is obtained by solving the humidity balance equation numerically for discrete time steps. The surface moisture content of the moisture buffering material is computed assuming constant indoor humidity during the time step. Analogous to transient heat transfer, the moisture buffering response of the material is modeled in two ways depending on the Biot number $(h_m S/\delta)$, where h_m is the convective mass transfer coefficient, S is a characteristic length and δ is the vapor permeability of the material. In this context, the Biot number relates the convective-surface resistance to the internal moisture transfer resistance. For cases where the Biot $\leq$ 0.1, a lumped parametric analysis is applied, which effectively means that there is no moisture gradient across the material, and the surface resistance is large compared to the internal resistance for moisture flow. However, this assumption is not applicable for a bulk material where moisture gradient across the thickness is expected. For this case (Biot $>>$ 0.1) the moisture exchange between the material and the indoor air is assumed to be in the few millimeter depth of the material. The surface moisture content of this thin layer is determined by solving the moisture balance equation for the material under no

moisture flow beyond the critical penetration depth assumption at the boundary $\left(\frac{\partial w}{\partial x} = 0\right)$. Unlike the models discussed above, this model has a dynamic link between the moisture buffering material response and the indoor air relative humidity condition. The challenge in this modeling approach is in defining the critical penetration depth, which could be arbitrary, and also the applicability of lumped-capacity assumption in real conditions.

3 THE NEED FOR HOLISTIC HYGROTHERMAL MODELING

During the design process, building engineers evaluate the performance of various design alternatives in terms of their durability, comfort and indoor air quality, as well as energy efficiency using building envelope, indoor and energy analysis tools, respectively. But, usually the analysis tools are standalone and used for the respective analysis without considering the effect of one on the other. Building envelope models are useful to evaluate the hygrothermal performance of an individual building component (wall, roof or floor), which could be subjected to wetting by condensation, rain penetration or air leakage.

The performance of a building envelope component is usually measured based on the moisture analysis of individual components (such as cladding, sheathing board and dry wall) for their drying potentials and likelihood of occurrence of problems associated with high moisture accumulation (Tariku et al. 2007). In the analysis, most building envelope models assume constant indoor boundary conditions based on Abranties and Freitas (1989) or Sanders (1995,1996) work. However, use of a stand-alone building envelope model without giving enough attention to the indoor environmental conditions may lead to a wrong conclusion. The application of accurate indoor boundary conditions are very important in the moisture performance analysis of building envelope components (TenWolde, 2001a; Tsongas et al., 1996). In the current simulation practice the indoor and outdoor boundary conditions are known quantities. The indoor boundary conditions (temperature and relative humidity) are predefined with two sets of constant

values for summer and winter periods or a set of value is assumed for the entire simulation period. Although the outdoor boundary conditions (weather data) are independent of the hygrothermal condition of the envelope, the indoor conditions are, as discussed in Section 2.2. This implies that the building envelope model needs to have a direct coupling with an indoor model, which will provide more accurate boundary conditions on the interior surface of the component. Moreover, this coupling enables one to take into account the interaction between different building envelope components in reference to their influence on the indoor boundary conditions. This is due to the fact that, the moisture and heat exchanges between the indoor air and the various building envelope components may vary depending on their orientations and inclinations. The main reasons for the variations can be due to the directional wind-driven rain and solar radiation loads (for example, the north wall will not get solar radiation as much as south wall) and/or the component type (window verses opaque wall).

Indoor temperature and relative humidity prediction models are important: 1) to keep the comfort level of the occupant, which is important as people spend most of the time indoors, 2) to improve indoor air quality and reduce health risk associated with mold growth, and 3) to keep and control the indoor humidity level in a specific range which is required due to the special use and operation need of the building. Examples of such buildings are art galleries, museum, library etc. To maintain the indoor humidity level within the design range, the building engineer may need to use indoor models to evaluate different ventilation strategies and/or moisture buffering materials, and decide on the appropriate equipment size and material choice. However, the success of the strategy may depend on the robustness of the indoor model used to predict the indoor conditions. Most of the current humidity models ignore or lack comprehensive analysis of moisture

exchange between the various building envelope components and the indoor air as discussed in section 2.2. To the contrary, various researchers (Simonson, 2004a,b; El Diasty et al., 1993; Jones, 1992) have emphasized the significance of this moisture exchange in determining the indoor humidity. El Diasty et al. (1992) and Jones (1995) suggested that as much as one third of the moisture release into the indoor air could be absorbed by interior moisture buffering materials. These materials have a potential of modulating the indoor humidity level (Simonson et al., 2004a,b), especially in cases where ventilation rate is low (TenWolde, 1988; Diasty et al., 1992). Thus, detailed account of the dynamic moisture absorption and release of moisture buffering materials is crucial to predict the indoor humidity level and fluctuation ranges more accurately. Moreover, Christian (1994) stated that moisture sources from construction (e.g. initial moisture content of concrete), and from wet soil through foundation walls and floor slabs could dominate all internal moisture sources. Despite their importance these moisture sources are not included in the current humidity models. To predict the indoor air conditions more accurately, though, the indoor model needs to be dynamically coupled with the building envelope model to capture these moisture sources and the dynamic moisture and heat exchange between the construction and indoor air.

Building envelope models can be used to assess the energy performance of a single component (wall and roof systems) with the same limitation stated above, which is the need for prescribed indoor boundary conditions. Inherently, these models do not consider the thermal interaction between different components of the building, which could have different thermal conditions throughout a day due to their orientation. For example, a wall oriented to the north does not receive as much solar radiation as the wall

oriented to the south. With these models, a comprehensive analysis of heating and cooling load calculation is not possible, and therefore cannot be used for HVAC design.

Currently, there are many energy simulation models such as EnegyPlus and ESP-r to evaluate the energy performances of alternative building designs and HVAC systems. These models determine the heating and cooling loads of the building as well as the indoor air temperature based on the whole building energy analysis. In these models the indoor temperature is an unknown quantity, unlike building envelope models. These energy simulation models, however, usually ignore the moisture effect on the thermal analysis (Mendes et al., 2003), and use constant thermal storage and transport (thermal conductivity and heat capacity, respectively) property values despite the fact that these properties can be strongly dependent on moisture content. For example, the thermal storage capacity of wood increases by 30%, compared to dry state value, as the moisture content increases to 10% (ASHRAE 2005), and also the thermal conductivity of lime silica brick increases more than twice as the moisture content increase to full saturation (Kuenzel et al., 2001). This implies that arbitrary choice of constant thermal transport and storage property values may result in incorrect prediction of heat flux through building enclosure as demonstrated in Hagentoft's (1996) simple calculation of heat fluxes with and without moisture in a structure. The other important effect of moisture in the energy calculation, which are quite often omitted in whole building energy analysis tools, are the latent heat transfer across the building enclosure and the local heating and cooling effects that are generated within the structure due to moisture phase changes (condensation and evaporation, respectively).

In the current energy simulations tools, the latent heat load is taken as instantaneous gain, and the indoor humidity load is calculated either with a very

simplified model for moisture storage capacity of interior furnishing or totally ignoring that phenomenon. However, the accurate prediction of indoor humidity, using a dynamic indoor humidity model, which takes into account the dynamic interaction of the indoor humidity and moisture buffering materials, is essential for a better calculation of the latent heat load. Knowledge of a more accurate latent heat load, in turn, helps to choose more appropriate cooling equipment size, which could result in operating cost savings (Isettti et al., 1988). The need for accurate prediction of indoor humidity for cooling equipment selection is more critical in hot-humid weather. Consequently, to perform a better energy analysis and select an appropriate HVAC system for a building, the effect of moisture on both building envelope components and indoor air has to be taken into account in the energy analysis. Thus, the integration of building envelope model, indoor model, and HVAC system model yields a more accurate prediction of the energy demand of the building. This integration can also yield a more accurate prediction of internal surface temperatures, which is important in defining the operative temperature of heating/cooling system.

The three aspects of building design: durability, indoor conditions, and energy performance, are interrelated. These three building performance parameters have to be considered simultaneously for optimized ventilation system design. For example, a design with low ventilation rate can have an advantage in energy saving, but could result in excessive indoor humidity, which consequently creates a problem in maintaining comfort and indoor air quality, and may also result in decay of wood products and corrosion of metal components. On the other hand, if the ventilation is excessive, it may result in high-energy demand and low occupant comfort.

3.1 Objective

The objective of this thesis is to carry out an integrated analysis of whole building performance and demonstrate the need for an integrated building design approach to attain optimized building performance. To achieve this objective, first, a whole building hygrothermal model is developed by which indoor conditions (temperature and humidity), building enclosure moisture performance and energy efficiency of a building are analyzed in an integrated manner on a single platform. The model is benchmarked before it is used to investigate the effects of various building design parameters on the overall performance of a building. Moreover, prediction of indoor humidity, development and application of two-dimensional building envelope model are also focuses of the research.

3.2 Thesis outline

The whole building hygrotherml model integrates various aspects of a building: building envelope enclosure, HVAC systems, and indoor heat and moisture generation mechanisms. The mathematical and numerical development of the two primary models namely, building envelope and indoor models, as well as the whole building hygrothermal model are presented in Chapter 4. Benchmarking of the building envelope model against analytical, numerical (comparison with other models), and experimental test cases are carried out in Chapter 5. The building envelope model can be used as a stand alone for simulating the coupled non-linear heat, air, and moisture transfer in building envelope components, or may be coupled with the indoor model to create the whole building hygrothermal model. In Chapter 6 the whole building hygrothermal

model simulation results are compared with internationally published results. The indoor humidity profiles of a real house that are generated by various humidity models are compared in Chapter 7. Subsequently, the hygrothermal responses of a building envelope section as it is exposed to the various indoor humidity profiles are compared. In Chapter 8, the effects of various building design variables on the overall performance of a house are investigated. Moreover, various building design options such as ventilation strategy and energy upgrade options are studied with the objective of achieving optimized building performance with respect to indoor humidity level, building envelope durability, and energy efficiency.

4 DEVELOPMENT OF WHOLE BUILDING HYGROTHERMAL MODEL

In whole building hygrothermal modeling the building is considered as an integrated system, which consists of building enclosure, indoor environment and mechanical systems, Figure 4-1. In this modeling approach the indoor environmental conditions, more specifically, temperature and relative humidity, are unknown quantities, and have to be determined from the heat and mass balance in the zone considering the following three mechanisms: 1) heat and mass transfer across the building enclosure, 2) internal heat and moisture generated by occupants and their activities, and 3) heat and moisture supply from mechanical systems (heating, cooling, humidification, dehumidification and ventilation) depending on the mode of operation of the building.

In this chapter, first, a building envelope model is developed to handle the heat and moisture exchanges between building enclosure and indoor air, as well as the effect of the outdoor climatic conditions on the indoor environment and building envelope components performance. The second and third heat and moisture transfer mechanisms, internal heat and moisture generations and mechanical systems outputs, are incorporated in the indoor model. The indoor model is presented in Section 4.2 in detail. Finally, the building envelope and indoor models are coupled to form a whole building hygrothermal model that can be used for an integrated analysis of indoor humidity, energy efficiency and building enclosure performance. The accuracy of the models is tested in Chapter 5 and 6 using internationally published benchmark exercises.

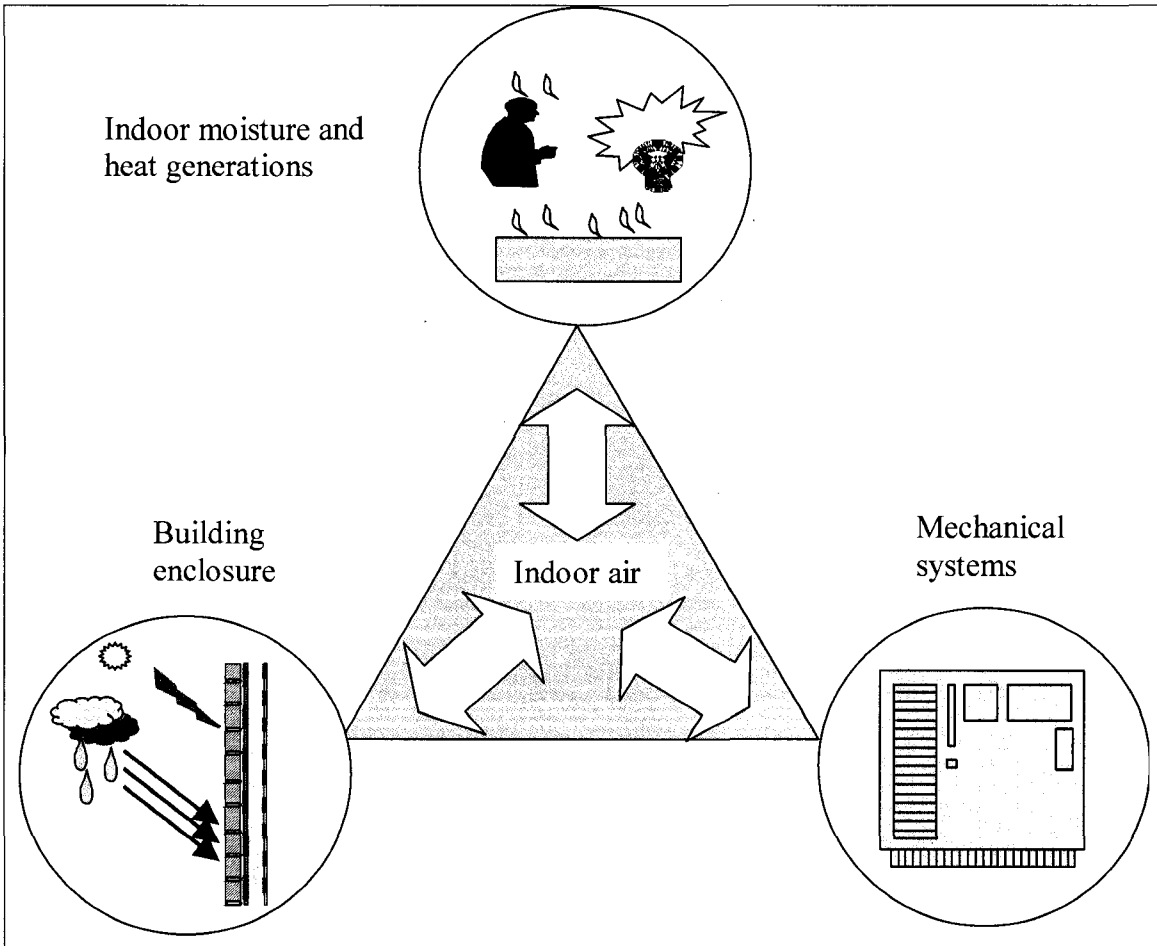

Figure 4-1 Dynamic interaction of building enclosure, indoor moisture and heat generations, and mechanical systems.

4.1 Building envelope model (HAMFit)

The thermal and moisture dynamic responses of building enclosures, which is one essential input of whole building hygrothermal model, have strong impact on the overall performance of the building. This is due to the fact that the moisture stored in the structure affects the indoor humidity and energy flow across the structure, and thereby HVAC equipment size. Moreover, the building enclosure can have significant influence on the indoor humidity level depending on the moisture buffering capacity of the interior lining materials. To accurately capture the dynamic influences of building enclosure on the indoor environment and HVAC systems, a transient HAM model that handles coupled heat, air and moisture transfer through multilayered porous media is essential.

Most building materials are porous, and composed of solid matrix and pores. In the pores, moisture can exist in any of the three thermodynamic states of matter, i.e. gas (vapor), liquid, and solid (ice) states. However, moisture movement is possible only in the vapor and liquid states. The main mechanisms of moisture transfer can be by vapor diffusion, capillary suction, or combination of both, depending on the moisture content of the material, Figure 4-2. Generally, the cutoff relative humidity for hygroscopic and capillary water regions may vary from material to material. In the hygroscopic region the pores are filled mainly with water vapor, Figure 4-3 (a), and consequently the moisture transport is mainly by vapor diffusion. Liquid water transport is possible for the case where the pores are filled with liquid water (Figure 4-3 (b)). This flow mechanism is very active in the capillary water region, where the relative humidity is over 95%. Both vapor and liquid transport can co-exist in the higher end of hygroscopic region, Figure 4-3 (c). In this region both vapor diffusion and capillary suction are active in large and small

pore, respectively. Vapor diffuses in the open pores and condenses on the capillary meniscus and at the other end of the meniscus it evaporates into the next open pore space. This moisture movement phenomenon implies that the diffusion path is reduced, which results in an increase in the transport process.

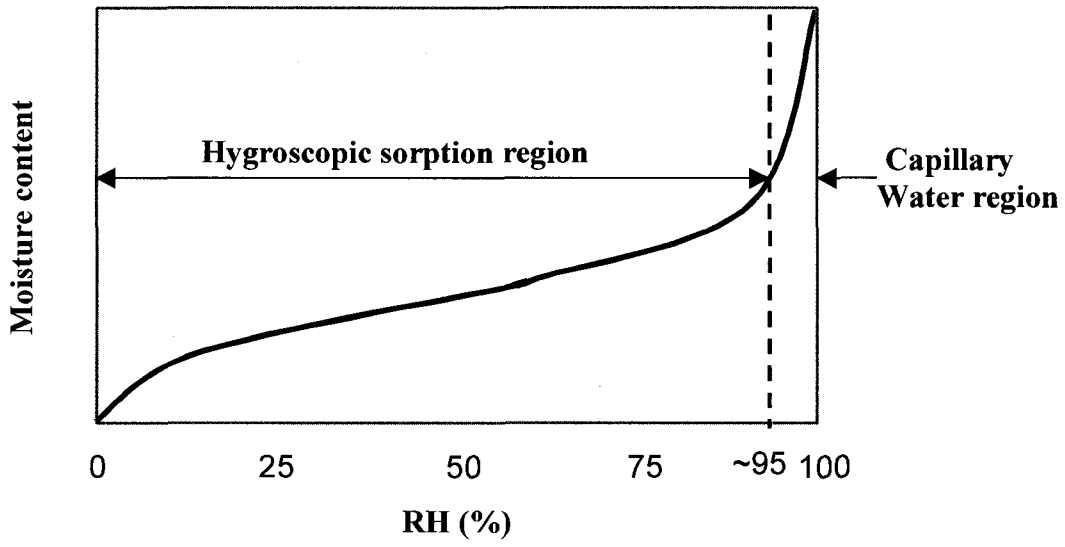

Figure 4-2 Equilibrium moisture content of a typical material at different relative humidity

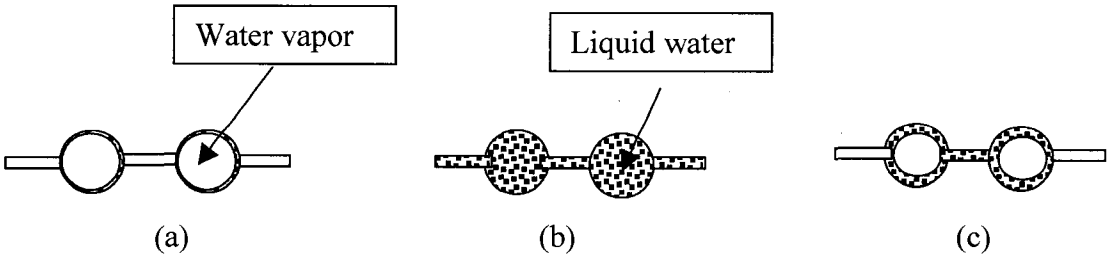

Figure 4-3 Moisture in idealized pores (Hagentoft, 1997).

(a) hygroscopic region, (b) capillary water region (c) high end of hygroscopic region

In the section below, a building envelope model is developed under the following assumptions. The fluid (air, water vapor and liquid water) in the pores and the local solid matrix are in thermal equilibrium. The general gas law defines the thermodynamic state of the air, water vapor and the water vapor-air mixture in the pores. The contact surfaces between two adjacent layers are assumed to be in perfect contact, consequently, the profiles of vapor pressure, suction pressure and temperature are continuous at the interface. The model is benchmarked in Chapter 5 and Tariku et. al. (2008).

4.1.1 Conservation equations

4.1.1.1 Conservation of Mass and Species

The governing equation for conservation of mass, which means that the total mass of a given control volume will not change, is given by Equation [4.1] (Bear, 1992).

$$\frac{\partial \rho}{\partial t} + div(\rho V) = 0 \qquad [4.1]$$

Although the total mass of the control volume will not change, there may be a gain and a loss of mass of individual components (water vapor and liquid water) due to phase change that occurs due to evaporation and condensation phenomena. The conservation of the individual fluids is governed by the general conservation of species equation, Equation [4.2], (Bear, 1992).

$$\rho\frac{\partial Y_i}{\partial t}+\rho div\left(VY_i\right)+div\left(j_i\right)=\dot{m}_c \qquad [4.2]$$

where: $\rho\frac{\partial Y_i}{\partial t}$ --The rate of net accumulation of species *i* in the control volume

$-\rho div\left(VY_i\right)$ --The rate of accumulation of species *i* in the control volume by convection (bulk flow velocity *V*)

$-div\left(j_i\right)$ --The rate of accumulation of species *i* in the control volume by molecular diffusion

$\dot{m}_c$ --The rate of production or destruction of species *i* in the control volume.

In building physics applications, the main components that constitute a porous control volume for above freezing temperature are the solid matrix, air, water vapor and liquid water, and their respective mass and mass fractions with reference to solid matrix mass are $m_m, m_a, m_v \text{ and } m_l$ and $Y_a=\frac{m_a}{m_m}, Y_v=\frac{m_v}{m_m} \text{ and } Y_l=\frac{m_l}{m_m}$, respectively. The apparent density of the control volume ρ is given by $\rho=\rho_m\left(1+Y_a+Y_v+Y_l\right)$, where ρ_m is density of the solid matrix. The reference moisture state for $\dot{m}_c$ (rate of mass change due to phase change) is liquid water, and consequently $\dot{m}_c$ is positive for condensation and negative for evaporation processes. Based on the general species equation (Equation [4.2]), the individual species conservation equation for water vapor, liquid water and air are given as follow:

Conservation equation for water-vapor:

$$\rho_m \frac{\partial Y_v}{\partial t} + \rho_m div(VY_v) + div(j_v) = -\dot{m}_c \qquad [4.3]$$

The water-vapor amount decreases if there is condensation

Conservation equation for liquid-water:

Equation [4.4] is the general governing equation for liquid flow.

$$\rho_m \frac{\partial Y_l}{\partial t} + \rho_m div(V_l Y_l) + div(j_l) = \dot{m}_c$$

The liquid flow by convection (second term) can be neglected since the liquid flow velocity in a porous media is negligible. Thus:

$$\rho_m \frac{\partial Y_l}{\partial t} + div(j_l) = \dot{m}_c \qquad [4.4]$$

The liquid water amount increase with condensation

Conservation equation for air:

$$\rho_m \frac{\partial Y_a}{\partial t} + \rho_m div(VY_a) + div(j_a) = 0 \qquad [4.5]$$

There is no production/destruction term.

4.1.1.2 Moisture balance equation

The governing equation for moisture flow can be derived by adding the vapor and liquid water species conservation equations, Equation [4.3] and [4.4], respectively.

$$\rho_m \frac{\partial Y_v}{\partial t} + \rho_m div(VY_v) + div(j_v) = -\dot{m}_c$$

$$+$$

$$\rho_m \frac{\partial Y_l}{\partial t} + div(j_l) = \dot{m}_c$$

Gives:

$$\rho_m \left(\frac{\partial Y_v}{\partial t} + \frac{\partial Y_l}{\partial t} \right) + \rho_m div(VY_v) + div(j_v) + div(j_l) = 0$$

Since $\rho_m \left(\frac{\partial Y_v}{\partial t} + \frac{\partial Y_l}{\partial t} \right) = \frac{\partial w}{\partial t}$, where w is moisture content in kg/m^3, the general governing equation for moisture transport can be given by Equation [4.6].

$$\frac{\partial w}{\partial t} + \rho_m div(VY_v) + div(j_v) + div(j_l) = 0 \qquad [4.6]$$

4.1.1.3 Energy balance equation

The conservation equation for internal energy and enthalpy are derived from the conservation equation of total stored energy (Kuo, 1986). The total stored energy (E) of a system is the sum of internal energy (U), kinetic energy (KE), and potential energy (PE),

$E = U + KE + PE$. The conservation equation for the total stored energy can be derived by considering a control volume, and accounting the rate of change of stored energy in the control volume (term *I*), transport of energy in and out of the control volume by convection (term *II*) and diffusion (term *III*) as well as the work done by external forces at the surface of the control volume viscous forces (term *IV*) and by gravity (body) force (term V) and heat source (or sink) (term *VI*).

$$\underbrace{\frac{\partial(\rho e)}{\partial t}}_{I} + \underbrace{div(\rho V e)}_{II} = \underbrace{-div(j_q)}_{III} + \underbrace{div(\hat{\tau} V)}_{IV} + \underbrace{\rho(\vec{g} \cdot V)}_{V} + \underbrace{\dot{Q}}_{VI} \qquad [4.7]$$

where e is energy per unit mass $\left(e = \frac{E}{m} = u + \frac{1}{2}|V^2| + g \cdot x_i\right)$ and ρe is energy per unit volume. After some mathematical manipulations (Kuo, 1986), the energy conservation equation, Equation [4.7], is rewritten in terms of enthalpy, Equation [4.8].

$$\frac{\partial(\rho h)}{\partial t} + div(\rho V h) = -div(j_q) + \dot{Q}_s \qquad [4.8]$$

4.1.2 Mathematical models implemented in the HAMFit model

4.1.2.1 Moisture transfer

The governing equation for moisture transfer (Equation [4.6]) can be written as Equation [4.9] after substituting the vapor diffusion, vapor convection and liquid conduction terms with expressions given in Appendix A-1 as Equation A-2, A-3 and A-4, respectively.

$$\frac{\partial w}{\partial t} + div\left(\rho_a V \omega\right) + div\left(-\delta_v \frac{\partial P_v}{\partial x_i}\right) + div\left(D_l\left(\frac{\partial P_s}{\partial x_i} + \rho_w g\right)\right) = 0 \qquad [4.9]$$

As shown in the above equation, Equation [4.9], various driving forces P_v and P_s and flow variables w and ω are present. In the numerical method adopted here it was important to express the driving forces and flow variables with a single flow potential. The chosen flow potential in this work is relative humidity since it is continuous at the interface of two layers of materials with different moisture storage properties (sorption and moisture retention), contrary to moisture content, which is discontinuous. This is illustrated in Figure 4-4 and Figure 4-5 as follows: the relative humidity of the contacting surfaces of material 1 and material 2 is the same since the vapor pressure and temperature are continuous at the interface. However, the equilibrium moisture contents of the respective contacting surfaces, W_1 and W_2, are different (Figure 4-4). Consequently, the moisture content profile becomes discontinuous as it jumps from W_1 to W_2 at the interface, Figure 4-5. On the other hand, relative humidity is continuous throughout the computational domain. As stated earlier, the numerical tool adopted in this thesis requires that all terms in the moisture balance equation be expressed in terms of a single driving

potential (relative humidity). The transformations of the terms in the moisture balance equation, similar to Hagentoft (2002), are presented below.

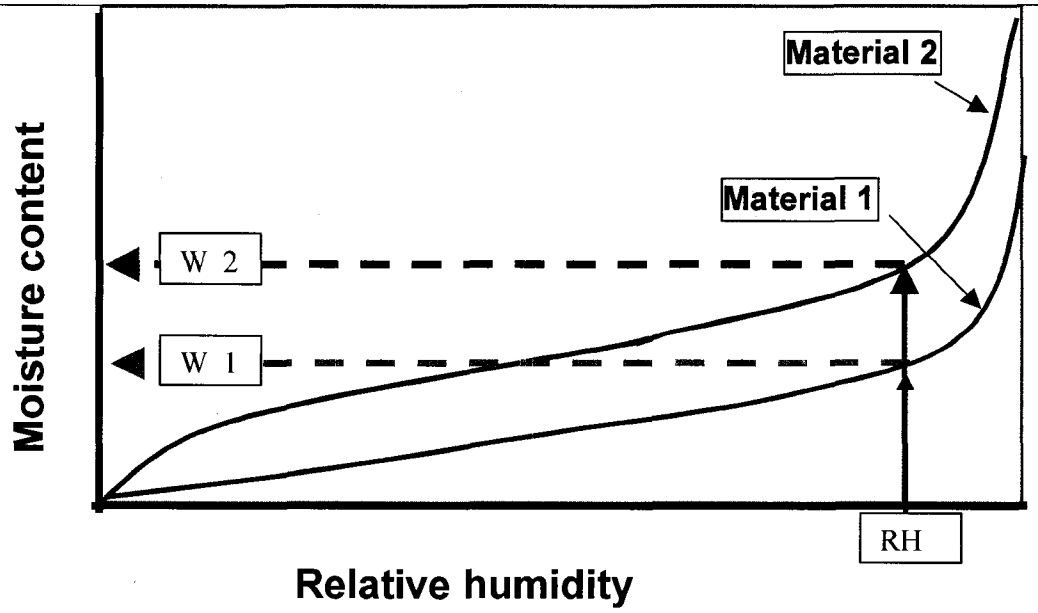

Figure 4-4 Sorption isotherm of two dissimilar materials

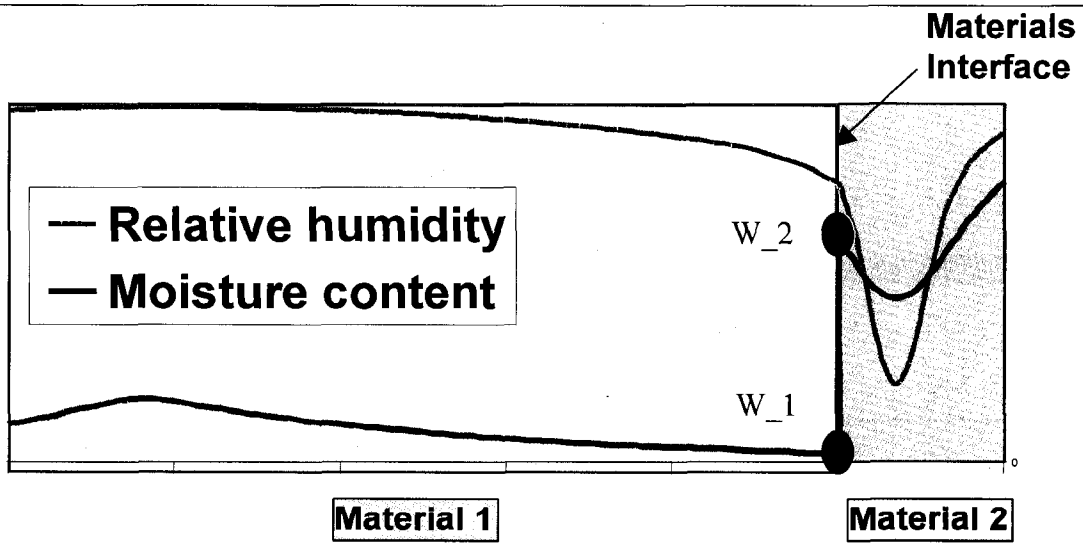

Figure 4-5 Relative humidity and moisture content profiles at the interface of two dissimilar materials.

The moisture content profile is discontinuous at the interface, but the relative humidity profile is not.

Transient term

$$\frac{\partial w}{\partial t} = \frac{\partial w}{\partial \phi} \cdot \frac{\partial \phi}{\partial t} \qquad \Theta = \frac{\partial w}{\partial \phi} \qquad \text{where } \Theta = \frac{\partial w}{\partial \phi} \text{ is the sorption capacity}$$

(Slop of sorption-moisture retention curve)

$$\frac{\partial w}{\partial t} = \Theta \frac{\partial \phi}{\partial t} \qquad [4.10]$$

Vapor diffusion term

$$\frac{\partial P_v}{\partial x_i} = \frac{\partial \left(\hat{P}(T) \cdot \phi \right)}{\partial x_i} = \phi \frac{\partial \hat{P}(T)}{\partial x_i} + \hat{P} \frac{\partial \phi}{\partial x_i}$$

$$\frac{\partial \hat{P}(T)}{\partial x_i} = \frac{\partial \hat{P}(T)}{\partial T} \cdot \frac{\partial T}{\partial x_i}$$

where $\hat{P}(T)$ is the saturation vapor pressure, which is a function of temperature T

$$\frac{\partial P_v}{\partial x_i} = \phi \frac{\partial \hat{P}}{\partial T} \cdot \frac{\partial T}{\partial x_i} + \hat{P} \frac{\partial \phi}{\partial x_i} \qquad [4.11]$$

Vapor convection term

$$\omega = \frac{0.622 \cdot P_v}{P_{atm} - P_v}; \quad P_{atm} - P_v \approx P_{atm} \; ; \; P_v = \hat{P}(T) \cdot \phi$$

$$\omega = \frac{0.622 \cdot \hat{P}(T) \cdot \phi}{P_{atm}}; \qquad C_c = \frac{0.622}{P_{atm}}$$

where P_{atm} is atmospheric pressure

$$\omega = C_c \hat{P} \cdot \phi \qquad [4.12]$$

Liquid water conduction term

From Kelvin's equation the suction pressure can be expressed as a function of temperature and relative humidity:

$$P_s(T,\phi) = -\frac{\rho_w RT}{M}\ln(\phi)$$

where R is the universal gas constant (8.314 $Jmol^{-1}$) and M is the molecular weight of water molecule (0.01806 kg mol^{-1}). Partial differentiation of suction pressure gradient yields Equation [4.13].

$$\frac{\partial P_s}{\partial x_i} = \frac{\partial P_s}{\partial T}\cdot\frac{\partial T}{\partial x_i} + \frac{\partial P_s}{\partial \phi}\frac{\partial \phi}{\partial x_i}$$

$$\frac{\partial P_s}{\partial T} = -\frac{\rho_w R}{M}\ln(\phi)$$

$$\frac{\partial P_s}{\partial \phi} = -\frac{\rho_w RT}{M}\cdot\frac{1}{\phi}$$

$$\frac{\partial P_s}{\partial x_i} = -\frac{\rho_w R}{M}\left(\ln(\phi)\frac{\partial T}{\partial x_i} + \frac{T}{\phi}\frac{\partial \phi}{\partial x_i}\right) \qquad [4.13]$$

Finally, substituting Equation [4.10] to [4.13] into Equation [4.9] gives:

$$\Theta\frac{\partial \phi}{\partial t} = \frac{\partial}{\partial x_i}\left(\delta_v\underbrace{\left[\phi\frac{\partial \hat{P}}{\partial T}\cdot\frac{\partial T}{\partial x_i} + \hat{P}\frac{\partial \phi}{\partial x_i}\right]}_{\frac{\partial P_v}{\partial x_i}} - \rho V_i\underbrace{\left[C_c\hat{P}\cdot\phi\right]}_{\omega}\right) + \frac{\partial}{\partial x_i}\left(D_l\underbrace{\frac{\rho_w R}{M}\left(\ln(\phi)\frac{\partial T}{\partial x_i} + \frac{T}{\phi}\frac{\partial \phi}{\partial x_i}\right)}_{\frac{\partial P_s}{\partial x_i}} - D_l\rho_w\vec{g}\right)$$

Rearranging terms:

$$\Theta\frac{\partial\phi}{\partial t}=\frac{\partial}{\partial x_i}\left(\underbrace{\left(\delta_v\hat{P}+D_l\frac{\rho_w R}{M}\frac{T}{\phi}\right)}_{D_\phi}\frac{\partial\phi}{\partial x_i}+\underbrace{\left(\delta_v\phi\frac{\partial\hat{P}}{\partial T}+D_l\frac{\rho_w R}{M}\ln(\phi)\right)}_{D_T}\frac{\partial T}{\partial x_i}\right)-\frac{\partial}{\partial x_i}\left(D_l\rho_w\vec{g}+\rho V_i\left(C_c\hat{P}\cdot\phi\right)\right) \qquad [4.14]$$

Thus, the mathematical model implemented in HAMFit for moisture transfer through building envelope components, written in short form, is:

$$\Theta\frac{\partial\phi}{\partial t}=\frac{\partial}{\partial x_i}\left(D_\phi\frac{\partial\phi}{\partial x_i}+D_T\frac{\partial T}{\partial x_i}\right)-\frac{\partial}{\partial x_i}\left(D_l\rho_w\vec{g}+\rho V_i C_c\hat{P}\cdot\phi\right) \qquad [4.15]$$

where $D_\phi=\left(\delta_v\hat{P}+D_l\frac{\rho_w R}{M}\frac{T}{\phi}\right)$ $D_T=\left(\delta_v\phi\frac{\partial\hat{P}}{\partial T}+D_l\frac{\rho_w R}{M}\ln(\phi)\right)$

The above equation (Equation [4.15]) can be reduced for a simpler case where the moisture transfer in a porous media is considered as isothermal, and with no airflow nor gravity effect as: $\Theta\frac{\partial\phi}{\partial t}=\frac{\partial}{\partial x_i}\left(D_\phi\frac{\partial\phi}{\partial x_i}\right)$. If moisture content is used as a flow variable, the moisture transfer equation can be written as: $\frac{\partial w}{\partial t}=\frac{\partial}{\partial x_i}\left(D_m\frac{\partial w}{\partial x_i}\right)$. Combining these equations provide a relationship between the moisture conduction coefficient D_ϕ and moisture diffusivity D_m. This relation helps to deduce the liquid conduction coefficient and liquid conductivity from measurable quantities of moisture capacity, vapor permeability and moisture diffusivity, Equation [4.16]. The vapor permeability is derived using the flow separation procedure as suggested in Kalagasidis (2004). In HAMFit

model the liquid conductivity is set to zero when the local temperature is below freezing point.

$$D_\phi = D_m \cdot \Theta = \left(\delta_v \hat{P} + D_l \frac{\rho_w R}{M} \frac{T}{\phi} \right) \qquad D_l = \frac{M}{\rho_w R} \cdot \frac{\phi}{T} \left(D_m \cdot \Theta - \delta_v \hat{P} \right) \qquad [4.16]$$

4.1.2.2 Heat transfer

The energy conservation equation (Equation [4.8]) can be written as Equation [4.17] after substituting the transient, convection and diffusion terms with expressions given in Appendix A-2 as Equation B-2, B-3 and B-4, respectively.

$$\underbrace{\rho_m \frac{\partial (h_m)}{\partial t} + \rho_m \left(h_a \frac{\partial}{\partial t} Y_a + Y_a \frac{\partial}{\partial t} h_a + h_v \frac{\partial}{\partial t} Y_v + Y_v \frac{\partial}{\partial t} h_v \right) + \rho_m \left(Y_l \frac{\partial}{\partial t} (h_l) + h_l \frac{\partial}{\partial t} (Y_l) \right)}_{Transient\ term} +$$

$$\underbrace{\rho_m \left(Y_a div(Vh_a) + h_a div(VY_a) + Y_v div(Vh_v) + h_v div(VY_v) \right)}_{Convection\ term} =$$

$$\underbrace{-\left(div\left(-\lambda_{eff} grad(T)\right) + h_a div(j_a) + j_a div(h_a) + h_v div(j_v) + j_v div(h_v) + h_l div(j_l) + j_l div(h_l) \right)}_{Diffusion\ term} + \dot{Q}_s$$

[4.17]

Rearranging terms:

$$\begin{aligned}
&\rho_m \left(\frac{\partial}{\partial t} h_m + Y_a \frac{\partial}{\partial t} h_a + Y_v \frac{\partial}{\partial t} h_v + Y_l \frac{\partial}{\partial t} h_l \right) \\
&+ \rho_m Y_a div(Vh_a) + \rho_m Y_v div(Vh_v) \\
&+ div\left(-\lambda_{eff} grad(T)\right) + j_a div(h_a) + j_v div(h_v) + j_l div(h_l) \\
&+ \rho_m \left\{ h_a \frac{\partial}{\partial t} Y_a + h_v \frac{\partial}{\partial t} Y_v + h_l \frac{\partial}{\partial t} (Y_l) + h_a div(VY_a) + h_v div(VY_v) \right\} \\
&= -div\left(h_a div(j_a) + h_v div(j_v) + h_l div(j_l) \right) + \dot{Q}_s
\end{aligned}$$

Moving the term in brace-bracket into right hand side and rearranging the terms gives:

$$\rho_m\left(\frac{\partial}{\partial t}h_m + Y_a\frac{\partial}{\partial t}h_a + Y_v\frac{\partial}{\partial t}h_v + Y_l\frac{\partial}{\partial t}h_l\right) + \rho_m Y_a div\left(Vh_a\right) + \rho_m Y_v div\left(Vh_v\right)$$

$$+div\left(-\lambda_{eff}grad\left(T\right)\right) + j_a div\left(h_a\right) + j_v div\left(h_v\right) + j_l div\left(h_l\right) =$$

$$-\left(\begin{array}{l} \underbrace{h_a\left(\rho_m\frac{\partial}{\partial t}Y_a + div\left(\rho_m VY_a\right) + div\left(j_a\right)\right)}_{I} \\ +\underbrace{h_v\left(\rho_m\frac{\partial}{\partial t}Y_v + div\left(\rho_m VY_v\right) + div\left(j_v\right)\right)}_{II} + \underbrace{h_l\left(\rho_m\frac{\partial}{\partial t}\left(Y_l\right) + div\left(j_l\right)\right)}_{III} \end{array}\right) + \dot{Q}_s$$

The above equation can be simplified by using (recalling) the species equations, Equation [4.3], [4.4] and [4.5] as follows:

Term *I*: $\rho_m\frac{\partial}{\partial t}Y_a + \rho_m div\left(VY_a\right) + div\left(j_a\right) = 0$ from Equation [4.5]

Term II: $\rho_m\frac{\partial}{\partial t}Y_v + \rho_m div\left(VY_v\right) + div\left(j_v\right) = -\dot{m}_c$ from Equation [4.3]

Term III: $\rho_m\frac{\partial}{\partial t}Y_l + div\left(j_l\right) = \dot{m}_c$ from Equation [4.4]

Thus, the reduced form of the conservation of energy equation is

$$\rho_m\left(\frac{\partial}{\partial t}h_m + Y_a\frac{\partial}{\partial t}h_a + Y_v\frac{\partial}{\partial t}h_v + Y_l\frac{\partial}{\partial t}h_l\right) + Y_a div\left(\rho_m Vh_a\right) + Y_v div\left(\rho_m Vh_v\right)$$

$$+div\left(-\lambda_{eff}grad\left(T\right)\right) + j_a div\left(h_a\right) + j_v div\left(h_v\right) + j_l div\left(h_l\right) = \dot{m}_c\left(h_v - h_l\right) + \dot{Q}_s \qquad [4.18]$$

Substituting the solid matrix, air, water vapor and liquid water enthalpies (h_m, h_a, h_v, h_l) with the corresponding expressions, which are presented in Appendix A-3 for completeness of the work, gives:

$$\rho_m\left(Cv_m\frac{\partial T}{\partial t}+Y_aCp_a\frac{\partial T}{\partial t}+Y_vCp_v\frac{\partial T}{\partial t}+Y_lCp_l\frac{\partial T}{\partial t}\right)+\rho_mY_aCp_a div(VT)+\rho_mY_vCp_v div(VT)$$

$$+div\left(-\lambda_{eff}grad(T)\right)+Cp_aj_a div(T)+Cp_vj_v div(T)+Cp_lj_l div(T)$$

$$=\dot{m}_c\left(\left(h_{fg}+Cp_vT\right)-Cp_lT\right)+\dot{Q}_s$$

Rearranging the terms and making use of the humidity ratio $\omega=\frac{Y_v}{Y_a}$ $Y_v=\omega Y_a$ yields:

$$\rho_m\underbrace{\left(Cv_m+Y_a\left(Cp_a+\omega Cp_v\right)+Y_lCp_l\right)}_{Cp_{eff}}\frac{\partial T}{\partial t}+\rho_a\left(Cp_a+\omega Cp_v\right)div(VT)$$

$$+div\left(-\lambda_{eff}grad(T)\right)+\left\{\left(Cp_aj_a+Cp_vj_v+Cp_lj_l\right)div(T)\right\}=\dot{m}_ch_{fg}+\dot{m}_cT\left(Cp_v-Cp_l\right)+\dot{Q}_s \quad [4.19]$$

Finally, the mathematical model implemented in HAMFit for heat transfer through building envelope components is given by Equation [4.20] assuming the term in the brace is negligible compared to the other terms.

$$\rho_mCp_{eff}\frac{\partial T}{\partial t}+\rho_a\left(Cp_a+\omega Cp_v\right)div(VT)+div\left(-\lambda_{eff}grad(T)\right)=\dot{m}_ch_{fg}+\dot{m}_cT\left(Cp_v-Cp_l\right)+\dot{Q}_s \quad [4.20]$$

where $Cp_{eff}=\underbrace{Cv_m+Y_a\left(Cp_a+\omega Cp_v\right)}_{C_o}+Y_lCp_l$ is the effective specific heat capacity of the control volume. C_o is referred as the dry heat capacity of the material. The rate of change of vapor concentration in the control volume can be neglected (Pederson, 1990) in vapor

species equation, Equation [4.3], and consequently the condensation term can be given by

$$\dot{m}_c = div\left(\delta_v \frac{\partial P_v}{\partial x_i}\right) - \rho_a div(V\omega).$$

4.1.2.3 Airflow through porous media

Airflow through a porous media can be expressed by using Poiseuille's law of proportionality (Hens, 2007), which relates pressure gradient and flow velocity (Equation [4.21].

$$V = -\frac{k_a}{\mu} div(P) \qquad [4.21]$$

where k_a and μ are the airflow coefficient and dynamic viscosity, respectively.

In building physics applications, the air is considered as incompressible due to very low airflow speed, and low pressure and temperature changes. The conservation equation for air mass balance under the above assumptions is given by:

$$div(\rho_a V) = 0 \qquad [4.22]$$

Combing the mass balance, Equation [4.22], and momentum balance, Equation [4.21], gives, Equation [4.23].

$$-div\left(\rho_a \frac{k_a}{\mu} div(P)\right) = -div(\delta_a div(P)) = 0 \qquad [4.23]$$

where $\delta_a = \rho_a \frac{k_a}{\mu}$ is air permeability

4.1.3 Development of a numerical tool for HAM analysis (HAMFit model)

The governing equations implemented in the building envelope model (HAMFit) are Equations [4.15], [4.20] and [4.23] for moisture, heat and air transport, respectively. The solution to the air balance equation is relatively easy if the air permeability of the medium is assumed to be constant, which is a general norm in building physics application. In this case, Equation [4.23] is solved independently for the pressure distribution in the medium of given boundary pressure conditions. Subsequently, Equation [4.21] is used to calculate the airflow velocity field. The known velocity field will then be used in the convection transport terms of moisture and energy equations, Equation [4.15] and [4.20] respectively.

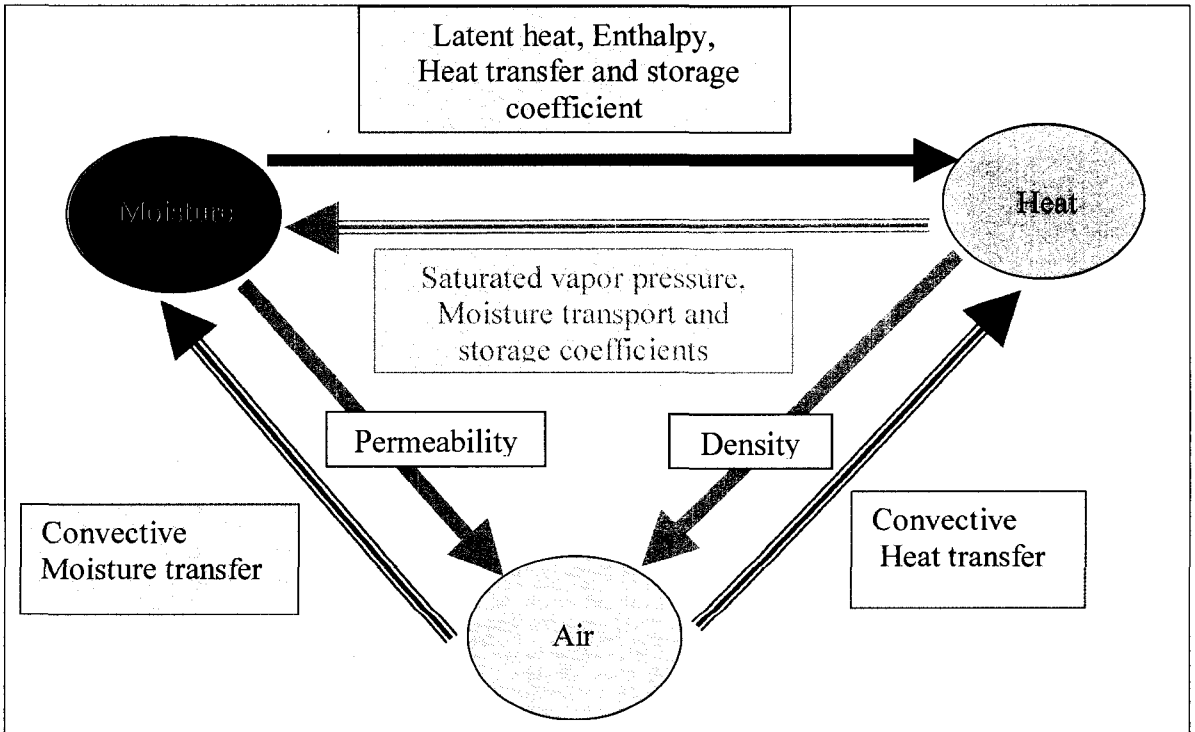

Figure 4-6 Interdependency of heat, air and moisture transports in a porous media. The arrow direction shows the influence of an entity on the transport of the linked entity through its effect on the parameters described in the accompanying text box.

The heat and moisture balance Equations [4.20] and [4.15], respectively, are highly coupled in a way that the heat transfer solution depends on the moisture balance solution and vise versa (Figure 4-6). In the heat balance equation, the thermal storage and transfer properties of materials (effective heat capacity, Cp_{eff} and apparent thermal conductivity, λ_{eff}) as well as the local heat source/sink (associated with moisture phase change, $\dot{m}_c$) depend on the moisture state of the domain. On the other hand, the temperature field affects the moisture transfer process due to the fact that the temperature gradient is one of the means of moisture transfer as indicated in the moisture balance (Equation [4.15]). Moreover, the vapor permeability, moisture transfer coefficients (D_ϕ and D_T) and saturated vapor pressure, which are important parameters in the moisture balance equation, are temperature dependent. In addition to the strong coupling of the heat and moisture balance equations, the equations themselves are highly non-linear, since the transfer and storage coefficients of the respective balance equations are not constant but rather function of the driving potentials. As an example, the moisture and heat transfer properties of a load bearing material (Hagentoft 2002), which is used in one of the benchmark exercises, are presented in Figure 4-7 and Figure 4-8, respectively. Figure 4-7 shows the non-linear curves of sorption capacity and vapor permeability as function of relative humidity as well as liquid diffusivity as function of moisture content. As moisture content increases the sorption capacity and liquid transport properties of the material increase significantly and the vapor permeability decreases to zero. Figure 4-8 shows the heat capacity and thermal conductivity of the same material as a function of moisture content. In the HAMFit model the hygrothermal properties of materials are

entered in MatLab database, and accessed by MatLab functions. Intermediate values are obtained by performing linear interpolation of adjacent data points.

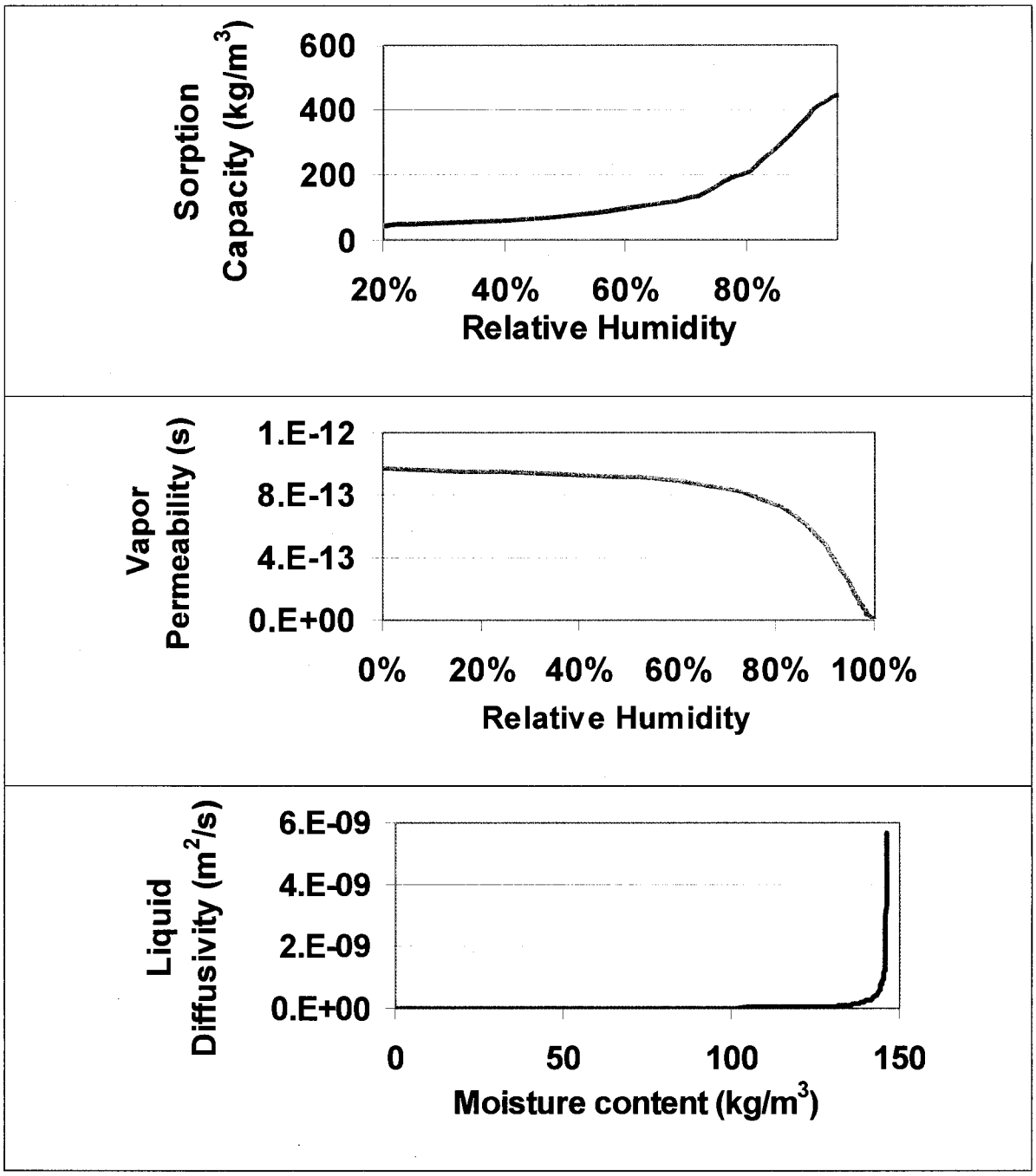

Figure 4-7 Typical moisture transport properties curves.

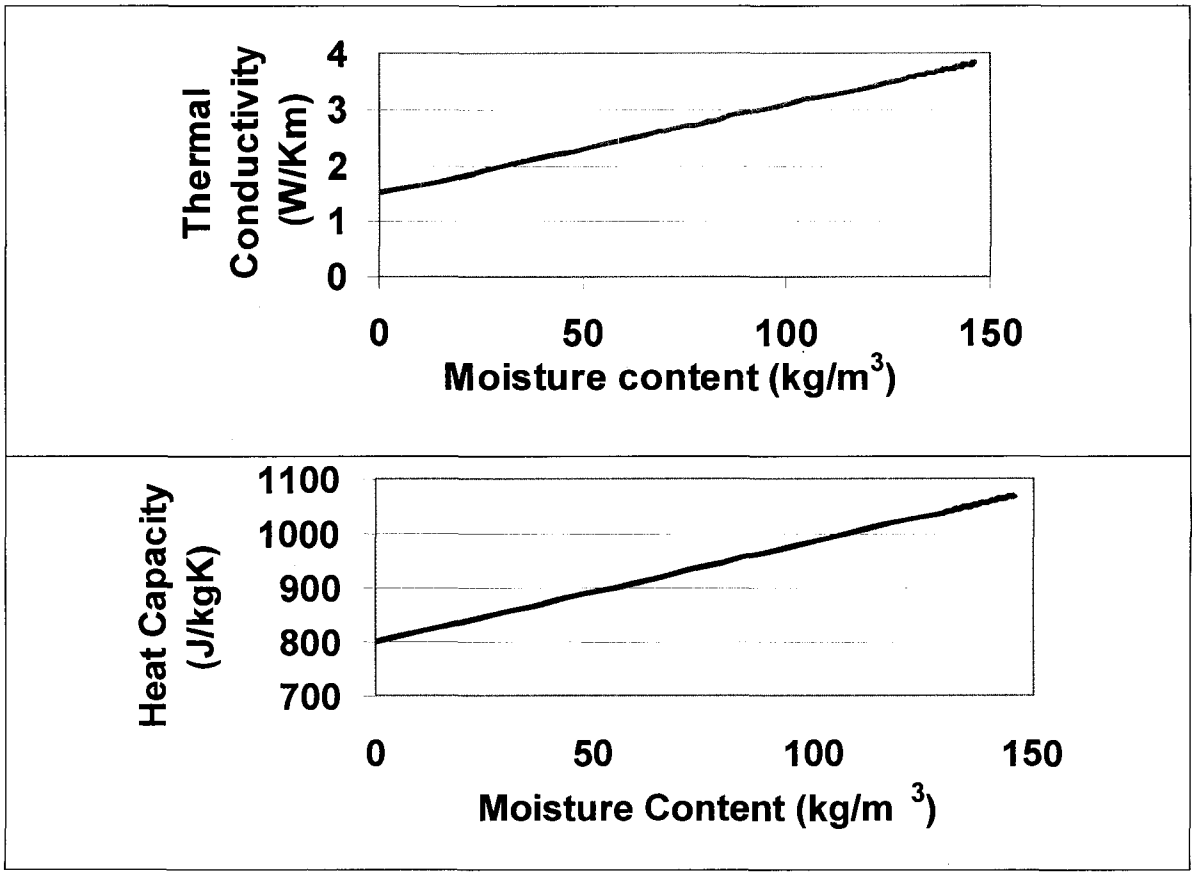

Figure 4-8 Typical thermal properties curves.

4.1.3.1 Numerical tool

To obtain the temperature and relative humidity field across the computational domain (building envelop component), the coupled and nonlinear partial differential equations (Equations [4.15], [4.20] and [4.23]) need to be solved simultaneously. Here, a finite-element based computational tool called COMSOL Multiphysics (COMSOL Multiphysics 2007) and MatLab (Mathworks 2007) are used to solve the three equations. COMSOL Multiphysics has a library of predefined models to solve familiar engineering problems such as convection diffusion problems, fluid dynamics, heat transfer and others, Figure 4-9. Also, it has a provision to create and solve user-developed models, which

may not be solved by the standard modules. This provision is identified in the list shown in Figure 4-9 as "PDE Modes". In this thesis, the building envelope model, HAMFit, is developed using the "PDE Modes".

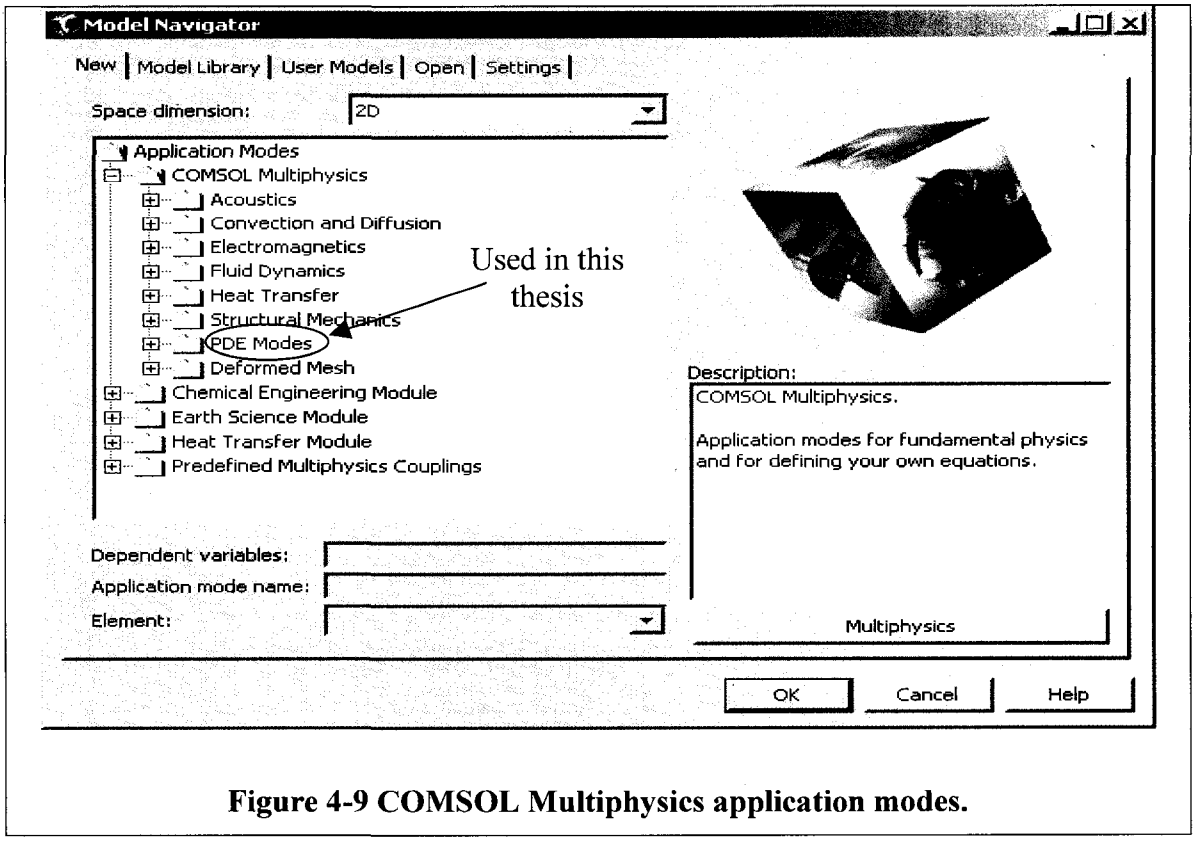

Figure 4-9 COMSOL Multiphysics application modes.

The "PDE modes" is an equation based modeling technique, where the user formulates the governing PDEs and directly implements it in the COMSOL Multiphysics working environment. Equation [4.24] describes the computational framework of the general form as it is written in the COMSOL Multiphysics Modeling Guide. The general form is "PDE modes", which is recommended for highly non-linear problems.

$$d_a \frac{\partial u}{\partial t} + \nabla \cdot \Gamma = F \qquad in\ \Omega$$

$$-n \cdot \Gamma = G + \lambda \qquad on\ \partial\Omega \qquad [4.24]$$

$$R = 0 \qquad on\ \partial\Omega$$

The first equation is the PDE, which defines the problem in the domain Ω and has a transient term, flux term, and source term. The flux term includes multi fluxes due to diffusion and convection transport processes. The second and third equations are the Neumann and Dirichlet boundary conditions, respectively, which are both satisfied on the boundary of the domain δΩ. n is the outward unit normal and is calculated internally. λ is an unknown vector-valued function called the Lagrange multiplier. This multiplier is also calculated internally and will be used only in the case of mixed boundary conditions. The terms d_a, F, G, and R are coefficients. They can be functions of the spatial coordinates, the solution u, or the space derivatives of u. The coefficients F, G, and R are scalar, whereas Γ is the flux vector. For the HAMFit model the heat, air and moisture equations, Equation [4.20], [4.23] and [4.15] respectively, are cast in the form of Equation [4.24], and solved using the time-dependent solver of the software. The solver is based on an explicit scheme with variable time stepping. The user can predefine the maximum time step so that it will match with the boundary condition change period. It has a possibility of solving any one of the three or all simultaneously. In addition to its efficient solver it has a graphical user interface (GUI) to create computational domain geometry, automatic and user controlled mesh generator, and it also has an integrated post processing capability for plotting, interpolating and integrating simulation results.

HAMFit model for building envelope HAM analysis

The newly developed building envelope model, HAMFit, is a transient model and has the capability of handling the non-linear and coupled HAM transfer through multilayered porous media by taking into account the non-linear hygrothermal properties of materials, moisture transfer in the vapor diffusion, capillary liquid water transport and convective heat and moisture transfers. Moreover, the model accounts for the effect of moisture in the thermal storage and transfer properties of materials as well as the local heating and cooling effects that are generated within the structure due to moisture phase changes (condensation and evaporation, respectively).

The model has two versions, HAMFit-1D and HAMFit2D. HAMFit-1D is used for one-dimensional heat, air and moisture analysis of building envelope components. And HAMFit2D is used to solve two-dimensional HAM problems that are caused by the geometry of the region of interest such as wall-floor junction (Figure 4-10–A) and two-dimensional corner section (Figure 4-10–B). And also in cases where the physical process itself has three-dimensional nature but can be approximated in two-dimension (for example airflow and gravitational moisture flow in the structure).

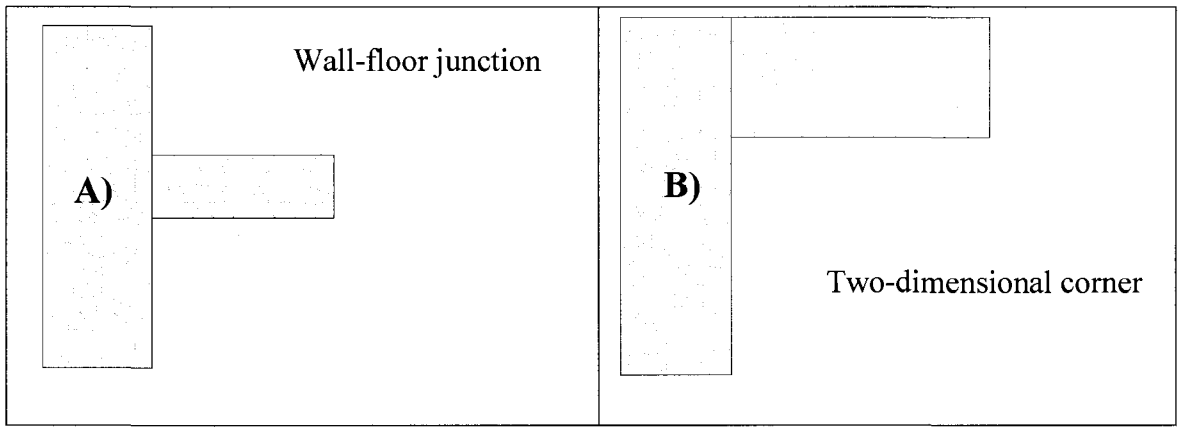

Figure 4-10 Examples of two-dimensional building envelope sections.

HAMFit model takes advantage of the smooth interfaces of COMSOL Multiphysics, MatLab and SimuLink computational tools, which all are from the same development environment. In fact COMSOL Multiphysics is one of the blocks in the SimuLink model library, and it is also possible to call MatLab functions from COMSOL Multiphysics working environment. Making use of these flexible simulation environments, HAMFit model is developed in such a way that a number of functions are created in MatLab; and these functions are called by COMSOL MultiPhysics multiple times during solving the HAM equations, which are cast in COMSOL MultiPhysics. The "PDE Modes" data structure of the problem including the geometry, mesh, PDEs and boundary conditions are embedded in the SimuLink S-function. Finally, the hygrothermal simulation (S-function) is run in the SimuLink simulation environment where the overall simulation parameters including outputs are controlled. S-function is a user-developed SimuLink block written in MatLab or C programming language, and where the developer sets the block's tasks, inputs and outputs. An example of COMSOL Multiphysics report that documents the hygrothermal numerical model, geometry, mesh, initial and boundary conditions, solver setting and other important information can be found in Appendix A-4.

The hygrothermal simulation environment of HAMFit-1D is shown in Figure 4-11. The latest simulation time is continuously updated and displayed at the left top corner of the working space. The simulation results (moisture content and temperature) are plotted in real time in the "Scope" block to monitor the simulation progress. The "Building Specification" block describes the general features of the building whose building envelope component is going to be hygrothermally assessed. Double clicking the block will open up the GUI for data input, Figure 4-12. The data that are entered in this

GUI are used mainly to calculate the pressure difference across the building component using the infiltration model and to estimate the wind-driven rain load on the component. The input data include: the building dimensions, orientation and inclination of the building envelop components, air tightness of each building envelope components, as well as the building site conditions including altitude. In the case of one-dimensional HAM analysis, the geometry of the computational domain is created by simply connecting multiple lines that represent the different layers of materials in the building component assembly. Consequently, there is no need to use COMSOL Multiphysics's GUI to create the geometry, and therefore, in the HAMFit-1D the geometry and mesh are specified right into the GUI window (Figure 4-13), which is created in SimuLink and opens up when double clicking the HAMFit-1D model. The default maximum element size at the boundaries and in the domains are 0.1 and 1 mm, respectively. All the necessary input data that are required for hygrothermal simulation of the component are defined in this window. These include the thickness and sequence of layers that make up the component, initial hygrothermal conditions (temperature and relative humidity) and internal heat and moisture sources in the component, heat and mass transfer coefficients of the boundary surfaces, the absorptivity and emissivity of the external surfaces. Moreover, the user can control the maximum time step size (usually matches the boundary condition time step) and frequency of the simulation results outputs. The simulation environment of the two-dimensional version of HAMFit model is similar to the one described above, except that in the HAMFit-2D the geometry, meshing and boundary conditions are implemented in the COMSOL Multiphysics GUI, and then exported to the MatLab work space and integrated in the HAMFit-2D SimuLink working

environment. The advantage of this modeling technique is that it allows simulating HAM transfers in any two-dimensional building envelope detail without geometric restriction.

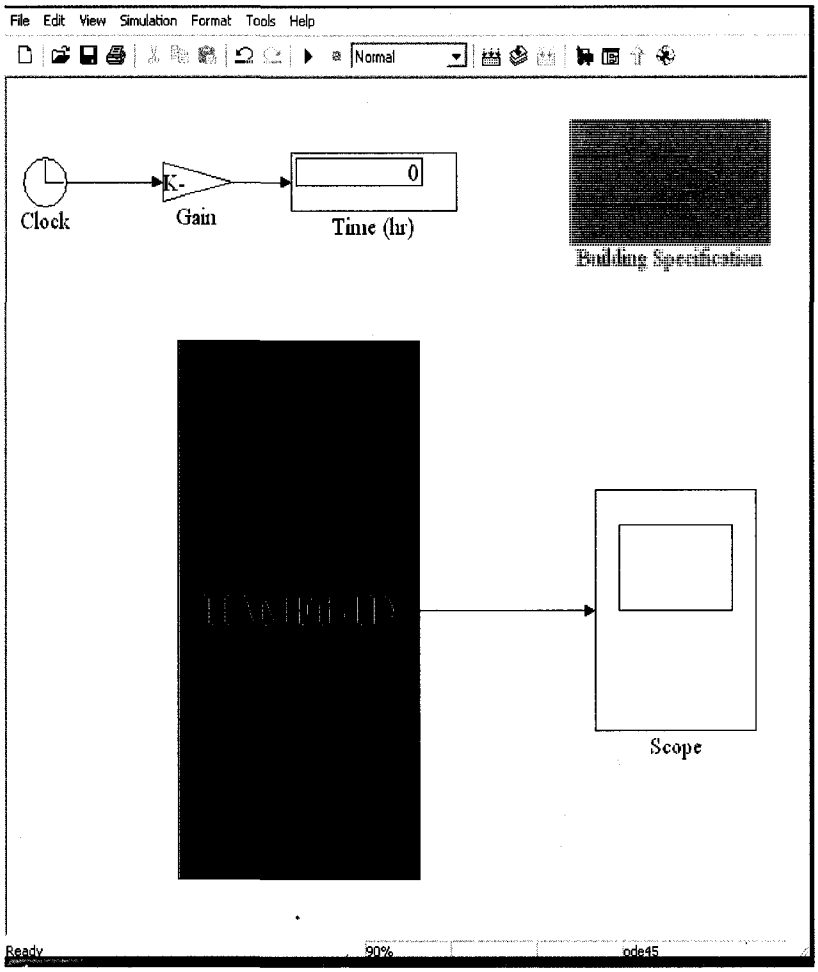

Figure 4-11 HAMFit-1D simulation environment

Limitation of the model

The model has limitations in the following regards: the hygrothermal properties of materials are time independent; the changes in the physical dimension and accompanying hygrothermal properties of materials due to thermal and moisture loads are not accounted for; the moisture storage characteristic of a material is defined by a single curve (neglecting hysteresis effect); effects of chemical reactions on HAM transport are not

considered; effects associated with phase change liquid to/from ice are neglected; layers of materials are assumed to be in perfect contact and airflow path in the structure is predefined. Moreover, the accuracy of the model's simulation result is limited to availability of complete information on construction details, boundary conditions, initial conditions, hygrothermal properties of the materials used and entry of input data correctly. User's understanding of the physical problem and adaptation of the problem in the numerical model are equally important.

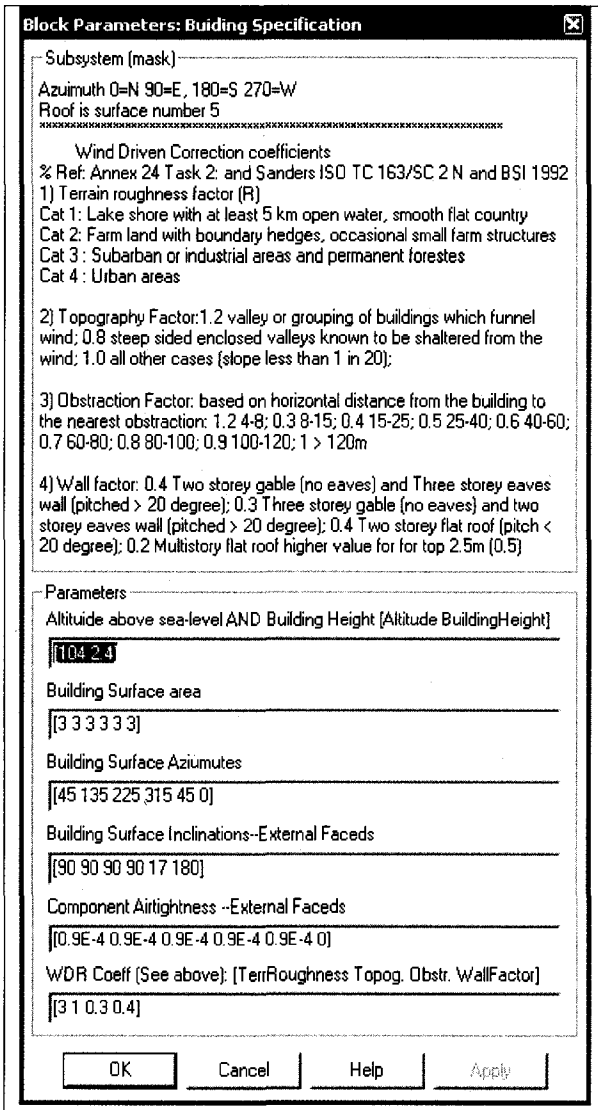

Figure 4-12 Building specification GUI

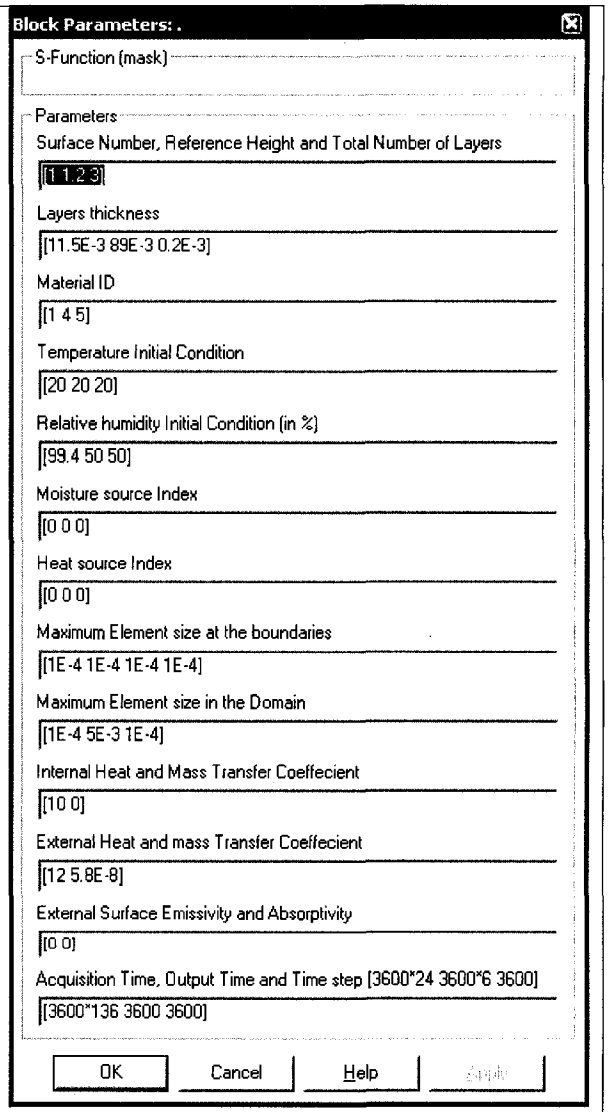

Figure 4-13 HAMFit-1D GUI

4.2 Indoor model

The indoor model is developed to predict the indoor temperature and humidity conditions based on the heat and moisture balance in the zone. The model accounts for the internal heat and moisture generations, mechanical systems outputs as well as the heat and moisture fluxes that cross the zone boundaries. These heat and moisture loads are discussed in detail below in the humidity and energy balance sections, respectively. The basic assumption of the model is that the indoor air is well mixed and can be represented by a single node. Based on this assumption, two linear first-order differential equations that govern the heat and moisture balances of a zone are, finally, developed.

4.2.1 Humidity balance equation

The humidity balance equation developed in this work incorporates the moisture absorption/desorption of hygroscopic internal lining of building envelope components and furniture $\left(\dot{Q}_b^m\right)$, moisture supply and removal from the zone by airflow $\left(\dot{Q}_v^m\right)$, moisture addition and removal by mechanical systems $\left(\dot{Q}_m^m\right)$, moisture addition into zone due to occupant activities $\left(\dot{Q}_o^m\right)$, evaporation from sink or bath tub $\left(\dot{Q}_e^m\right)$, and moisture removal due to moisture condensation on surfaces $\left(\dot{Q}_c^m\right)$. The mathematical representation of the humidity balance model used is presented in Equation [4.25] below. Where ω, ρ_a and $\tilde{V}$ are the humidity ratio (kg/kg air), density of air (kg/m^3) and volume of the zone (m^3).

$$\rho_a \tilde{V} \frac{d\omega}{dt} = \dot{Q}_b^m + \dot{Q}_v^m + \dot{Q}_m^m + \dot{Q}_o^m + \dot{Q}_e^m + \dot{Q}_c^m \qquad [4.25]$$

The six moisture exchange mechanisms that affect the indoor humidity conditions are discussed below:

4.2.1.1 Moisture absorption/desorption $\left(\dot{Q}_b^m\right)$

The moisture absorption/desorption term $\left(\dot{Q}_b^m\right)$ represents the moisture exchange between moisture buffering materials such as interior furnishing and furniture with the indoor air. This term is one of the two coupling terms, where a two-way dynamic exchange of data between the building envelope and indoor models is done. The net moisture gain or loss to the indoor air from i number of surfaces is given by the summation of each surface's contribution, Equation [4.26]. This way the dynamic interaction between the indoor space and every single construction can be made.

$$\dot{Q}_b^m = \sum_i A_i h_i^m \left(p_i^s - p\right) \qquad [4.26]$$

where A_i (m^2) is the surface area of surface i,

h_i^m (kg/s m^2 Pa) is the surface mass transfer coefficient of surface i,

p_i^s (Pa) is the surface vapor pressure of surface i, and

p (Pa) is the zone vapor pressure

The equation can be rewritten in terms of humidity ratio, Equation [4.27] by transforming vapor pressure into humidity ration using the relation $\omega = 0.622\frac{p}{P_a - p} \approx 6.22\times10^{-6}\,p$; where P_a is the atmospheric pressure (Pa).

$$\dot{Q}_b^m = \frac{10^6}{6.22}\sum_i A_i h_i^m \left(\omega_i^s - \omega\right) \qquad [4.27]$$

The surface humidity ratio (ω_i^s) is determined from a moisture balance calculation of the building envelope model using the indoor humidity condition as an interior moisture boundary condition and outside weather as an external boundary condition. In doing so, this term accounts for: i) the moisture exchange between the outside and indoor space due to convection and diffusion transport mechanism, ii) moisture migration to the indoor space during drying of building envelope components which have high initial construction moisture content, iii) rain penetration or capillary liquid flow from wet soil. Accounting to these moisture transfer mechanisms is an improvement to the earlier humidity models where the moisture exchange is limited to few millimeters of the internal surfaces, or the moisture buffering effect is represented with empirical equations. This term couples the moisture balance equations of the building envelope and indoor models.

4.2.1.2 Moisture supply and removal from the zone by airflow $\left(\dot{Q}_v^m\right)$

The moisture exchange by airflow between the outside and indoor space in a single zone can be given by Equation [4.28].

$$\dot{Q}_v^m = \dot{m}\left(\omega_e - \omega\right) \qquad [4.28]$$

where $\dot{m}$, ω_e and ω are the mass flow rates of dry air (kg/s), humidity ratio (kg/kg of air) of exterior and indoor zone, respectively. The airflow to/from the indoor zone is the sum of an intentional airflow through cracks and holes, commonly called air leakage, and intentional airflow by means of natural ventilation (e.g. opening of window) and forced ventilation by mechanical systems. The effective air flow rate is calculated by doing air mass balance in the zone considering: the external driving force (wind pressure), pressure gradient created due to temperature difference across a building envelope component (stack pressure), air-tightness of the building or building components, intentional openings areas and locations, and the supply and exhaust fan pressure or air flow rate. Due to dynamic variation of wind speed and direction in the weather, the effective airflow rate may change according to time.

4.2.1.3 Moisture addition and removal by mechanical systems $\left(\dot{Q}_m^m\right)$

To increase occupant comfort level or due to the requirement of the building operation, the indoor humidity levels of some buildings are controlled by using a humidistat. These buildings require a mechanical system that works continuously and maintain the indoor

humidity level within the set points by adding moisture when the indoor humidity level is below the lower set point, and removing moisture when it is above the upper set point. The amount of moisture addition or removal during humidification and dehumidification respectively is given by Equation [4.29].

$$\dot{Q}_m^m = \frac{\rho_a \tilde{V}}{\Delta t}(\tilde{\omega} - \omega) \qquad [4.29]$$

where $\tilde{\omega}$ and Δt are the set point humidity ratio and time step, respectively.

4.2.1.4 Moisture addition into zone due to occupant activities $\left(\dot{Q}_o^m\right)$

This term represents the moisture production rate by human respiration and perspiration, moisture generating activities such as cooking and washing, and also moisture release by pets and plants in the zone. These types of moisture productions are independent of the indoor humidity condition, unlike evaporation or condensation, and estimated from literature. The diurnal moisture generation rate schedule is usually used in the indoor humidity calculations to reflect the occupant activity at various times. For example, an office where occupancy is expected between 9:00 and 17:00 h, the moisture generation schedule can be represented as shown in Figure 4-14.

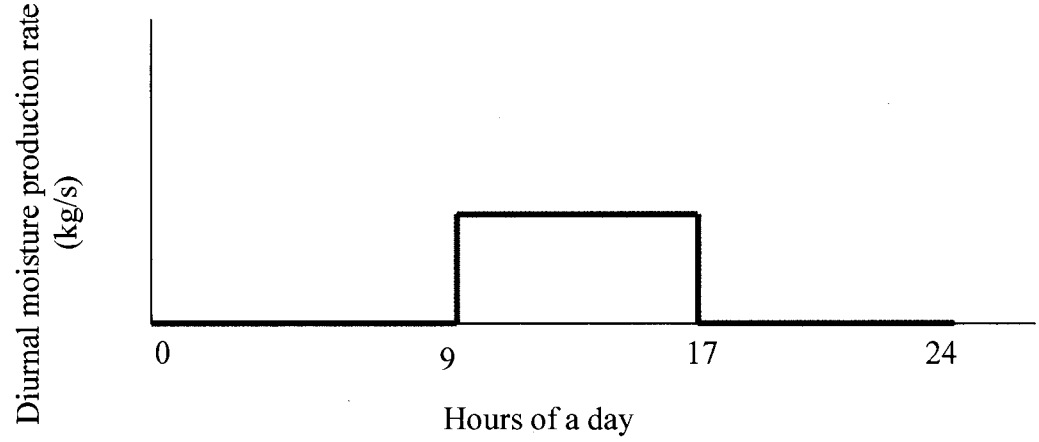

Figure 4-14 Typical diurnal moisture generation schedule.

4.2.1.5 Evaporation $\left(\dot{Q}_e^m\right)$

Evaporation $\left(\dot{Q}_e^m\right)$ term accounts for the sum of moisture addition to the indoor air due to evaporation of water from a reservoir (such as fish tank), and condensate surface. The evaporation rate is a function of the water temperature (or saturated vapor pressure), indoor air vapor pressure and airflow velocity in the zone.

$$\dot{Q}_e^m = \sum_e A_e h_e^m \left(\hat{p}_e - p\right)$$

where A_e (m^2) and $\hat{p}_e$(Pa) are the water surface area and saturated vapor pressure of water in reservoir e, respectively. The mass transfer coefficient for evaporation h_e^m (kg/s m^2 Pa) is influenced by the indoor airflow speed. Rewriting the above equation in terms of the humidity ratio yields Equation [4.30].

$$\dot{Q}_e^m = \frac{10^6}{6.22} \sum_e A_e h_e^m \left(\hat{\omega}_e - \omega\right) \qquad [4.30]$$

4.2.1.6 Condensation $\left(\dot{Q}_c^m\right)$

Moisture can be removed from the indoor air due to water vapor condensation on cold surfaces, where the surface temperature is below the dew point temperature of the indoor air. This usually happens on the inside surfaces of glazing units and building envelope components where thermal bridges occur. The total condensation rate in the zone can be determined using Equation [4.31], which is similar to the evaporation rate equation.

$$\dot{Q}_c^m = \frac{10^6}{6.22}\sum_c A_c h_c^m \left(\hat{\omega}_c - \omega\right) \qquad [4.31]$$

where A_c (m^2), $\hat{\omega}_c$ (kg/kg of air) and h_c^m (kg/s m^2 Pa) are the surface area, saturated humidity ratio and mass transfer coefficient of the condensation surface , respectively. Substituting Equations [4.27]-[4.31] into the general humidity balance equation, Equation [4.25] yields the final form of the humidity balance equation used in the indoor model, Equation [4.32].

$$\rho_a \tilde{V}\frac{d\omega}{dt} = -\omega\left(\frac{10^6}{6.22}\left[\sum_i A_i h_i^m + \sum_e A_e h_e^m + \sum_c A_c h_c^m\right] + \dot{m} + \frac{\rho_a \tilde{V}}{\Delta t}\right) + \left(\frac{10^6}{6.22}\left[\sum_i A_i h_i^m \omega_i^s + \sum_e A_e h_e^m \hat{\omega}_e + \sum_c A_c h_c^m \hat{\omega}_c\right] + \dot{m}\omega_e + \frac{\rho_a \tilde{V}}{\Delta t}\tilde{\omega} + \dot{Q}_o^m\right) \qquad [4.32]$$

The humidity balance equation has the form: $a\frac{d\omega}{dt} + b\omega + c = 0$ where a, b and c are constants during a time step.

4.2.2 Energy balance equation

The general energy balance equation for the indoor air considers the energy exchange between the building envelope internal surfaces and the indoor air $\left(\dot{Q}_b^h\right)$, the energy carried by the air flow into and out of the zone $\left(\dot{Q}_v^h\right)$, the heat supply and removal (heating/cooling) by mechanical systems to maintain the room in the desired temperature range $\left(\dot{Q}_m^h\right)$, the internal heat generated due to occupant activities (e.g. cooking) and building operation (e.g. lighting) $\left(\dot{Q}_o^h\right)$,and the energy supplied and removed from the interior space due to enthalpy transfer by moisture movement $\left(\dot{Q}_h^h\right)$, and heat gain through fenestration system $\left(\dot{Q}_f^h\right)$. The contribution of each terms in the total energy balance equation are described below. For the purpose of energy balance, the indoor air is assumed to be a mixture of only dry air and water vapor. Hence, the energy balance equation for the indoor air is written in terms of the mixture enthalpy balance, Equation [4.33].

$$\rho_a \tilde{V} \frac{dh}{dt} = \dot{Q}_b^h + \dot{Q}_v^h + \dot{Q}_m^h + \dot{Q}_o^h + \dot{Q}_h^h + \dot{Q}_f^h \qquad [4.33]$$

Assuming the dry air and vapor act as an ideal gas, the specific enthalpies of dry air $\left(h_a\right)$and water vapor $\left(h_v\right)$ at a reference temperature of 0°C can be give as $h_a = Cp_a T$ and $h_v = Cp_v T + h_{fg}$, and the mixture enthalpy (h) is given by $h = h_a + \omega h_v = T\left(Cp_a + \omega Cp_v\right) + \omega h_{fg}$.

4.2.2.1 Heat exchange with building envelope surfaces $\left(\dot{Q}_b^h\right)$

The term $\dot{Q}_b^h$, heat exchange between building envelope surfaces and indoor air, couples the energy balance equations of building envelope and indoor models. The total heat exchange between the interior surface of building envelope components and indoor air is given by summation of each surfaces contribution, Equation [4.34].

$$\dot{Q}_b^h = \sum_i A_i h_i^h \left(T_i^s - T\right) \qquad [4.34]$$

where A_i (m^2) is the surface area of surface i,

h_i^h ($W/m^2 K$) is the surface heat transfer coefficient of surface i,

T_i^s (^oC) is the surface temperature of surface i, and

T (^oC) is the zone temperature.

The surface temperature (T_i^s) is determined from the energy balance calculation of the building envelope model, using the indoor temperature and humidity as interior boundary conditions and outside weather as external boundary conditions. The building envelope model takes into consideration the thermal load due to solar radiation, long wave radiation, and enthalpy transfer by moisture movement, in addition to the convection and diffusion heat transfer mechanisms. Moreover, the model considers the effect of moisture on the heat storage capacity and thermal conductivity of building components. The inclusion of enthalpy transfer and use of moisture dependent material properties in the energy balance equation can give a more accurate surface temperature values, and can be considered as an improvement to energy simulation models, which use dry material properties and ignore latent heat transfer. This term is one of the two coupling terms,

where a two-way dynamic exchange of data between the building envelope and indoor models is done.

4.2.2.2 Heat supply and removal from the zone by airflow $\left(\dot{Q}_v^h\right)$

Intentional and unintentional airflows that could occur across building enclosure components may bring and remove heat into and out of the zone, respectively. Although the entering and leaving mass flow rates are the same for a single zone model, the humidity ratios and the temperatures of the entering and leaving are not the same. Hence, the net energy contribution of 'dry-airflow' is determined by considering the enthalpy exchange of the incoming $\left(h_a^e\right)$ and outgoing air $\left(h_a\right)$ as shown in Equation [4.35].

$$\dot{Q}_v^h = \dot{m}\left(h_a^e - h_a\right) = \dot{m}Cp_a\left(T_e - T\right) \qquad [4.35]$$

As mentioned earlier, the dynamic effective air flow rate is calculated by doing air mass balance in the zone; considering the external driving force (wind pressure), pressure gradient created due to temperature difference across a building envelope component (stack pressure), air-tightness of the building or building components, intentional openings area and location, and the supply and exhaust fan pressure (air flow rate). The incoming enthalpy $\left(h^e\right)$ is purely dependent on the outside temperature.

4.2.2.3 Heating and cooling mechanical systems $\left(\dot{Q}_m^h\right)$

The thermal load on the exterior surface of building enclosure components varies significantly from season to season due to the high ambient temperature and solar radiation variations throughout a year. Unless mechanical systems are used for heating and cooling, the indoor temperature will follow the exterior weather condition, which would result in low temperature in the winter and high temperature in the summer time. This free-float temperature could be out of the acceptable indoor comfort temperature range, especially in cold and hot climate regions during the winter and summer seasons, respectively. Moreover, surface condensation and mold growth could be facilitated. To provide a comfortable and healthy indoor condition, the indoor temperature should be controlled by thermostat, and the required heating and cooling energy should be provided if the indoor operative temperature is below and above a set point, respectively. Depending on the mechanical heating system used, the energy addition could be by convection heating, radiant heating, or both. However, only the convective heating portion of the total heat supply is used for the energy balance of indoor space. The rest (radiating portion) is assumed to elevate the inside surface temperature of the building envelope, and ultimately, transfers the heat to the indoor air by convection. The direct heating/cooling energy required to maintain the indoor air temperature within the set points is given by Equation, [4.36]. In this formulation the energy addition or removal will not change the moisture content of the air, ω.

$$\dot{Q}_m^h = \frac{\rho_a \tilde{V}}{\Delta t}\left(Cp_a + \omega Cp_v\right)\left(\tilde{T} - T\right) \qquad [4.36]$$

where $\tilde{T}$ and Δt are the set point temperatures and time step, respectively. In practical application, the maximum heating and cooling capacity of the mechanical system $\dot{Q}^h_{m\_\max}$ is limited. Thus, the sum of convective and radiative heating at any give time must be less than or equal to the maximum system capacity, $\frac{\dot{Q}^h_m}{F^h_m} \le \dot{Q}^h_{m\_\max}$ where F^h_m is the fraction of convective heating (1 for air convection system and 0.7 for hydronic heating system (Kalagasidis, 2004).

4.2.2.4 Internal heat generation $\left(\dot{Q}^h_o\right)$

This term includes the internal heat gain due to lighting, cooking, equipment, occupant body temperature, etc. Since the time and duration of lighting, cooking or doing other activities depends on the occupant daily routine, it is usually given in diurnal schedule. For example for an office building, where lighting will be turned off and no occupancy is expected during 17:00 to 9:00 h next morning, an internal heat release may have a schedule similar to the profile shown in Figure 4-15. The thermal energy released from the heat source can contribute directly to the indoor air space heating by convection, radiated to the surrounding surfaces, or by a combination of both. As mentioned in the previous section, only the convective fraction of the total heat gain is used in the energy balance equation of the indoor air space, and the rest of the thermal load is applied on the interior surface of the building envelope surfaces as radiative heat fluxes.

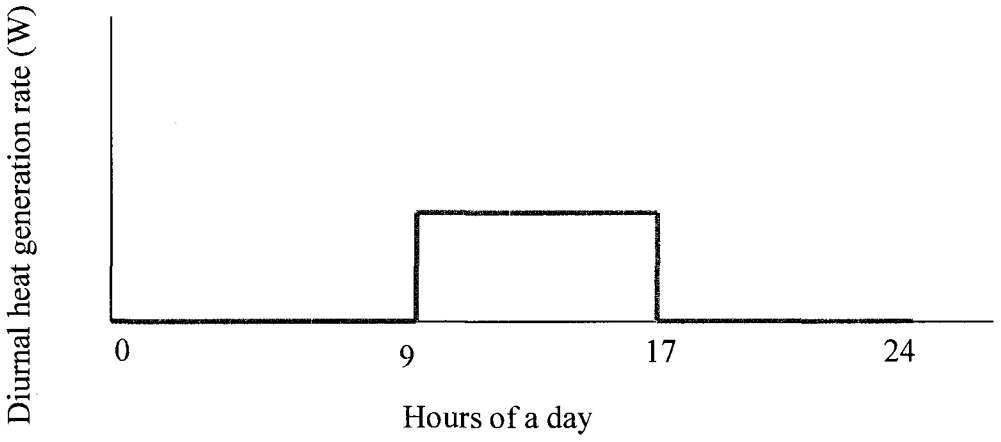

Figure 4-15 Typical diurnal heat generation rate schedule.

4.2.2.5 Enthalpy transfer by moisture movement $\left(\dot{Q}_h^h\right)$

Moisture carries energy (enthalpy) as it comes into or removed from the indoor space. The energy contribution of moisture is given by Equation [4.37]. This term accounts for the energy transfer due to moisture movement by ventilation $\left(\dot{Q}_v^m\right)$ and convection at the building envelope surfaces $\left(\dot{Q}_b^m\right)$; moisture gain or removal from the indoor space by mechanical systems (humidification/dehumidification) $\left(\dot{Q}_m^m\right)$, and also other means: occupant activity $\left(\dot{Q}_o^m\right)$, evaporation $\left(\dot{Q}_e^m\right)$ and condensation $\left(\dot{Q}_c^m\right)$.

$$\dot{Q}_h^h = \dot{Q}_b^m h_v^{b*} + \underbrace{\dot{m}\left(\omega_e h_v^{ev} - \omega h_v\right)}_{by\ airflow(ventilation)} + \dot{Q}_m^m h_v^{m*} + \dot{Q}_o^m h_v^o + \dot{Q}_e^m h_v^e + \dot{Q}_c^m h_v \qquad [4.37]$$

where h_v is the indoor air water-vapor enthalpy

h_v^{ev} is the outdoor air water-vapor enthalpy

h_v^o is the enthalpy of the moisture released by the indoor moisture source

h_v^e is the enthalpy of evaporated moisture

h_v^{b*} depends on the moisture transfer between interior building envelope surface and indoor air. For moisture absorption by building envelope surfaces h_v^{b*} is the indoor air water-vapor enthalpy h_v, for desorption h_v^{b*} is the enthalpy of the moisture at the building envelope surface $\left(h_v^b\right)$

h_v^{m*} depends on whether the mechanical system is used for humidification or dehumidification of the indoor air. If the system is used for humidification, h_v^{m*} is the enthalpy of the moisture released by the mechanical system, and if it is used for dehumidification h_v^{m*} is the indoor air water-vapor enthalpy h_v.

Equation [4.37] can be transformed into Equation [4.38], when the enthalpy of the vapor is expressed as the sum of sensible and latent heat as defined above $h_v = Cp_vT + h_{fg}$.

$$\dot{Q}_h^h = \dot{Q}_b^m\left(Cp_vT^{b*} + h_{fg}\right) + \dot{m}\left(\omega_e\left(Cp_vT^{ev} + h_{fg}\right) - \omega\left(Cp_vT + h_{fg}\right)\right) +$$
$$\dot{Q}_m^m\left(Cp_vT^{m*} + h_{fg}\right) + \dot{Q}_o^m\left(Cp_vT^o + h_{fg}\right) + \dot{Q}_e^m\left(Cp_vT^e + h_{fg}\right) + \dot{Q}_c^m\left(Cp_vT + h_{fg}\right)$$

After rearranging terms:

$$\dot{Q}_h^h = \underbrace{\dot{Q}_b^m Cp_v T^{b*} + \dot{m}\left(\omega_e Cp_v T^{ev} - \omega Cp_v T\right) + \dot{Q}_m^m Cp_v T^{m*} + \dot{Q}_o^m Cp_v T^o + \dot{Q}_e^m Cp_v T^e + \dot{Q}_c^m Cp_v T}_{Sensible\ heat} +$$

$$\underbrace{h_{fg}\left(\dot{Q}_b^m + \dot{m}\left(\omega_e - \omega\right) + \dot{Q}_m^m + \dot{Q}_o^m + \dot{Q}_e^m + \dot{Q}_c^m\right)}_{Latent\ heat}$$

In short form:

$$\dot{Q}_h^h = \dot{Q}_{hs}^h + \dot{Q}_{hl}^h \qquad [4.38]$$

where $\dot{Q}_{hs}^h$ and $\dot{Q}_{hl}^h$ are the sensible and latent heats defined as:

$$\dot{Q}_{hs}^h = \underbrace{\dot{Q}_b^m Cp_v T^{b*} + \dot{m}\left(\omega_e Cp_v T^{ev} - \omega Cp_v T\right) + \dot{Q}_m^m Cp_v T^{m*} + \dot{Q}_o^m Cp_v T^o + \dot{Q}_e^m Cp_v T^e + \dot{Q}_c^m Cp_v T}_{Sensible\ heat}$$

[4.39]

$$\dot{Q}_{hl}^h = \underbrace{h_{fg}\left(\dot{Q}_b^m + \dot{m}\left(\omega_e - \omega\right) + \dot{Q}_m^m + \dot{Q}_o^m + \dot{Q}_e^m + \dot{Q}_c^m\right)}_{Latent\ heat} \qquad [4.40]$$

The subscripts for the temperatures T^{b*}, T^{ev}, T^{m*}, T^o, and T^e follow the definition of enthalpies in the above paragraph (h_v^{b*}, h_v^{ev}, h_v^{m*}, h_v^o, and h_v^e).

4.2.2.6 Heat gain through fenestration $\left(\dot{Q}_f^h\right)$

The heat gains to the indoor air space through fenestration are the solar heat gain and the heat flow due to temperature difference between the indoor and outdoor temperatures. In

this thesis, fenestrations are represented as single-glazing unit but with the apparent U-value and solar heat gain coefficient of the fenstration system considered. Figure 4-16 shows the general schematic diagram of heat flow through a single-glazing unit. For deatiled analysis of mult-glazed fenestration sysstems see Athienitis and Santamouris (2002). As solar radiation reaches the exterior surface of the fenestration (I_o), parts of the incident radiation will be transmitted (I_t), reflected (I_r) and the rest will be absorbed (I_a), depending on the effective transmissivity (τ), reflectivity (ρ) and absortivity (α) properties of the fenestration system ($\tau + \alpha + \rho = 1$).

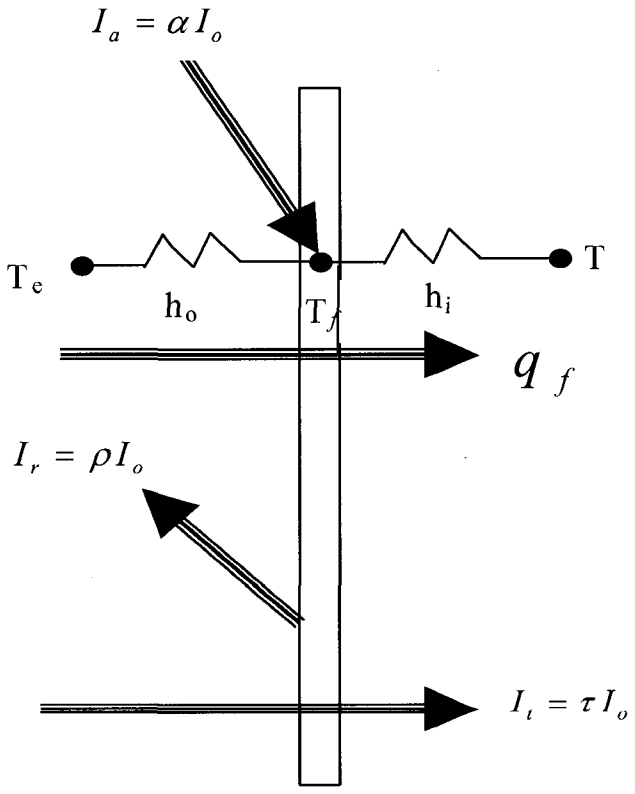

Figure 4-16 Heat flow mechanisms through a sigle-glazing unit

Usually, the heat storage and thermal resistance of the fenestration are neglected, and the heat gain is assumed to be instantaneous. Under this assumption the heat flow through a sigle-glazing unit q_f can be determined by carrying out a steady state heat balance (Heat gain at the exterior surface = heat loss at the interior surface) as follows:

$$q_f = h_o\left(T_e - T_f\right) + I_a = h_i\left(T_f - T\right) \qquad [4.41]$$

Solving for glass temperature T_f:

$$T_f = \frac{h_o}{h_i + h_o}T_e + \frac{h_i}{h_i + h_o}T + \frac{1}{h_i + h_o}I_a$$

The oveall heat transfer coeffcient (U-value) of a sigle-glazing unit is given by:

$$U = \frac{1}{\left(\frac{1}{h_i} + \frac{1}{h_o}\right)} = \frac{h_i h_o}{h_i + h_o}$$

Hence, the glass temperature can be rewritten as:

$$T_f = \frac{U}{h_i}T_e + \frac{U}{h_o}T + \frac{U}{h_i h_o}I_a \qquad [4.42]$$

Finally, the heat transfer $\left(q_f\right)$ is determined using Equation [4.41] and [4.42]:

$$q_f = h_i\left(T_f - T\right) = h_i\left(\frac{U}{h_i}T_e + \frac{U}{h_o}T + \frac{U}{h_i h_o}I_a - T\right)$$

$$q_f = \underbrace{U\left(T_e - T\right)}_{due\ to\ temperature\ difference} + \underbrace{\frac{U}{h_o}\alpha I_o}_{due\ to\ absorbed\ solar\ radiation} \qquad [4.43]$$

The absorbed solar radation will be dissipated to the indoor and outdoor environment by convection. The fraction of absorbed solar radiaton, which is dissipated to the indoor air space as derived in Equation [4.43], is $\frac{U}{h_o} I_a = \frac{U}{h_o} \alpha I_o$. The apparent heat gain to the indoor space due to solar radiation, which is usally called 'Solar Heat Gain - SHG', is the sum of the trasmitted solar radition and the fraction of absorbed solar radiation given by Equation [4.44].

$$q_s = \tau I_o + \frac{U}{h_o} \alpha I_o \qquad [4.44]$$

Using the *F*-factor (Athienitis and Santamouris, 2002), which is the ratio of the solar heat gain to the incident solar radiation $F = \frac{q_s}{I_o} = \tau + \frac{U}{h_o} \alpha$, the solar heat gain can be given as:

$$q_s = F I_o \qquad [4.45]$$

The *F*-factor encapsulates the transmissivty, absorptivity, and conductance properties of the fenestration system.

In the indoor air energy balance equation (Equation [4.33]), the instantaneous heat gain to the indoor air through fenestration $\left(\dot{Q}_f^h\right)$ is the sum of heat flow through the fenestarion according to Equation [4.43] and a fraction of transmitted solar radiation $\left(f_{sa} I_t\right)$ which instantly heat the indoor air. f_{sa} is the solar air factor $f_{sa} I_t = f_{sa} \tau I_o$, and A_w is window area.

$$\dot{Q}_f^h = A_w \times \left[\underbrace{U\left(T_e - T\right)}_{due\ to\ temperature\ difference} + \underbrace{\frac{U}{h_o} \alpha I_o}_{fraction\ of\ absorbed\ solar\ radiation} + \underbrace{f_{sa} \tau I_o}_{fraction\ of\ transmited\ solar\ radiation} \right] \qquad [4.46]$$

According to the European Standard pEN ISO 13791, the fraction of the transmitted solar radiation that will be availabe as an immediate energy input to the indoor air $\left(f_{sa}I_t\right)$ depends on the quantity of very low thermal capacity items such as, carpets and furniture inside the room. The suggested values for the solar to air factor $\left(f_{sa}\right)$ are 0, 0.1 and 0.2, for no furniture, small amount of furniture and large amount of furniture, respectively. The rest of the transmitted radiaton will be absorbed by the interior surfaces which later transfer part of the heat to the indoor air by convection.

Assembling terms

Substituiting Equation [4.38] for the enthalpy transfer by moisture movement $\left(\dot{Q}_h^h\right)$ term in the energy balance equation, Equation [4.33] gives:

$$\rho_a \tilde{V} \frac{dh}{dt} = \underbrace{\dot{Q}_{hl}^h + \dot{Q}_{hs}^h}_{\dot{Q}_h^h} + \dot{Q}_b^h + \dot{Q}_v^h + \dot{Q}_m^h + \dot{Q}_o^h + \dot{Q}_f^h \qquad [4.47]$$

The energy balance equation can be simplified by substituting Equation [4.40] for the latent heat $\left(\dot{Q}_{hl}^h\right)$ term, and representing the air-vapor mixture enthalpy as defined in previous paragraph: $h = h_a + \omega h_v = T\left(Cp_a + \omega Cp_v\right) + \omega h_{fg}$:

$$\rho_a \tilde{V} \frac{d\left(T\left(Cp_a + \omega Cp_v\right) + \omega h_{fg}\right)}{dt} = h_{fg}\left(\dot{Q}_b^m + \dot{m}\left(\omega_e - \omega\right) + \dot{Q}_m^m + \dot{Q}_o^m + \dot{Q}_e^m + \dot{Q}_c^m\right) + \dot{Q}_{hs}^h + \dot{Q}_b^h + \dot{Q}_v^h + \dot{Q}_m^h + \dot{Q}_o^h + \dot{Q}_f^h$$

Expanding terms:

$$\rho_a \tilde{V}\left(Cp_a + \omega Cp_v\right)\frac{dT}{dt} + \underbrace{h_{fg}\rho_a \tilde{V}\frac{d\omega}{dt}}_{I} = h_{fg}\left(\dot{Q}_b^m + \dot{m}\left(\omega_e - \omega\right) + \dot{Q}_m^m + \dot{Q}_o^m + \dot{Q}_e^m + \dot{Q}_c^m\right) + \dot{Q}_{hs}^h + \dot{Q}_b^h + \dot{Q}_v^h + \dot{Q}_m^h + \dot{Q}_o^h + \dot{Q}_f^h \quad [4.48]$$

Moving the second term of the right hand side (*I*) to the left side:

$$\rho_a \tilde{V}\left(Cp_a + \omega Cp_v\right)\frac{dT}{dt} = h_{fg}\left[\underbrace{\dot{Q}_b^m + \dot{m}\left(\omega_e - \omega\right) + \dot{Q}_m^m + \dot{Q}_o^m + \dot{Q}_e^m + \dot{Q}_c^m - \rho_a \tilde{V}\frac{d\omega}{dt}}_{II}\right] + \dot{Q}_{hs}^h + \dot{Q}_b^h + \dot{Q}_v^h + \dot{Q}_m^h + \dot{Q}_o^h + \dot{Q}_f^h$$

Recall the humidity balance equation, Equation [4.49]:

$$\rho_a \tilde{V}\frac{d\omega}{dt} = \dot{Q}_b^m + \dot{m}\left(\omega_e - \omega\right) + \dot{Q}_m^m + \dot{Q}_o^m + \dot{Q}_e^m + \dot{Q}_c^m .$$

Based on the humidity balance equation the term *II* in the left hand side of the above equation will be zero, and consequently the latent heat contribution of moisture in the indoor air energy balance equation will disappear. The simplified energy balance equation will be:

$$\rho_a \tilde{V}\left(Cp_a + \omega Cp_v\right)\frac{dT}{dt} = \dot{Q}_b^h + \dot{Q}_v^h + \dot{Q}_m^h + \dot{Q}_f^h + \dot{Q}_{hs}^h + \dot{Q}_o^h \quad [4.50]$$

where the terms $\dot{Q}_b^h$, $\dot{Q}_v^h$, $\dot{Q}_m^h$, $\dot{Q}_{hs}^h$ and $\dot{Q}_f^h$ as derived in Equation [4.34], [4.35], [4.36], [4.39], and [4.46], respectively:

$$\dot{Q}_b^h = \sum_i A_i h_i^h \left(T_i^s - T\right)$$

$$\dot{Q}_v^h = \dot{m}\left(h_a^e - h_a\right) = \dot{m}Cp_a\left(T_e - T\right)$$

$$\dot{Q}_m^h = \frac{\rho_a \tilde{V}}{\Delta t}\left(Cp_a + \omega Cp_v\right)\left(\tilde{T} - T\right)$$

$$\dot{Q}_{hs}^h = \dot{Q}_b^m Cp_v T^{b*} + \dot{m}\left(\omega_e Cp_v T^{ev} - \omega Cp_v T\right) + \dot{Q}_m^m Cp_v T^{m*} + \dot{Q}_o^m Cp_v T^o + \dot{Q}_e^m Cp_v T^e + \dot{Q}_c^m Cp_v T$$

$$\dot{Q}_f^h = A_w \times \left[U\left(T_e - T\right) + \frac{U}{h_o}\alpha I_o + f_{sa}\tau I_o\right]$$

The final form of the energy balance equation implemented in the HAMFitPlus indoor model is Equation [4.51].

$$\rho_a \tilde{V} h_s \frac{dT}{dt} = -T\left(\sum_i A_i h_i^h + \dot{m}Cp_a + \frac{\rho_a \tilde{V}}{\Delta t}h_s + UA_w + \dot{m}\omega_e Cp_v + \dot{Q}_c^m Cp_v\right) + \left(\sum_i A_i h_i^h T_i^s + \dot{m}Cp_a T_e + \frac{\rho_a \tilde{V}}{\Delta t}h_s \tilde{T} + A_w\left[UT_e + \frac{U}{h_o}\alpha I_o + f_{sa}\tau I_o\right] + \dot{m}\omega_e Cp_v T^{ev} + \dot{Q}_b^m Cp_v T^{b*} + \dot{Q}_m^m Cp_v T^{m*} + \dot{Q}_o^m Cp_v T^o + \dot{Q}_e^m Cp_v T^e\right) \quad [4.51]$$

where $h_s = Cp_a + \omega Cp_v$ is the sensible heat of the air-water vapor mixture.

The energy balance equation has the form: $a\frac{dT}{dt} + bT + c = 0$ where a, b and c are constants during the time step. Finally, the two fundamental equations of the indoor model in HAMFitPlus, which are derived from humidity and energy balance Equations [4.32] and [4.51], respectively, are solved simultaneously for indoor humidity and temperature

4.3 Development of a whole building hygrothermal model (HAMFitPlus)

The schematic representations of the hygrothermal loadings that are considered in the whole building hygrothermal model, HAMFitPlus are shown Figure 4-17. In this modeling approach the building is considered as a system, which is exposed to the local weather conditions including wind-driven rain and solar radiation on the outside, and internal heat and moisture generations as well as solar gain at the inside, and also involves mechanical systems for heating/cooling, de/humdification as well as ventilation to maintain the balance of the desired indoor environmental conditions (temperature and relative humidity

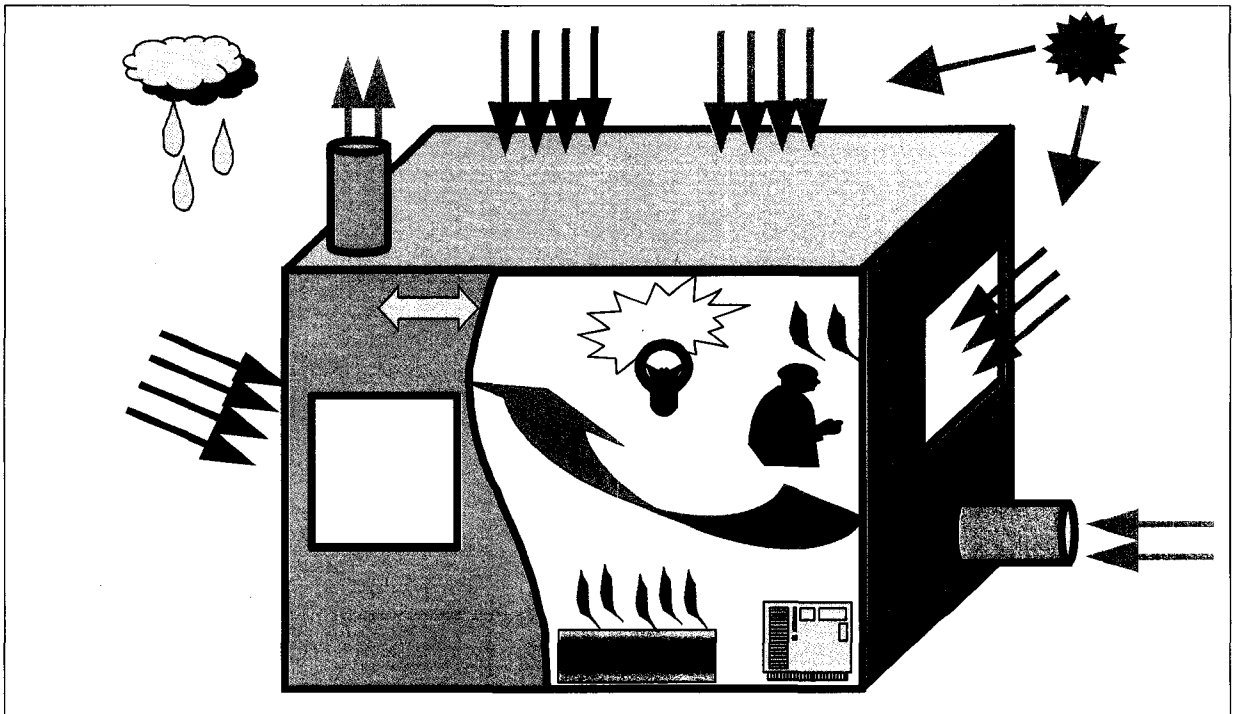

Figure 4-17 Typical hygrothermal loadings on a building.

In the previous sections, the governing equations for HAM transport through building enclosure, Equation [4.20], [4.23] and [4.15], and the indoor heat and moisture balance equations, Equation [4.32] and [4.51], are stated. Integration of these equations in a single platform forms the basis of the whole hygrothermal model, HAMFitPlus. The heat and moisture balance equations of the building enclosure are coupled with the corresponding indoor heat and moisture balance equations through the hygrothermal conditions (temperature and relative humidity) of the interior surfaces. Consequently, during solving these coupled equations, a solution with interior surfaces temperatures and relative humidity that satisfy both the building enclosure and indoor model equations is sought. Graphical representation of the whole building hygrothermal model is shown in Figure 4-18. The hygrothermal responses of a building (indoor temperature and relative humidity, energy consumption and building enclosure hygrothermal conditions) are the consequences of the dynamic interactions of various elements shown in Figure 4-18. The building enclosure may constitute many layers of different thickness, which may have unique non-liner hygrothermal properties. A change in the building enclosure design, say painting interior surface or additional of insulation, or climatic conditions will affect the indoor air conditions, which in turn affect the HVAC system outputs, say dehumidification or heating demand. Likewise, a change in the indoor heat and moisture generations or HVAC system output affects the indoor air conditions, which in turn affect the hygrothermal performance of the building enclosure. The whole building hygrothermal model, HAMFitPlus, deals with these interrelated and coupled effects in a single platform, and predicts the indoor temperature and relative humidity conditions, moisture and temperature distributions in the building envelope components as well as the heating and cooling loads.

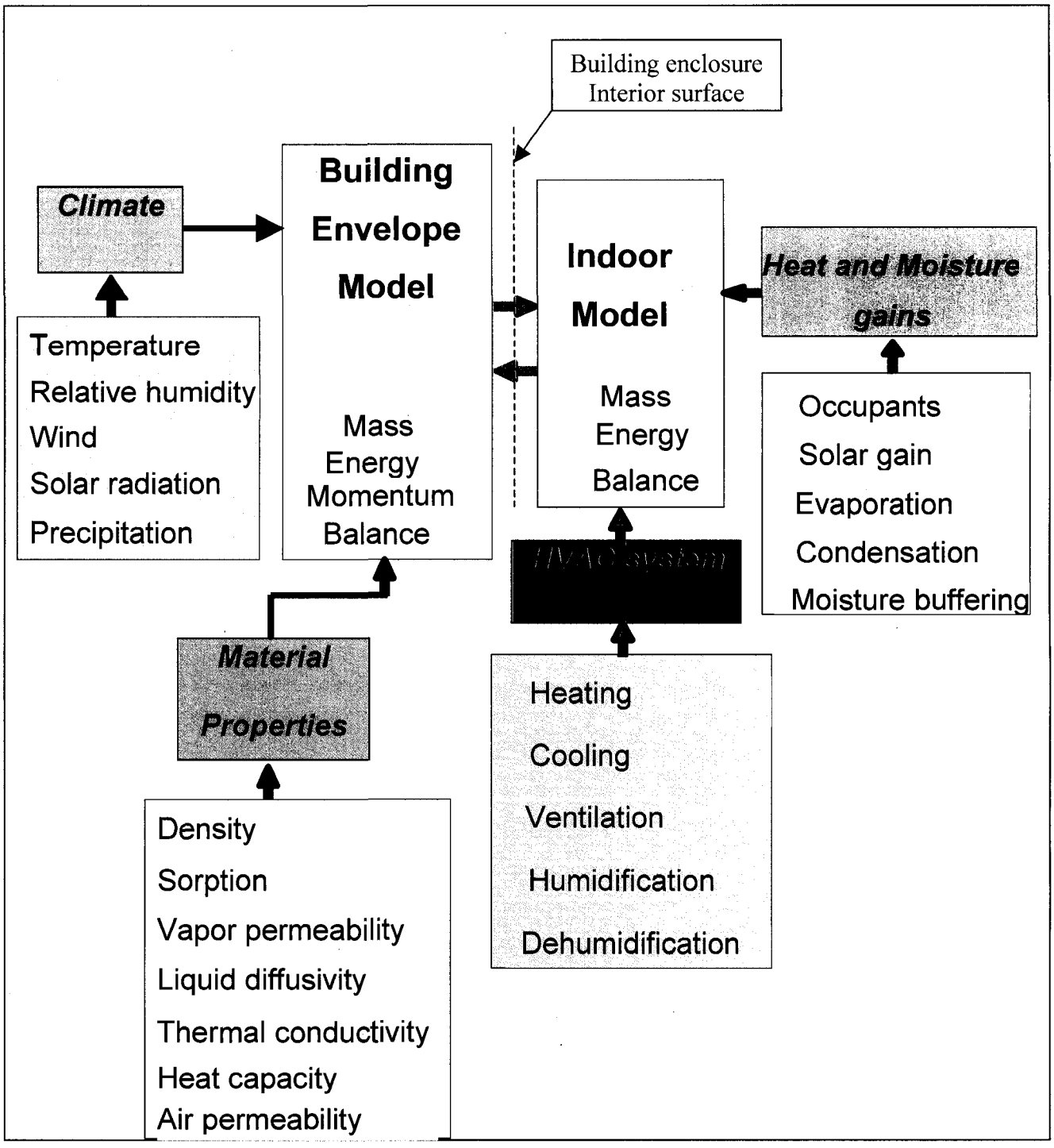

Figure 4-18 Schematic diagram of HAMFitPlus model.

4.3.1 HAMFitPlus model

HAMFitPlus is developed on SimuLink simulation environment, which has smooth interface with COMSOL Multiphysic and MatLab computational tools. The simulation environment allows full integration and dynamic coupling of building envelope and indoor models that are developed in Section 4.1 and 4.2, respectively. The model comprises five primary blocks. These are, "Building", "Zone Enclosure", Window", "Furniture" and "Mechanical systems and Heat and Moisture gains" block, Figure 4-19. The blocks are "user-developed" block types, where the task, inputs and outputs of each block are written in S-function, and embedded in the respective blocks. This approach permits full control of the simulation environment and is particularly useful in the whole building hygrothermal analysis where there is large time scale variation between building enclosure and HVAC systems response (Schijndel and Hensen, 2005). Consequently, HAMFitPlus can be classified as a hybrid model with continuous part for indoor model and a discrete part for building envelope model. The simulation update time for the discrete part is user specified, and can vary from seconds to hours depending on the boundary conditions. The blocks have GUI to enter user specified data.

Limitation of HAMFitPlus

In addition to the limitations that were stated for HAMFit in Section 4.1.3.1, HAMFitPlus has the following additional limitations: it is a single zone model where the indoor temperature and humidity conditions are assumed to be uniform through out the room (well mixed assumption); a combined convective and longwave radiation exchange

coefficient is used for the interior surface (in the current version); for exterior surface the longwave radiation exchange is computed using International Standard ISO 15927-1:2003(E), Annex B; the indoor solar gain is distributed proportional to interior surface areas.

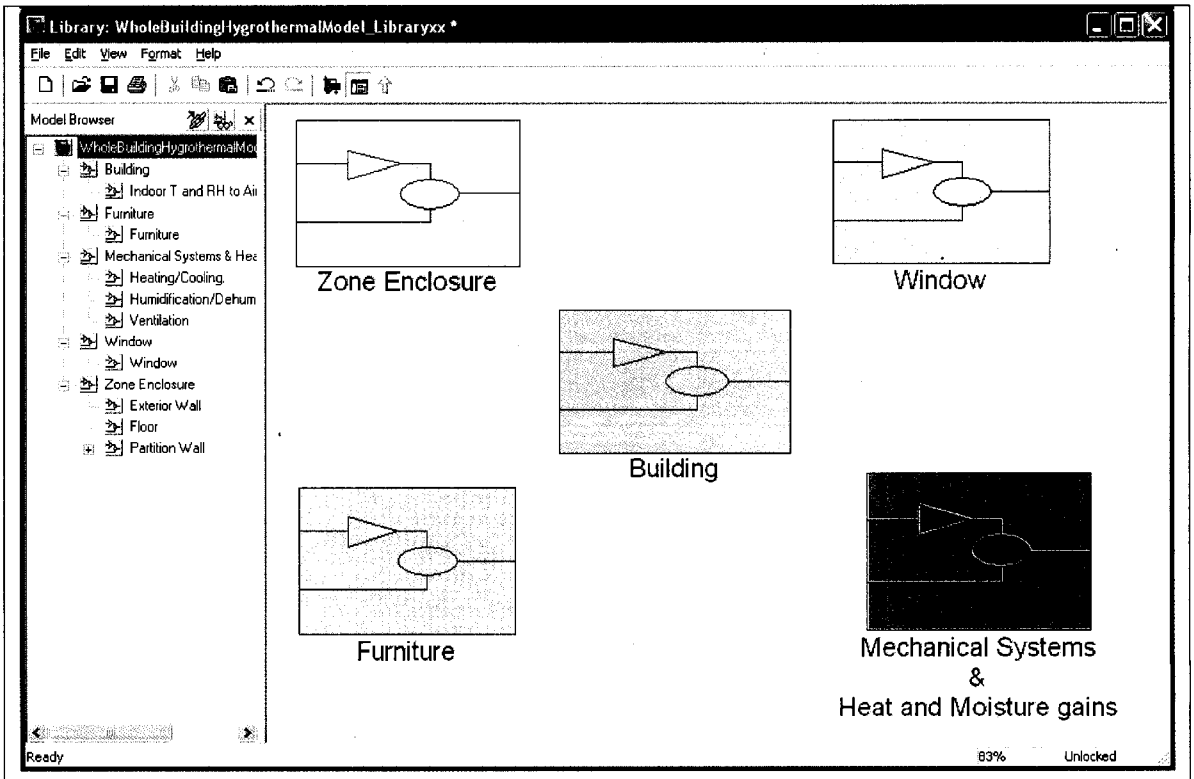

Figure 4-19 HAMFitPlus primary building blocks

The general specification of the building including the building site (latitude, longitude, altitude, topography and surrounding environment), building size and orientation, building envelop components surface area, orientation, inclination and air tightness are specified in the "Building" block. The zone humidity and energy balance equations are encapsulated in this block. The integration of different blocks creates a virtual simulation environment similar to Figure 4-20, which represents a certain building operation scenario, Figure 4-17. Figure 4-20 consists of a "Building enclosure" block for

opaque building envelope components, "Window" block, a block for internal heat and moisture sources that can be represented as a lumped system (for example, evaporation of water from a sink or cooling of heated pan), "Furniture" block, a block that encloses the mechanical systems for heating, cooling, humidification, dehumidification and ventilation and indoor heat and moisture generations, and finally the "Zone Humidity and Energy balance" block.

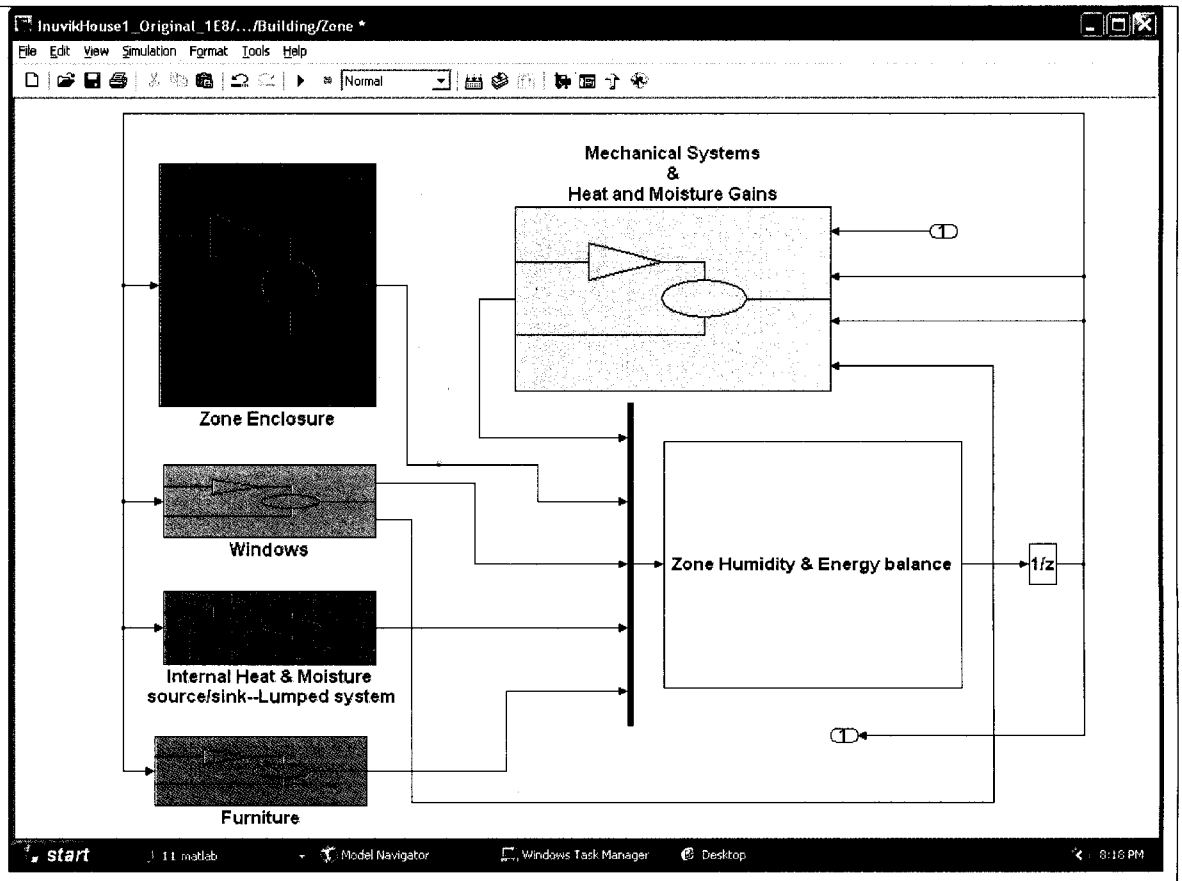

Figure 4-20 Virtual building as represented in HAMFitPlus model

The six building envelope components that are encapsulated in the "Zone Enclosure" block are shown in Figure 4-21. For example here, the South and East walls are exterior walls, the North and West walls are partition walls that are adjacent to

hallway and next room, respectively, and the other two components are ceiling and floor. Due to high computational cost, the building envelope components are represented as one-dimensional elements and consequently a modified version of HAMFit is used instead of HAMFit2D (the two dimensional version of HAMFit). The building components can be composed of different layer of materials and thickness, and can also be exposed to different exterior boundary conditions. The inputs to each components block are the indoor temperature and relative humidity, and the outputs of the blocks are the interior surface temperature and humidity conditions of the components. The GUI of the component blocks is similar to the GUI presented for HAMFit model in Figure 4-13.

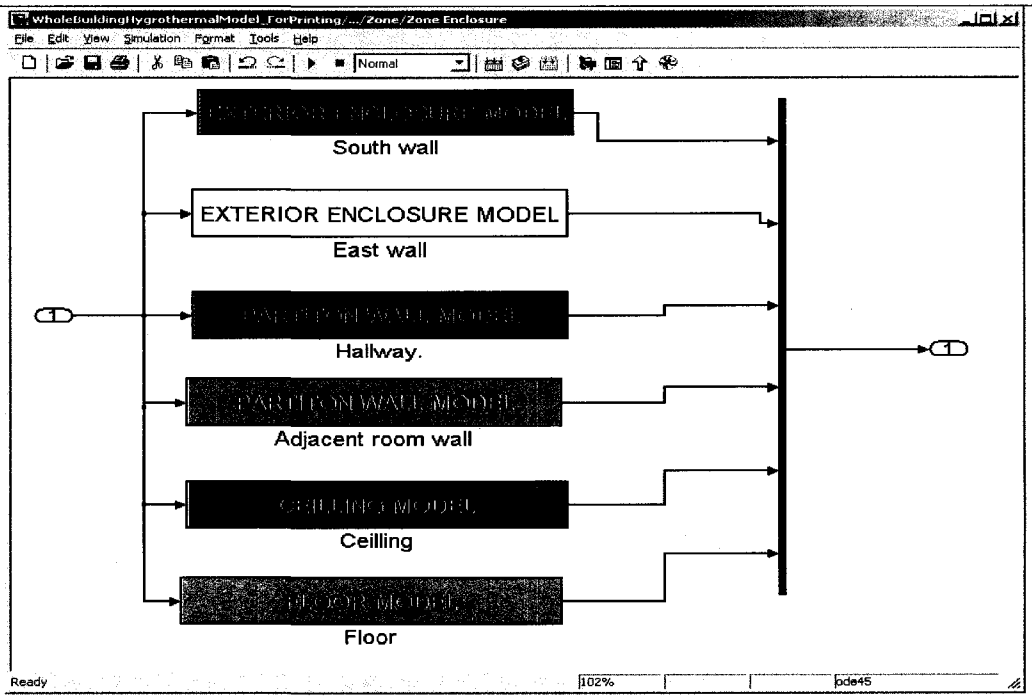

Figure 4-21 Building envelope components

As shown in Figure 4-22 the "Mechanical systems and Indoor heat and moisture gains" block encapsulates the mechanical system for heating/cooling, humidification/dehumidification, ventilation, and indoor moisture and heat generation

blocks. The inputs of the fist two blocks are indoor temperature and humidity conditions, and the corresponding outputs are the thermal (heating/cooling) and moisture (addition/removal) loads. The outputs of the blocks, which subsequently are passed to the indoor heat and moisture balance model, depend on the respective mechanical system set points and capacity. The specifications of the heating/cooling and humidification/ dehumidification equipments are defined in Figure 4-23 and Figure 4-24, respectively. The third block outputs the effective ventilation rate of a house, which could be due to the combined effects of natural and mechanical ventilations. The heat and moisture loads that are independent of the indoor environment conditions (temperature and humidity) are represented in the last two blocks (examples of these loads are heat gain from light bulbs and moisture release by plants). The outputs of these blocks are only function of time and are scheduled based on assumed occupants' daily routine activities.

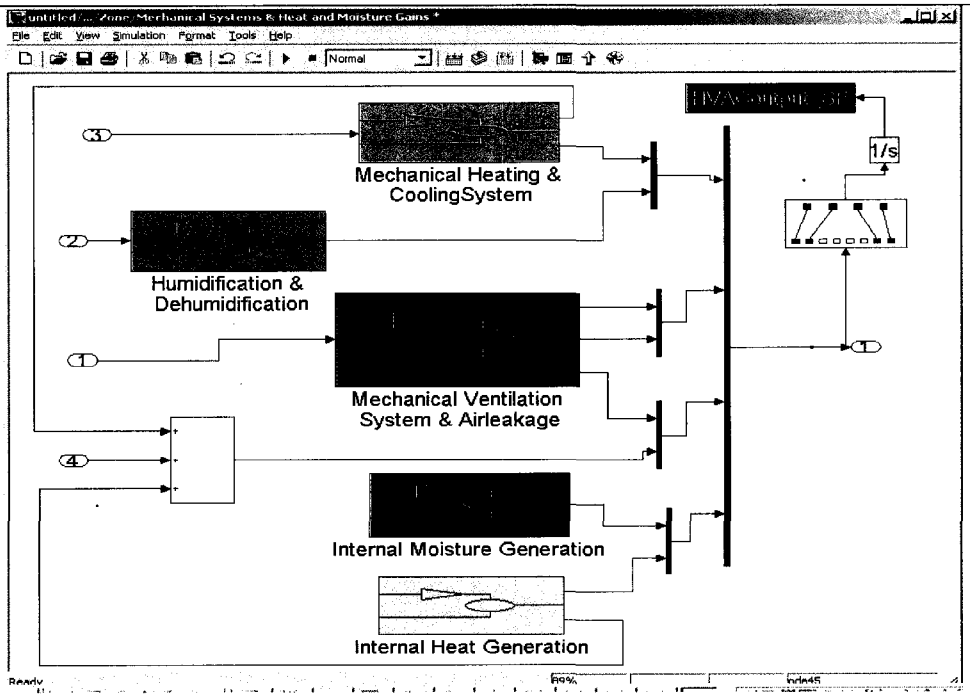

Figure 4-22 Mechanical systems and Indoor heat and moisture gains

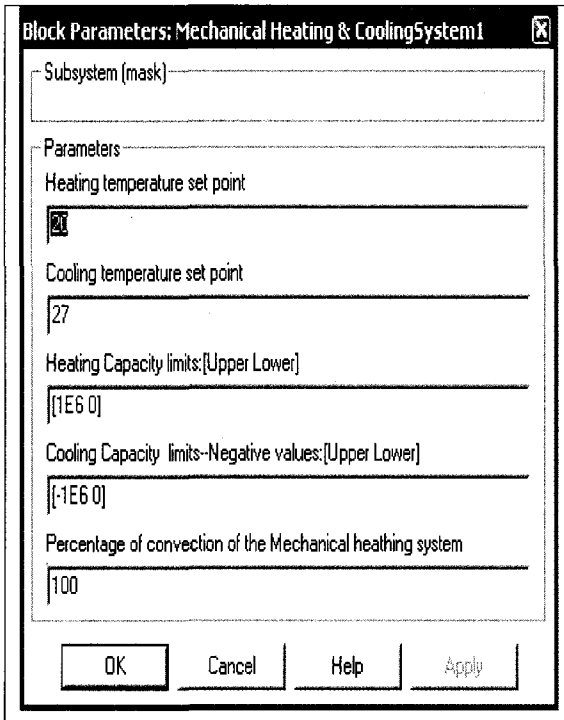

Figure 4-23 Heating/Cooling system GUI

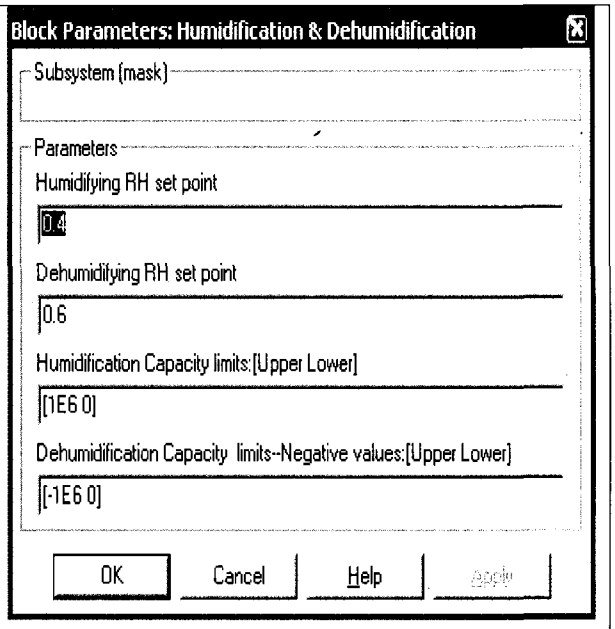

Figure 4-24 Humidification/Dehumidification GUI

Indoor furniture can play an important role on regulating the indoor humidity condition of the house through its moisture buffering potential. In HAMFitPlus, it is represented by "Furniture" block, Figure 4-20, and approximated as an interior building envelope component, whose exterior surfaces are exposed to the indoor environmental conditions. Thus, the inputs and outputs of this block are the indoor temperature and humidity conditions and the surface temperature and moisture conditions, respectively. The outputs are passed to the indoor heat and moisture balance model. The "Window" block represents one of the very important building envelope components, which is window. The outputs of the block, which are the heat flux and window condensation rate, can influence the humidity and energy balance of the zone. The specifications of the windows on the four orientations are separately specified using the GUI shown in Figure 4-25.

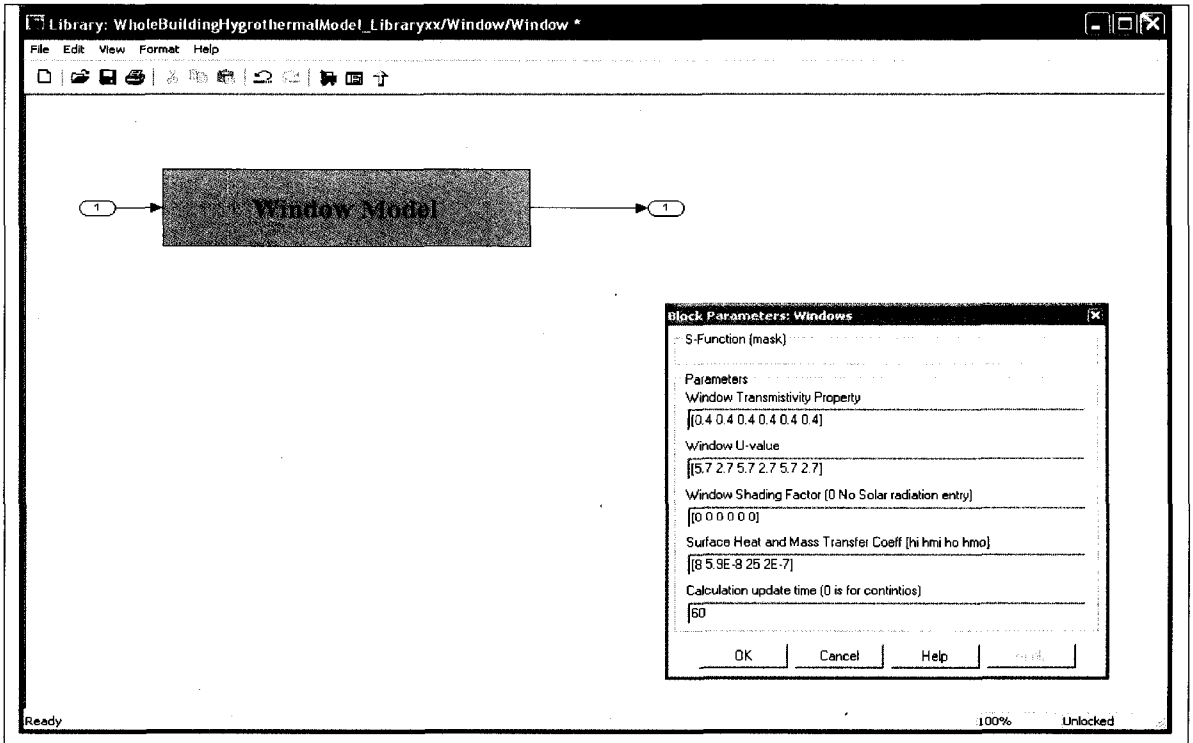

Figure 4-25 GUI to specify windows properties

Finally, as shown in Figure 4-20, the outputs of all the blocks are passed to the "Zone Humidity and Energy balance" block, which is where the two linear first-order differential equations for heat and moisture balances (Section 4.2, Equation [4.32] and [4.51], respectively) are solved for the indoor temperature and humidity ratio.

The outputs of HAMFitPlus simulation include:

- Transient temperature and moisture distribution across each building envelope components.
- Transient indoor temperature and relative humidity conditions
- Transient heating and cooling loads

Hence, the model can be used to assess building enclosure's performance, indoor environmental conditions (temperature and relative humidity), and also energy efficiency of a building in an integrated manner. But, before using the model for practical

applications as it is used in Chapter 7 and 8, it needs to be benchmarked against the internationally published test cases. Consequently, the following two chapters are devoted to benchmark, first, the building enveloped model (HAMFit) and then the whole building hygrothermal model (HAMFitPlus).

5 BENCHMARKING OF BUILDING ENVELOPE MODEL (HAMFit)

In this section, the newly developed building envelope model, HAMFit, is benchmarked against published test cases. This is an important step that must be carried out before integrating it with an indoor model to form the whole building hygrothermal model. The benchmark exercises are carried out using the HAMFit simulation environment and graphical user interfaces that are presented in Figure 4-11, Figure 4-12 and Figure 4-13. The test cases comprise an analytical verification, comparisons with other models (four test cases) and validation of simulation results with experimental data. Judkoff and Neymark (1995) recommend these three classes of model evaluation methods for testing the robustness of numerical models. Since the HAM transfers processes and dynamic responses of a building envelope component are non-linear and complex, analytical solutions are possible only for very simplified cases. In the case of comparative test, the dynamic responses of the HAMFit model for a well-defined heat and moisture transfer problem are compared with other models' simulation results. The prerequisite for such type of comparative analysis is that all model input parameters including geometrical representation, dimensions, initial conditions, internal and external boundary conditions, and material properties of the building envelope systems have to be prescribed and consistently used by all participating models The drying experiment that is carried out by Maref et al (2002) is used for validation and testing of HAMFit. The model's prediction is compared with this laboratory controlled measured data.

HAMSTAD Benchmark exercises

Here, the five benchmark exercises that are designed under the European project called HAMSTAD are used for analytical verification and comparative tests of the newly developed model. HAMSTAD stands for Heat, Air and Moisture Standards Development. One of the objectives of the HAMSTAD project was to develop standard test cases, by which the accuracy of the existing and newly developed hygrothermal models can be evaluated (Hagentoft, 2002). The exercises are designed to have at least two-transfer mechanisms and cover a wide range of complicated non-linear HAM transport processes that result from the various combinations of climate, material properties and construction.

To limit the scope of evaluation of models to the mathematical and numerical implementation of building physics, the geometrical representation, dimensions, initial conditions and material properties of the building envelope systems are prescribed in detail. Moreover, the internal and external boundary conditions are well defined. In some cases, the input data have only theoretical significance. These values are formulated in such a way that the resulting HAM transport processes are more complex and thereby more challenging for the models to simulate. In each of the five exercises, the simulation results of HAMFit are superimposed on the corresponding solutions that are provided by the HAMSTAD project participants.

5.1 Analytical verification -- HAMSTAD Benchmark Exercise #2

In this exercise, the isothermal drying process of a relatively wet homogeneous layer structure, which has 200 mm thickness, is considered, Figure 5-1. The initial hygrothermal conditions of the structure are 20°C and 95% temperature and relative humidity, respectively. The relative humidity level of the surrounding environment is changed so that the structure dries out by moisture redistribution and release to the surrounding. The top (exterior) and bottom (interior) surfaces of the structure are exposed to 45% and 65% relative humidity, respectively, while the temperature is kept constant at 20°C. The heat and mass transfer coefficients for both surfaces are 25W/m^{2}K and 1E-3 s/m, respectively. The material properties of the structure are given in Table 5-1 below. The full description of the benchmark exercise is given in (Hagentoft, 2002). This benchmark exercise is a test case that has an analytical solution. This is possible due to the fact that the drying process is isothermal, boundary conditions and hygrothermal properties of the material are assumed to be constant.

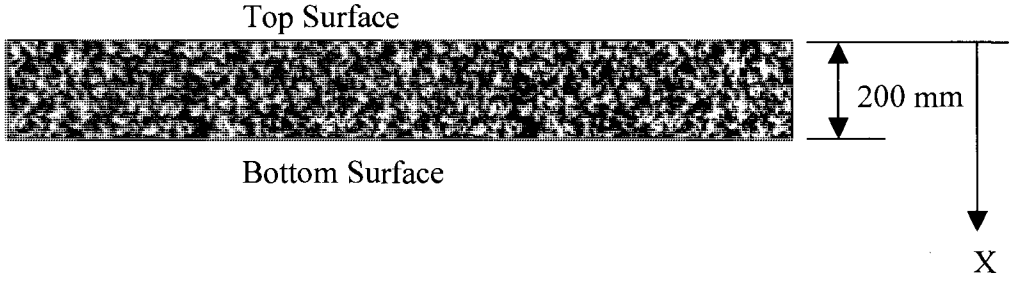

Figure 5-1 Benchmark two: Monolithic structure

The initial moisture content of the structure is 80.8 kg/m^3 (95% relative humidity), and the top and bottom boundary conditions are 45% and 65% relative humidity, respectively.

Table 5-1 Benchmark two: Material properties

Sorption isotherm	$w = \frac{116}{\left(1 - \frac{1}{0.118}\ln(\phi)\right)^{0.869}}$ kg/m^3
Vapor diffusion	10^{-15} s
Moisture diffusivity	6 x 10^{-10} m^2/s
Thermal conductivity	0.15 W/mK
Heat capacity	4.2 x 10^5 J/m^{3}K

The accuracy of the numerical model in simulating the drying process of the structure is verified by comparing the model results with the analytical solutions, which are provided in the HAMSTAD project. The transient moisture profiles (moisture content in kg/m^3) across the structure, which result due to the continuous release of moisture from the structure to the surrounding through its boundary surfaces, are used as verification parameters. Figure 5-2 shows the moisture distribution across the wall at 100, 300 and 1000 hours. The moisture distributions at the mid section of the wall at 100, 300 and 1000 hours are presented in Figure 5-3 to Figure 5-5. As can be seen in these figures, the newly developed building envelope model, HAMFit, produced excellent results, which agreed very well with the analytical and other models solutions (labeled 1 to 6).

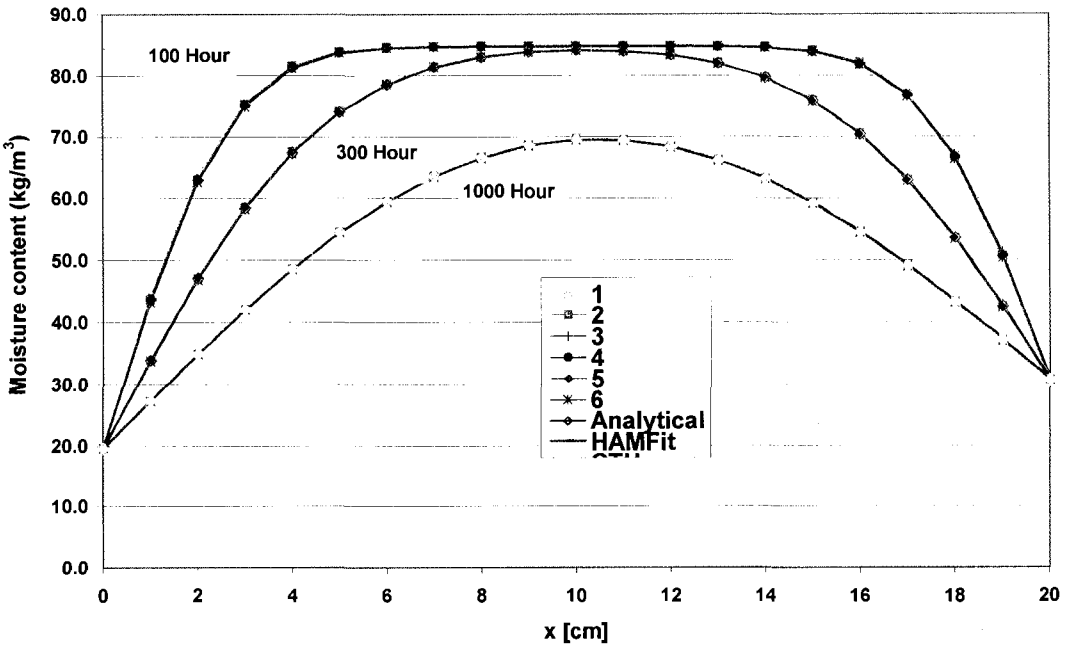

Figure 5-2 Moisture distribution across the wall at 100, 300 and 1000 hours

(The relative humidity of the top and bottom environments reduced from 95% to 45% and 65%, respectively.)

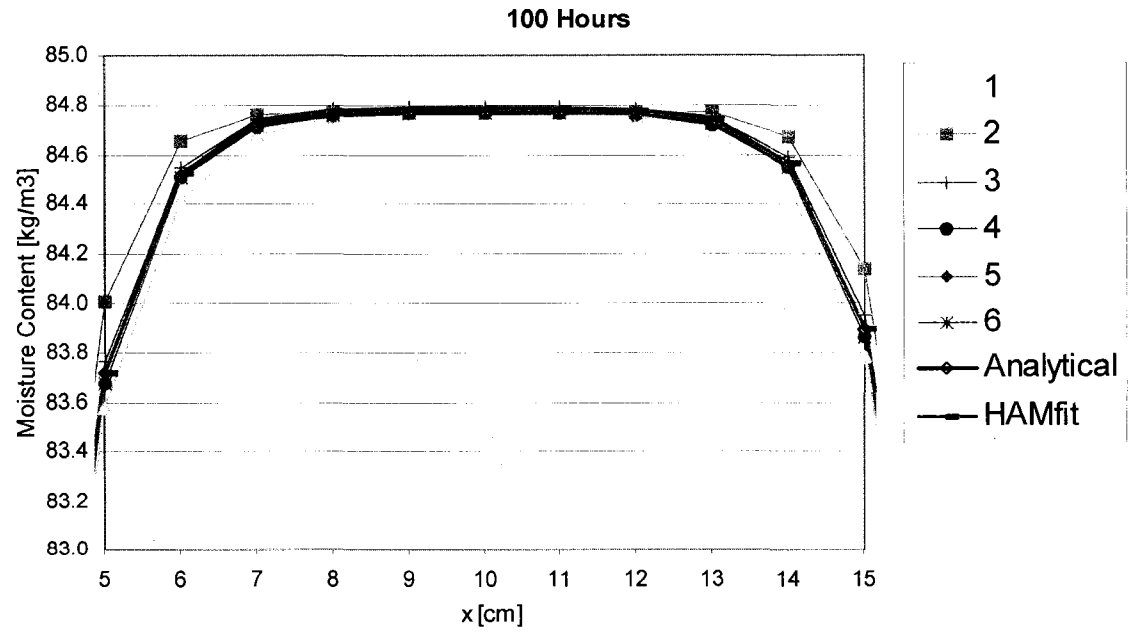

Figure 5-3 Expanded view of the moisture distribution at the middle cross-section of the wall at 100 hours

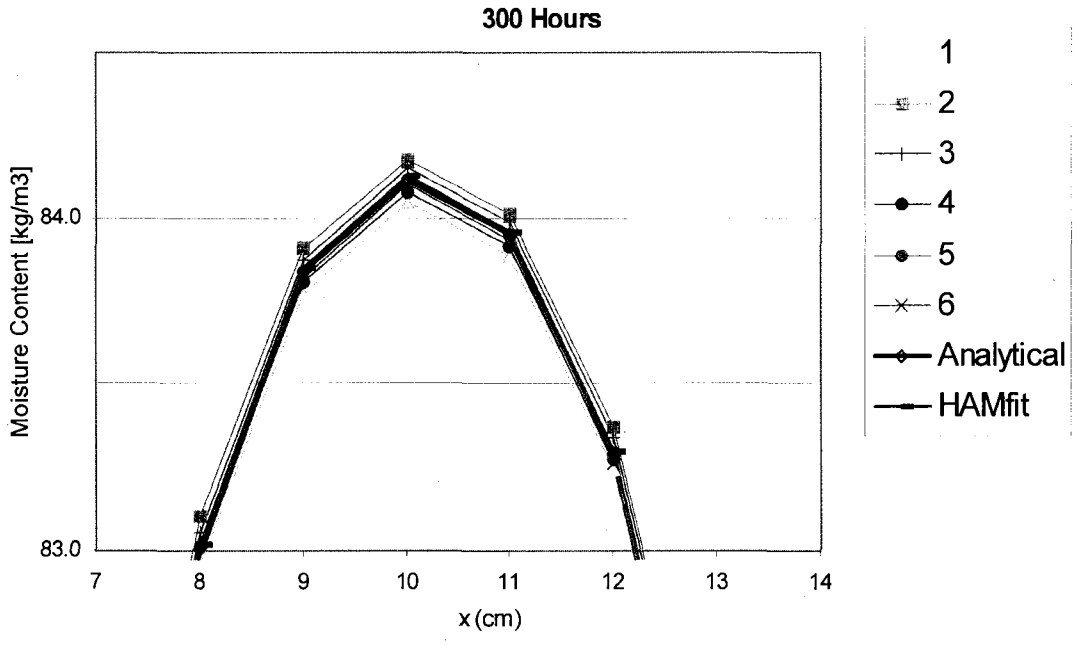

Figure 5-4 Expanded view of the moisture distribution at the middle cross-section of the wall at 300 hours

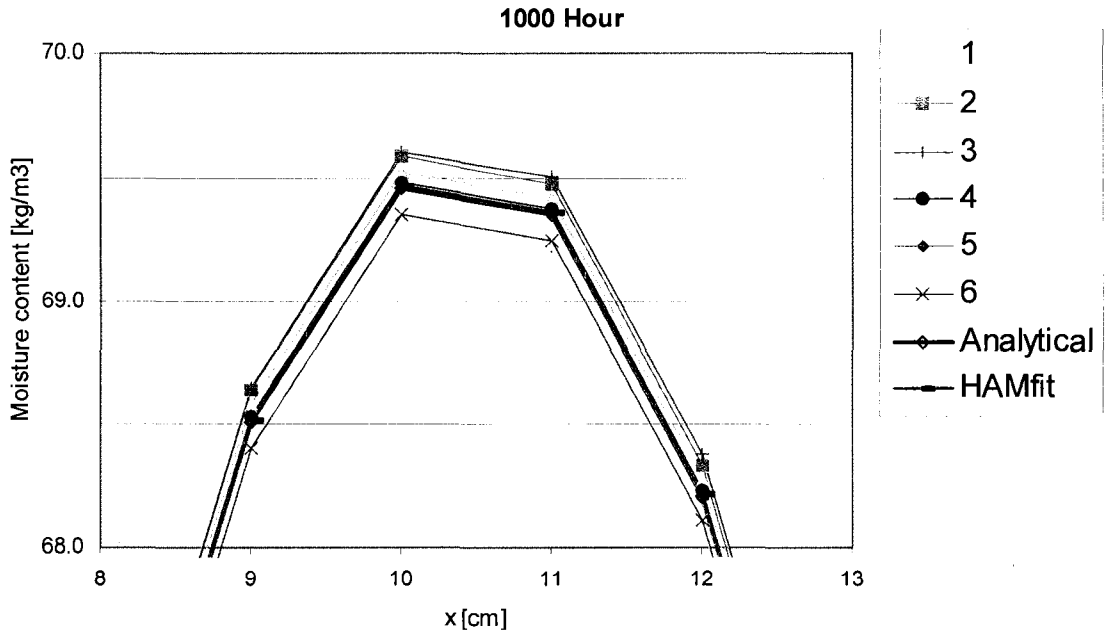

Figure 5-5 Expanded view of the moisture distribution at the middle cross-section of the wall at 1000 hours

5.2 Comparative Analysis 1—HAMSTAD Benchmark Exercise #3

In benchmark #3, the effect of airflow (exfiltration and infiltration) on the wetting (accumulation of moisture) and drying of a lightweight structure is analyzed. Although the main moisture transfer mechanism in this exercise is by airflow, moisture is transported due to temperature and moisture gradient across the monolithic wall layer. The schematic diagram of the structure considered is shown in Figure 5-6 below. The pressure gradients across the wall, which causes heat and moisture transfer by convection, in both infiltration and exfiltration periods are 30 Pa, Figure 5-7. The exterior surface of the structure is vapor tight (painted), whereas the interior surface is open. Accordingly the mass transfer coefficients of the exterior and interior surfaces are 7.38E-12 and 2E-7 s/m, respectively. The heat transfer coefficients for both surfaces are 10 W/m^2K.

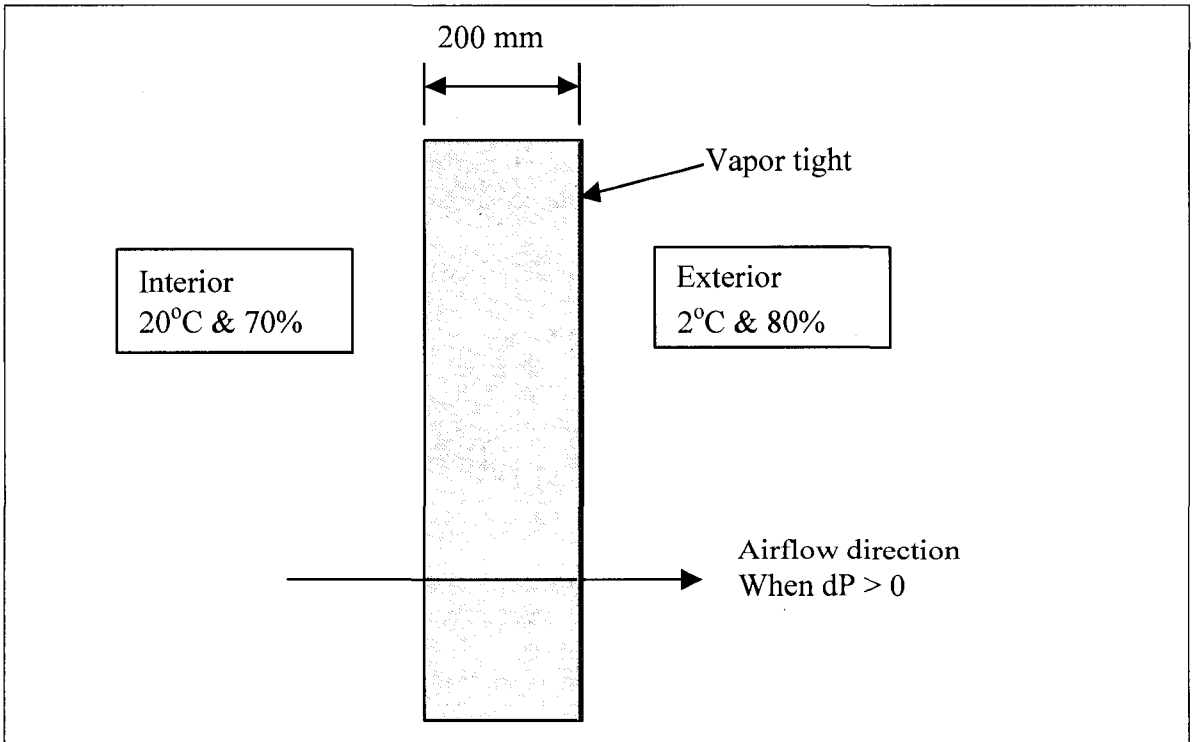

Figure 5-6 Benchmark three: Lightweight wall with vapor tight exterior surface

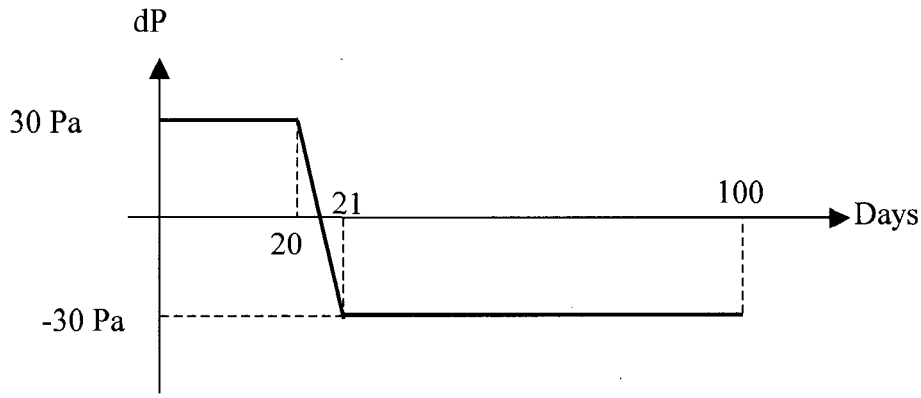

Figure 5-7 Pressure gradient across the wall as a function of time

The initial hygrothermal conditions of the structure are 20°C and 95% temperature and relative humidity, respectively. In the first 20 days the airflow is from inside to outside (exfiltration) and the airflow is reversed in the next 80 days (infiltration). The interior temperature and relative humidity conditions are 20°C and 70%, respectively. Whereas, the exterior temperature and relative humidity conditions are 2°C and 80%, respectively. These boundary conditions are maintained constant for the 100 days of simulation period. The density and specific heat capacity of the monolithic layer are 212 kg/m^3 and 1000 J/kgK, respectively. The full description of this benchmark exercise is given in Hagentoft (2002). The time history of moisture content and temperature at different cross-section of the wall, i.e. at 0.05, 0.1, 0.15, 0.17 and 0.19 m, are used for model comparisons. For comparison purpose, the HAMFit simulation results are superimposed on the solutions provided by the HAMSTAD participants. The full solution of HAMFit for this test case along with the moisture storage characteristics (sorption isotherm and water retention curve), vapor permeability, liquid diffusivity and moisture dependent thermal conductivity of the material are presented in Appendix B-1. Here, the temperature and moisture content variations with time for the left and right

section of the wall, 0.05 and 0.19 m respectively, are presented in Figure 5-8 to Figure 5-11. As can be seen in these figures and Appendix B-1, the HAMFit simulation results agree very well with the other models solutions (labeled 1 to 4).

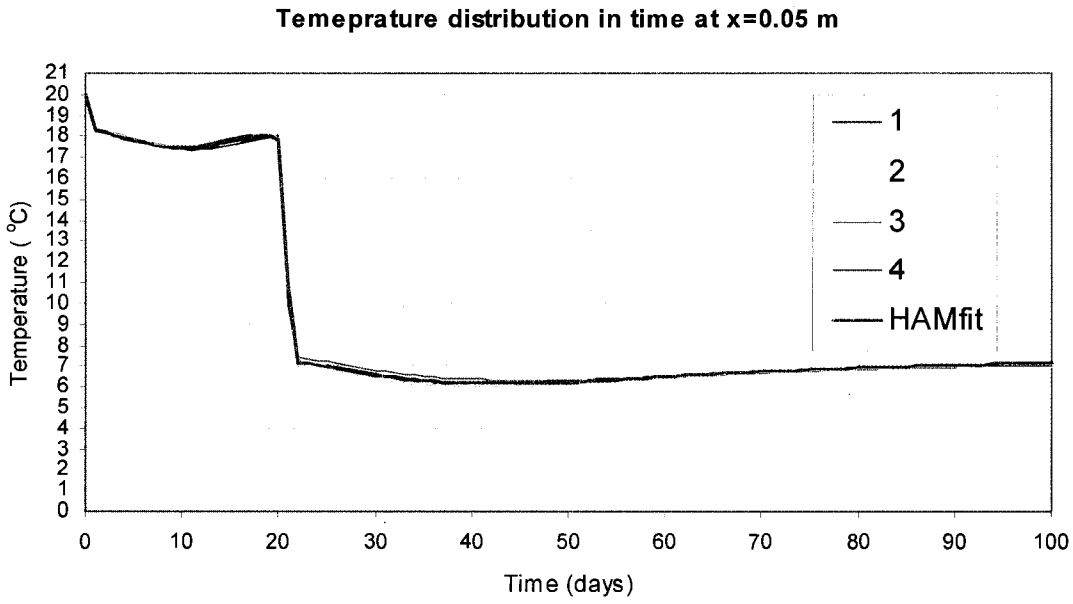

Figure 5-8 Temperature variations in time at 0.05 m cross-section of the wall.

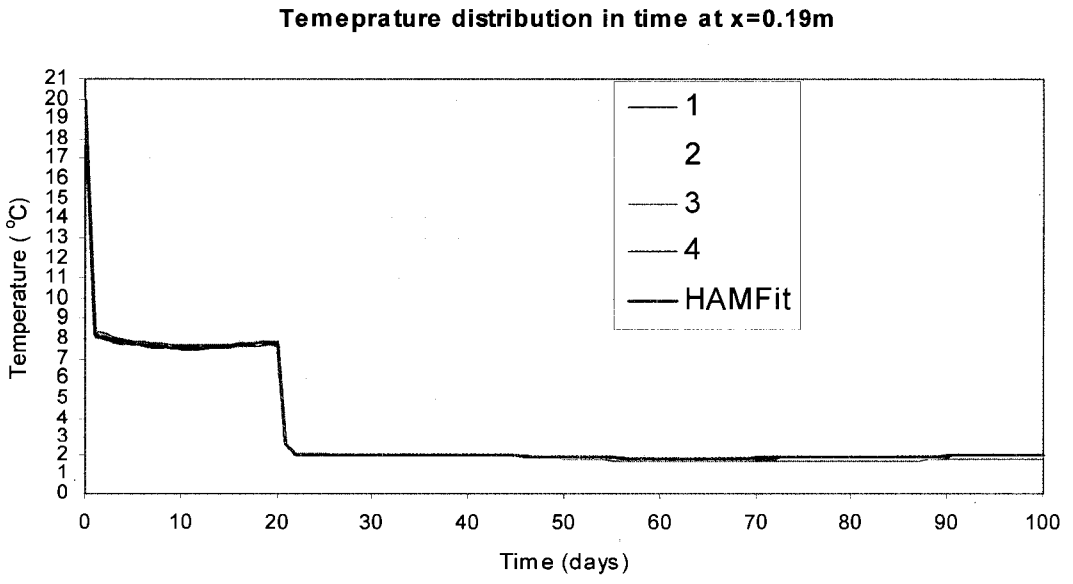

Figure 5-9 Temperature variations in time at 0.19 m cross-section of the wall.

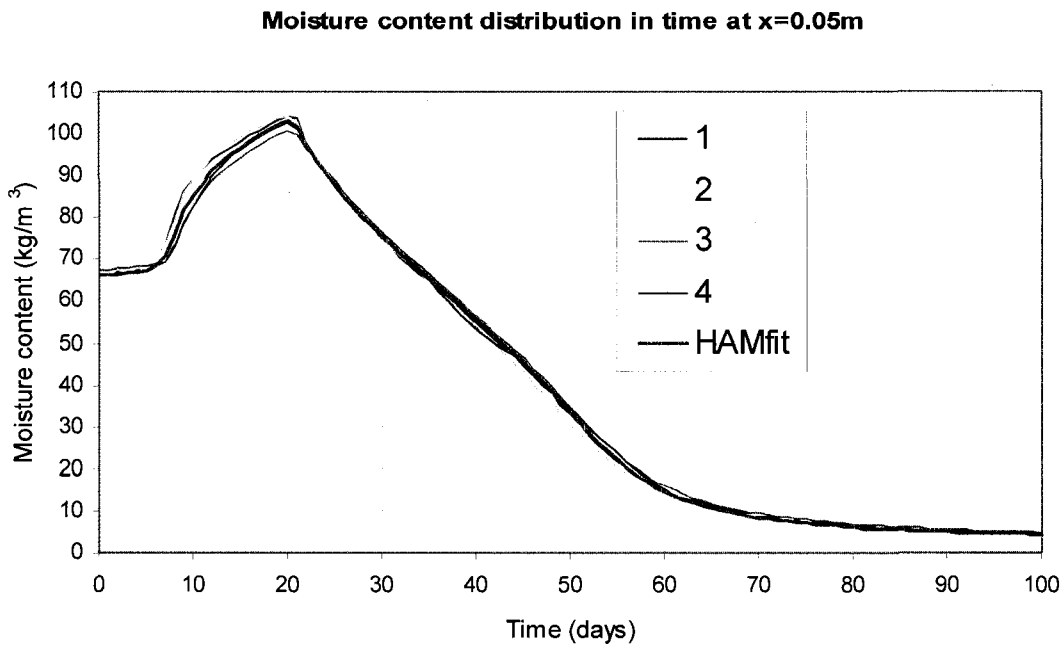

Figure 5-10 Moisture content variations in time at 0.05 m cross-section of the wall.

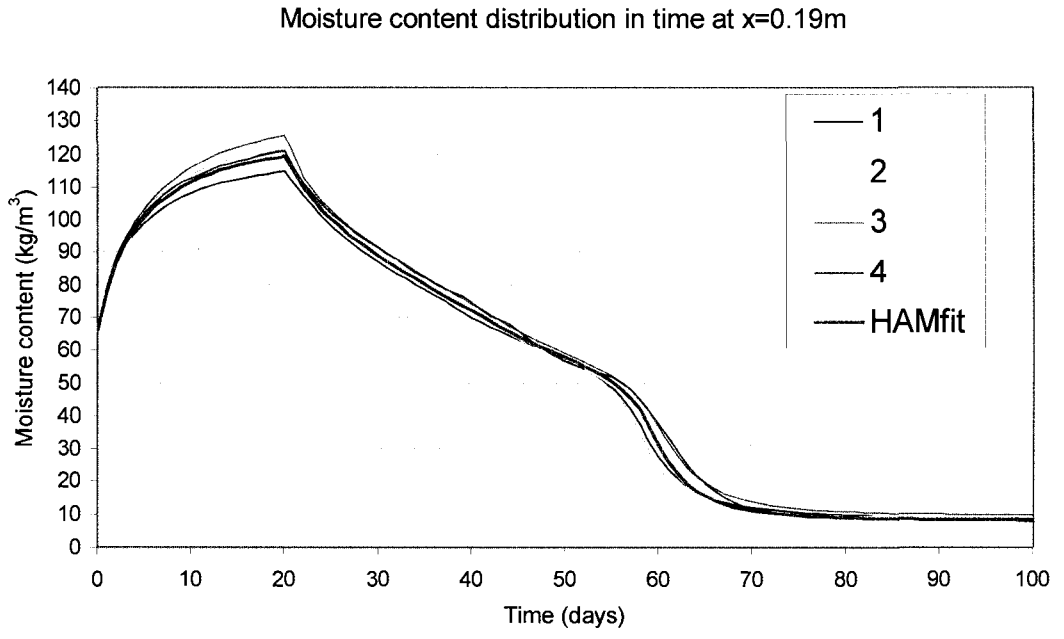

Figure 5-11 Moisture content variations in time at 0.19 m cross-section of the wall.

5.3 Comparative Analysis 2—HAMSTAD Benchmark Exercise #5

In this exercise, moisture redistribution in three layers wall system is analyzed. The three layers of the wall are: 365 mm brick at the exterior as a load-bearing layer, followed by 15 mm mortar, and finally 40 mm insulation layer at the interior. The schematic diagram of the wall is shown in Figure 5-12. The two special features of this exercise are: the insulation layer is capillary active, and the difference in thermal conductivity of insulation and brick is large. At dry condition, the thermal conductivity of the insulation is 11 times higher than that of the brick. The initial hygrothermal conditions of all three layers are 25°C and 60% temperature and relative humidity, respectively.

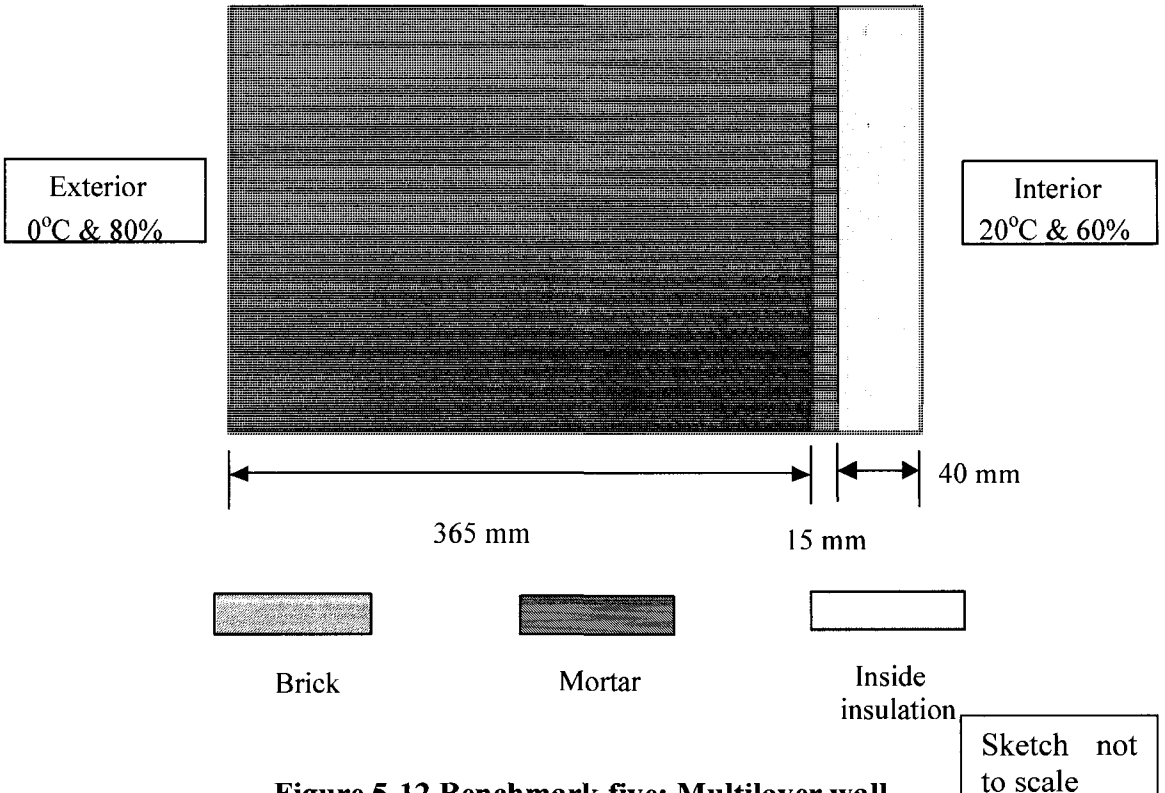

Figure 5-12 Benchmark five: Multilayer wall

Table 5-2 Density and specific heat capacities of brick, mortar and insulation layers.

Material	Density (kg/m^3)	Specific heat capacity (J/kgK)
Brick	1600	1000
Mortar	230	920
Insulation	212	1000

The wall is exposed to constant boundary conditions (temperature and relative humidity conditions) on both interior and exterior surfaces of the wall for 60 days of simulation period. The interior temperature and relative humidity conditions are 20°C and 60%, respectively. Whereas the exterior temperature and relative humidity conditions are 0°C and 80%, respectively. The mass transfer coefficients of the interior and exterior surfaces are 5.882E-8 and 1.838E-7 s/m, respectively, whereas the heat transfer coefficients are 8 and 25 W/m^2K, respectively. The density and specific heat capacity of the layers are given in Table 5-2 above. The hygrothermal properties of the insulation are the same as the ones presented in HAMSTAD Benchmark exercise #3. The full description of this benchmark exercise including the moisture storage characteristics (sorption isotherm and water retention curve), vapor permeability, liquid diffusivity and moisture dependent thermal conductivity of the brick and mortar are given in Hagentoft (2002). The moisture content and relative humidity profiles across the wall section at the end of the simulation period (sixty days) are used for model comparisons. In Figure 5-13 and Figure 5-14 the simulation results of HAMFit are superimposed on the HAMSTAD project participants results. As can be seen in the figures, HAMFit prediction of relative

humidity, Figure 5-13, and moisture content, Figure 5-14, profiles across the wall section agree very well with the other models solutions (labeled 1 to 6).

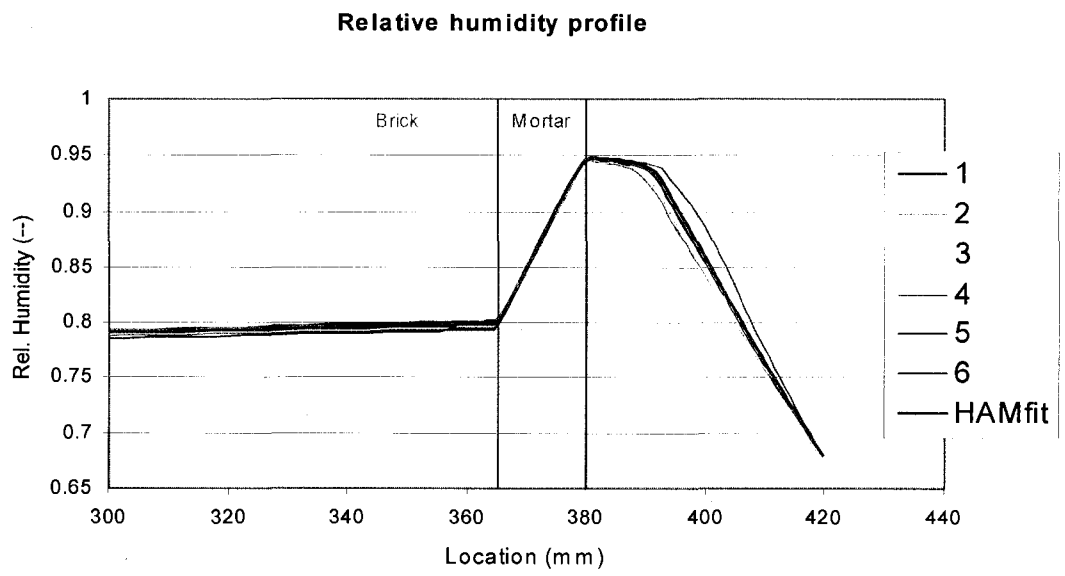

Figure 5-13 Relative humidity profiles across the wall section.

The wall is exposed to 0°C and 80% RH at the exterior and 20°C and 70% RH at the interior surfaces.

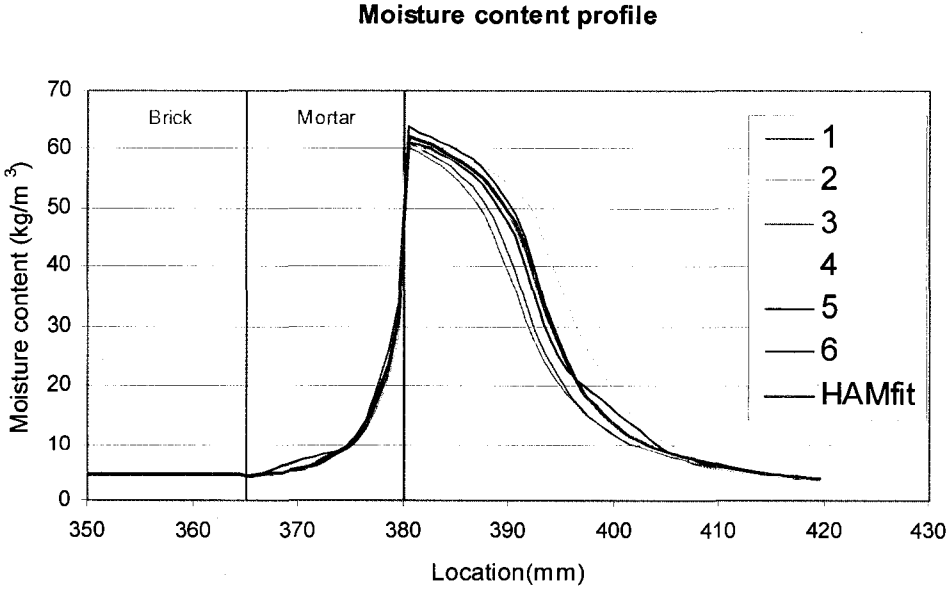

Figure 5-14 Moisture content profiles across the wall section.

5.4 Comparative analysis 3—HAMSTAD Benchmark Exercise #4

The third comparative analysis deals with heat and moisture transfer in a two-layer wall system exposed to realistic internal and external boundary conditions. The schematic diagram of the wall system, which is composed of load-bearing layer on the exterior and finishing layer on the interior, is shown in Figure 5-15. Realistic time dependent boundary conditions that are applied at the external and internal surfaces of the wall are shown in Figure 5-16- Figure 5-18. The variable heat and moisture loads on the exterior surface, which are due to solar radiation and rain, respectively, are represented by equivalent outdoor temperature (Figure 5-16) and wind–driven rain flux (Figure 5-18). The time dependent indoor moisture load, which may be related to occupant activities, is represented by variable indoor vapor pressure (Figure 5-17). The outdoor air temperature and vapor pressure, as well as the indoor air temperature are held constant with values of 10°C, 1150 Pa, and 20°C respectively. The moisture storage characteristics (sorption isotherm and water retention curve), vapor permeability, liquid diffusivity and moisture dependent thermal conductivity of the load-bearing and finishing layers are documented in Appendix B-2. This test case is more challenging (Hagentoft et al., 2004) as it involves severe climatic load that causes surface condensation on the exterior surface due to nighttime cooling (low equivalent temperature), and frequent occurrences of wetting and drying of the wall due to the alternating rain and solar radiation loads. Moreover, the problem involves rapid rainwater absorption at the interfaces and fast moisture movement within the layers due to the extremely high liquid water absorption property of the load-bearing layer.

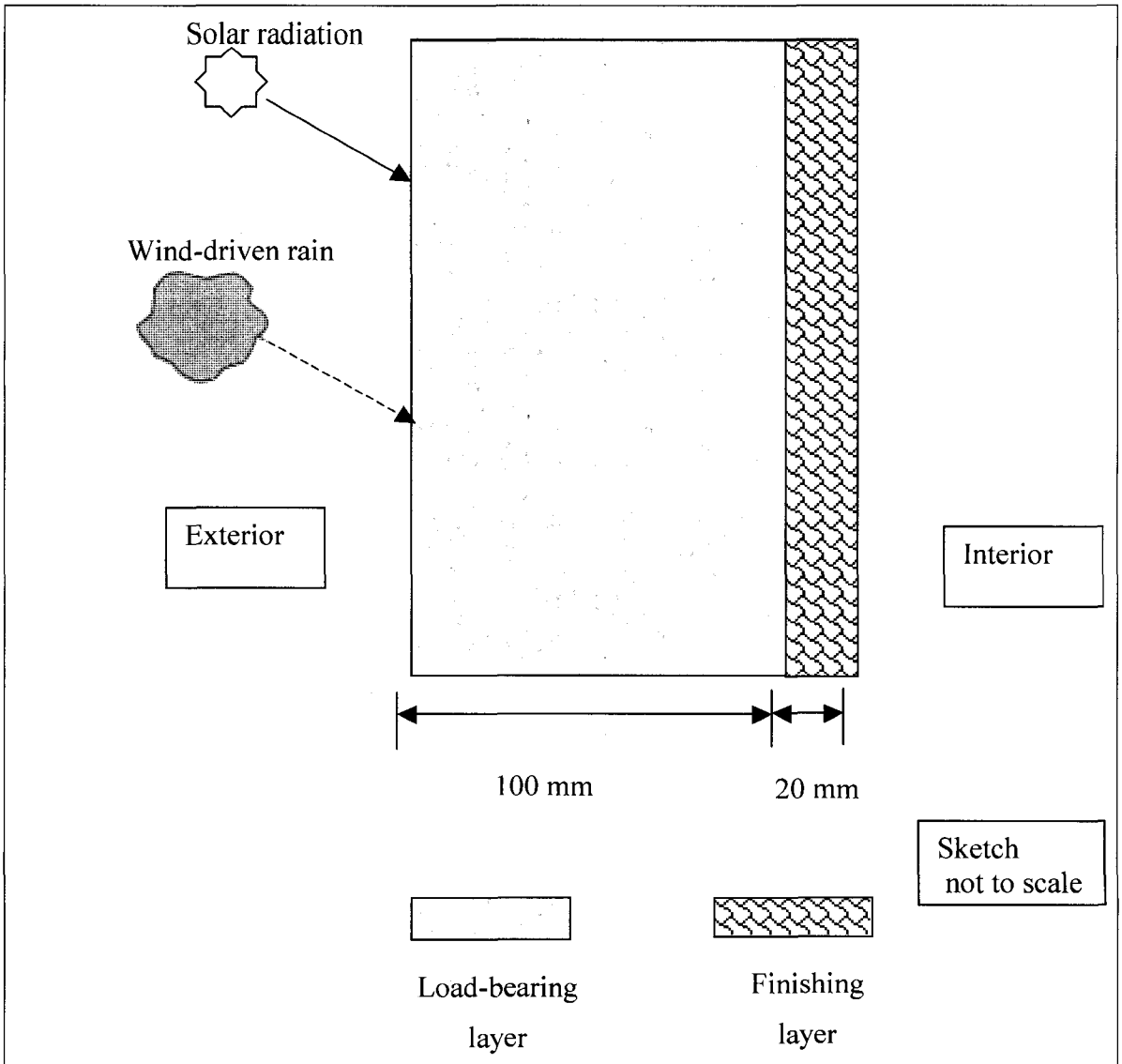

Figure 5-15 Benchmark four: Load-bearing wall exposed to time varying boundary conditions

Table 5-3 Density and specific heat capacities of load-bearing and finishing materials

Material	Density (kg/m^3)	Specific heat capacity (J/kgK)
Load-bearing	2050	840
Finishing material	790	870

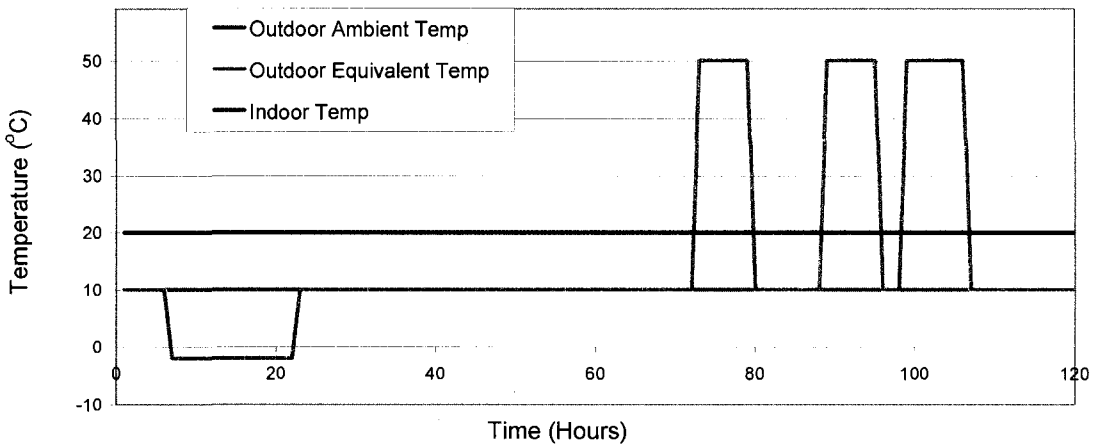

Figure 5-16 Indoor and outdoor temperatures

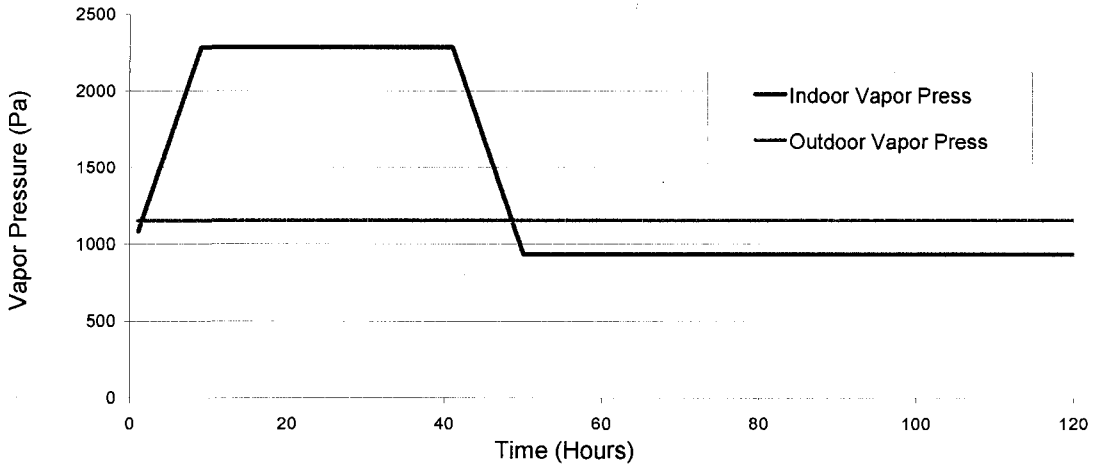

Figure 5-17 Indoor and outdoor vapor pressure

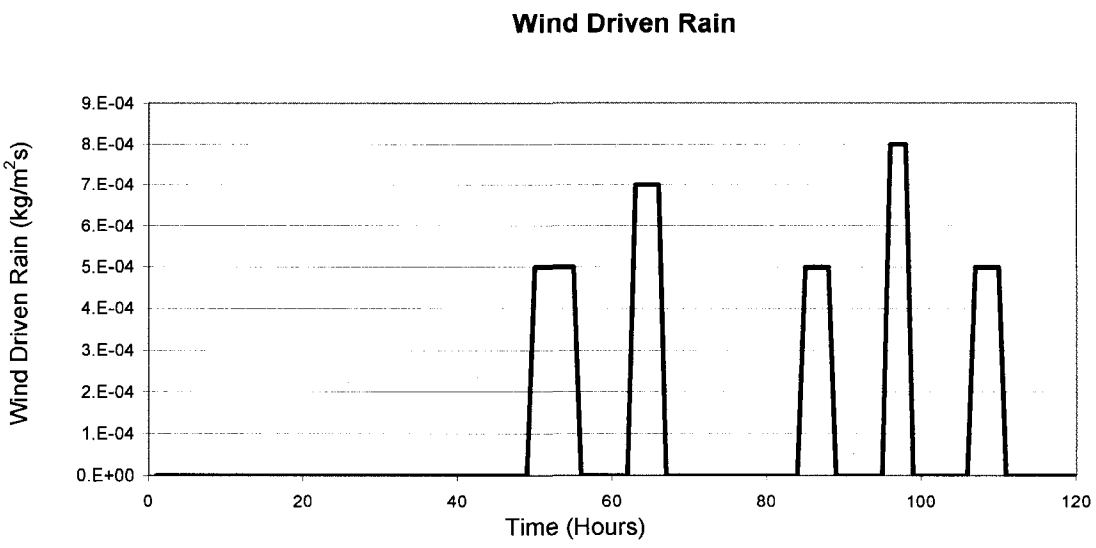

Figure 5-18 Wind-driven rain load on the exterior surface of the wall

The initial hygrothermal conditions of the two layers are 20°C and 40% temperature and relative humidity, respectively. The mass transfer coefficients of the interior and exterior surfaces are 3E-8 and 2E-7 s/m, respectively. The heat transfer coefficients for the corresponding surfaces are 8 and 25 W/m^2K, respectively. The density and specific heat capacity of the layers are given in Table 5-3. The full description of this benchmark exercise is given in Hagentoft (2002). The required simulation results for comparison of the models are: 1) the hourly values of internal and exterior surface temperatures and moisture contents for the whole simulation period of 5 days (120 hours), and 2) the temperature and moisture content profiles of the wall cross-section at every 6 hours. The complete solutions of HAMFit for this benchmark exercise are presented in Appendix B-2. For comparison purpose, the simulation results of HAMFit are superimposed on the corresponding HAMSTAD project participants' solutions. Here the transient surface moisture contents and temperatures of the outer and

inner surfaces of the wall for the entire simulation period are presented, Figure 5-19 to Figure 5-22. Moreover, the moisture content and temperature profiles of the wall system after 96 hours are presented in Figure 5-23 and Figure 5-24, respectively. As can be seen in the full solution, provided in the Appendix B-2, as well as the typical results presented here, the simulation results of HAMFit agree very well with the other six models solutions (labeled 1 to 6). In whole building hygrothermal modeling, the coupling of building enclosure and indoor environment is through interior surfaces, and therefore, it is important to accurately predict the hygrothermal states of these surfaces to obtain useful results.

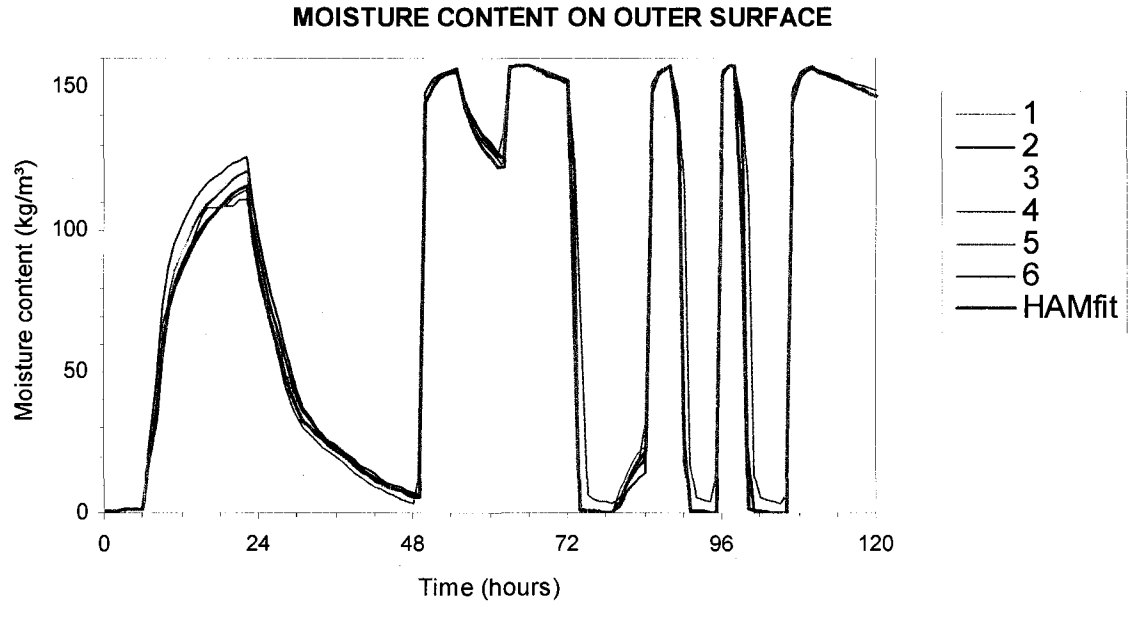

Figure 5-19 Surface moisture contents of the outer surfaces of the wall verses time

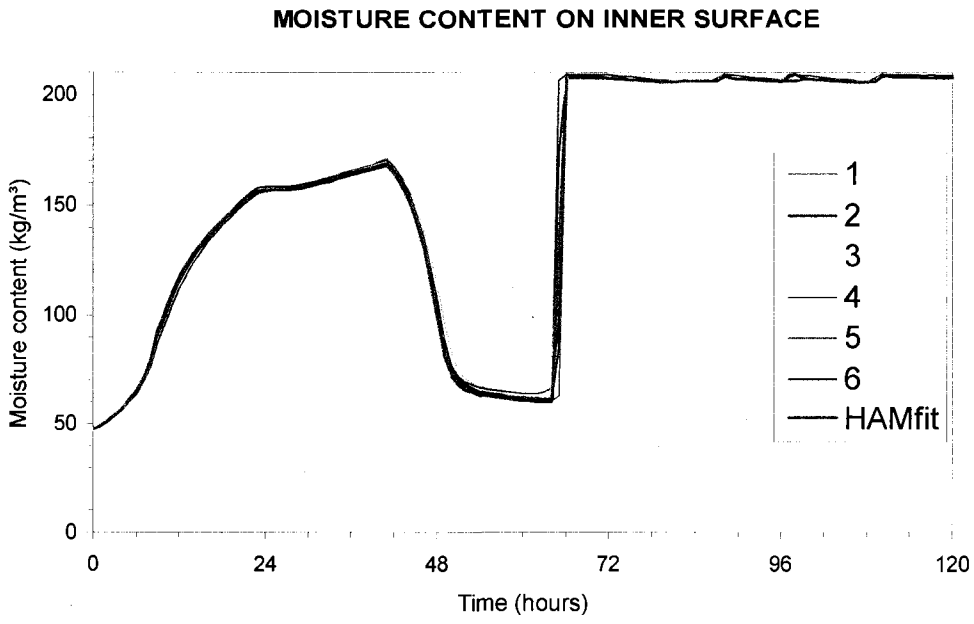

Figure 5-20 Surface moisture contents of the inner surfaces of the wall verses time

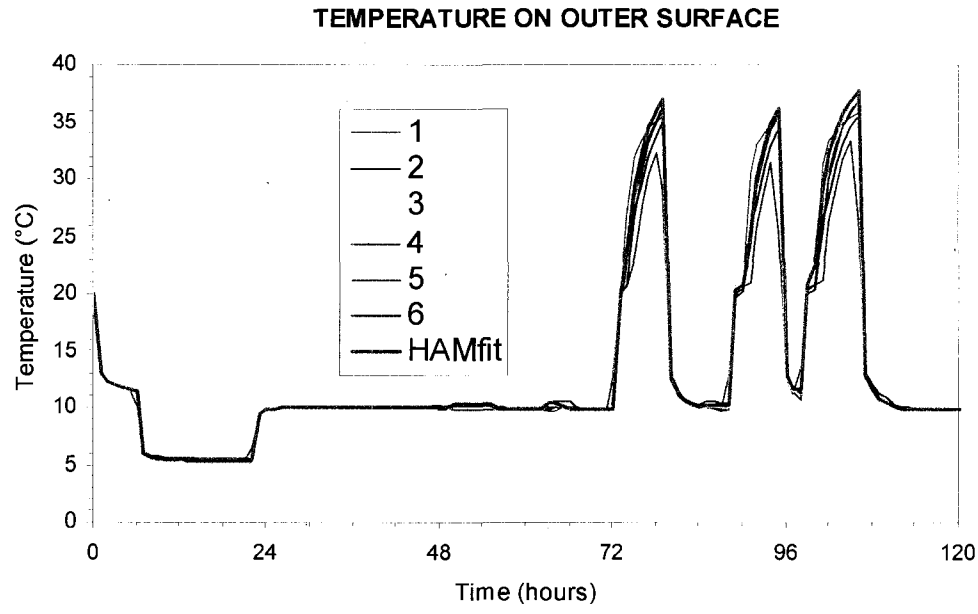

Figure 5-21 Surface temperatures of the outer surface of the wall verses time

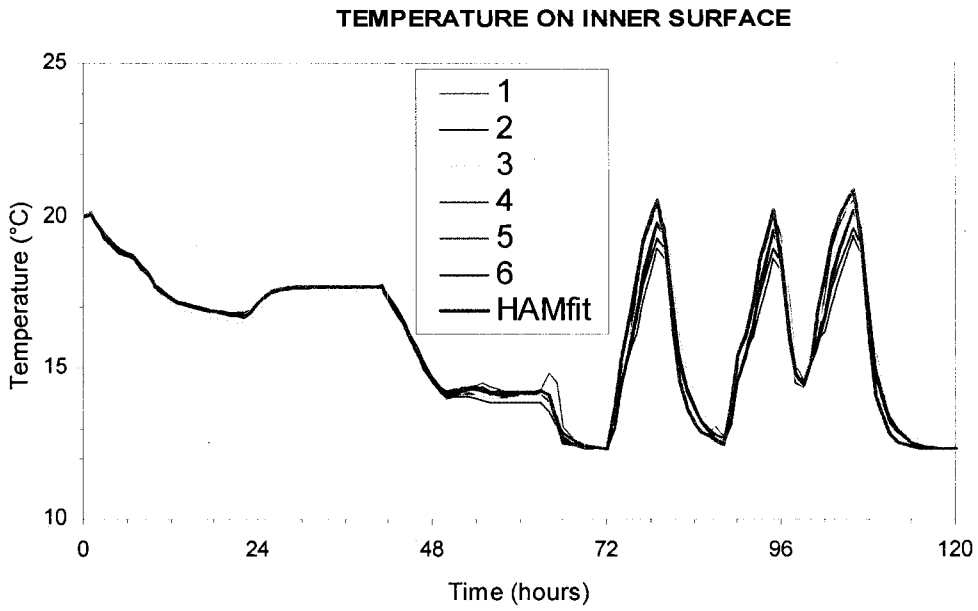

Figure 5-22 Surface temperatures of the inner surface of the wall verses time

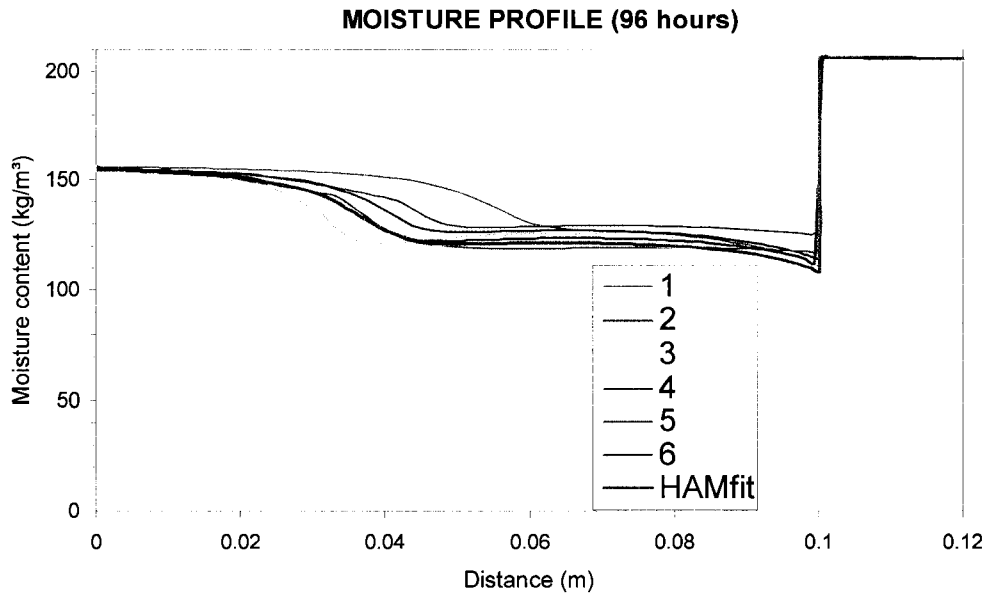

Figure 5-23 Moisture profiles across the wall section at 96 hours

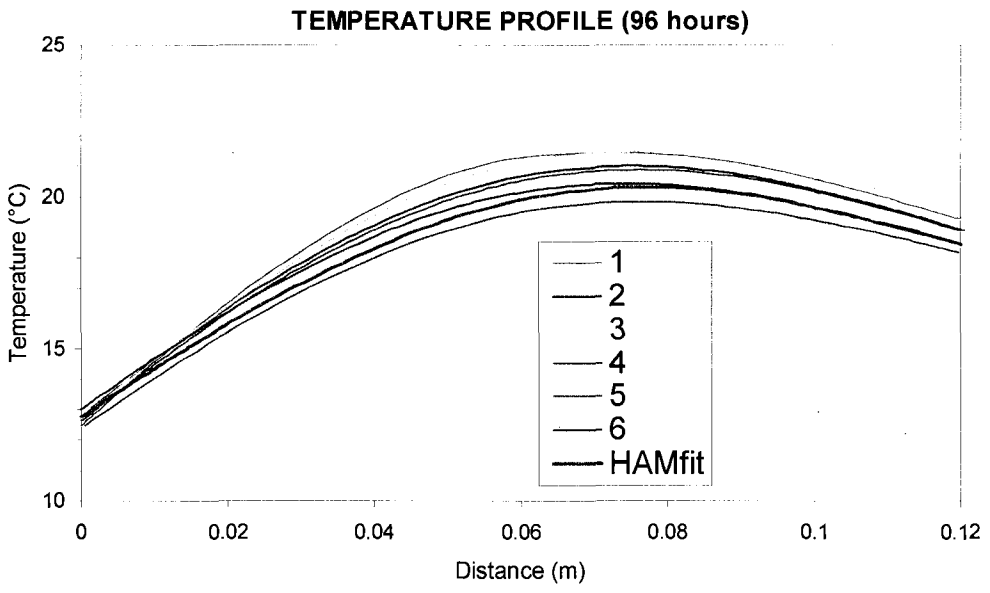

Figure 5-24 Temperature profiles across the wall section at 96 hours

5.5 Comparative Analysis 4—HAMSTAD Benchmark Exercise #1

This last comparative analysis exercise deals with a roof system shown in Figure 5-25. The hygrothermal properties of the adjacent layers are quite different: the load-bearing layer is capillary active and has high moisture storage capacity; on the contrary the insulation is capillary non-active (no liquid flow) and has low moisture storage capacity. The thermal conductivity of the insulation is 50 times higher than that of the load-bearing. In this roof system, the load-bearing structure lies above the insulation layer, which results in temperature fluctuation in the load-bearing layer following the outdoor weather conditions. The exterior surface of the roof is sealed with a roofing-membrane to prevent water from getting into the structure. Moreover, it prohibits vapor

exchange with the outdoor. In such kind of roof system, there is a potential of interstitial condensation during winter. This is due to the fact that the load- bearing will be cold, and drying to the outside will not be possible due to the presence of vapor-tight membrane. The condensate will redistribute into inner section of the load-bearing layer (capillary-active layer) during winter, and evaporate (dry) to the inside during summer. This well known interstitial condensation problem is simulated using the North-European weather conditions on the exterior and a common dwelling climate in the interior as a realistic boundary conditions, shown in Figure 5-26 and Figure 5-27. The outdoor climate conditions are represented by the outdoor vapor pressure and equivalent temperature, which accounts for solar radiation and long-wave radiation exchange. Whereas, the indoor climate is represented by variable vapor pressure and constant temperature (20°C).

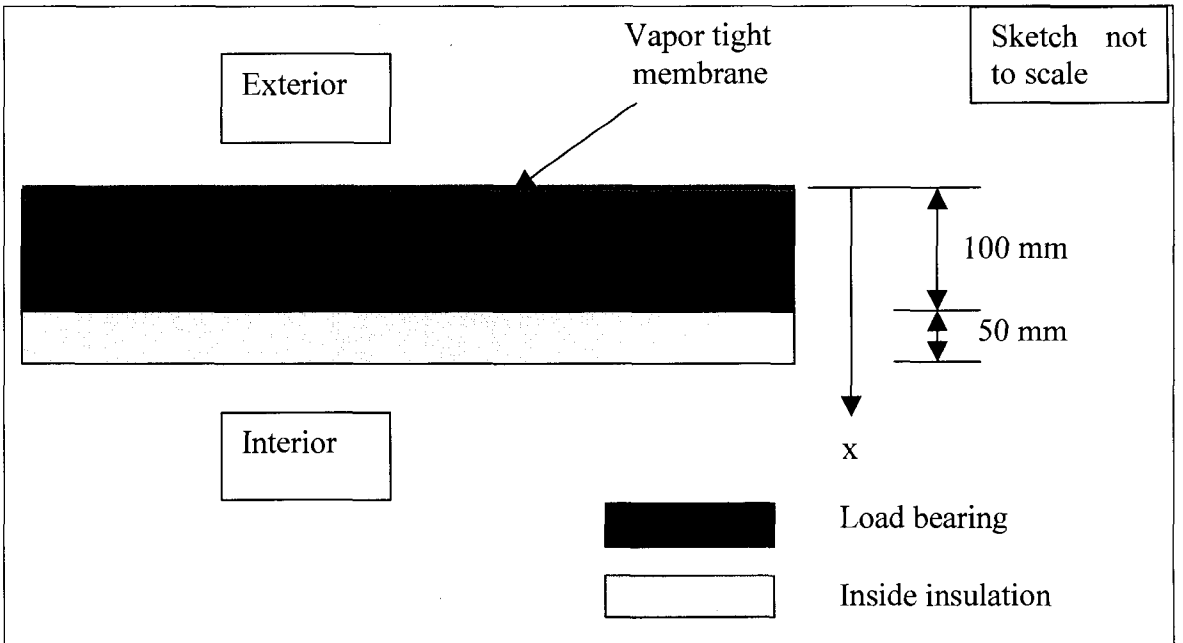

Figure 5-25 Benchmark one: Insulated roof structure exposed to time varying boundary conditions.

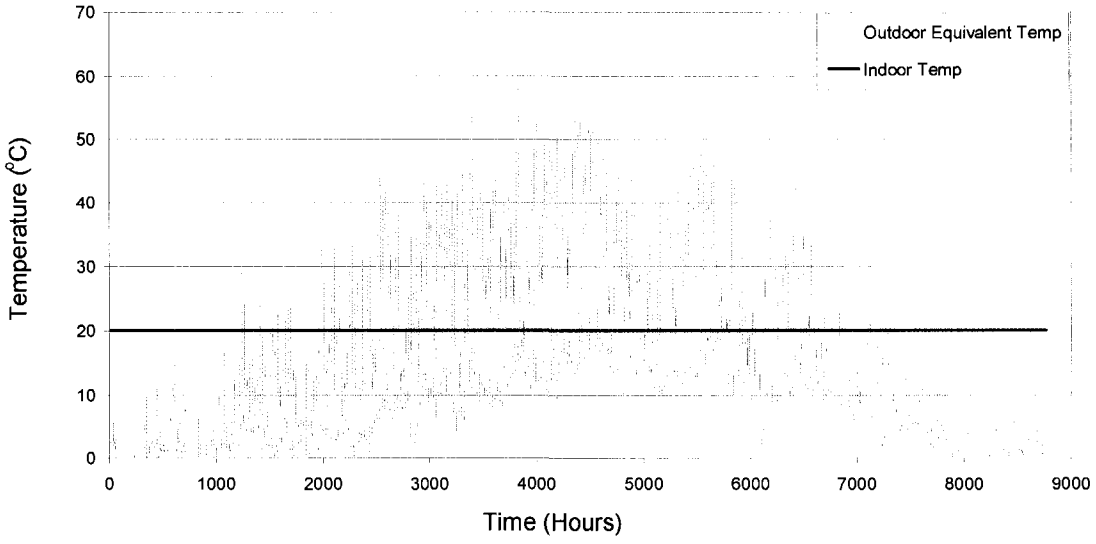

Figure 5-26 Indoor and outdoor temperature conditions

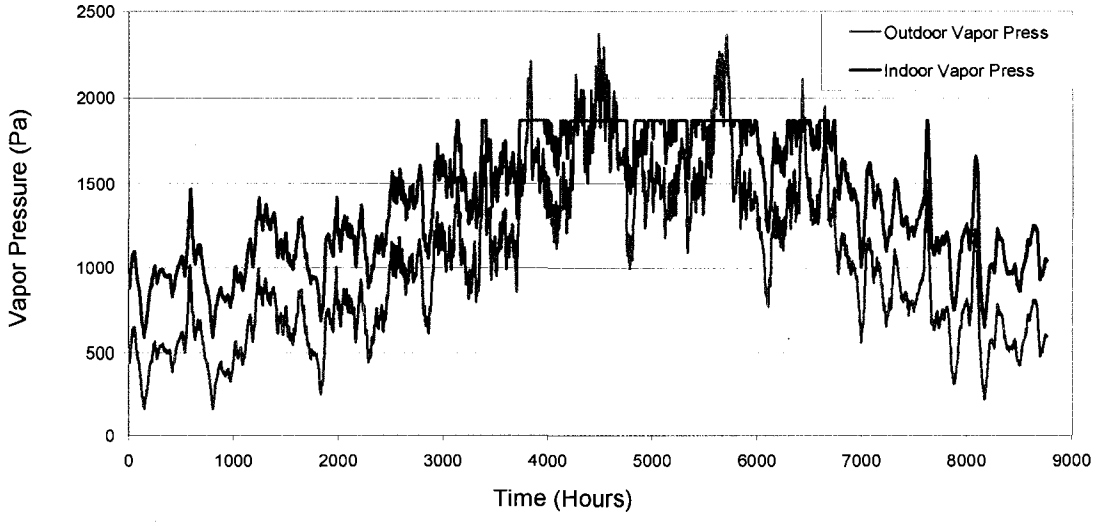

Figure 5-27 Indoor and outdoor vapor pressure conditions

The initial moisture conditions of the load bearing and insulation are 145 and 0.065 kg/m^3, respectively, and the initial temperature of this relatively wet roof system is 10°C. The mass transfer coefficients of the interior and exterior surfaces are 2E-8 and 0 s/m, respectively, whereas the heat transfer coefficients are 7 and 25 W/m^2K, respectively. The heat capacities of the load bearing and insulation layers are 1824 and 73.9 kJ/m^3K, respectively. The full description of this benchmark exercise including the moisture storage characteristics (sorption isotherm and water retention curve), vapor permeability, liquid diffusivity and moisture dependent thermal conductivity of the load-bearing and insulation layers is documented in Hagentoft (2002). The transient moisture content profiles of the load bearing and insulation layers during the first year of simulation period are shown in Figure 5-28 and Figure 5-29, respectively. In these figures the simulation results of HAMFit for this benchmark exercise are superimposed on the solutions provided by the HAMSTAD project participants. The total moisture profiles of the load bearing and insulation layers predicted by HAMFit simulation agree very well with the other participant models. Moreover, the HAMFit simulation results lie within the established band of acceptance as shown in Figure 5-30 and Figure 5-31. The band of acceptance is defined as the 99.9% confidence intervals that are established based on statistical analysis of the participants' simulation results.

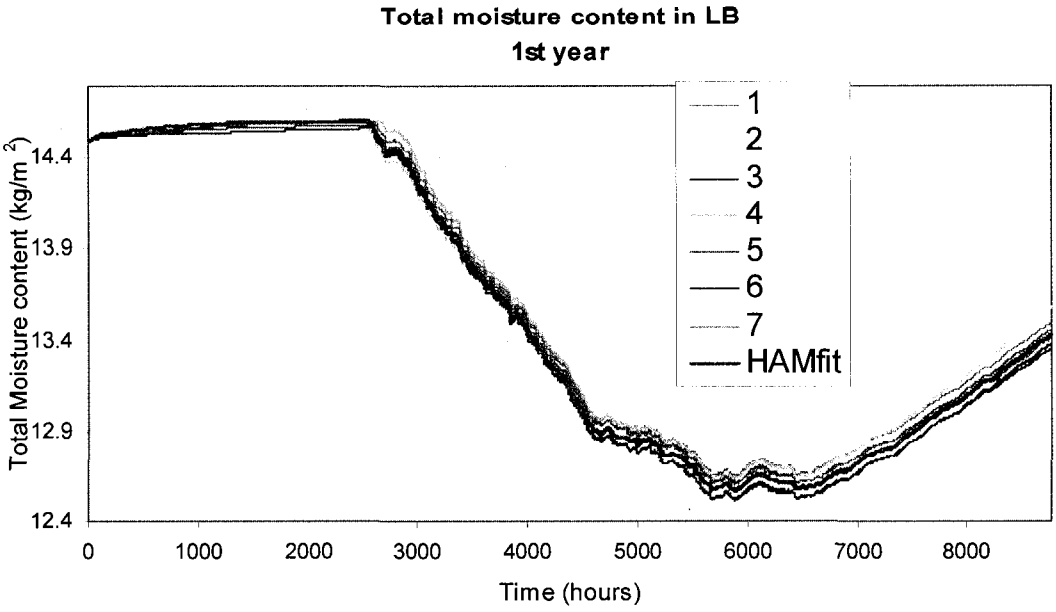

Figure 5-28 Total moisture content profile of load bearing layer during the firstyear

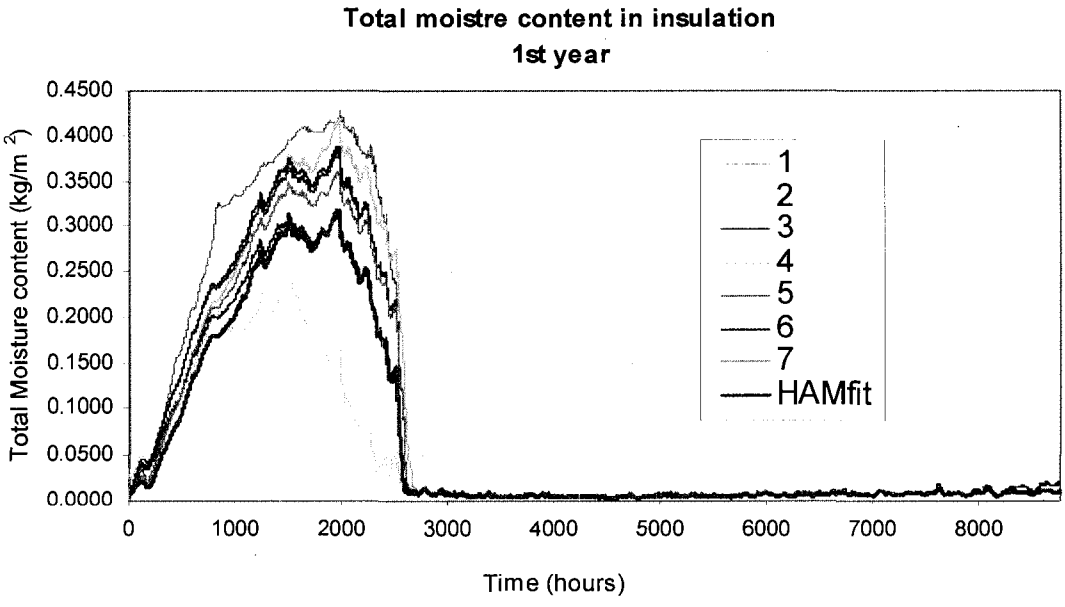

Figure 5-29 Total moisture content profile of insulation layer during the first year

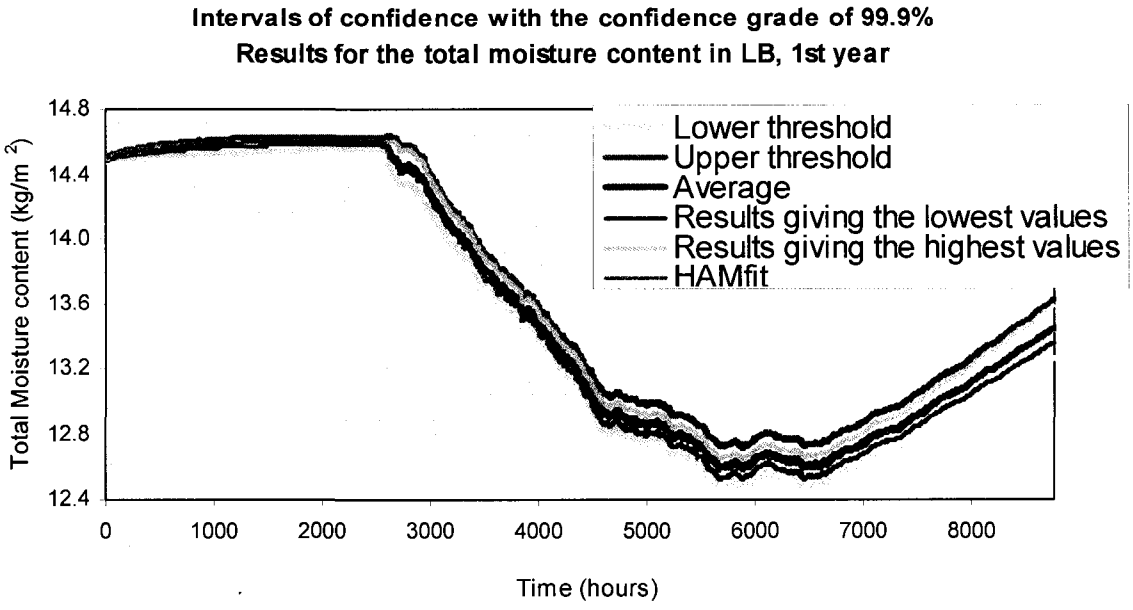

Figure 5-30 The 99.9% confidence intervals for the total moisture content of load-bearing layer

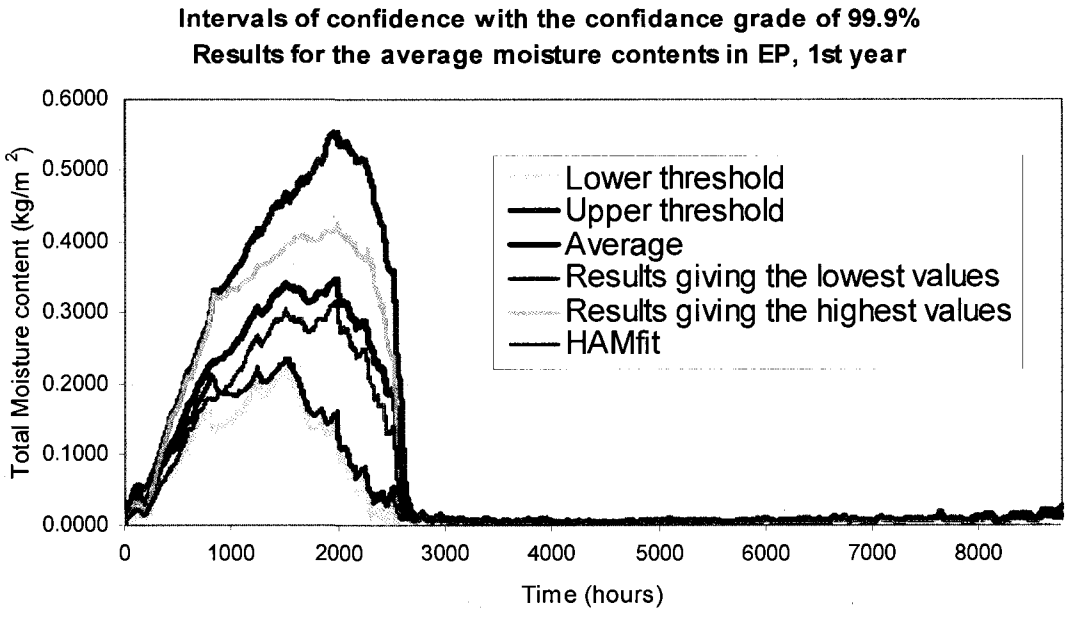

Figure 5-31 The 99.9% confidence intervals for the total moisture content of insulation layer

5.6 Experimental validation—Laboratory controlled drying experiment

In this section the drying experiment that is carried out by Maref et al (2002) is used for validation and testing of HAMFit. The model's prediction is compared with this laboratory controlled measured data. In fact, the main objective of their experiment was to provide measured data by which building envelope models can be tested and validated. The experiment is done in full-scale size wall that has equal height and width of 2.43 m. The wall system comprises of a wood frame, sheathing board (11.5 mm thick OSB) and vapor barrier (polyethylene sheet) that are installed on the outside and interior surfaces of the frame, respectively. The cavity between the studs is filled with glass fiber insulation. The vertical cross-section of the wall system under consideration is shown in Figure 5-32.

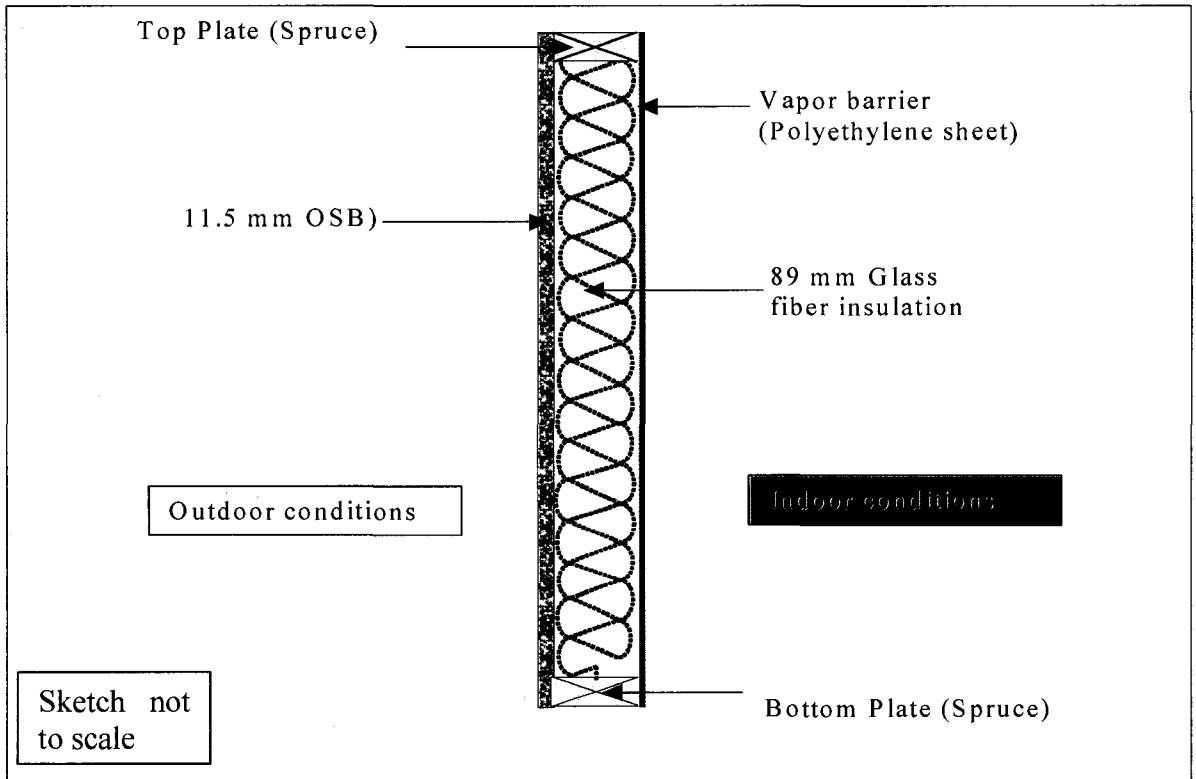

Figure 5-32 Schematic diagram of the wall section used in the drying experiment

The experiment is designed to measure the drying rate of a wetted sheathing board (OSB) as it is exposed to controlled indoor and outdoor boundary conditions. At the beginning of the experiment, the equilibrium moisture content of the wetted OSB was 330 kg/m^3, which is equivalent to 99.6% relative humidity. This initial moisture condition is attained by carrying out preconditioning process that involves; soaking of the OSB in a water bath, and then wrapping it up with polyethylene sheet to allow moisture redistribution across the thickness. As part of the experiment setup, the entire surfaces of the wood frame were coated with vapor tight paint to restrict moisture exchange with the surrounding including with the OSB. Furthermore, the edges of the OSB were sealed to prevent moisture loss through these surfaces. These preliminary actions suggest that the drying process is one-dimensional that takes place through the OSB planer surfaces. Hence, the one-dimensional version of HAMFit is used to mimic the experiment. During the experiment, any weight loss recorded by the weighing system is interpreted as moisture loss (drying) of the OSB to the outdoor environment. The basis for this assumption are the following: 1) the wood-frame weight remains the same since its moisture exchange with the surrounding is restricted by the paint, 2) moisture accumulation in the insulation is insignificant due to its non-hygroscopic nature 3) condensation on the exterior surface of the polyethylene sheet is insignificant since the indoor and outdoor temperature conditions are nearly the same.

The OSB used in this experiment has a density of 650 kg/m^3, thermal conductivity of 9.41E-02 W/mK and specific heat capacity of 1880 J/kgK. Its moisture storage and transport properties that include the sorption isotherm, vapor permeability and liquid diffusivity are given in Figure 5-33 to Figure 5-35. The density, thermal conductivity, heat capacity and vapor permeability of the glass fiber insulation are 11 kg/m^3, 3.66E-02

W/mK, 1256 J/kgK and 1.30E-10 kg/s.Pa.m, respectively. Since the insulation is non-hygroscopic its moisture storage capacity is very low, and therefore neglected in the modeling. Moreover due to its capillary non-active nature, the liquid water transport property is set to zero. The vapor permeability of polyethylene sheet is 2.29E-15 kg/s.Pa.m. As far as hygrothermal modeling is concerned vapor permeability is the most important hygrothermal property of polyethylene sheet, but all the rest including moisture storage, thermal storage, liquid permeability and thermal resistance values can be set to zero. Since the polyethylene sheet is directly exposed to the indoor boundary conditions, it is possible to model it as a surface vapor resistance rather than as a layer. In fact in the HAMFit modeling the mass transfer coefficient of the interior surface is calculated by superimposing the vapor resistance of polyethylene sheet on the vapor flow resistance created by moist-air boundary layer.

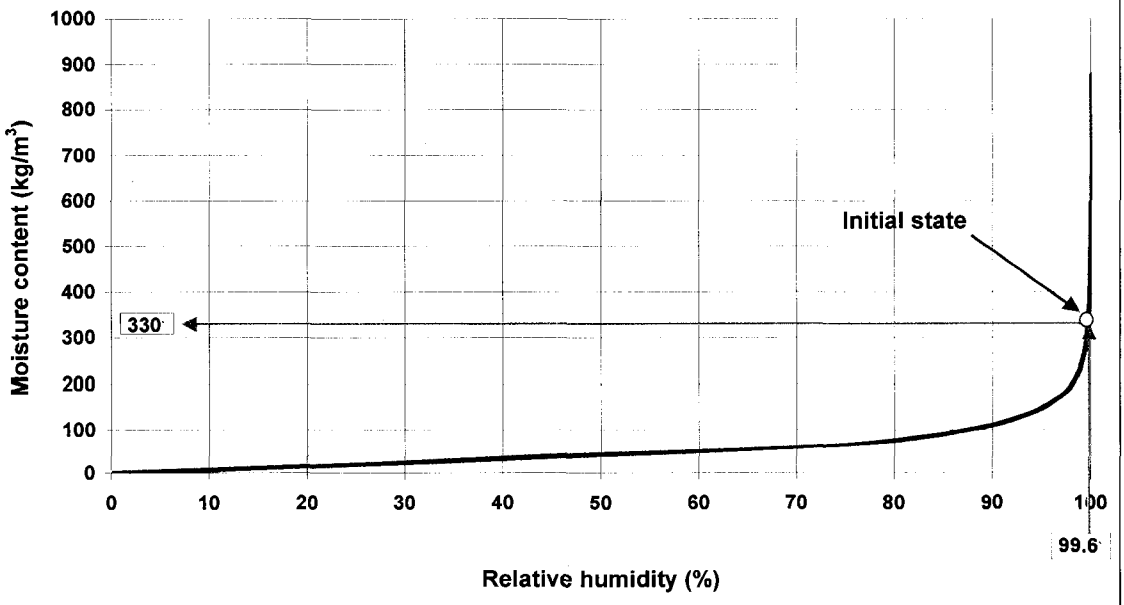

Figure 5-33 Sorption isotherm and moisture retention curve of OSB

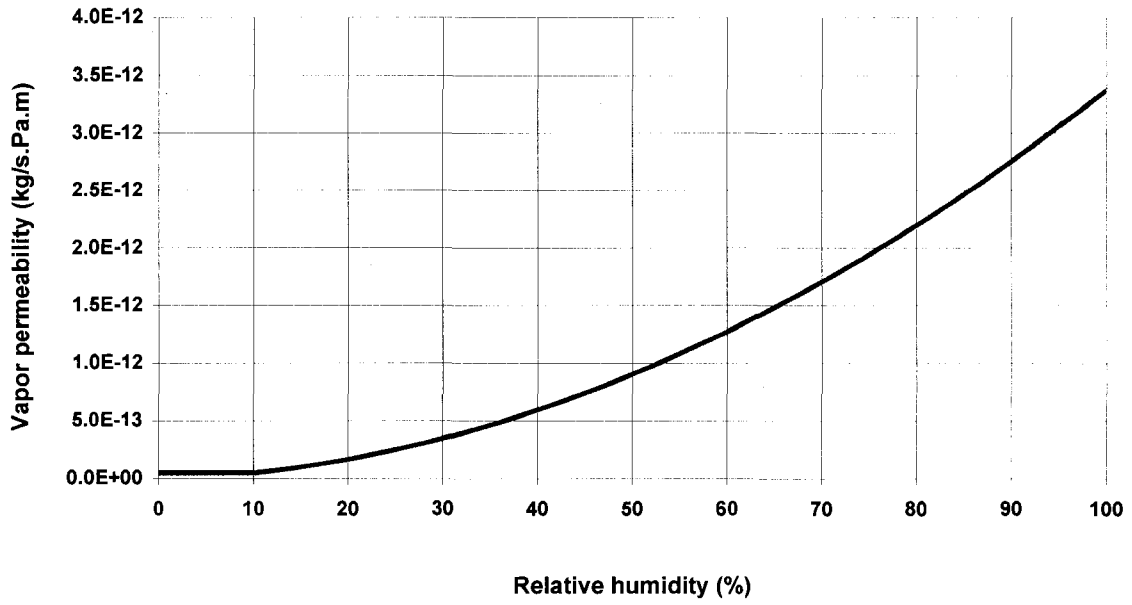

Figure 5-34 Vapor pereability of OSB

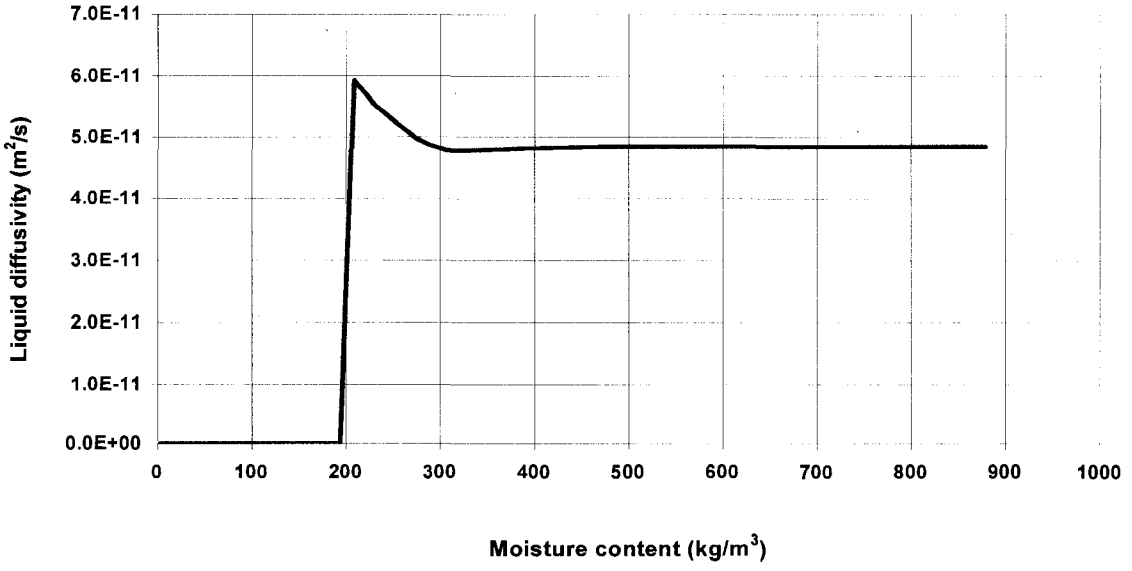

Figure 5-35 Liquid diffusivity of OSB

The initial equilibrium moisture content of the OSB is 330 kg/m^3, and the corresponding relative humidity (from sorption isotherm curve) is 99.6%. In the HAMFit simulation, the initial moisture content is assumed to be uniform across the OSB thickness. This assumption is based on the step taken during preconditioning process, more specifically, wrapping of the wetted OSB with polyethylene sheet to allow moisture redistribution. The initial temperature condition of the wall system is assumed to be 25°C and uniform across the thickness. The boundary conditions to which the wall system is exposed to are controlled and measured. The thirty days time history of temperature and relative humidity of the exterior boundary conditions are shown in Figure 5-36. Figure 5-37 shows the indoor temperature and relative humidity conditions for the same period of time. As can be seen in Figure 5-36, the temperature and relative humidity conditions of the outdoor environment are fairly constant at 25°C and 25%, respectively. In most of the time, the temperature difference across the wall is between 1–2°C. This small temperature difference coupled with the presence of insulation in the cavity makes the drying process nearly an isothermal process. The indoor relative humidity is generally higher and variable than the outdoor relative humidity. However, its effect on the drying process is very limited due to the presence of polyethylene sheet, which essentially create an interior adiabatic boundary condition for moisture transfer. In the HAMFit simulation, heat transfer coefficient of 8 W/m^{2}K is used for both interior and exterior surfaces of the wall, and mass transfer coefficients of 1.53E-11 and 5.80E-8 s/m are used for the corresponding surfaces.

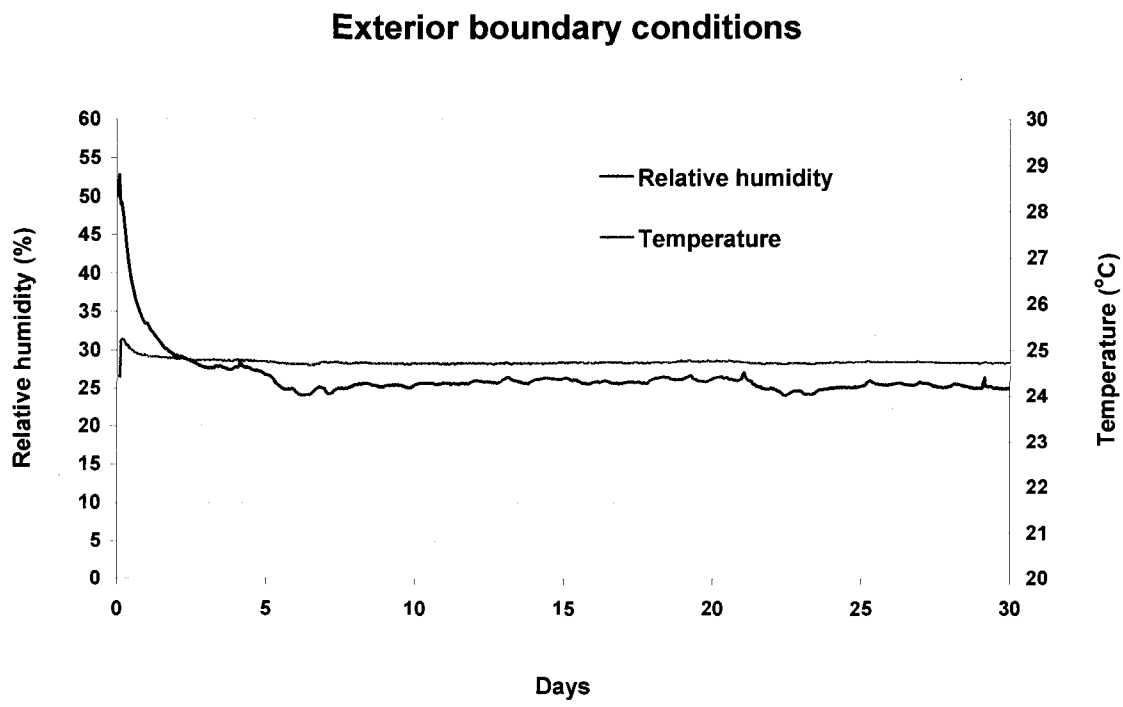

Figure 5-36 Exterior relative humidity and temperature conditions

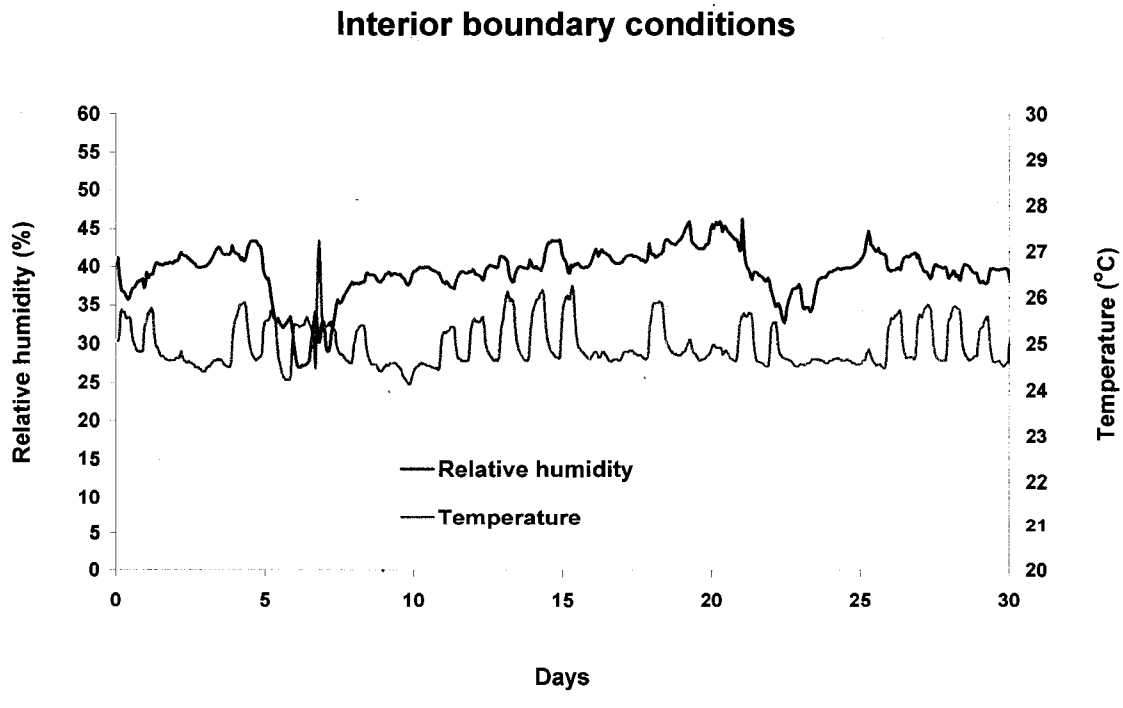

Figure 5-37 Interior relative humidity and temperature conditions

In Figure 5-38 the simulation result of HAMFit is superimposed on the laboratory determined drying curve of OSB. The drying curve shows the transient moisture content of the OSB at different times of the drying period. As can be seen in the figure, HAMFit prediction is in excellent agreement with the experimental result for the entire drying period. During this period, the OSB lost 2.5 kg of moisture per meter square area of OSB. The average moisture content of the OSB by weight reduces from 51% (initial state) to 16% (end of experiment). One of the main advantages of numerical modeling is that once the model gives satisfactory result, as the case presented here, more detailed information about the problem in space and time can be extracted easily. Here, the moisture distributions across the thickness of the OSB at various times of the drying period are extracted from the HAMFit simulation and presented in Figure 5-39. As shown in this figure, the moisture gradient near the exterior surface is higher (steeper relative humidity profile) in all moisture profile curves than any other region of the OSB thickness. Moreover, the gradient decreases as the drying period progress, which consequently results in a lower drying rate (as can be seen in Figure 5-39). At the 30^{th} day of the drying period at least 60% of the OSB thickness has a relative humidity below 90%. At the same time the wettest part of the OSB (near the polyethylene sheet) has a moisture content of 229 kg/m^3, which is reduced from the initial moisture content of 330 kg/m^3.

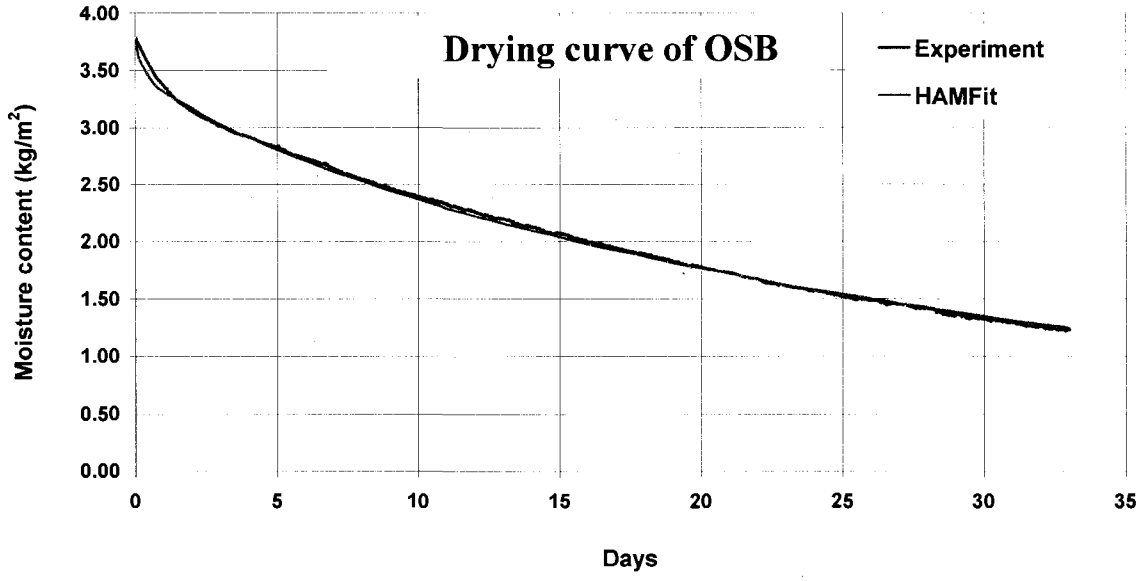

Figure 5-38 Comparison of the experimentally measured and simulated (using HAMFit) drying curves of OSB

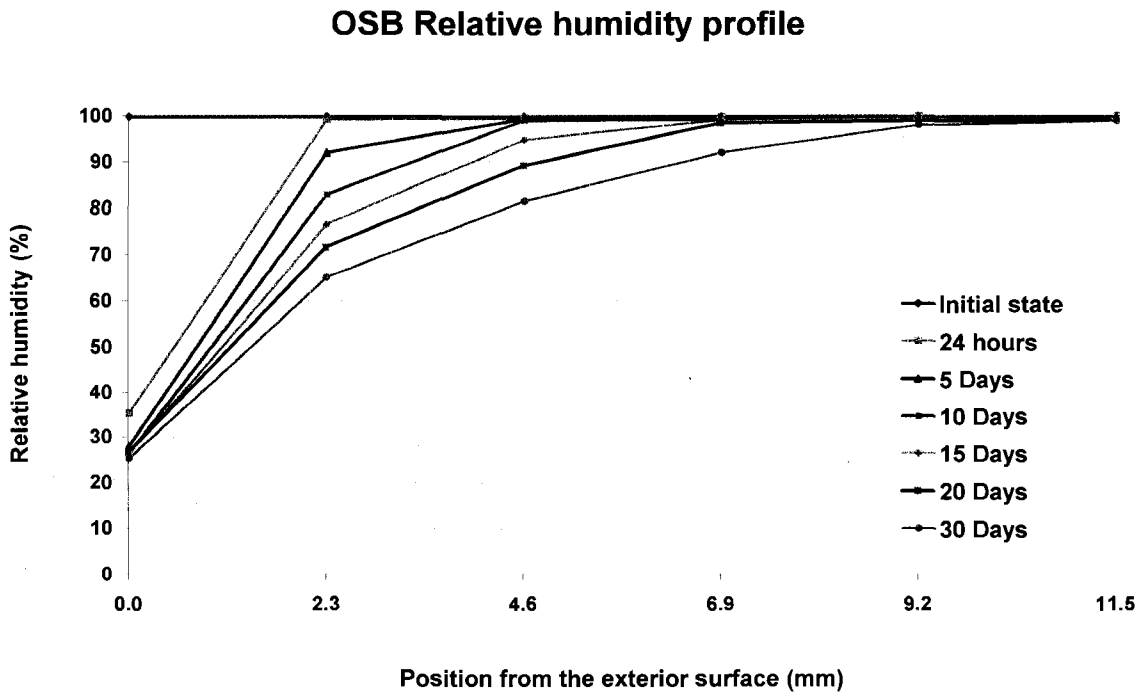

Figure 5-39 Moisture distribution across the thickness of OSB at various times

In this section, the transient HAM model, HAMFit, is successfully benchmarked against six internationally published test cases that comprise analytical verification, comparisons with other models and validation with experimental results. The good agreements obtained with the respective test cases suggest that the model development and implementation are satisfactory, and therefore, can be coupled with the indoor model to create the whole building hygrothermal model, HAMFitPlus. The benchmarking of HAMFitPlus, utilizing this transient model as one of its building block, is presented in the next chapter.

6 BENCHMARKING OF WHOLE BUILDING HYGROTHERMAL MODEL (HAMFitPlus)

The newly developed hygrothermal model, HAMFitPlus, couples the building envelope and indoor air models. The integrated model predicts the hygrothermal condition of the building enclosure as well as indoor air for a given outdoor climatic conditions and indoor heat and moisture sources. The model solves the coupled PDEs that govern the heat and moisture transfer in building envelope components (Equation [4.20] and [4.15]), as well as the indoor humidity and energy balance equations (ODEs Equation [4.32] and [4.51]) of the indoor air simultaneously. In this chapter, the whole building hygrothermal model is benchmarked against internationally published test cases. The benchmark exercises are carried out using the HAMFitPlus simulation environment and graphical user interfaces that are discussed in Section 4.3.1. Due to the strong coupling of the heat and moisture transfer processes that occur within in building envelope components and indoor air as well as dynamic interaction among the two; the HAMFitPlus model is benchmarked in two steps. In the first step, the heat and moisture transfer processes are decoupled. This is achieved by considering test cases with no moisture transfer (sealed building enclosure surfaces) or no heat transfer across the envelope (isothermal case). In the second step, the coupled heat and moisture transfer across the envelope due to varying boundary conditions are considered. A total of seven benchmark exercises are presented here. The benchmark exercises consist of two analytical verifications, three comparison with other models and two validations with experimental results. Judkoff and Neymark (1995) recommended these three classes of

tests to evaluate the robustness of a model by comparing the model (HAMFitPlus) simulation results with the corresponding test case solutions.

6.1 Benchmark step 1: Decoupled whole building energy and moisture analysis

6.1.1 Comparative test 1 – Whole building energy analysis

For the purpose of evaluating whole building energy analysis models such as HAMFitPlus, IEA Solar Heating and cooling Task 12, Subtask B (Model evaluation and improvement) and IEA Energy Conservation in Buildings and Community Systems Annex 21, Subtask C (Reference cases and evaluation procedures) developed a joint research project called BESTEST (Building Energy Simulation Test) (Judkoff and Neymark, 1995). The test cases developed under the BESTEST project forms the basis for the later developed ASHRAE Standard 140P, *Standard Method of Test of the Evaluation for Building Energy Analysis Computer Programs* (ANSI/ASHRAE 2001). In this section two of the BESTEST cases are considered for evaluation of HAMFitPlus. The first case is referred to as the BESTEST case 600FF (FF stands for free float). In this simulation case there is no heating or cooling equipment, and therefore, there the indoor temperature fluctuates freely in response to the outdoor climate conditions. In the second case (BESTEST case 600) the indoor temperature is controlled in a limited range of 20 – 27°C using mechanical systems that provides heating and cooling. The typical simulation variables that are used for evaluating numerical models are indoor temperature, annual

heating and cooling loads as well as their daily profiles. In both test cases the effect of moisture on energy is ignored. Consequently, there is no coupling of heat and moisture transport equations and therefore, only the energy PDE and ODE need to be solved.

Building description

The schematic diagram of the building, which is considered for the whole building energy analysis, is shown in Figure 6-1. The building is a lightweight construction (wood and insulation) with a dimension of 8 m width, 6 m length and 2.7 m high. On the south wall, it has two identical windows, which have dimensions of 3 m width and 2 m height. The exterior walls consists of 12 mm thick plasterboard on the interior, followed by 66 mm thick fiberglass insulation, and finally wood siding of 9 mm thick on the exterior. The roof has the same series of layers as the exterior walls but with different thickness: 10, 111.8 and 19 mm for the plasterboard, fiberglass insulation and wood siding, respectively. The emissivity and absorptivity of the external opaque surfaces (wood siding) are 0.9 and 0.6, respectively. The floor is composed of 25 mm timber flooring and 1003 mm of insulation. The physical and thermal properties of all these materials are presented in Table 6-1 below. The south facing windows have an overall thermal conductance of (U-value) 3.00 W/Km^2, shading coefficient of 0.916 and solar heat gain coefficient of 0.787.

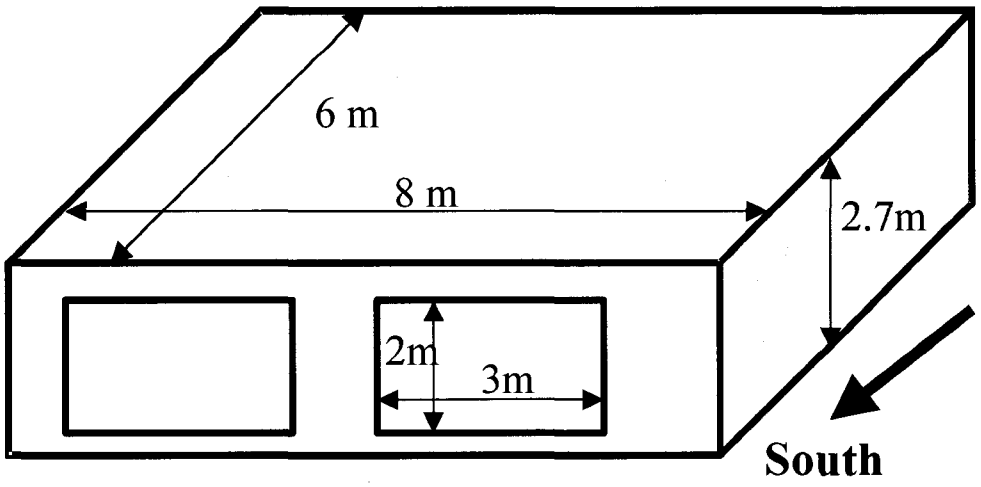

Figure 6-1 Schematic diagram of a building that is considered for whole building energy analysis

Table 6-1 Physical and thermal properties of materials that make up the building

	K (W/mK)	Thickness (m)	U (W/m^2K)	R (m^2K/W)	Density (kg/m^3)	Cp (J/kgK)	Area (m^2)
Exterior wall (inside to outside)							63.60
Int surf coeff			8.29	0.121			
Plasterboard	0.160	0.012	13.333	0.075	950.0	840.0	
Fiberglass quilt	0.040	0.066	0.606	1.650	12.0	840.0	
Wood siding	0.140	0.009	15.556	0.064	530.0	900.0	
Ext surf coeff			29.300	0.034			
Total air+air			0.514	1.944			
Total surf surf			0.559	1.789			
Floor (inside to outside)							48.00
Int surf coeff			8.29	0.121			
Timber flooring	0.140	0.025	5.600	0.179	650.0	1200.0	
Insulation	0.040	1.003	0.040	25.075			
Total air+air			0.039	25.374			
Total surf surf			0.040	25.254			
Roof (inside to outside)							48.00
Int surf coeff			8.29	0.121			
Plasterboard	0.160	0.010	16.000	0.063	950.0	840.0	
Fiberglqss quilt	0.040	0.1118	0.358	2.794	12.0	840.0	
Wood siding	0.140	0.019	7.368	0.136	530.0	900.0	
Ext surf coeff			29.300	0.034			
Total air+air			0.318	3.147			
Total surf surf			0.334	2.992			

Boundary conditions and building operating conditions

The building is exposed to Denver, Colorado weather conditions. Denver is located at 39.8° north latitude, 104.9° west longitude, and at an altitude of 1609 m. The typical metrological year (TMY) weather data of Colorado is used for the whole building energy simulation. TMY consists of an hourly data of ambient temperature, relative humidity, wind speed and direction, solar radiation, cloud cover, as well as other metrological data for a period of a year. The TMY weather data is available at the National Renewable Energy Laboratory, U.S. Department of Energy. The exterior boundary conditions for the walls and roof are generated from the weather data file, whereas for the floor a constant 10°C ground temperature is assumed.

The building is assumed to operate with a constant ventilation rate of 0.5 ACH (air-exchange per hour), and constant internal sensible heat gain of 200 W. 60% of the total heat gain is assumed to be radiative and the remaining 40% is convective. The full description of the BESTEST cases can be obtained in Judkoff and Neymark (1995).

Simulation results

The simulation results of HAMFitPlus for the two test cases (600FF and 600) are presented along with the statistical summary results of seven reference programs, which were selected in the BESTEST project. The programs were, namely: BLAST, DOE2, ESP, SERIRES, S3PAS, TASE and TRANSYS. The simulation parameters that are used for comparison of HAMFitPlus with the reference programs were the maximum, minimum and annual mean free-floating temperatures for the BESTEST case 600 FF, and the annual heating and cooling and peak heating and cooling loads for the BESTEST case

600. But first, the solar radiation calculation performed by HAMFitPlus is compared with that of the reference programs' since it is an important parameter that can influence the simulation results of the two test cases (600FF and 600).

Solar radiation

The annual total incident global solar radiation on the four wall surfaces and roof are shown in Table 6-2. For comparison purpose, the minimum, maximum and mean values of the reference programs, as presented in the BESTEST project, are listed in the table along with HAMFitPlus calculated values. For all five surfaces, the HAMFitPlus predictions are within the range (minimum and maximum values) of the reference programs predictions. The HAMFitPlus results deviates from the mean values by 8.4, 4.7, 4.1, 0.7 and 0.2% for the north, east, west, south and horizontal surfaces, respectively.

Table 6-2 Total incident global solar radiation on the four walls and roof

	Total Incident Global Solar radiation (kWh/m^2)				
	NORTH	EAST	WEST	SOUTH	HORIZONTAL
BESTEST Minimum	367	959	857	1456	1797
BESTEST Maximum	457	1217	1090	1566	1832
BESTEST Mean	429	1080	1018	1490	1827
HAMFitPlus	465	1131	976	1480	1831

The solar radiation profiles on the south wall for January 4th (cold day) and July 27th (hot day) are shown in Figure 6-2 below. Observation of the two solar radiation profiles suggests that the peak solar radiation is higher on January 4th (0.929 kW/m^2) compared to the hot summer day of July 27th (0.462 kW/m^2). Thus, in the northern hemisphere, having a window oriented to south has an advantage of collecting more solar radiation during winter season, subsequently reducing heating load.

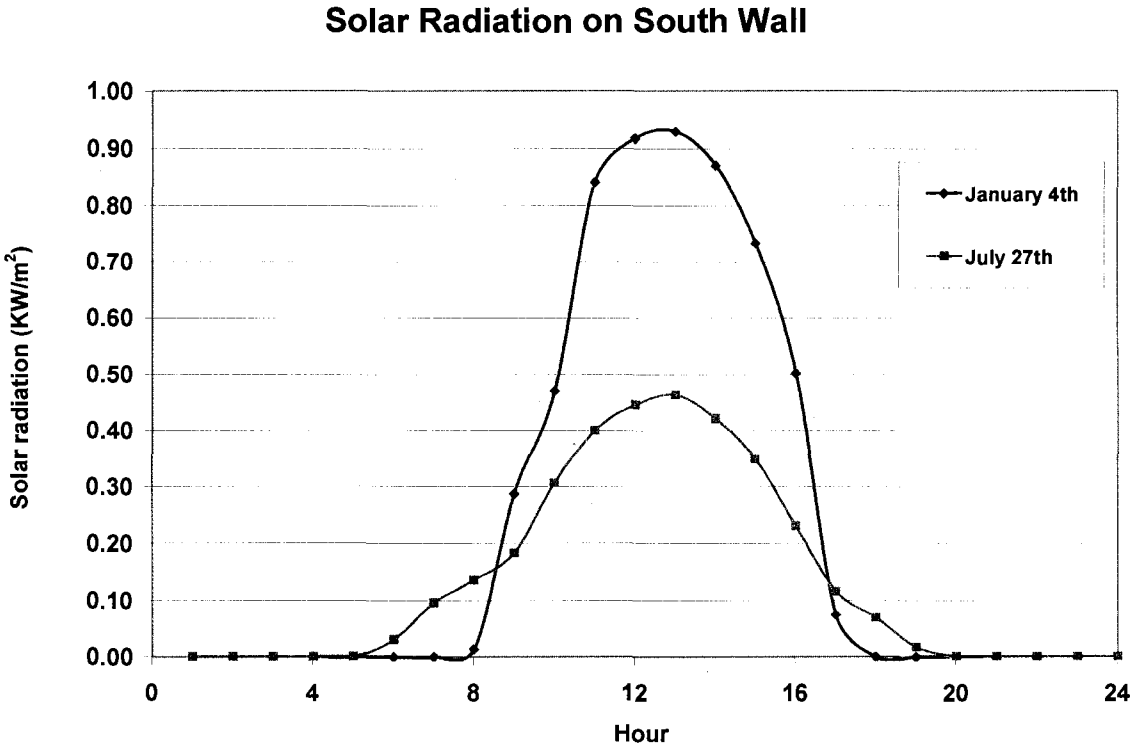

Figure 6-2 Solar raiation on south wall on January 4th and July 27th

BESTEST Case 600FF Results

In this test case there are no mechanical systems for heating or cooling, consequently, the indoor temperature fluctuates freely in response to the outdoor ambient temperature and solar radiation changes. The HAMFitPlus prediction of indoor temperature profiles for January 4th and July 27th are shown in Figure 6-3 and Figure 6-4, respectively. On both days, the indoor temperature reaches its highest value at 16:00 h, and to its lowest value at 7:00 h. The maximum, minimum and the annual average indoor temperatures, predicted by HAMFitPlus were 65.5, -16.7 and 25.8°C, respectively. The maximum and minimum temperatures were on the 17th of October at 16:00 h and 4th of January at 7:00 h, respectively.

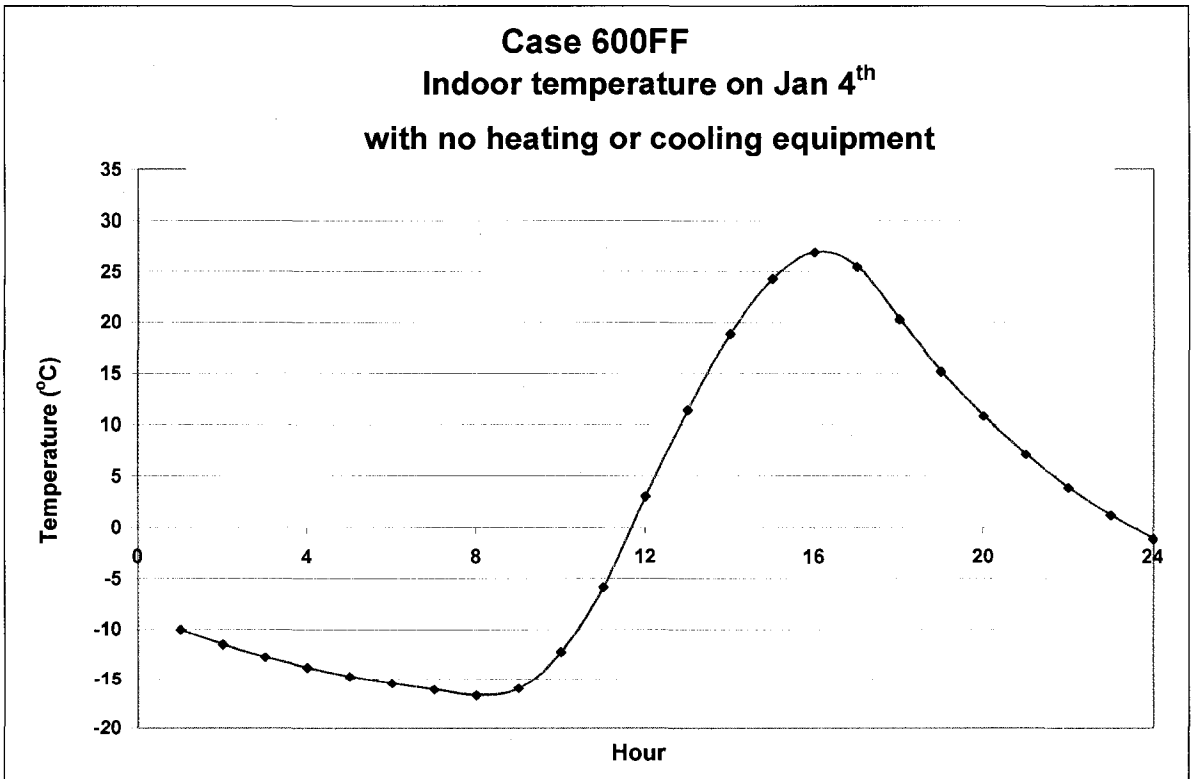

Figure 6-3 HAMFitPlus prediction of indoor temperature profile for January 4th

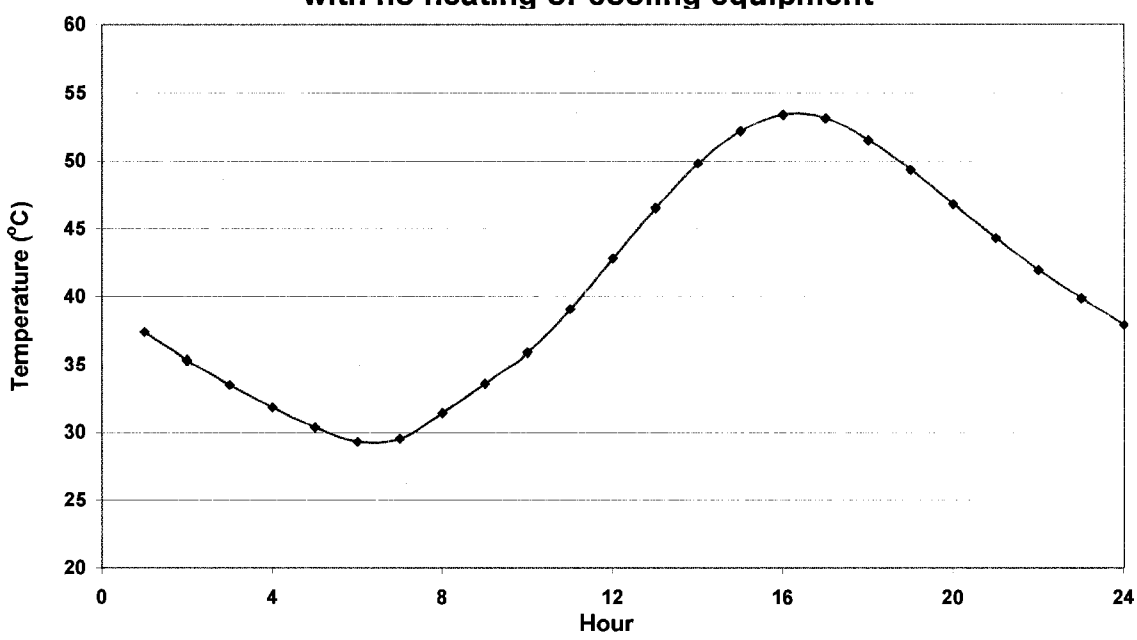

Figure 6-4 HAMFitPlus prediction of indoor temperature profile for July 27^{h}

Table 6-3 summarizes the BESTEST programs (minimum, maximum and mean values) and HAMFitPlus prediction of the annual minimum, maximum and mean indoor temperature. As shown in Table 6-3, all HAMFitPlus predicted values were with the range of the reported reference programs' values. The deviations of HAMFitPlus from the mean values of the reference programs were 0, 1.8 and 2.7% for the annual minimum, maximum and mean values, respectively.

Table 6-3 Annual mean indoor temperature for Case 600FF.

	Indoor temperature (°C)		
	Annual Minimum	Annual Maximum	Annual Mean
BESTEST Minimum	-18.8	64.9	24.2
BESTEST Maximum	10.0	69.8	25.9
BESTEST Mean	-16.7	66.7	25.1
HAMFitPlus	-16.7	65.5	25.8

BESTEST Case 600 Results

In the second whole building energy simulation exercise, the indoor temperature is controlled to be in a range between 20 and 27°C. To maintain the indoor temperature in the desired narrow band (20 to 27°C), there is a need for mechanical systems that provide heating and cooling as required. As noted in the simulation results of the previous exercise (BESTEST case 600FF), the indoor temperature has the possibility of fluctuating between –16.7 and 65.5°C. The mechanical system that is provided for this simulation exercise has the following features: it is thermostat controlled, 100% convective air system with an infinite sensible heating and cooling, but zero latent heat capacities; it provides heating if the air temperature is less than 20°C, and cooling if the air temperature is above 27°C; the operation of the thermostat is solely governed by the indoor air temperature.

The indoor temperature profiles for January 4th and July 27th as predicted by HAMFitPlus are shown in Figure 6-5. Moreover the energy demands for heating (positive value) and cooling (negative value) for the corresponding days are shown in Figure 6-6. In January 4th there is a rather cooling demand from 12:00 to 16:00 h, which is due to the higher solar gain through the south window (Figure 6-2). The annual heating and cooling loads as predicated by HAMFitPlus were 5057 and 7229 kWh; and also the hourly integrated peak heating and cooling demands were 4.348 and 6.455 kW, respectively. The highest heating and cooling demands occurred on January 4th at 2:00 h and October 17th at 13:00 h, respectively.

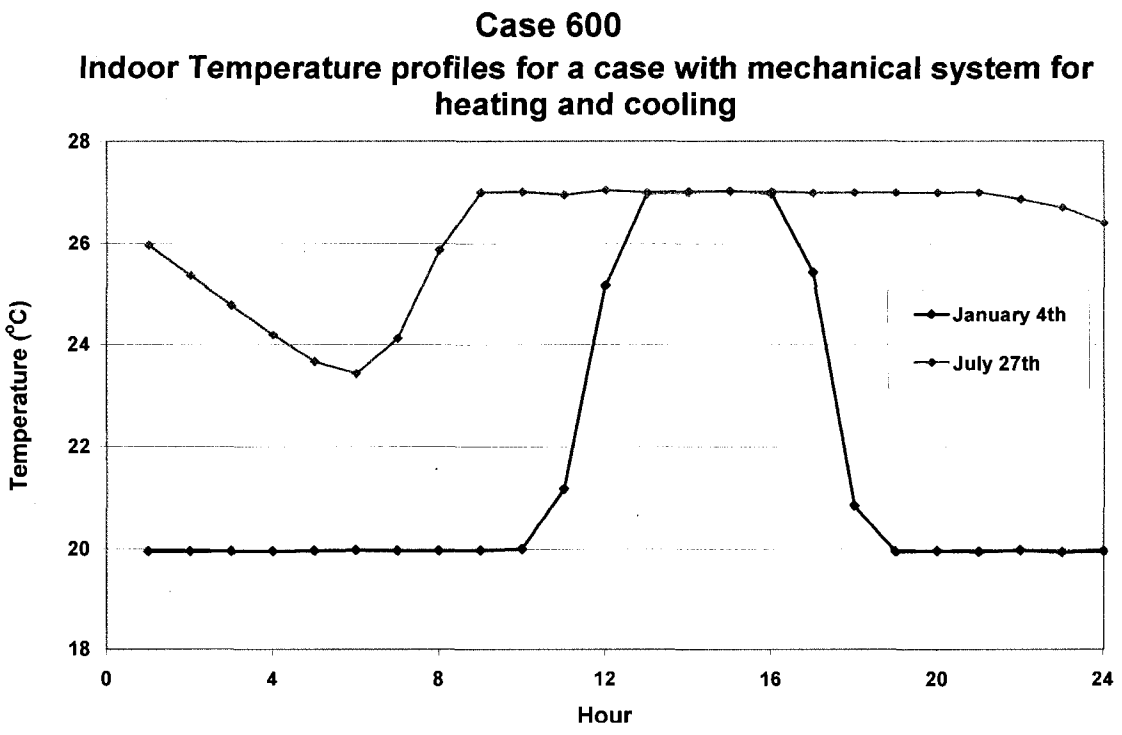

Figure 6-5 HAMFitPlus predictions of indoor temperature profiles for January 4th and July 27 (Case 600)

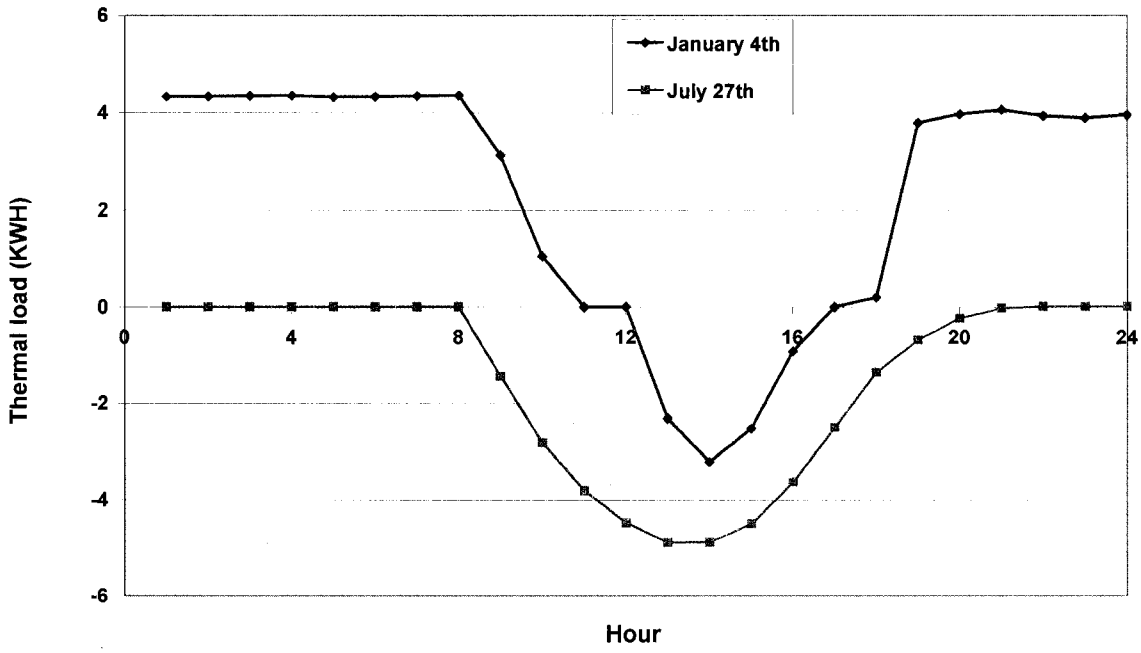

Figure 6-6 HAMFitPlus predictions of heating and cooling loads for January 4th and July 27th (Case 600)

Table 6-4 summarizes the BESTEST programs (minimum, maximum and mean values) and HAMFitPlus prediction of the annual heating and cooling loads as well as the hourly integrated peak heating and cooling loads. As shown in the table, all HAMFitPlus predicted values were within the range of the BESTEST reference programs values. The deviations of HAMFitPlus from the mean values of the reference programs were 0.65, 5.81, 7.67 and 2.15% for the annual heating, cooling, peak heating and cooling loads, respectively.

Table 6-4 Annual heating and cooling and hourly integrated peak heating and cooling loads.

(HAMFitPlus compared to those obtained from the BESTTEST programs for Case 600)

	Annual thermal loads			
	Annual heating load (kWh)	Annual cooling load (kWh)	Hourly integrated Peak heating load (kW)	Hourly integrated Peak cooling load (kW)
BESTEST Minimum	4296	6137	3.437	5.965
BESTEST Maximum	5709	7964	4.354	6.812
BESTEST Mean	5090	6832	4.038	6.597
HAMFitPlus	5057	7229	4.348	6.455

As presented in Table 6-2, Table 6-3 and Table 6-4, all of the HAMFitPlus predicated values were with in the reference programs range, and therefore, it can be concluded that in these model comparative tests (BESTEST case 600 and 600FF) the newly developed model performed very well.

6.1.2 Analytical verification –Moisture buffering

In this section, analytical verification of HAMFitPlus is carried out using test cases for which analytical solutions are available. The test cases considered here are referred to as 'Moisture BESTEST' Case 0A and Case 0B. These test cases are formulated in the Annex 41 project (Ruut and Rode 2004, 2005) and later published by Rode et al (2006). In both cases, moisture exchange between the indoor air and the building envelope components at an isothermal condition is analysed. Hence, only the whole building moisture transfer equations are solved by decoupling the heat transfer PDE and ODE. Consequently, the local heating and cooling that may occur during moisture phase change inside building envelope component are neglected.

In these exercises, the quasi-steady indoor humidity conditions of the simplified building shown in Figure 6-7 are calculated. The whole building components (walls, roof and floor) are constructed from monolithic layer of 150 mm thick aerated concrete. The material properties of the aerated concrete, represented in a simplistic manner, are given in Table 6-5. The building does not have window and all external surfaces are exposed to the outdoor air conditions, including the exterior surface of the floor. Furthermore, the following assumptions are made in both exercises (Case 0A and Case 0B). The initial conditions (temperature and relative humidity) of the building envelope components (walls, roof and floor) as well as the indoor air are at 20°C and 30%, respectively. The outdoor boundary conditions are also constant with a temperature of 20°C and relative humidity 30%. The indoor temperature is held constant at 20°C during the simulation period, which results in isothermal moisture absorption and desorption processes. The building is assumed to operate with a constant ventilation rate of 0.5 ACH (air-exchange

per hour), and 500 g/hr indoor moisture gain during the time between 9:00 to 17:00 h. The schematic diagram of the diurnal moisture production schedule is shown in Figure 6-8. The complete description of the exercises is given in Peuhkuri and Rode (2004).

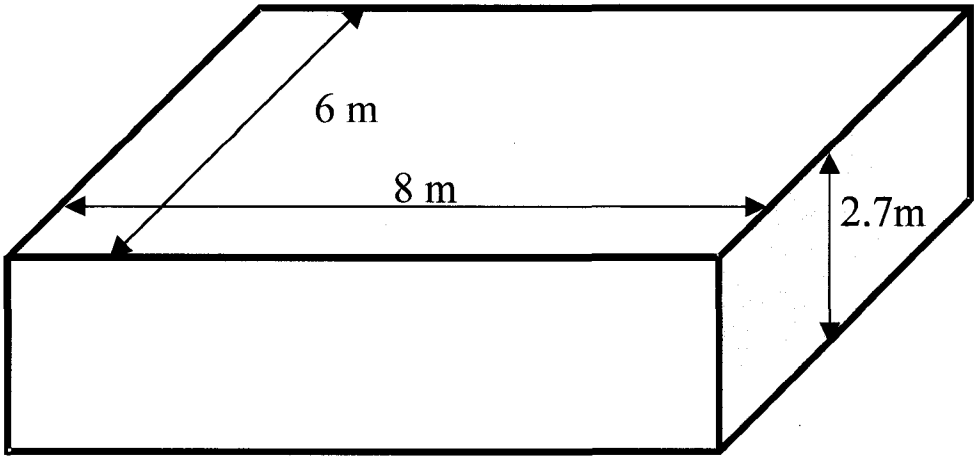

Figure 6-7 Schematic diagram of the simplified building considered in 'MOISTURE BESTEST' Case 0A and 0B

Table 6-5 Simplified material properties of aerated concrete used in 'MOISTURE BESTEST' Case 0A and 0B.

Thickness (m)	Density (kg/m^3)	Conductivity (W/mK)	Heat Capacity (J/kgK)	Water vapour permeability (kg/m.s.Pa)	Sorption curve (kg/m^3)
0.15	650	0.18	840	3E-11	$w = 42.965\phi$

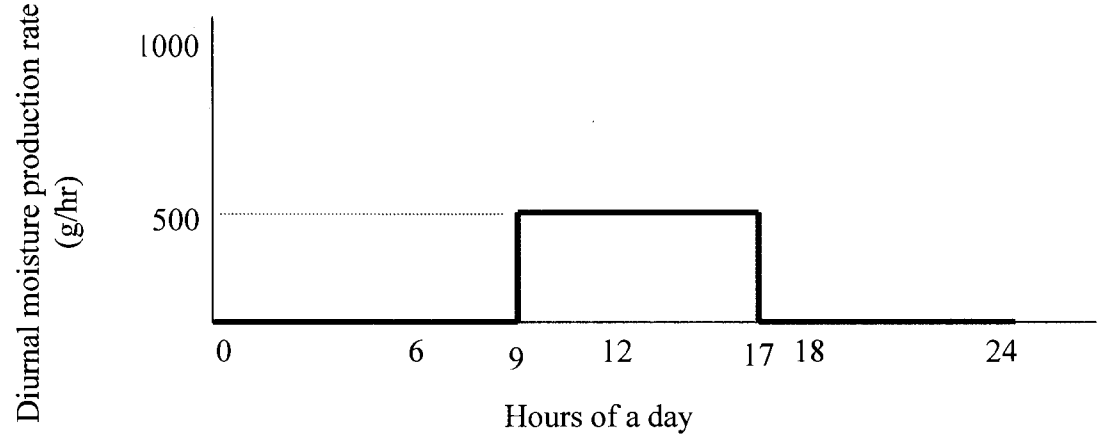

Figure 6-8 Diurnal moisture production schedule.

Simulation results

For comparison purpose, the simulation results of HAMFitPlus are superimposed on the corresponding analytical solutions developed by Bednar and Hagentoft (2005). The simulation results of the other participants are also included in the presentation of HAMFitPlus results to highlight the variability of the simulation results. Derivation of analytical solutions for indoor relative humidity were possible due to the various simplifying assumptions made on the building geometry, boundary conditions, hygrothermal material properties, and also building operation.

MOISTURE BESTEST Case 0A

In this case, the external and internal surfaces of all building envelope components; walls, roof and floor, are covered with vapour tight membrane, which results in vapour exchange neither to the indoor nor to the outdoor air (Figure 6-9).

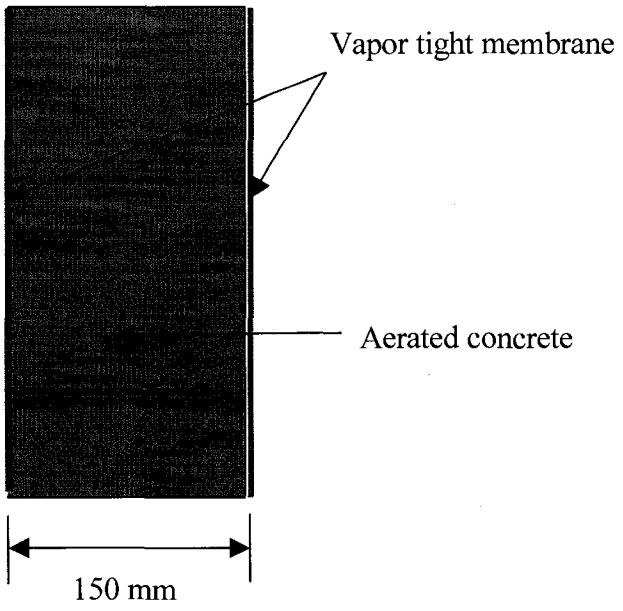

Figure 6-9 Typical building envelope components for Case 0A
(Both interior and exterior surfaces are vapor tight.)

The hourly average relative humidity of the indoor air is used to compare HAMFitPlus's simulation result with the analytical solution developed by Bednar and Hagentoft, (2006). In Figure 6-10 the simulation result of HAMFitPlus and the analytical solution are shown in red and blue curves, respectively. Moreover, the simulation results of other fourteen models that are introduced in this common exercise are shown in gray lines. The indoor relative humidity steadily increases from 30% to 73% during the moisture generation period (9:00-17:00 h), and then decreases and completes the cycle (reduce to 30%), due to the presence of ventilation (0.5 ACH) and absence of moisture generation. This quasi-steady state indoor relative humidity profile is attained after 24 hours of simulation. As can be seen in Figure 6-10, HAMFitPlus prediction of indoor humidity is in excellent agreement with the analytical solution.

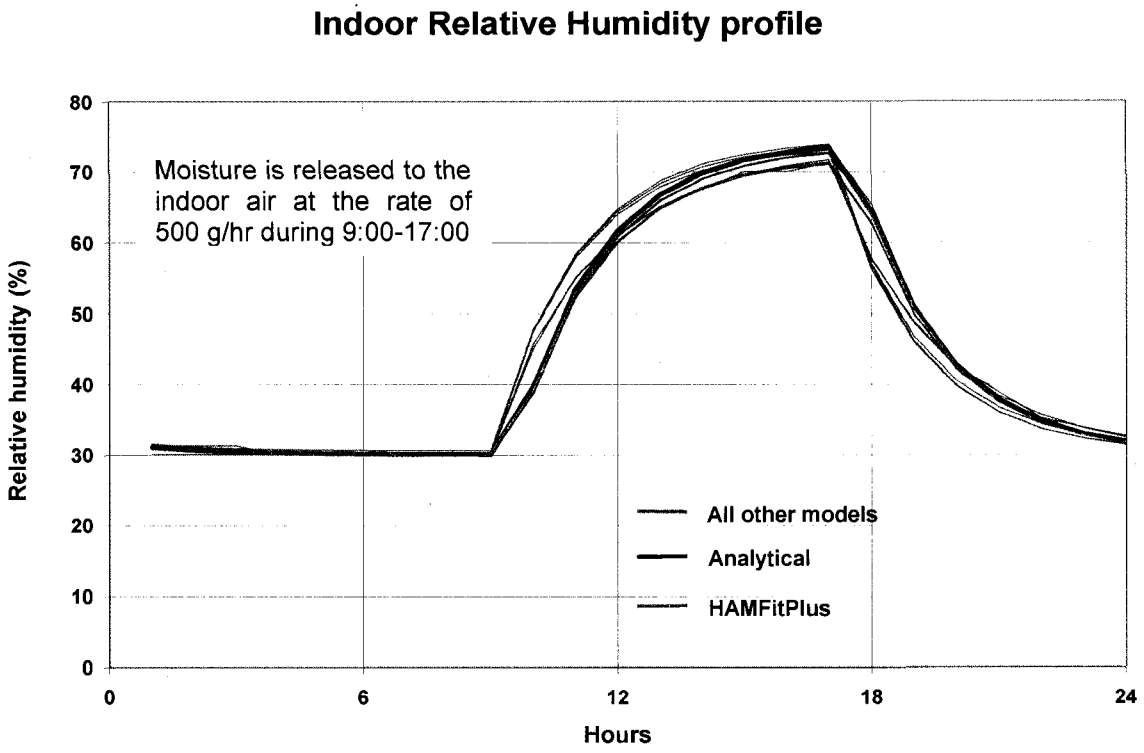

Figure 6-10 The diurnal indoor relative humidity profile for 'MOISTURE BESTEST' Case 0A

(Both interior and exterior surfaces are vapor tight)

MOISTURE BESTEST Case 0B

In this case, the external surfaces of all building envelope components; walls, roof and floor, are covered with vapour tight membrane to avoid vapour loss from inside to outside. However, the interior surfaces of all building envelope components are open, where vapour exchange with the indoor air is possible (Figure 6-11). The mass transfer coefficient for the interior surfaces is 2E-8 m/s.

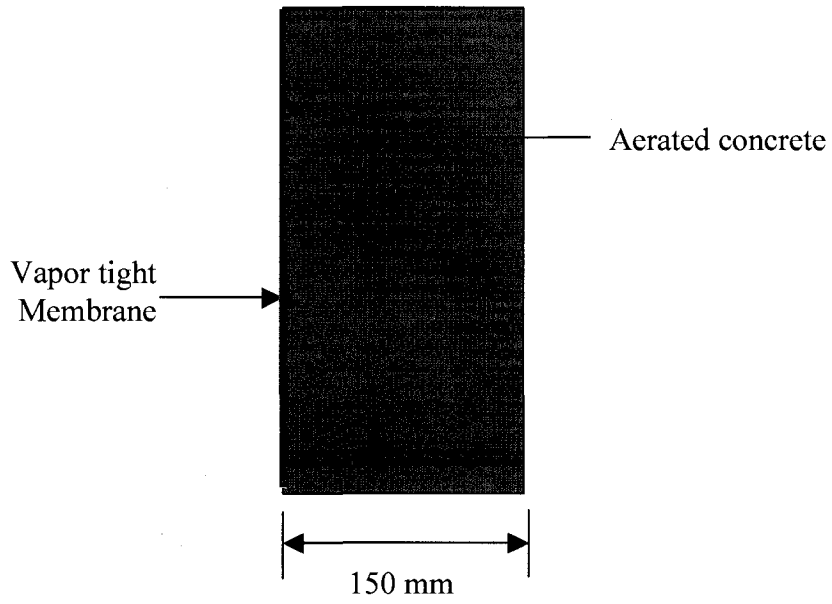

Figure 6-11 Typical building envelope components for Case 0B.
(The interior surface is open and the exterior surface is vapor tight)

Again, the hourly average relative humidity of the indoor air after quasi-steady state condition is reached is used to compare HAMFitPlus with the established analytical solution. The same colour code used in presenting the solutions in Case 0A is adopted here. Hence, the HAMFitPlus, analytical and the other fourteen models results are represented in Figure 6-12, red, blue and grey lines, respectively. The indoor relative humidity has the same profile as Case 0A, but with different magnitudes. The indoor relative humidity steadily increases from 41.5% to 49% during the moisture generation period (9:00-17:00 h), and then decreases and completes the cycle (reduce to 41.5%), which is due to the presence of ventilation (0.5 ACH) and absence of moisture generation. In this test case scenario, quasi-steady condition is obtained after a simulation period of a year and half. Again the HAMFitPlus prediction of indoor humidity is in

excellent agreement with the analytical solution as shown in Figure 6-12, The solutions of the other models, shown in the same figure, deviate from the analytical solution more in Case 0B than in Case 0A, even though both cases were isothermal and involved simplified geometry and material properties. The higher deviation observed in Case 0B implies that whole building hygrothermal modelling with moisture exchange between building envelope components and indoor air can be a challenging task. One of the possible reasons for the variation could be computational domain representation. For example some models divide the building component into two; the innermost as a penetration layer and the rest as bulk layer; whereas the others fully discritize the component. Mesh size, time step, material and boundary conditions' representations could also contribute towards the variations.

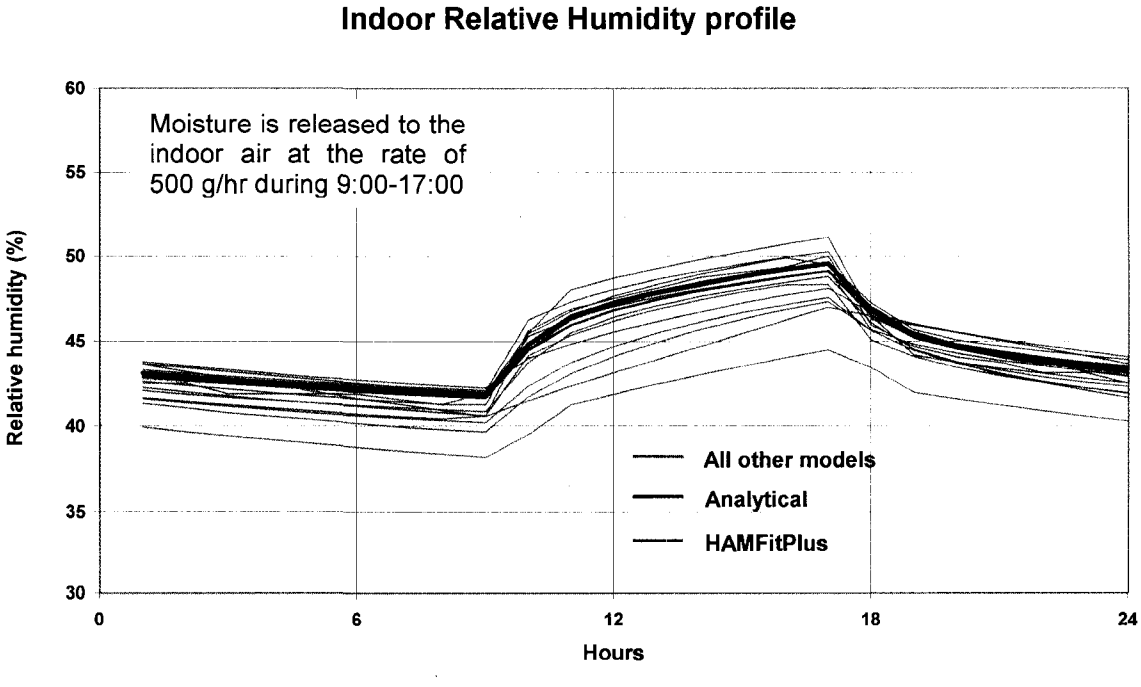

Figure 6-12 The diurnal indoor relative humidity profile for 'MOISTURE BESTEST' Case 0B

In Figure 6-13 below, the relative humidity profile of the building for Case 0A and 0B are superimposed to see the moisture buffering effect of building envelope components. The moisture profiles in red and blue correspond to Case 0A with no moisture buffering and Case 0B with moisture buffering, respectively. As can be seen in the figure, the amplitude of the indoor humidity in Case 0B is 7.5%, which is far less than the 43% exhibited in Case 0A. This is due to the humidity modulation effect of the building envelope components. Moisture buffering materials absorb moisture during high indoor humidity periods, and hence, reduce the peak relative humidity level (from 72 to 49%), and later releases back the absorbed moisture at times when the indoor humidity is low. Due to this moisture transfer dynamics, the building components in Case 0B not only reduce the peak humidity level but also increase the lower indoor humidity level compared to Case 0A (41.5 versus 30). Subsequently, the indoor relative humidity fluctuation amplitude reduces. From this simplified exercise, it can be concluded that building envelope components can have a measurable influence on the indoor humidity level. Hence, it is essential to incorporate their moisture buffering effects in the whole building hygrothermal modeling to realistically predict the indoor humidity condition of a building. Accurate prediction of indoor humidity level may benefit for assessing occupants' comfort, perceived indoor air quality, and also for designing an appropriate equipment size and strategy for ventilation and/or latent heat load removal.

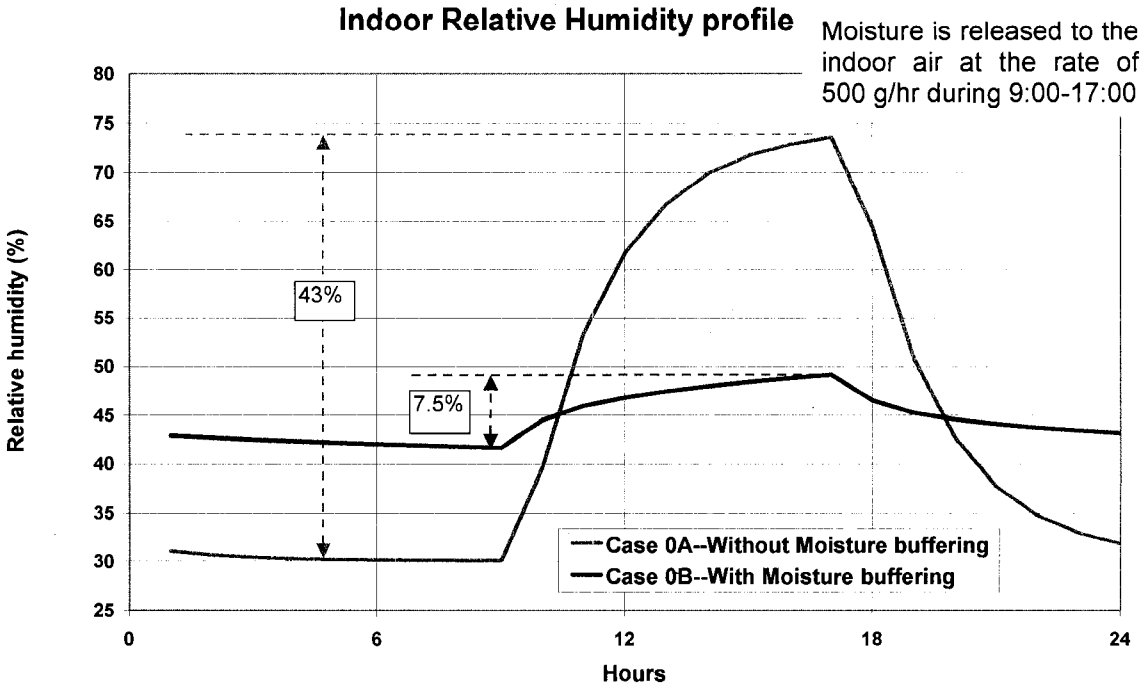

Figure 6-13 Indoor relative humidity profiles with and without moisture buffering effecs of building envelope components.

6.2 Benchmark step 2: Coupled whole building energy and moisture analysis

In the previous sections (Section 6.1.1 and 6.1.2) HAMFitPlus was benchmarked against test cases where the thermal and humidity conditions of a building are decoupled and predicted independently. In this section, the heat and moisture transfer in building envelope components as well as in a zone are considered simultaneously. Hence, the interdependence and effect of one on the other transport process is taken into account.

6.2.1 Comparative test 2 –Whole building hygrothermal analysis

In this sub-section an integrated analysis of energy, indoor humidity, and moisture condition of building envelope components using a whole building hygrothermal model is demonstrated. The accuracy of HAMFitPlus in predicting these quantities is assessed in comparison with other models' simulation results. The test case used here is referred to as Common exercise 1, case 3. This test case is formulated in the `Moisture BESTEST` (Peuhkuri and Rode, 2005) as part of the Annex 41 project and later published by Rode et al. (2006). Common exercise 1, case 1 and 2 are relatively simpler as they include neither solar gain by the exterior surfaces of the building and indoor air through the windows; nor longwave radiation exchange of the building surfaces with the surroundings. Case 3 is deemed to be more complex as it includes these effects, and subsequently used in this thesis for model comparison. In this exercise the building geometry, dimensions, orientation, windows size and location are the same as the test case used in the whole building energy analysis (shown in Figure 6-14). However difference lies on the material used for the building enclosure, geographic location of the building site, moisture buffering potential of building components, boundary conditions for the floor and solar heat gain coefficient of the window. In this test case the building envelope components (walls, roof and floor) are constructed from monolithic layer of 150 mm thick aerated concrete. The hygrothermal properties of this layer are more realistic (taken from Kumaran, 1996) than those used in the moisture buffering test case (Section 6.1.2), where the moisture storage and transport properties are given in simplistic manner. The density, conductivity and heat capacity of the aerated concrete used in this exercise

are 600 kg/m^3, 0.18 W/mK and 840 J/kgK, respectively. The sorption isotherm and vapour permeability curves are shown in Figure 6-15 and Figure 6-16 below.

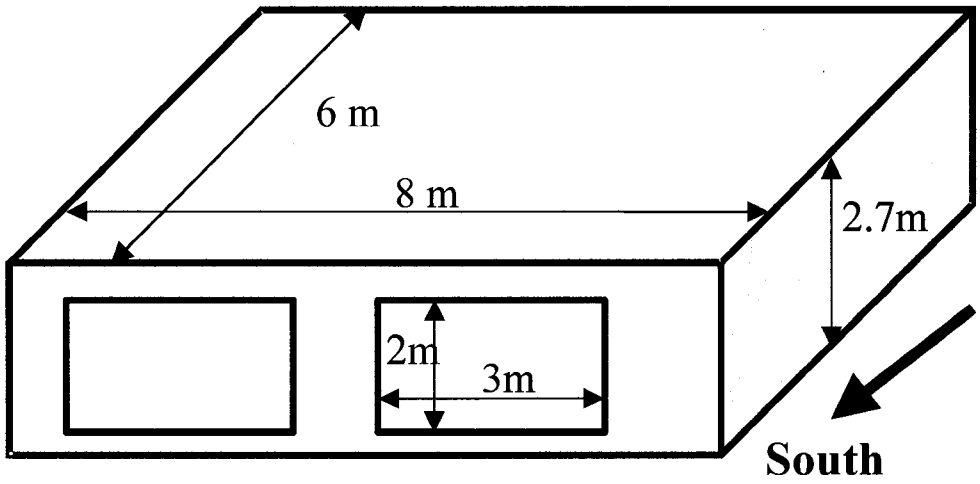

Figure 6-14 Schematic diagram of a building that is considered for whole building heat and moisture analysis

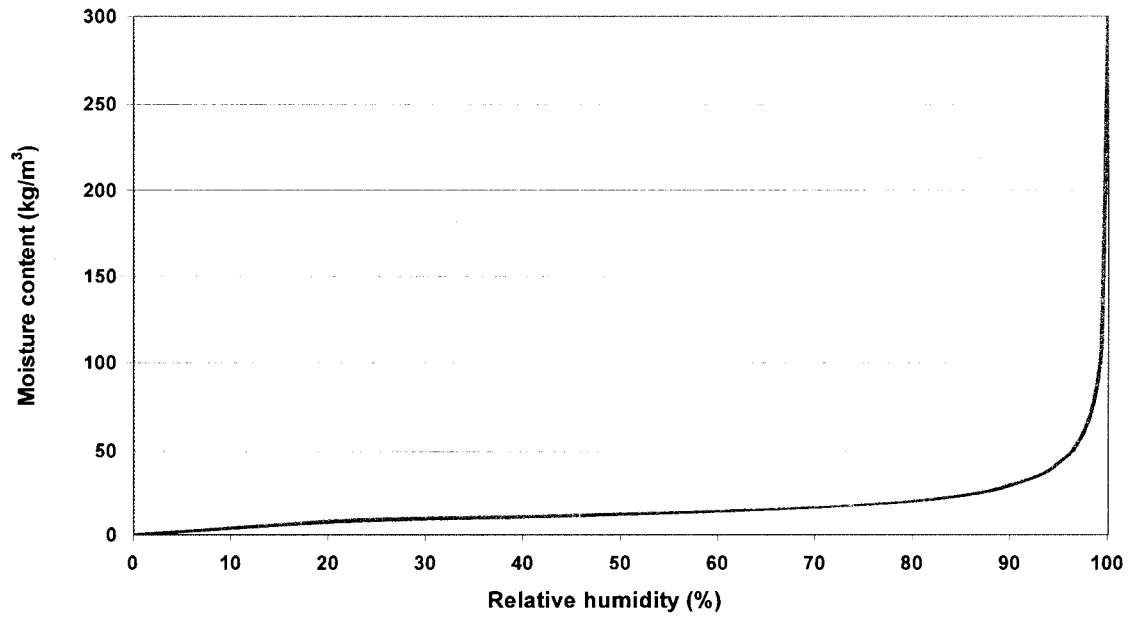

Figure 6-15 Sorption isotherm curve of aerated concrete (Kumaran, 1996).

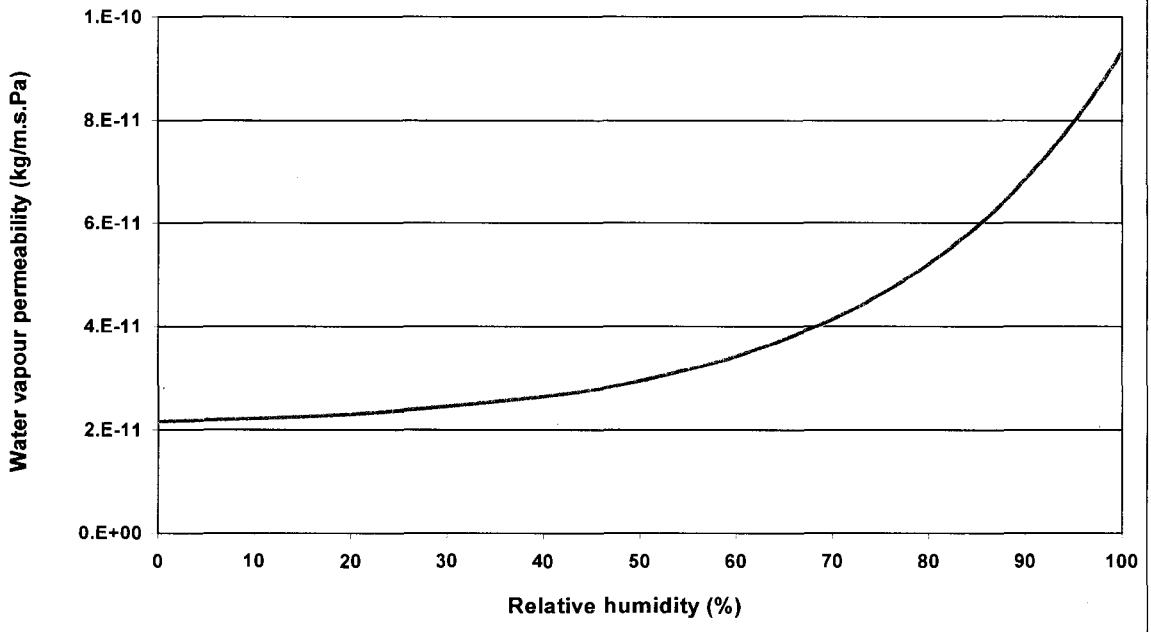

Figure 6-16 Vapor permeability curve of aerated concrete (Kumaran, 1996).

Boundary and initial conditions

The building is exposed to Copenhagen, Denmark weather conditions. Copenhagen is located at 12^{0} 40' longitude and 55^{0} 37' latitude, and has an altitude of 5 m from sea level. The weather data including ambient temperature, relative humidity, wind speed and direction, as well as solar radiation and cloud data are taken from the IWEC weather files (ASHRAE 2001). IWEC stands for International Weather for Energy Calculation, and the data file consists of the typical local weather conditions for a location. The building is assumed to be on an open flat country site with a ground reflectivity (a parameter which is used in solar radiation calculation) of 0.2. The additional modifications considered in this exercise ('MOISTURE BESTEST' Case 3) in

relation to the thermal BESTEST case are the following: 1) the exterior surface of the floor in this test building is exposed to ambient temperature and relative humidity, contrary to ground boundary condition used in BESTEST cases; 2) the windows in this exercise have a solar heat gain coefficient of one; 3) the building envelope components can exchange moisture with both outdoor and indoor air as these surfaces are open for vapour transport. Subsequently, the dynamic moisture buffering effects of these components can influence the indoor humidity condition of the building. The heat and mass transfer coefficients of the interior surfaces are 8.3 $W/m^2 K$ and 2E-8 kg/s.m.Pa, respectively; and the respective transfer coefficients for the exterior surfaces are 29.3 $W/m^2 K$ and 6.25E-8 kg/s.m.Pa, respectively. These heat transfer coefficients represent the combined coefficients of heat transfer by convection and long-wave radiation heat exchange. The initial hygrothermal conditions of all building envelope components and indoor air are assumed to be the same. These are 20°C temperature and 80% relative humidity. These initial conditions imply that the simulation starts with relatively moist construction and indoor conditions.

Building operating conditions

The building is assumed to operate with a constant ventilation rate of 0.5 ACH (air-exchange per hour), and indoor moisture and heat gains per diurnal schedules shown in Figure 6-17 and Figure 6-18, respectively. The heat and moisture gains occur between 9:00 to 17:00 h, everyday at constant rates of 800 W and 500 g/hr, respectively. The heat gain is assumed to be 100% convective sensible heat.

The indoor temperature is maintained between 20 and 27°C using a thermostat controlled mechanical system, which has similar features as the one described in

BESTEST Case 600. It is 100% convective air system with an infinite sensible heating and cooling, but zero latent heat capacities. The system provides heating if the air temperature is less than 20°C, and cooling if the air temperature is above 27°C. The indoor air temperature governs the operation of the thermostat.

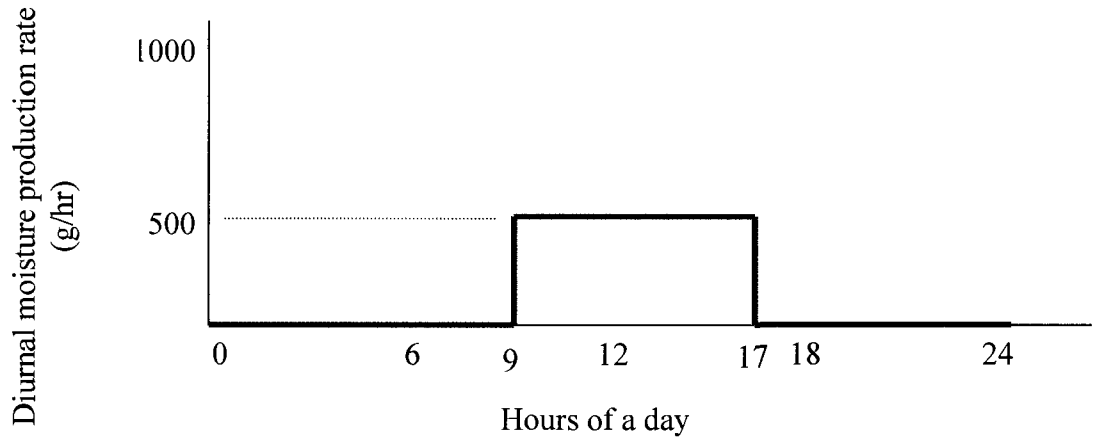

Figure 6-17 Diurnal moisture production schedule.

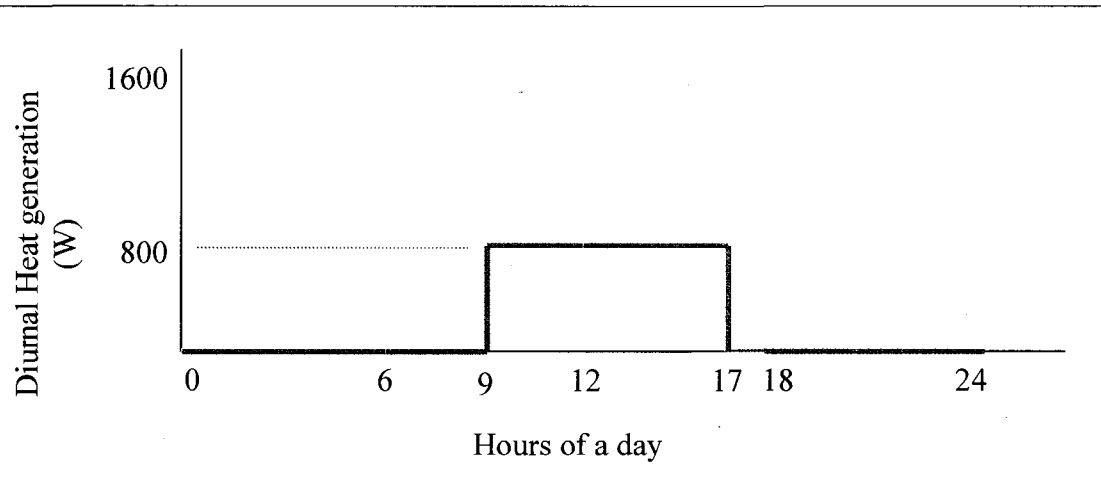

Figure 6-18 Diurnal heat gain schedule.

Simulation results

This exercise deals with the interaction of indoor environment, building envelope and HVAC systems. Hence, the simulation results are based on integrated analysis of these three components. The parameters that are used for inter-model comparison cover the three aspects of whole building performance assessment. These are: 1) indoor environment: prediction of indoor temperature and relative humidity, 2) building envelope hygrothermal condition, viz. temperature and relative humidity conditions of the exterior surface of the roof, 3) energy consumption, viz. estimation of the heating and cooling loads that are required to maintain the indoor temperature in the desired range. HAMFitPlus generates all these outputs simultaneously. Simulation results of the twelve common exercise participants are published in Rode and Peuhkuri (2005) and Rode et al. (2006). These results are used for inter-model comparison and benchmarking of HAMFitPlus. For comparative purpose, the simulation results of HAMFitPlus are superimposed on the corresponding simulation results of the participants' models (Figure 6-19 to Figure 6-25).

Indoor temperature and relative humidity

The indoor temperature and relative humidity profiles of the building for July 5th are shown in Figure 6-19 and Figure 6-20, respectively. The simulation results of HAMFitPlus are shown in red, and that of all other models` in gray curves. Generally, the indoor temperature predictions are more scattered when the indoor temperature is in free-float situation, Figure 6-19. This situation arises when the overall thermal balance of the building with no heating or cooling input from the mechanical system results in an indoor temperature within the set limits (20 – 27°C). Although the deviations of the indoor

relative humidity prediction of six of the twelve models are relatively small (less than 5%), the overall difference during the cooling period can be as high as 23%, Figure 6-20. As shown in Figure 6-19 and Figure 6-20, HAMFitPlus predictions of indoor temperature and relative humidity profiles are within the range of the participant models' solutions. In fact, the model is in close agreement with the batch of models, whose solutions are close to one another. HAMFitPlus simulation result indicates that the indoor relative humidity fluctuation for the day of July 5th is 11%, with minimum and maximum values of 44 and 55%, respectively.

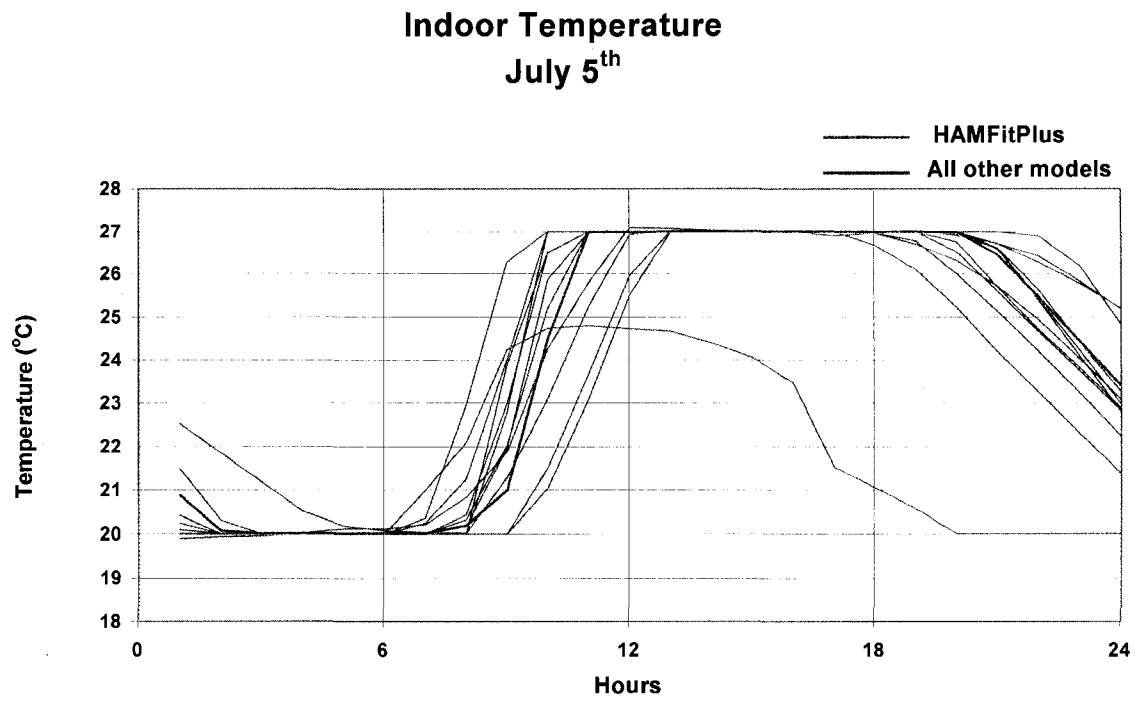

Figure 6-19 Indoor temperature profile on July5th as predicted by HAMFitPlus and other participating models.

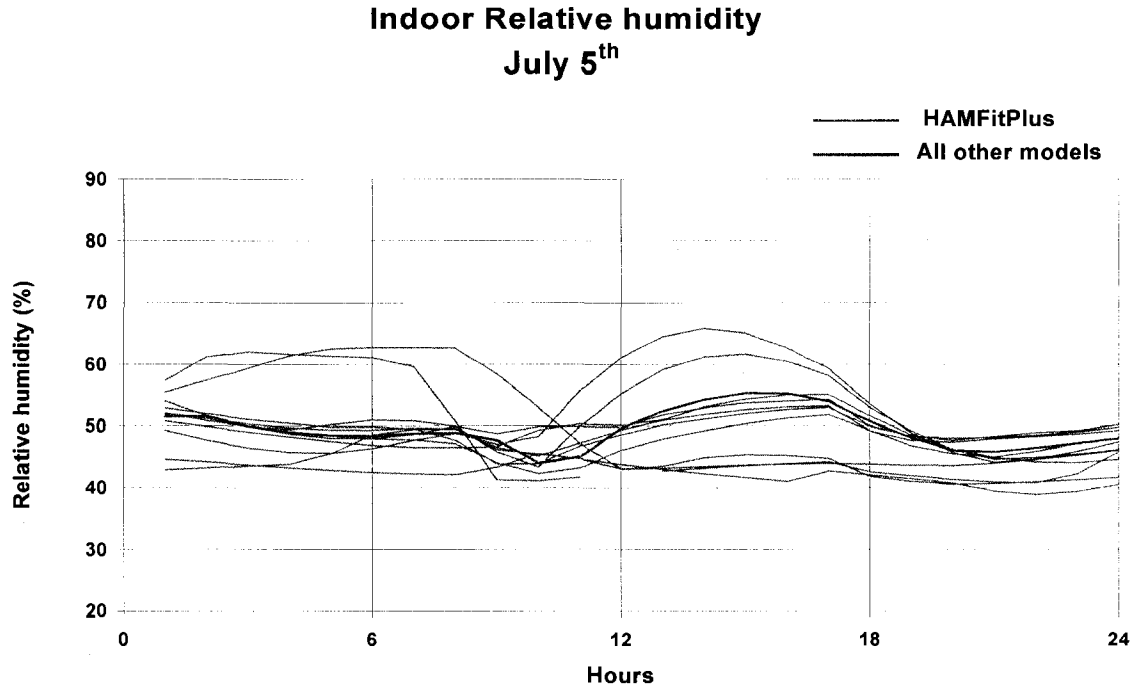

Figure 6-20 Indoor relative humidity profile on July5th as predicted by HAMFitPlus and other participating models

Building envelope hygrothermal condition

The temperature and relative humidity conditions of the exterior surface of the roof for July 5th are shown in Figure 6-21 and Figure 6-22, respectively. The HAMFitPlus results (shown in red curve) are superimposed on the solutions provided by the twelve Annex 41 participants (shown in grey curves). The surface temperature and relative humidity predicated by the participant models, with the exception of one model in each case, have similar profiles. As can be seen in Figure 6-21 and Figure 6-22, HAMFitPlus shows good agreement with the majority of the models in terms of predicted profile as well as magnitudes. The simulation results of HAMFitPlus suggests that the roof surface temperature can get as low as 12°C, during night time, and as high as 39°C at

13:00 h when the solar radiation is maximum. This temperature fluctuation can dictate the direction of moisture flow, and subsequently result in cyclic moisture condensation and evaporation in the roof structure. The highest moisture accumulation (corresponding to 76% relative humidity) is observed at the time when the roof surface temperature is the lowest. This is due to the fact that vapour flows from the inside (high vapour pressure area) to the outside surface (low vapour pressure area). During this transport process, part of the vapour condenses and increases the local moisture content. The amount of condensation increases with a decrease in local temperature. As the roof surface temperature gets warmer, the moisture starts to flow in the reverse direction. This is because, at this time, the exterior surface of the roof has a higher temperature and moisture content, which translates to high vapour pressure. The high vapour pressure drives the accumulated moisture to the interior surface of the roof. Consequently, at the time when the solar radiation is the highest (13:00 h), the exterior surface of the roof experiences drying (corresponding to as low as 15% relative humidity).

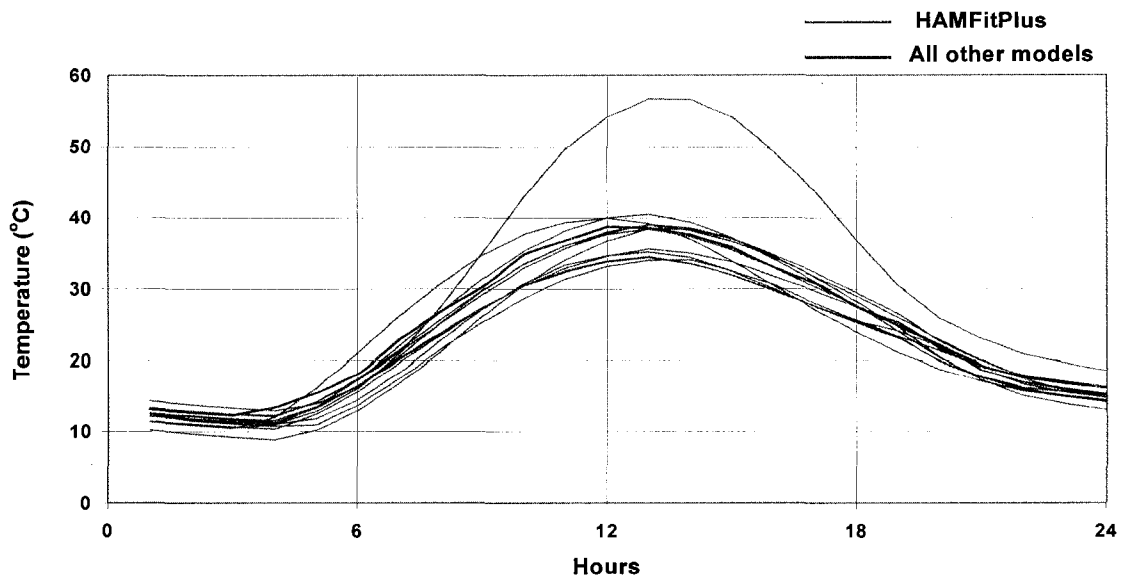

Figure 6-21 Roof surface temperature profile on July5th as predicted by HAMFitPlus and other participating models

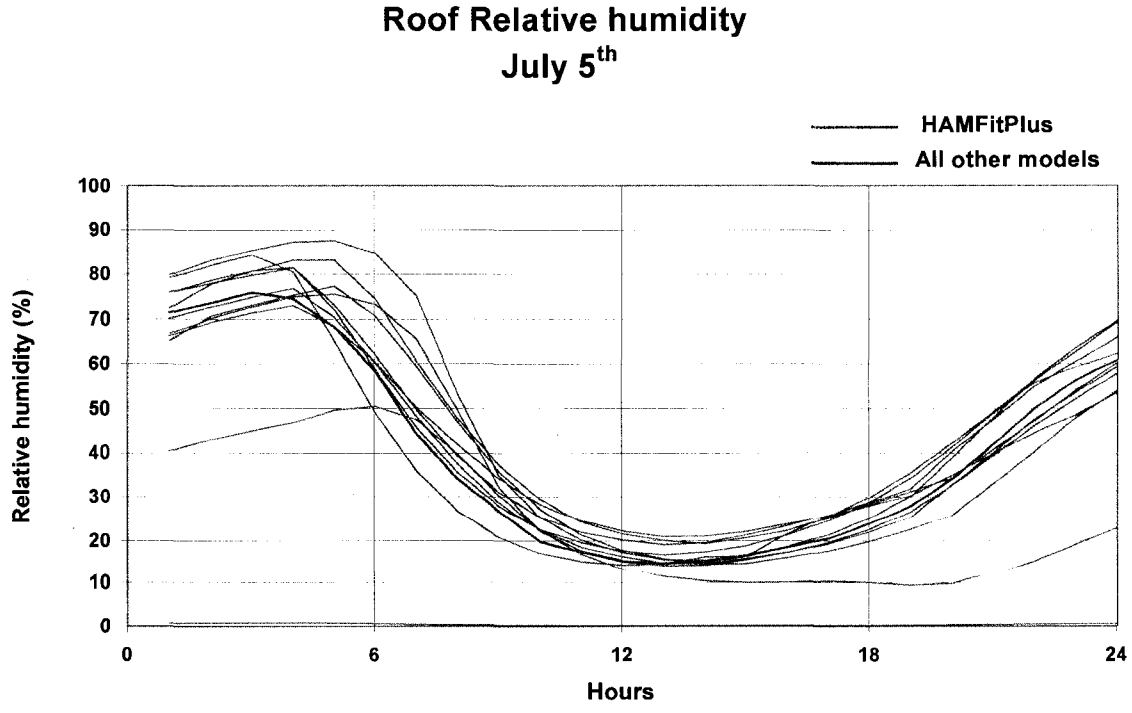

Figure 6-22 Roof surface relative humidity profile on July5th as predicted by HAMFitPlus and other participating models

Energy—Heating and cooling loads

The heating and cooling loads for July 5th are shown in Figure 6-23 and Figure 6-24, respectively. The HAMFitPlus results (shown in red curve) are superimposed on the solutions provided by the twelve Annex 41 participants (shown in grey curves). In general, the heating and cooling load predictions of the models are rather scattered. One of the reasons could be due to differences in solar radiation calculations as presented in Figure 6-25. As can be seen in this figure, there is no agreement among the various models in the calculation of the solar gain through the window. In all cases, however, HAMFitPlus predictions of heating and cooling load profiles fall within the range of the other participant models results (Figure 6-23 and Figure 6-24). HAMFitPlus simulation results suggest that on July 5th the building requires heating from 1:00 to 9:00 h and cooling from 10:00 to 21:00 h. The hourly peak heating and cooling demands for that day are 1.16 and 5.68 kWh, respectively. These energy demands occur at 5 and 14 h, respectively. Moreover, the annual heating and cooling loads are estimated to be 15420 and 1880 kWh, respectively.

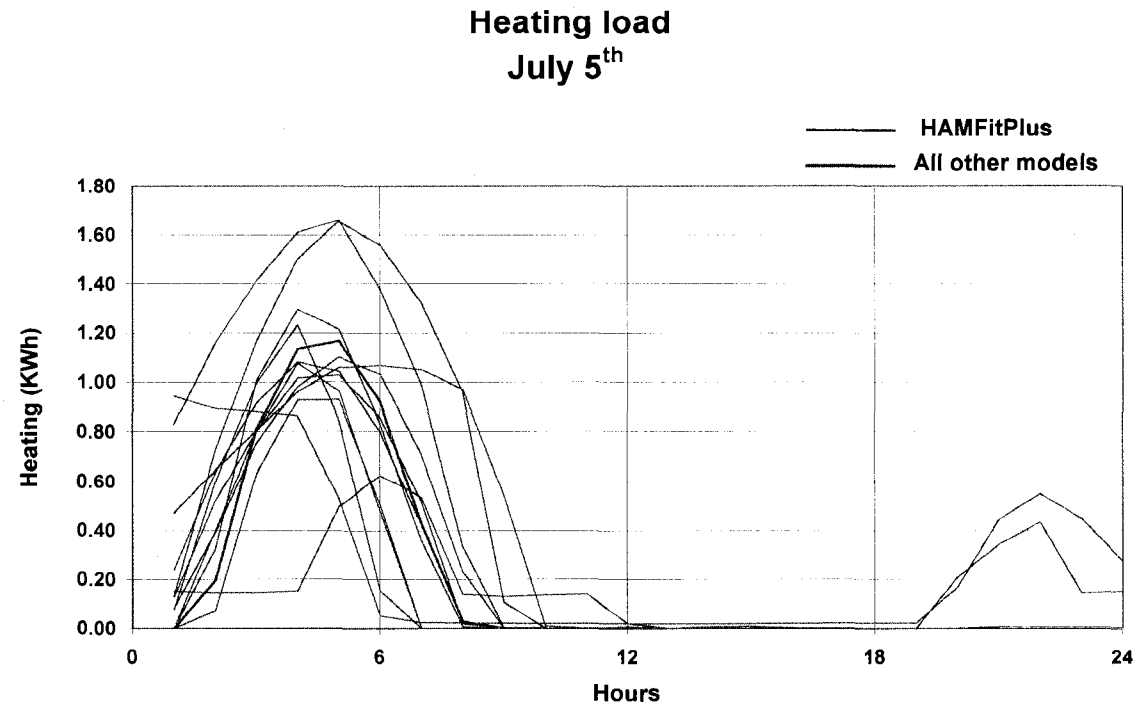

Figure 6-23 Heating load on July5th as prediacted by HAMFitPlus and other participating models

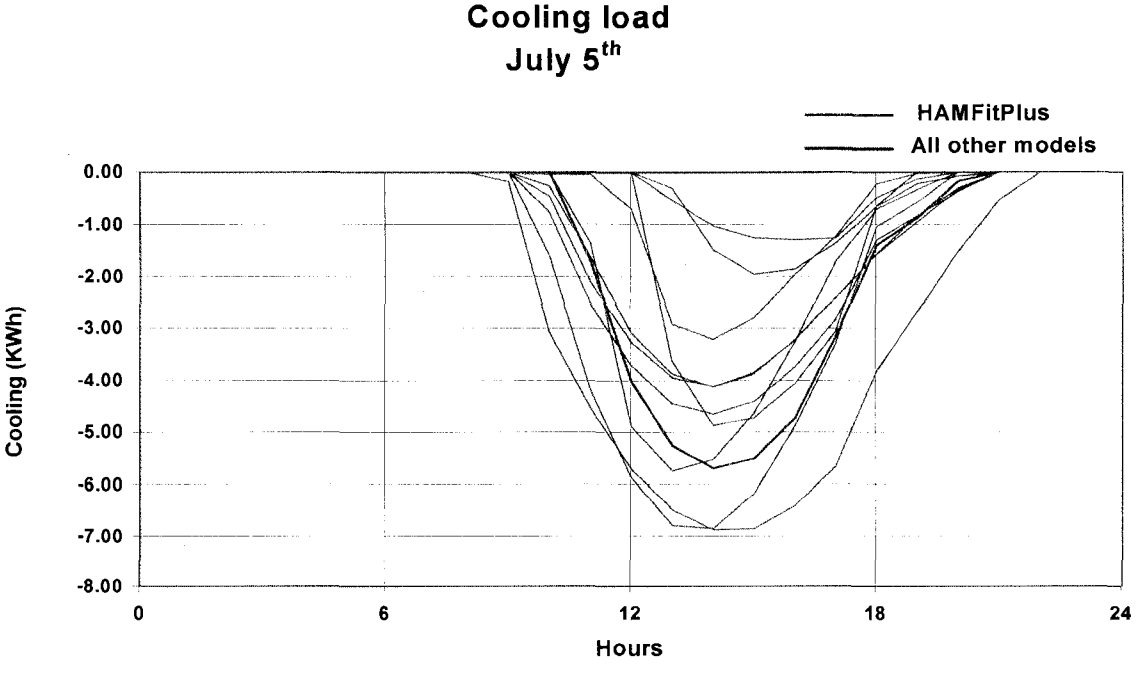

Figure 6-24 Cooling load on July5th as prediacted by HAMFitPlus and other participating models

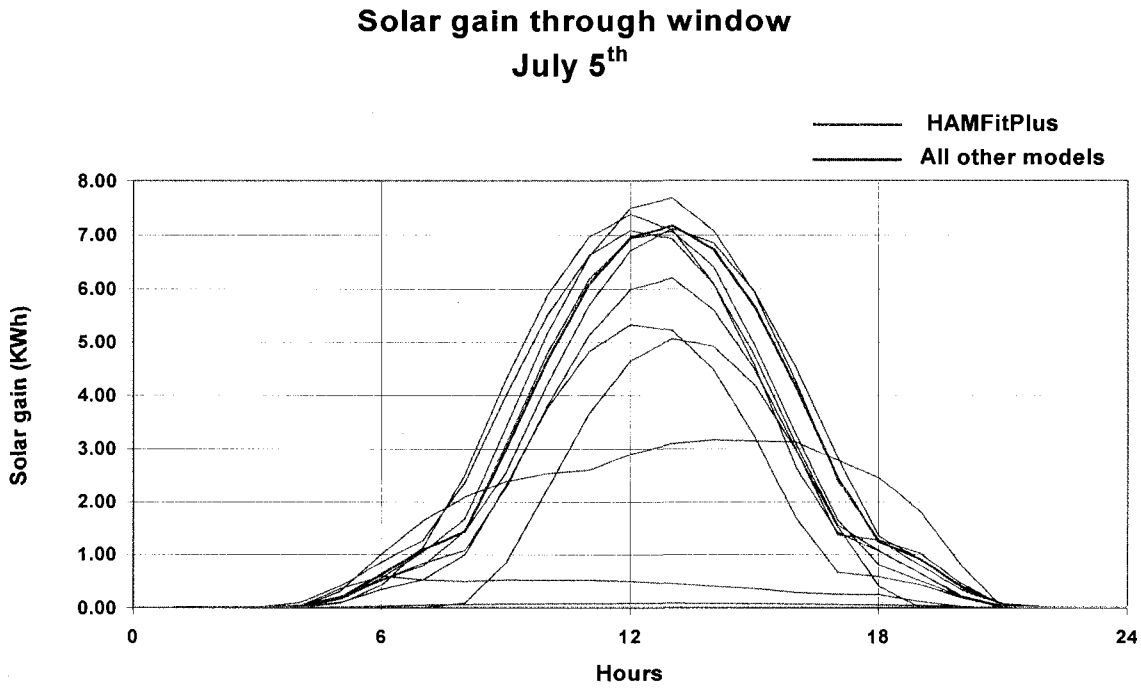

Figure 6-25 Solar gain through window on July5th as prediacted by HAMFitPlus and other participating models

In comparison with the twelve models considered here, HAMFitPlus simulation results of the indoor humidity and temperature conditions, hygrothermal conditions of the exterior roof surface and energy demands to maintain the desired indoor temperature are all well within the range of the solutions provided by the participants. The wide variations of simulation results, which are observed in Figure 6-19 and Figure 6-24, underline the complexity of modeling the interaction of indoor air, HVAC system and building envelope components.

6.2.2 Experimental validation—Two rooms with real climatic exposure

In this section HAMFitplus is benchmarked with the field experimental data collected at FhG (Fraunhofer-Instituite of building physics), Holzkirchen, Germany. The experiment was carried out as part of Annex 41 project initiatives with the objective of providing experimental data for evaluation and validation of whole building hygrothermal models (Lenz and Holm, 2005). The field measurements and simulation results of various models, including that of HAMFitPlus, are published in Holm and Lengsfeld (2007) and Annex 41 final report (2008).

Rooms' descriptions

In this experiment, two rooms that have identical geometry, dimensions, and orientation as well as boundary conditions are considered. Each room has a floor area of 19.34 m^2 and volume of 48.49 m^3. Figure 6-26 shows the schematic diagram of the rooms' floor plan. One of the rooms is designated as a reference room and the other one as a test room. The surfaces, designated by letters 'ABCDE' for the reference room and 'EFGHI' for the test room, are exterior walls. These surfaces are exposed to the time varying real weather conditions. The surfaces 'AL', 'EK' and 'IJ' are partition walls, whereas 'JK' and 'KL' are walls adjacent to hallway. The exterior wall (Figure 6-27) consists of the following layers, in sequence from exterior to interior: 5 mm mineral fiber, 70 mm polystyrene, 15 mm mineral plaster, 240 mm brick, 20 mm old inside plaster and 10 mm of gypsum plaster. The layers that make up the partition walls, wall adjacent to the hallway, ceiling and floor are summarized in Table 6-6.

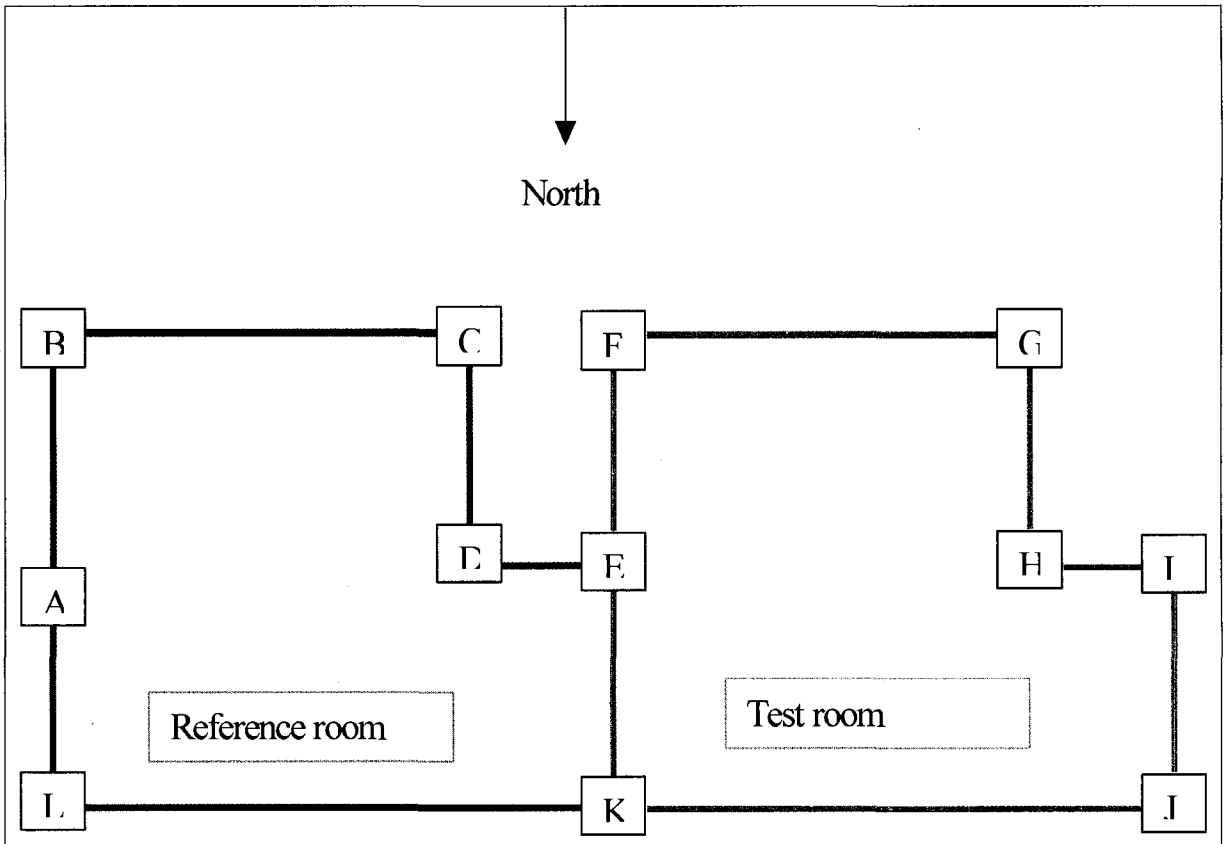

Figure 6-26 Schematic diagram of the reference and test rooms floor paln

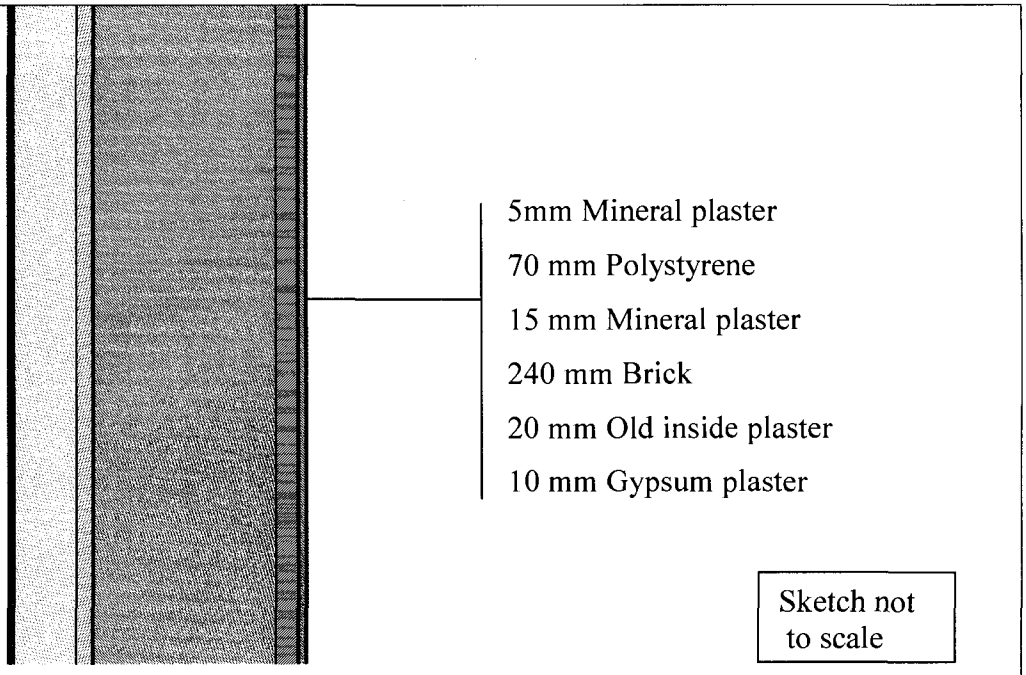

Figure 6-27 Schematic diagram of exterior wall

Table 6-6 Sequence of materials that make up the various building envelope components

Exterior → Interior					
Partition Wall	Gypsum plaster (10 mm)	Solid brick (115 mm)	Mineral wool (100 mm)	Solid brick (115 mm)	Gypsum plaster (10 mm)
Hallway Wall	Gypsum board (12.5 mm)	Polystyrene (50 mm)	Lime silica brick (175 mm)		Gypsum plaster (15 mm)
Ceiling	Wood (25 mm)	Concrete screed (50 mm)	Polystyrene (20 mm)	Concrete (175 mm)	Gypsum plaster (15 mm)
Floor	Concrete (25 mm)	Polystyrene (20 mm)	Concrete screed (50 mm)		PVC linoleum (3mm)

Each room has a double pane window of size 1.41 m high and 1.94 m wide. The overall heat transfer coefficient of the window is 1.1 W/m^2K. To restrict solar radiation transmission into the room, the windows are covered with wool cloth. Hence the window solar heat gain coefficient is assumed to be zero. The rooms also have doors, which have dimension of 1.94 m high and 0.82 m wide, located on the wall adjacent to the hallway. To reduce heat flow through the door (avoid thermal bridge), it is manufactured with 50 mm thick polystyrene insulation as a core material.

Material properties

The hygrothermal properties of the materials used in the construction of the experimental rooms are given in Table 6-7 below. The moisture storage and transport properties of materials, for the full hygroscopic range, are derived using the parameters given in the table. The vapor permeability of a material is derived from the corresponding vapor resistance factor, μ. The vapor resistance factor of a material is defined as the ratio of the vapor permeability of stagnant air and the material at the same temperature and pressure. The vapor permeability of stagnant air (δ_a) is defined by Schimer's equation, $\delta_a = 5.65 \times 10^{-8} T^{-1}$ where T is the ambient temperature in degree Kelvin (Kalagasidis, 2004). The moisture storage properties of the materials as a function of relative humidity (ϕ) are approximated using Equation [6.1] (WUFI User manual). The parameter 'b' is defined using the given equilibrium moisture content of the material at 80% relative humidity (W_{80}) and capillary saturation (W_f). Moreover, using the given absorption coefficient (A_f) values, the moisture diffusivity (D_w) of the materials as a function of

moisture content are approximated by Equation [6.2] (Kumaran 1996, WUFI User manual)

$$w(\phi) = w_f \frac{(b-1)\cdot\phi}{b-\phi} \qquad [6.1]$$

$$D_w(w) = 3.8\left(\frac{A_f}{w_f}\right)\cdot 1000^{\frac{w}{w_f}-1} \qquad [6.2]$$

Table 6-7 Hygrothermal properties of materials used in reference and test rooms

Materials	Density (kg/m^3)	Heat Capacity (J/kgK)	Thermal conductivity (W/mK)	μ_dry (-)	W_{80} (kg/m^3)	W_f (kg/m^3)	A_f ($kg/m^2s^{1/2}$)
Mineral plaster	1900	850	0.8	25	45	210	0.002
Polystyrene	30	1500	0.04	50	0	0	0
Brick	1650	850	0.6	9.5	9	370	0.4
Old inside plaster	1721	850	0.2	13	1.8	264	0.3
Gypsum plaster	850	850	0.2	8.3	6.3	400	0.3
Mineral wool	60	850	0.04	1.3	0	0	0
Gypsum board	850	870	0.16	6	35	400	0.3
Lime silica brick	1900	850	1	28	25	250	0.045
Wood	400	1500	0.09	200	60	575	0
Concrete screed	1950	850	1.6	75	38	155	
Concrete	2300	850	1.6	180	85	150	0.02
PVC Linoleum	1000	1500	0.16	15000	0	0	0
Aluminum foil				10000	0	0	0

Boundary conditions

The exterior surfaces of the reference room 'ABCDE' and test room 'EFGHI', shown in Figure 6-26, are exposed to real weather conditions of Holzkirchen, Germany. Holzkirchen is located at 47.88° north latitude and 11.73° east longitude, and has an elevation of 600 m. The weather data during the experiment period are provided. It includes ambient temperature, relative humidity, wind speed and direction, solar radiation as well as rain and cloud conditions. The temperature and relative humidity conditions that are recorded values of the space adjacent to the hall way ('JK' and 'KL') and ceiling are used as boundary conditions for the respective surfaces. The boundary conditions of the partition walls ('AL' and 'IJ') are the air conditions of the adjacent room (50% relative humidity and 20°C). The ground temperature is assumed to be 2°C. The emissivity and absorptivity of the exterior and interior surfaces of the building components are 0.9 and 0.4, respectively. A heat transfer coefficients of 8 W/m^2K is used for both internal and external surfaces of the partition walls, ceiling and hallway walls as well as the internal surfaces of the exterior walls and floor. The exterior surface heat transfer coefficients of the latter two (exterior walls and floor) are 18 and 100 W/m^2K, respectively.

Rooms' operating conditions

During the experiment, the indoor temperatures of the two rooms are desired to be 20±0.2°C. To achieve this condition, a radiator heater that has a capacity 1000 W is installed in each room. A thermostat controls the operation of the radiator. The electrical power consumption by the radiator, to maintain the indoor temperature in the specified

range, is recorded. Since the experiment is done in heating season, no mechanical cooling equipment is required. The reported air exchange rates per hour due to both infiltration and mechanical ventilation system are 0.63 and 0.68 for the reference and test rooms, respectively. The rooms are subjected to identical indoor moisture load of 2.4 kg per day. The estimated daily total moisture production (2.4 kg/day) is distributed throughout the day in varying magnitude and duration to reflect the daily activity of the occupants. The diurnal moisture production schedule used in the experiment is shown Figure 6-28. According to this schedule, the occupants' morning activities (such as taking shower) generates a peak moisture production rate of 400 g/hr for two hours (6:00-8:00 h). Whereas their evening activities (such as cooking and washing dishes) result in a moderate moisture production rate of 200 g/hr for six hours (16:00-22:00 h). For the rest of the day a 25 g/hr moisture production rate, which represents moisture generation by other than occupants' activity (such as pets or plants), is assumed.

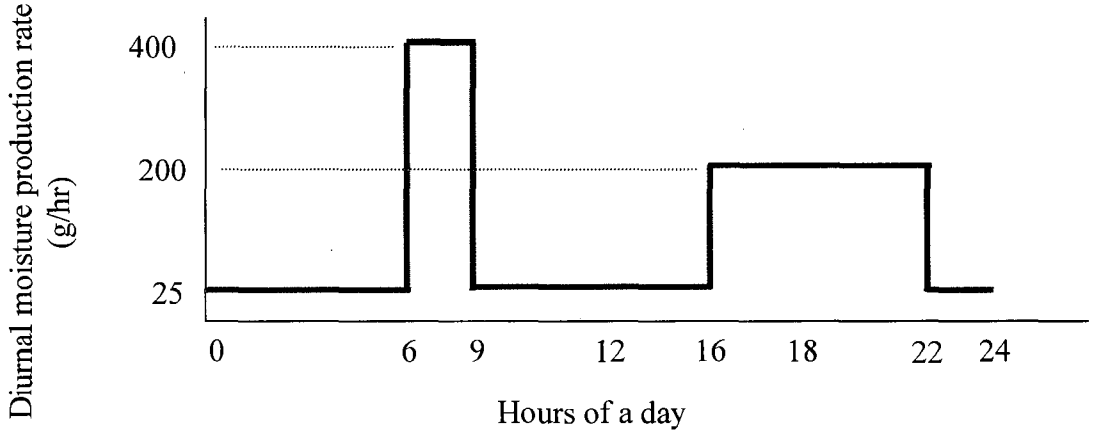

Figure 6-28 Diurnal moisture production schedule

Simulation results

Step 1

The first step of the experiment takes place from January 17th to February 2nd 2005. During this period the interior surfaces of the walls and ceiling of the test room is covered with aluminum foil (estimated vapor diffusion thickness of 1000 m). Similarly, the interior surfaces of the reference room are painted with latex paint (estimated vapor diffusion thickness of 0.15 m). In the HAMFitPlus simulation the mass transfer coefficients of these interior surfaces are deduced from the vapor permeance values of the corresponding paints. Hence, mass transfer coefficients of 1.93E-14 and 1.29E-9 s/m are used for the test and reference rooms, respectively. This experiment represents cases with limited interaction between building envelope components and indoor air (reference room), and an extreme case where the building envelope is decoupled from the indoor air (test room). The experimental results of these two cases are shown in Figure 6-29. Generally, the indoor relative humidity amplitude of the reference room is relatively smaller than that of the test room. This implies that a room even with a limited moisture buffering capacity (reference room) has a potential of modulating the indoor humidity conditions. To the contrary, the test room does not have moisture-buffering capacity, and therefore, the indoor relative humidity is less by about 4% and higher by about 2% of the lower and upper values of the reference room, respectively.

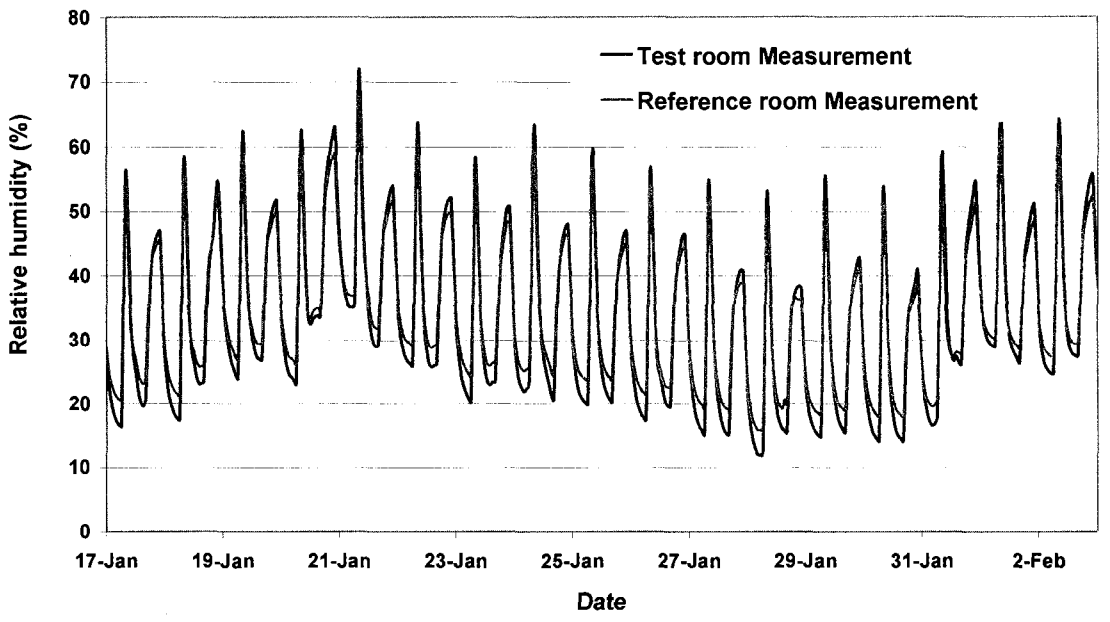

Figure 6-29 Measured indoor relative humidity conditions of the Test and Reference rooms (Step 1 experiment)

For comparison purpose the HAMFitPlus simulation results are superimposed on the experimentally measured indoor relative humidity of the test and reference rooms accordingly. In all figures, the HAMFitPlus simulation results are designated in red and the measured data in blue curves Figure 6-30 and Figure 6-31 show the indoor humidity profiles of the corresponding rooms for the entire simulation period. Whereas in Figure 6-32 and Figure 6-33, the humidity profiles of the respective rooms on January 25th are presented for detailed view. As can be seen in the figures, the indoor relative humidity prediction of the HAMFitPlus is in good agreement with the measured values. In general a better agreement between measured and simulated results is obtained for the test room than the reference room. The simulation consistently underestimates the indoor relative

humidity peak of the reference room by 2-6% RH. This suggests that the actual vapor diffusion thickness of the latex paint (in the reference room) might be higher than the value given (used) for simulation.

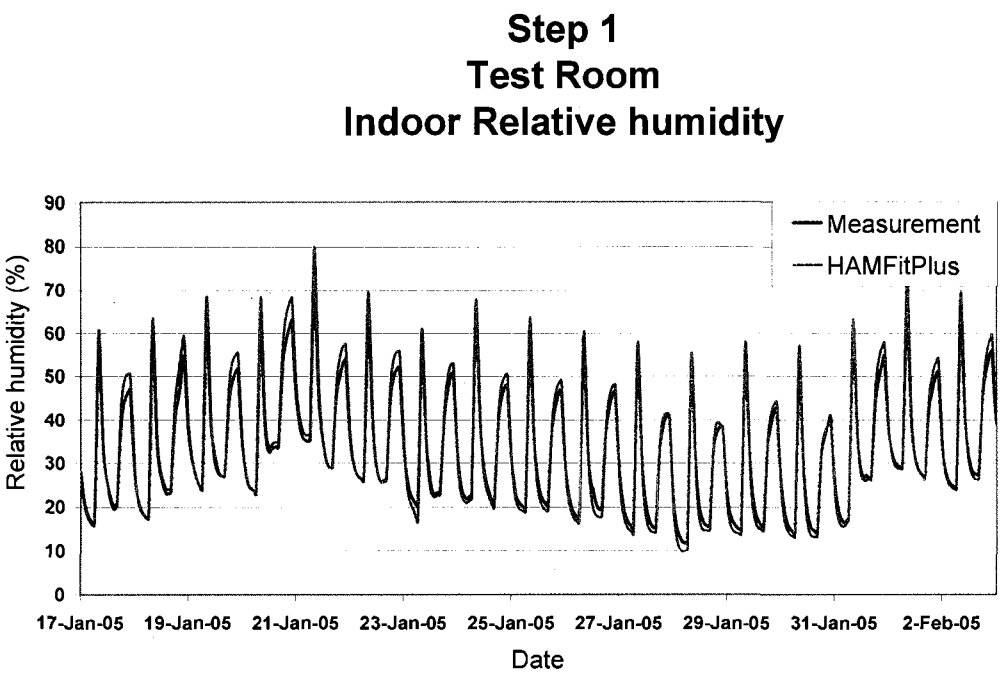

Figure 6-30 Measured and simulated indoor humidity of the test room (Step 1 experiment)

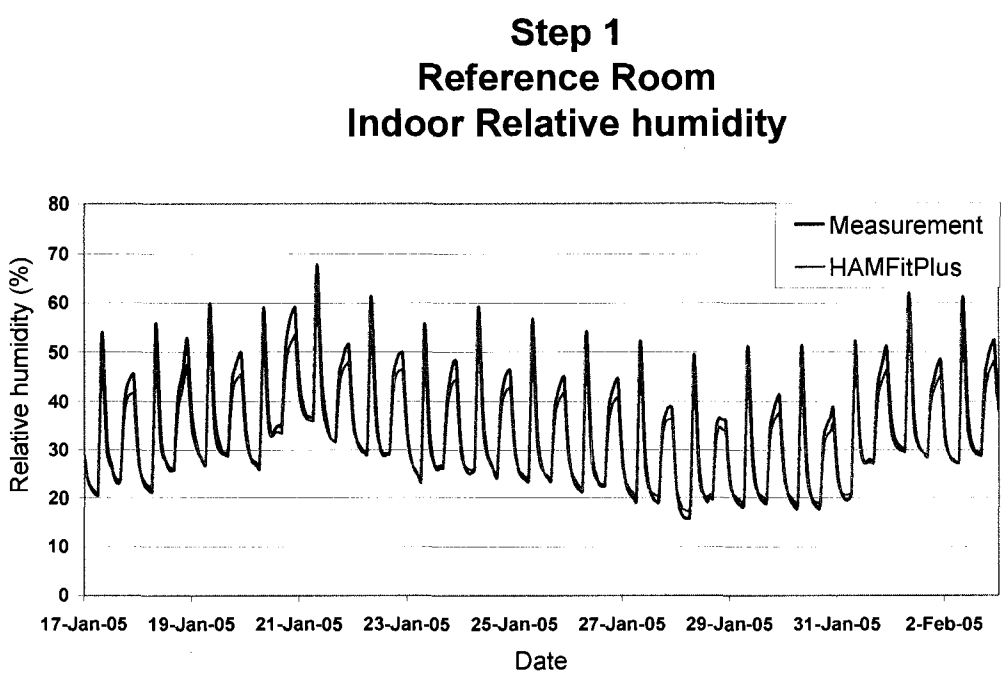

Figure 6-31 Measured and simulated indoor humidity of the Reference room (Step 1 experiment)

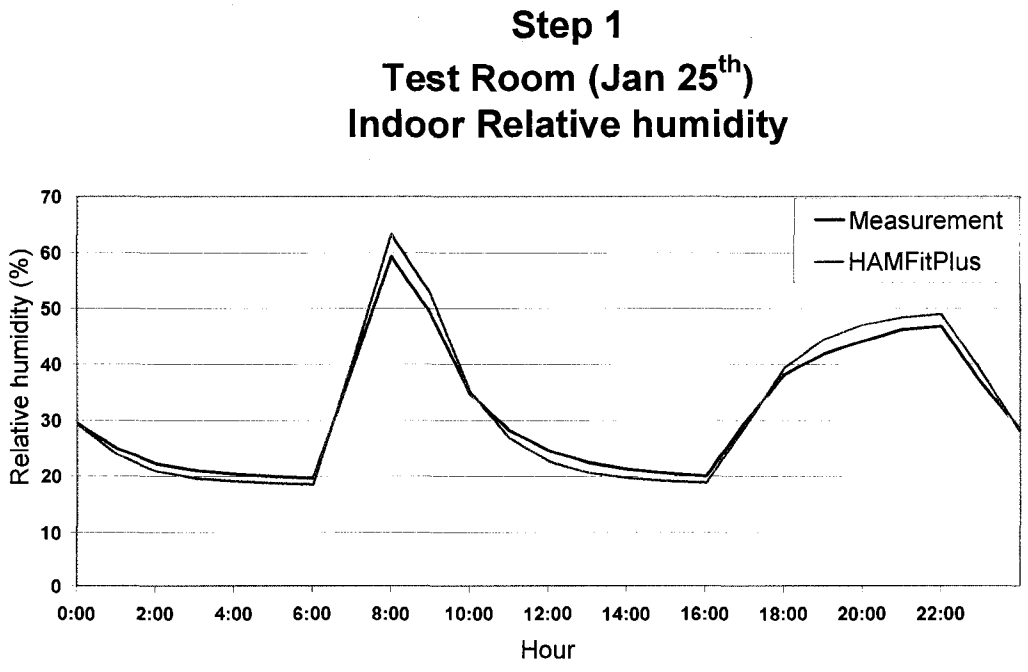

Figure 6-32 Measured and simulated indoor humidity of the Test room on January 25th (Step 1 experiment)

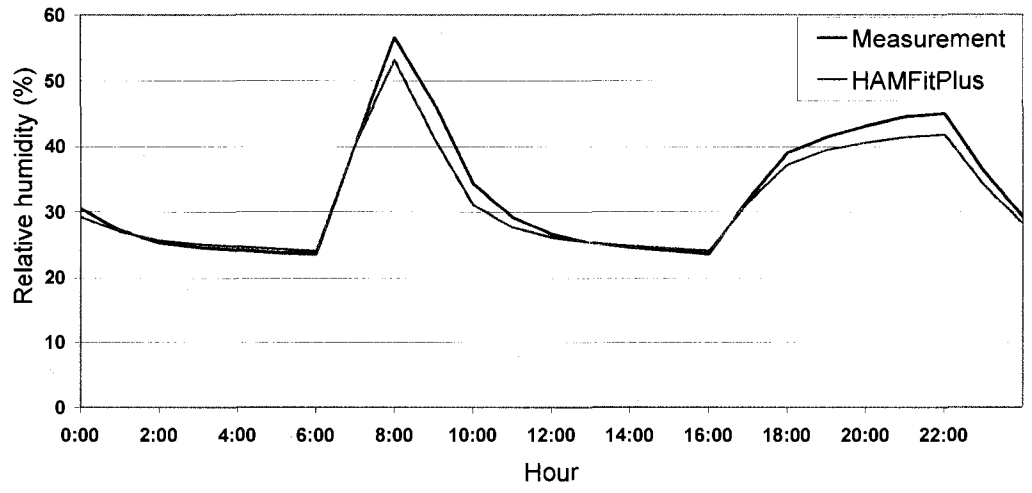

Figure 6-33 Measured and simulated indoor humidity of the Reference room on January 25th (Step 1 experiment)

Step 2

The second step of the experiment takes place from February 14th to March 20th 2005. In this experiment the reference room is left as it is with no change on the interior furnishing (gypsum finished with latex paint). But the test room is modified in such a way that the walls that are covered with aluminum foil are now covered with 12.5 mm thick unpainted gypsum board. Subsequently, the test room will have a high moisture buffering capacity in this step of the experiment compared to the first step (walls with aluminum foil). Hence, the dynamic interaction between building envelope components and indoor air is more important in this step than in the first step of the experiment. The hygrothermal properties of the gypsum board that is used for covering the 50 m^2 area of

the walls, are given in Table 6-8. In the HAMFitPlus simulation, a mass transfer coefficient of 5E-8 s/m is used for the interior surfaces of the test room walls (newly installed gypsum surfaces). Since there is no change in the interior surfaces of walls and ceiling of the reference room (Step 1 versus Step 2 experiment), the corresponding mass transfer coefficients defined (for these surfaces) in the first step simulation are used.

Table 6-8 Hygrothermal properties of gypsum board that is installed in Test room for moisture buffering

Materials	Density (kg/m^3)	Heat Capacity (J/kgK)	Thermal conductivity (W/mK)	μ_dry (-)	W_{80} (kg/m^3)	W_f (kg/m^3)	A_f ($kg/m^2s^{1/2}$)
Gypsum board	710	850	0.31	8	9.5	400	0.3

For comparison purpose the HAMFitPlus simulation results are superimposed on the experimentally measured indoor relative humidity of the test and reference rooms, Figure 6-34 to Figure 6-37. In the figures, the HAMFitPlus simulation results are designated in red and the measured data in blue curves. The first two figures (Figure 6-34 and Figure 6-35) show the indoor humidity profiles of the rooms for the entire simulation period, and the other two, Figure 6-36 and Figure 6-37, present expanded views of a sample humidity profile for February 17th. As can be seen in these figures, the simulation results of HAMFitPlus are in good agreement with the corresponding measured data of the test and reference rooms. The good agreement obtained here underlines the importance of coupling building envelope components and indoor environment to accurately predict the indoor humidity of a building (using whole building hygrothermal

model). Furthermore, the experimental and simulation results in this section demonstrate the significance of moisture buffering materials in modulating and reducing the indoor humidity level of a house. For example, the maximum and minimum indoor relative humidity of the reference room, which has a limited moisture buffering capacity, on February 17th are 57 and 24%, respectively (Figure 6-37). Whereas in the case of the test room, that has a higher moisture buffering capacity, the corresponding values are 47 and 27%, respectively (Figure 6-36). Consequently, the indoor relative humidity amplitudes of the two respective rooms are 33 to 20%. This result suggests that materials with high moisture buffering capacity provide a more stable indoor humidity condition (low fluctuation amplitude).

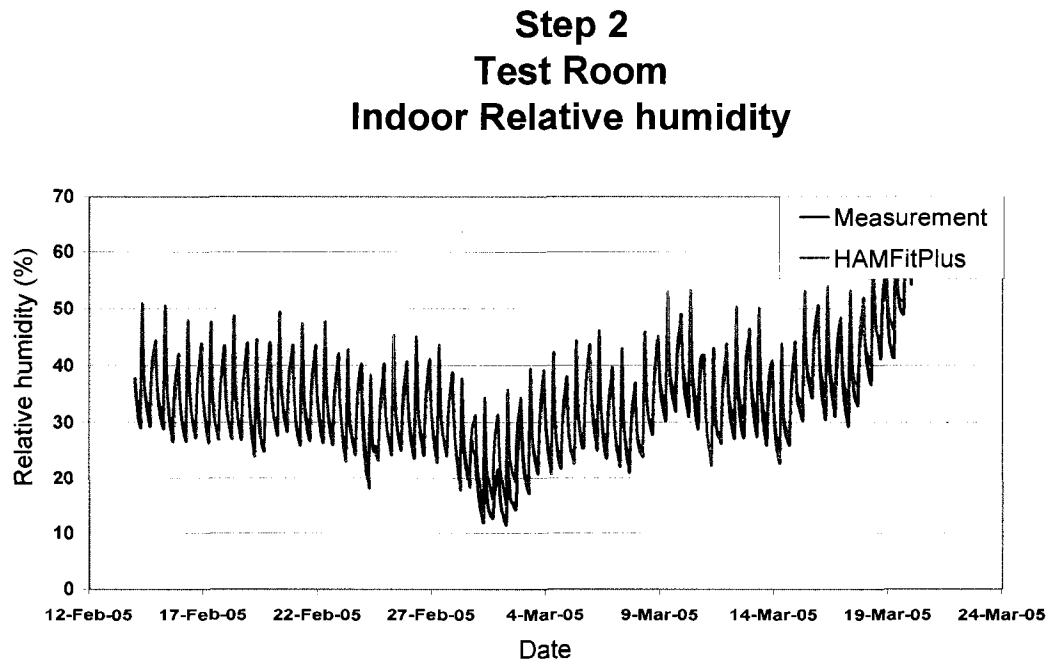

Figure 6-34 Measured and simulated indoor humidity of the Test room (Step 2 experiment)

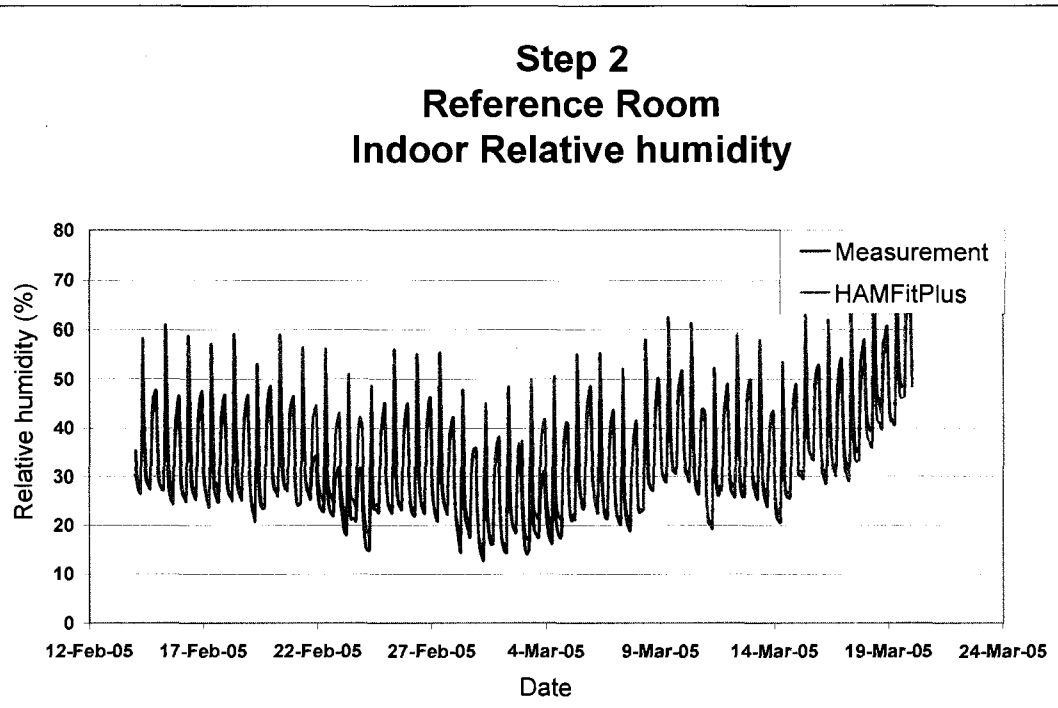

Figure 6-35 Measured and simulated indoor humidity of the Reference room (Step 2 experiment)

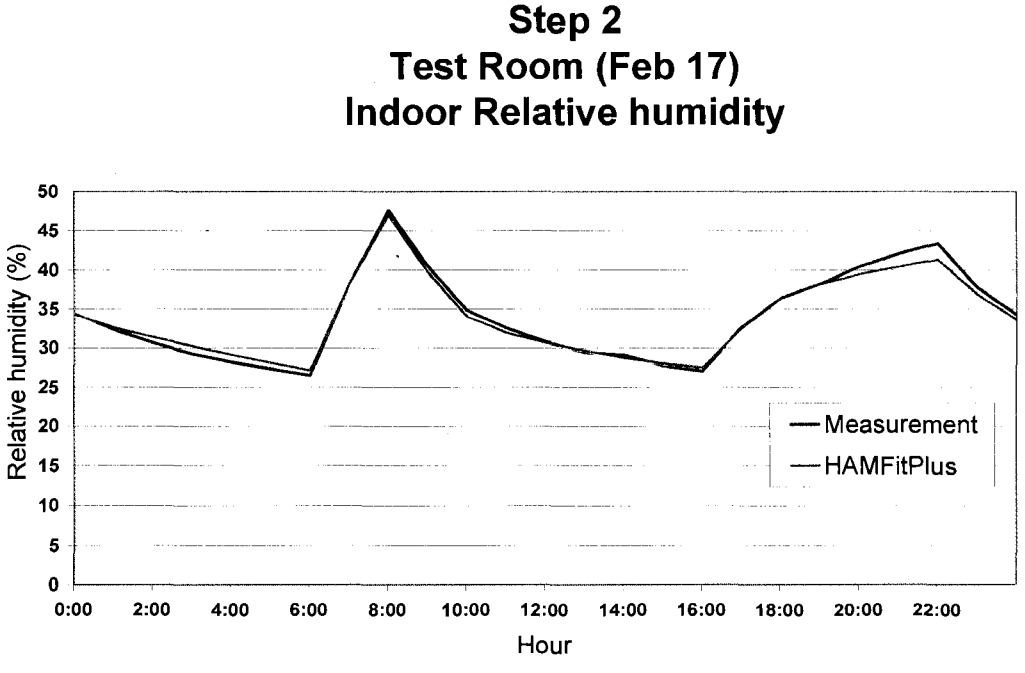

Figure 6-36 Measured and simulated indoor humidity of the Test room on February 17th (Step 2 experiment)

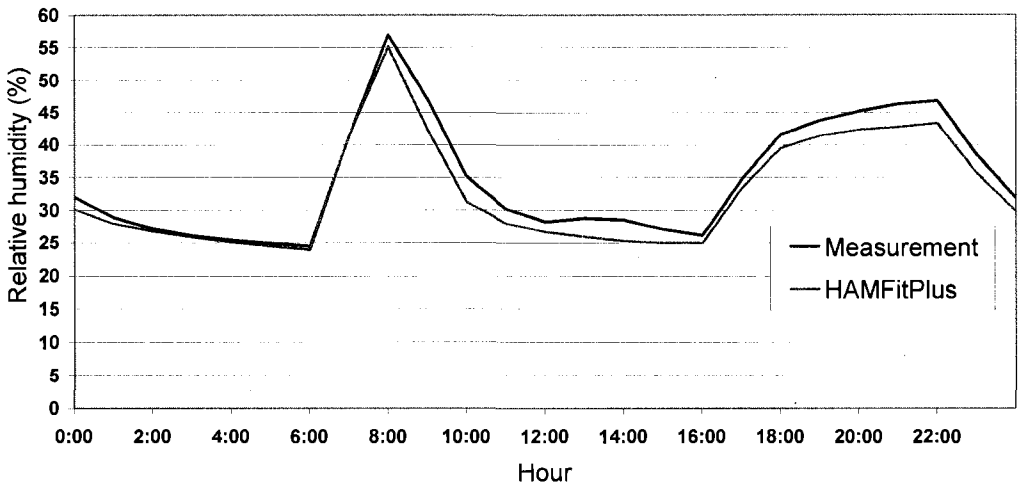

Figure 6-37 Measured and simulated indoor humidity of the Reference room on February 17th (Step 2 experiment)

Heating energy

The HAMFitPlus prediction of heating energy demand during the first step of experiment is shown in Figure 6-38. The measured data is the electric power consumed, not the direct heat input to the rooms to maintain the temperature at 20°C. Therefore the simulation and the measured results cannot be compared readily, but their profiles might. In actuality, the radiator heat release rate to the indoor air should be less than the electrical power input (second law of thermodynamics –efficiency of a device is always less than 100%). Consequently, the measured results are expected to be higher than the predicted values.

As shown in the Figure 6-38, the measured values are higher and have distinct peaks every morning around 7:00 h. This consistent pattern is created independent of the

outdoor temperature conditions, and therefore the simulation cannot reproduce them. Ignoring the peaks and recalling that the mechanical efficiency of the radiator is less than 100%, the profiles of the simulated heating energy and measured electric consumption are similar.

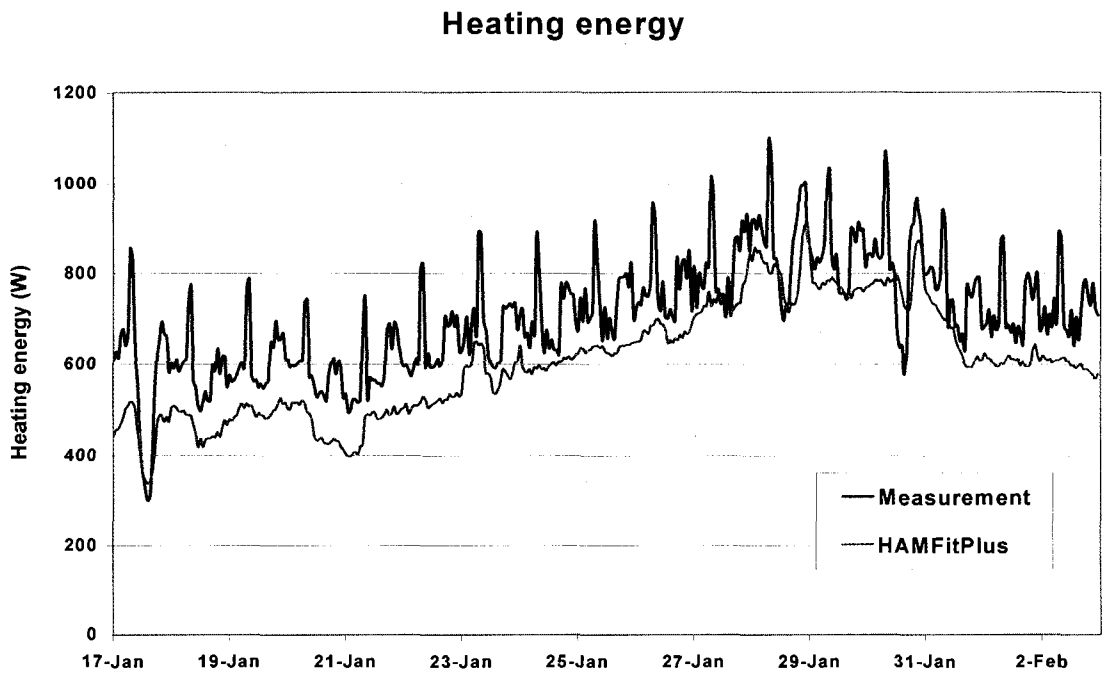

Figure 6-38 Approximated (from measurement) and simulated energy demands during Step 1 experiment

In this section, the capability of the model in predicting indoor temperature and relative humidity, energy demands for heating and cooling as well as hygrothermal conditions of building component in an integrated manner is demonstrated. The simulation results of HAMFitPlus, for the seven benchmark exercises that are carried out in this section, are in good agreement with the corresponding reference solutions. In the next two Chapters, the model is used for whole building hygrothermal simulation of "real" case scenarios.

7 INDOOR HUMIDITY AND BUILDING ENVELOPE PERORMANCE ANALYSIS

After a series of successful verification and validation of the HAMFitPlus model, in this section, the model is used to predict the indoor humidity condition of an occupied dwelling. The simulated indoor humidity of the house is compared with predictions of two other indoor humidity models that are referred in ASHRAE Standard 160P (2006) and European Standard (EN ISO 13788), as well as experimentally measured values. The objective, here, is to show the degree of indoor humidity variations that can be expected in using advanced and simpler models for the house and monitoring period considered. Moreover, the effect of indoor humidity on the hygrothermal performance of a building envelope component, and the need for accurate indoor humidity modeling are discussed.

The residential building considered here is one of the twenty-four houses that are monitored by the Institute for Research in Construction (IRC) researchers under a Panel of Energy Research and Development (PERD) project. The ultimate objective of this research project is to design and develop buildings that are energy efficient and durable under the extreme climatic conditions. The houses are located in northern Canada, more specifically, in Prince Rupert (British Columbia), Inuvik (Northwest Territories) and Carmacks (Yukon Territories). In each location, the indoor relative humidity and temperature conditions of eight houses, and the corresponding outdoor temperature and relative humidity are measured for four consecutive weeks. The indoor temperature and relative humidity measuring devices (HOBO Pro Series sensors) are placed in two locations of the following five choices for each dwelling: living room, bedroom, kitchen,

storage and bathroom. The complete descriptions of the monitoring protocol along with the survey results of the twenty-four houses are documented in Hood (2006). Twenty-one of the twenty-four houses are heated by radiating heating systems; such as electrical baseboard, wood stove or hydronic systems. In these houses, mixing of various rooms indoor air takes place by buoyancy, which are not effective as the mechanical air-distribution system that is equipped with ducts and fan. Thus, due to the limited indoor air mixing, representation of the indoor air by a single node will not be appropriate. Consequently, HAMFitPlus cannot be used to model the indoor humidity condition of these houses. Among the three remaining houses, the indoor humidity of a house in Carmacks seems reasonably uniform, and therefore considered for further analysis in this section. The house is a single-storey house equipped with an air-distribution system and, as shown in Figure 7-1, the indoor humidity measurements at two locations of the house (kitchen and living room) are very close.

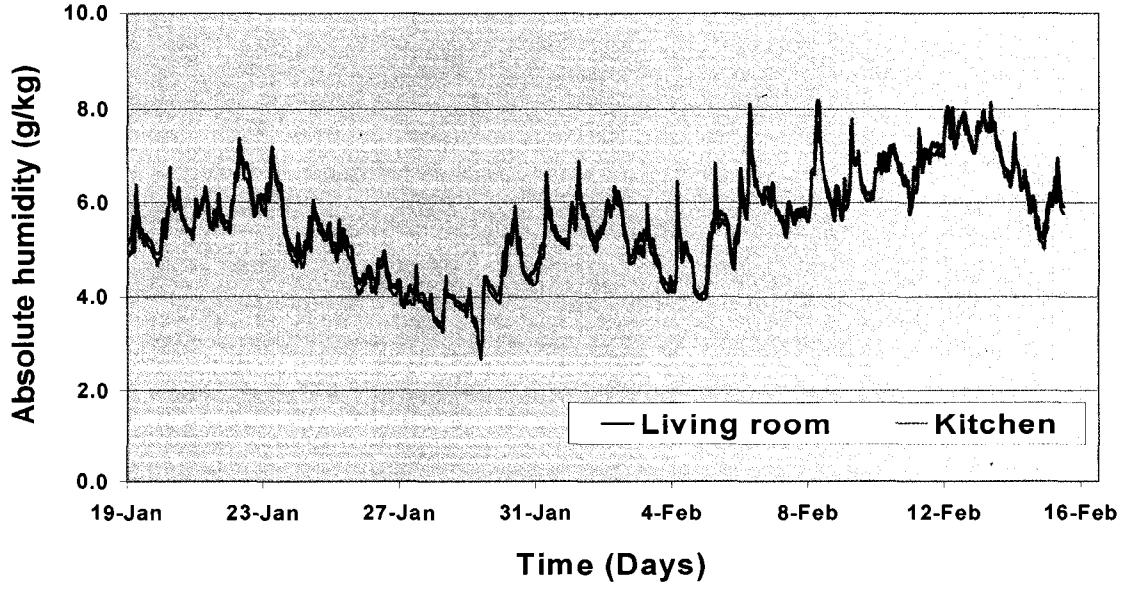

Figure 7-1 Measured indoor absolute humidity in the living room and kitchen of a house considered for further analysis

Carmacks is located in the northwestern part of Canada in Yukon Territories at latitude of 62° 7' north and longitude of 136° 11' west and has an elevation of 543 m above sea level. In the map of Canada, shown in Figure 7-2, Yukon Territories is identified in red color. The residential building considered here is subjected to extreme loadings in both indoor and outdoor. The high indoor and outdoor loadings are due to the high occupancy of the house, which is five during the day and six at nighttime; and to the extremely cold outdoor temperature, respectively. Hence, the building may have a challenge in maintaining the required indoor humidity conditions for a better and healthy indoor air quality and building enclosure durability, while being energy efficient at the same time.

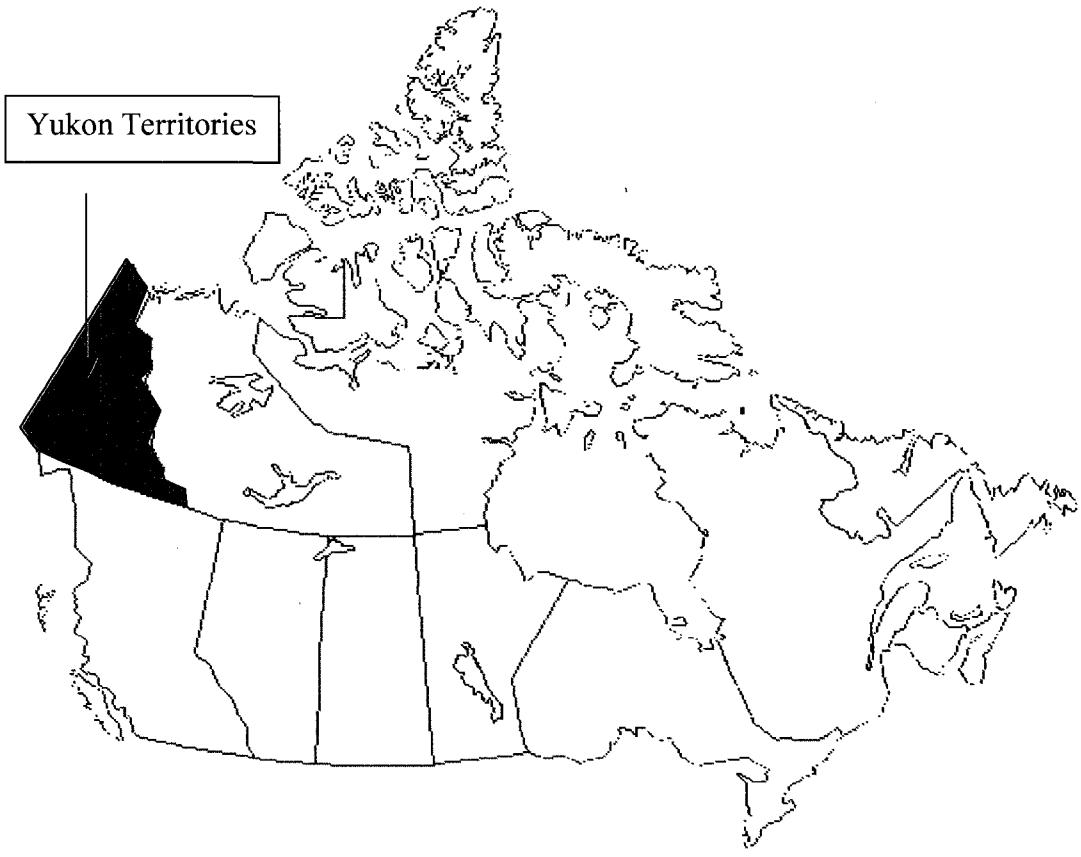

Figure 7-2 Map of Canada.

Local weather conditions

In general, the weather parameters that are required for whole building hygrothermal analysis are hourly ambient temperature, relative humidity, wind speed and direction, solar radiation (global and diffusive horizontal radiations) precipitation and sky (cloud) conditions. However, for the house considered in this study, the effect of precipitation can be ignored due to the fact that the exterior layer of the house (cladding) is sheet metal and no rain absorption is possible. The weather station in Carmacks records only ambient temperature and wind conditions –wind speed and directions. The relative humidity of the ambient air is measured as part of the field monitoring tasks of the PERD project. Hence, the only weather parameter that needs to be estimated to carry out the whole building hygrothermal modeling is solar radiation data. The hourly average temperature and relative humidity of the outdoor air that are imposed on the building envelope as part of the external boundary conditions are shown in Figure 7-3 and Figure 7-4, respectively. Generally, the outdoor temperature is very cold with the hourly average maximum and minimum temperature of 6.5 and -42.2°C, respectively. The monitoring period (January 19th – February 20th) average temperature is -19.0°C. The hourly relative humidity of the ambient air varies from 45 to 95%, with an average value of 73% for the monitoring period. About 30% of the time, the outdoor air is calm. For all other times, the wind directions are categorized into eight subsections each subtended by 45° angle, and plotted as percentage of occurrence, Figure 7-5. As can be seen in the figure, the predominant wind blowing direction during the monitoring period is southeast (25%), followed by the west (18%) and northwest (17%) directions. These orientations coincide with the orientation of the largest surface areas of the house. The mean wind speed during the monitoring period is 6.7 km/hr (1.86 m/s). However, the mean wind speeds in the

separate eight subsections vary from 2.3 to 11 km/hr as shown in Figure 7-6. Based on these figures (Figure 7-5 and Figure 7-6) it can be said that during the monitoring period, wind blows to the southeast direction more frequently at higher speed than any other directions.

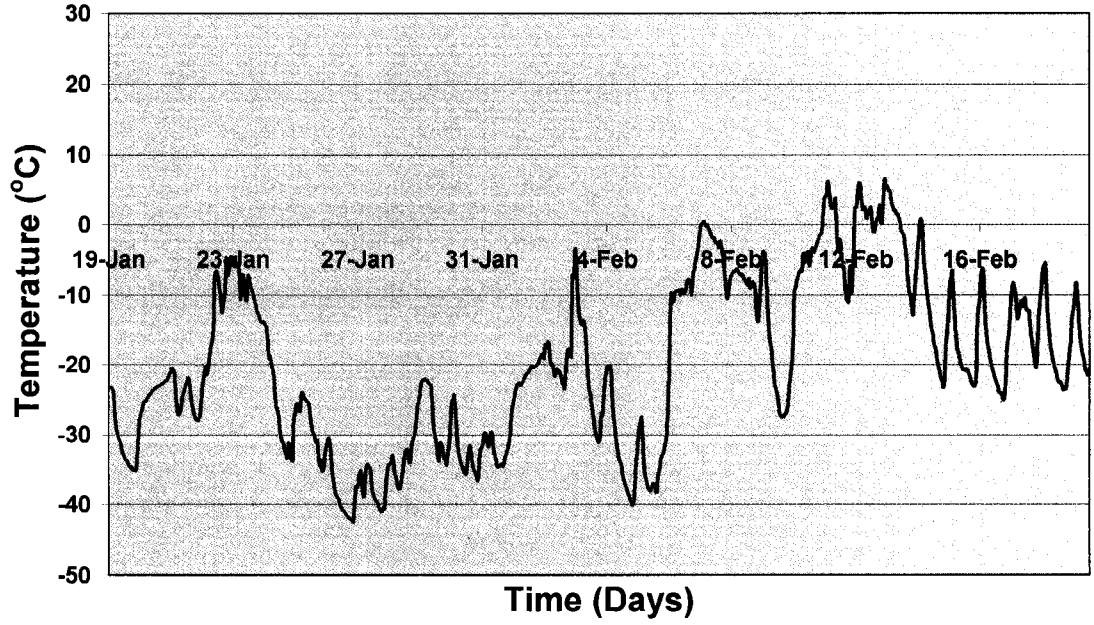

Figure 7-3 Hourly average temperature of Carmacks.

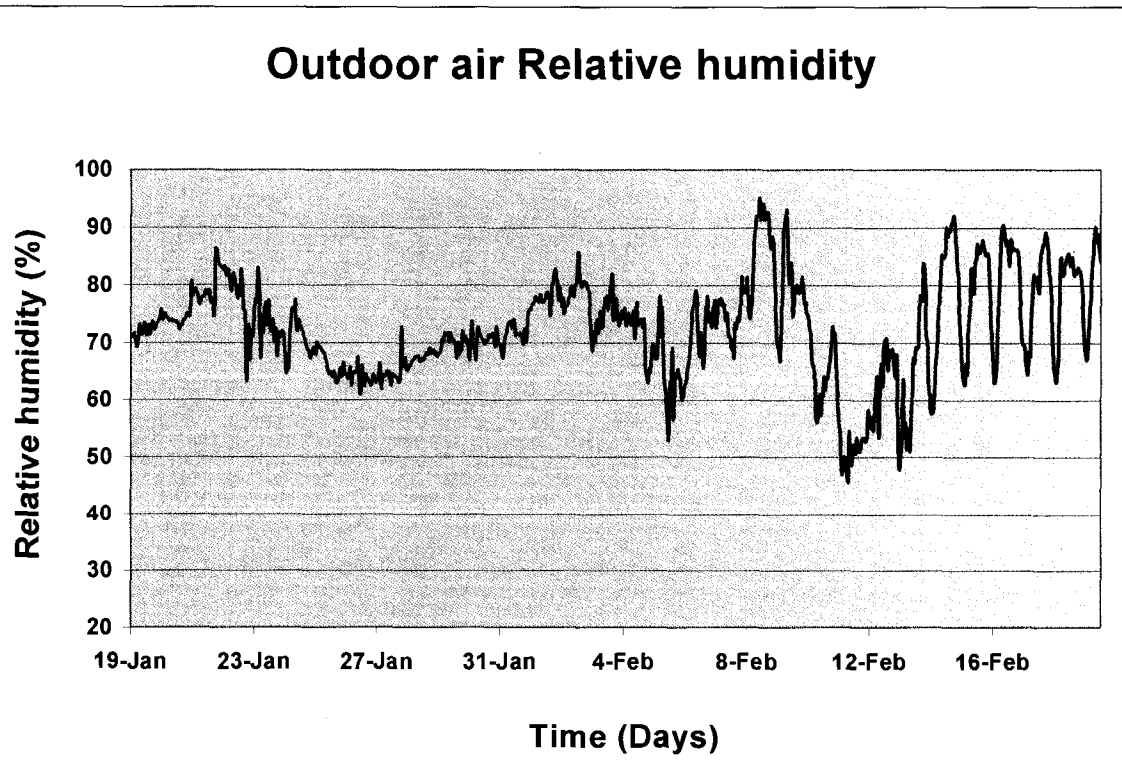

Figure 7-4 Hourly average relative humidity of Carmacks.

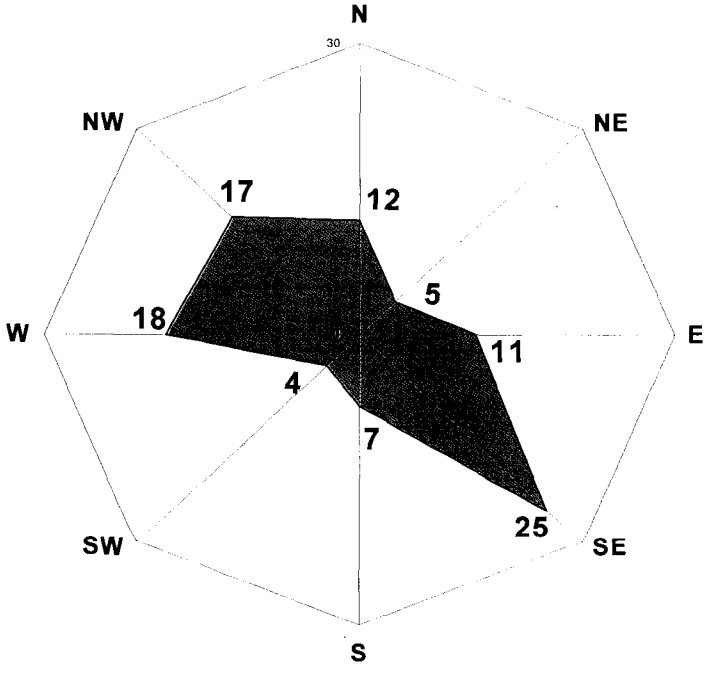

Figure 7-5 Frequency of wind blowing in the respective eight directions (in %)

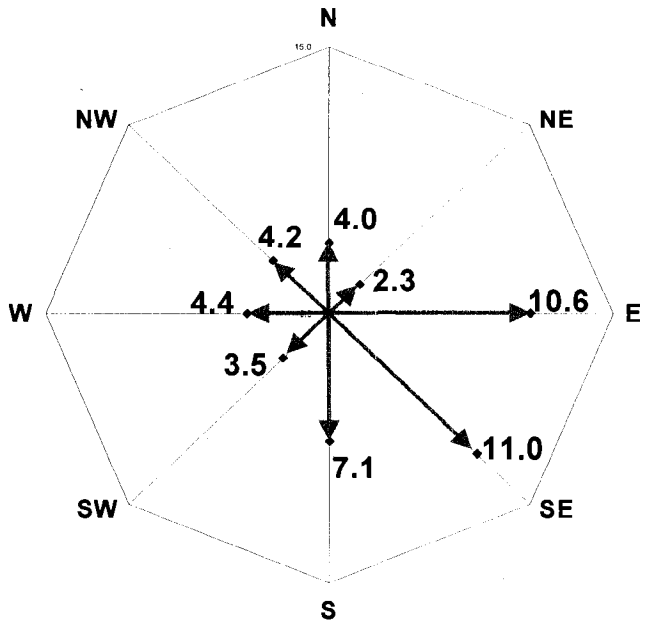

Figure 7-6 Mean wind speeds in the respective eight directions (in km/hr).

The hourly direct and diffusive horizontal solar radiations for a given location are usually estimated using solar model. One of the important parameters that are required by the solar model is the cloud cover index, which is determined based on human observation of the sky condition. Unfortunately, this information is not available for Carmacks, and therefore it is approximated using the observation made in the nearby weather stations located in the same territory, Figure 7-7. The three weather stations are Mayo (Latitude: 63° 37' N Longitude: 135° 52' W), Whitehorse (Latitude: 60° 42' N Longitude: 135° 4' W) and Burwash Landing (Latitude: 61° 22' N Longitude: 139° 3'). The weather files of these locations are downloaded from the Environment Canada web site http://www.climate.weatheroffice.ec.gc.ca/climateData/canada_e.html

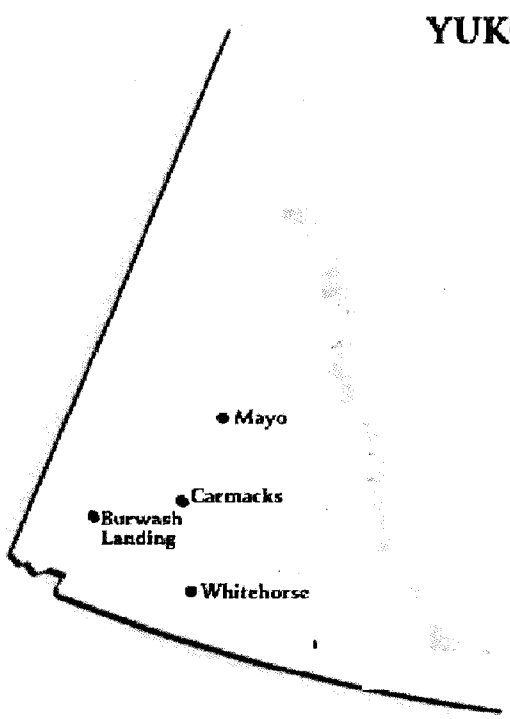

Figure 7-7 Yukon Territory and weather stations near by Carmacks

In the weather files of these three locations, the sky conditions are recorded in text form: clear, mainly clear, mostly cloudy and cloudy. These text descriptions can be conveniently translated to numerical values (amount of cloud covering the dome of the sky in tenths) using Environment Canada classification indices (http://www.climate.weatheroffice.ec.gc.ca/Glossary-popup_e.html#weather). Here, the following equivalent numeric values shown in bracket are adopted for a further analysis of solar radiations: Clear (0), Mainly clear (2), Mostly cloudy (8), Cloudy (10) and partially cloudy (5) for a missing data. Since the three locations are about the same distance from Carmacks (168 to 173 Km), the Carmacks sky condition is assumed to be the average of the sky conditions of the three near by weather stations.

The hourly horizontal global solar radiation is estimated using Zhang and Huang solar model (2002), Equation [7.1]. The required input data for this model include solar data (solar altitude angle and cloud cover) and other climatic conditions such as temperature, relative humidity and wind speed. The calculated horizontal global solar radiations are expected to be greater than or equal to zero but less than the solar constant (1355 W/m^2).

$$I_{ghz} = \left[I_{sc} \sin\beta \left\{ c_o + c_1 CC + c_2 CC^2 + c_3 \left(T_n - T_{n-3} \right) + c_4 \phi + c_5 V_w \right\} + d \right] / k \qquad [7.1]$$

where

I_{ghz} : Estimated hourly solar radiation in W/m^2

I_{sc} : Solar constant, 1355 W/m^2

β : Solar altitude angle, the angle between horizontal and the line to the sun

CC : Cloud cover in tenths

ϕ : Relative humidity in %

T_n and T_{n-3} : Temperatures at hours n and n-3, respectively

V_w : Wind sped in m/s

and the correlation coefficients $c_o, c_1, c_2, c_3, c_4, c_5, d$ and k are given by:

$$c_o = 0.5598,\ c_1 = 0.4982,\ c_2 = -0.6762,\ c_3 = 0.02842,$$
$$c_4 = -0.00317,\ c_5 = 0.014,\ d = -17.853, k = 0.843$$

Figure 7-8 shows the horizontal global solar radiation calculated based on the solar model suggested by Zhang and Huang (2002).

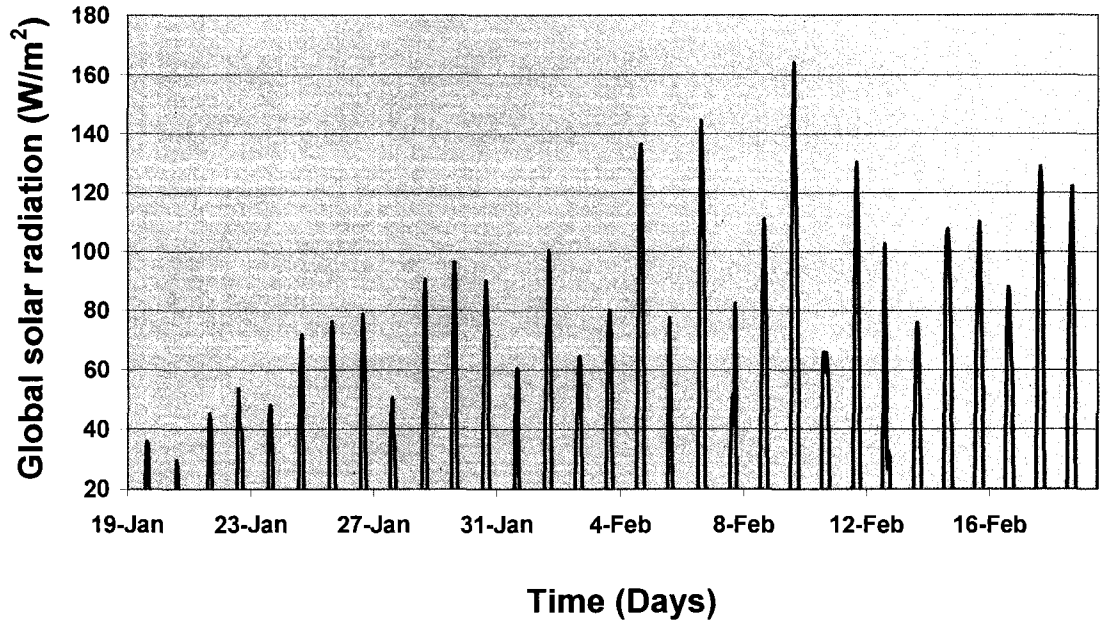

Figure 7-8 Calculated horizontal global solar radiation for the monitoring period

The horizontal components of the direct normal $\left(I_{dn\_hz}\right)$ and diffusive $\left(I_{df\_hz}\right)$ solar radiation are estimated from the calculated global horizontal radiation (Equation [7.1]) using Watanabe et al. (1983) model, which is given by Equation [7.2].

$$I_{dn\_hz} = I_{sc} \sin\beta K_{DS}\left(1-K_T\right)/\left(1-K_{DS}\right)$$

$$I_{df\_hz} = I_{sc} \sin\beta\left(K_T - K_{DS}\right)/\left(1-K_{DS}\right) \qquad [7.2]$$

where:

$$K_T = I_{ghz}/\left(I_{sc}\sin\beta\right) \qquad K_{TC} = 0.4268 + 0.1934\sin\beta$$

$$K_{DS} = K_T - \left(1.107 + 0.03569\sin\beta + 1.681\sin^2\beta\right)\left(1-K_T\right)^2, \text{ when } K_T = K_{TC}$$

$$K_{DS} = \left(3.996 - 3.862\sin\beta + 1.54\sin^2\beta\right)K_T^{\,3}, \qquad \text{when } K_T < K_{TC}.$$

Once the horizontal components of the direct normal $\left(I_{dn\_hz}\right)$ and diffusive $\left(I_{df\_hz}\right)$ solar radiation are estimated, the solar gains of all opaque surfaces that are oriented at different directions and inclinations, as well as indoor air space through the fenestration system can be calculated following the calculation procedures described in Goswami (2004). The calculation procedure considers the orientation and inclination of the surface, the geographic location of the site (latitude and longitude), the hour of the day and the day of the year.

7.1 Indoor humidity models

In this subsection, the indoor humidity condition of the house, which is exposed to Carmacks weather conditions on the exterior and additional hygrothermal loadings in the interior, is simulated using four models. These are: the Class-model (Sandberg, 1995), ASHRAE Standard 160P proposed Simple and Intermediate models (ASHRAE Standard 160P, 2006) and the newly developed whole building hygrothermal model, HAMFitPlus. These models cover the three indoor humidity calculation procedures. These are: empirical, steady state and transient humidity calculation methods. The simulations are carried out for the time period when experimental data are available. Subsequently, the indoor humidity profiles of the house as simulated by the four approaches are compared to one another, and benchmarked against experimentally measured data. Detailed

descriptions on how these models are implemented, to predict the indoor humidity condition of the house, are discussed below.

7.1.1 Class-Model

Sandberg (1995) developed the indoor humidity Class-model based on the large-scale field survey results. Later on, the model is adopted in the European Standard (EN ISO 13788) to generate the indoor humidity boundary condition that is required in the hygrothermal performance assessment of building envelope components. In this method the indoor humidity conditions of buildings are classified into five classes: very-low, low, medium, high and very high (shown in Figure 7-9). For a given monthly mean outdoor temperature, each class is bound by minimum and maximum possible values of indoor and outdoor vapor pressure differences. The corresponding representative building types are: storage area, offices, normal family house, high-occupancy house and swimming pool, respectively. The first and very important step of this method is cataloging a given house into one of these classes. Although buildings with extreme humidity conditions (very-low and very-high) might easily be classified based on the intended use of the building (for instance storage and swimming pool respectively), in the rest of the cases, however, the classification can be subjective. For example, the medium class represents a "normal family house". However the characteristics of this house in terms of measurable variables such as number of occupants per square floor area and/or airthightness of the building are not defined. Without such measuring variable, categorizing a given family house into low, medium or high classes can be misleading since there is no basis to compare the house with a reference house, say "normal family house". The indoor

humidity level of the house considered in this study can be expected to lie in the medium or high humidity level, based on the available data on the use and number of occupancy of the building. As mentioned earlier, each class is bound by a minimum and maximum value. Thus, the probable region of interest for the house considered in this study is the shaded part of Figure 7-9. Since the indoor humidity prediction and comparison with the experimentally measured values are done during wintertime, where the monthly mean temperature is below 0°C (-19.0°C), the specific region of interest in this study is, therefore, the rectangular area shown in the same figure bounded by red lines. Consequently, for the house and time period considered here, the lower and upper limits of indoor and outdoor vapor pressure differences are 540 and 1080 Pa, respectively.

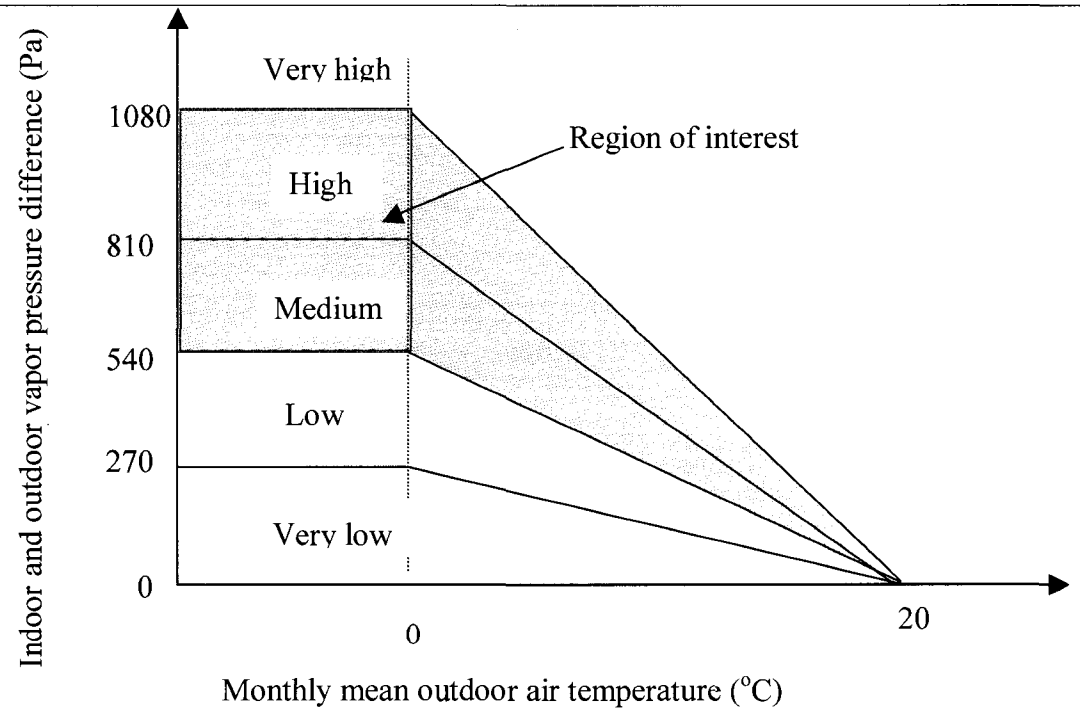

Figure 7-9 Indoor humidity classifications in Class model (Sandberg, 1995).

Thus, the indoor vapor pressure can be calculated from Equation [7.3].

$$\Delta p_v = p_v^i - p_v^o \qquad [7.3]$$

where: Δp_v is the indoor and outdoor vapor pressure difference, Pa

p_v^i is the indoor air vapor pressure, Pa

p_v^o is the outdoor air vapor pressure, Pa

The indoor humidity condition of the house can be expressed in terms of relative humidity, Equation [7.4], by rewriting Equation [7.3] and making use of the definition of relative humidity (ratio of vapor pressure and saturated vapor pressure).

$$p_v^i = \Delta p_v + p_v^o$$

$$\phi^i = \left(\frac{\Delta p_v + p_v^o}{p_{v\_sat}^i} \right) \times 100 \qquad [7.4]$$

where: ϕ^i is the indoor relative humidity, %

$p_{v\_sat}^i$ is the saturated vapor pressure of the indoor air, Pa

As observed from the experimental measurement, the indoor temperature of the house is nearly constant at 20°C, and the corresponding saturated vapor pressure $\left(p_{v\_sat}^i \right)$ is 2337 Pa. Consequently, the lower and upper bounds of the indoor relative humidity are defined by Equation [7.5] and [7.6], respectively.

For lower bound: $\Delta p_v = 540\,Pa$

$$\phi^i = \left(\frac{540 + p_v^o}{2337}\right) \times 100 \qquad [7.5]$$

For upper bound: $\Delta p_v = 1080\,Pa$

$$\phi^i = \left(\frac{1080 + p_v^o}{2337}\right) \times 100 \qquad [7.6]$$

The only variable in these equations is the outdoor vapor pressure, which is available in the local weather data.

7.1.2 ASHRAE Standard 160P Simple indoor humidity model

ASHRAE Standard 160P (2006) outlines a standard procedure for hygrothermal performance evaluation of building envelope components. In this standard, methods for setting-up outdoor and indoor climatic loadings are proposed. For the indoor hygrothermal loading, three indoor models are proposed, namely: Simplified, Intermediate and Full Parametric calculation methods. The graphical representation of the Simplified method is shown in Figure 7-10. In this model, the indoor relative humidity is kept constant at 40% (P_1) and 70% (P_2) when the 24-hour average outdoor temperature is below -10°C and above 20°C, respectively. At times when the 24-hour average outdoor temperature lies between -10 and 20°C, the indoor humidity is determined by performing a linear interpolation of the two points 'P_1' and 'P_2'. The step line that joins these two points has a slope of one and y-intercept value of 50%. The only set of data that is required to calculate the indoor relative humidity of the house under consideration is outdoor temperature, which is available in the weather data file.

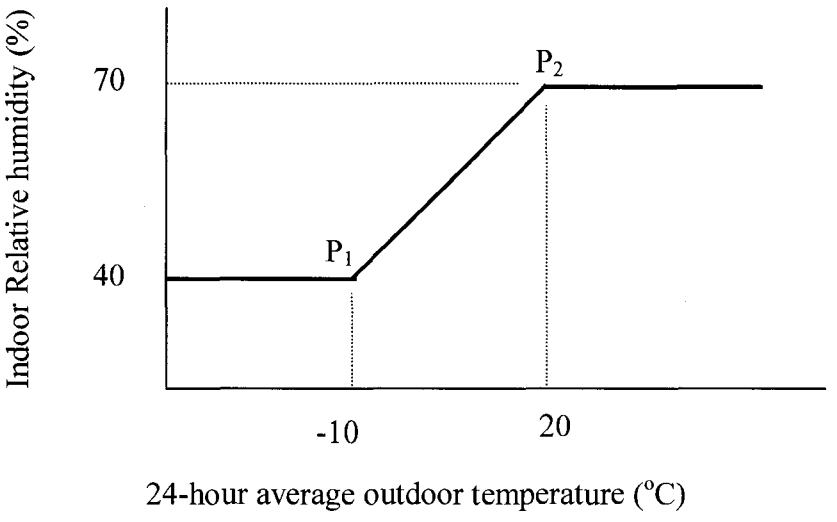

Figure 7-10 ASHRAE Standard 160P Simple humidity model.

7.1.3 ASHRAE Standard 160P Intermediate indoor humidity model

Unlike the Simplified calculation method, which depends only on outdoor temperature, the Intermediate model accounts for four important building parameters; these are: building size, local weather conditions, moisture generation, and ventilation rates. The model equation, which applies for classes of buildings that operate without dehumidification or air-conditioning (as the house considered here), is given by Equation [7.7]. The calculation procedure is similar to the steady-state model used in Loudon (1971), except that in the ASHRAE Intermediate model a 24-hour running average outdoor vapor pressure is used instead of instantaneous vapor pressure that is used in Loudon (1971).

$$p_v^i = p_{v\_24h}^o + \frac{c\dot{m}}{Q_{ventilation}} \qquad [7.7]$$

where:

p_v^i is the indoor air vapor pressure, Pa

$p_{v\_24h}^o$ is the 24-hour running average outdoor air vapor pressure, Pa

c is a constant 1.36×10^5 m^2/s^2

$\dot{m}$ is the moisture generation rate (kg/s)

$Q_{ventilation}$ is the ventilation rate, m^3/s

As explicitly stated in the ASHRAE standard 160P (2006), the basis for using running average instead of instantaneous vapor pressure is to "account for moisture buffering effects of materials". This is, though, a simplistic approach of modeling the moisture buffering effects of building envelope components. The moisture generation rate ($\dot{m}$) is determined based on the data assembled from the work done in the IEA Annex XIV (IEA 1991) and TenWolde (1994a, b), and latter compiled in TenWolde and Walker (2001) and presented in the ASHRAE standard 160P (2006) as in Table 7-1. The table shows the estimated daily moisture production rates of occupants living in the same house. These rates are: 8 kg/day for 1 or 2 adult; 4 kg/day for the first child; 2 kg/day for second child, and 1 kg/day for additional child. According to the standard, the total daily moisture production rate of a building is calculated from Table 7-1 based on the number of occupants. As reported in the survey document, a family of two adults and four children occupies the house under consideration. Following up the moisture generation estimation scheme, the total daily moisture production by the household is estimated to be 16 kg/day.

Table 7-1 Estimated moisture generation rates based on number of occupants

	Number of Occupants	Moisture generation rate	
		L/day	g/s
1 bedroom	2	8	0.09
2 bedrooms	3	12	0.14
3 bedrooms	4	14	0.16
4 bedrooms	5	15	0.17
Additional bedrooms	+1 per bedroom	+1	+0.01

The indoor relative humidity of the house can be written in the form of Equation [7.8], after substituting the assumed daily moisture generation rate 16 kg/day (1.85E-4 kg/s) and indoor saturated vapor pressure (2337 Pa) in Equation [7.7]

$$\phi^i = \frac{1}{23.37}\left(p^o_{v\_24h} + \frac{25.18}{Q_{ventilation}} \right) \qquad [7.8]$$

The reduced ASHRAE Intermediate model, Equation [7.8], suggests that for a house of known size and occupancy, the indoor relative humidity of the house depends on the outdoor vapor pressure, which can be constructed from the outdoor temperature and relative humidity data (available in the weather data file), and ventilation rate. The calculation procedure for estimating the time varying ventilation rate will be discussed in the whole building hygrothermal modeling section below.

7.1.4 Whole building hygrothermal model—HAMFtiPlus

Whole building hygrothermal modeling is referred to in ASHRAE Standard 160P as a "Full Parameter Calculation Method". Unlike the Intermediate model, where the moisture source is a lumped sum and moisture exchange (addition or removal from the indoor space) takes place only by ventilation, a whole building hygrothermal model implements these factors in a more detailed manner and also deals with the dynamic interaction between indoor environment and the building enclosure. The advanced model incorporates among other things the following: moisture buffering effects of materials which could act as a moisture source and sink; moisture removal due to condensation on cold surfaces such as on windows; moisture addition by evaporation from water reservoirs and from building envelope components that have higher initial moisture content, as well as moisture exchange through building envelope components by convection and diffusion. Thus, to perform a whole building hygrothermal analysis, the building envelope components, indoor heat and moisture sources as well as mechanical systems need to be characterized in detail.

Full implementation of the newly developed whole building hygrothermal model, HAMFitPlus, to predict the indoor humidity condition of the house under consideration, is discussed in detail below. Some parameters such as solar radiation, air leakage due to wind pressure and internal heat gain profiles are discussed in detail for completeness of the work although they are not dominant factors in the case considered here (winter period, high latitude location, low wind speed compared stack effect and heating system with infinite heating capacity). The basic input parameters of the model are: 1) building description in terms of its geometry, orientation and building site (local topography and

weather conditions); 2) building enclosure, which includes building components (walls, roof, floor, windows and doors), configurations of layers of materials and their hygrothermal properties; 3) internal heat and moisture generation rates; and 4) types and capacities of mechanical systems for heating, cooling, humidification, dehumidification and ventilation. In this study, though, only heating and ventilation systems are relevant since cooling, humidification and dehumidification equipments are reportedly not present in the house. Most of the necessary input data are extracted from the survey report (Hood, 2006), and any additional input data that are required but not documented in the survey report are taken from literature. The four basic input data are discussed in the following sections.

Building description

The building is a pre-manufactured single detached house, which has a rectangular shape and 18° sloped roof. It is placed on a deck that is 0.914 m above ground and enclosed with OSB sheathing boards that create unheated crawl space underneath. The house is surrounded by trees in the northeast and northwest directions. This information is important to define the wind speed profiles in the respective directions, and subsequently to calculate the air leakage rate due to wind pressure. The local climatic conditions to which the house is exposed are discussed at the beginning of this chapter.

The floor area and volume of the house are 81.9 m^2 and 196 m^3, respectively. Knowledge of the actual floor plan of the house is important to estimate the interior partition walls areas that might play an active role in moisture absorption and desorption, and thus affect the indoor humidity of the house. Unfortunately, this information is not documented in the survey report. Consequently, the assumed floor plan is constructed

based on the information available in the survey report such as floor area, number of bedrooms, bathrooms, windows size and locations, photos, and typical floor plans of manufactured houses of the same floor area that are advertised in manufacturers website (for example http://www.palmharbor.com/our-homes/floor-plans). The orientation and the assumed floor plan of the house are shown in Figure 7-11. The house is 19.5 m long and 4.2 m wide, and its front elevation is oriented to the northwest direction. The house has two bedrooms, a living room, a kitchen and a bathroom. The total surface areas of the exterior and partition walls are 118.68 and 76 m^2, respectively. The partition wall surface area includes the surface areas of both sides of the wall since these surfaces have the same moisture buffering effect on the indoor air humidity

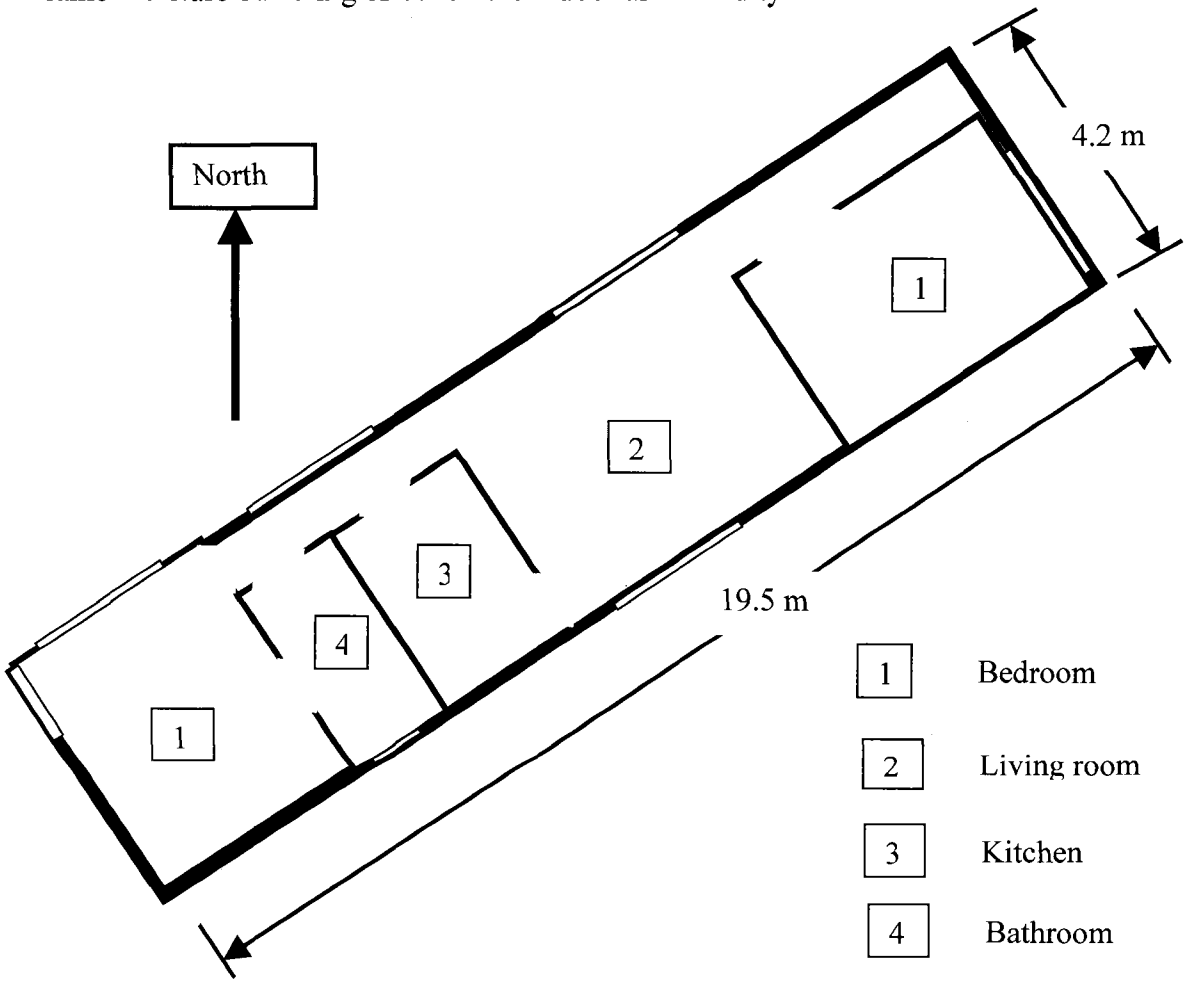

Figure 7-11 Floor plan and orientation of the house

Building enclosure

The house is built with a typical wood-frame construction with layers of materials to control heat, air and moisture movement through the building components. The exterior walls, floor and roof are all made of wood frame structures with layers of materials in sequence listed in Table 7-2 below. The wood frames of exterior walls, floor and roof are constructed from 2" by 6'', 2" by 8" and 2" by 4" cross-section spruces, respectively. The exterior wall comprises of sheet metal (as a cladding material), sheathing membrane, sheathing board, insulation in the stud cavity, vapor barrier and finally gypsum board as a finishing layer. The roof is protected from rain penetration into the structure with asphalt-shingles that are installed on top of the sheathing board. To control vapor flow, the vapor barrier is installed at the interior surface of the insulation. The floor is covered with linoleum tile, which is installed on top of the interior sheathing board and act as a vapor barrier. The cavity between the floor sheathing board and the belly wrap, which is exposed to the crawl space, is filled with glassfiber insulation.

Table 7-2 Materials used for building envelope components

	Exterior Wall	Roof	Floor
Interior layer	12.5 Gypsum board	12.5 Gypsum board	12.5 Plywood
Vapor barrier	Polyethylene sheet	Polyethylene sheet	Linoleum tile *
Butt insulation	RSI 3.5 (m^2K/W)	RSI 7.0 (m^2K/W)	RSI 4.9 (m^2K/W)
Sheathing board	12.5 mm OSB	12.5 mm OSB	--
Weather barrier	Building paper	--	--
Exterior layer	Sheet metal	Asphalt shingles	Paper board

* The tile is installed on top of plywood

The hygrothermal properties of the OSB, plywood, gypsum board and insulation are taken from the ASHRAE Research project RP-1018 *'A Thermal and Moisture Transport Database for Common Building and Insulating Materials'* (Kumaran et al., 2002). The moisture storage capacity, heat capacity, liquid permeability and thermal resistance of the membranes, linoleum tile, sheet metal and asphalt shingles are assumed to be negligible. The vapor permeability of the polyethylene sheet and building paper are taken from ASHRAE Fundamental (2005), and infinite vapor flow resistance is assumed for linoleum tile, sheet metal and asphalt shingles. In fact, these materials can be replaced by equivalent surface transfer coefficients for the purpose of model calculations. The absorptivity and emissivity of the external walls and roof surfaces are estimated to be 0.40 and 0.60, and 0.90 and 0.96, respectively.

The interior-finishing layer of the walls and ceiling, that is gypsum board, interacts with the indoor air and modulates the indoor humidity. Its moisture absorption or desorption as well as moisture movement through this layer depends on the temperature distribution across its thickness. To accurately establish the temperature profile across the gypsum board, the energy balance equation need to be solved for the whole building envelope component. However, for the problem at hand (indoor humidity prediction) the moisture balance equation needs to be solved only for the gypsum board since it is decoupled, in terms of moisture flow, from the rest of the building component layers by the polyethylene sheet at the back, which creates near closed boundary condition and limits moisture flow to and from the cavity. Subsequently, the single most important material whose moisture storage and transport properties need to be defined well is the gypsum board.

The house has seven windows with a total area of 15% of the floor area. The orientation and size (shown in bracket) of these windows are as follows: two windows on southeast wall (1.58 and 0.46 m^2); one window on southwest wall (1.08 m^2); three windows on northwest wall (1.3, 1.58 and 3.72 m^2) and one window on northeast wall (2.7 m^2). As reported in the survey document, the windows are standard double-glazed windows with air space between glazing, and vinyl frame. Accordingly, the overall heat transfer coefficient (U-value) and solar heat gain coefficient of the windows are assumed to be 2.87 W/m^2K and 0.6, respectively (ASHRE Fundamental, 2005). The house has two external doors (1.87 m^2 area each) that are installed on the northeast and northwest walls. It is reported that the core material of the doors is polystyrene, and the effective thermal resistance of the door is estimated to be 0.98 m^2K/W.

Indoor heat and moisture generations

The house is occupied by a family of two adults and four children. The number of occupants in the daytime is five, and six in the evening six. At a given time, the heat and moisture production in the house vary depending on the number of occupants and type of activities they are engaged in. Unfortunately, the types and schedules of occupants' indoor activities in a typical day were not part of the survey questions, and consequently, the heat and moisture generation profiles are not readily available. These profiles are essential to predict the indoor humidity and temperature conditions of the house using the whole building hygrothermal model, HAMFitPlus. Here, the best possible profiles are outlined based on information documented in the survey report and available in the literature. The daily moisture generation profile is developed as follows: the total daily moisture production (16.0 kg/day) is distributed through out the day based on assumed

occupants daily routine and the associated moisture production rates of each activity. Christian (1994) gave the breakdown of the daily moisture production rates of family of four (two adults and two children) due to occupants' main activities such as dishwashing, cooking, taking shower, and respiration and perspiration of occupants (shown in Table 7-3). The original data, which is for a family of four, is extrapolated to a family of six to reflect the occupant size in this study. The extra moisture source (4.01 kg/day), which is the difference between the total moisture production in the house as estimated per ASHRAE standard 160P (2006) and the sum of the extrapolated moisture production in Table 7-3, is assumed to be a background moisture release. This moisture source is assumed to be released constantly throughout the day, and accounts for moisture release from floor mopping, water sinks, laundry (washing and drying), plants and other unforeseen sources. As documented by the surveyor, significant amount of window condensation is frozen on the window frame (as the average outdoor temperature during the simulation period is $-19^{o}C$) and the lower portion of the walls under the windows have shown visible moisture problem. Moisture release to the indoor air from these surfaces is assumed to be part of the 4.01 kg/day background moisture source.

Table 7-3 Daily moisture productions by occupants' activities

Activity	Family of Four (kg/day)	Extrapolated for family of six (kg/day)
Dishwashing	0.5	0.80
Cooking	1.62	2.50
Shower	1	1.50
People respiration/perspiration	5	7.50 (six people-night time) 6.25 (five people-day time)

Once again, the moisture production of each activity is broken-down in time, based on the assumed occupants' daily activities. Figure 7-12 shows the moisture production profile of the house along with the assumed occupants' activities in a typical day. The numbers in the boxes indicate the amount of moisture production during an activity that is carried on from the beginning to the end of the box in kilogram. In this schedule, dishwashing at breakfast, lunch and dinner preparation times are assumed to generate 0.1, 0.35 and 0.35 kg of moisture, respectively. Addition of these distributed moisture productions gives the daily total moisture production during dishwashing (0.8 kg/day), which is set in Table 7-3. All occupants are assumed to take showers in the morning between 6:00-9:00 h, which consequently results in a release of 1.5 kg of moisture and a peak in the diurnal moisture load profile. Assuming light cooking in the morning compared to lunch and dinner times, the total moisture production due to cooking (2.5 kg/day) is distributed into 0.5, 0.9 and 1.1 kg, in the respective periods. The moisture production by occupants due to respiration and perspiration between 9:00-17:00 h is assumed to be 2.08 kg (when the number of occupants is five), and 5 kg for the rest of the time (when the number of occupants is six). The background moisture production (4.01 kg), which accounts for all the unknown moisture sources, is uniformly spread over 24-hour duration. Finally the constructed diurnal moisture generation schedule looks like in Figure 7-12. The maximum moisture generation (1184 g/hr) occurs during the morning period between 6:00-9:00 h, followed by dinnertime (17:00-20:00 h) at the rate of 968 g/hr. The occupants are assumed to be at rest from 13:00 to 17:00 h (after lunch until the time to prepare dinner), and consequently, the moisture generation rate at this period is the lowest (432 g/hr).

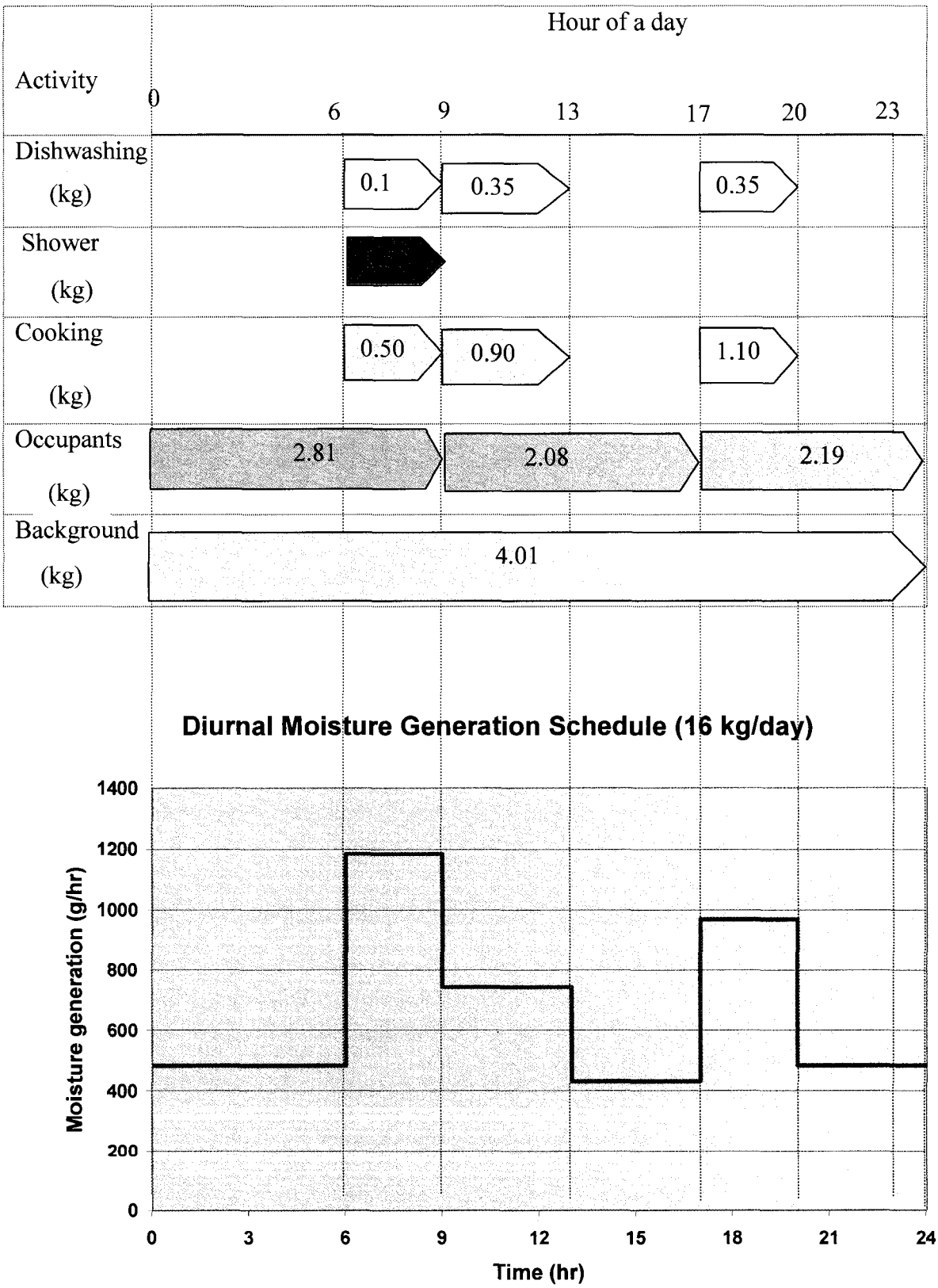

Figure 7-12 Daily moisture generation profile

The diurnal heat generation schedule shown in Figure 7-13 is formulated in the same fashion as the moisture production rate, which is based on assumed occupants' daily routines. This information is specifically important for simulation cases where the indoor temperature and energy demand are computed. Occupants are one of the heat sources that can raise the indoor temperature. In this work, the sensible heat gain from an occupant is approximated to be 67 W, which is adopted from Athienitis and Satamouris (2002). Assuming constant and equal heat release rates for all occupants, the total sensible heat gain during 9:00-17:00 h (five occupants) and all other time (six occupants) are approximated to be 335 W and 402 W, respectively. The periodic heat source that is associated with cooking can significantly raise the indoor temperature as well. The corresponding heat release to the indoor air space during breakfast (6:00-9:00 h), lunch (9:00-13:00 h) and dinner (17:00-20:00 h) preparations time are approximated to be 750, 2000 and 2000 Watt-hour, respectively. Moreover, the family is assumed to use a computer between lunch and dinnertime (13:00-17:00 h), whose heat generation rate is approximated to be 125 W (ASHRAE Fundamental, 2005). During the evening (17:00-23:00 h), lighting and entertainment appliances such as television are assumed to generate an additional heat gain of 350 W. Assembling these heat generation items yields a typical diurnal heat generation schedule for the house under consideration, Figure 7-13. The numbers in the boxes indicate the heat generation during an activity that is carried on from the beginning to the end of the box in Watt-hour. The lowest heat generation rate (402 Watts) occurs during sleeping time (23:00-6:00 h next morning), and the maximum (1419 Watts) during dinnertime (17:00-20:00 h). In the HAMFitPlus simulations, the internal heat gain at a time (from the developed heat generation profile) is assumed to be composed of 50% radiative and 50% convective heat gains.

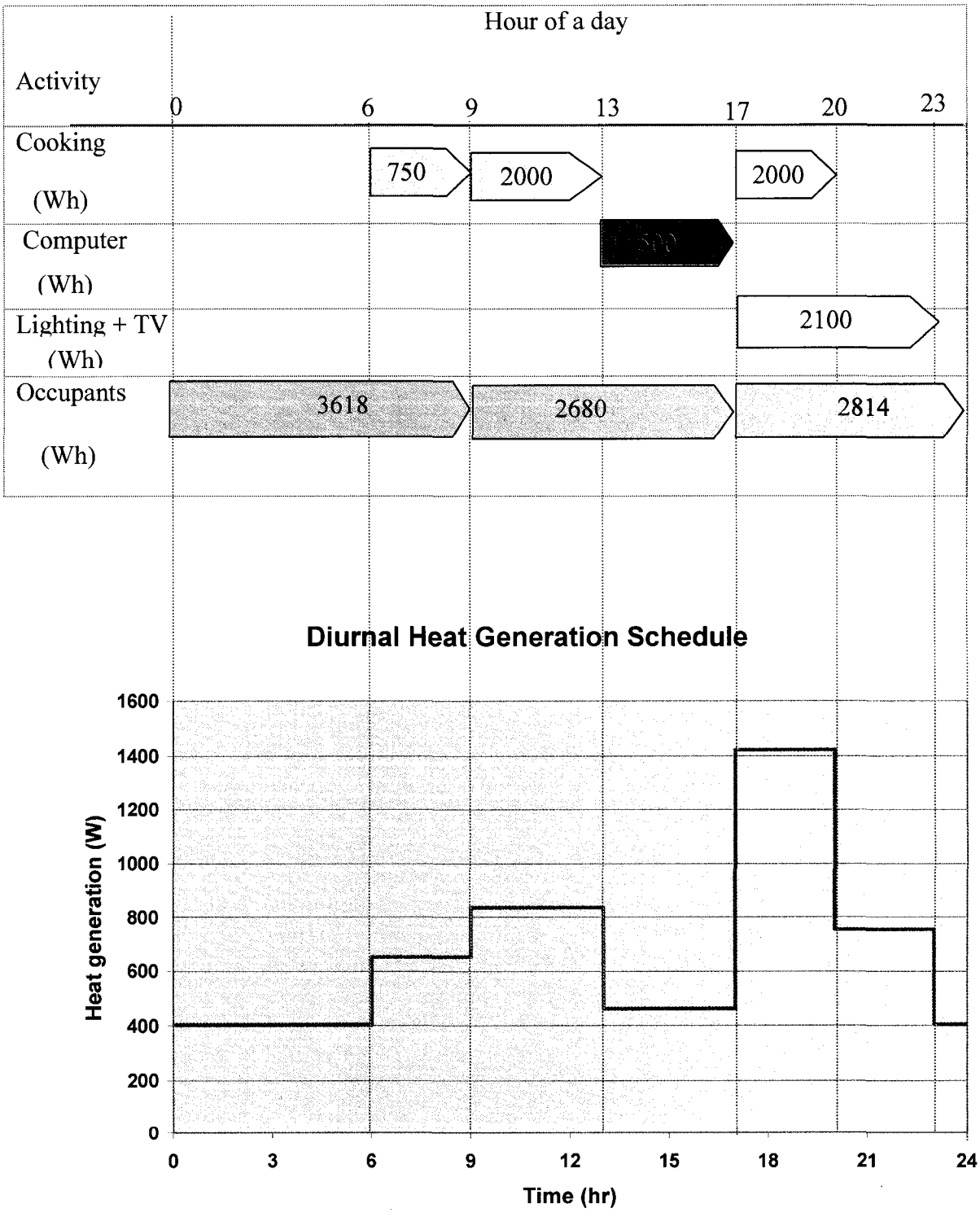

Figure 7-13 Daily heat generation profile

Mechanical systems

The house is equipped with a mechanical heating system, which consists of oil fired-furnace and forced air heat distribution system (fan and ducts). The actual heating capacity of the heating system is not reported in the survey document, but the measured indoor air temperature of the house during the monitoring period suggests that the system has enough heating capacity to maintain the indoor air temperature at least at 20°C. Subsequently, an infinite heating capacity is assumed for simulations cases (using HAMFitPlus) where heating loads are calculated based on an indoor temperature around 20°C. The basic assumption, here, is that the heating demand is always less than the actual heating capacity of the equipment. The house also has a mechanical ventilation system, more specifically exhaust fans. The fans are installed in the bathroom and kitchen. However, as the surveyor reported, they are not usually operational due to malfunction, otherwise kept turned-off to avoid the noise that is generated from their operation. Consequently, the apparent means of ventilation takes place by natural ventilation mechanisms through unintended openings (airleakage) and/or through intentional openings (e.g. window openings). For the simulation period considered in this study, that is when the outdoor temperature is very cold and opening of windows is impractical, the natural ventilation is assumed to occur by only airleakage. The air exchange rate due to the time varying wind and stack pressure is calculated using a simple single zone infiltration model. The model is developed based on conservation of mass (the total mass flow rates of infiltrated and exfiltrated air across the building envelope are equal) as outlined in Hutcheon and Handegord (1995). In the model the neutral pressure level is first determined to compute the stack pressure at any given height of the building envelope component. Moreover, the wind pressure at the surfaces

of the four walls and roof are determined from the local wind velocity profile and wind pressure coefficient of the respective surface. The wind pressure coefficient for a surface depends on the angle between the line perpendicular to the surface and the wind direction (Orme et al. 1998). The other input data that are essential to estimate the natural ventilation rate of the house are the air leakage characteristics of the different building envelope components (walls and roof). These data are generated based on the air-tightness test results of the whole house. The test is carried out by depressurization of the house. The total airleakge rate of the house at 50 Pa depressurization is 5.04 ACH (air exchange per hour), which is equivalent to 0.2744 m^3/h (Hood, 2006). Although the total airleakage rate for the house at the test condition is known, the proportion of airleakage through the exterior walls, roof, floor, wall window interface, wall door interface and other openings are not known. In this work, for lack of better data, it is assumed that two-third of the total airleakage is through the exterior walls, and the rest through the roof. The floor is assumed to be airtight since the top layer is airtight. Subsequently, the proportion of airleakage through the exterior walls and roof are 3.36 ACH (0.1829 m^3/hr) and 1.68 ACH (0.0915 m^3/hr), respectively. And the airleakage coefficient of the respective building envelope components, C, can be calculated using Equation [7.9].

$$Q_a^v = A \times C \times \Delta P^n \qquad [7.9]$$

where:

Q_a^v is the airleakag rate (kg/s)

A is the airleakage area (m^2)

C is the airleakage coefficient ($kg/s.m^2.Pa^n$)

ΔP is the pressure difference across the building envelope component (Pa)

n is the flow exponent (dimensionless)

For instance, the airleakge coefficients for the exterior walls is determined as follow:

-The total volume of the house is 196 m^3.

-The total airleakage at 50 Pa depressurization test is 5.04 ACH or

in volume flow rate $\left(\frac{Building\ volume\left(m^3\right) \times ACH\left(m^3/m^3hr\right)}{3600}\right)$=0.2744 m^3/s

-The total mass flow rate $\left(Q_a^v = Volume\ flow\ rate \times air\ density\right)$ is 0.32928 kg/s,

where the density of air at the test condition is 1.20047 kg/m^3.

-The airleakage through exterior walls $\left(Q_{a\_w}^v = \frac{2}{3}Q_a^v\right)$ is 0.21952 kg/s.

- The flow coefficient for the exterior walls (C_w) is calculated by rewriting Equation [7.9] into: $C_w = \frac{Q_{a\_w}^v}{A_w \times \Delta P^{n_w}}$ where, A_w is the total area of the exterior surfaces (118.68 m^2), n_w is the flow exponent for the exterior walls (0.67) and ΔP is the pressure difference across the surfaces (50 Pa).
- Finally, the flow coefficient for the exterior walls is 1.4595E-4 $kg/s.m^2.Pa^{0.67}$

The flow coefficient for the roof is determined in a similar fashion as the exterior walls, and is equal to 9.7302E-05 $kg/s.m^2.Pa^{0.67}$. Figure 7-14 shows the calculated natural ventilation rates of the house during the monitoring period. During this period the

airleakage rate varies from 0.13 to 0.34 ACH, while the average is 0.23 ACH. The infiltration model involves determination of the neutral pressure level, local wind speed, surface pressure coefficients and airleakage coefficients of building envelope components. Except for the determination of the airleakage coefficients of the building envelope component, which need to be defined once, all the other steps are repeated whenever the wind or the temperature conditions changes. In the simulation case considered here where the indoor temperature is nearly stable and the weather data is hourly, the air exchange rate computations are done hourly. These calculated air exchange rate values are used as well in the ASHRAE Standard 160P Intermediate model to predict the indoor humidity of the house under consideration.

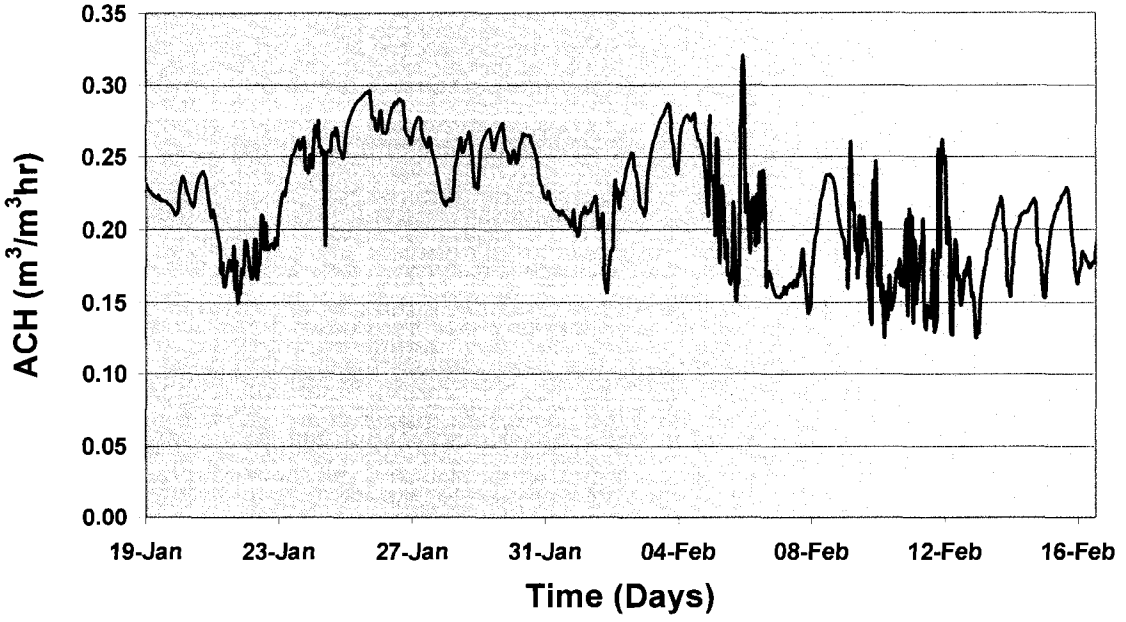

Figure 7-14 Natural ventilation rate of the house during the monitoring period

7.2 Indoor humidity prediction and discussion

The hourly averaged, measured, indoor temperature and relative humidity of the test house during the monitoring period of January 19 to February 15 are shown in Figure 7-15 and Figure 7-16, respectively. In general, the indoor temperature is relatively stable with 3°C fluctuation range from the average value, which is 19.7°C. The lowest and highest indoor temperatures are 12.9°C and 22.6°C, which are recorded on January 29 and February 9, 2006, respectively. Unlike, the temperature that is controlled by thermostat and adjusted by the mechanical heating system, the house has neither an indoor humidity control system nor auxiliary unit for addition or extraction of moisture to/from the indoor space. Hence, the relative humidity profile of the house is rather variable compared to the temperature profile. The average indoor relative humidity for the monitoring period is 39.8%, while the hourly values can vary from the lowest value of 23.8% to the maximum value 57.3%. As can be shown in the Figure 7-16, the indoor relative humidity is in decreasing trend (from 50 to 23.8%) during January 23 and January 28. In about the same period, the outdoor temperature, Figure 7-3, is also in decreasing trend (–4 to –40°C). This results in an increase in temperature difference between the indoor and outdoor, thereby increasing the stack pressure and consequently the natural ventilation (airleakage) (Figure 7-14). Since the moisture content of the outdoor air at this period (low temperature) is insignificant, the high ventilation rate takes away more moisture than it brings in to the indoor space, resulting in decreasing relative humidity as shown in Figure 7-16. Relatively high indoor relative humidity level is observed in the second week of February. During this period the outdoor temperature is relatively higher, which results in low stack pressure (ventilation). For the house and

climate considered in this study, the outdoor temperature plays a major effect in regulating the indoor humidity conditions through its predominant effect on stack pressure—ventilation. Low humidity level is expected during very cold outdoor temperature (due to enhanced stack effect-ventilation) and relatively high humidity in cold outdoor temperature conditions (minimized stack effect-ventilation). This implies that problems associated with high indoor humidity such as mold growth and possibly degradation of building envelope components can be expected during warm winter periods (early or late periods of winter). In other words, a weather condition that does not permit enough natural ventilation by opening windows as is the case in summer, or that creates a high natural ventilation due to very cold outdoor temperature (stack pressure), may pose problems associated with high indoor humidity unless mechanical ventilation is used.

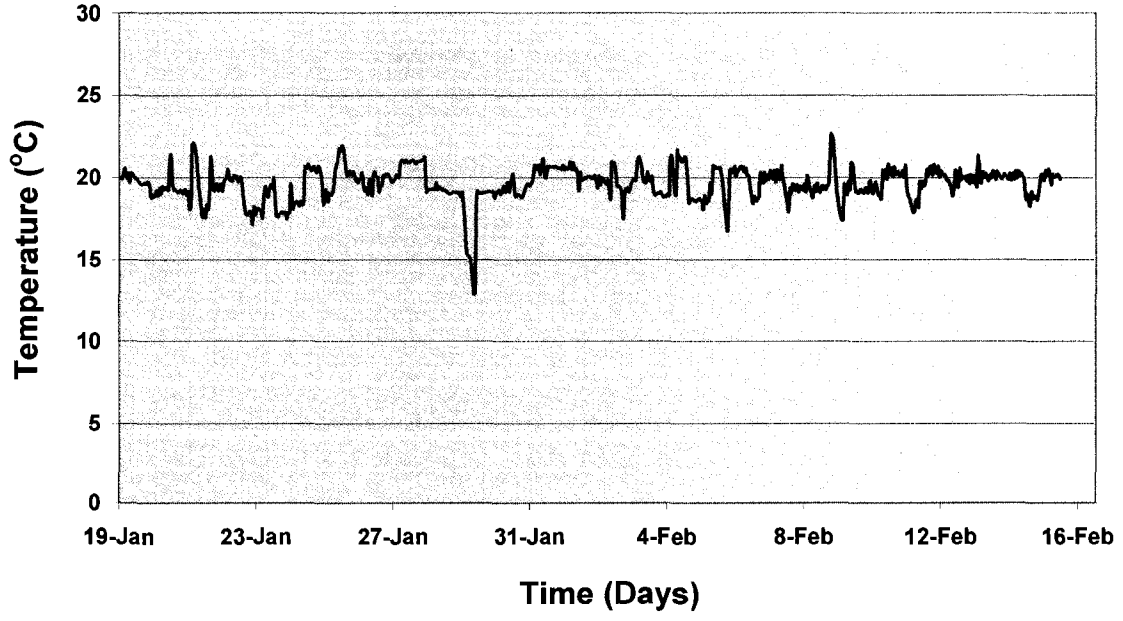

Figure 7-15 Measured indoor temperature of the house

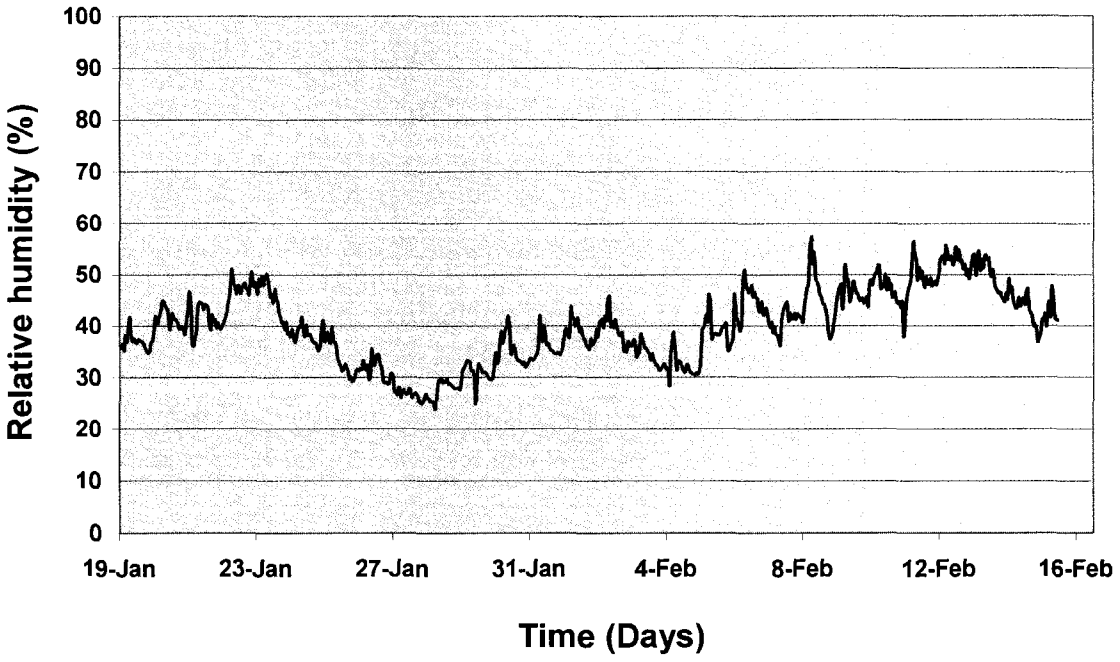

Figure 7-16 Measured indoor relative humidity of the house

The indoor relative humidity of the test house as predicted by Class Model is presented along with the measured data in Figure 7-17. The hourly-averaged measured indoor relative humidity is shown in blue; and the upper and lower bounds of the relative humidity as predicted by the Class model are shown in pink and green curves, respectively. As explained in Section 7.1.1, this model is an empirical model that gives the possible indoor relative humidity range of an assumed class of building type rather than a definite value. The base relative humidity values of the lower and upper bounds, which are the limiting cases in Equation [7.5] and [7.6] when the outdoor vapor pressure is zero, are 23 and 46%, respectively. This creates a bandwidth of 23% relative humidity. Observation of the outdoor temperature, Figure 7-3, and the predicted lower and upper bound relative humidity values suggested that, generally, the relative humidity increases

with outdoor temperature. This is because the level of increase of relative humidity from a base value depends on the humidity level of the outdoor air (vapor pressure), which is generally higher at relatively warm temperature due to its higher moisture carrying capacity.

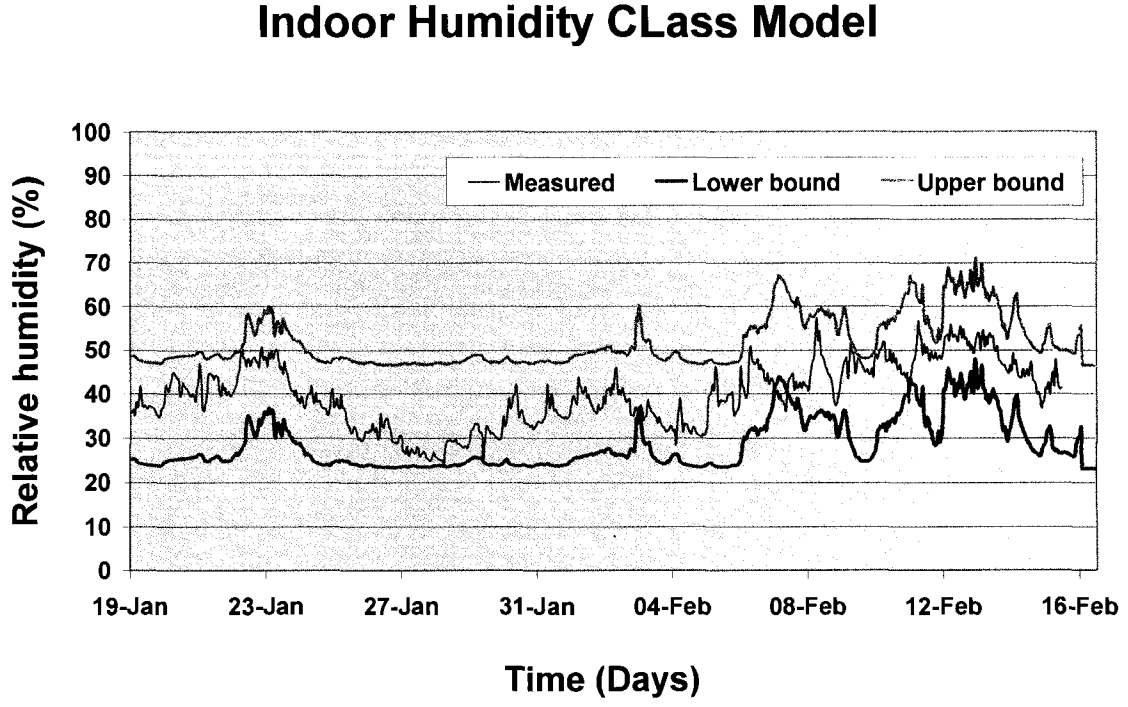

Figure 7-17 Indoor relative humidity of the house as predicated by Class model

As can be seen in Figure 7-17, the measured indoor relative humidity values lie between the upper and lower bound values. Indeed, a median of the two bound values may agree better with the measured data than either of the two bounds, which consistently over and underestimate the indoor relative humidity values, respectively. However, this information is deduced only after comparing with (looking at) the measurement data, and cannot be said before hand. In fact, classification of a given

building to one of the five categories is the basic problem of the Class model. There is no definite classification guideline, for example floor area per occupant to classify a house of interest whether it is normally or over-crowdedly occupied. This kind of guidelines can help avoid the arbitrarily assignment of a building to different classes (say Class three or four), and subsequently used a quick estimation of a possible indoor humidity range of a building. But the model still will not be a deterministic tool since it grossly assumes that all buildings of a given category in a given location exhibit identical indoor relative humidity conditions regardless of the specific features of the building under investigation such as: building site, orientation, size, airtightness, occupants' behavior, building materials, construction details such as window type and size (windows can remove moisture by condensation), size and type of interior furnishing materials, which might have moisture buffering effects, HVAC system (presence and type of mechanical ventilation, humidification and dehumidification systems) and any other specific features of the building of interest.

The indoor relative humidity prediction of the house using the ASHRAE Standard 160P Simple and Intermediate models along with the measured data are shown in Figure 7-18. Again here, the measured data is represented in blue line and the Simple and Intermediate models are in orange and cyan color lines, respectively. As can be seen in the figure, the Simple model predicts 40% indoor relative humidity for most of the monitoring period, which is the model's lowest cutoff value. This is due to the fact that the twenty-four hours average outdoor temperature is below $-10^{o}C$ for most of the time. At times when the average outdoor temperature is over $-10^{o}C$ (in the linear region of Figure 7-10) a better agreement with the measured data is observed. Although, the prediction of the Simple model is good for the case considered here, in general the model

should be limited to first-order approximation of indoor humidity. This is due to the fact that the model ignores the specific features of the house under consideration similar to the Class model and solely depends on outdoor air temperature condition. According to this model, all houses in Carmacks will still have the same indoor relative humidity regardless of the level of occupancies, airthighness or any other factors, which may not be the case in reality. The Intermediate model, as the name implies, is an advanced model compared to the Simple model. However, for the problem considered here, the Simple model predicts results rather reasonable and relatively close to the measured indoor relative humidity when compared to those of the Intermediate model, Figure 7-18. As shown in the figure, the Intermediate model consistently over-predicted the indoor relative humidity of the house during the entire monitoring period. Since the ventilation (airleakage) rate, which is one of the important parameters of this model, is strongly influenced by the outdoor temperature. The indoor relative humidity, in general, follows the outdoor temperature profile (Figure 7-3).

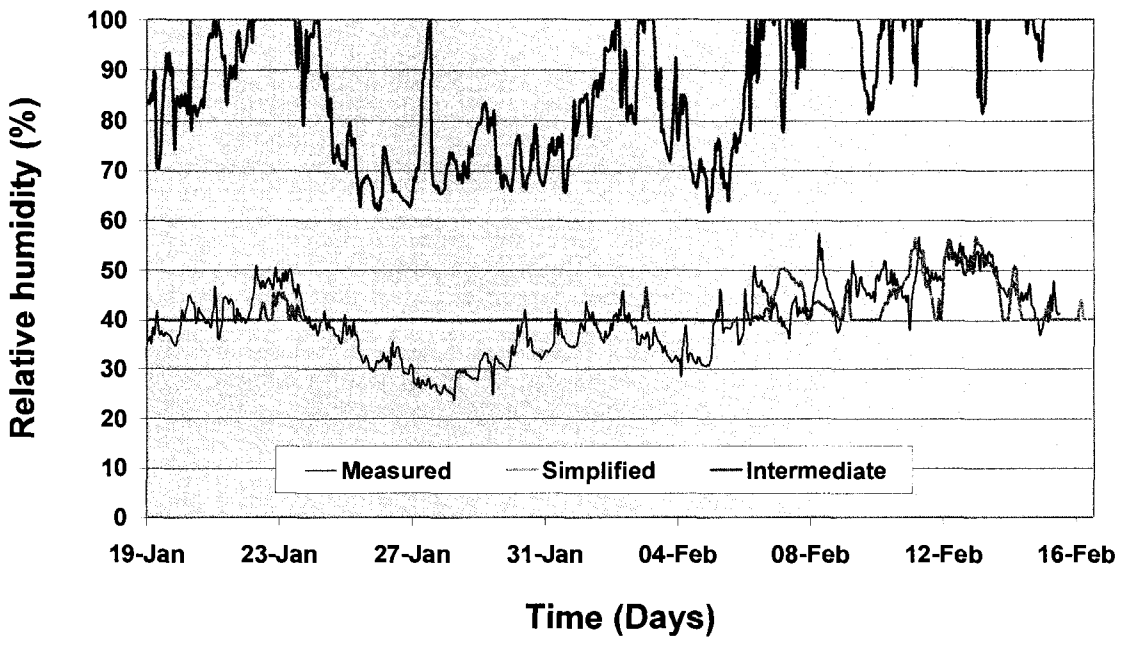

Figure 7-18 Indoor relative humidity of the house as predicated by ASHRAE Standard 160P Simple and Intermediate models

As can be seen in Figure 7-18, the Intermediate model's prediction of the indoor relative humidity of the house is excessively high when compared with the measured data. The main reasons for the unrealistic high prediction are because the model: 1) does not incorporate moisture removal by window condensation, which is important in cold climate and 2) does not have established upper and lower threshold values similar to the Simple model. Without these modifications the applicability of the model is limited to low occupancy houses, and seasons when no or little window condensation is expected. For the house (occupancy and weather conditions) considered in this study, a significant amount of moisture that is generated in the house is removed from the indoor air by

condensing on the window, Figure 7-19. The outdoor temperature is so cold that the condensate is frozen on the window surface and frame.

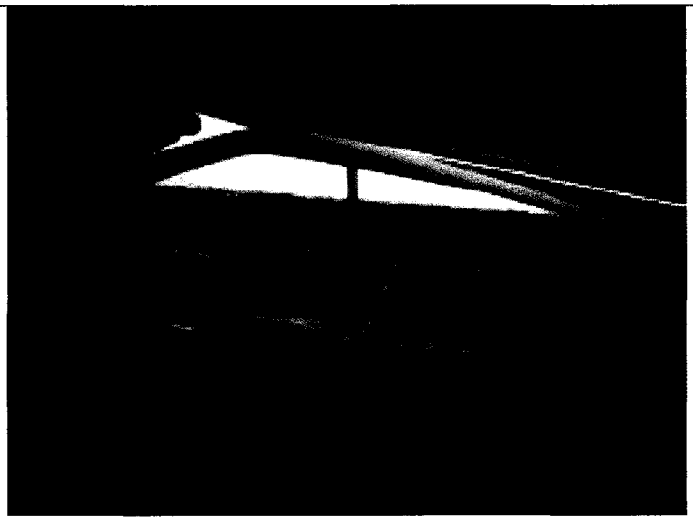

Figure 7-19 Excessive window condensation (Stad 2006)

The prediction of the indoor relative humidity of the house using the whole building hygrothermal model, HAMFitPlus, is proven to be the best of all the models considered in this study as seen in Figure 7-20. Unlike the empirical and ASHRAE Standard 160P models, HAMFitPlus takes into account the specific features of the house including building materials used, moisture and heat generation profiles, moisture removal due to window condensation, and moisture absorption and desorption effects of building envelope components and furnishing. In the present simulation, the furnishing materials are represented as an interior partition walls (if detailed information is available on furnishing separately, this can be directly used as an input). In general, the model treats the house as a system and integrates the mechanical systems, building envelope components, and indoor heat and moisture sources/sinks. Modeling of these components dynamic interactions yields simulation results that agree very well with the measured data.

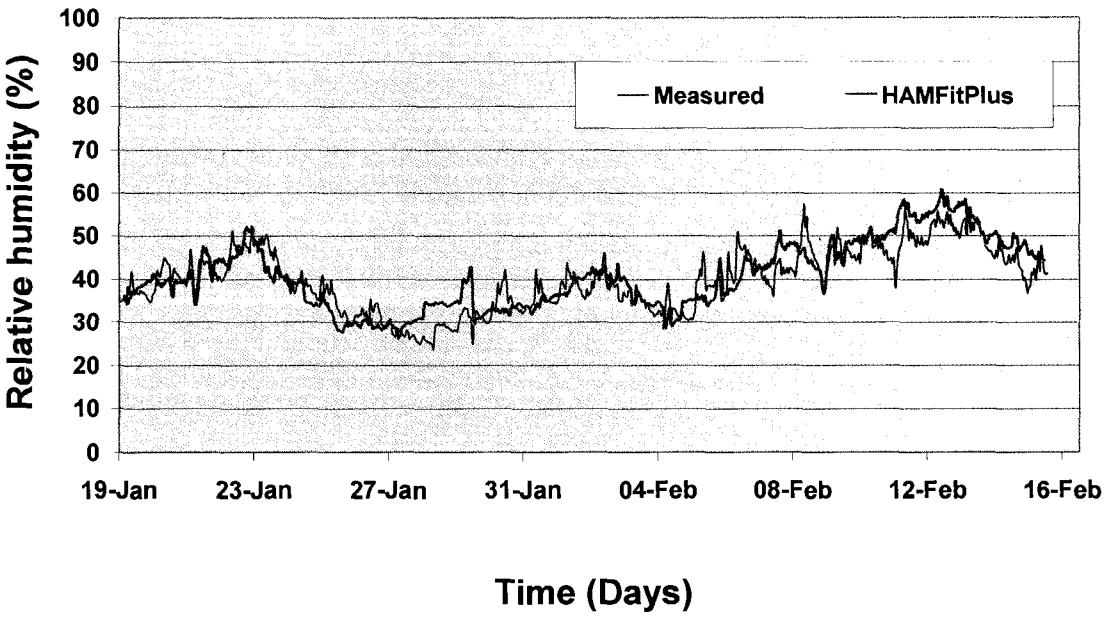

Figure 7-20 Indoor relative humidity of the house as predicated by HAMFitPlus

The calculation results of ASHRAE Standard 160P Intermediate model show that ignoring window condensation and moisture buffering effects of materials results in unrealistically high indoor humidity predictions. Figure 7-21 shows the simulation results of HAMFitPlus for a case where window condensation is considered but not the moisture buffering effect of materials. As can be seen in this figure, the deviation of the simulation and measured data is pronounced at times when the ventilation rate is low and the indoor humidity is relatively high. The only difference between the simulation cases whose results are shown in Figure 7-20 and Figure 7-21 is the inclusion or exclusion of moisture buffering effects of materials, and consequently the higher deviations observed in Figure 7-21 must be due to the absence of moisture absorption/desorption effects of building

envelope components. Thus, incorporation of moisture buffering effects of materials in indoor humidity modeling is very important to accurately predict the indoor humidity condition of a building.

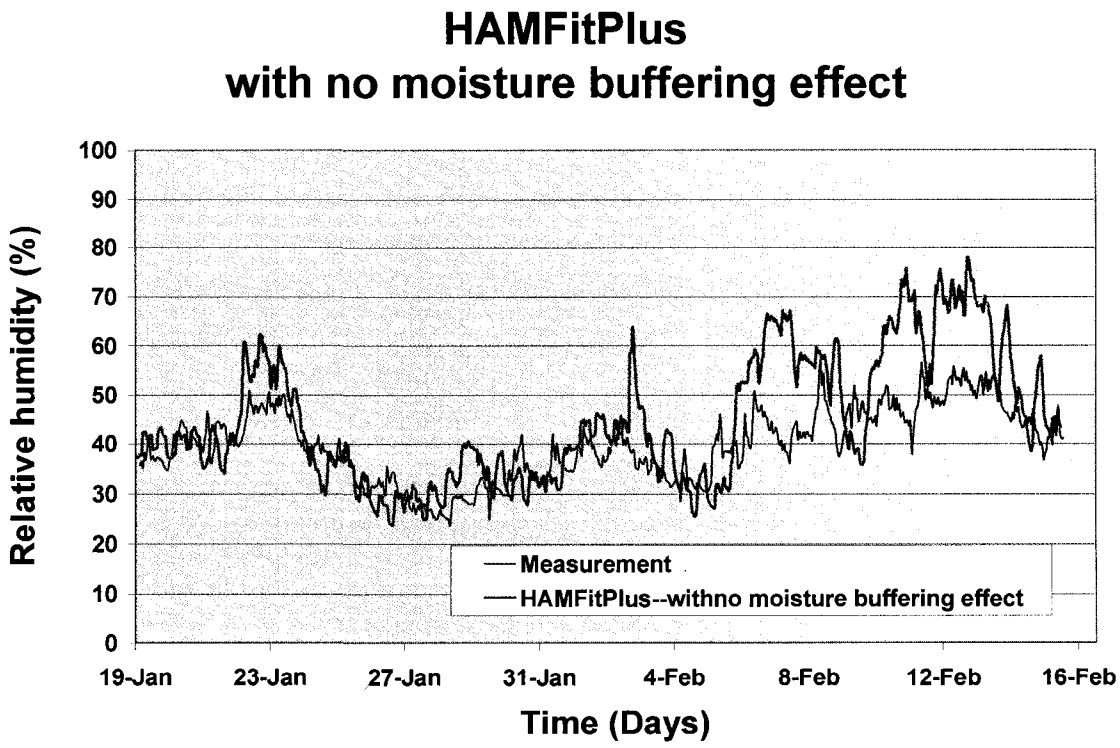

Figure 7-21 Indoor relative humidity of the house as predicted by HAMFitPlus for a case with no moisture buffering effect.

A statistical summary of the indoor humidity models used in this study is given in Table 7-4. The mean predicted indoor relative humidity values of the HAMFitPlus and ASHRAE Standard 160P Simplified models (40.5 and 41.9%, respectively) are close to the corresponding mean measured value (39.8%). The highest and lowest predicted mean relative humidity values are 86.5 and 28.6%, respectively, which correspond to ASHRAE Standard 160P Intermediate model and lower bound of the Class model results,

respectively. The minimum indoor relative humidity value predicted by the Intermediate model is 61.8%, which is very high when compared to the actual measured minimum value (23.8%). Moreover, the Intermediate model predicated the highest indoor relative humidity value of 100% while the maximum measured value is 57.3%. HAMFitPlus's minimum and maximum indoor relative humidity values are 27.6 and 60.6%, respectively, which are close to the corresponding measured values (23.8 and 57.3%, respectively).

Table 7-4 Statistical summary of the indoor relative humidity values obtained from measurements and numerical models.

	Measured RH values (%)	CLASS Model		ASHRAE Standard 160P		HAMFitPlus (%)
		Lower Bound (%)	Upper Bound (%)	Simplified (%)	Intermediate (%)	
Mean	39.8	28.6	51.7	41.9	86.5	40.5
Minimum	23.8	23.3	46.4	40.0	61.8	27.6
Maximum	57.3	47.6	70.7	56.5	100.0	60.6

The correlations between the indoor relative humidity measurement and simulation results of the three humidity models are graphically presented in Figure 7-22-Figure 7-24. The blue line in the figures represents an ideal case where the measured and predicted values are in perfect agreement. The closer the data plot to this line, the more accurate is the prediction of indoor relative humidity obtained by the model. As shown in Figure 7-22, the data points of the Upper and Lower bounds of the Class model lie above and below the blue line, respectively. This implies that the corresponding bounds over-

and underestimate the indoor relative humidity of the house, respectively. The ASHRAE Standard 160P Intermediate model consistently overestimates the indoor relative humidity of the house, whereas the Simple model shows a good correlation with the measured data, Figure 7-23. The best correlation between the measured and predicted values is obtained from the whole building hygrothermal analysis using HAMFitPlus, Figure 7-24, where most of the data are very close to the perfect-correlation line. The absolute errors[1] of the three models are summarized in Table 7-5. For almost half of the simulation period, the relative humidity difference between the measured and HAMFitPlus predicted values (absolute errors) are less than 3% (relative humidity), Table 7-5. While for 77.54% (nearly three-quarter) of the simulation period, the relative humidity difference is below 5% (relative humidity). Furthermore, the absolute errors for nearly the entire simulation period (98.18%) are less than 10% (relative humidity). Thus, the indoor humidity simulation result of HAMFitPlus can be considered as satisfactory. The second best model for the problem considered here is the ASHRAE Standard 160P Simple model where the absolute errors of 57.8% of the predicated values are less than 5% (relative humidity). And the worst model of all, for the problem under consideration, is the ASHRAE Standard 160P Intermediate model where the absolute errors of the predicted values are more than 10% (relative humidity). The relative errors[2] of the three models are summarized in Table 7-6. As shown in this table, 65.55% and 97.42% of the HAMFitPlus predicted values have relative errors below 10 and 25%, respectively.

---

[1] $absolute\ error = |measured - simulated|$

[2] $relative\ error = 100 \times \left| \frac{measured - simulated}{measured} \right| \%$

Whereas, 82% of the Simple model predicated values have relative error under 25%. And almost all predicated values of Intermediate model have relative errors over 50%.

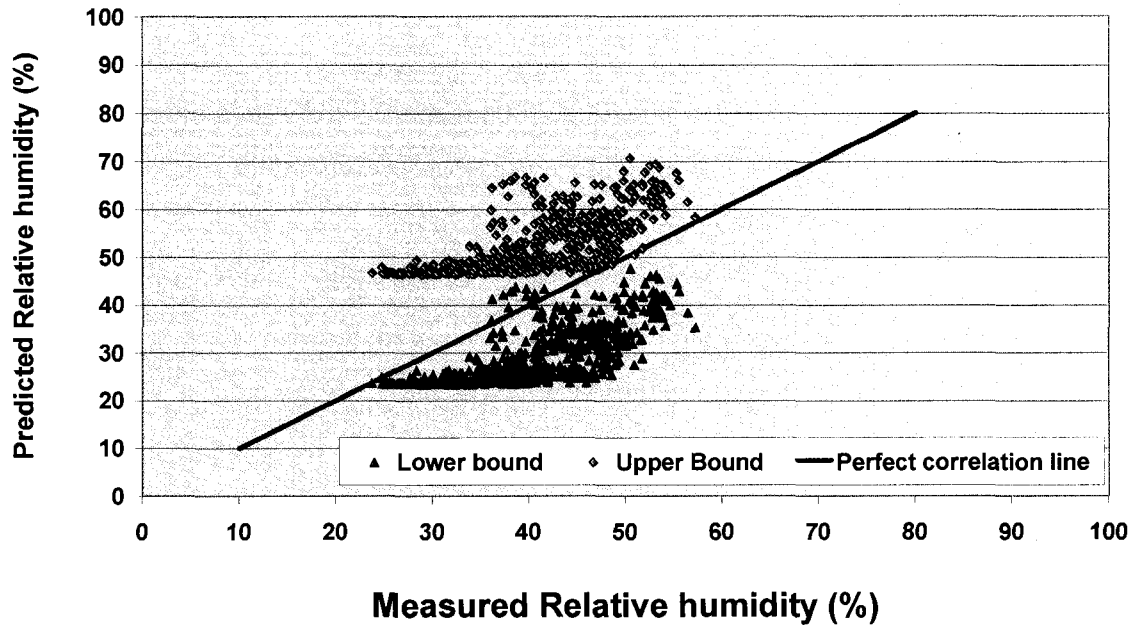

Figure 7-22 Correlation between measured and predicted indoor relative humidity values—Class model

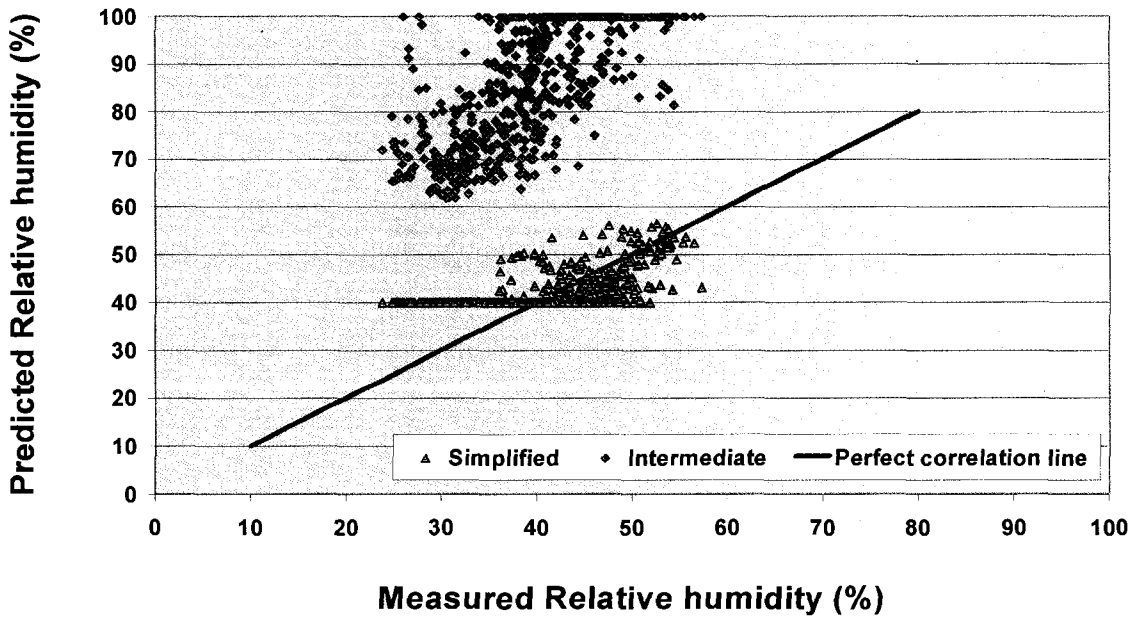

Figure 7-23 Correlation between measured and predicted indoor relative humidity values—ASHRAE Standard 160P models

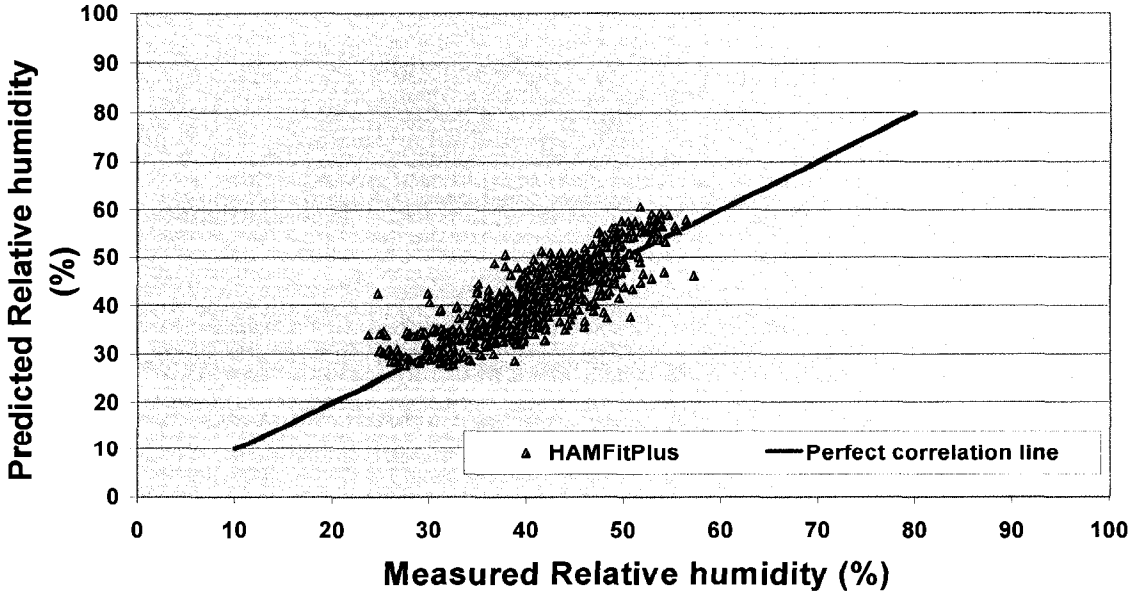

Figure 7-24 Correlation between measured and predicted indoor relative humidity values—HAMFitPlus

Table 7-5 Summary of the absolute error of the models with reference to the measured indoor relative humidity values.

Absolute Difference (%)	CLASS Model		ASHRAE Standard 160P		HAMFitPlus (%)
	Lower Bound (%)	Upper Bound (%)	Simplified (%)	Intermediate (%)	
< 3	5.46	3.49	37.03	0.00	49.47
< 5	11.08	7.89	57.81	0.00	77.54
< 10	39.30	36.72	87.71	0.00	98.18
> 10	60.70	63.28	12.29	100.00	1.82

Table 7-6 Summary of the relative errors of the models with reference of the measured indoor relative humidity values.

Relative Error (%)	CLASS Model		ASHRAE Standard 160P		HAMFitPlus (%)
	Lower Bound (%)	Upper Bound (%)	Simplified (%)	Intermediate (%)	
< 10	5.31	7.74	50.83	0.00	65.55
< 25	37.48	41.73	82.09	0.00	97.42
< 50	100.00	82.40	96.66	0.15	99.85
> 50	0.00	17.60	3.34	99.85	0.15

7.3 Indoor humidity and building envelope component performance

The performance of a building envelope component depends on the indoor and outdoor boundary conditions that it is exposed to. Thus, establishing boundary conditions that represent the 'real' indoor and outdoor climatic conditions with which the building envelope component performance is assessed is very important. The outdoor boundary conditions are usually well defined based on measured weather data. The weather data that is available for a location can be used for hygrothermal assessment of different building enclosure types that are built in the same location. But the indoor climatic conditions of those buildings can vary depending on the number of occupants, amount of indoor heat and moisture gains, type of interior furnishing, HVAC system and other factors. In fact, the outdoor boundary conditions themselves influence the indoor boundary conditions. Subsequently, the indoor boundary conditions are usually highly variable with time, and are the result of heat and moisture balance of the indoor air. In building performance analysis, assumption of indoor boundary conditions with simple indoor boundary conditions profiles such as constant temperature and relative humidity conditions or one set of values for winter and another set for summer may not be appropriate. The current trend is to use humidity models such as Class model or ASHRAE Standard 160P models to define the indoor boundary conditions. However, as discussed in Section 7.2 the indoor humidity profiles obtained from these models can vary significantly; use of one or the other model for hygrothermal performance assessment of a building component may result in different conclusions. In this section, the indoor humidity profiles that are developed in Section 7.2 including the whole building hygrothermal model, HAMFitPlus, are used for hygrothermal performance

assessment of a building envelope component. In doing so, the influence of indoor humidity on the hygrothermal performance of the building envelope component is shown. The importance of an accurate indoor humidity model in hygrothermal performance evaluation of the building envelope component is emphasized.

7.3.1 HAMFit2D Simulation

The south corner section of the house is considered for this study. The effect of the indoor humidity on the building envelope component performance is evaluated. The schematic diagram of this two-dimensional corner section is shown in Figure 7-25. This building envelope section is chosen because it has high mold growth potential as confirmed by the Surveyor (Hood 2006). This region is relatively cold as a result of the thermal bridge that is created by the corner post and studs. Such cold bridge section promotes condensation and increases moisture accumulation, which subsequently results in mould growth in the region. As shown in the Figure 7-25, the exterior surfaces of the corner section are covered with sheet metal. The sheet metal is attached to the sheathing board, which is 12.5 mm thick OSB. The wall sections are insulted with 152.4 mm fiberglass insulation. The vapor barrier (Polyethylene sheet), which is installed behind the 12.5 mm gypsum board, is assumed to be continuous. Thermal bridge is created by the two studs (50.8 x 152.4 mm) and a corner post (152.4 X 152.4 mm).

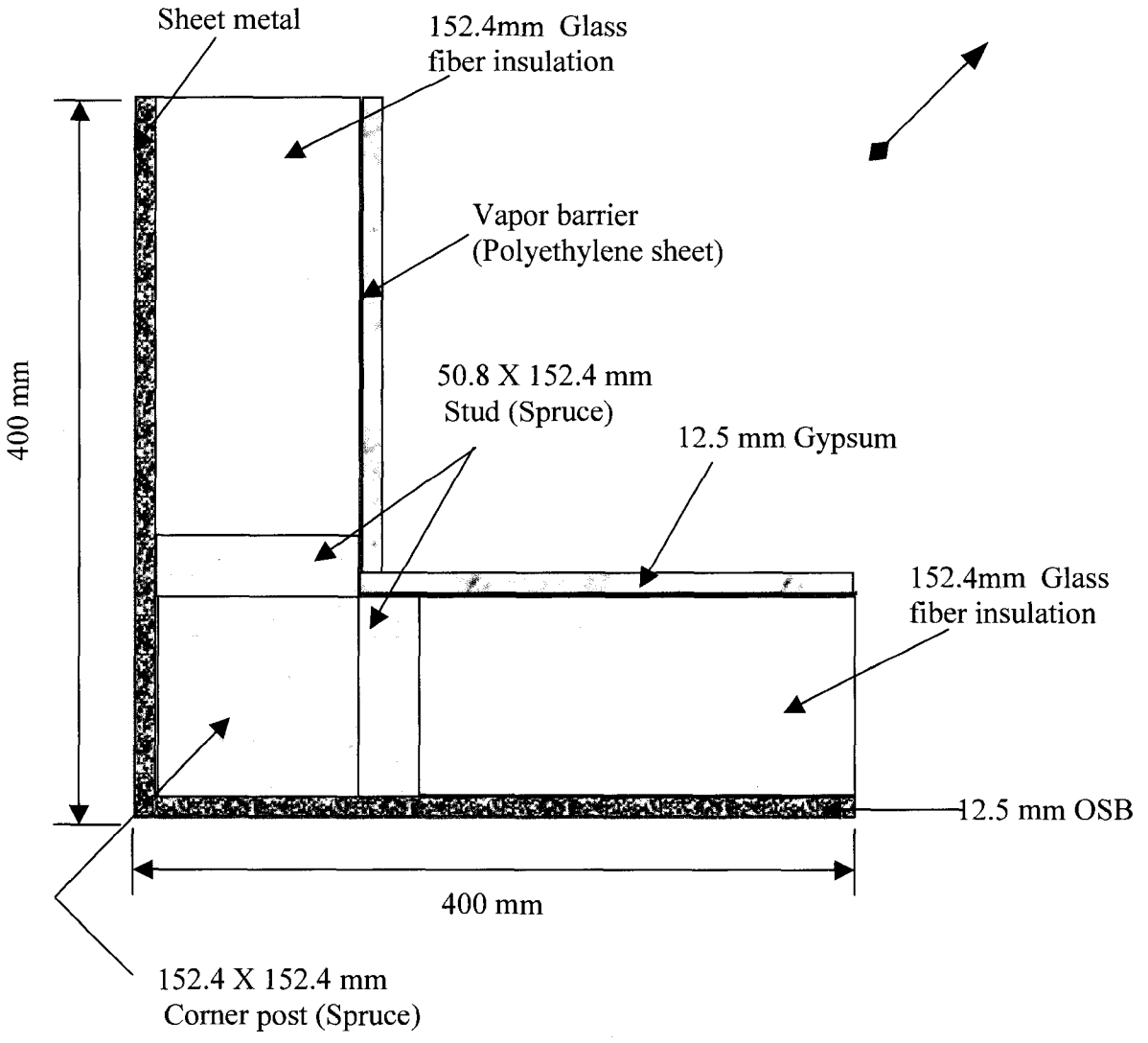

Figure 7-25 The schematic diagram of two-dimensional corner section that is considered for hygrothermal performance analysis.

The hygrothermal simulations are performed using the two-dimensional version of the newly developed building envelope model (HAMFit2D) in Chapter 4. The simulations are carried out for the same period for which the indoor humidity profiles are predicted in Section 7.2 (January 19 to February 16, 2006). The hygrothermal properties of all the layers are discussed in Section 7.1.4, *Building enclosure*. The computational domain of

the corner section is descritized into 1920 quadratic elements, Figure 7-26. To control the overall mesh density (avoid excessively small and/or large number of elements) each layer is meshed independently, but in conformity with the other. This procedure is necessary due to the high variation in the thickness of the layers, for instance the insulation is about 1000 times thicker than the thinnest layer (Polyethylene sheet).

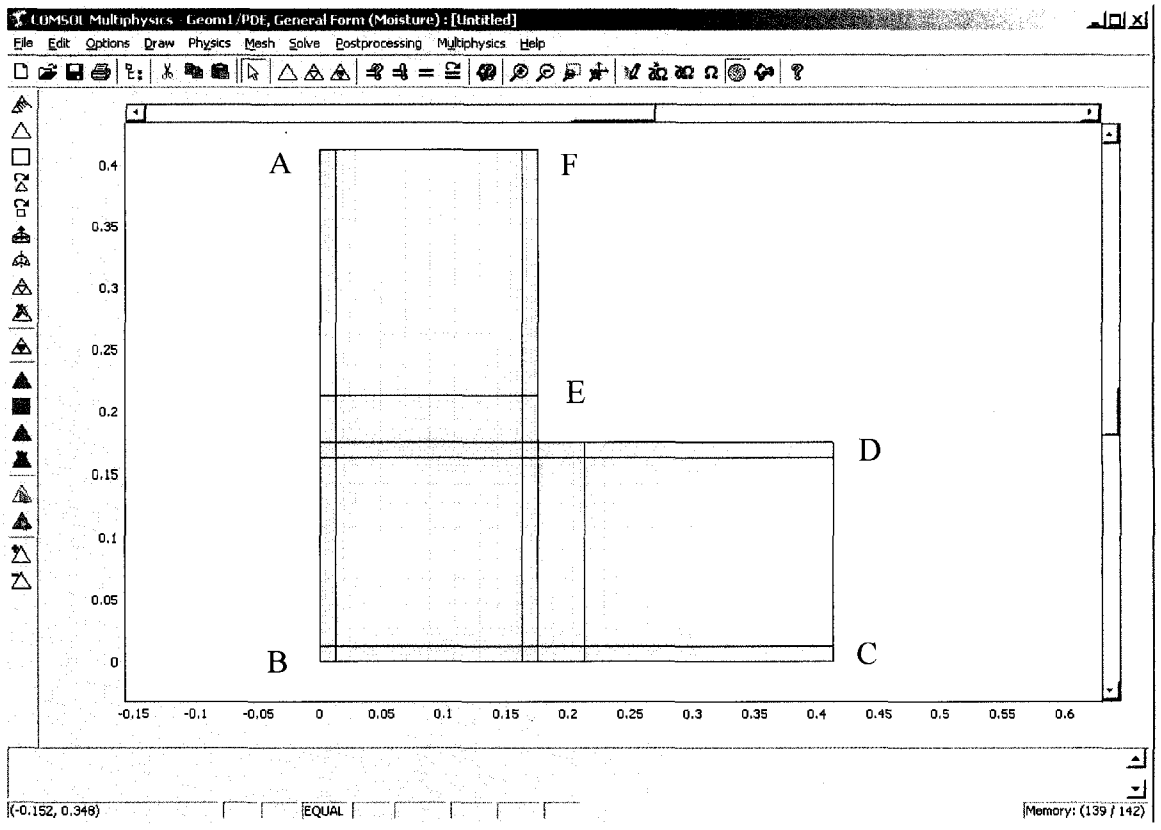

Figure 7-26 Quadratic mesh of the corner section of the house

The boundary conditions that are applied on all surfaces are Neumann type boundary conditions, where moisture and heat fluxes are used instead of surface temperature and relative humidity conditions (Dirichlet type boundary conditions). For surfaces A-F and C-D, shown in Figure 7-26, adiabatic/closed boundary conditions (zero flux) are assumed

for both heat and moisture transfers. This is based on an assumption that the temperature and moisture gradients in the lateral directions of the walls become negligible at the mid section of a cavity, 400 mm from the corner point. The heat and moisture fluxes at the interior surface of the domain (D-E-F) are calculated from the indoor climate data, which are determined in Section 7.2 by the respective humidity model, and using heat and moisture transfer coefficients. The heat transfer coefficient of the two-dimensional corner surfaces is estimated to be 6 W/Km^2 (Sanders 1996, IEA Annex 14 1991). The moisture transfer coefficient of the corresponding surface is 2E-8 s/m, which is estimated based on Lewis relation (ASHRAE Fundamental 2005). The heat transfer coefficient accounts for both convection and long-wave radiation heat exchanges. The external surfaces (A-B-C) are exposed to the local weather conditions. Since these surfaces are metal sheets, wind-driven rain load and moisture exchange with the surrounding is zero. Consequently a zero-flux condition for moisture exchange is assumed for these external surfaces. The effective heat flux on these boundary are calculated by adding the heat gain due to solar radiation and the net heat exchange between the surfaces and the surrounding environment due to longwave radiation and convective heat exchange mechanisms. For these external boundaries, the convective and longwave radiation heat exchanges are treated independently. The convective heat transfer coefficient depends on wind speed, and approximated by Equation [7.10] (Sanders 1996). The longwave radiation heat exchange is estimated based on International Standard ISO 15927-1:2003(E), Annex B.

$$\begin{aligned} h_c^o &= 5.82 + 3.96\,V & V \le 5\ m/s \\ h_c^o &= 7.68\,V^{0.75} & V > 5\ m/s \end{aligned} \qquad [7.10]$$

where V is the wind speed measured at 10 m 'adjacent' to the house.

7.3.2 Simulation results

Figure 7-27 shows the typical temperature profile of the corner section of the house on January 29th, 2006. On this particular date, the daily average outdoor and indoor air temperatures were –40.4°C and 17.5°C, respectively. Observation of the temperature profile suggests that the coldest spot on the interior gypsum is a region around the junction of the two perpendicular gypsum boards. Similar temperature profiles are observed in all four simulation cases where the Lower bound (Class model), HAMFitPlus, ASHRAE Standard 160P Simple model and the Upper bound (Class model) indoor humidity profiles are used. This is expected since the indoor temperature is the same in all four cases. But the moisture distributions on the back of the gypsum board, more specifically at the region of interest, are quite different. The moisture distributions across the corner section of the house at the time that corresponds to the temperature profile presented are shown in Figure 7-28 to Figure 7-31. In these figures the moisture distributions are represented in terms of relative humidity, and plotted in the same scale for comparison purpose. At this particular time, the daily average indoor relative humidity as predicted by the Lower bound (Class model), HAMFitPlus, ASHRAE Standard 160P Simple model and the Upper bound (Class model) are 25, 34, 40 and 48%, respectively.

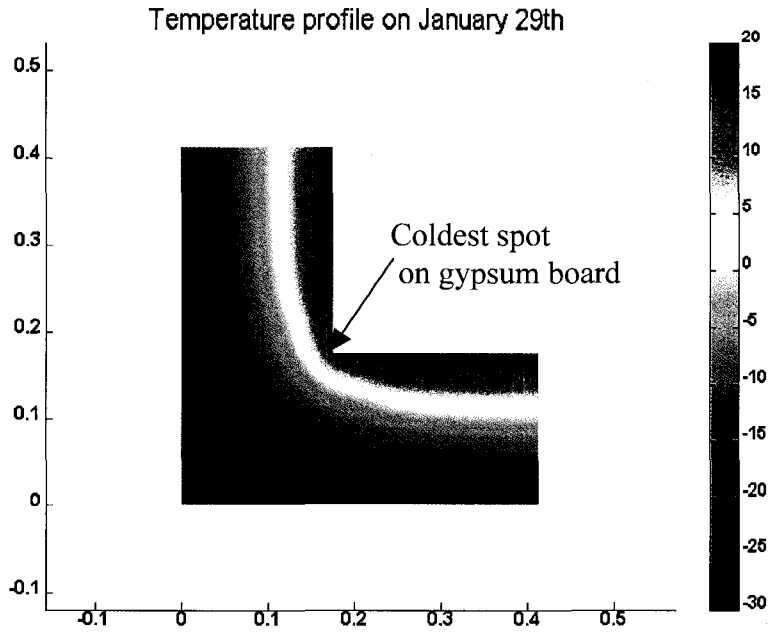

Figure 7-27 Temperature profile of the corner section of the house on January 29th

In all the four cases the moisture profile in the OSB and insulation layers does not change. This is because these layers do not exchange moisture neither with the internal nor external environmental conditions as they are sealed with polyethylene and metal sheets in the interior and exterior surfaces, respectively. But, the gypsum board dynamically interacts with the corresponding indoor environmental conditions. As can be seen in all four relative humidity profile plots, the gypsum at the junction region experiences elevated moisture accumulation compared to the corresponding adjacent gypsum section. The figures also show various degree of moisture accumulation (at the junction region) for the four indoor humidity profiles used. The corresponding relative humidities are: 56% (Lower bound of Class model-Figure 7-28), 73 % (HAMFitPlus model-Figure 7-29), 94% (ASHRAE Standard 160P Simple model-Figure 7-30), and finally 96% (Upper bound of Class model-Figure 7-31). The implies that the relative

humidity at the junction region can vary from 56 to 96% depending on the indoor humidity profile that is assumed for the house under consideration. This wide range of simulation results reinforces the need for accurate determination of indoor humidity that can be used as indoor boundary condition in the analysis of building envelope components performance.

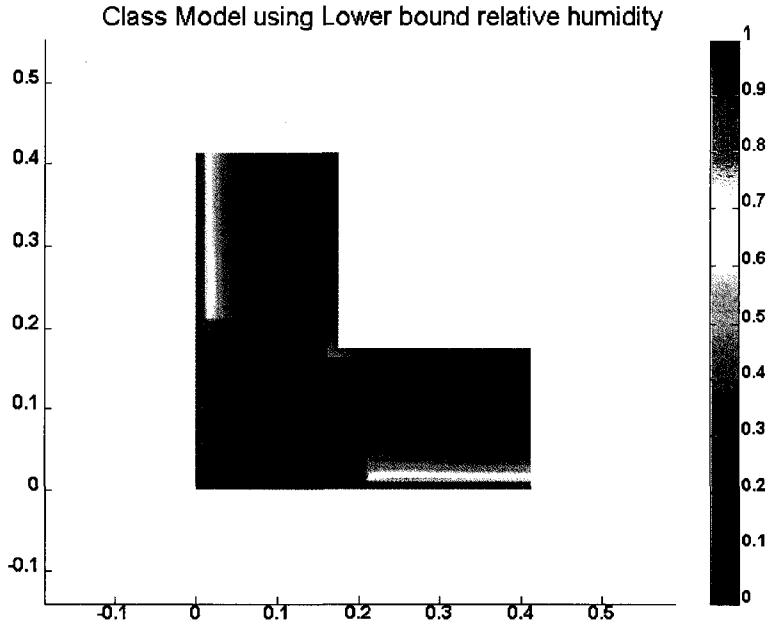

Figure 7-28 Relative humidity profile of the corner section using indoor humidity profile generated by Lower bound of Class model

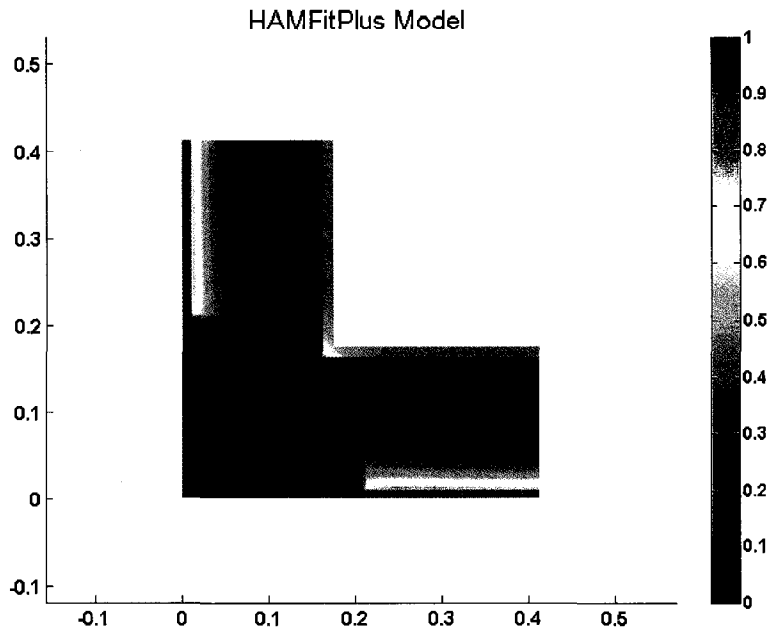

Figure 7-29 Relative humidity profile of the corner section using indoor humidity profile generated by HAMFitPlus

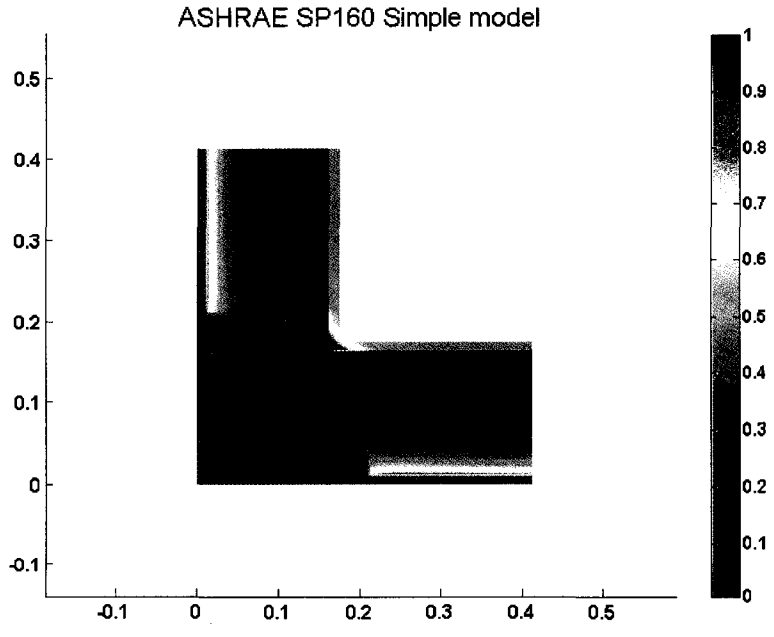

Figure 7-30 Relative humidity profile of the corner section using indoor humidity profile generated by ASHRAE Standard 160P Simple model

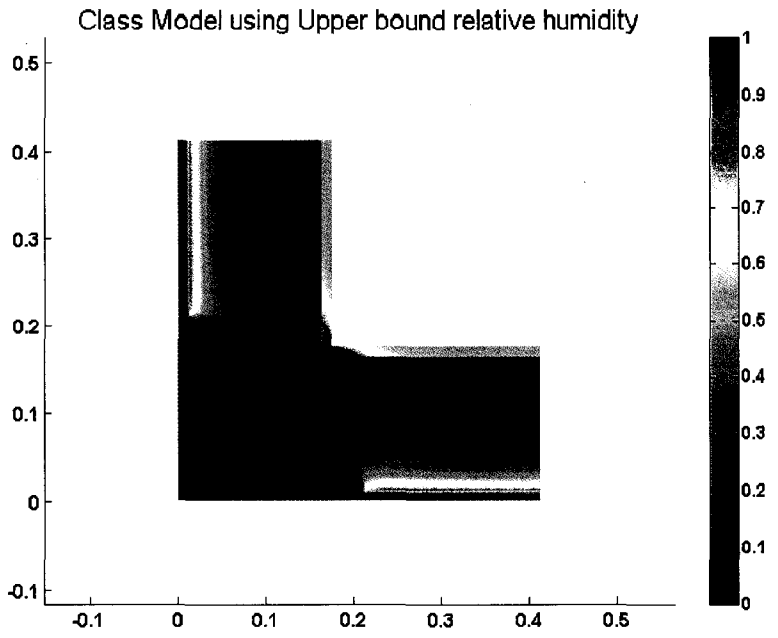

Figure 7-31 Relative humidity profile of the corner section using indoor humidity profile generated by Upper bound of Class model

Consequently, this region is an area of interest for comparative analysis of the four indoor humidity models. The low temperature in this region may promote indoor moisture condensation and increases moisture accumulation in the gypsum board, and subsequently creates a favorable condition for mold growth. The temperature and moisture time history of this critical location are extracted from the hygrothermal simulation results and further analyzed. Figure 7-32 shows the temperature time history of the outermost junction point of the two joining gypsum boards. The temperature of this location varies between 2.4°C on January 29th and 15.7°C on February 12, 2006. Generally, it is believed that temperature over 0°C creates a favorable condition for mold growth if accompanied with high relative humidity for long enough time (Viittanen and Salonvaara, 2001). Accordingly, this critical location might satisfy one of the criteria for

mold growth. The relative humidity profiles of the same critical location as exposed to the four indoor humidity conditions are shown in Figure 7-33.

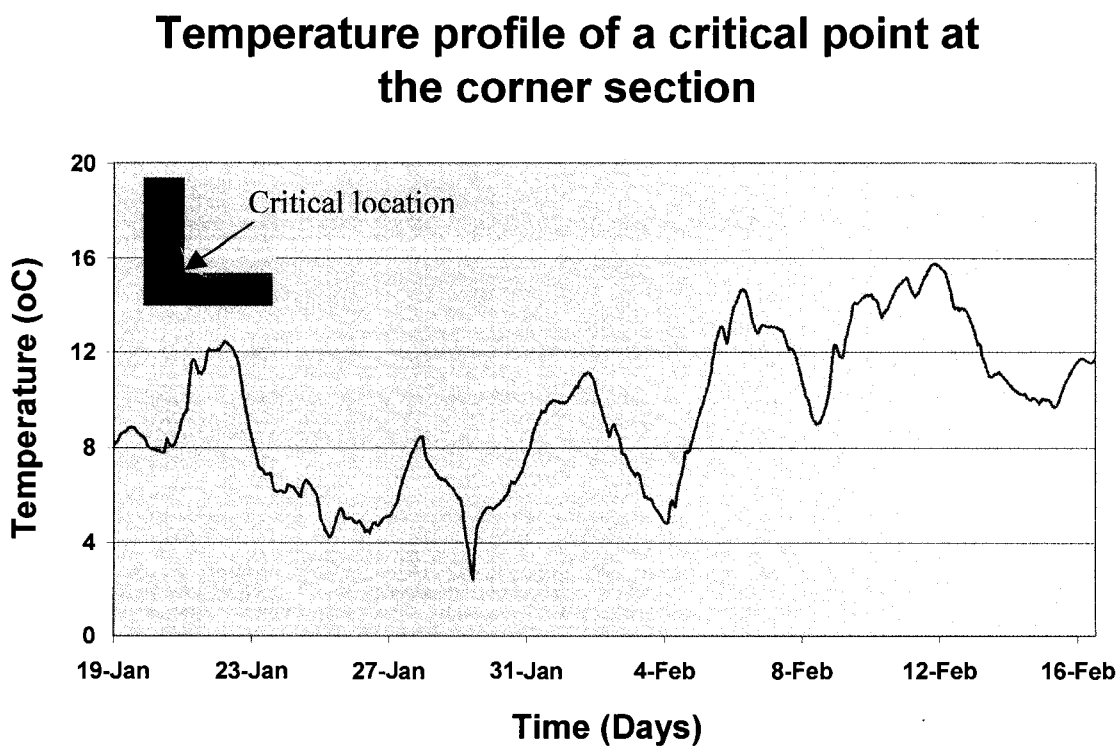

Figure 7-32 Temperature profile at the rear junction point of the two gypsum boards

The hygrothermal simulation results presented in Figure 7-33 suggest that the amount of moisture accumulation in the corner gypsum depends on the type of indoor humidity model used to generate the indoor boundary conditions. The combination of the cold outdoor temperature, which promotes condensation, and the higher indoor humidity predicted by the Upper bound (Class model) brings the relative humidity profile of the corner piece to a high level. In the simulation case where the indoor humidity predicted by the Lower bound (Class model) is used as an indoor humidity boundary condition, the

same location experiences the lowest level of moisture accumulation. For most of the simulation period, the moisture profiles of the critical point in cases with HAMFitPlus and ASHRAE 160P Simple models are close to each other, and lie more or less in the middle of the Upper and Lower bounds (Class model) results. Their deviations are pronounced for about a week (26^{th} of January to 2^{nd} of February) when the ASHRAE Standard 160P Simple model over predicted the indoor humidity level. At this time the HAMFitPlus indoor relative humidity prediction reaches its lowest value of 23% due to the high ventilation rate that is caused by the relatively cold outdoor temperature, while the ASHRAE Standard 160P Simple model maintains the lower cutoff value of 40%. In general, the relative humidity of the critical point during the entire simulation period is less than 80% in the case of Lower bound (Class model) and 90% in the case of HAMFitPlus. In Table 7-7 the percentage of time at which the relative humidity of the corner piece is over 80 and 90% in the four indoor humidity models considered are presented. As shown in the table, the critical location experiences a relative humidity over 90% for 70 percent of the simulation period in the case of the Upper bound (Class model) and 26% of the simulation period in the case of the ASHRAE Standard 160P Simple model. The percentage of time in which this critical location has a relative humidity over 80% are 93, 47 and 30% for cases with the Upper bound (Class model), ASHRAE Standard 160P Simple model and HAMFitPlus, respectively. The average relative humidity of the critical point for the cases with Upper bound (Class model), HAMFitPlus, ASHRAE Standard 160P Simple model and Upper bound (Class model) are 56, 76, 78 and 90%, respectively. Vittanen and Salonvaara (2001) suggested that a gypsum board with relative humidity over 80% might create a favorable condition for mold growth. If one uses this relative humidity threshold as a measure of building

envelope performance, the use of one or the other indoor humidity profiles that are generated by the various indoor models may yield different conclusions about the hygrothermal performance of the building envelope component. For instance, in the cases considered here, the gypsum board can be assessed as it is at high mold growth risk (if one used the Upper bound Class model) or no risk (if one uses Lower bound Class model). As these simulation results suggest, it is very important to use a more accurate indoor model, which is based on whole building heat and moisture balance, to generate the indoor humidity profile that will be used as boundary condition in the hygrothermal performance analysis of building envelope components.

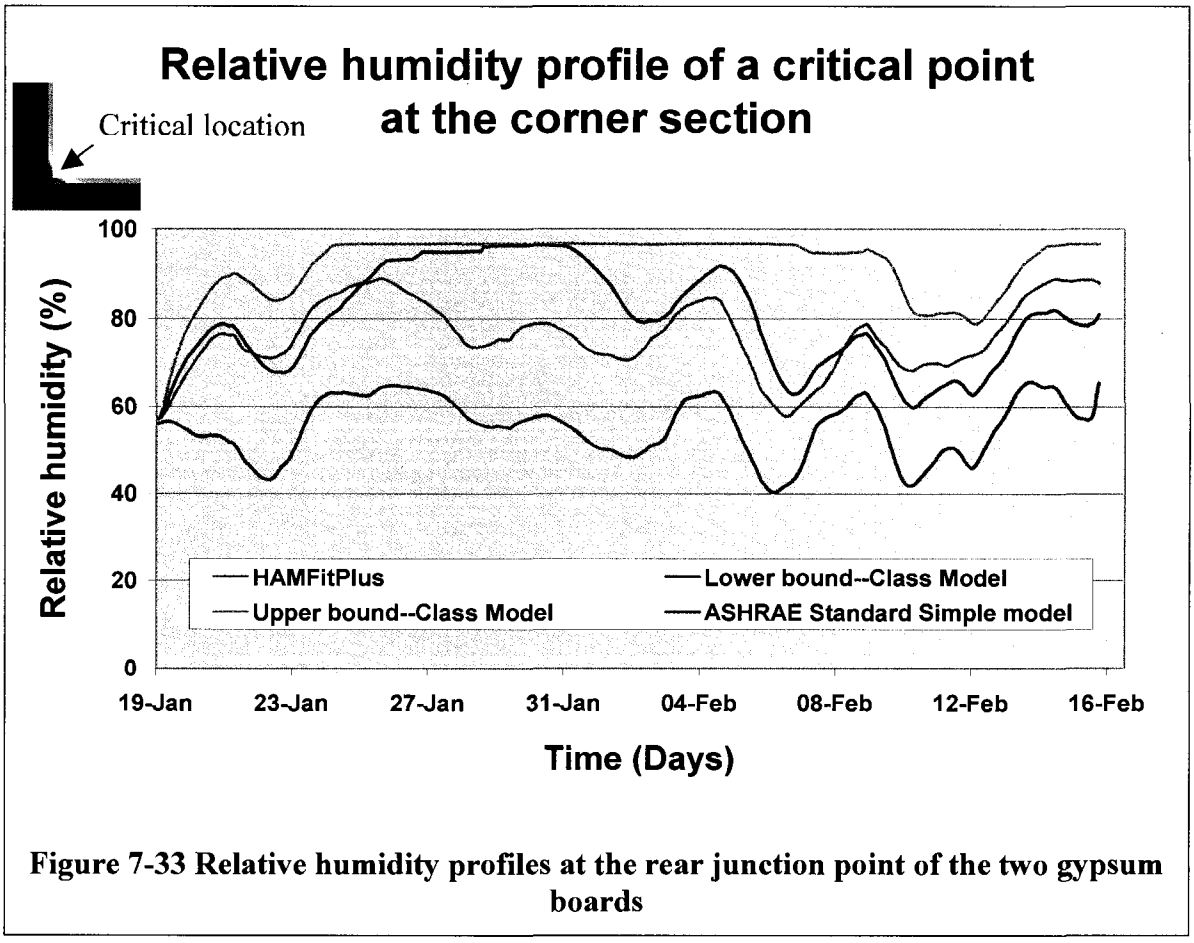

Figure 7-33 Relative humidity profiles at the rear junction point of the two gypsum boards

Table 7-7. The percentage of time for which the critical location attains a relative humidity over 80 and 90%.

Relative humidity (%)	CLASS Model		ASHRAE Standard 160P Simplified (%)	HAMFitPlus (%)
	Lower Bound (%)	Upper Bound (%)		
> 80	0	93	47	30
> 90	0	70	26	0

In the next section, various retrofit options for the residential house considered in this section are assessed using HAMFitPlus. The model is used to choose design parameters that can lead to reduction in energy consumption while maintaining the indoor humidity at an acceptable level for occupants' comfort and health as well as building envelope components performance.

8 WHOLE BUILDING HYGROTHERMAL PERFORMANCE ANALYSIS

One of the advantages of numerical models is that they can be used to evaluate different design scenarios more economically and efficiently. But first, the models need to be validated and benchmarked. As presented in Chapters 6, HAMFitPlus is successfully benchmarked against experimental results, verified with analytical solutions, and also compared with other models. In this section, the usefulness of the model for evaluation of various building design options that may alter the overall performance of a specific building is presented. The indoor humidity level, energy consumption, window condensation and moisture in building envelope components during one winter month period are used to evaluate the design variable on the overall performance of the building. The objective is to choose design parameters that can lead to reduction in heating load while maintaining the indoor humidity at an acceptable level for the occupants and for the durability of the building envelope components.

The house described in Chapter 7 is taken as a reference house and various parameters are varied to see their level of influence on the overall house performance. The parameters considered are: interior layer material, interior layer surface finish, ventilation, thermostat setback, window-type, insulation and combinations of these parameters. The detailed description of the house including building envelope components, indoor heat and moisture gains, mechanical systems and weather conditions are given in Chapter 7. The house is subjected to extreme loads in both outdoor and indoor: very cold outdoor temperature and very high indoor moisture gain.

8.1 Moisture buffering effects of surface finish

To investigate the effect of surface finish, more specifically paints, on the indoor humidity profile of the house, three surface finishing options are considered. In the first two cases, the interior layer (gypsum board) is finished with acrylic and latex paints. In both cases the paints are applied on top of primer coat. The third option represents a case where the gypsum is not painted or painted with a paint that has insignificant vapor resistance. The vapor permeance of the acrylic and latex paints, along with the base primer, are taken from Roels et al. (2006). For these paints, they formulate an analytical expression (Equation [8.1]) that captures the relationship between relative humidity and the corresponding vapor resistance factors. The values of the coefficients 'a', 'b' and 'c' are given in Table 8-1

$$\mu = \frac{1}{a + b \cdot \exp(c\phi)} \qquad [8.1]$$

Table 8-1 Coefficients for acrylic and latex paints vapor resistance factors

	Thickness (m)	A	B	C
Acrylic paint	1.00E-04	2.50E-04	1.35E-05	5.65
Latex paint	1.00E-04	2.50E-05	4.22E-07	8.17

In the simulations, paints are treated as vapor resistance layers. Consequently, the effective surface vapor resistance for each simulation case is calculated by adding the vapor resistances of the corresponding paint at 50% relative humidity and the surface

resistance created by the moisture boundary layer. Based on Equation [8.1], the vapor resistance values $\left(\frac{\mu \cdot t}{\delta_a}\right)$ of the acrylic and latex paints at 50% humidity are 1.08E+09 and 1.03E+10 m/s, respectively. In the above expression 't' is the paint thickness and 'δ_a' is the vapor permeability of air, which is given by Schirmer's Equation (Kalagasidis, 2004). The vapor permeability of air at standard atmospheric pressure and 21°C is 1.94E-10 kg m^{-1} s^{-1} Pa^{-1}. The vapor resistance due to the boundary layer is assumed to be 2E+07 m/s. The effective vapor transfer coefficients of the three paint options are calculated in accordance to the European standard EN ISO12572:2001, Annex E, and presented in the last column of Table 8-2. As the last column in the Table shows, the surface vapor transfer coefficient of the acrylic paint is less than that of the reference case (no paint) by a factor of fifty and the coefficient of the latex paint is one order of magnitude less than that of the acrylic paint.

Table 8-2 Effective mass transfer coefficients of the three surface-finish options.

	Boundary layer resistance (Z_b) m/s	Paint resistance (Z_c) m/s	Total resistance ($Z_T = Z_b + Z_c$) m/s	Effective vapor transfer coefficient ($1/Z_T$) s/m
No Paint	2.0E+07	-	2.0E+07	5.00E-08
Acrylic paint	2.0E+07	1.08E+09	1.10E+09	1.00E-09
Latex paint	2.0E+07	1.03E+10	1.03E+10	1.00E-10

8.1.1 Indoor humidity—Simulation results

In the three simulation cases, the indoor temperature is controlled by a thermostat, which activates the heating system whenever the indoor temperature goes below 21°C. In all the three cases, the calculated indoor temperatures are nearly constant (fluctuates between 20.96 to 21°C). As expected, the total heating loads for the entire simulation period in the three simulation cases are equal, which is 2796 kWh. The indoor relative humidity profiles of the house for the three finishing options are presented in Figure 8-1.The simulation results suggest that the type of paint used, acrylic or latex paint, does not make a significant difference in the indoor relative humidity. However, as can be seen in the figure, the reference case (with no paint) tends to damp the high indoor humidity fluctuation and it provides the maximum possible moisture buffering capacity as far as the surface finishing is concerned. The presence of the paints lowers the moisture buffering capacity of the interior layer and creates a condition for the indoor humidity to be sensitive to a small change in ventilation rate. The natural ventilation rate, which is the same in all the three cases, is shown in Figure 8-2. For instance, during the simulation period of 44 to 95 hour the ventilation rate is relatively low. During this time the indoor humidity in cases with paints show significant increase while the reference case shows a moderate increase. This is because at low ventilation rate, the cases with paints tend to accumulate the excess moisture in the indoor air, but in the reference case, part of the excess moisture is absorbed by the interior surface of the gypsum and reduces the possible indoor humidity increase in the indoor air.

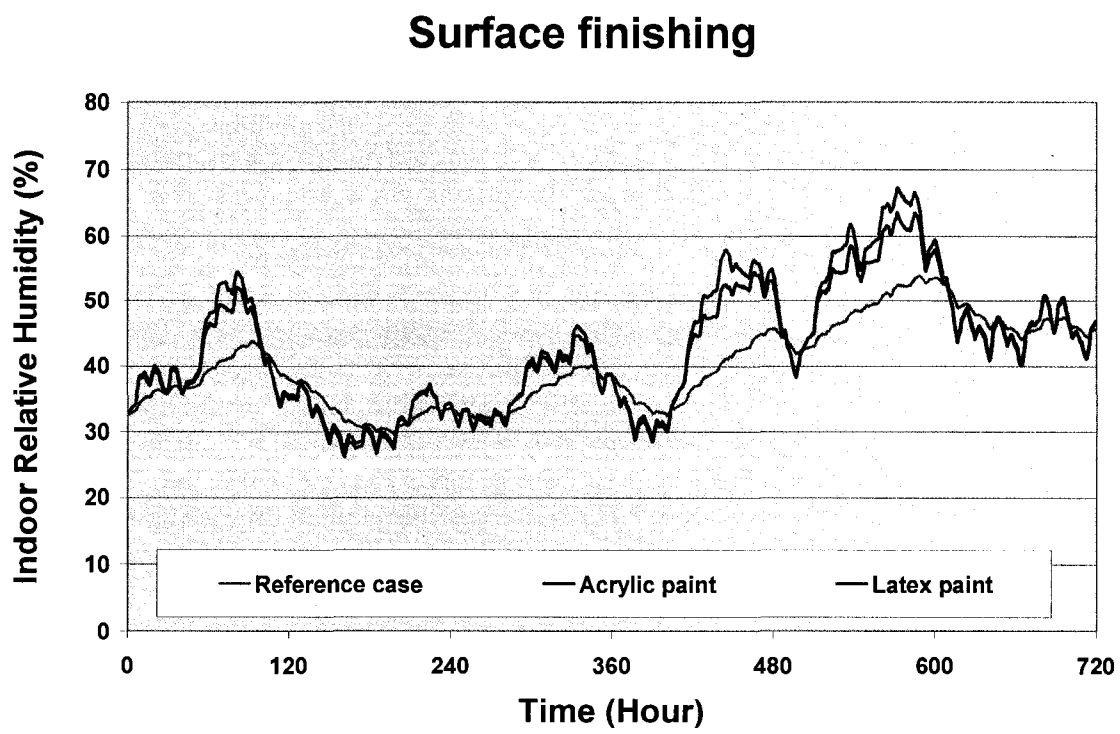

Figure 8-1 Relative humidity of the house for the three surface finishing options

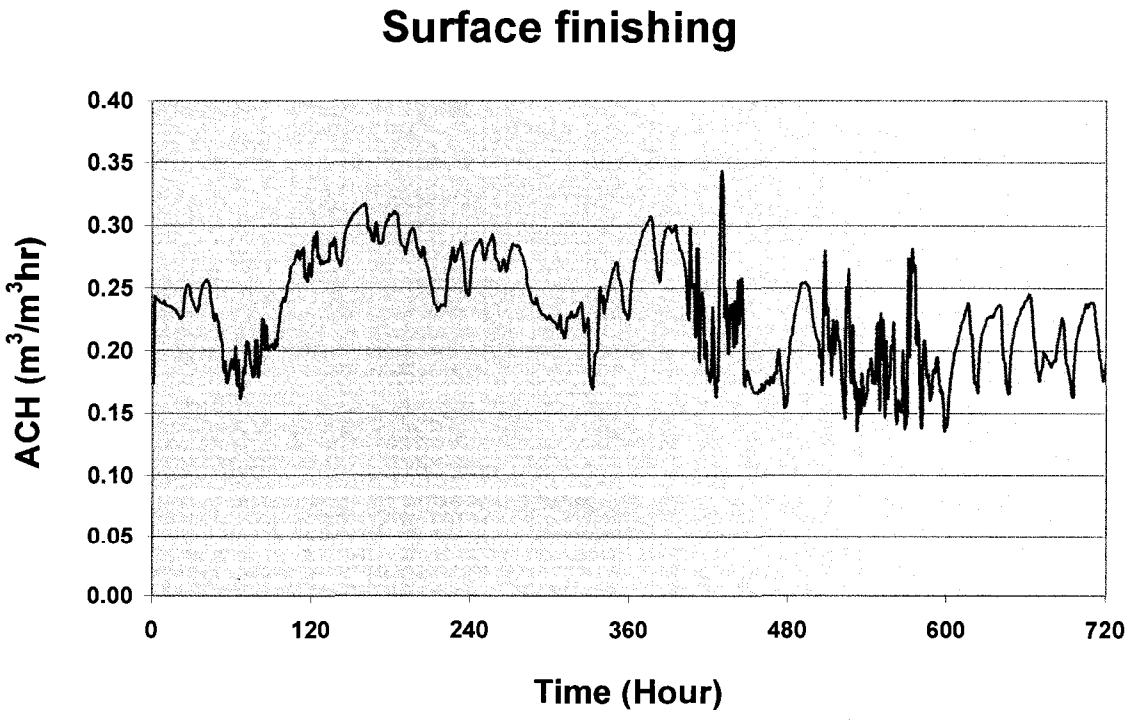

Figure 8-2 Natural ventilation rate of the house during the simulation period.

8.1.2 Window condensation

The low outdoor temperature has dual effects: a) increasing the natural ventilation, due to an increase in stack pressure (for this cold climate, as mentioned earlier, the main driving force for natural ventilation is stack effect), and b) high window condensation due to low inside window surface temperature. Both factors result in reduced indoor humidity level. Since the ventilation rates and window's surface temperature are the same in all the three cases (bare gypsum and two painted gypsum cases) there is no significant difference among the respective window condensation rates, Figure 8-3. Slight variations are observed when the outdoor temperature is relatively cold or relatively warm. At cold periods (for instance 96 to 161 hour), the window condensation rate in the case with bare gypsum is slightly higher than that of the painted cases. This is due to the fact that the indoor relative humidity in the reference case is slightly higher than the other two cases. The reason for the slight increase in the indoor relative humidity in the reference case is because the bare gypsum absorbs moisture during high indoor humidity periods and releases moisture back to the indoor air when the indoor humidity tends to be low. On the other hand, at the relatively warmer outdoor temperature (for instance 500 to 600 hour), more window condensation occurred in the painted cases than the reference case. At this time the ventilation rate is low and the indoor relative humidity tends to increase. Since painted gypsum has very limited moisture buffering potential, part of the excess moisture that is absorbed by the bare gypsum in the reference case condenses on the window surfaces and the rest increase the indoor humidity level. The magnitude and frequency of the indoor moisture condensation on the window surfaces for the three surface finishing options are summarized in Table

8-3. Among the three options, the interior finish with latex paint results in more condensation (7.241 kg/day) and also occurs more frequently (80% of the time) than the other two. The least window condensation occurs in the reference case (6.576 kg/day), which also happens less frequently (61% of the time). In all the three cases, significant percentage of the moisture generated in the house (41 – 45.2%) condenses on the window surfaces and freezes. This is consistent with the surveyor's observation (Stad, 2006) where he reported considerable condensation on windows and ice buildup, and also moisture staining and possible deterioration of lower portion of the walls below windows.

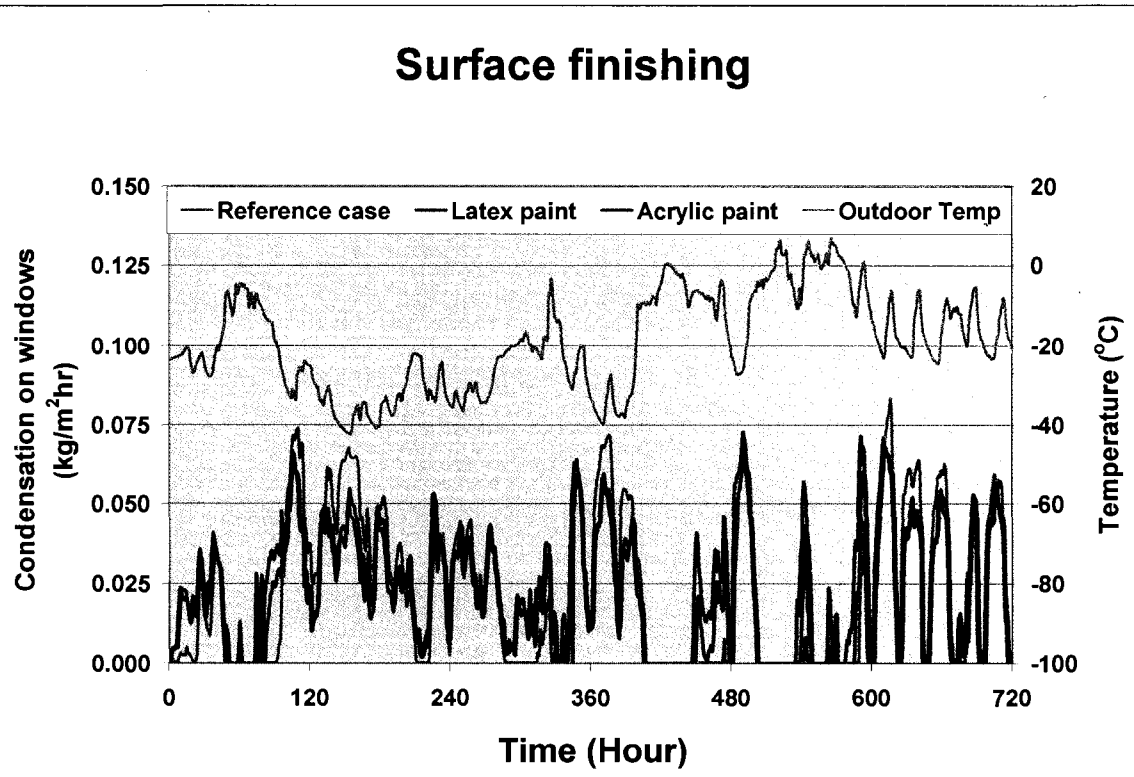

Figure 8-3 Outdoor temperature and window condensation rates for the three surface finishing options.

Table 8-3 Window condensation for the three surface finishing options

	Average window condensation (kg/day)	Moisture supply that is condensed (%)	Condensation occurrence (%)
Reference case (No paint)	6.576	41.0	61
Acrylic paint	6.792	42.4	76
Latex paint	7.241	45.2	80

8.1.3 Moisture in building envelope component--Case of surface finishing

To examine the effect of paints on the durability of building envelope components, the two-dimensional corner section, which is represented in Figure 7-25 is considered for investigation. The mesh and material properties of the layers are the same as the ones used in Section 7.3. The two dimensional hygrothermal analyses are performed (using HAMFit2D) by applying adiabatic/closed boundary conditions at the cut-sections of the walls, and Carmacks' weather data on the exterior surface of the corner section. The interior surface of the section is exposed to the relative humidity and temperature conditions that are expected from the respective surface finish options. The expected indoor boundary conditions of the three cases (no paint, acrylic and latex paints) are, in fact, the output of the whole building hygrothermal analysis shown in Figure 8-1.

The outer most junction point of the two gypsum boards, which is the same point of interest in Section 7.3, is used to compare the effect of paints on the hygrothermal

performance of building envelope components. At this critical location high moisture accumulation, which may favor mold growth and degradation of building envelope components, is expected. The temperature-time history of the critical location in all the three cases is identical, Figure 8-4. The temperature fluctuates from the lowest 5.15°C at 170 hour, to the highest 16.22°C at 584 hour. Generally, it is believed that temperature over 0°C creates a favorable condition for mold growth if accompanied with high relative humidity for long enough time (Viitanen and Salonvaara, 2001). This implies that this critical location might satisfy one of the criteria for mold growth.

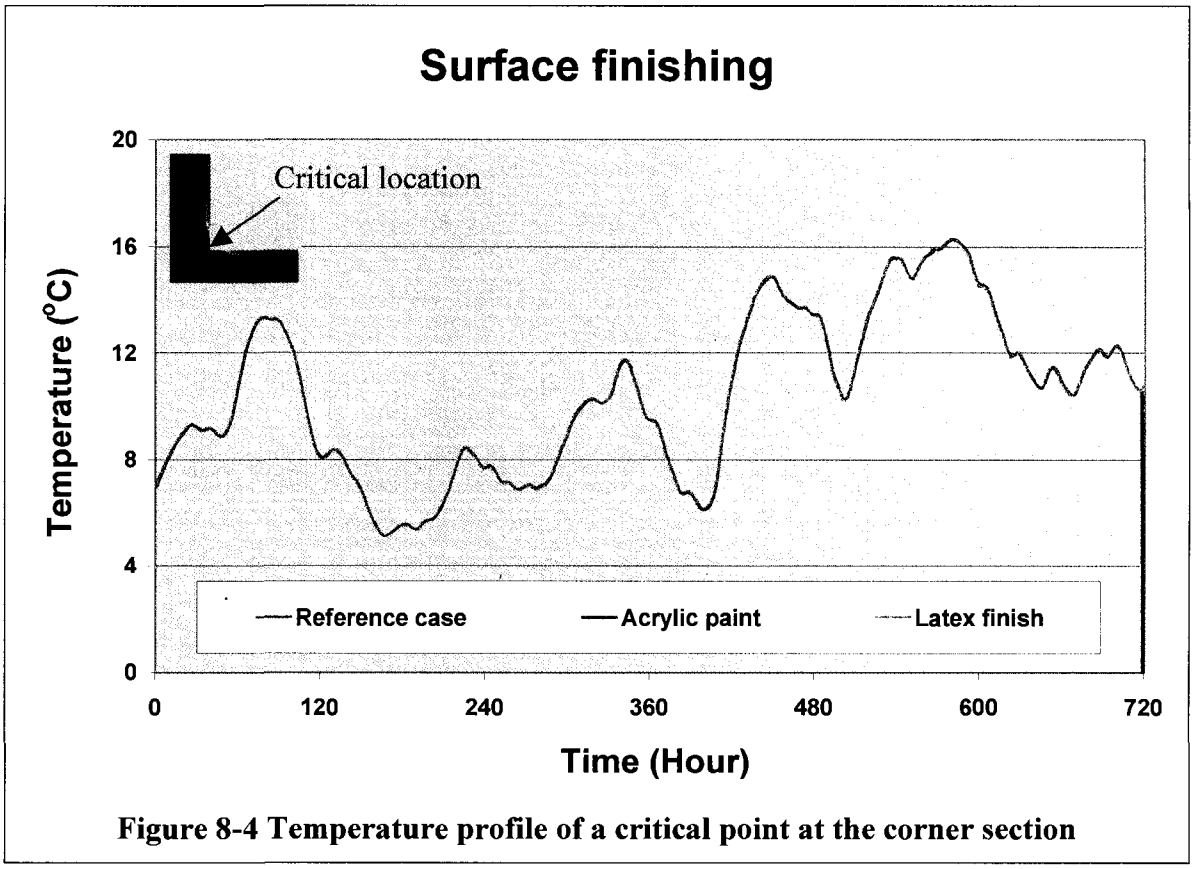

Figure 8-4 Temperature profile of a critical point at the corner section

The relative humidity of the critical point for the three cases is shown in Figure 8-5 below. The moisture accumulation profile in the case with latex paint is relatively lower than the case with acrylic paint. The relative humidity of corner gypsum in the case with no paint shows a higher fluctuation of wetting and drying in response to the indoor humidity condition compared to the cases with paints. As presented in Figure 8-1, the indoor humidity level in the case with the acrylic paint is high, which consequently results in higher moisture absorption by the interior layer compared to the case with latex paint. But, its drying potential (moisture release to the indoor environment) is low compared to the case with no paint. These moderate moisture absorption and release properties of the acrylic paint results in a higher and continuously sustained relative humidity condition. The other two cases are better for different reasons: in the case with no paint, the indoor humidity is generally low and consequently moisture absorption by the interior layer is low, and drying of the layer to the interior is possible; whereas, in the case with latex paint, the indoor humidity is relatively high as the case with acrylic case. However, moisture absorption by the interior layer is very limited since the latex paint is more vapor tight. The average relative humidity of the corner gypsum for the last 600 hours are 77, 79 and 71% for the case with no paint, acrylic and latex paints, respectively. Based on Viitanen and Salonvaara's (2001) mold growth criteria, the case with acrylic paint, whose vapor tightness lies between the more vapor tight (latex) and open surface (reference case), can probably has high mold growth risk compared with the other surface finishing.

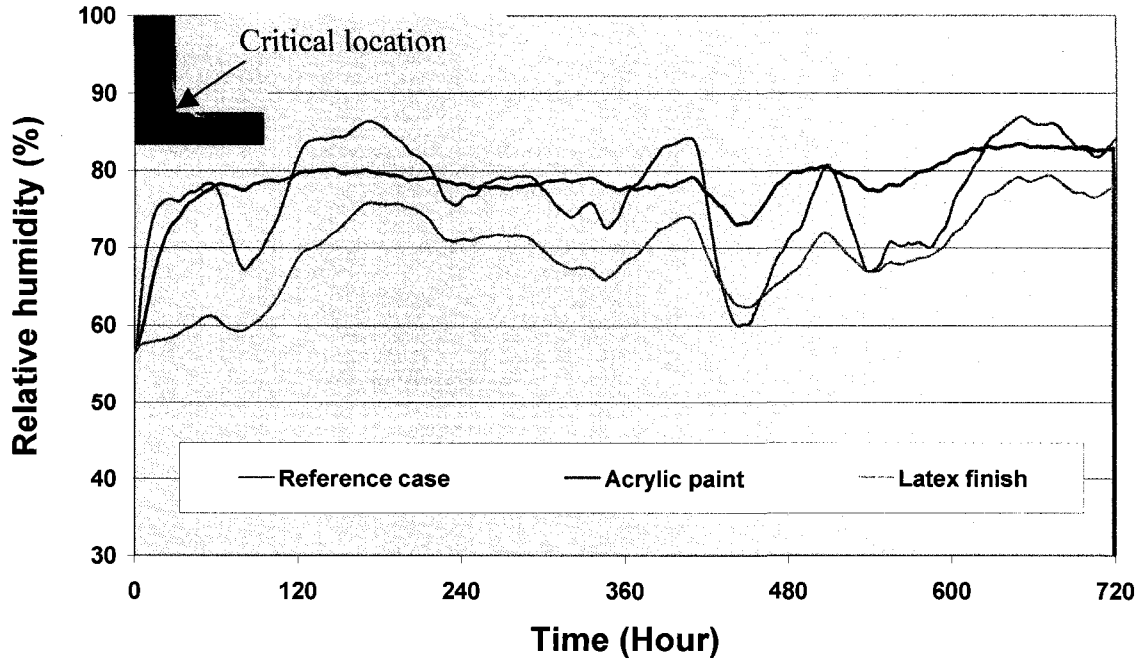

Figure 8-5 Relative humidity profile of a critical point at the corner section

8.2 Influence of interior layer materials

The second series of simulations are performed to examine the degree of influence of interior layer materials on the hygrothermal performance of the house: indoor humidity, energy consumption, and durability. The materials considered are gypsum board (reference case), plywood and fiberboard, and their hygrothermal properties are taken from Kumaran (2002). All simulation parameters including building parameters, HVAC systems and heat and moisture gains are the same in all the three cases. Consequently, the simulated indoor temperature profiles and total energy required for heating are equal to the values reported in the reference case, which are nearly constant (fluctuates between 20.96 to 21°C) and 2796 kWh, respectively. Figure 8-6

shows the indoor relative humidity of the house for the corresponding interior layer of materials. In general, there is no significant difference in the indoor humidity level of the house among the three cases. Slight differences are observed during higher indoor relative humidity periods (95, 342, 481 and 589 hours). In comparison with plywood, the fiberboard reduces the peak relative humidity by as much as 3% and increases by 2% during high and low relative humidity periods, respectively. The high indoor humidity modulating potential of fiberboard in comparison with other materials is noted as well in the laboratory experiment (Wu et al. 2008) and field measurement (Holm and Kunzel 2006).

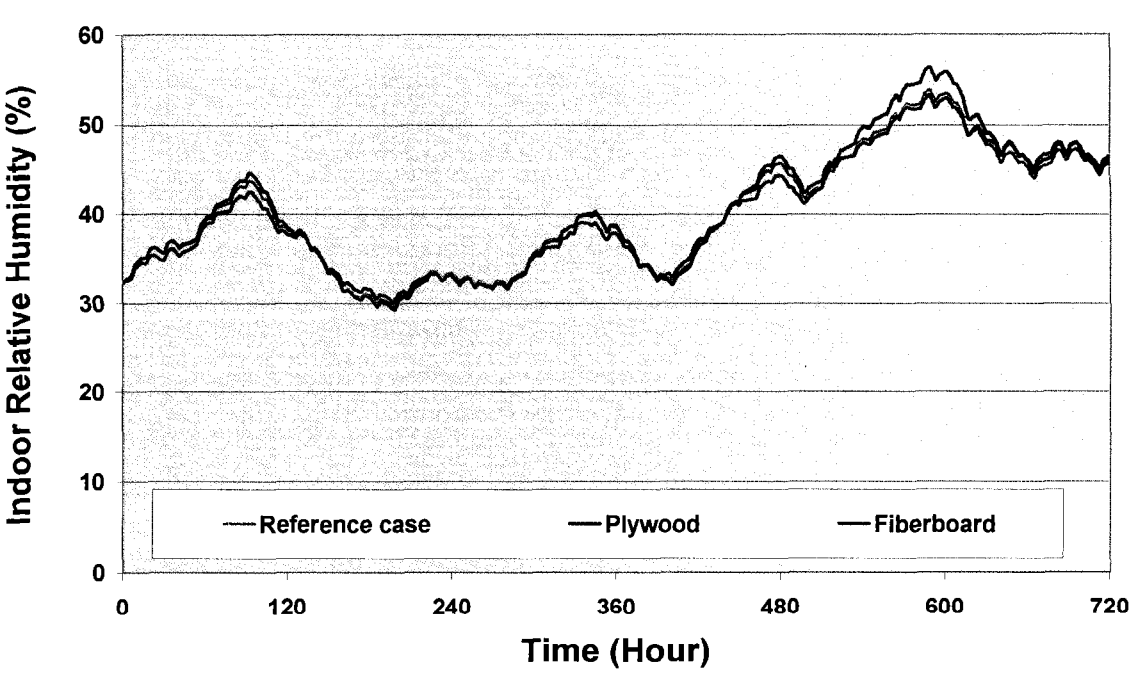

Figure 8-6 Indoor relative humidity of the house for the three interior layers

As Table 8-4 shows below, there is no significant difference in the amount and frequency of window condensation among the three cases. But generally, use of plywood in comparison of the other two lining gives relatively higher moisture condensation on the window surfaces (7.021 kg/day), and also more frequent occurrences of window condensation (63% of the time).

Table 8-4 Window condensations for the three interior layers

	Average window condensation (kg/day)	Moisture supply that is condensed (%)	Condensation occurrence (%)
Reference case	6.576	41.0	61
Plywood	7.021	43.8	63
Fiberboard	6.545	40.9	59

8.3 Mechanical ventilation capacity

Generally, the indoor humidity of the reference house is high. In some cases the relative humidity reaches as high as 58%. As demonstrated in Section 8.1.3, the average relative humidity at the corner section of the reference case can be as high as 77%. The high indoor humidity might affect the occupants' comfort, perceived indoor air quality, health related to mold growth and durability of building envelope components. To avoid such problems in very cold climate, the National Building Code of Canada (2005) sets the upper indoor relative humidity level of residential houses in winter season to 35%.

One of the means for the reference house to achieve the code requirement is by introducing mechanical ventilation systems. The amount of ventilation (or ventilation capacity) that is required to lower the indoor humidity to a level close to 35% needs to be determined. Three mechanical ventilation rates 15, 30 and 45 L/m^{3}s are considered. The effective (combined) ventilation rate is estimated by quadratic superposition of mechanical and natural ventilation rates, Equation [8.2] (ASHRAE Fundamental 2005).

$$Q_t = \sqrt{Q_m^2 + Q_l^2} \qquad [8.2]$$

where Q_t, Q_m and Q_l are the total, mechanical and natural ventilation rates in m^3/s, respectively. Figure 8-7 shows the calculated effective ventilation rates of the house during the monitoring period.

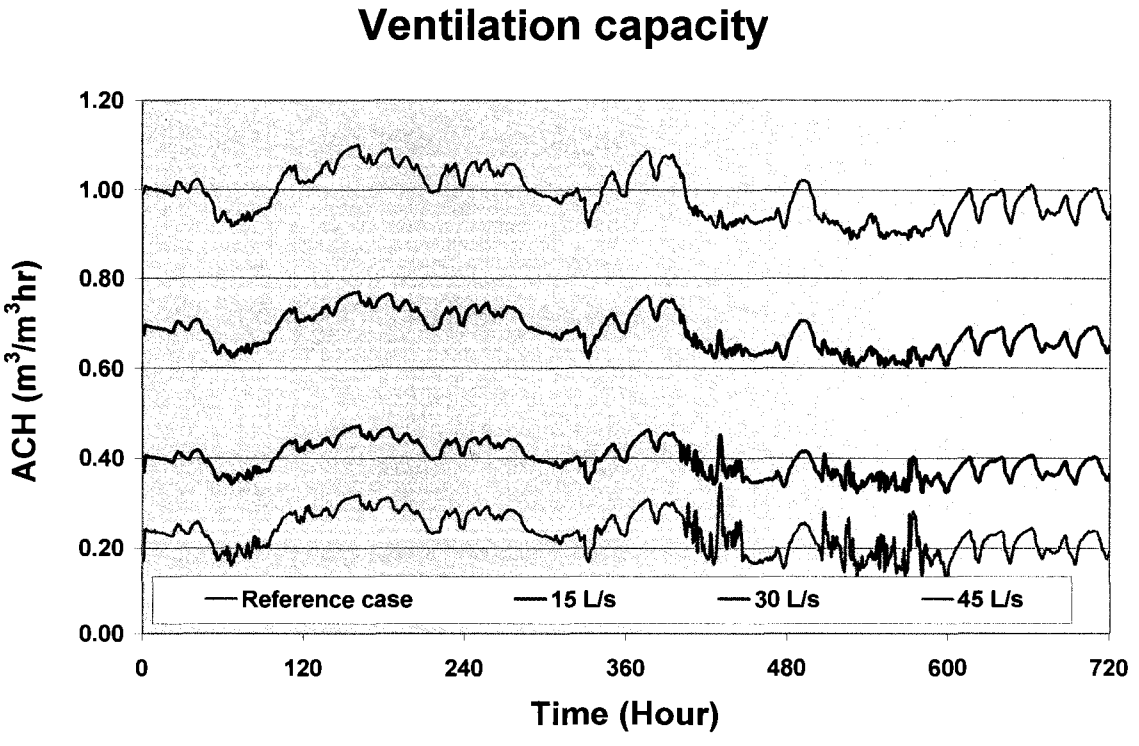

Figure 8-7 Ventilation rates that are considered to lower the indoor relative humidity level below 35%.

The indoor humidity levels of the reference house and three cases with mechanical ventilation systems of 15, 30 and 45 L/s are shown in the Figure 8-8. The maximum relative humidity, which is at 590 hour, reduces from 53% to 46%, 37% and 31% while the mechanical ventilation rates increases from 0, 15, 30 and 45 L/s, respectively. Likewise, the indoor relative humidity ranges (maximum minus minimum) narrow down from 24 to 18, 14 and 10%, respectively.

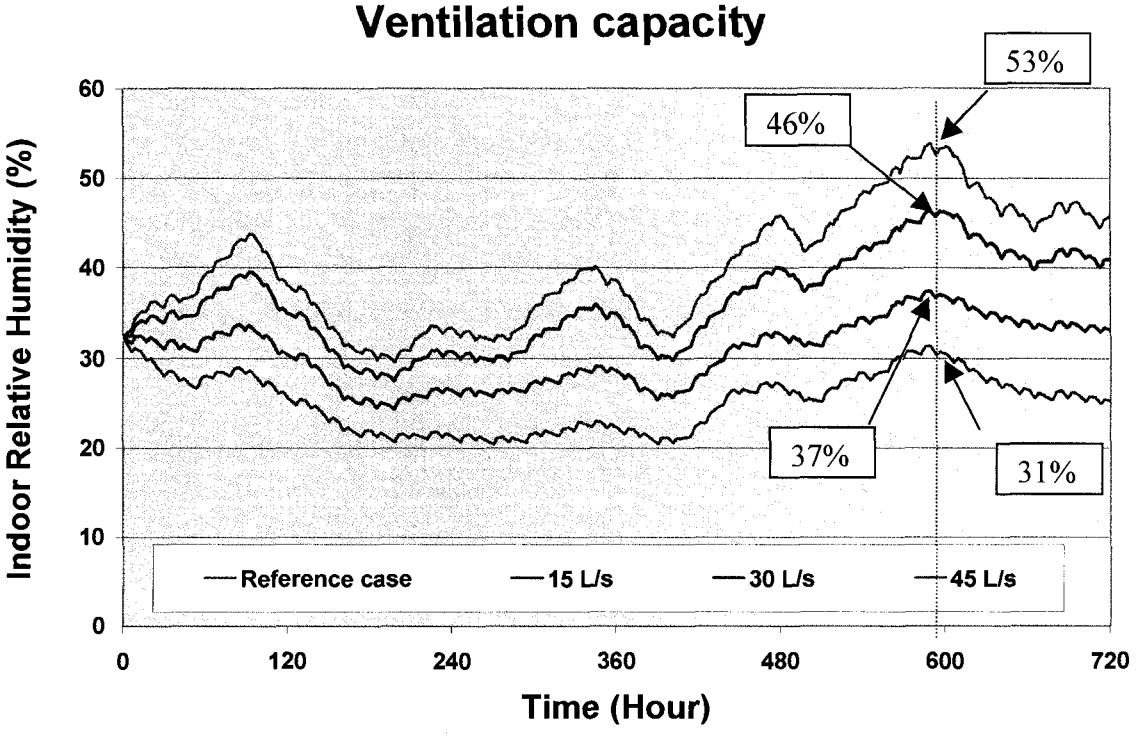

Figure 8-8 Relative humidity profiles of the house for cases with different mechanical ventilation rates

Window condensation decreases significantly as the ventilation rate increases, Table 8-5. Window condensation occurrences decreases from 61 percent to 48, 25 and 5 percent of the time. Likewise, the amount of condensation decreases. In the case of high

continuous ventilation rate (45 L/s), only 0.6 percent of the moisture supply condenses on the window surface. This is very small compared to the condensate amount in the reference case (41.0% of the moisture supply).

Table 8-5 Window condensation for cases with different mechanical ventilation rates

	Average window condensation (kg/day)	Moisture supply that is condensed (%)	Condensation occurrence (%)
Reference (No mechanical ventilation)	6.576	41.0	61
15 L/s	3.862	24.1	48
30 L/s	0.941	5.8	25
45 L/s	0.097	0.6	5

Although the indoor moisture conditions (indoor humidity level and window condensation) can be managed by introducing mechanical ventilation systems, the energy cost that is required to keep the house at 21°C temperature increases with ventilation rate. The total heating load of the reference house for the thirty days is 2796 kWh. The energy demand increase by 51% if a mechanical ventilation system with 45 L/s is adopted, Table 8-6. This implies that there is a need for ventilation strategy that minimizes the energy demand and at the same time maintains acceptable level of indoor humidity conditions. In the next section three ventilation strategies are considered.

Table 8-6 Heating load for cases with different mechanical ventilation rates

	Heating load (kWh)	Percentage of increase in heating load (%)
Reference (No mechanical ventilation)	2796	-
15 L/s	3094	11
30 L/s	3633	30
45 L/s	4211	51

8.4 Ventilation strategy

Four ventilation strategies are considered for evaluation of both indoor humidity and energy performances of the house. The first one is the reference case, which is with no mechanical ventilation. In the second case, the ventilation system is set to operate in continuous mode with a constant ventilation rate of 30 L/s. In the third strategy, the ventilation system operates continuously, but the ventilation rate is time dependent. The ventilation schedule of a typical day is shown in Figure 8-9. Depending on the hour of the day, the ventilation system operates at 15, 30 or 45 L/s, which represent the low, medium and high ventilation rates. The ventilation rates are selected in response to the indoor moisture generation rates. The daily moisture production profile of the house is presented in Figure 7-12. During the morning hours (6:00-9:00 h), high moisture production is expected, and consequently the ventilation system is assumed to operate at the higher ventilation rate. During house keeping and lunch preparation period (9:00-13:00 h) and evening hours (17:00-21:00 h) moderate moisture production is assumed, hence the

ventilation rate is set to medium rate. In the rest of the day, the ventilation system is assumed to operate at low ventilation rate. Relative humidity controlled ventilation (RHCV) is the fourth ventilation strategy that is considered in this section. In this strategy, the ventilation system has a ventilation capacity of 45 L/s and its operation depends on the indoor relative humidity level, turned on when the indoor humidity relative level is over 35% and turned off when it is below 35%.

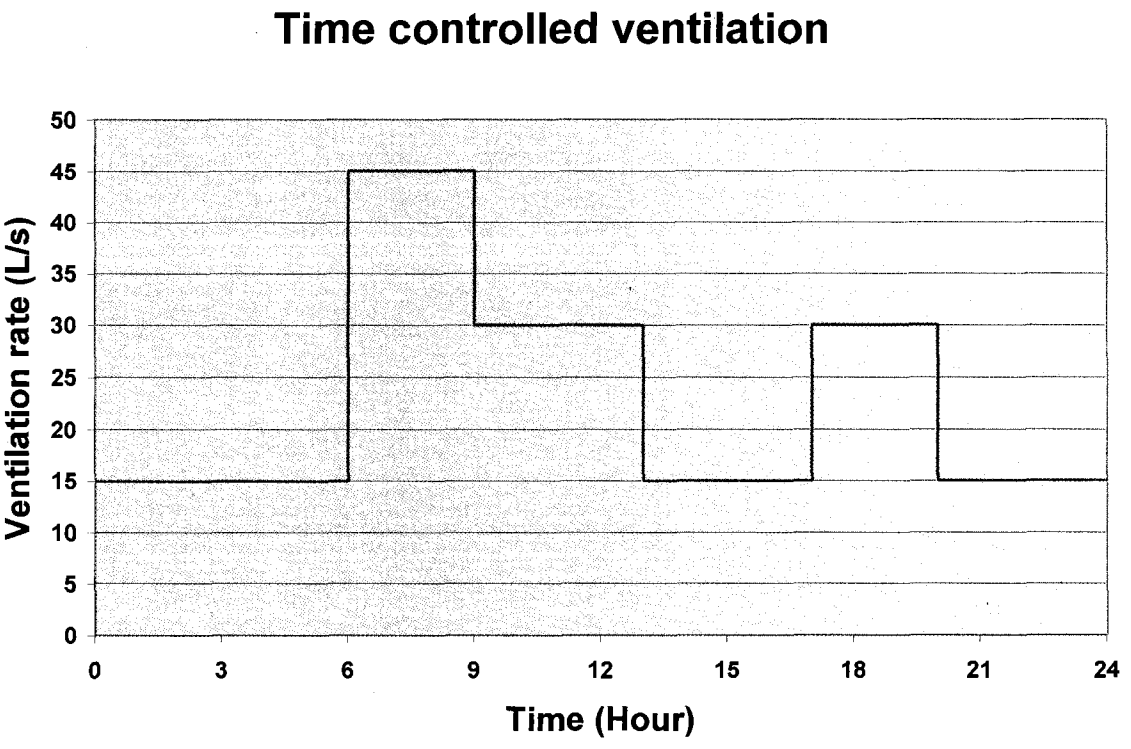

Figure 8-9 Ventilation schedule of a typical day

Figure 8-10 shows the indoor relative humidity profiles of the house for cases with different ventilation strategies. In the reference case, where no mechanical ventilation is incorporated, the indoor relative humidity exceeds the upper limit (35%) for

most of the time (71% of the simulation period). The time-controlled ventilation strategy maintains the indoor humidity level below the set point for most of the period. However, this ventilation strategy could not maintain the desired humidity level after 510 hour. This is due to the fact that this ventilation strategy is time controlled, and does not have a feed back mechanism that gives the state of the indoor humidity condition. The continuous and RHCV strategies manage to maintain the indoor humidity level below the upper limit with the exception of a few hours. In the case of continuous ventilation strategy, however, there is no dynamic coupling between the ventilation system and the indoor humidity level. Subsequently this ventilation strategy has a tendency of over-ventilating, which results in low indoor humidity level compared to other ventilation strategies. The indoor humidity level is close to the set point and more stable in the case of the RHCV strategy.

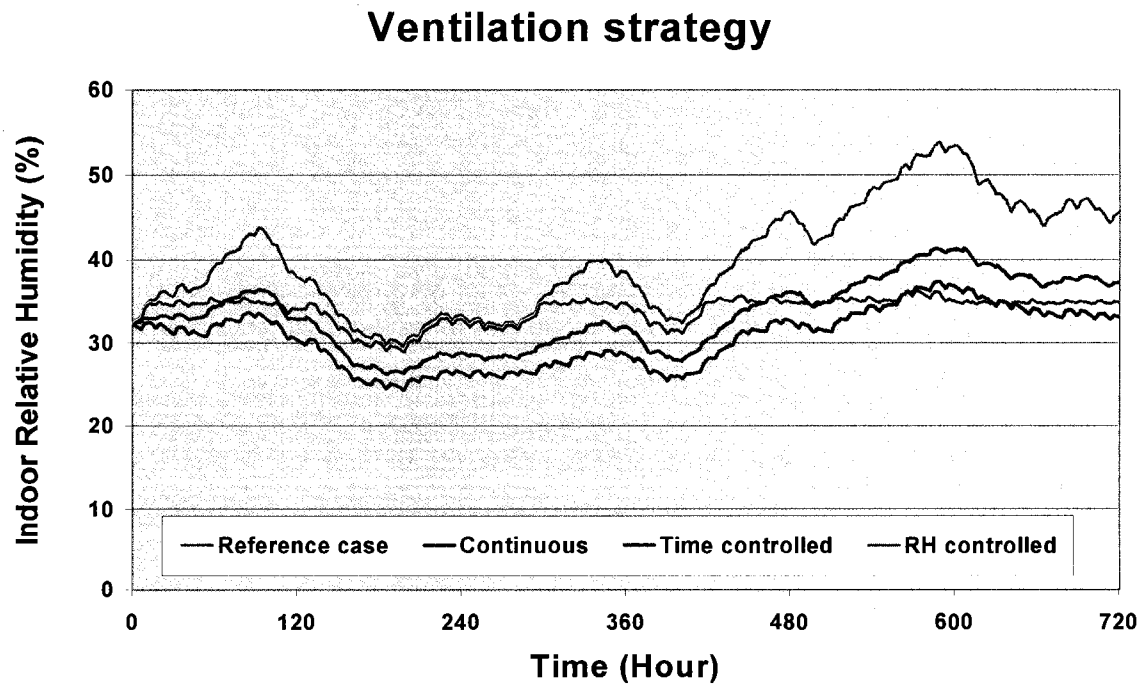

Figure 8-10 Relative humidity profiles of the house for cases with different ventilation strategies

The condensation on the windows is summarized in the Table 8-7. The condensate amount is reduced by about half and by one-third of the reference case when RHCV and time-controlled ventilation strategies, respectively, are adopted. The lowest amount (0.941 kg/day) and number of condensation occurrences (25% of the time) are obtained in the case of continuous ventilation strategy.

Table 8-7 Window condensation for cases with different ventilation strategies

	Average window condensation (kg/day)	Moisture supply that is condensed (%)	Condensation occurrence (%)
Reference (No mechanical ventilation)	6.576	41.0	61
Continuous ventilation	0.941	5.9	25
Time controlled ventilation	2.200	13.7	41
RHCV	3.379	21.1	43

Although the continuous ventilation strategy yields less window condensation, it requires 29.92% more energy than that of the reference case, Table 8-8. Only 13.75% additional energy is required if the RHCV strategy is adopted. The additional energy demand in the case of time-controlled ventilation is in between the continuous and RHCV strategies (20.08%).

Table 8-8 Heating load for cases with different ventilation strategies

	Heating load (kWh)	Percentage of increase in heating load (%)
Reference (No mechanical ventilation)	2796	-
Continuous ventilation	3633	29.92
Time controlled ventilation	3358	20.08
RHCV	3181	13.75

8.4.1 Combination of RHCV and moisture buffering

For the case where the indoor humidity level is controlled by mechanical ventilation at the expense of extra energy, materials with higher moisture buffering capacity might contribute to energy saving. This is due to the fact that these materials can absorb part of the extra humidity, and hence reduce the required ventilation and the energy required for heating. As the indoor humidity profile of the house shown in Figure 8-6 indicates, fiberboard has a relatively higher moisture buffering capacity compared to plywood and gypsum board (reference case). Simulation results suggest that replacing the interior layer, gypsum board, with the more moisture-buffering layer, fiberboard, in the case of RHCV strategy yields a relative energy saving of 1.5%. This implies that the extra energy that is required will be 12.04% of the reference case, which is less than the case with gypsum board (13.75% Table 8-8).

8.4.2 Moisture in building envelope component—Case of RHCV strategy

Moisture management of building envelope components is one of the four parameters for evaluation of whole building performance, indoor humidity, energy efficiency and window condensation being the other three parameters. As shown above, mechanical ventilation can be used to regulate the indoor humidity condition of the houses to the desired level. The ventilation strategy that can provide the desired humidity level at the minimum additional energy cost is the RHCV strategy. Choosing this ventilation strategy can also result in a better moisture management of the building envelope component. This is demonstrated by simulating the dynamic response of the two-dimensional corner section of the house (shown in Figure 7-25) using HAMFit2D. All the simulation parameters are the same as described in Section 7.3 except for the indoor humidity boundary condition. The indoor humidity condition is obtained from whole building analysis of the house with RHCV strategy shown in Figure 8-8. Figure 8-11 shows the moisture condition at the rear junction point of the two gypsum boards. . As shown in the figure, the relative humidity of the critical location is lower throughout the simulation period in the case of RHCV than the reference case, where no mechanical ventilation is installed. During the last 600 hours, the critical section has an average relative humidity of 77% (reference case) and 67% (RHCV case). Moreover, when RHCV is introduced in the reference house, the percentage of time that this critical location attains relative humidity over 80% decreases from 35% to 9%. The lowest relative humidity in the reference case is 60%, which is high compared to the 48% that is obtained in adopting the RHCV system. These data suggest that in the case of RHCV,

where the average relative humidity is 67% and the relative humidity of the location is over 80% only 9% of the time, the building envelope component is at less risk for mold growth compared with the reference case. In general, RHCV yields a better building component performance by promoting faster drying compared to the reference case.

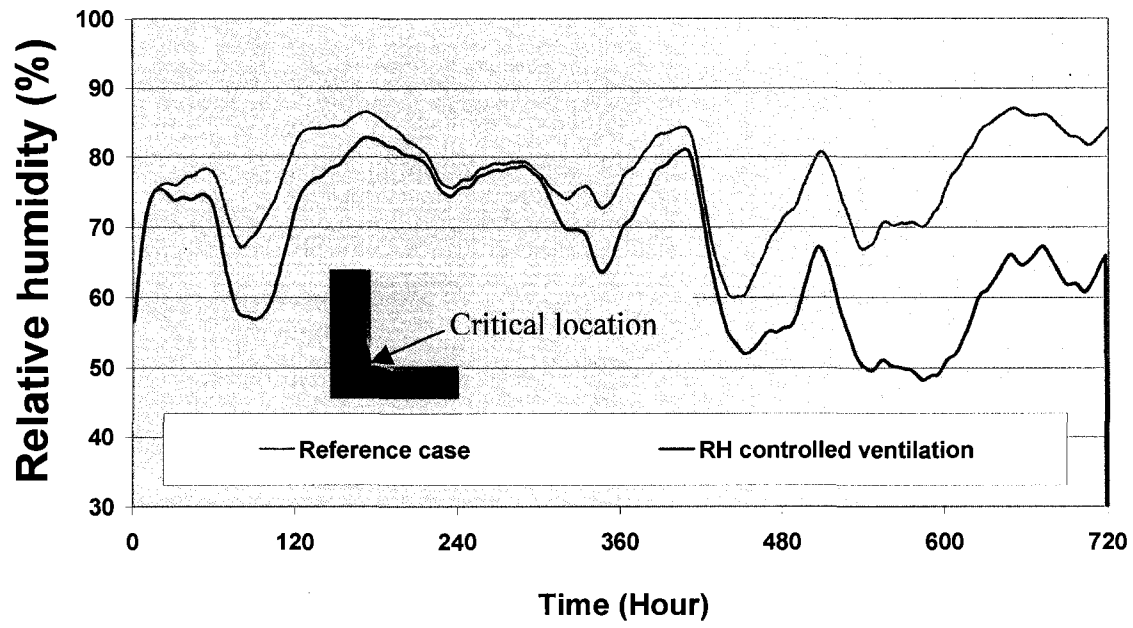

Figure 8-11 Relative humidity profile of a critical point at the corner section: comparison of Reference and RHCV cases

8.5 Thermostat setback

One of the strategies for conservation of energy for the house considered here is decreasing the operative indoor temperature, which thereby reduces the heating demand The house considered here is assumed to be occupied throughout the day. Hence, the only time the indoor temperature can be reduced is during sleeping time (21:00-7:00 h), when

the occupants use additional insulation (blankets) to maintain their thermal comfort. Figure 8-12 shows three thermostat settings considered here. The first thermostat setting belongs to the reference case where the indoor temperature is maintained constant at 21°C at all time (no set-back). In the second thermostat-setting scheme, the indoor temperature is maintained at 21°C from 7:00 to 21:00 h, and then setback to 17°C for the remaining hours (21:00 to 7:00 h). This scheme is referred as single-step up since the indoor temperature increases in a single step from 17 to 21°C at 7:00 h. The third thermostat-setting scheme is similar to the second scheme except that the increment of the indoor temperature from 17 to 21°C is done in three steps (1.5, 1.5 and 1°C increments at 5, 6 and 7 h, respectively) as opposed to the second option where a single step (4°C increment) is used. The third option is referred to as multiple-steps up.

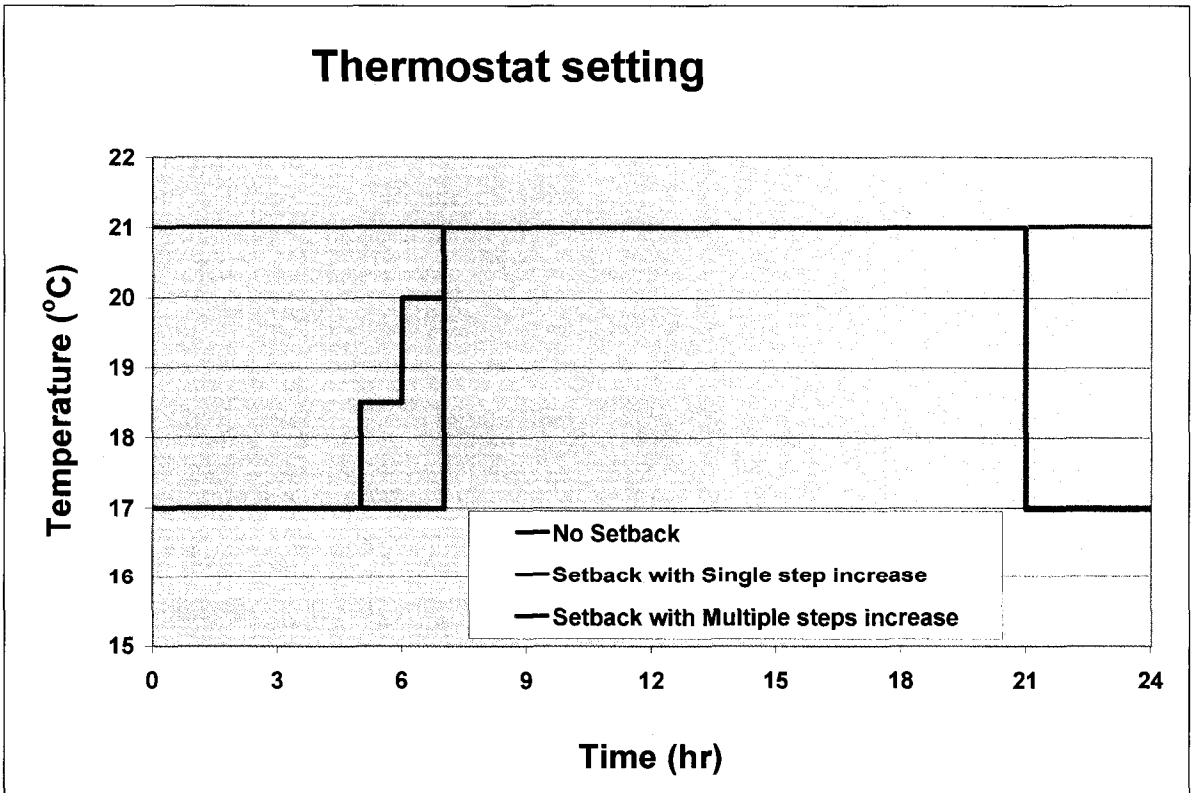

Figure 8-12 Thermostat setting schemes for a typical day.

Energy analysis of the three thermostat-setting schemes suggests that implementation of thermostat with temperature setback reduces heating energy consumption by as much as 4.42% (single-step up case) when compared to the case with a constant temperature setting (reference case). Adoption of the third thermostat-setback scheme (multiple-steps up) results in 3.62% heating energy saving compared with the reference case. Although a relatively higher energy saving is obtained by choosing the single-step rather than multiple-steps up scheme, the peak energy demand at the transition of indoor temperature from 17 to 21°C is significantly higher in the single-step up scheme. Figure 8-13 shows a typical daily energy consumption profile of the house. In the two cases where thermostat setback schemes are considered, heating is not needed for about two hours (21:00–23:00 h). The energy demand in the reference case is nearly uniform throughout the day. But, the peak energy demands in the cases of single step and multiple-step schemes are 21.01 and 13.16 kW, respectively. These results imply that indoor temperature control with thermostat setback can decrease energy consumption, but may require a heating system with a higher heating capacity to maintain the desired indoor temperature quickly. In the case considered here, the heating capacity needs to be increased by 77 and 183% of the reference case if the multiple-step and single-step schemes are chosen, respectively. Among the thermostat-setback scheme considered, the multi-step scheme might be preferable since it represents a compromise between the energy saving and equipment size.

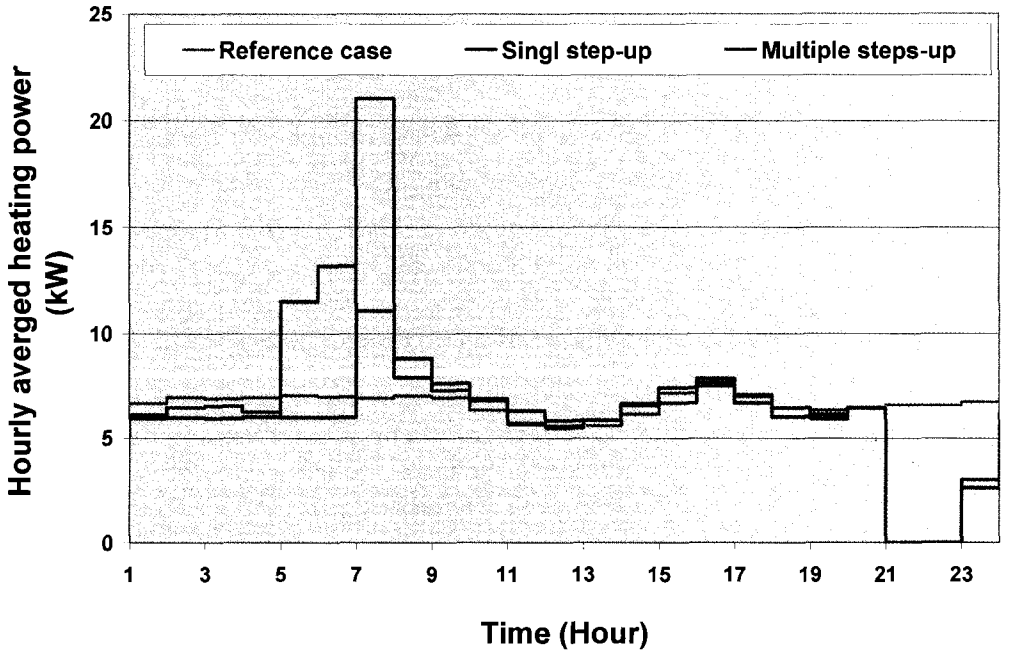

Figure 8-13 Typical day energy consumption of the house under different thermostat setback scheme

HAMFitPlus solves energy and indoor humidity balance equations simultaneously, and therefore, consequence of energy upgrade by chosen retrofit option on the indoor humidity and durability of the envelope can be investigated. Figure 8-14 shows the indoor relative humidity profiles of the house for the three thermostat settings. The cases with thermostat-setback options, single- and multiple steps up, have fluctuating profiles. The typical day indoor relative humidity profiles for the cases with the three thermostat setback schemes are shown in Figure 8-15. In cases with thermostat-setback, the indoor relative humidity reaches to the maximum during the period when the temperature setback is effective. The differences in the relative humidity daily peaks between the cases with and without thermostat-setback options can be as high as 12%. And the

maximum indoor relative humidity, which is attended at 605 hour by the cases with thermostat-setback option, is 65%.

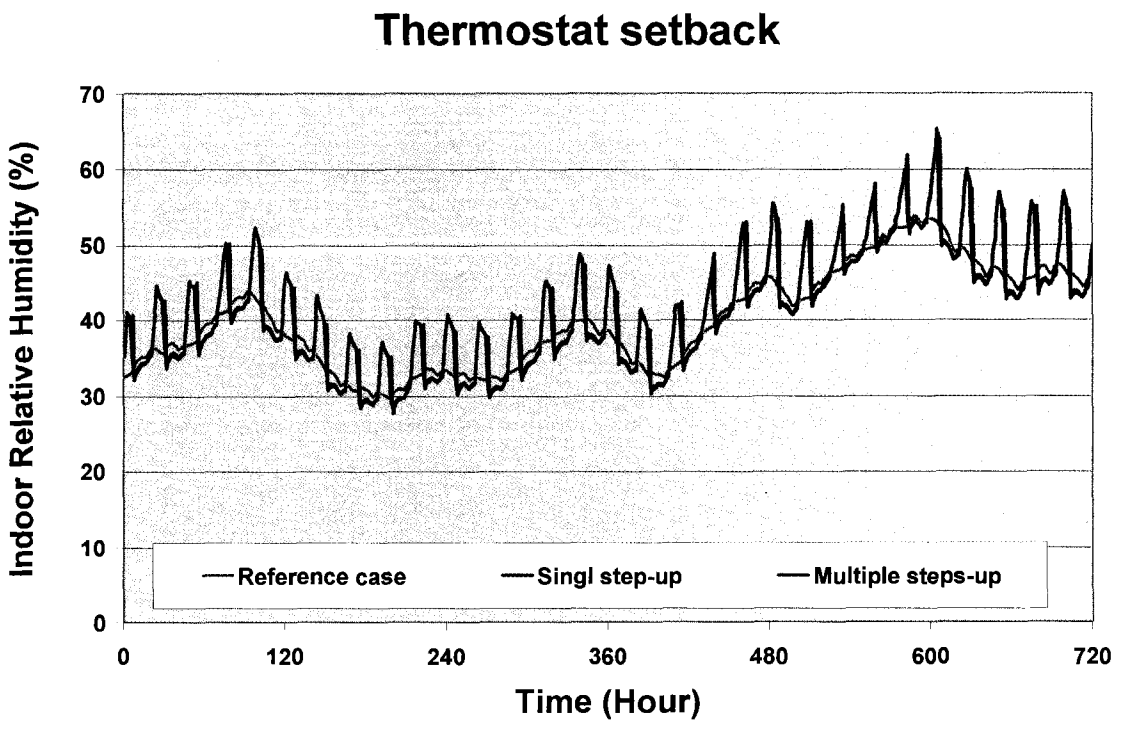

Figure 8-14 Indoor relative humidity profiles of the house for the three thermostat setback schemes

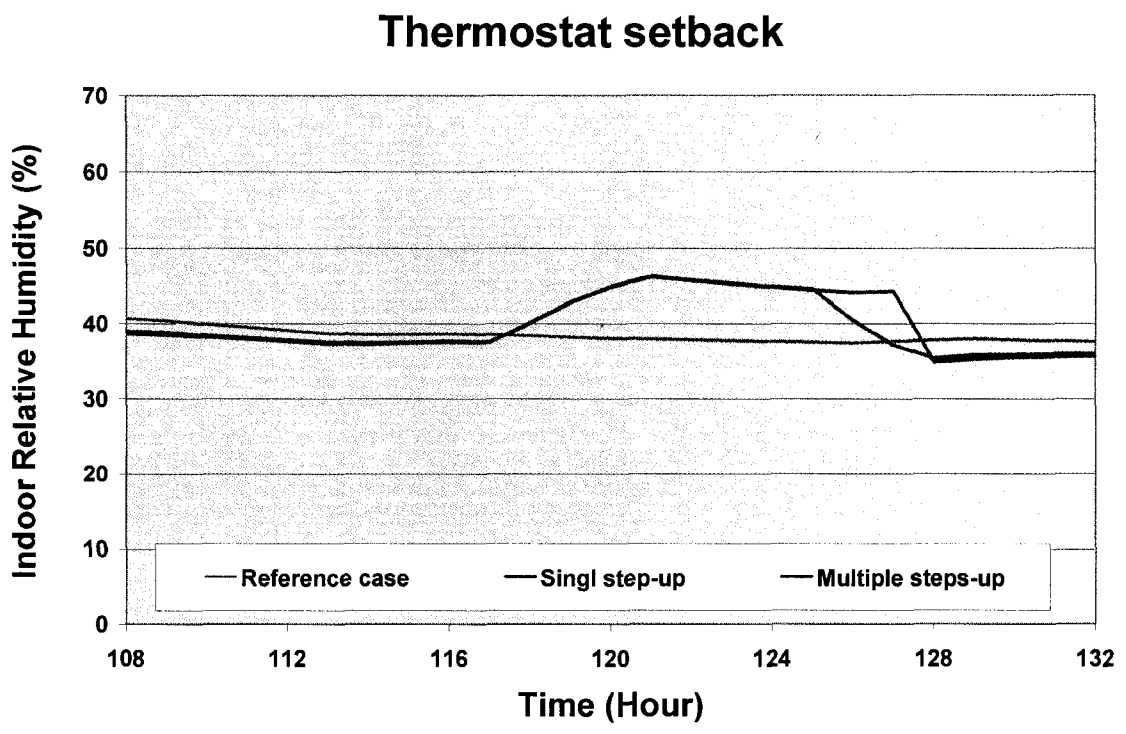

Figure 8-15 Indoor relative humidity profiles of the house for the three thermostat setback schemes—Detailed view

8.5.1 Moisture in building envelope component—Case of Thermostat setback

Although the thermostat setback improves the energy efficiency of the house as demonstrated here, the effect of high indoor relative humidity fluctuation on the durability of building envelope components might also need consideration. This is because the low indoor temperature coupled with unchanged moisture supply results in more condensation on windows surfaces and building envelope components. The amount of condensate on the window surfaces increases by 2.10 and 1.82% for the single-step and multi-steps-up cases, respectively, compared to the reference case. Hygrothermal

simulation of the corner section of the house indicates that the building envelope components experience additional cyclic moisture loading in cases where thermostat setback is used. This is shown in Figure 8-16 where the moisture condition at the back of the gypsum board is presented for cases with and without thermostat setback. The corresponding indoor humidity boundary conditions are shown in Figure 8-14. Although the overall trend of the relative humidity responses of the reference and thermostat setback cases are similar, in the later case the relative humidity increases by about 3% from the reference case during the night time when the thermostat setback period is on. These cyclic moisture loadings with short amplitude and frequency may have an effect on the durability of the component.

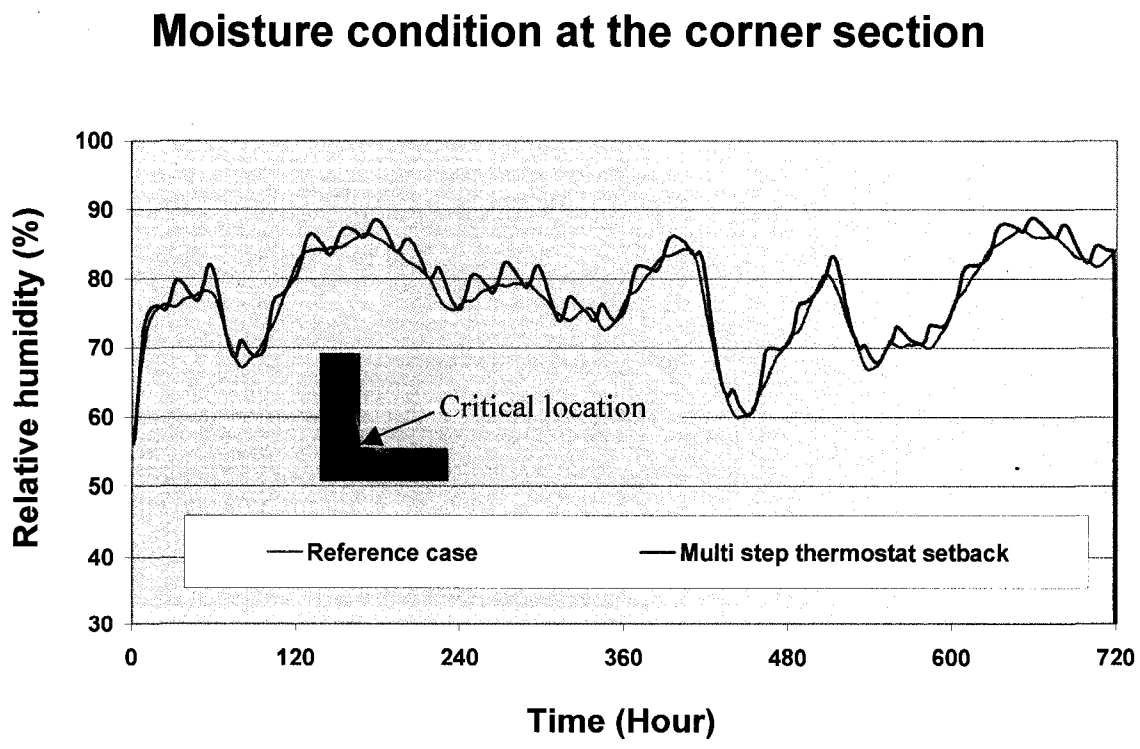

Figure 8-16 Relative humidity profile of a critical point at the corner section: comparison of cases with and without thermostat-setback

8.6 Combination of RHCV and thermostat setback

As presented above, thermostat with nighttime temperature setback yields an energy saving of 3.62% in the case with multi-step up scheme. However, this setting results in a higher indoor humidity level, as high as 65%, which increases window condensation by 1.82% and exhibits short amplitude moisture accumulation cycles in the building envelope component. These conditions might affect the occupant comfort, health and durability of the building envelope. On the other hand, introduction of mechanical ventilation system to lower the indoor humidity level of the house to the recommended value requires additional heating energy. A possible building performance-upgrading scenario, which combines moisture control and energy saving strategies, is considered here: combination of mechanical ventilation and thermostat setback. Based on previous simulation results, a mechanical ventilation system with RHCV strategy to maintain the indoor relative humidity below 35%, and a thermostat with multiple-step-up setback scheme, which resulted in less peak energy demand, are implemented. The three cases considered here are: a case with neither thermostat setback nor mechanical ventilation system (reference case); RHCV system but with no thermostat setback (case 2), and a case where both thermostat setback with multiple-step-up scheme and RHCV system (case 3) are implemented.

Table 8-9 and Table 8-10 show the heating load and window condensation results of the respective upgrade options. In the third case, the energy saved by thermostat setback (3.62%) is taken by the energy demand for heating the extra ventilation that is required during temperature setback period. During thermostat-setback period the relative humidity is generally high as shown in Figure 8-14. Consequently, there is no significant

energy saving in adopting RHCV system with thermostat setback option when compared to the case with only RHCV option. The energy demands for the respective cases are 3181 and 3170 kWh, respectively (13.75 and 13.36% more of the reference case, respectively). Although there is no noticeable energy saving gain in case 3 compared to case 2, the amount of window condensation is reduced by 21.2% from case 2. Hence, case 3 can be considered a better choice as it provides a controlled indoor humidity level, provides more ventilation, and reduces window condensation for about the same energy demand as of case 2.

Table 8-9 Heating energy demand for cases with RHCV and thermostat setback options

	Heating load (kWh)	Percentage of increase in heating load (%)
Reference (No mechanical ventilation)	2796	-
RHCV	3181	13.75
RHCV + Thermostat setback with Multiple-step-up scheme	3170	13.36

Table 8-10 Window condensation for cases with RHCV and thermostat-setback options

	Average window condensation (kg/day)	Moisture supply that is condensed (%)	Condensation occurrence (%)
Reference (No mechanical ventilation)	6.576	41.00	61
RHCV	3.379	21.11	43
RHCV + Thermostat setback with Multiple-step-up scheme	2.660	16.62	45

8.7 External Insulation

One of the means of increasing energy efficiency of the house is by increasing the thermal resistance of the exterior components of the building envelope. In the following section, the thermal and moisture performances of the reference house, as it is retrofitted with external insulation, are examined. The material used for external insulation is expanded-polystyrene. The density, specific heat capacity, and thermal conductivity of the insulation are 20 kg/m^3, 1470 J/K.kg and 0.034 W/Km, respectively (Kumaran, 2002). Three whole building hygrothermal simulations (using HAMFitPlus) are carried out with different insulation thickness. All the simulation parameters of these three cases are the same as the reference case except that in these cases the house is additionally insulated on the exterior by 25, 50, or 100 mm thick expanded polystyrene.

Analysis of the simulation results indicates that there is no substantial change in the indoor humidity profiles nor the amount and frequency of window condensation in cases with external insulation when compared to that of the reference case. But a substantial energy saving is obtained as the external insulation thickness increases, Figure 8-17. Using the reference case (no external insulation) as a basis, the percentage of energy savings obtained by retrofitting the house with 25, 50 and 100 mm thick insulation are 9, 16 and 26%, respectively. In comparison with thermostat setback, the energy saving obtained by introducing external insulation is significant. However, the cost of the latter energy upgrade is substantially higher compared to installing a thermostat with automatic control. To determine an optimal insulation thickness, a cost-benefit analysis of the initial investment (additional material cost) and long–term operation (heating cost saving) of the house due to an increase in insulation thickness may need to be carried out. In addition to this cost-benefit analysis, the effect of insulation on the moisture performance of the building envelope components has to be considered simultaneously.

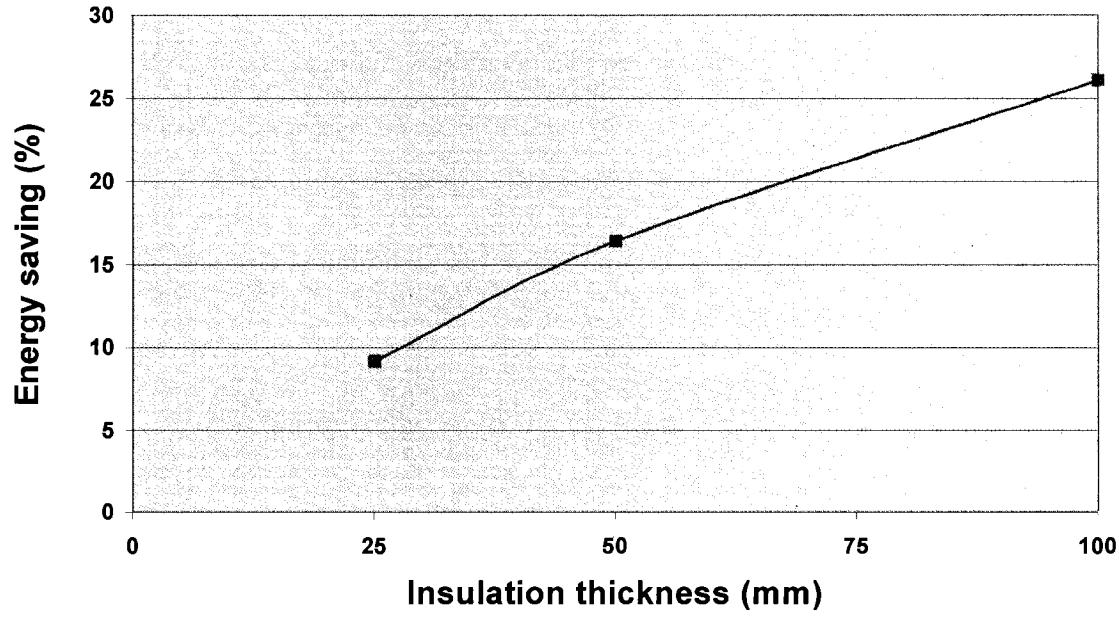

Figure 8-17 Energy saving as a function of external insulation thickness

8.7.1 Moisture in building envelope component—Case of External insulation

As demonstrated from the HAMFitPlus simulation results, addition of external insulation yields a better energy performance of the house without significant change in the level of indoor humidity or occupant comfort. This retrofit option can have an effect on the hygrothermal performance of building envelope components. To investigate this, a two-dimensional vertical section of the northeast wall is considered, Figure 8-18. The wall is assumed to have crack openings of 3 mm width at the exterior sheathing board (at the neutral pressure level) and interior gypsum board. These openings created an airflow path between the outdoor and indoor air through the insulation. The airleakage rate is

governed by Poiseuille's law of proportionality (Hens 2007), which is defined here by the pressure difference at the two openings and the flow resistance of the cavity. The flow resistance of the cavity is approximated by the flow resistance property of the glass fiber insulation. The air permeability of the glass fiber insulation is approximately 2.5E-04 kg m^{-1} s^{-1} Pa^{-1} (Kumaran, 2002).

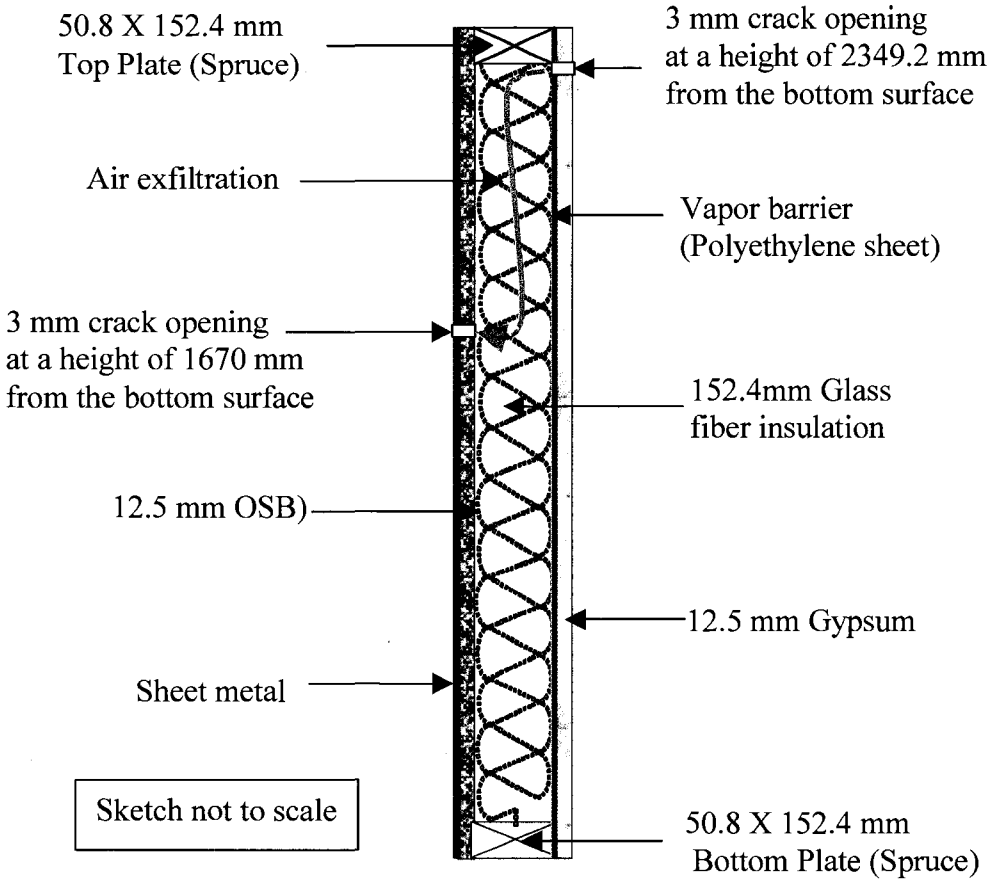

Figure 8-18 A cross-section view of the reference case wall section (with no external insulation)

8.7.1.1 HAMFit2D simulation

The hygrothermal performance of the wall with airflow through the structure is assessed with HAMFit2D simulation. The outdoor and indoor surfaces of the wall are exposed to Carmacks weather conditions, and indoor relative humidity and temperature conditions that are predicted by HAMFitPlus. The pressure difference across the wall is determined based on the outdoor and indoor pressure conditions. It is calculated for each hour (as the weather data is hourly) using the infiltration model described in Section 7.1.4. The model considers the building site, geometry, orientation as well as the driving forces due to wind and stack pressures. The simulation runs for a period of thirty days starting January 19th, 2006. The top and bottom boundary conditions for heat and moisture transfer are assumed to be under adiabatic/closed boundary conditions. The left and right boundary surfaces are subjected to Neumann type boundary conditions, where the moisture and heat fluxes are applied on the surfaces. The effective heat flux on the exterior surface is calculated by adding the heat gain due to solar radiation and the net heat exchange between the surfaces and the surrounding environment due to longwave radiation and convective heat exchange mechanisms. The convective and longwave radiation heat exchanges are treated independently. The convective heat transfer coefficient depends on wind speed, and is approximated by Equation [7.10] (Sanders 1996). The longwave radiation heat exchange is estimated based on International Standard ISO 15927-1:2003, Annex B. Since the exterior surface is sheet metal, which is impermeable for moisture flow, the wind-driven rain load and moisture exchange with the surrounding are neglected in the HAMFit2D simulation. The heat and mass transfer coefficients of the interior boundary surface are 8 W/Km^2 and 5E-8 s/m, respectively.

The heat transfer coefficient accounts for both convection and long-wave radiation heat exchanges. The indoor relative humidity and temperature profiles that are generated by HAMFitPlus for the case 'External insulation' are used as indoor boundary conditions. The indoor relative humidity is the same as the reference case (shown in Figure 8-1), and the temperature is nearly constant at 21°C. All boundary surfaces are assumed to be impermeable, except at the crack opening locations. The pressure boundary conditions at the crack opening are given by the pressure difference of the two locations, Figure 8-19. The hygrothermal properties of all the layers are the same as discussed in Section 7.1.4, *Building enclosure*.

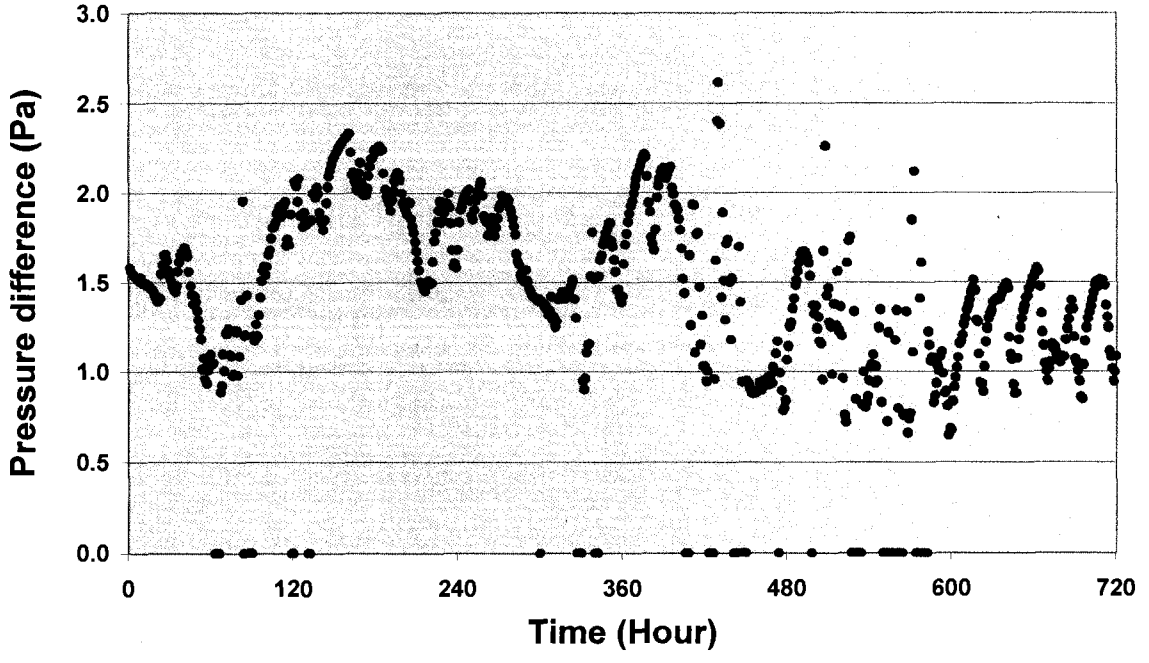

Figure 8-19 Pressure difference between the two crack openings (exfiltration)

Due to high variation in the thickness of the layers, a controlled mesh is applied to each component. This procedure results in discritization of the sheathing board (OSB), cavity insulation, and top and bottom plates into 2160 quadratic elements. Figure 8-20 shows the mesh at the upper section of the wall. Presentation of the entire wall mesh was not possible due to the high aspect ratio, height to thickness ratio of the wall.

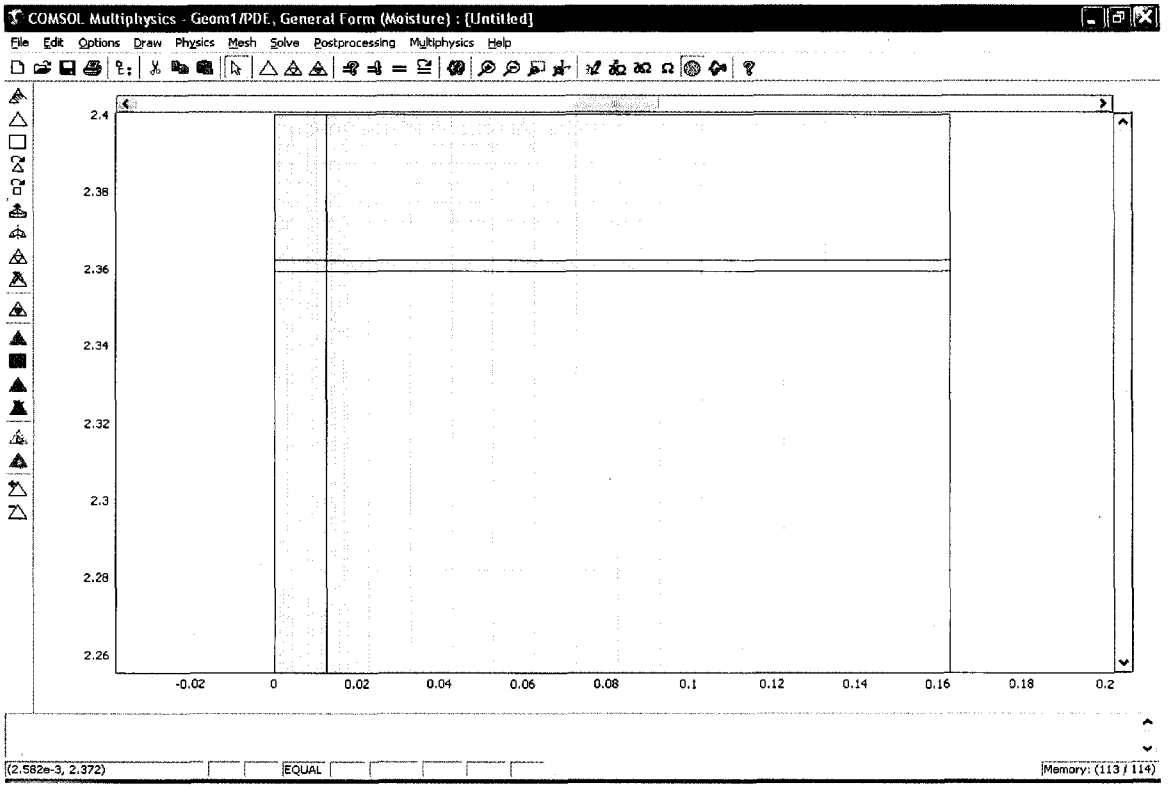

Figure 8-20 Discritization of the upper section of the wall

8.7.1.2 Simulation results

Four scenarios were simulated to investigate the effect of external insulation and airleakage on the hygrothermal performance of a wall in cold climate. The first case is the reference case where there is no external insulation. In the other three cases, the wall is

padded with an external insulation of 25, 50 or 100 mm thick expanded-polystyrene. The relative performances of the four walls are assessed based on the hygrothermal conditions of the sheathing board (OSB) and top/bottom plates. The temperature and moisture (relative humidity) profiles across the walls section on January 24th are presented in Figure 8-21 and Figure 8-22, respectively, as hygrothermal snapshots samples. In Figure 8-21, the temperature contour plots of the upper section of the OSB, cavity insulation and top plate are shown. The first contour plot is for the reference case wall (no external insulation installed), and the following three contour plots are for the walls retrofitted with external insulation of 25, 50 and 100 mm thickness At this particular time, the temperature difference of the coldest spot on the sheathing board of the reference case wall and that of the highly insulated wall is significantly high (21^{o}C). As the level of external insulation thickness increases, the coldest spot temperature increases from –25, which is the case in the reference wall, to -16, -8, and -4^{o}C for the walls padded with external insulation thickness of 25, 50 and 100 mm, respectively.

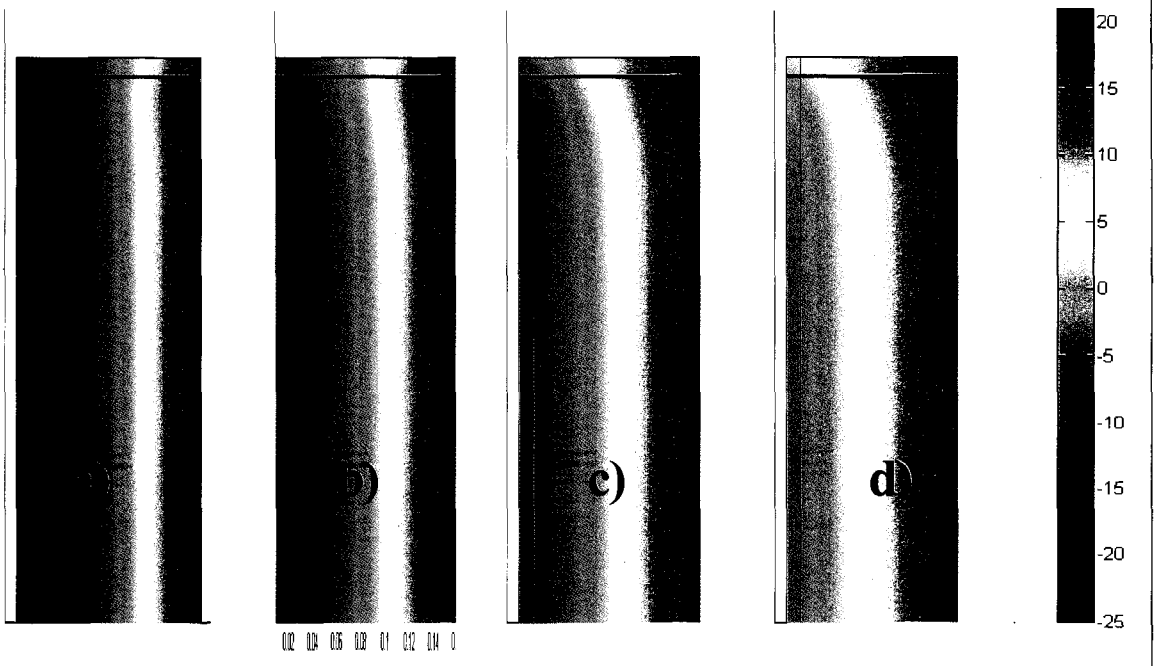

Figure 8-21 Temperature profiles of the upper section of the wall on January 24th:
a) no external insulation b) 25 mm external insulation c) 50 mm external insulation d) 100 mm external insulation

Figure 8-22 shows the moisture profiles of the upper sections of the reference case wall and the three retrofitted walls with external insulation thickness of 25, 50 and 100 mm. In the figure, the respective walls are designated as wall 'a', 'b', 'c' and 'd'. As the temperature control plots of the four walls (Figure 8-21) shows, the OSB and its adjacent areas are relatively colder than the center or the right end section of the wall. In all four cases, relatively high moisture accumulations are observed in this region, more specifically at the top section, due to the exfiltration of the relatively moist indoor air to this cold area. At this time, the moisture laden indoor air jet impinges the cold OSB surface, and loses a significant amount of moisture by condensation and subsequently freezes on the interior surface of the OSB (if the corresponding temperature is below

0°C). As the air flows down the cavity it loses its moisture along the way. The condensation amount near the OSB surface depends on the level of external insulation that the wall has. For instance, at the time when the relative humidity snap shot is taken, i.e. January 24th, the relative humidity around the OSB in the reference wall and the wall that is retrofitted with only 25 mm external insulation have already attained 100% (shown in Figure 8-22 'a' and 'b' in red). In cases where the walls are retrofitted with 50 and 100 mm thick external insulation, the relative humidities of the same location are relatively low (83 and 70%, respectively). This implies that addition of extra insulation can improve the durability of the building envelope component in cases when moisture flows from indoor to outdoor by either diffusion or airlakage

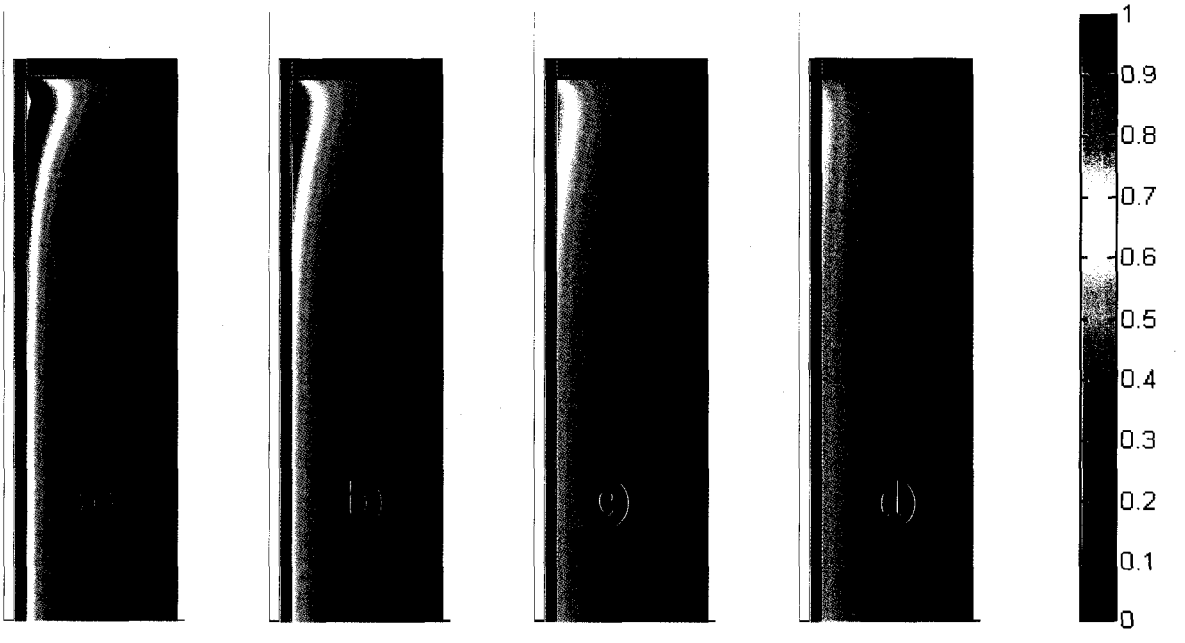

Figure 8-22 Relative humidity profiles of the upper section of the wall on January 24th: a) no external insulation b) 25 mm external insulation c) 50 mm external insulation d) 100 mm external insulation

For a further comparison, the temperature and moisture time history of two critical points, which are located in a region where high moisture accumulation in all four cases is observed, are investigated. One of the points of interest is on the OSB surface located at 100 mm from the top and the other one on the interior surface of the top plate located 15 mm away from the interior surface of OSB are looked at. Figure 8-23 shows the relative humidity time history of a point on the top plate. The moisture accumulation increases continuously with time in the reference wall and the wall retrofitted with 25 mm insulation. In these walls, the relative humidity of the spruce surface, which is 15 mm away from the interior surface of OSB, increases from 35% at the initial state to 82% in the reference wall and 74% in the latter wall at the end of the simulation period. As the external insulation increases from 25 to 50 and 100 mm, the top plate is kept at relatively warm temperatures, which consequently results in relatively less moisture condensation and high drying potential. The highest moisture accumulations in these walls occur at 240 and 380 hours for the retrofitted walls with 50 and 100 mm exterior insulation, respectively. The corresponding maximum relative humidity values are 55% and 47%, respectively. These walls have far less moisture accumulations. Their moisture profiles have alternating wetting and drying patterns, when compared with the reference wall and the wall with 25 mm exterior insulation that have consistently increasing moisture accumulations.

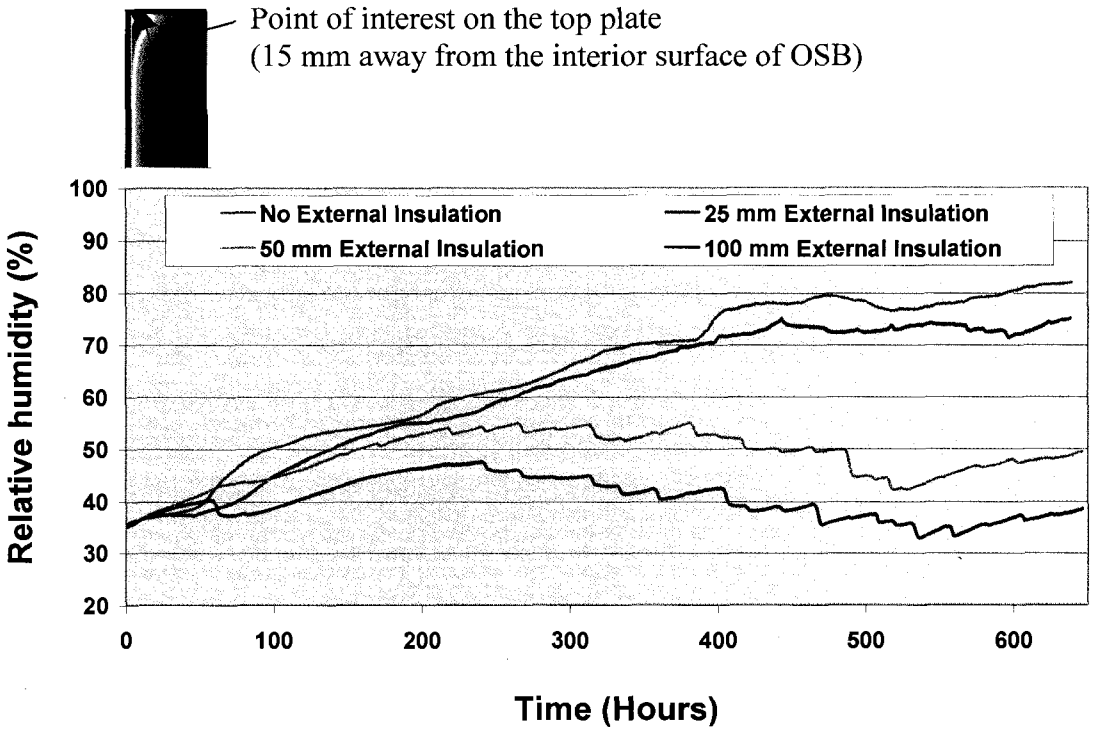

Figure 8-23 Relative humidity profile of the critical point on the top plate—Case with exterior insulation

The relative humidity of a point on the OSB fluctuates highly in response to the outdoor temperature and airleakage conditions. To compare the moisture profiles of the region of interest in the four walls that have different exterior insulation thickness, the calculated relative humidity data is smoothed by performing a twenty-four hours running average. Figure 8-24 shows the relative humidity time history plot of the point of interest for the four cases. In the reference case (no insulation), the region of interest is saturated only after 90 hours of simulation (less than four days). Moreover, this region remains under saturation state for 68% of the simulation period. Retrofitting of the wall with 25 mm external insulation does not produce a significant improvement on moisture accumulation on the OSB as it does on the top plate (Figure 8-23). In this case, although

it may not have any significance, saturation of the OSB starts at a later time (pushed to 141 hours which is about six days), and the percentage of time that this region remains under saturation is reduced by half (34%). But for most of the time the region remains at high moisture content (over 95% relative humidity). A significant improvement, however, is obtained when the wall is retrofitted with 50 or 100 mm thickness of external insulations. In fact, the highest relative humidity are 84 and 71% for the walls retrofitted with 50 and 100 mm thick insulation, respectively. As can be seen in Figure 8-24, the OSBs in these cases are relatively dry. The case with the highest external insulation thickness (100 mm) accumulates relatively less moisture and dries out to the lowest relative humidity level (28%) compared to anyone of the walls considered here.

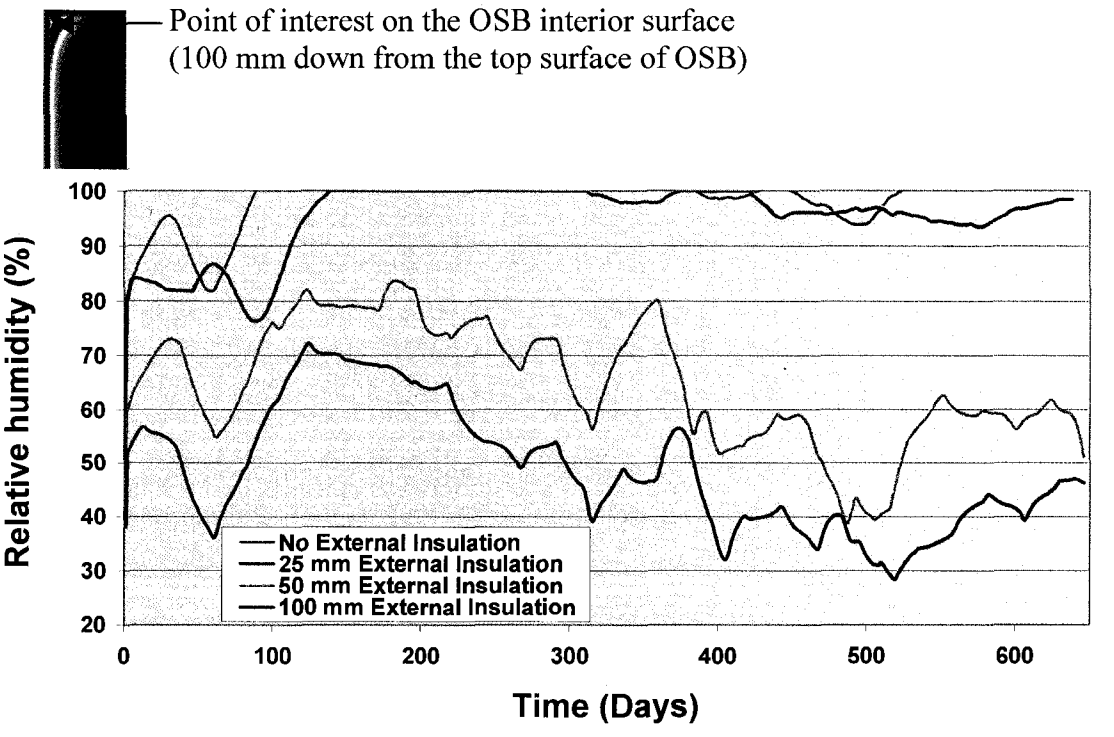

Figure 8-24 Relative humidity profile of the critical point on the OSB surface—Case with exterior insulation

The simulation results of the four cases suggest that addition of extra insulation on exterior walls enhance not only on the overall energy performance of the house, but also the durability of the building envelope components. As presented above, a significant amount of moisture condensed on the OSB of the reference wall and the wall with only 25 mm thick external insulation. The condensed and frozen moisture will meltdown when the cladding is warmed up by solar radiation and ambient temperature in the spring season, resulting in cyclic freezing and melting of high moisture accumulation (freeze-thaw), which can affect the durability of the OSB and the house at large. These simulations suggest that the moisture conditions of the building envelope components need to be assessed, taking into account outdoor and indoor climatic conditions, in determining the required insulation thickness. Thus, integrated analysis of energy efficiency of the whole building, durability of building envelope components, and investment cost (insulation material cost) may be essential for designing high performance buildings in cold climates.

8.8 Window upgrade

The third energy upgrade option is to replace the existing windows with more thermally efficient windows. As stated in the building description section the windows of the reference house are regular double-glazed windows on vinyl frame, which have U-value of 2.87 W/m^2K. To see the effect of windows on the overall performance of the house, in regard to indoor humidity and energy consumption, two window upgrade options are considered here. The properties of these windows are taken from ASHRAE (2005). The first one is a double glaze window with low e-coating (0.1) and U-value of

2.52 W/m^{2}K. It is referred here as a "medium" efficiency window. The second one is a triple glazing window with low e-coating (0.1) and U-value of 1.89 W/m^{2}K. This window is referred to here as a "high" efficiency window. All the simulation parameters including moisture source is the same as the reference case, except that the windows in the four orientations are replaced by the chosen window upgrade options.

The simulation result indicated that a 7% energy saving is obtained when the existing window is replaced with a "medium" efficient window, Table 8-11. The energy saving is almost doubled (13%) when "high" efficient window is replaced. This energy upgrade option provides a better energy saving compared to the thermostat options, and the "high" efficient window upgrade provides energy saving as good as padding the house with 50 mm external insulation.

Table 8-11 Heating loads for cases with window upgrades

	Heating load (kWh)	Percentage of increase in heating load (%)
Reference (Regular double glaze window)	2796	-
Medium efficiency window	2607	-7
High efficiency window	2424	-13

The whole building hygrothermal simulations results indicate that, although upgrading the existing window yields energy savings, the indoor humidity increases as the thermal efficiency of the windows increases as shown in Figure 8-25. The maximum

indoor relative humidity for the reference case, "medium" and "high" efficiency windows are 53, 57 and 62%, respectively. The indoor relative humidity curves of the "medium" and "high" efficiency windows are consistently over by about 4 and 9% from the reference case, respectively. These high indoor humidity profiles are attributed to the less moisture removal from the indoor space by window condensation. Generally, a window with a higher thermal efficient results in a higher indoor window surface temperature, which consequently reduces the frequency and amount of window condensation potentials, Table 8-12. Comparing with the reference window, the window condensate amount reduces by 26 and 57% when the windows are replaced by the "medium" and "high" efficient windows, respectively. Like wise, the frequency of window condensation occurrence reduces by 11 and 20% respectively.

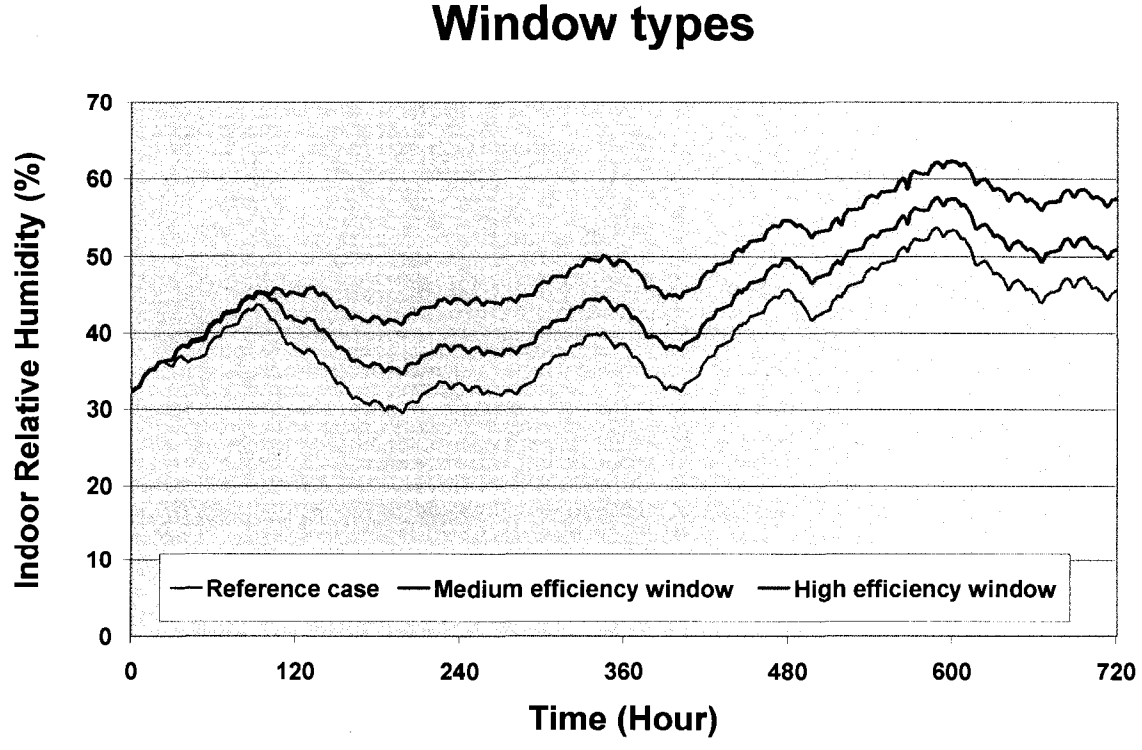

Figure 8-25 Relative humidity profiles of the house for cases with window upgrades

Table 8-12 Window condensations for cases with window upgrades

	Average window condensation (kg/day)	Moisture supply that is condensed (%)	Condensation occurrence (%)
Reference (Regular double glaze window)	6.576	41.10	61
Medium efficiency window	4.816	30.10	50
High efficiency window	2.806	17.53	41

Similar to a case with addition of external insulation, the window upgrading option also requires cost-benefit analysis to decide whether this energy upgrade option is necessary, and if so, to choose an appropriate window type that has high thermal performance and is cost effective. In addition to the cost-benefit analysis related to the window upgrade (investment) and energy costs, the change in the indoor humidity level as a consequence of the window upgrade and its effect on the IAQ and durability of the building components has to be looked at simultaneously.

8.8.1 Moisture in building envelope component—Case of Window upgrade

As observed in the HAMFitPlus simulation results of the two window types considered here, window upgrading increases the indoor humidity level. The high indoor humidity may affect the durability of the building components as the high humid air diffuses and/or is transported by convection through the building envelope components.

This is investigated by simulating the dynamic response of the two-dimensional corner section of the house shown in Figure 7-25 using HAMFit2D for the three cases: reference, "medium" and "high" efficiency window types. All the simulation parameters are the same as described in Section 7.3 except the indoor humidity boundary conditions. The indoor humidity conditions of the three cases (shown in Figure 8-25) are obtained from HAMFitPlus simulations of the respective cases. In all three cases, the temperature profiles at the critical location, which is at the rear junction point of the two gypsum boards, are similar to the result presented in Figure 8-4, with minimum and maximum values of 5.2 and 16.2°C. The dynamic moisture responses of this critical location for the three cases are shown in Figure 8-26. From the figure it is evident that as the efficiency of the window increases, the moisture accumulation on the critical section increases. As shown in Table 8-13, the average relative humidity increases from 77% in the reference case to 87 and 95% in the "medium" and "high" efficiency window cases, respectively. Moreover, the percentage of times that the relative humidity of the critical location is over 80% increases from 35% in the reference case to 69 and 88% for the "medium" and "high" efficiency windows, respectively. In the reference case, the relative humidity of the critical location is always under 90%, whereas in the "medium" and "high" efficiency window cases the same location attains over 90% relative humidity for about 42 and 66% of the simulation period, respectively. These results suggest that although significant energy saving is obtained by upgrading the windows to "medium" and "high" efficiency windows, the accompanying high indoor humidity can cause a serious damage on the building envelope components as well as the well-being of the occupants due to the significant number of occurrence of relative humidity over 80%, which might create a favorable condition for mold growth and health risk.

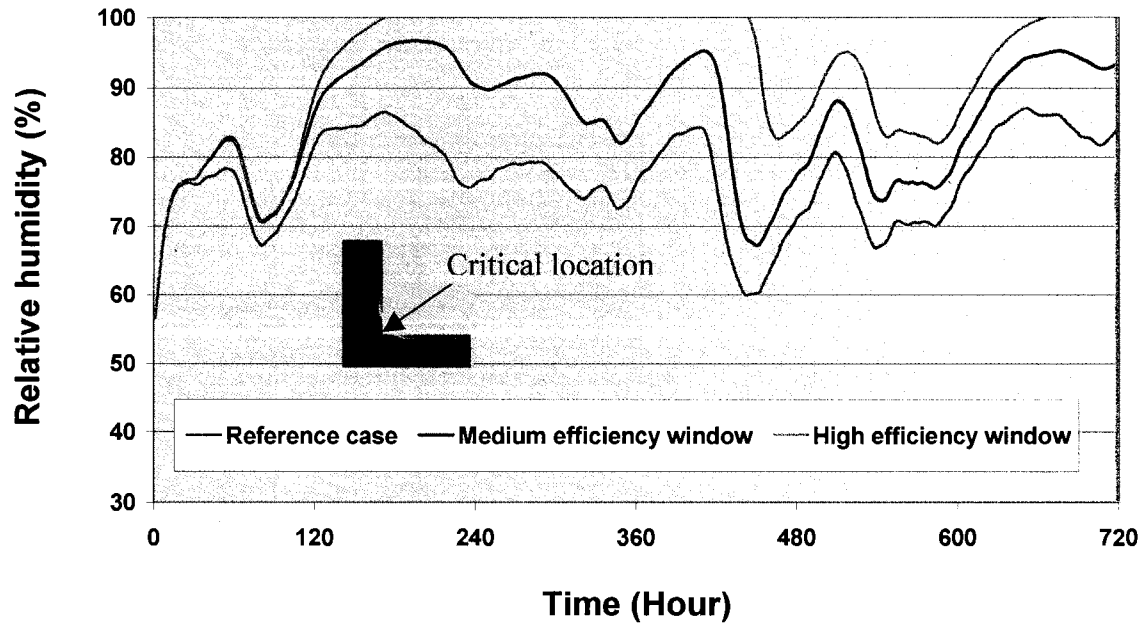

Figure 8-26 Relative humidity profile at the rear junction point of the two gypsum boards (critical point)-- Case with window upgrades

Table 8-13 Summary of moisture condition at the rear junction point of the two gypsum boards (critical location)—Case for window upgrades

	Average Relative humidity (%)	Percentage of time Relative humidity greater than 80% (%)	Percentage of time Relative humidity greater than 90% (%)
Reference (Regular double glaze window)	77	35	0
Medium efficiency window	87	69	42
High efficiency window	95	88	66

8.9 Combination of RHCV and Window upgrades

As demonstrated above, upgrading of the original window to more energy efficient window results in an energy saving of up to 9% in the case of "high" efficiency windows, while at the same time the indoor humidity level reaches levels as high as 62%. The high indoor humidity level has negative effect on the IAQ and durability of building envelope components (Figure 8-26). For the building to have all round optimized performance (energy + indoor AQ + durability), the indoor humidity level needs to be considered as one of the optimization parameters along with durability and energy efficiency of the building. The most efficient way of achieving the desired indoor humidity level is by introducing mechanical ventilation. Of course, this approach compromises the energy saving, which might be obtained as a consequence of window upgrading. But it is essential to achieve an optimized design of a house that is energy efficient, and has acceptable indoor humidity level and long service life (building envelope durability). As presented in Section 8.4, the RHCV has a better performance in regard to energy and indoor humidity control when compared with the other ventilation strategies (no mechanical ventilation, continuous ventilation, and time controlled ventilation). Consequently, a mechanical ventilation system that has a ventilation capacity of 45 L/s and its operation is controlled by the indoor humidity level (turned on when the indoor relative humidity level is over 35%, otherwise turned off), is adopted in this section.

Figure 8-27 shows the indoor humidity profiles of three cases, namely: reference case, a case with "high" efficiency windows, and finally a case with a combination of RHCV and "high" efficiency window. The energy consumption and window

condensation of the corresponding cases are summarized in Table 8-14 and Table 8-15. The indoor humidity profile of the case with a combination of RHVC and "high" efficiency window is nearly constant at the set value of 35%. However, to bring down the high indoor humidity level of the case with "high" efficiency window (shown in green line) to the 35% level requires a significant amount of ventilation. The additional heating energy that is required in this option (RHCV and "high" efficiency window) is 10.34% of the reference case heating load, Table 8-14. This implies that the heating load reduction (-13.0% of the reference case heating load) that is achieved by upgrading the reference house window to "high" efficiency windows (see Table 8-11) is used to heat part of the incoming fresh air due to RHCV operation.

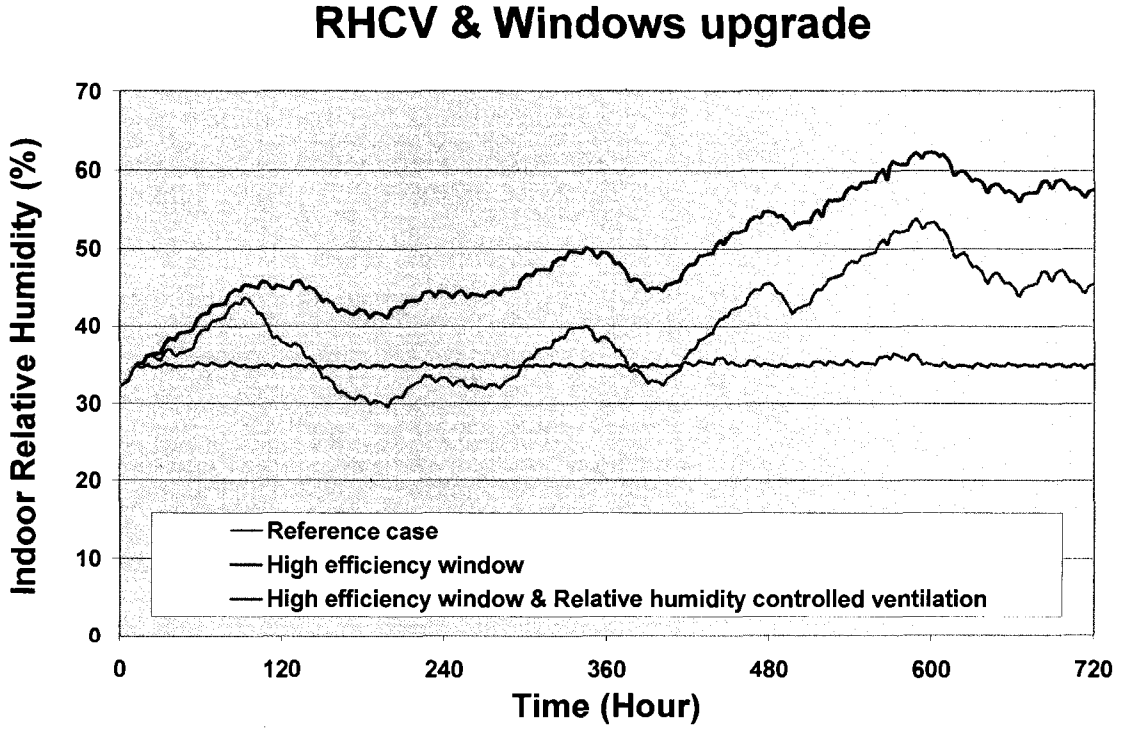

Figure 8-27 Indoor relative humidity of the house for cases with RHCV and window upgrade

Although the simulation results in Table 8-14 indicate that there is no substantial energy gain in adopting RHCV with "high" efficiency window verses RHCV only, the amount of window condensation and fresh air supply can be much better, Table 8-15. In fact, in the case where both RHCV and "high" efficiency window upgrade options are implemented there is no window condensation at all, which is remarkable in contrast to the case with RHCV only where window condensation occurs 43% of the simulation period at an average rate of 3.379 kg/day, Table 8-15. It can be concluded that measures taken with only energy upgrade (window upgrade) can result in IAQ and durability problem. On the other hand, the measure to control indoor humidity level (controlled ventilation system) results in higher energy demand. Combination of the two measures can result in a controlled indoor humidity level, a better IAQ, and durability of building envelope components. Particularly, the case with the combination of RHCV and "high" efficiency window options gives a constant indoor humidity level with no window condensation and moisture accumulation in building envelope components at the expense of modest additional energy cost.

Table 8-14 Heating load summary of the cases with RHCV and window upgrade

	Heating load (kWh)	Percentage of increase in heating load (%)
Reference (No mechanical ventilation)	2796	-
RH controlled ventilation	3181	13.75
High efficiency window	2424	-13.33
RH controlled ventilation Plus High efficiency window	3086	10.34

Table 8-15 Window condensation summaries of the cases with RHCV and window upgrade

	Average window condensation (kg/day)	Moisture supply that is condensed (%)	Condensation occurrence (%)
Reference (No mechanical ventilation)	6.576	41.1	61
RH controlled ventilation	3.379	21.1	43
High efficiency window	2.806	17.5	41
RH controlled ventilation Plus High efficiency window	0.000	0.00	0

8.10 Comprehensive upgrade for Indoor humidity, Energy and building envelope performance

As discussed in the previous sections, for the reference house to maintain the indoor humidity level at the desired range, be durable and more energy efficient; it has to be retrofitted with energy upgrading options along with a RHCV system. In the previous sections, only one energy upgrade option per case is considered. In this section, three retrofitting strategies, which involve more than one energy upgrade options per case, are evaluated. The first one is a case with thermostat setback (multiple-step-up scheme) and external insulation of 50 mm thickness, and the second one is the same as the first case except that the windows are upgraded to "medium" efficiency windows. In the third case the windows are upgraded to "high" efficiency windows, otherwise the same as case the other two. In all the three cases the indoor humidity level is controlled with a RHCV system, which ensures that the indoor humidity profiles of the three cases are similar, nearly constant at 35%. Consequently, the hygrothermal conditions of the respective building envelope components options will be similar as well since they are exposed to the same indoor and outdoor boundary conditions. The simulation results in Section 8.7.1, *Moisture in building envelope component—Case of External insulation*, suggests that addition of insulation on the exterior surfaces of the house is critical in this cold climate (Carmacks) to avoid excessive moisture condensation and freeze-thaw phenomena that may cause (speed-up) deterioration of the building envelope components. Hence, the building envelope components of the three cases considered here are padded with the minimum insulation thickness that can maintain the sheathing board (OSB) relatively dries (less than 80% relative humidity). From the three insulation

thickness considered in Section 8.7.1, *Moisture in building envelope component—Case of External insulation*, the 50 mm insulation is the minimum insulation thickness that can avoid high moisture accumulation on the sheathing board, and therefore, it is adopted here.

Under these simulation scenarios, the house will have a constant indoor temperature of 21°C and 35% relative humidity. The amounts of energy saving and moisture condensation on windows surfaces are given in Table 8-16 and Table 8-17, respectively. In the first retrofit option that includes a RHCV system, thermostat setback and external insulation but with no window upgrade yields a considerable improvement in the house performance. The indoor relative humidity is maintained at 35%, an energy saving of 2.32% of the total heating load of the reference case is achieved, and also the amount and frequency of window condensation occurrence reduce by 60% and 17%, respectively, from that of the reference case. In the second case where the house is further retrofitted by replacing the reference windows with the "medium" efficiency windows, the indoor relative humidity is also maintained at 35%, a higher energy saving (4.31% of the total heating load of the reference case) is obtained, and the amount and frequency of window condensation occurrence reduce by 88.5% and 41%, respectively, from that of the reference case. Adoption of the third retrofit option, which is an upgrade version of the second option where the "medium" efficiency windows are replaced by the "high" efficiency windows, can be regarded as the best comprehensive retrofit option as it provides a controlled indoor relative humidity, higher energy saving (9.33% from the reference case), no moisture condensation on the window surfaces and also no excess moisture accumulation in the building envelope component (condensation on the sheathing board). In this case, the average ventilation rate per person is 6.0 L/s, which is

quite close to the ASHRAE's recommended value of 7.5 L/s (ASHRAE Standard 62.2-2003 "*Ventilation and Acceptable Indoor Air Quality in Low-rise Residential Buildings*"). Whereas in the reference (original) case, the average ventilation rate is 2.0 L/s per person, which may not be sufficient to maintain satisfactory indoor air quality.

Table 8-16 Heating load summary of the house with comprehensive upgrades

	Heating load (kWh)	Percentage of increase in heating load (%)
Reference case	2796	-
Multiple-step-up Thermostat setback + RHCV + 50 mm External Insulation	2732	-2.32
Multiple-step-up Thermostat setback + RHCV + 50 mm External Insulation + "Medium" efficiency window	2676	-4.31
Multiple-step-up Thermostat setback + RHCV + 50 mm External Insulation + "High" efficiency window	2536	-9.33

Table 8-17 Window condensation summary of the house with comprehensive upgrades

	Average window condensation (kg/day)	Moisture supply that is condensed (%)	Condensation occurrence (%)
Reference case	6.576	41.1	61
Multiple-step-up Thermostat setback + RHCV + 50 mm External Insulation	2.621	16.4	44
Multiple-step-up Thermostat setback + RHCV + 50 mm External Insulation + "Medium" efficiency window	0.757	4.7	20
Multiple-step-up Thermostat setback + RHCV + 50 mm External Insulation + "High" efficiency window	0.000	0.00	0

In this section, HAMFitPlus is used to investigate the effect of various retrofit options on the overall performance of a residential house. Table 8-18 summarizes the simulation results of the whole building hygrothermal model under the respective modeling assumptions discussed above. The table shows the effects of interior surface finish, interior layer material, ventilation capacity, ventilation strategy, thermostat setback, window-type, insulation thickness and combinations of these parameters on the energy efficiency, indoor humidity and building enclosure performance. It has to be noted here that the analysis and the results presented in this section are only intended to show the need for an integrated building performance analysis, and not to be generalized as the study focuses on a specific building operation during one winter month. The long-term overall performance of the building, however, can be investigated by running HAMFitPlus for an extended simulation period (usually more than two years) before such generalizations are made.

Table 8-18 Summary results of the different options considered

Modifications on the reference house	Energy	Indoor humidity	Durability	
	Percentage of increase in heating load (%)	Indoor Relative humidity under 35%	Percentage of decrease in window condensation (%)	Sheathing board RH < 80%
Acrylic paint	0	NO	-3.3	NO
Latex paint	0	NO	-10.1	NO
Plywood	0	NO	-6.7	NO
Fiber board	0	NO	-0.5	NO
15 L/s	11	NO	41	NO
30 L/s	30	YES	85	NO
45 L/s	51	YES	98	NO
Continuous ventilation	29	YES	85	NO
Time controlled ventilation	20	NO	66	NO
RHCV	13	YES	48	NO
RHCV + Thermostat setback with Multiple-step-up scheme	13	YES	59	NO
"Medium" efficiency window	-7	NO	26	NO
"High" efficiency window	-13	NO	57	NO
25 mm insulation	-9	NO	0	NO
50 mm insulation	-16	NO	0	YES
100 mm insulation	-26	NO	0	YES
RHCV + "High" efficiency window	10	YES	100	NO
Multiple-step-up Thermostat setback + RHCV + 50 mm External Insulation	-2.3	YES	60	YES
Multiple-step-up Thermostat setback + RHCV + 50 mm External Insulation + "Medium" efficiency window	-4.31	YES	88	YES
Multiple-step-up Thermostat setback + RHCV + 50 mm External Insulation + "High" efficiency window	-9.33	YES	100	YES

9 CONCLUSION

Buildings are designed to create an isolated space from the surrounding environment and provide desired interior environmental conditions for the occupants. In addition to fulfilling the function of creating a favorable indoor environmental condition, they are expected to be durable and energy efficient. In this thesis a whole building hygrothermal model (HAMFitPlus) is developed on a single development platform and used for an integrated analysis of these three building functions. The model and the work accomplished in this thesis are summarized as follow:

- HAMFitPlus considers a building as an integrated system and takes into account the dynamic interactions of building enclosure, indoor air, HVAC system and indoor heat and moisture generation mechanisms is developed. At the current development HAMFitPlus is a single zone model but will be extended to multi-zone model in the future.
- HAMFitPlus is developed on SimuLink simulation environment, which has a smooth interface with COMSOL Multiphysics and MatLab computational tools.
- The simultaneous outputs of the model include indoor temperature and humidity, temperature and moisture content in the building envelope components and building energy demand to maintain the intended indoor environmental conditions (temperature and humidity).
- The building envelope model (HAMFit) accommodates non-linear transfer and storage properties of materials, moisture transfer by vapor diffusion, capillary liquid water transport and convective heat and moisture transfer through multi-layered

porous media. The model can be used for HAM analysis of two-dimensional building envelope component (detail) without geometric shape restriction.

- Although the two-dimensional version of HAMFit can be used in HAMFitPlus, in this thesis the one-dimensional version is used to reduce the high computational time demand. The two-dimensional version is used separately for hygrothermal performance analysis of building envelope components.
- The building envelope (HAMFit) and whole building hygrothermal (HAMFitPlus) models are successfully benchmarked against a number of internationally published test cases that comprise an analytical verification, comparisons with other models and validation of simulation results with experimental data.
- As presented in Chapter 7, the indoor humidity profiles obtained from simple indoor humidity models can vary significantly, and use of one or the other model's result for hygrothermal performance assessment of a building component may result in different conclusions. Consequently, it is very important to use a more accurate model, which is based on whole building hygrothermal analysis, to generate the indoor humidity profile.
- In Chapter 8, the whole building hygrothermal model is effectively used to investigate the effect of various retrofit options on the overall performance of the house in terms of energy efficiency, indoor humidity and building enclosure performance.
- The results presented in Chapter 8 are only intended to show the need for an integrated building performance analysis, and not to be generalized as the study focuses on a specific building operation during one winter month. The long-term overall performance of the building can be investigated, however, by running

HAMFitPlus for an extended simulation period (usually more than two years) before such generalizations are made

- The extensive whole building heat and moisture analyses that are carried out in this research work underlines the importance of an integrated design approach in designing new buildings or retrofitting existing buildings in order to attain an optimized building performance (as upgrading or changing in design of one aspect of the building might affect the other building performance).

10 FUTURE WORK

In this thesis a whole building hygrothermal model is developed, benchmarked and used for practical application. However, it is limited to a single zone building. The model can be further improved in the following areas.

1) Further development on Whole building heat and moisture model
   a. Extend the capability of the model so that it can be used for multi-zone, multi-story buildings. This task requires coupling of the model with multi-zone airflow model.
   b. Coupling the model with CFD so that indoor conditions variation across a large zone or a zone with limited air movement can be effectively modeled
   c. Characterization of heat and moisture generation mechanisms and creating database of typical occupants activities profiles
2) Further development on Building envelop hygrothermal model
   a. Extension of the building envelope model to 3D HAM model to deal with building envelope details such as 3D corners
   b. Modeling of airflow in building envelope cavity
   c. Coupling of HAM and CFD for a better assessment of wind-driven rain effect
   d. Characterization of ageing effect on the hygrothermal properties of materials.
3) Benchmarking of models
   a. Laboratory controlled experiments for validation of building component and whole building hygrothermal models.
   b. Validations of building envelop and whole building models

4) Further HAM models applications

   a. Development of risk assessment criteria for building enclosure performance

   b. Overall building performance assessment of multi-zone buildings

   c. Extended the application of whole building model for trains and aircraft cabins

11 REFERENCE

Abranties, V; Freitas, V. (1989). User Influence Upon Building Indoor Humidity, *Housing Science*, Vol. 13 (4) pp 277-282

Athenatis, A.; Santamouris, M. (2002). Thermal Anaylsis and Design of Passive Solar Buildings. *Published by James & James* (science Publishers) Ltd., London, UK, ISBN 1-902916-02-6

ASHRAE Handbook of Equipment (1988). Humidifiers, *Chapter 5*, American Society of Heating, Refrigeration, and Air-Conditioning Engineers, Atlanta

ASHRAE Standard 55-1992. Thermal Environmental Conditions for Human Occupancy. American Society of Heating, Refrigeration, and Air-Conditioning Engineers, Atlanta

ASHRAE Standard 62-1992. Ventilation for Acceptable Indoor Air Quality. American Society of Heating, Refrigeration, and Air-Conditioning Engineers, Atlanta

ASHRAE. 2001. *International Weather for Energy Calculation (IWEC Weather Files) Users Manual and CD-Rom*, Atlanta

ASHRAE Standard 62.2-2003. Ventilation and Acceptable Indoor Air Quality in Low-rise Residential Buildings. American Society of Heating, Refrigeration, and Air-Conditioning Engineers, Atlanta

ASHRAE Handbook of Fundamentals (2005). American Society of Heating, Refrigeration, and Air-Conditioning Engineers, Atlanta

ASHRAE Standard 60P. (2006). Design Criteria for Moisture Control in Buildings. *Draft*

Bear, J. (1992). Modeling Transport Phenomena in Porous Media. *Elsevier Science Publishers B.V.* ISBN 0 444 89498-5. pp 15-60

Bedner, T. and Dreyer, J. (2006). The Influence of Construction Material Moisture on the Indoor Humidity and surface Conditions. *Proceeding of the 3rd International Building Physics /Engineering Conference*, August 26-31, Montreal, Canada, pp 549-552.

Bednar, T.; Hagentoft, C. (2005). Analytical Solution for Moisture Buffering Effect Validation Exercises for Simulation Tools. *Nordic Symposium on Building Physics*, Reykjavik, June 13-15.

Burch, D.M.; Thomas, W.C.; Mathena, L.R.; Licitra, B.A.; Ward, D.B. (1989). Transient Heat and Moisture Transfer in Multi-Layer, Non-Isothermal Walls—Comparison of Predicted and Measured Results. *Proceedings of Thermal Performance of the Exterior Envelopes of Buildings IV*, Dec. 4-7, Clearwater Beach, Florida, USA pp. 513-531.

Burch, D. M.; TenWolde, A. (1993). A Computer Analysis of Moisture Accumulation in the Walls of Manufactured Housing. *ASHRAE Transactions*, Vol. 99, Part 2

Burch, D. M. (1993) An Analysis of Moisture Accumulation in subjected to Hot and Humid Climates. *ASHRAE Transactions*, Vol. 99, Part 2

Christian, J.E. (1994). Moisture Sources. Moisture Control in Buildings, ASTM Manual Series: MNL 18, pp. 176-182.

Clausen, G.; Rode, C.; Bornehag, C.-G.; Sundell, J. (1999). Dampness in Buildings and Health. Interdisciplinary Research at the National Center for Indoor Environment and Energy. *Proceeding of the 5th Symposium of Building Physics in The Nordic Countries*

COMSOL Multiphysics: http://www.comsol.com/

DIN 4108. 1981. Thermal Insulation in Buildings, (DIN-Norm), p.48, Berlin, Germany.

Djebbar, R.; van Reenen, D.; Tariku, F. (2002). Hygrothermal Performance of Building Envelope Retrofit Options. Task 3a - Hygrothermal Performance Analysis of High-Rise Masonry Wall Assemblies, *Client Report B-1137.3*, pp. 67.

El Diasty, R.; Fazio, P.; Budaiwi, I. (1992). Modelling of Indoor Air Humidity: The Dynamic Behaviour with in Enclosure. *Energy and Buildings*, Vol. 19, pp.61-73

El Diasty, R.; Fazio, P.; Budaiwi, I. (1993). The Dynamic Modeling Air Humidity Behavior in a Multi-Zone Space. *Building and Environment*, Vol. 28, pp.33-55

European Standard prEN ISO 13791 (2004). Thermal Performance of Buildings – Calculation of Internal Temperatures of a Room in Summer Without Mechanical Cooling –General Criteria and Validation Procedures. *ISO/FDIS 13791:2004*

Fang, L. Clausen, G and Fanger, P.O. (1998a). Impact of Temperature and Humidity on the Perception of Indoor Air Quality, *Indoor Air*, Vol. 8, pp. 80-90.

Fang, L. Clausen, G and Fanger, P.O. (1998b). Impact of Temperature and Humidity on the Perception of Indoor Air Quality During and Longer Whole-Body Exposures, *Indoor Air*, Vol. 8, pp. 276-284.

Fang, L. (2002). Temperature, Humidity And Perception of Indoor Air Quality, *Journal of Australian Institute of Refrigeration Air Conditioning and Heating*, pp. 20-24.

Fazio, P. (2004). Building Envelope Design/Building Enclosure. *Course pack*, Concordia University, Department of Building, Civil and Environmental Engineering, Archives 1002-02-4536

Gerbasi, D. (2008). CONDENSE User Manual. GES Technologies Inc., Montreal

Grunewald, J.; Plagge, R.; Roels, S. (1999). Full Documentation of the Numerical Simulation Program DIM3.1, *Vol. 5 of the Final Report of the Brite-Euram Project BRPR-96-0229*, Dresden, Germany

Goswami, D. (2004). Energy Resources: Solar energy resources, *The CRC Handbook of Mechanical Engineering*, 2nd Edition, ISBN13: 9780849308666, Publisher CRC

Gu, L.; Swami, M.; Fairey, P. (1993). Multiphase Transport in Porous media, *ASME Winter Annual Meeting*, New Orleans, LA., Nov. 28-Dec. 3. pp. 47-55

Hagentoft, C-E, (1992). Simplified analysis of combined heat, moisture and air transport for one-dimensional cases. *IEA/Annex 24 Internal Report,* T1-S-92.

Hagentoft, C-E, (1996). Heat, Air and Moisture Transfer through New and Retrofitted Insulated Envelope Parts, *IEA Annex 24 HAMTIE*, Final Report, Vol.5, Task5: Performances and Practice, ISBN 90-75741-04-9

Hagentoft, C. (1997). Building Physics Fundamentals, *Report R-97:1*, Department of Building Physics, Chalmers University of Technology, Sweden

Hagentoft, C-E. (2002). HAMSTAD – Final report: Methodology of HAM-modeling, *Report R-02:8*. Gothenburg, Department of Building Physics, Chalmers University of Technology.

Hagentoft, C-E.; Kalagasidis, A.; Adl-Zarrabi, B.; Roels, S.; Carmeliet, J.; Hens, H; Grunewald, J.; Funk, M.; Becker, R.; Shamir, D.; Adan, O.; Brocken, H.; Kumaran, K.; Djebbar, R. (2004). Assessment Method of Numerical Prediction Models for Combined Heat, Air and Moisture Transfer in Building Components: Benchmarks for One-dimensional Cases. *Journal of Thermal Envelope and Building Science*. Vol. 27 (4), pp. 327-352.

Hens, H. (1996). Heat, Air and Moisture Transfer through New and Retrofitted Insulated Envelope Parts, *IEA Annex 24 HAMTIE*, Final Report, Vol.1, Task1: Modeling, ISBN 90-75741-02-2

Hens, H. (2007). Building Physics-Heat, Air and Moisture, Fundamentals and Engineering Methods with Examples and Exercises, *Published by Ernst & Sohn A Wiley Com.* ISBN 978-3-433-01841-5.

Holm, A.; Kunzel, H.M. (2006). Experimental Investigation of the Hygric Buffering Capacity of Wood Based Interior Paneling. *Proceeding of the 3rd International Building Physics /Engineering Conference*, August 26-31, Montreal, Canada, pp 3-10

Holm, A.; Lengsfeld, K. (2007). Moisture-Buffering Effect—Experimental Investigations and Validation. *Proceedings of Thermal Performance of the Exterior Envelopes of Whole Buildings X International Conference.* Dec. 2-7, Clearwater, FL.

Hood, I. (2006). Field Survey of Indoor and Outdoor Climatic Conditions and Airtightness Level Prevailing in Two Northern Housing Regions *Status Report: Carmacks Survey*, Vancouver, BC

Hutcheon, N.; Handegord, G. (1995). Chapter 12: Water and Buildings, *Building Science for a Cold Climate*, National Research Council of Canada

IEA-Annex 14 (1991). Sourcebook, *Annex 14 Final Report*, Vol. 1, Leuven, Belgium

IEA-Annex 41 (2003). Whole Building Heat, Air and Moisture response (MOIST-ENG). *Report Kick-off Meeting*, November 26-28, Leuven, Belgium.

Isetti, C.; Laurenti, L; Ponticiello, A. (1988). Predicting Vapor Content of the Indoor Air and Latent Loads for Air-Conditioned Environments: Effect of Moisture Storage Capacity of the Walls. *Energy and Buildings*, Vol. 12, pp. 141-148.

ISO 13788:2000. Hygrothermal performance of Building Components and building Elements –Internal Surface Temperature to Avoid Critical Surface Humidity and Interstitial Condensation Calculation Method. *ISO/FDIS 13788:2000(E)*

ISO 12572:2001 Hygrothermal Performance of Building Materials and Products -- Determination of Water Vapour Transmission Properties. *ISO/FDIS* 12572:2001, Annex E

ISO 15927-1:2003 Hygrothermal performance of buildings -- Calculation and presentation of climatic data -- Part 1: Monthly means of single meteorological elements. *ISO/FDIS* 15927-1:2003, Annex B

Janssens, F. (1998). Reliable Control of Interstitial Condensation in Lightweight Roof Systems, *Ph.D. Thesis*. Catholic University of Leuven, Belgium

Jones, R. (1993). Modeling Water Vapor Conditions in Buildings. *Building Services Engineering Research and Technology*, Vol. 14 (3), pp.99-106.

Jones, R. (1995). Indoor Humidity Calculation Procedures. *Building Services Engineering Research and Technology*, Vol. 16 (3), pp.119-126.

Judkoff, R.; Neymark, J. (1995). Building Energy Simulation test (BESTEST) and diagnostic method. *NREL/TP-472-6231*. Golden, CO National Renewable Energy Lab

Kalagasidis, A. (2004). HAM-Tools: An Integrated Simulation Tool for Heat, Air and Moisture Transfer Analysis in Building Physics. *Ph.D. Thesis*, Chalmers University of Technology, Sweden

Karagiozis, A. (1993). Overview of the 2D Hygrothermal Heat-Moisture Transport Model LATENITE. *Internal Report*, Institute for Research in Construction, National Research Council Canada, Ottawa.

Karagiozis, A. (2001). Advanced hygrothermal modeling MOISTURE-EXPERT, ver: 1. *Proceeding of the 35th International Particle board/Composite Symposium*. April 3-5.

Karagiozis, A.; Kuenzel, H.M.; Holm, A. (2001). WUFI-ORNL/IBP - A North American Hygrothermal Mode. *Proceedings for Performance of Exterior Envelopes of Whole Buildings VIII: Integration of Building Envelopes*, Dec. 2-7, Clearwater Beach, FL

Karagiozis, A.; Salonvaara, M. (2001) Hygrothermal System-Performance of Whole Building,. Building and Environment, Vol. 36, pp. 779-787.

Kohonen, R. (1984). Transient Analysis of the Thermal and Moisture Physical Behavior of Building Constructions. *Building and Environment*, Vol. 19 (1), pp 1-11

Kuenzel, H.M. (1995). Simultaneous Heat and Moisture Transport in Building Components: One- and Two- dimensional calculation using simple parameters, *PhD. Thesis*, University of Stuttgart, Germany.

Kuenzel, H.M.; Kiessl, K. (1997). Calculation of Heat and Moisture Transfer in Exposed Building Components, *International Journal of Heat and Mass Transfer*, Vol. 40 (1), pp. 159-167.

Kuenzel, H.M. (1998). The Smart Vapor Retarder : An Innovation Inspired by Computer Simulations, *ASHRAE Transactions*, Part 2, pp. 903-907.

Kuenzel, H.; Karagiozis, A., Holm, A. (2001). A Hygrothermal Design Tool for Architects and Engineers, *Moisture Analysis and Condensation Control in Building Envelopes*, ASTM Manual series 50: Chapter 9.

Kuenzel, H.M.; Zirkelbatch, D.; Sedlbauer, K. (2003). Predicting Indoor Temperature and Relative Humidity Conditions Including Hygrothermal Interactions with the Building Envelope. *Proceeding of 1st International Conference on Sustainable Energy and Green Architecture*, Building Science Research Center (BSRC), Oct. 8-10

Kumaran, M.K. (1992). Heat, Air and Moisture Transport through Building Materials and Components: Can We Calculate and Predict? *Proceeding of the 6th Conference on Building Science and Technology*, Waterloo, Canada, pp. 103-144

Kumaran, M.K.; Mitalas, G.P.; Bomberg, M.T. (1994). Fundamentals of transport and storage of moisture in building materials and components, *Moisture Control in Buildings, ASTM Manual Series*, MNL-18, Philadelphia, PA, (ISBN: 0803120516): American Society for Testing and Materials, pp. 3-17

Kumaran, K. (1996). Heat, Air and Moisture Transfer through New and Retrofitted Insulated Envelope Parts, *IEA Annex 24 HAMTIE*, Final Report, Vol.3, Task 3: Material Properties.

Kumaran, K.; Lackey, J.; Normandin, N.; Tariku, F.; van Reenen, D. (2002). A Thermal and Moisture Transport Property Database for Common Building and Insulating Materials, *Final Report—ASHRAE Research Project 1018-RP, pp.229*

Kumaran, M.K. (2005). Indoor Humidity as a Boundary Condition for Whole Building HAM Analysis. *Annex 41 Working Document*, A41-T3-C-05-1

Kuo, K. (1986). Principles of Combustion, *Published by John Wiley & Sons Inc.* ISBN 0-471-09852-3

Kusuda, T. (1983). Indoor Humidity Calculations, *ASHRAE Transactions*, DC-83-12

Lenz, K.; Holm, A. (2005). Common Exercise 3 'Two real exposure rooms at FhG'. IEA, Annex 41, Task 1, Modeling common exercise.

Loudon, A.G. (1971). The Effect of Ventilation and Building Design Factors on the Risk of Condensation and Mould Growth in Dwellings. *The Architects' Journal*, Vol. 153 (20), pp. 1149-1159

Luikov, A.V. (1966). Heat and mass transfer in capillary – porous bodies, *Pergamon Press*, New York.

Manufactured home: http://www.palmharbor.com/our-homes/floor-plans

Matlab: http://www.mathworks.com

Maref, W.; Lacasse, M.A.; Kumaran, M.K.; Swinton, M.C. (2002) Benchmarking of the advanced hygrothermal model-hygIRC with mid-scale experiments. *eSim 2002 Proceedings*, University of Concordia, Montreal, pp. 171-176

Mendes, N.; Winkelmann, F.C.; Lamberts, R.; Philippi, P.C. (2003). Moisture Effects on Conduction Loads, *Energy and Buildings*, Vol. 35, pp. 631-644

Mukhopadhyaya, P.; Tariku, F. (1999). Modeling Drying Potential of Accidentally Entered Moisture from Wall Cavity, *MEWS Consortium: Technical Report T7-06,* (NRCC-44274)

National Building Code of Canada (2005). National Research Council Canada, Ottawa.

Ojanen, T. and Kohonen, R. (1989). Hygrothermal Influences of Air Convection in Wall Structures, *Proceedings of Thermal Performance of the Exterior Envelopes of Buildings IV*, Dec 4-7, Clearwater Beach, Florida, pp. 234-242

Ojanen, T.; Kohonen, R.; Kumaran, K. M. (1994). Modeling Heat, Air and Moisture Transport Through Building Materials and Components, *ASTM Manual Series MNL 18, Chapter 2: Moisture Control in Buildings*, H. Trechsel, Ed., Philadelphia

Orme, M.; Liddament, W. (1998). Numerical data for air infiltration and natural ventilation calculations- Table 3.5. *AIVC TN 44*, pp.100.

Oreszczyn, T.; Pretlove, S. (1999). Condensation Targeter II: Modeling surface relative humidity to predict mould growth in dwellings. *Proceeding CIBSE: Building Services Engineering Research and Technology*, Vol.20 (3), pp. 143-153.

Pederson, C. R.(1990). Combined Heat and Moisture Transfer in Building Constructions, *Ph.D. Thesis*, Report no. 214, Thermal Insulation Laboratory, Technical University of Denmark.

Pederson, C. R.(1992). Prediction of Moisture Transfer in Building Constructions, *Building and Environment*, Vol. 27(3), pp. 387-397.

Philip, J.R.; De Vries, D.A. (1957). Moisture Movement in Porous Material Under Temperature Gradients. *Transactions, American Geophysical Union.* Vol. 38 (2), pp 222-232

Quirouette, R.L. (1983) Moisture Sources in Houses, *Building Science Insight '83*, Division of Building Research, National Research Council of Canada, pp. 15-28.

Rivard, H. (1993). CONDENSE Version 2.0: User's Manual, Quebec Building Envelope Council, Montreal, Canada.

Rode, C. (2003). Whole Building Hygrothermal Simulation Model. ASHRAE Transactions: Symposia

Rode, C.; Ruut, P.; Woloszyn, M. (2006). Simulation Tests in whole Building Heat and Moisture Transfer, *Proceeding of the 3rd International Building Physics /Engineering Conference*, August 26-31, Montreal, Canada, pp 527-534

Ruut P.; Rode, C. (2004). Common Exercise 1 – Case 0A and 0B Revised. IEA, Annex 41, Task 1, Modeling common exercise.

Ruut P.; Rode, C. (2005). Common Exercise 1 "Realistic" Case. IEA, Annex 41, Task 1, Modeling common exercise.

Roels, S.; Janssen, H.; Carmeliet, J.; Diepens, J.; de Wiy, M. (2006). Hygric Buffering Capacities of Uncoated and Coated Gypsum Board. *Proceeding of the 3rd International Building Physics /Engineering Conference*, August 26-31, Montreal, Canada, pp 27-34

Sandberg, P.J. (1995). Building Components and Building Elements—Calculation of Surface Temperature to Avoid Critical Surface Humidity and Calculation of Interstitial Condensation. *Draft European Standard CEN/TC 89/W 10 N 107*

Sanders, C. (1995). Design Parameters Used to Avoid Interstitial Condensation for a Range of Climates. *ASHRAE Transactions: Symposia*, pp. 627-638.

Sanders, C. (1996). Heat, Air and Moisture Transfer through New and Retrofitted Insulated Envelope Parts, *IEA Annex 24 HAMTIE*, Final Report, Vol.2, Task2: Environmental Conditions, ISBN 90-75741-03-0

Salonvaara, M. (1993). Moisture Potentials: numerical Analysis of Two Differential Equations. *Internal Reports*. Annex 24, T1-SF-93/01

Salonvaara, M.; Karagiozis, A. (1994). Moisture Transport in Building Envelopes Using an Approximate Factorization Solution Method. *Proceeding of the Second Annual Conference of the CFD Society of Canada*, Toronto, Canada, pp. 317-326.

Salonvaara, M. Karagiozis, A. (1996). The Influence of Water-proof Coating on the Hygrothermal Performance of a Brick Facade Wall System. *ASTM STP 1314*

Sawers (1983) Condensation in the Home: Where, Why, and What to Do About It, *Canada Mortgage and Housing Corporation (CMHC)*, ISBN 0-662-51645-1

Schijndel, A.W.M; Hensen J.L.M. (2005). Integrated Heat, Air and Moisture Modeling Toolkit in MatLab. *Proceeding of the ninth International IBPSA Conference.* August 15-18, Montreal, Canada, pp 1107-1113.

Schuyler, G. D.; Swinton, M.; Lankin, J. (1989). WALLDRY—A computer Model that Simulates Moisture Migration Through Wood Frame Walls—Comparison to Field Data, *Proceedings of Thermal Performance of the Exterior Envelopes of Buildings IV*, Dec 4-7, Clearwater Beach, Florida, pp. 492-505

Shaw, C.Y. and Kim, A. (1984). Performance of Passive Ventilation Systems in a Two-Story House, *5th AIC conference*, October 1-4, Reno, Nevada, USA

Simonson, C.; Salonvaara, M.; Ojanen, T. (2004a). Heat and Mass Transfer Between Indoor Air and a Permeable and Hygroscopic Building Envelope: Part 1 – Field Measurements. *Journal of Thermal Envelope and Building Science*, Vol. 28 (1), pp. 63-101.

Simonson, C.; Salonvaara, M.; Ojanen, T. (2004b). Heat and Mass Transfer Between Indoor Air and a Permeable and Hygroscopic Building Envelope: Part II – Varification and Numerical Studies. *Journal of Thermal Envelope and Building Science*, Vol. 28 (2), pp. 161-185.

Stad, T. (2006). Energuide and Condition Report Summary, Carmacks, Yukon, pp 16

Sterling, E.M.; Arundel, A.; Sterling, T.D. (1985). Criteria for human exposure to humidity in occupied buildings. *ASHRAE Transactions*, 91 (1B)

Straube, J.; Burnett, E. (2001). Overview of Hygrothermal (HAM) Analysis Methods, *Moisture Analysis and Condensation Control in Building Envelopes*, ASTM Manual series 50: Chapter 5

Talukdar, P.; James, C.; Simonson, C. (2006). Modeling Exercise on Transient Heat and Moisture Transfer in a Bed of Gypsum Board (Phase 1). *Annex 41 Subtask 2 Common Exercise*, Mechanical Engineering Department, University of Saskatchewan, Canada

Tariku, F.; Kumaran, M.K. (1999a). Application of IRC's Advanced Hygrothermal Model to Assess the Role of an Air Cavity in a Drying Process, *MEWS Consortium: Technical Report T7-02,* (NRCC-44269)

Tariku, F.; Kumaran, M.K. (1999b). Assessment of the Role of Air Cavity, Building Membrane and Water Vapor Retarder in the Drying Process of a Full Scale Wall System Exposed to Ottawa Weather, *MEWS Consortium: Technical Report, T7-05,* (NRCC-44273)

Tariku, F.; Kumaran, M. K. (2002). Experimental and Analytical Investigations on the Drying Process Undergone by Aerated Concrete, *A Thermal and Moisture Transport Property Database for Common Building and Insulating Materials, Appendix II* Final Report ASHRAE Research Project 1018-RP

Tariku, F.; Kumaran, M. K. (2006). Hygrothermal Modeling of Aerated Concrete Wall and Comparison With Field Experiment. *Proceeding of the 3rd International Building Physics /Engineering Conference*, August 26-31, Montreal, Canada, pp 321-328

Tariku, F.; Kumaran, M.K.; Fazio, P. (2006). Whole building heat and moisture analysis. *IEA Annex 41 Lyon meeting*, 18 pages, October 25-27.

Tariku, F.; Cornick, S.; Lacasse, M. (2007). Simulation of Wind-Driven Rain Effects on the Performance of a Stucco-Clad Wall. *Proceedings of Thermal Performance of the Exterior Envelopes of Whole Buildings X International Conference.* Dec. 2-7, Clearwater, FL

Tariku, F.; Kumaran, M.K.; Fazio, P. (2008). Development and benchmarking of a new hygrothermal model. Paper accepted to *The 11th International Conference on Durability of Building Materials and Components*, Istanbul, Turkey, May.11-14

TenWolde, A. (1988). Mathematical Model for Indoor Humidity in Houses during Winter, *Proceedings of Symposium on Air Infiltration, Ventilation and Moisture Transfer*, Washington DC: Building Thermal Envelope Coordinating Council.

TenWolde, A. (1994). Ventilation, Humidity, and Condensation in Manufactured Houses During Winter. *ASHRAE Transactions*, 100(t): 103-115

TenWolde, A. (2001). Manual Analysis Tools, *Moisture Analysis and Condensation Control in Building Envelopes*, ASTM Manual series 50: Chapter 7

TenWolde, A. (2001a). Interior Moisture Design Loads for Residences. *Building VIII: Performance of exterior envelopes of whole buildings.* Dec. 2-7, Clearwater, FL

TenWolde, A; Pilon, C.L. (2007). The Effect of Indoor Humidity on Water Vapor Release in Homes. *Proceedings of Thermal Performance of the Exterior Envelopes of Whole Buildings X International Conference.* Dec. 2-7, Clearwater, FL

Toftum, J.; Fanger, P.O. (1998). Air Humidity Requirements for Human Comfort. ASHRAE Transactions, Vol. 105 (2), pp 641-647.

Trechsel, H.R. (2001). Moisture Primer, *Moisture Analysis and Condensation Control in Building Envelopes*, ASTM Manual series 50: Chapter 1

Trowbridge, J.; Ball, K.; Peterson, J.; Hunn, B.; Grasso, M. (1994). Evaluation of strategies for controlling humidity in residences in humid climates. *ASHRAE-Transactions*. Vol.100 (2). pp 59-73

Tsongas, G.; Burch, D.; Roos, C.; Cunningham, M. (1996). A Parametric Study of Wall Moisture Contents Using a Revised Variable Indoor Relative Humidity Version of the MOIST Transient Heat and Moisture Transfer Model. *Proceedings of the Thermal Performance of Exterior Envelopes VI Conference*, Dec. 4-8, Clearwater Beach, FL

Viitanen, H.; Salonvaara, M. (2001). Failure criteria. *Moisture Analysis and Condensation Control in Building Envelopes*, ASTM Manual series 50: Chapter 4

Wang, J (2003). Heat and Moisture Transfer in Built Structures – Numerical Analyses, *Ph.D. Thesis*, Department of Building Physics, Chalmers University of Technology, Sweden, ISBN 91-7291-269-3

Watanabe, T.; Urano, Y.; Hayashi, T. (1983). Procedures for Separating Direct and Diffuse Isolation on a Horizontal Surface and Prediction of Isolation on Tilted Surfaces. Transactions, No. 330, *Architectural Institute of Japan*, Tokyo, Japan.

Wu, Y.; Fazio, P.; Kumaran, K. (2008). Moisture Buffering Capacities of Five North American Building Materials. *Journal of Testing and Evaluation* Vol. 36 (1)

Zhang, Q.Y.; Huang, Y.J. (2002). Development of Typical Year Weather Files for Chimese Locations, LBNL-51436, ASHRAE Transaction, Vol. 108, part 2.

APPENDIX A-1

Terms in the moisture balance equation

The governing equation for moisture transport is given by Equation (A-1) and the corresponding terms are given below:

$$\frac{\partial w}{\partial t} + \rho_m div(VY_v) + div(j_v) + div(j_l) = 0 \qquad \text{(A-1)}$$

I. Vapor diffusion $div(j_v)$

The diffusion term $div(j_v)$ represents the molecular diffusion of a water-vapor through the control volume. The driving potentials for this type of transport could be concentration and/or temperature gradients.

$$j_v = -D_v^M \rho_m \frac{\partial}{\partial x_i}(Y_v) - D_v^T \frac{\partial}{\partial x_i}(\ln T)$$

where D_v^M and D_v^T are the vapor diffusion and thermal diffusion coefficient, respectively. The first term is due to concentration gradient and governed by Fick's law, and the second term is due to temperature gradient (Soret effect). The later term is usually neglected in building physics application because of its limited contribution in the vapor transfer when compared with the first term (due to concentration gradient) (Kumaran, 1992; Hens, 1996). Consequently, it is omitted here as well.

The mass fraction of water vapor (Y_v) in the diffusion equation can be expressed by the partial pressure of water-vapor (P_v) using ideal gas law:

$$\frac{P_v}{\rho_v} = RT \quad -->\frac{P_v}{RT} = \rho_v \qquad \rho_v = \rho_m Y_v \quad ==> \quad Y_v = \frac{P_v}{\rho_m RT}$$

and substituting $Y_v = \frac{P_v}{\rho_m RT}$ into the diffusion term: $j_v = -D_v^M \rho_m \frac{\partial}{\partial x_i}(Y_v)$ gives:

$$j_v = -\frac{D_v^M}{RT}\frac{\partial}{\partial x_i}(P_v) = -\delta_v \frac{\partial}{\partial x_i}(P_v) \tag{A-2}$$

where $\delta_v = \frac{D_v^M}{RT}$ is the water vapor permeability of the material.

II. <u>Vapor convection</u> $\rho_m div(VY_v)$

The mass fraction of the vapor can be expressed in terms of air density (ρ_a) and humidity ratio (ω): $\omega = \frac{Y_v}{Y_a}$ $\quad Y_v = Y_a\omega$ $\quad \rho_a = Y_a\rho_m$ $\quad Y_a = \frac{\rho_a}{\rho_m}$ $\quad Y_v = \omega\frac{\rho_a}{\rho_m}$

Substituting $Y_v = \omega\frac{\rho_a}{\rho_m}$ into the convection term yields:

$$\rho_m div(VY_v) = \rho_m div\left(V\,\omega\frac{\rho_a}{\rho_m}\right) = div(\rho_a V\,\omega) \tag{A-3}$$

III. Liquid conduction $div(j_l)$

In a porous media, liquid water transports due to suction pressure gradient and gravity force is given by Equation (A-4).

$$j_l = D_l\left(\frac{\partial P_s}{\partial x_i} + \rho_w g\right) \tag{A-4}$$

where: D_l -liquid permeability (s) and P_s -suction pressure (Pa)

ρ_w -density of liquid water (kg/m^3), $g = \vec{u}\cdot\vec{g}$ -is the dot product of the acceleration due to gravity (m/s^2) acting on the downward direction ($\vec{g}$) and the unit vector ($\vec{u}$) of the principal coordinate. The suction pressure is estimated based on capillary theory of hypothetical cylinder pore geometry, Figure A-1.

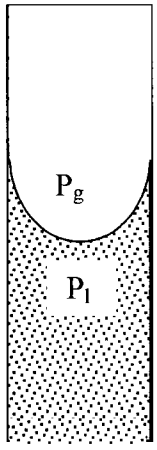

Figure A-1 Capillary force in idealized cylindrical pore geometry

The curvature of the meniscus depends on the equilibrium condition of the vapor pressure (relative humidity) above the meniscus and the pore pressure. The relationship between the vapor pressure over the meniscus and pore pressure is given by Kelvin's equation below.

$$P_l = \frac{RT\rho_w}{M_w} \ln \phi$$

where P_l is pore pressure (Pa), R is the gas constant (8.314 J/Kmol),

M_w is the molar mass of water (0.018 kg/mol); ρ_w is the density of water (kg/m^3)

ϕ is the relative humidity in fraction

The suction pressure is given by $P_s = -P_l$ assuming the atmospheric pressure is negligible compared with the pore pressure.

APPENDIX A-2

Terms in the energy conservation equation

The governing equation for conservation of energy is given by Equation (B-1), and the corresponding terms are given below:

$$\frac{\partial(\rho h)}{\partial t} + div(\rho V h) = -div(j_q) + \dot{Q}_s \qquad \text{(B-1)}$$

I. Transient term $\dfrac{\partial(\rho h)}{\partial t}$

The rate of change of the total enthalpy of the control volume for temperature above freezing ($H = \rho h$) is the summation of the rate of changes of the enthalpies of the solid matrix, air and moisture (water-vapor and liquid water). Each constitutes have a different energy storing capacity and mass fraction.

$$\frac{\partial(\rho h)}{\partial t} = \frac{\partial}{\partial t}\left(\rho_m \underbrace{Y_m h_m}_{solid\,matrix} + \rho_m \underbrace{h_a Y_a}_{air} + \rho_m \underbrace{h_v Y_v}_{water-vapor} + \rho_m \underbrace{h_l Y_l}_{liquid-water} \right)$$

where ρ_m is the density of the solid matrix (dry material) and Y_a, Y_v and Y_l are the mass fraction of air, water vapor and liquid water, respectively, defined on the basis of solid matrix (dry material) weight $\left(Y_a = \dfrac{m_a}{m_m} \quad Y_v = \dfrac{m_v}{m_m} \quad Y_l = \dfrac{m_l}{m_m} \right)$

Hence,

$$\frac{\partial(\rho h)}{\partial t} = \rho_m \frac{\partial}{\partial t}\left(\underbrace{h_m}_{solid\ matrix} + \underbrace{h_a Y_a}_{air} + \underbrace{h_v Y_v}_{water-vapor} + \underbrace{h_l Y_l}_{liquid-water} \right)$$

Expanding the terms gives:

$$\frac{\partial(\rho h)}{\partial t} = \underbrace{\rho_m \frac{\partial(h_m)}{\partial t}}_{material\ matrix} + \underbrace{\rho_m \left(h_a \frac{\partial}{\partial t} Y_a + Y_a \frac{\partial}{\partial t} h_a + h_v \frac{\partial}{\partial t} Y_v + Y_v \frac{\partial}{\partial t} h_v \right)}_{Air\ and\ water-vapor} + \underbrace{\rho_m \left(Y_l \frac{\partial}{\partial t}(h_l) + h_l \frac{\partial}{\partial t}(Y_l) \right)}_{liquid\ water} \tag{B-2}$$

II. <u>Convection term</u> $div(\rho V h)$

Among the four possible entities of a given control volume: solid matrix, air, water vapor, liquid water, only the air and water vapor enthalpies can be transported by convection, the rest won't move by the low airflow velocity.

$$div(\rho V h) = \rho_m \left(div(V Y_a h_a) + div(V Y_v h_v) \right)$$

Expanding the terms gives:

$$div(\rho V h) = \rho_m \left(Y_a div(V h_a) + h_a div(V Y_a) + Y_v div(V h_v) + h_v div(V Y_v) \right) \tag{B-3}$$

III. Diffusion term $div(j_q)$

The diffusion term, j_q, is the sum of two components $(j_q = j_c + j_d)$.

1) The first component, j_c, is heat transfer by conduction and can be determined by using Fourier's law, $j_c = -\lambda_{eff} grad(T)$, where λ_{eff} is the apparent thermal conductivity of the control volume, considering the solid matrix, air and moisture mass fraction.

2) The second component, j_d, is due to transfer of extra enthalpy across the control volume surface due to concentration gradient (Dufour effect). It is given by $j_d = \sum_i h_i j_i$, where h_i is the specific enthalpy of component *i*, and j_i is the diffusion flux of component *i*. The participating components in the Dufour effect are entities that could transport in the control volume, these are: air, water-vapor and liquid water. $j_d = \sum_i h_i j_i = h_a j_a + h_v j_v + h_l j_l$

Then the total diffusion term is given by:

$$div(j_q) = div\left(\underbrace{-\lambda_{eff} grad(T)}_{j_c} + \underbrace{h_a j_a + h_v j_v + h_l j_l}_{j_d} \right)$$

$$div(j_q) = div\left(-\lambda_{eff} grad(T)\right) + div\left(h_a j_a + h_v j_v + h_l j_l\right)$$

Expanding the terms gives:

$$div(j_q) = div\left(-\lambda_{eff} grad(T)\right) + h_a div(j_a) + j_a div(h_a) + h_v div(j_v) + j_v div(h_v) + h_l div(j_l) + j_l div(h_l) \quad \text{(B-4)}$$

APPENDIX A-3

Specific enthalpies

I. Solid matrix:

The specific enthalpy of dry material can be obtained from the basic definition of enthalpy and specific heat:

$$h_m = u_m + Pv_m \qquad \frac{dh_m}{dT} = \frac{d(u_m + Pv_m)}{dT} = \frac{du_m}{dT} + \underbrace{v_m \frac{dP}{dT} + P\frac{dv_m}{dT}}_{=0 \text{ For solid}} = \frac{du_m}{dT}$$

$$but \quad \frac{du_m}{dT} = c_{v_m} \qquad and$$

$$dh_m = c_{v_m} dT$$

II. Air:

The enthalpy of dry air is given by the product of temperature and specific heat capacity with a reference enthalpy value of zero at 0°C and standard atmospheric pressure.

$$h_a = Cp_a T$$

III. Water vapor:

The specific enthalpy of water vapor can be approximated by sum of the latent heat of evaporation (h_{fg}) at a reference temperature of 0°C and sensible enthalpy (product of temperature and specific heat capacity of vapor).

$$h_v = h_{fg} + Cp_v T$$

IV. Liquid water

The specific enthalpy of liquid water is approximated by the sensible enthalpy of liquid water (product of temperature and specific heat capacity of liquid water). The specific enthalpy of water is assigned to be zero at the triple point (0.01°C).

$$h_l = Cp_l T$$

APPENDIX A-4

COMSOL Multiphysics Model Report

1. TABLE OF CONTENTS

2. MODEL PROPERTIES

Property	Value
Model name	2D Corner HAM Analysis
Author	Fitsum Tariku
Company	
Department	
Reference	
URL	
Saved date	
Creation date	Apr 20, 2008 1:02:30 PM
COMSOL version	COMSOL 3.3.0.405

Application modes and modules used in this model:

- Geom1 (2D)
    - PDE, General Form
    - PDE, General Form

3. CONSTANTS

Name	Expression	Value	Description
cp_l	4200		
Gconst	-7.245E-5		
hg	2500000		
cp_air	1005		
rho_air	1.2		
cp_v	1880		
BC_step	3600		

4. GEOMETRY

Number of geometries: 1

4.1. Geom1

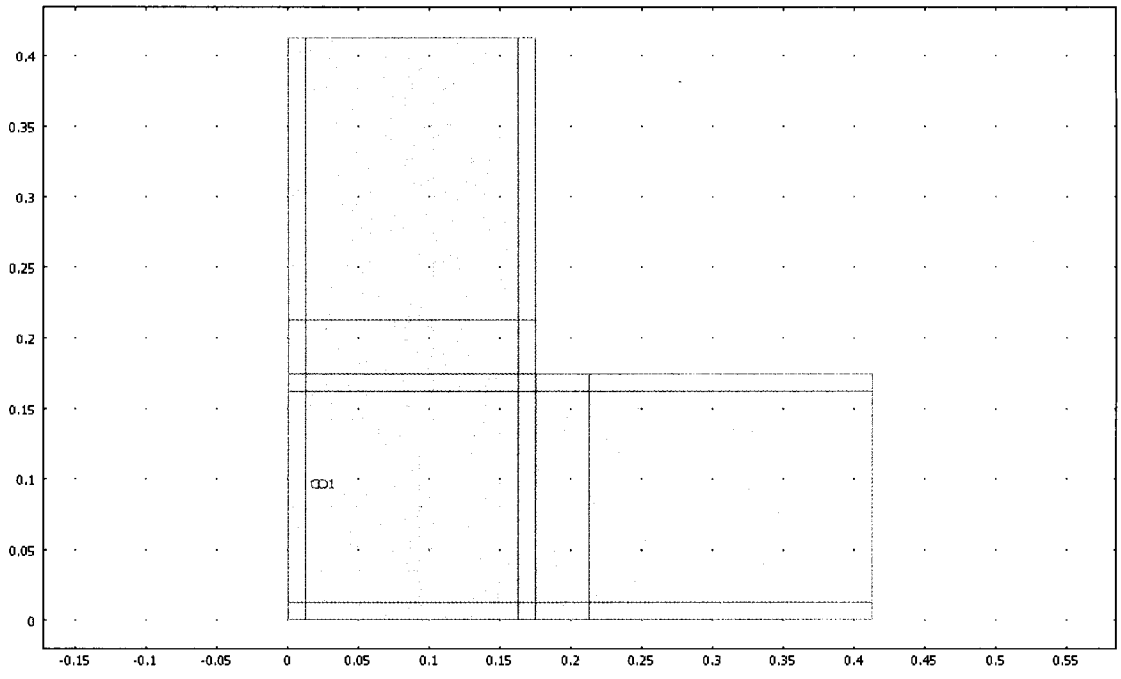

4.1.1. Point mode

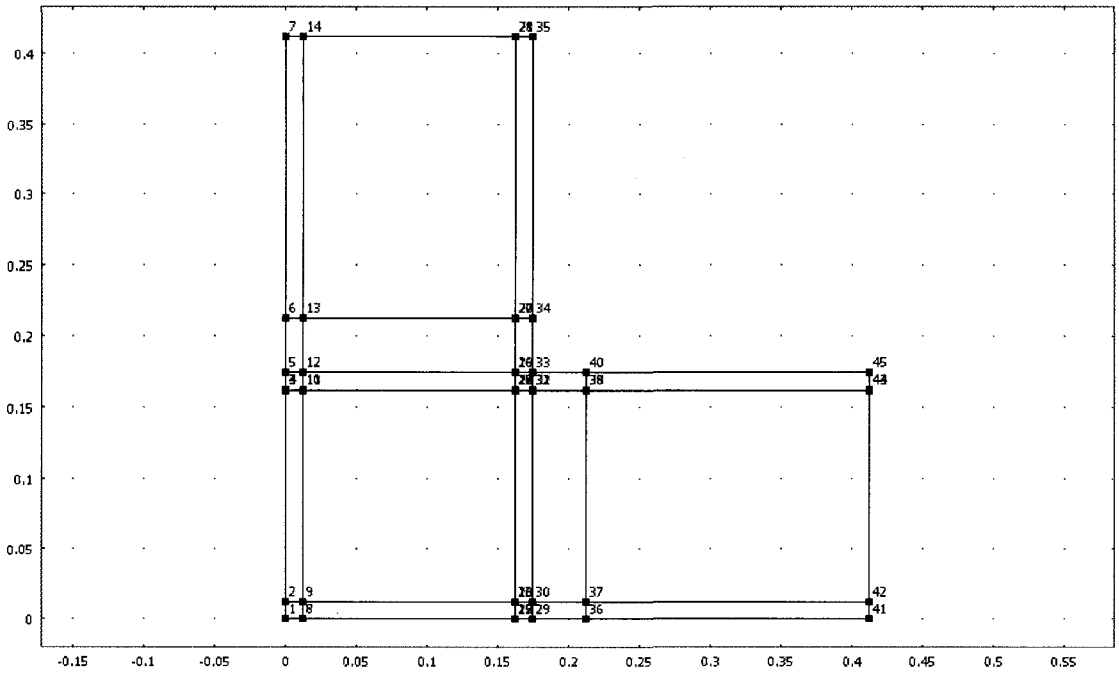

4.1.2. Boundary mode

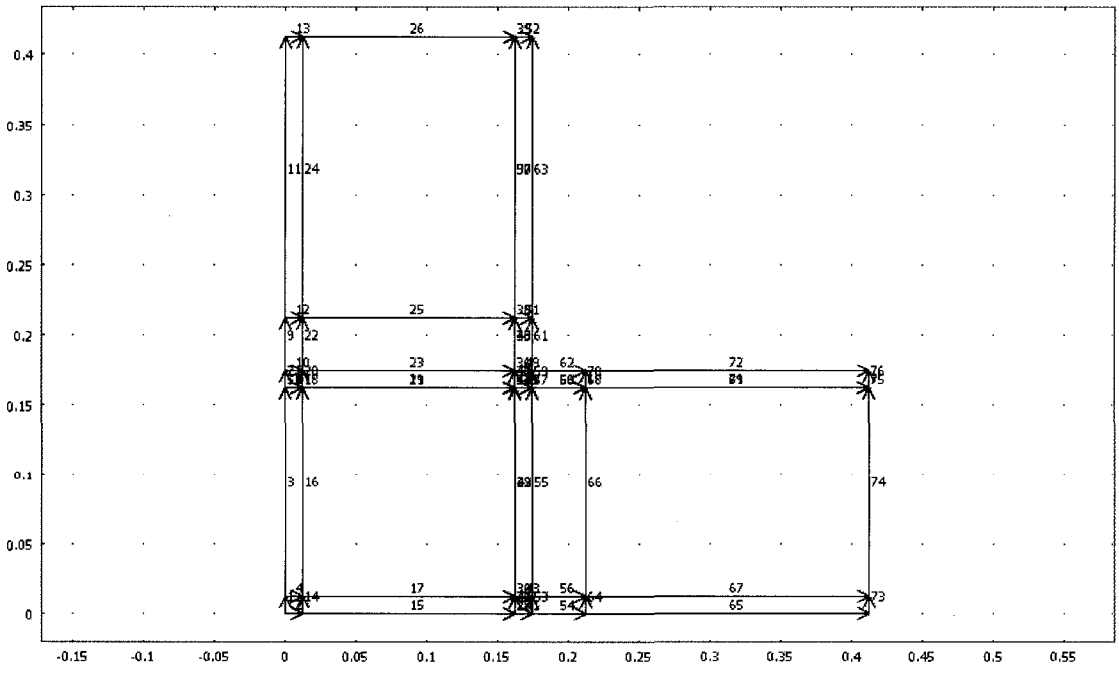

4.1.3. Subdomain mode

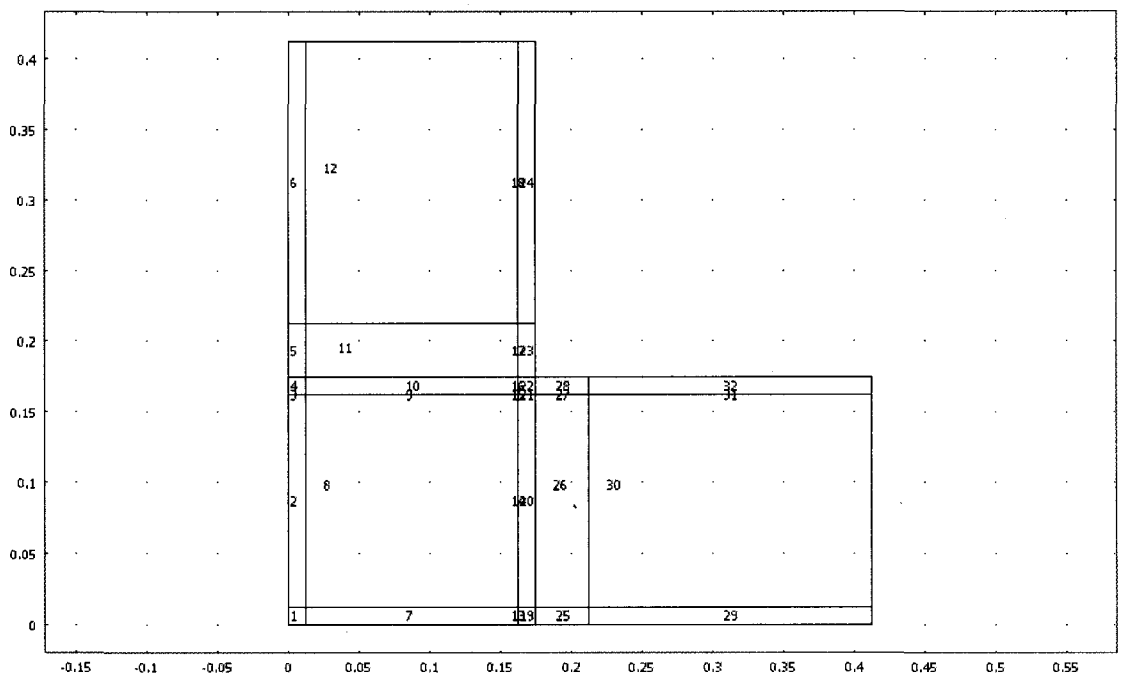

5. GEOM1

Space dimensions: 2D

Independent variables: x, y, z

5.2. Expressions

5.3. Mesh

5.3.1. Mesh Statistics

Number of degrees of freedom	15738
Number of mesh points	2015
Number of elements	1920
Triangular	0
Quadrilateral	1920

Number of boundary elements	590
Number of vertex elements	45
Element area ratio	0

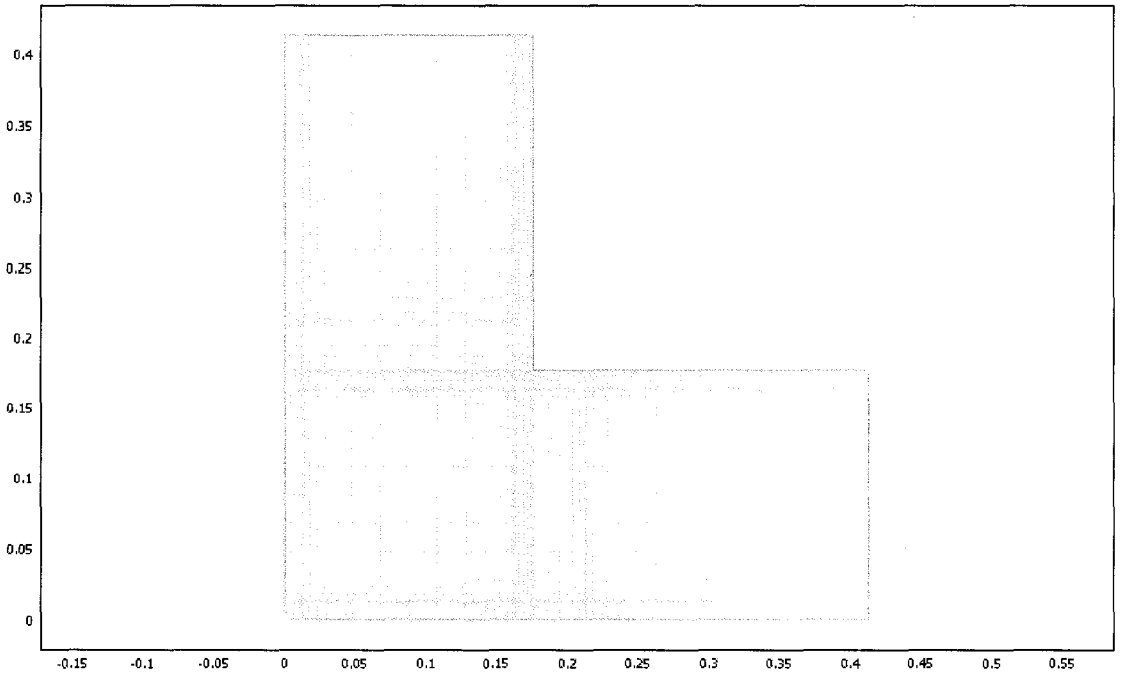

5.4. Application Mode: PDE, General Form (Moisture)

Application mode type: PDE, General Form

Application mode name: Moisture

5.4.1. Application Mode Properties

Property	Value
Default element type	Lagrange - Quadratic
Wave extension	Off
Frame	Frame (xy)
Weak constraints	Off

5.4.2. Variables

Dependent variables: phi, phi_t

Shape functions: shlag(2,'phi')

Interior boundaries not active

5.4.3. Boundary Settings

Boundary	1-3, 5, 7, 9, 11, 15, 28, 41, 54, 61-63, 65, 72	13, 26, 39, 52, 73-76
Type	Dirichlet boundary condition	Neumann boundary condition
(g)	**MOS_BC**	0
(r)	**(1-phi).*(phi>1)**	**(1-phi).*(phi>1)**
Integration order (wcgporder)	**{}**	**{}**

5.4.4. Subdomain Settings

Locked Subdomains: 1-32

Subdomain	1-32
Shape functions (shape)	**shlag(2,'phi')**
Damping/Mass coefficient (da)	**M_C**
Source term (f)	**QMS**
Conservative flux source term (ga)	**{{'-D_M_M.*phix-D_T_M.*Tx+M_air_x.*C_c1.*phi';'-D_M_M.*phiy-D_T_M.*Ty+D_M_G.*phi+M_air_y.*C_c1.*phi'}}**

Subdomain initial value	1-32
phi	initial_phi

5.5. Application Mode: PDE, General Form (Energy)

Application mode type: PDE, General Form

Application mode name: Energy

5.5.1. Application Mode Properties

Property	Value

Default element type	Lagrange - Quadratic
Wave extension	Off
Frame	Frame (xy)
Weak constraints	Off

5.5.2. Variables

Dependent variables: T, T_t

Shape functions: shlag(2,'T')

Interior boundaries not active

5.5.3. Boundary Settings

Boundary	1-3, 5, 7, 9, 11, 15, 28, 41, 54, 61-63, 65, 72	13, 26, 39, 52, 73-76
Type	Neumann boundary condition	Neumann boundary condition
(g)	**ENG_BC**	0
Integration order (wcgporder)	**{}**	**{}**

5.5.4. Subdomain Settings

Locked Subdomains: 1-32

Subdomain	1-32
Shape functions (shape)	**shlag(2,'T')**
Damping/Mass coefficient (da)	**H_C**
Source term (f)	**QHS**
Conservative flux source term (ga)	**{{'-D_T_T.*Tx-D_M_T.*phix+M_air_x.*cp_air.*T+C_cond.*M_air_x.*C_c1.*phi';'-D_T_T.*Ty-D_M_T.*phiy+M_air_y.*cp_air.*T+C_cond.*M_air_y.*C_c1.*phi'}}**

Subdomain initial value	1-32
T	initial_T

6. SOLVER SETTINGS

Solve using a script: off

Auto select solver	On
Solver	Stationary
Solution form	Automatic
Symmetric	auto
Adaption	Off

6.1. Direct (UMFPACK)

Solver type: Linear system solver

Parameter	Value
Pivot threshold	0.1
Memory allocation factor	0.7

6.2. Advanced

Parameter	Value
Constraint handling method	Elimination
Null-space function	Automatic
Assembly block size	5000
Use Hermitian transpose of constraint matrix and in symmetry detection	Off
Use complex functions with real input	Off
Stop if error due to undefined operation	On
Type of scaling	Automatic
Manual scaling	
Row equilibration	On
Manual control of reassembly	Off
Load constant	On
Constraint constant	On
Mass constant	On
Damping (mass) constant	On
Jacobian constant	On
Constraint Jacobian constant	On

7. EQUATIONS

7.1. Point

Dependent variables: phi, T

7.1.1. Point: 1-45

weak term (weak)

0
0

dweak term (dweak)

0
0

constr term (constr)

0
0

7.2. Boundary

Dependent variables: phi, T

7.2.1. Boundary: 1, 3, 5, 7, 9, 11

q coefficient

phi	T
-diff(MOS_BC,phi)	-diff(MOS_BC,T)
-diff(ENG_BC,phi)	-diff(ENG_BC,T)

g coefficient

MOS_BC
ENG_BC

h coefficient

phi	T
-diff((1-phi)*(phi>1),phi)	-diff((1-phi)*(phi>1),T)
0	0

r coefficient

(1-phi)*(phi>1)
0

constr term (constr)

0
0

7.2.2. Boundary: 2, 15, 28, 41, 54, 65

q coefficient

phi	T
-diff(MOS_BC,phi)	-diff(MOS_BC,T)
-diff(ENG_BC,phi)	-diff(ENG_BC,T)

g coefficient

MOS_BC
ENG_BC

h coefficient

phi	T
-diff((1-phi)*(phi>1),phi)	-diff((1-phi)*(phi>1),T)
0	0

r coefficient

(1-phi)*(phi>1)
0

weak term (weak)

0
0

dweak term (dweak)

0
0

constr term (constr)

0
0

7.2.3. Boundary: 4, 6, 8, 10, 12-14, 16-27, 29-40, 42-53, 55-60, 64, 66-71, 73-76

q coefficient

phi	T
0	0
0	0

g coefficient

0
0

h coefficient

phi	T
0	0
0	0

r coefficient

0
0

weak term (weak)

0
0

dweak term (dweak)

0

0

constr term (constr)

0
0

7.2.4. Boundary: 61-63, 72

q coefficient

phi	T
-diff(MOS_BC,phi)	-diff(MOS_BC,T)
-diff(ENG_BC,phi)	-diff(ENG_BC,T)

g coefficient

MOS_BC
ENG_BC

h coefficient

phi	T
-diff((1-phi)*(phi>1),phi)	-diff((1-phi)*(phi>1),T)
0	0

r coefficient

(1-phi)*(phi>1)
0

weak term (weak)

0
0

dweak term (dweak)

0
0

constr term (constr)

0
0

7.3. Subdomain

Dependent variables: phi, T

7.3.1. Subdomain: 1-7, 13, 19, 25, 29 [locked]

Diffusion coefficient (c)

phi	T
-diff(M_air_x*C_c1*phi-D_M_M*phix-D_T_M*Tx,phix), -diff(M_air_y*C_c1*phi-D_M_M*phiy-D_T_M*Ty+D_M_G*phi,phix), -diff(M_air_x*C_c1*phi-D_M_M*phix-D_T_M*Tx,phiy), -diff(M_air_y*C_c1*phi-D_M_M*phiy-D_T_M*Ty+D_M_G*phi,phiy)	-diff(M_air_x*C_c1*phi-D_M_M*phix-D_T_M*Tx,Tx), -diff(M_air_y*C_c1*phi-D_M_M*phiy-D_T_M*Ty+D_M_G*phi,Tx), -diff(M_air_x*C_c1*phi-D_M_M*phix-D_T_M*Tx,Ty), -diff(M_air_y*C_c1*phi-D_M_M*phiy-D_T_M*Ty+D_M_G*phi,Ty)
-diff(C_cond*M_air_x*C_c1*phi-D_T_T*Tx-D_M_T*phix+M_air_x*cp_air*T,phix), -diff(C_cond*M_air_y*C_c1*phi-D_T_T*Ty-D_M_T*phiy+M_air_y*cp_air*T,phix), -diff(C_cond*M_air_x*C_c1*phi-D_T_T*Tx-D_M_T*phix+M_air_x*cp_air*T,phiy), -diff(C_cond*M_air_y*C_c1*phi-D_T_T*Ty-D_M_T*phiy+M_air_y*cp_air*T,phiy)	-diff(C_cond*M_air_x*C_c1*phi-D_T_T*Tx-D_M_T*phix+M_air_x*cp_air*T,Tx), -diff(C_cond*M_air_y*C_c1*phi-D_T_T*Ty-D_M_T*phiy+M_air_y*cp_air*T,Tx), -diff(C_cond*M_air_x*C_c1*phi-D_T_T*Tx-D_M_T*phix+M_air_x*cp_air*T,Ty), -diff(C_cond*M_air_y*C_c1*phi-D_T_T*Ty-D_M_T*phiy+M_air_y*cp_air*T,Ty)

Absorption coefficient (a)

phi	T
-diff(QMS,phi)	-diff(QMS,T)
-diff(QHS,phi)	-diff(QHS,T)

Source term (f)

QMS
QHS

Damping/Mass coefficient (da)

phi	T
M_C	0
0	H_C

Conservative flux convection coeff. (al)

phi	T
-diff(M_air_x*C_c1*phi-D_M_M*phix-D_T_M*Tx,phi), -diff(M_air_y*C_c1*phi-D_M_M*phiy-D_T_M*Ty+D_M_G*phi,phi)	-diff(M_air_x*C_c1*phi-D_M_M*phix-D_T_M*Tx,T), -diff(M_air_y*C_c1*phi-D_M_M*phiy-D_T_M*Ty+D_M_G*phi,T)
-diff(C_cond*M_air_x*C_c1*phi-D_T_T*Tx-D_M_T*phix+M_air_x*cp_air*T,phi), -diff(C_cond*M_air_y*C_c1*phi-D_T_T*Ty-D_M_T*phiy+M_air_y*cp_air*T,phi)	-diff(C_cond*M_air_x*C_c1*phi-D_T_T*Tx-D_M_T*phix+M_air_x*cp_air*T,T), -diff(C_cond*M_air_y*C_c1*phi-D_T_T*Ty-D_M_T*phiy+M_air_y*cp_air*T,T)

Convection coefficient (be)

phi	T
-diff(QMS,phix), -diff(QMS,phiy)	-diff(QMS,Tx), -diff(QMS,Ty)
-diff(QHS,phix), -diff(QHS,phiy)	-diff(QHS,Tx), -diff(QHS,Ty)

Conservative flux source term (ga)

M_air_x*C_c1*phi-D_M_M*phix-D_T_M*Tx, M_air_y*C_c1*phi-D_M_M*phiy-D_T_M*Ty+D_M_G*phi
C_cond*M_air_x*C_c1*phi-D_T_T*Tx-D_M_T*phix+M_air_x*cp_air*T, C_cond*M_air_y*C_c1*phi-D_T_T*Ty-D_M_T*phiy+M_air_y*cp_air*T

weak term (weak)

0
0

dweak term (dweak)

0
0

constr term (constr)

0
0

Ultraweak term (bnd.weak)

0
0

7.3.2. Subdomain: 8-11, 14, 20, 26 [locked]

Diffusion coefficient (c)

phi	T
-diff(M_air_x*C_c1*phi-D_M_M*phix-D_T_M*Tx,phix), -diff(M_air_y*C_c1*phi-D_M_M*phiy-D_T_M*Ty+D_M_G*phi,phix), -diff(M_air_x*C_c1*phi-D_M_M*phix-D_T_M*Tx,phiy), -diff(M_air_y*C_c1*phi-D_M_M*phiy-D_T_M*Ty+D_M_G*phi,phiy)	-diff(M_air_x*C_c1*phi-D_M_M*phix-D_T_M*Tx,Tx), -diff(M_air_y*C_c1*phi-D_M_M*phiy-D_T_M*Ty+D_M_G*phi,Tx), -diff(M_air_x*C_c1*phi-D_M_M*phix-D_T_M*Tx,Ty), -diff(M_air_y*C_c1*phi-D_M_M*phiy-D_T_M*Ty+D_M_G*phi,Ty)
-diff(C_cond*M_air_x*C_c1*phi-D_T_T*Tx-D_M_T*phix+M_air_x*cp_air*T,phix), -diff(C_cond*M_air_y*C_c1*phi-D_T_T*Ty-D_M_T*phiy+M_air_y*cp_air*T,phix), -diff(C_cond*M_air_x*C_c1*phi-D_T_T*Tx-D_M_T*phix+M_air_x*cp_air*T,phiy), -diff(C_cond*M_air_y*C_c1*phi-D_T_T*Ty-D_M_T*phiy+M_air_y*cp_air*T,phiy)	-diff(C_cond*M_air_x*C_c1*phi-D_T_T*Tx-D_M_T*phix+M_air_x*cp_air*T,Tx), -diff(C_cond*M_air_y*C_c1*phi-D_T_T*Ty-D_M_T*phiy+M_air_y*cp_air*T,Tx), -diff(C_cond*M_air_x*C_c1*phi-D_T_T*Tx-D_M_T*phix+M_air_x*cp_air*T,Ty), -diff(C_cond*M_air_y*C_c1*phi-D_T_T*Ty-D_M_T*phiy+M_air_y*cp_air*T,Ty)

Absorption coefficient (a)

phi	T
-diff(QMS,phi)	-diff(QMS,T)
-diff(QHS,phi)	-diff(QHS,T)

Source term (f)

QMS
QHS

Damping/Mass coefficient (da)

phi	T
M_C	0
0	H_C

Conservative flux convection coeff. (al)

phi	T
-diff(M_air_x*C_c1*phi-D_M_M*phix-D_T_M*Tx,phi), -diff(M_air_y*C_c1*phi-D_M_M*phiy-D_T_M*Ty+D_M_G*phi,phi)	-diff(M_air_x*C_c1*phi-D_M_M*phix-D_T_M*Tx,T), -diff(M_air_y*C_c1*phi-D_M_M*phiy-D_T_M*Ty+D_M_G*phi,T)
-diff(C_cond*M_air_x*C_c1*phi-D_T_T*Tx-D_M_T*phix+M_air_x*cp_air*T,phi), -diff(C_cond*M_air_y*C_c1*phi-D_T_T*Ty-D_M_T*phiy+M_air_y*cp_air*T,phi)	-diff(C_cond*M_air_x*C_c1*phi-D_T_T*Tx-D_M_T*phix+M_air_x*cp_air*T,T), -diff(C_cond*M_air_y*C_c1*phi-D_T_T*Ty-D_M_T*phiy+M_air_y*cp_air*T,T)

Convection coefficient (be)

phi	T
-diff(QMS,phix), -diff(QMS,phiy)	-diff(QMS,Tx), -diff(QMS,Ty)
-diff(QHS,phix), -diff(QHS,phiy)	-diff(QHS,Tx), -diff(QHS,Ty)

Conservative flux source term (ga)

M_air_x*C_c1*phi-D_M_M*phix-D_T_M*Tx, M_air_y*C_c1*phi-D_M_M*phiy-D_T_M*Ty+D_M_G*phi
C_cond*M_air_x*C_c1*phi-D_T_T*Tx-D_M_T*phix+M_air_x*cp_air*T, C_cond*M_air_y*C_c1*phi-D_T_T*Ty-D_M_T*phiy+M_air_y*cp_air*T

weak term (weak)

0
0

dweak term (dweak)

0
0

constr term (constr)

0
0

Ultraweak term (bnd.weak)

0
0

7.3.3. Subdomain: 12, 30 [locked]

Diffusion coefficient (c)

phi	T
-diff(M_air_x*C_c1*phi-D_M_M*phix-D_T_M*Tx,phix), -diff(M_air_y*C_c1*phi-D_M_M*phiy-D_T_M*Ty+D_M_G*phi,phix), -diff(M_air_x*C_c1*phi-D_M_M*phix-D_T_M*Tx,phiy), -diff(M_air_y*C_c1*phi-D_M_M*phiy-D_T_M*Ty+D_M_G*phi,phiy)	-diff(M_air_x*C_c1*phi-D_M_M*phix-D_T_M*Tx,Tx), -diff(M_air_y*C_c1*phi-D_M_M*phiy-D_T_M*Ty+D_M_G*phi,Tx), -diff(M_air_x*C_c1*phi-D_M_M*phix-D_T_M*Tx,Ty), -diff(M_air_y*C_c1*phi-D_M_M*phiy-D_T_M*Ty+D_M_G*phi,Ty)
-diff(C_cond*M_air_x*C_c1*phi-D_T_T*Tx-D_M_T*phix+M_air_x*cp_air*T,phix), -diff(C_cond*M_air_y*C_c1*phi-D_T_T*Ty-D_M_T*phiy+M_air_y*cp_air*T,phix), -diff(C_cond*M_air_x*C_c1*phi-D_T_T*Tx-D_M_T*phix+M_air_x*cp_air*T,phiy), -diff(C_cond*M_air_y*C_c1*phi-D_T_T*Ty-D_M_T*phiy+M_air_y*cp_air*T,phiy)	-diff(C_cond*M_air_x*C_c1*phi-D_T_T*Tx-D_M_T*phix+M_air_x*cp_air*T,Tx), -diff(C_cond*M_air_y*C_c1*phi-D_T_T*Ty-D_M_T*phiy+M_air_y*cp_air*T,Tx), -diff(C_cond*M_air_x*C_c1*phi-D_T_T*Tx-D_M_T*phix+M_air_x*cp_air*T,Ty), -diff(C_cond*M_air_y*C_c1*phi-D_T_T*Ty-D_M_T*phiy+M_air_y*cp_air*T,Ty)

Absorption coefficient (a)

phi	T
-diff(QMS,phi)	-diff(QMS,T)
-diff(QHS,phi)	-diff(QHS,T)

Source term (f)

QMS
QHS

Damping/Mass coefficient (da)

phi	T
M_C	0
0	H_C

Conservative flux convection coeff. (al)

phi	T
-diff(M_air_x*C_c1*phi-D_M_M*phix-D_T_M*Tx,phi), -diff(M_air_y*C_c1*phi-D_M_M*phiy-D_T_M*Ty+D_M_G*phi,phi)	-diff(M_air_x*C_c1*phi-D_M_M*phix-D_T_M*Tx,T), -diff(M_air_y*C_c1*phi-D_M_M*phiy-D_T_M*Ty+D_M_G*phi,T)
-diff(C_cond*M_air_x*C_c1*phi-D_T_T*Tx-D_M_T*phix+M_air_x*cp_air*T,phi), -diff(C_cond*M_air_y*C_c1*phi-D_T_T*Ty-D_M_T*phiy+M_air_y*cp_air*T,phi)	-diff(C_cond*M_air_x*C_c1*phi-D_T_T*Tx-D_M_T*phix+M_air_x*cp_air*T,T), -diff(C_cond*M_air_y*C_c1*phi-D_T_T*Ty-D_M_T*phiy+M_air_y*cp_air*T,T)

Convection coefficient (be)

phi	T
-diff(QMS,phix), -diff(QMS,phiy)	-diff(QMS,Tx), -diff(QMS,Ty)
-diff(QHS,phix), -diff(QHS,phiy)	-diff(QHS,Tx), -diff(QHS,Ty)

Conservative flux source term (ga)

M_air_x*C_c1*phi-D_M_M*phix-D_T_M*Tx, M_air_y*C_c1*phi-D_M_M*phiy-D_T_M*Ty+D_M_G*phi
C_cond*M_air_x*C_c1*phi-D_T_T*Tx-D_M_T*phix+M_air_x*cp_air*T, C_cond*M_air_y*C_c1*phi-D_T_T*Ty-D_M_T*phiy+M_air_y*cp_air*T

weak term (weak)

0
0

dweak term (dweak)

0
0

constr term (constr)

0
0

Ultraweak term (bnd.weak)

0
0

7.3.4. Subdomain: 15-18, 21, 27, 31 [locked]

Diffusion coefficient (c)

phi	T
-diff(M_air_x*C_c1*phi-D_M_M*phix-D_T_M*Tx,phix), -diff(M_air_y*C_c1*phi-D_M_M*phiy-D_T_M*Ty+D_M_G*phi,phix), -diff(M_air_x*C_c1*phi-D_M_M*phix-D_T_M*Tx,phiy), -diff(M_air_y*C_c1*phi-D_M_M*phiy-D_T_M*Ty+D_M_G*phi,phiy)	-diff(M_air_x*C_c1*phi-D_M_M*phix-D_T_M*Tx,Tx), -diff(M_air_y*C_c1*phi-D_M_M*phiy-D_T_M*Ty+D_M_G*phi,Tx), -diff(M_air_x*C_c1*phi-D_M_M*phix-D_T_M*Tx,Ty), -diff(M_air_y*C_c1*phi-D_M_M*phiy-D_T_M*Ty+D_M_G*phi,Ty)
-diff(C_cond*M_air_x*C_c1*phi-D_T_T*Tx-D_M_T*phix+M_air_x*cp_air*T,phix), -diff(C_cond*M_air_y*C_c1*phi-D_T_T*Ty-D_M_T*phiy+M_air_y*cp_air*T,phix), -diff(C_cond*M_air_x*C_c1*phi-D_T_T*Tx-D_M_T*phix+M_air_x*cp_air*T,phiy), -diff(C_cond*M_air_y*C_c1*phi-D_T_T*Ty-D_M_T*phiy+M_air_y*cp_air*T,phiy)	-diff(C_cond*M_air_x*C_c1*phi-D_T_T*Tx-D_M_T*phix+M_air_x*cp_air*T,Tx), -diff(C_cond*M_air_y*C_c1*phi-D_T_T*Ty-D_M_T*phiy+M_air_y*cp_air*T,Tx), -diff(C_cond*M_air_x*C_c1*phi-D_T_T*Tx-D_M_T*phix+M_air_x*cp_air*T,Ty), -diff(C_cond*M_air_y*C_c1*phi-D_T_T*Ty-D_M_T*phiy+M_air_y*cp_air*T,Ty)

Absorption coefficient (a)

phi	T
-diff(QMS,phi)	-diff(QMS,T)
-diff(QHS,phi)	-diff(QHS,T)

Source term (f)

QMS
QHS

Damping/Mass coefficient (da)

phi	T
M_C	0
0	H_C

Conservative flux convection coeff. (al)

phi	T
-diff(M_air_x*C_c1*phi-D_M_M*phix-D_T_M*Tx,phi), -diff(M_air_y*C_c1*phi-D_M_M*phiy-D_T_M*Ty+D_M_G*phi,phi)	-diff(M_air_x*C_c1*phi-D_M_M*phix-D_T_M*Tx,T), -diff(M_air_y*C_c1*phi-D_M_M*phiy-D_T_M*Ty+D_M_G*phi,T)
-diff(C_cond*M_air_x*C_c1*phi-D_T_T*Tx-D_M_T*phix+M_air_x*cp_air*T,phi), -diff(C_cond*M_air_y*C_c1*phi-D_T_T*Ty-D_M_T*phiy+M_air_y*cp_air*T,phi)	-diff(C_cond*M_air_x*C_c1*phi-D_T_T*Tx-D_M_T*phix+M_air_x*cp_air*T,T), -diff(C_cond*M_air_y*C_c1*phi-D_T_T*Ty-D_M_T*phiy+M_air_y*cp_air*T,T)

Convection coefficient (be)

phi	T
-diff(QMS,phix), -diff(QMS,phiy)	-diff(QMS,Tx), -diff(QMS,Ty)
-diff(QHS,phix), -diff(QHS,phiy)	-diff(QHS,Tx), -diff(QHS,Ty)

Conservative flux source term (ga)

M_air_x*C_c1*phi-D_M_M*phix-D_T_M*Tx, M_air_y*C_c1*phi-D_M_M*phiy-D_T_M*Ty+D_M_G*phi
C_cond*M_air_x*C_c1*phi-D_T_T*Tx-D_M_T*phix+M_air_x*cp_air*T, C_cond*M_air_y*C_c1*phi-D_T_T*Ty-D_M_T*phiy+M_air_y*cp_air*T

weak term (weak)

0
0

dweak term (dweak)

0
0

constr term (constr)

0
0

Ultraweak term (bnd.weak)

0
0

7.3.5. Subdomain: 22-24, 28, 32 [locked]

Diffusion coefficient (c)

phi	T
-diff(M_air_x*C_c1*phi-D_M_M*phix-D_T_M*Tx,phix), -diff(M_air_y*C_c1*phi-D_M_M*phiy-D_T_M*Ty+D_M_G*phi,phix), -diff(M_air_x*C_c1*phi-D_M_M*phix-D_T_M*Tx,phiy), -diff(M_air_y*C_c1*phi-D_M_M*phiy-D_T_M*Ty+D_M_G*phi,phiy)	-diff(M_air_x*C_c1*phi-D_M_M*phix-D_T_M*Tx,Tx), -diff(M_air_y*C_c1*phi-D_M_M*phiy-D_T_M*Ty+D_M_G*phi,Tx), -diff(M_air_x*C_c1*phi-D_M_M*phix-D_T_M*Tx,Ty), -diff(M_air_y*C_c1*phi-D_M_M*phiy-D_T_M*Ty+D_M_G*phi,Ty)
-diff(C_cond*M_air_x*C_c1*phi-D_T_T*Tx-D_M_T*phix+M_air_x*cp_air*T,phix), -diff(C_cond*M_air_y*C_c1*phi-D_T_T*Ty-D_M_T*phiy+M_air_y*cp_air*T,phix), -diff(C_cond*M_air_x*C_c1*phi-D_T_T*Tx-D_M_T*phix+M_air_x*cp_air*T,phiy), -diff(C_cond*M_air_y*C_c1*phi-D_T_T*Ty-D_M_T*phiy+M_air_y*cp_air*T,phiy)	-diff(C_cond*M_air_x*C_c1*phi-D_T_T*Tx-D_M_T*phix+M_air_x*cp_air*T,Tx), -diff(C_cond*M_air_y*C_c1*phi-D_T_T*Ty-D_M_T*phiy+M_air_y*cp_air*T,Tx), -diff(C_cond*M_air_x*C_c1*phi-D_T_T*Tx-D_M_T*phix+M_air_x*cp_air*T,Ty), -diff(C_cond*M_air_y*C_c1*phi-D_T_T*Ty-D_M_T*phiy+M_air_y*cp_air*T,Ty)

Absorption coefficient (a)

phi	T
-diff(QMS,phi)	-diff(QMS,T)
-diff(QHS,phi)	-diff(QHS,T)

Source term (f)

QMS
QHS

Damping/Mass coefficient (da)

phi	T
M_C	0
0	H_C

Conservative flux convection coeff. (al)

phi	T
-diff(M_air_x*C_c1*phi-D_M_M*phix-D_T_M*Tx,phi), -diff(M_air_y*C_c1*phi-D_M_M*phiy-D_T_M*Ty+D_M_G*phi,phi)	-diff(M_air_x*C_c1*phi-D_M_M*phix-D_T_M*Tx,T), -diff(M_air_y*C_c1*phi-D_M_M*phiy-D_T_M*Ty+D_M_G*phi,T)
-diff(C_cond*M_air_x*C_c1*phi-D_T_T*Tx-D_M_T*phix+M_air_x*cp_air*T,phi), -diff(C_cond*M_air_y*C_c1*phi-D_T_T*Ty-D_M_T*phiy+M_air_y*cp_air*T,phi)	-diff(C_cond*M_air_x*C_c1*phi-D_T_T*Tx-D_M_T*phix+M_air_x*cp_air*T,T), -diff(C_cond*M_air_y*C_c1*phi-D_T_T*Ty-D_M_T*phiy+M_air_y*cp_air*T,T)

Convection coefficient (be)

phi	T
-diff(QMS,phix), -diff(QMS,phiy)	-diff(QMS,Tx), -diff(QMS,Ty)
-diff(QHS,phix), -diff(QHS,phiy)	-diff(QHS,Tx), -diff(QHS,Ty)

Conservative flux source term (ga)

M_air_x*C_c1*phi-D_M_M*phix-D_T_M*Tx, M_air_y*C_c1*phi-D_M_M*phiy-D_T_M*Ty+D_M_G*phi
C_cond*M_air_x*C_c1*phi-D_T_T*Tx-D_M_T*phix+M_air_x*cp_air*T, C_cond*M_air_y*C_c1*phi-D_T_T*Ty-D_M_T*phiy+M_air_y*cp_air*T

weak term (weak)

0
0

dweak term (dweak)

0
0

constr term (constr)

0
0

Ultraweak term (bnd.weak)

0
0

8. VARIABLES

8.1. Subdomain

Name	Description	Expression
absphix_Moisture	|grad(phi)|	sqrt(phix^2+phiy^2)
absga1x_Moisture	|ga1x|	sqrt(ga1x^2+ga1y^2)
absTx_Energy	|grad(T)|	sqrt(Tx^2+Ty^2)
absga2x_Energy	|ga2x|	sqrt(ga2x^2+ga2y^2)

APPENDIX B-1

HAMSTAD Benchmark Exercise #3

In benchmark #3, the effect of airflow (exfiltration and infiltration) on the wetting (accumulation of moisture) and drying of a lightweight structure is analyzed. Although the main moisture transfer mechanism in this exercise is by airflow, moisture transports due to temperature and moisture gradient across the monolithic wall layer. The schematic diagram of the structure considered is shown in Figure B-1 below. The pressure gradients across the wall, which causes heat and moisture transfer by convection, in both infiltration and exfiltration periods are 30 Pa, Figure B-2 . The exterior surface of the structure is vapor tight (painted), whereas the interior surface is open. Accordingly the mass transfer coefficients of the exterior and interior surfaces are 7.38E-12 and 2E-7 s/m, respectively. The heat transfer coefficients for both surfaces are 10 W/m^2K. The initial hygrothermal conditions of the structure are 20°C and 95% temperature and relative humidity, respectively. In the first 20 days the airflow is from inside to outside (exfiltration) and the airflow is reversed in the next 80 days (infiltration). The interior temperature and relative humidity conditions are 20°C and 70%, respectively. Whereas the exterior temperature and relative humidity conditions are 2°C and 80%, respectively. These boundary conditions are maintained constant for the 100 days of simulation period. The density and specific heat capacity of the monolithic layer are 212 kg/m^3 and 1000 J/kgK, respectively. The moisture storage characteristics (sorption isotherm and water retention curve), vapor permeability, liquid diffusivity and moisture dependent thermal conductivity of the material are shown in Figure B-3. The full description of this benchmark exercise is given in Hagentoft (2002). The time history of moisture content

and temperature at different cross-section of the wall, i.e. at 0.05, 0.1, 0.15, 0.17 and 0.19 m, are used for model comparisons. As shown in Figure B-4 and Figure B-5, temperature and moisture content variations with time at different cross-sections of the wall, the simulation results of HAMFit agrees very well with the other models solutions (labeled 1 to 4).

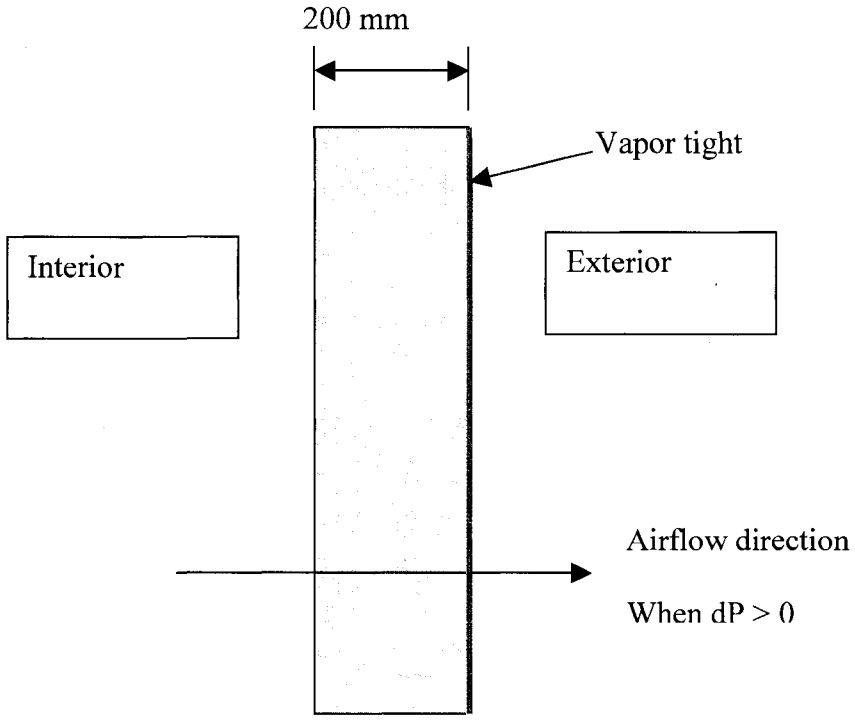

Figure B-1 Benchmark three: Lightweight wall

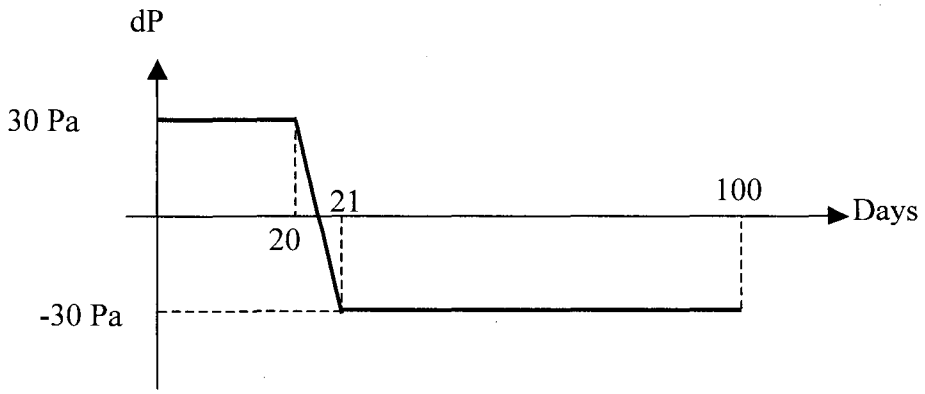

Figure B-2 Pressure gradient across the wall

Hygrotherrmal properties

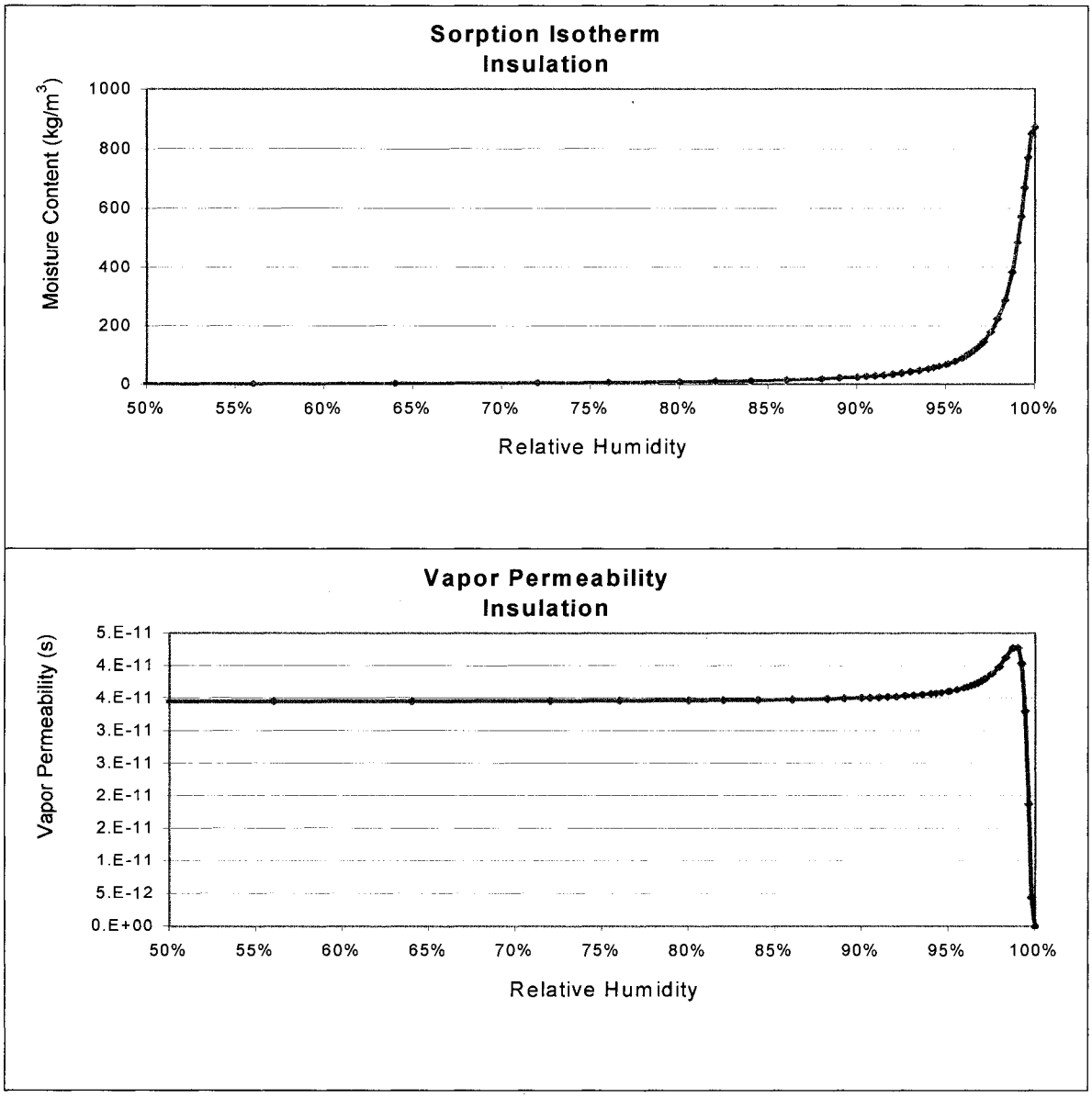

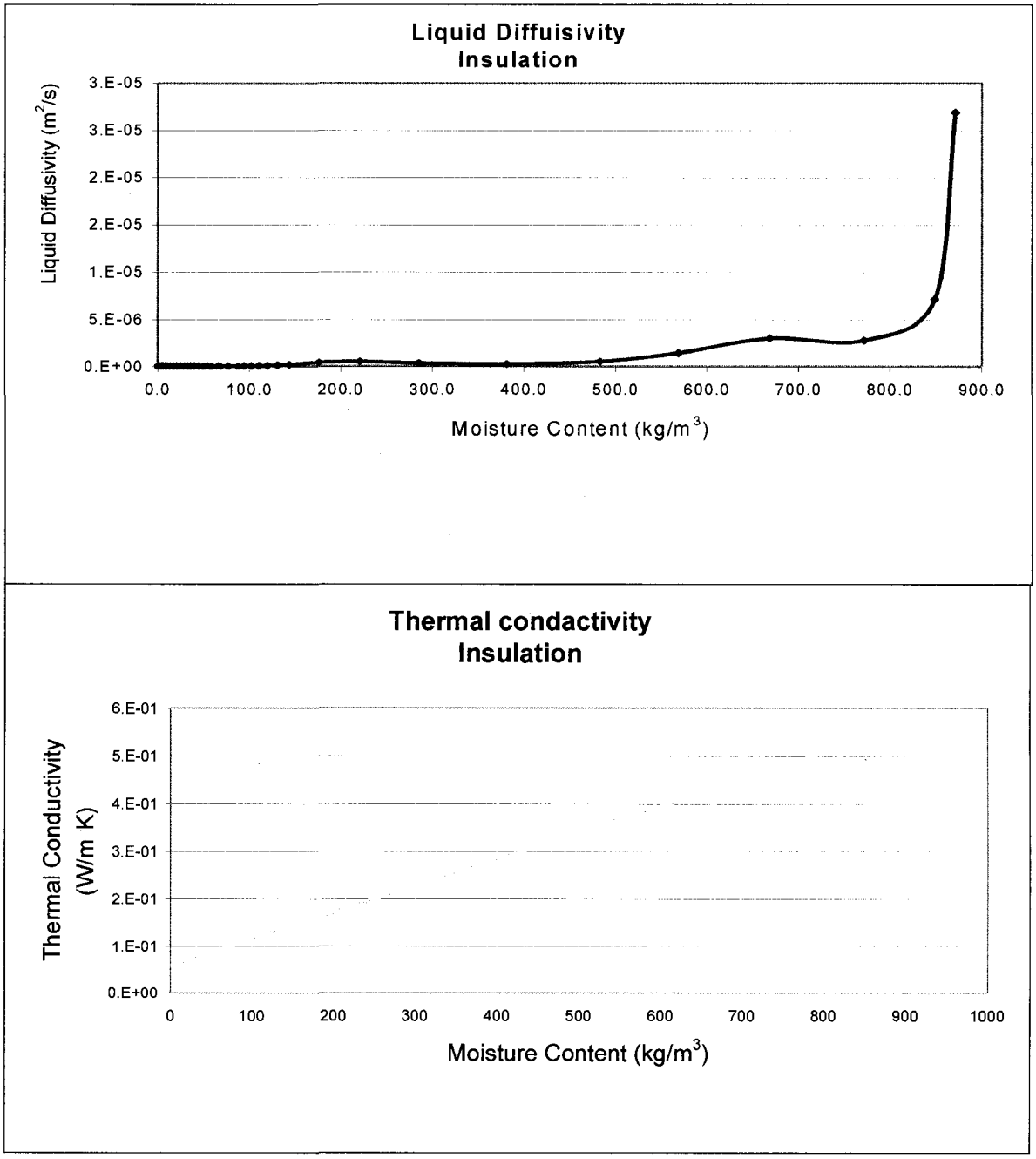

Figure B-3 Sorption-isotherm, vapor permeability, liquid diffusivity and moisture dependent thermal conductivity properties of the lightweight wall

Temperature profiles at different cross-section

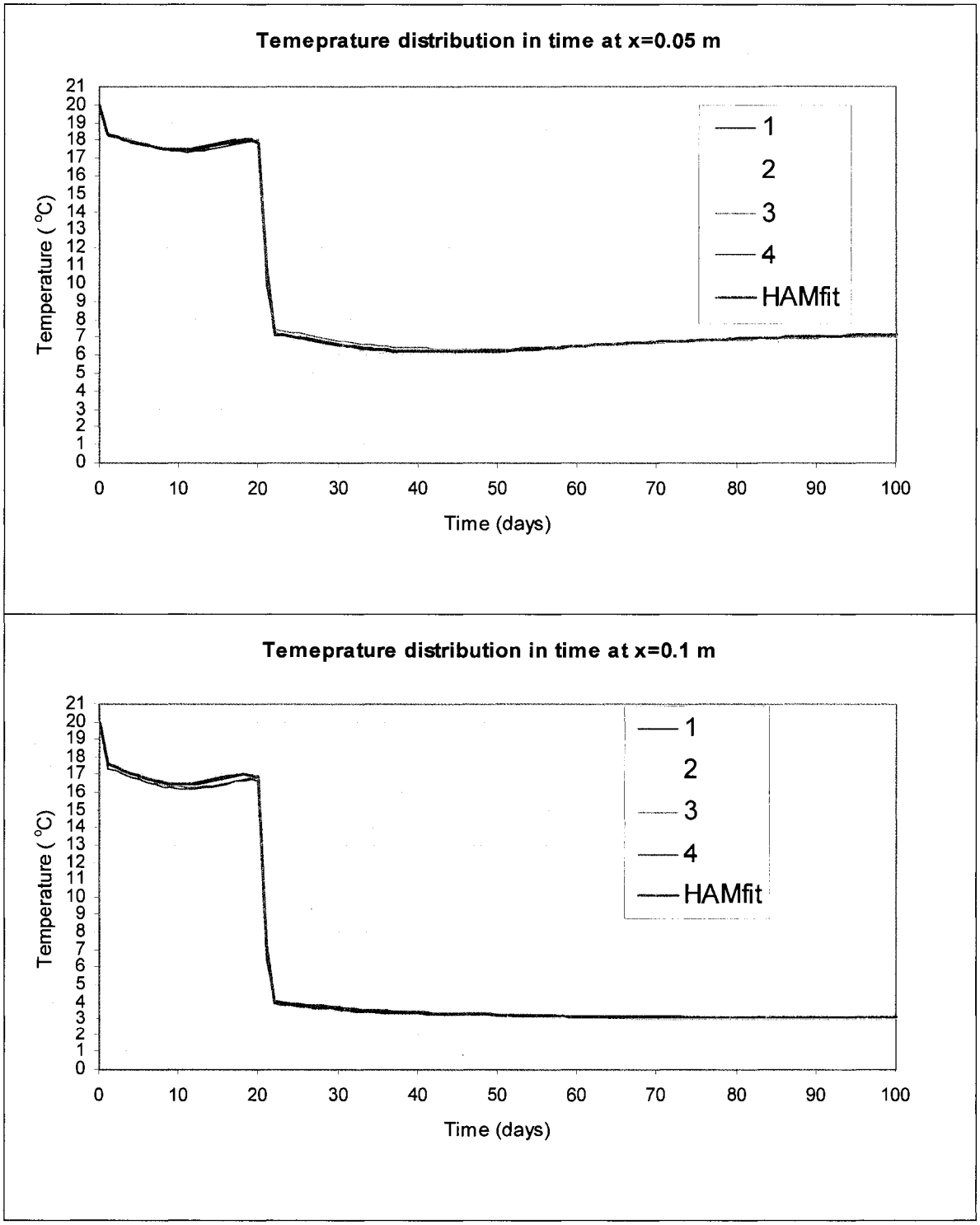

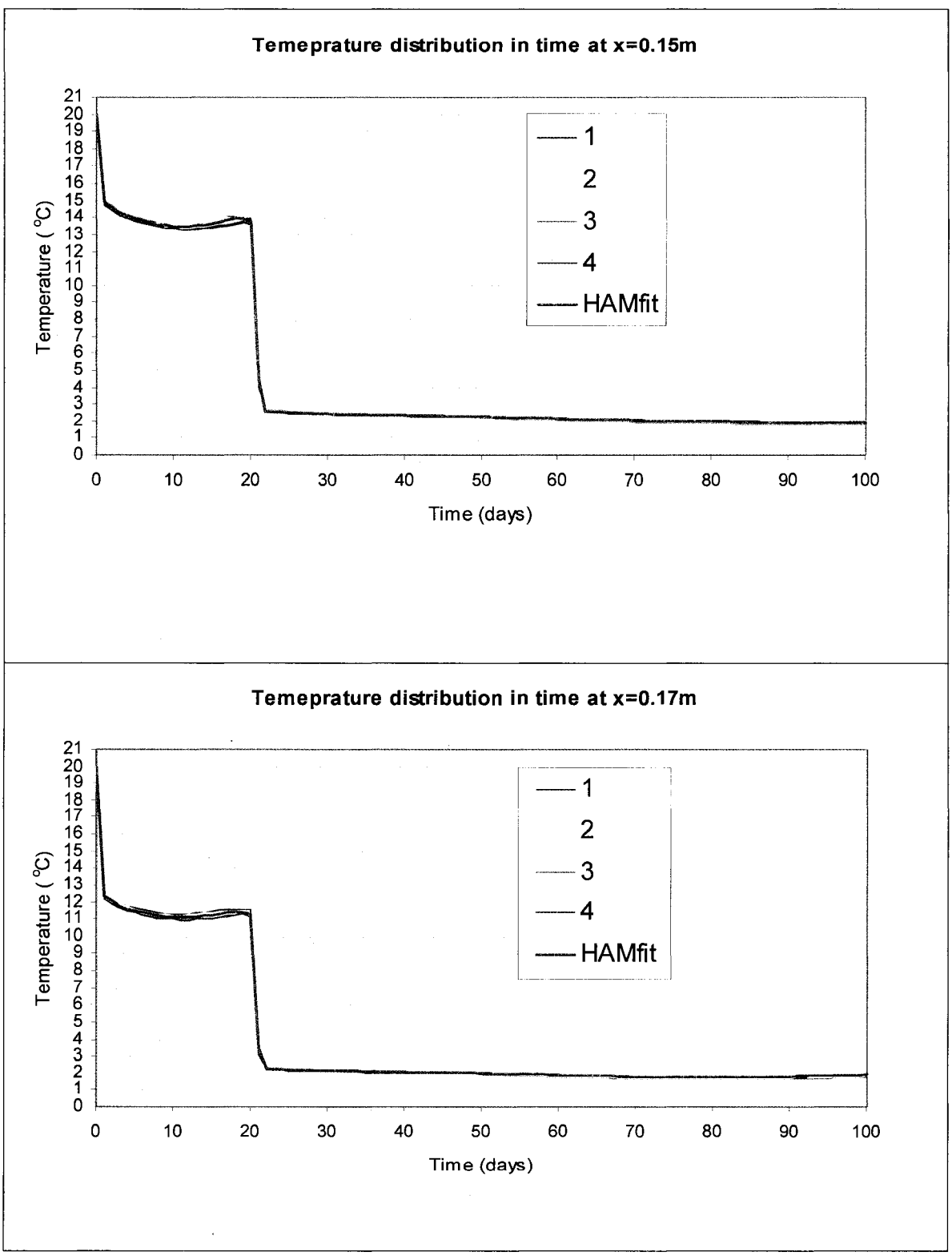
Temeprature distribution in time at x=0.15m
Temperature (°C)
Time (days)
1
2
3
4
HAMfit
Temeprature distribution in time at x=0.17m
Temperature (°C)
Time (days)
1
2
3
4
HAMfit

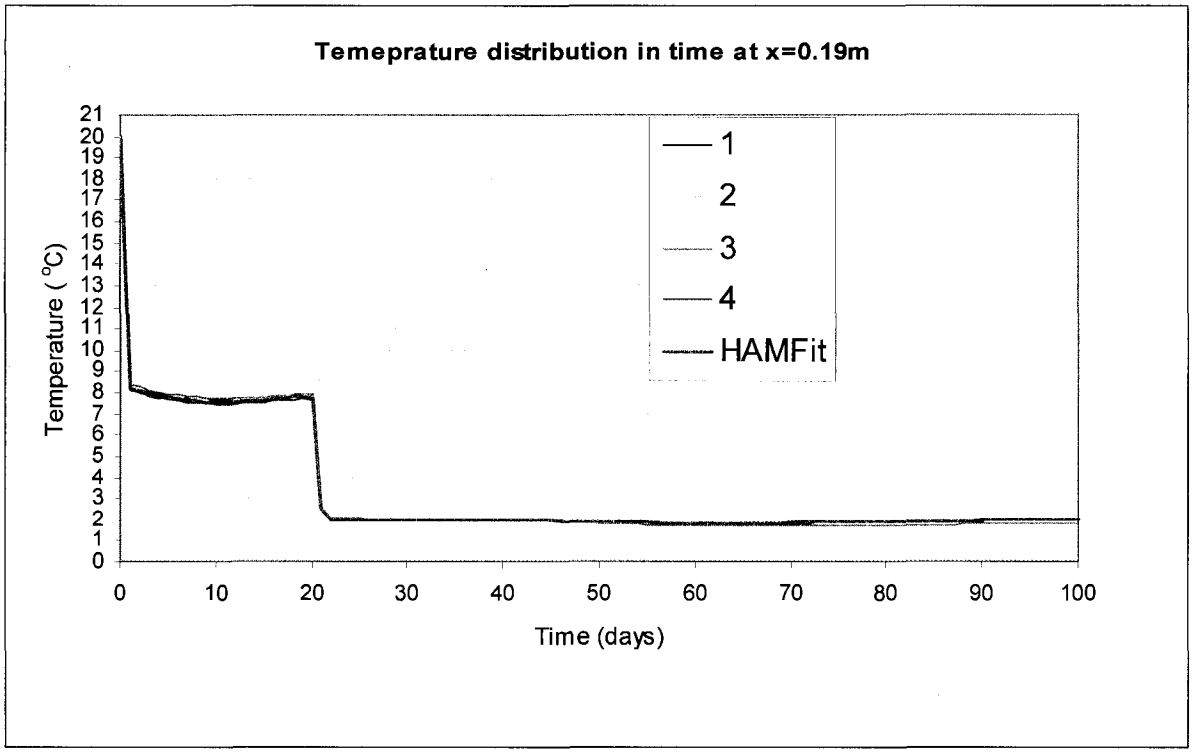

Figure B-4 Temperature variations in time at 0.05, 0.10, 0.15, 0.17 and 0.19 m cross-section of the wall

Moisture content profiles at different cross-section

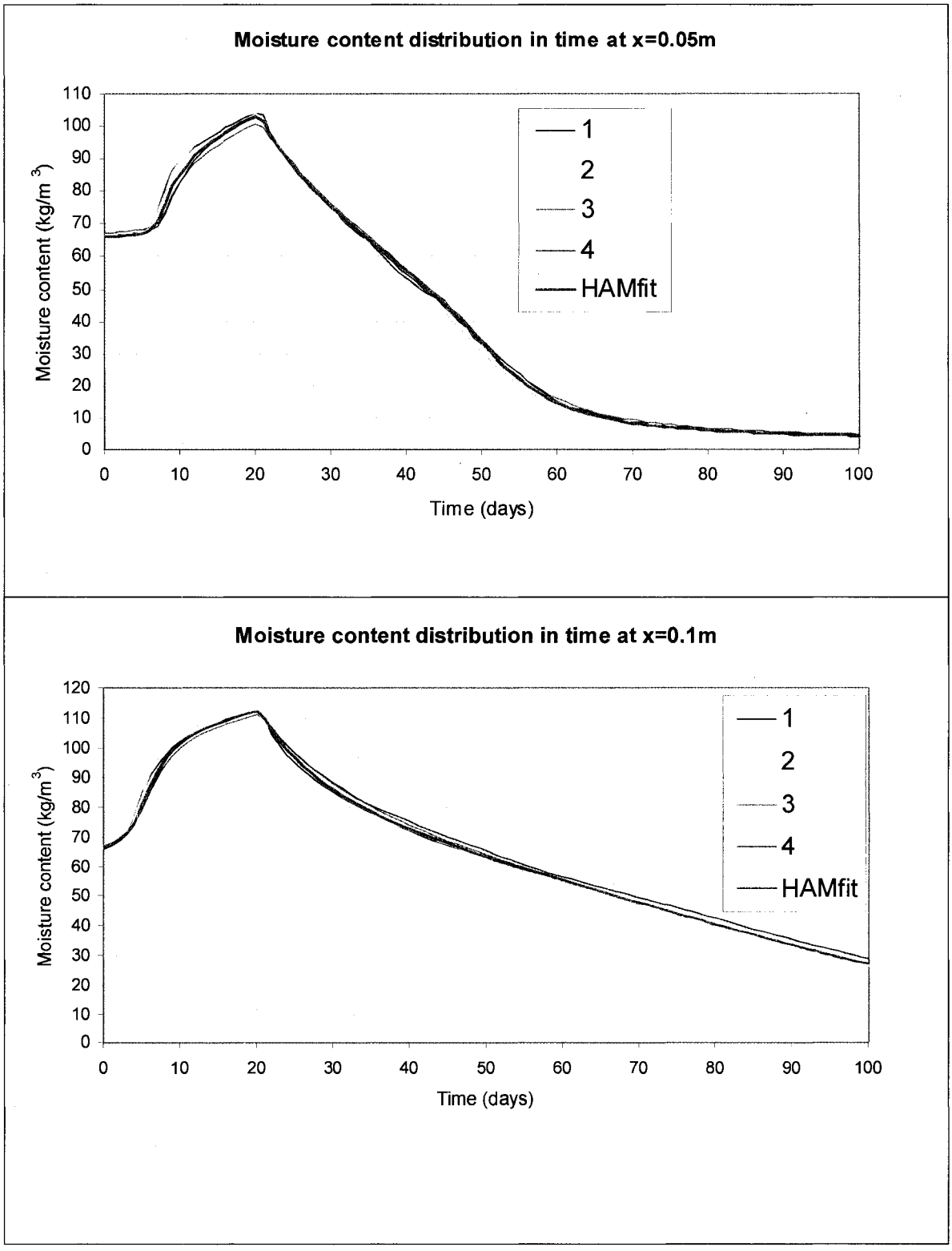

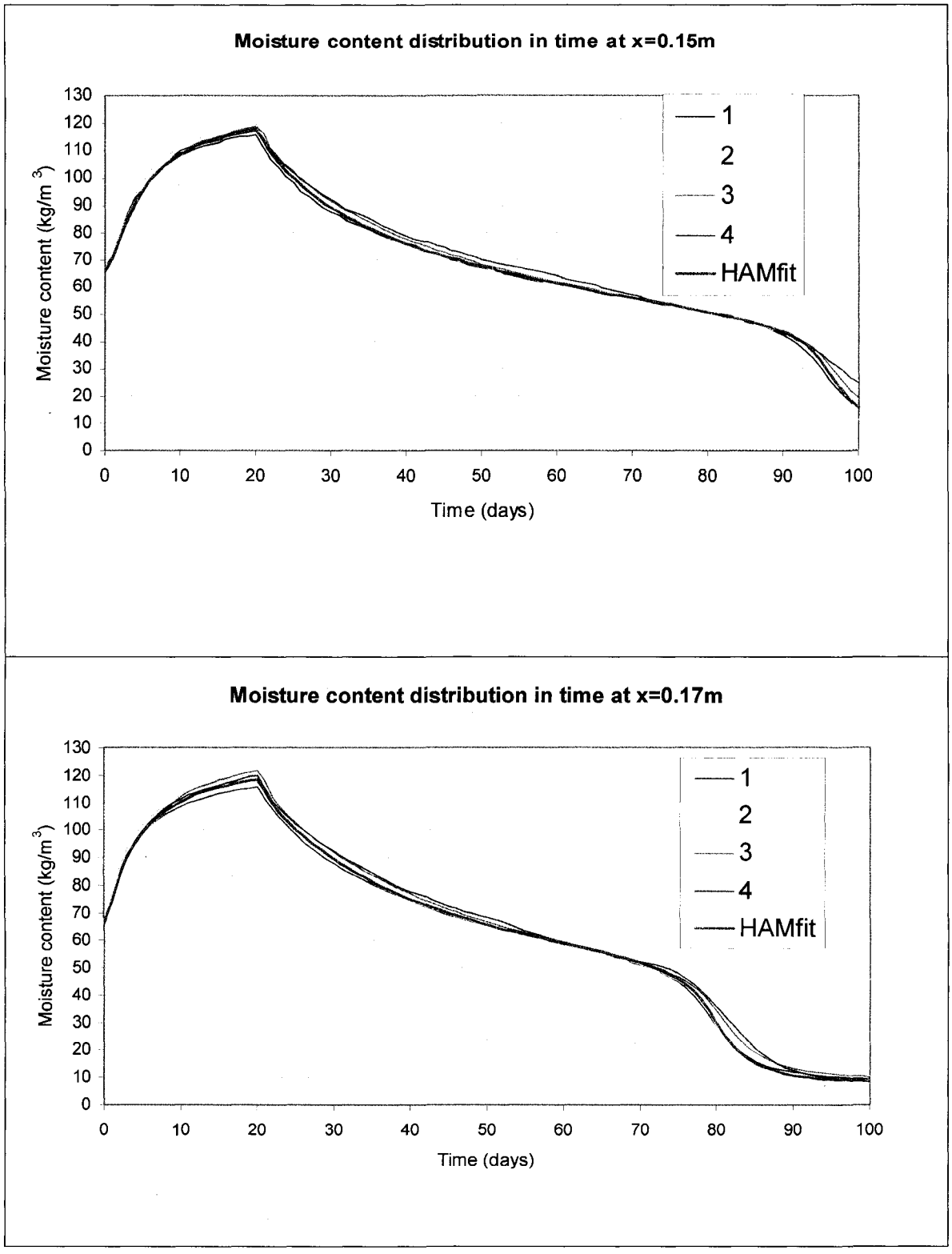
Moisture content distribution in time at x=0.15m
Moisture content (kg/m3)
Time (days)
1
2
3
4
HAMfit
Moisture content distribution in time at x=0.17m
Moisture content (kg/m3)
Time (days)
1
2
3
4
HAMfit

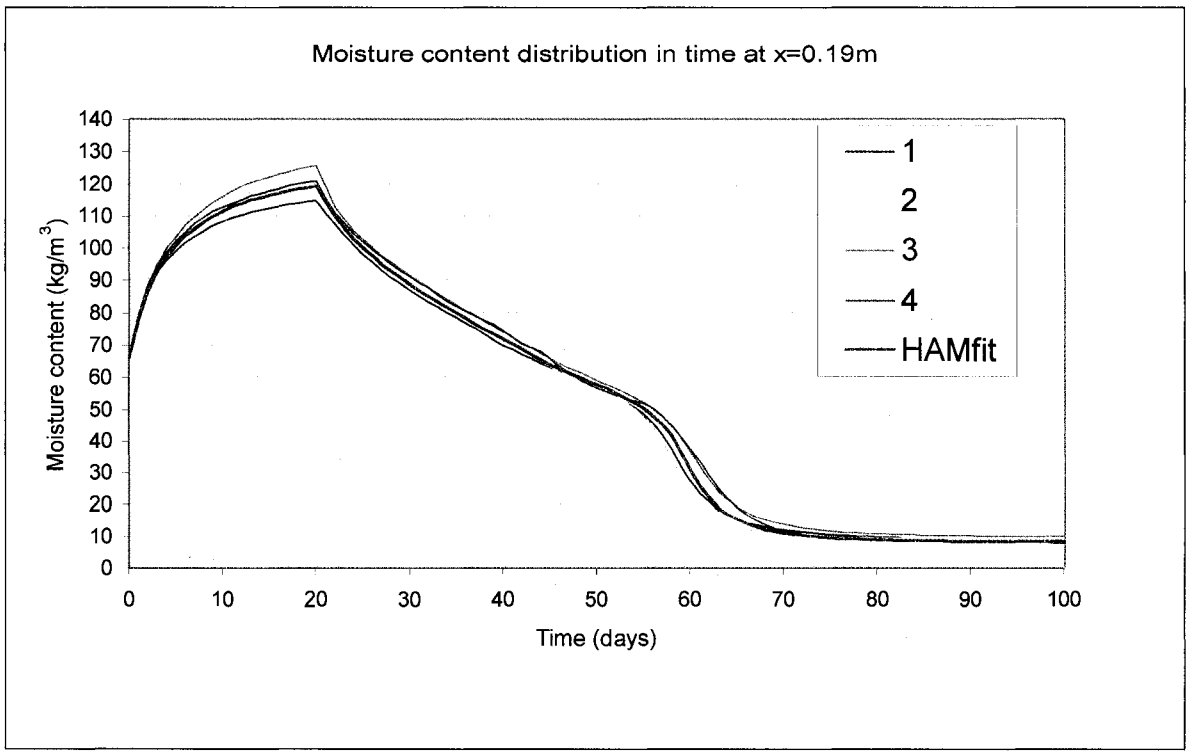

Figure B-5 Moisture content variations in time at 0.05, 0.10, 0.15, 0.17 and 0.19 m cross-section of the wall

APPENDIX B-2

HAMSTAD Benchmark Exercise #4

The fourth benchmark exercise deals with heat and moisture transfer in a two-layer wall system exposed to realistic internal and external boundary conditions. The schematic diagram of the wall system, which is composed of load-bearing layer at the exterior and finishing layer at the interior, is shown in Figure B-6. Realistic time dependent boundary conditions, which are applied at the external and internal surfaces of the wall, are shown in Figure B-7. The variable heat and moisture loads on the exterior surface, which are due to solar radiation and rain, respectively, are represented by equivalent outdoor temperature and wind–driven rain flux. The time dependent indoor moisture load, which is due to occupant activity, is represented by variable indoor vapor pressure. The outdoor air temperature and vapor pressure, as well as the indoor air temperature are hold constant with values of 10°C, 1150 Pa, and 20°C respectively. As Hagentoft et al. (2004) described the problem; the climatic load is severe, causing surface condensation on the exterior surface due to nighttime cooling (low equivalent temperature), and frequent occurrence of wetting and drying of moisture in the wall due to the alternative rain and solar radiation loads. Moreover, rainwater absorption and moisture movement within the layers and at the interfaces are rapid, due to the extremely fast liquid water absorption property of the load-bearing layer. The initial hygrothermal conditions of the two layers are 20°C and 40% temperature and relative humidity, respectively. The mass transfer coefficients of the interior and exterior surfaces are 3E-8 and 2E-7 s/m, respectively, whereas the heat transfer coefficients are 8 and 25 W/m^2K, respectively. The density and specific heat capacity of the layers are given in Table B-1

below. The moisture storage characteristics (sorption isotherm and water retention curve), vapor permeability, liquid diffusivity and moisture dependent thermal conductivity of the load-bearing and finishing layers are shown in Figure B-8 and Figure B-9, respectively. The full description of this benchmark exercise is given in Hagentoft (2002). The required simulation results for comparison of the models are: 1) the hourly values of internal and exterior surface temperatures and moisture contents for the whole simulation period of 5 days (120 hours), and 2) the temperature and moisture content profiles of the wall cross-section at every 6 hours. The HAMFit results for the surface moisture content and temperature, as well as the moisture and temperature profiles across the wall sections are shown in Figure B-10-Figure B-13. As can be seen from the figures the simulation results of HAMFit agrees very well with the other six models solutions (labeled 1 to 6).

Table B-1 Density and specific heat capacities of load-bearing and finishing materials

Material	Density (kg/m^3)	Specific heat capacity (J/kgK)
Load-bearing	2050	840
Finishing material	790	870

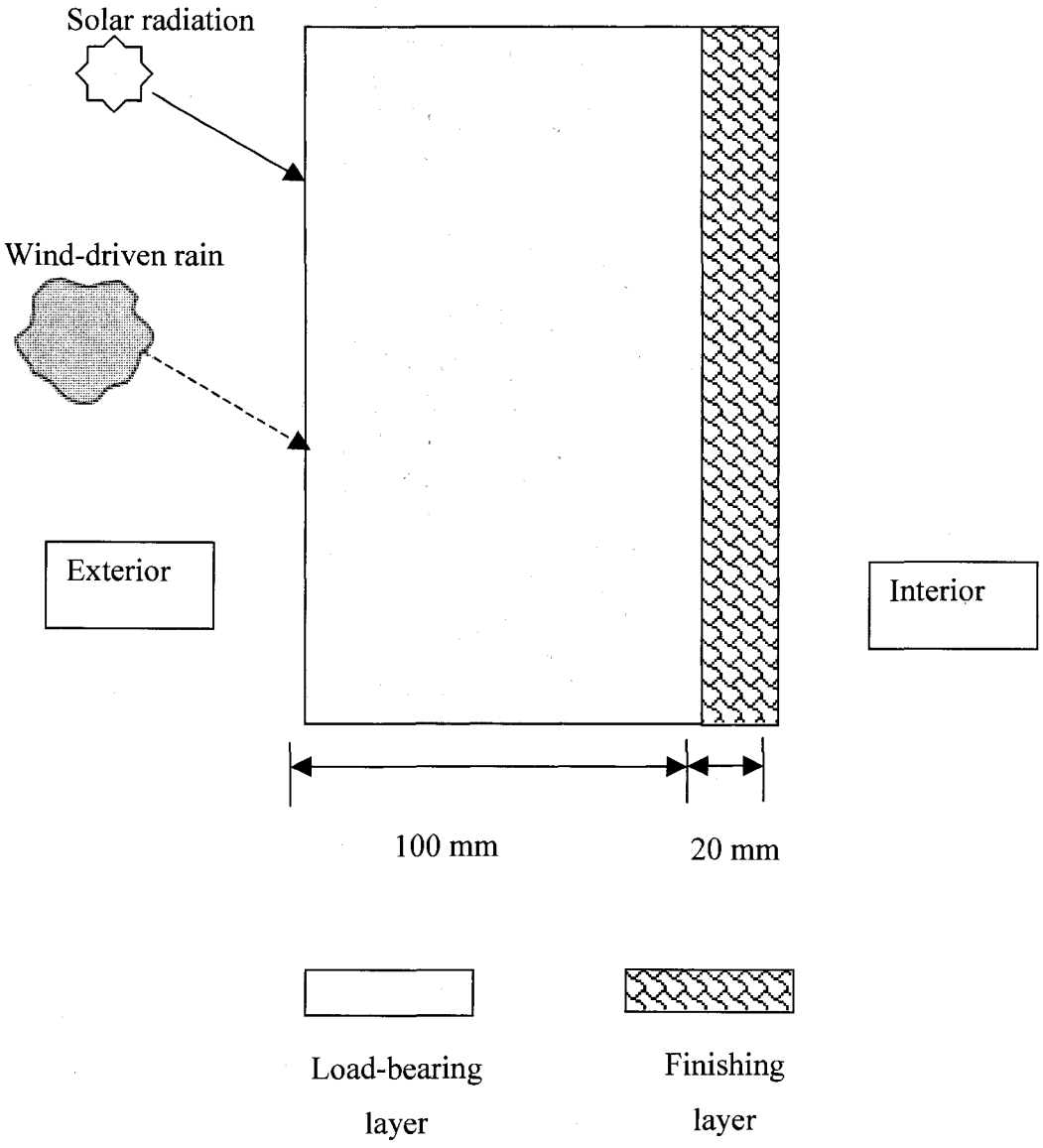

Figure B-6 Benchmark four: Load-bearing wall

Boundary conditions

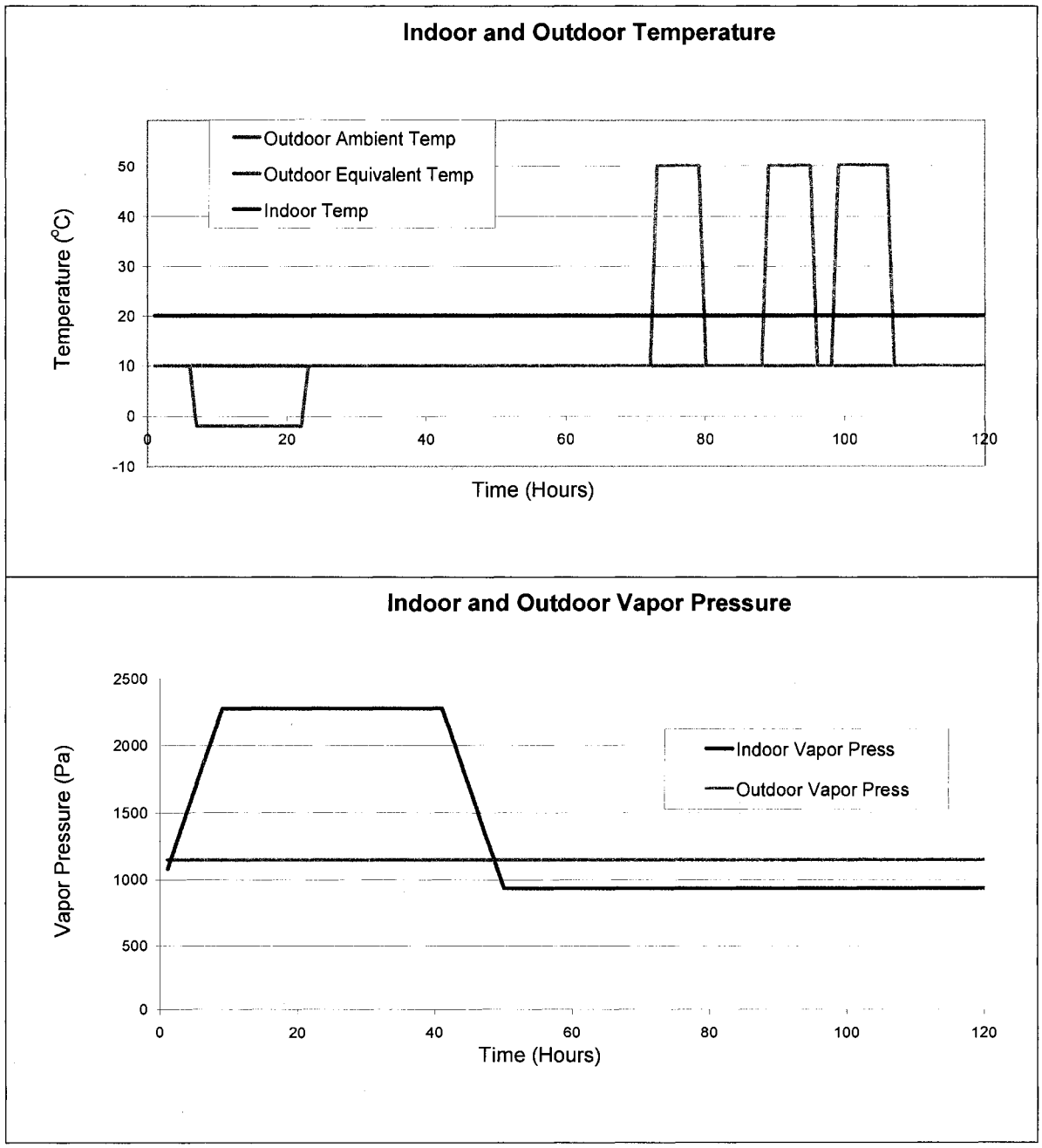

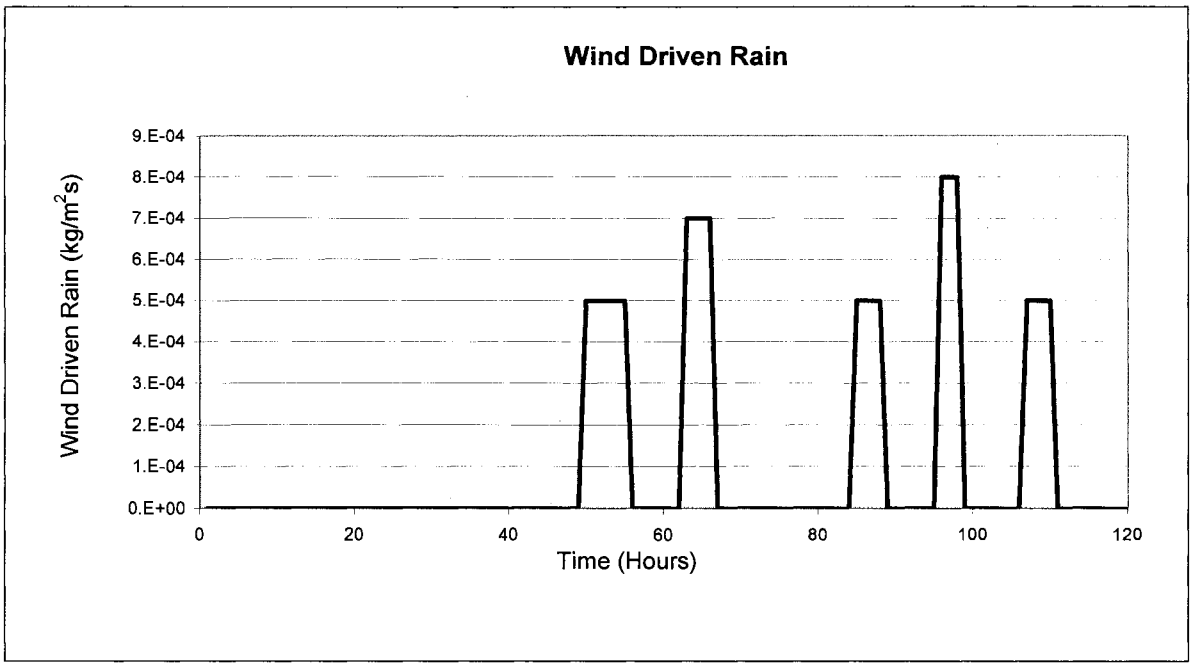

Figure B-7 Realistic boundary conditions: Indoor and outdoor temperatures, vapor pressures and wind–driven rain

Hygrotherrmal properties of the load-bearing layer

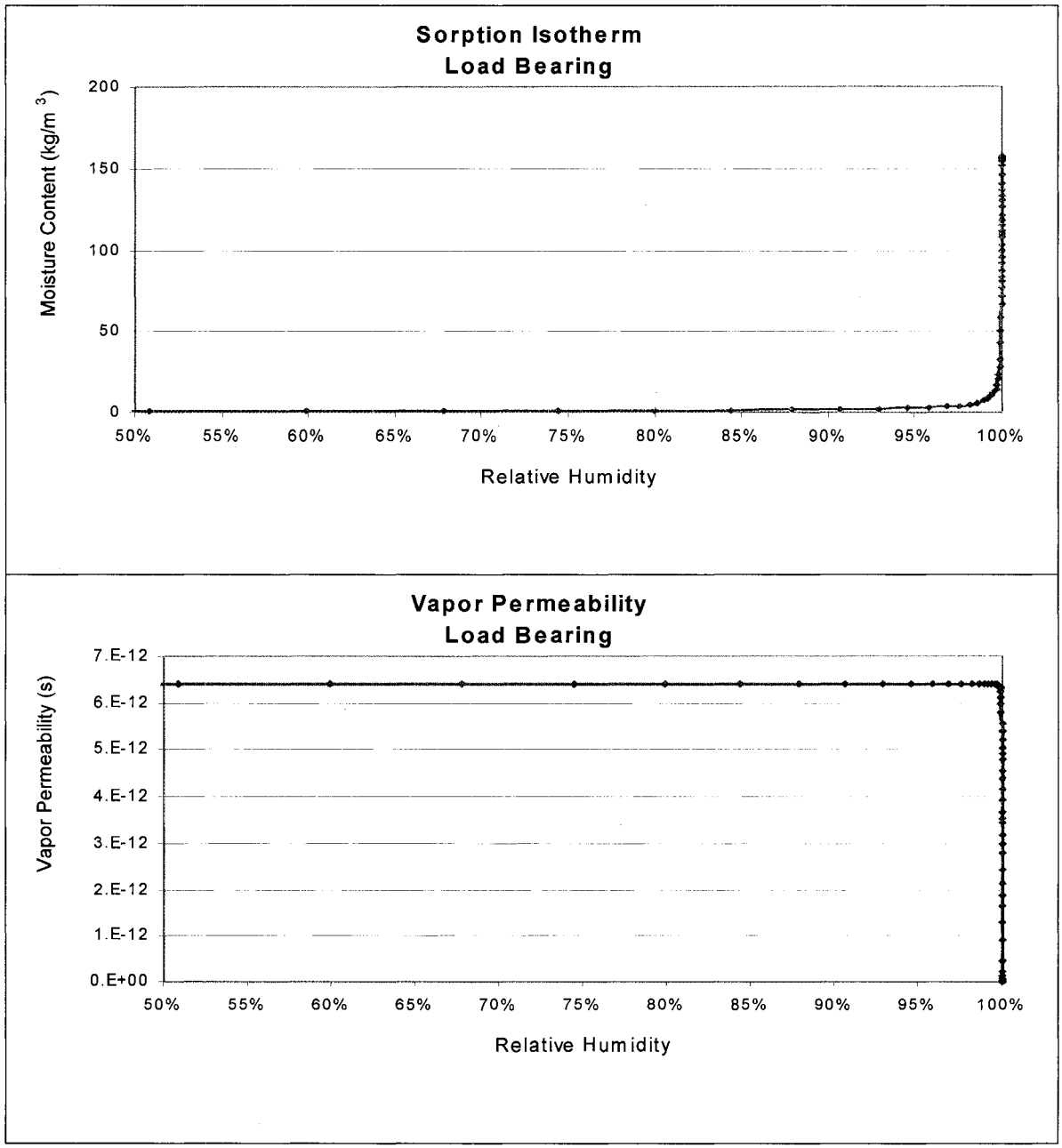

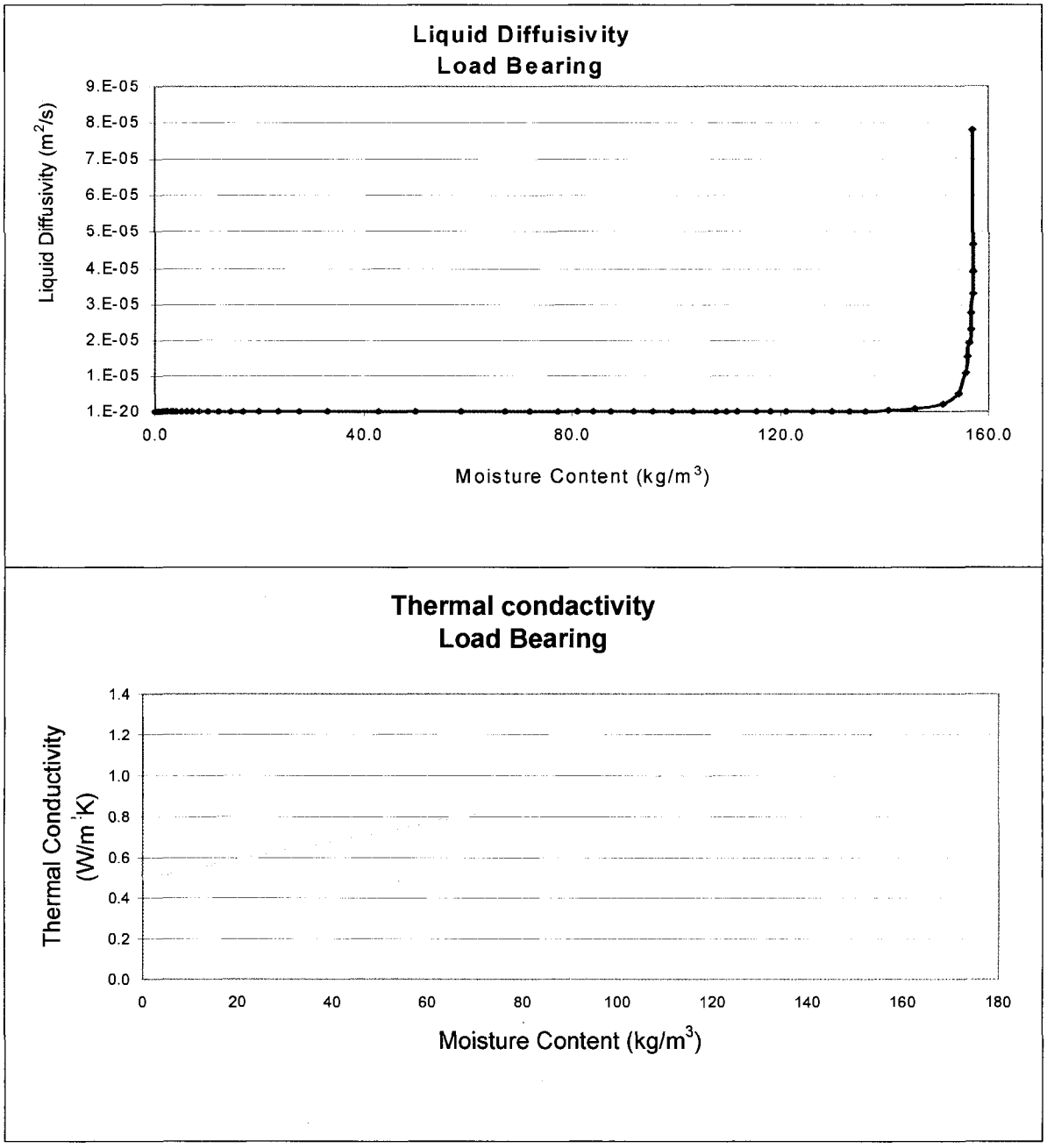

Figure B-8 Sorption-isotherm, vapor permeability, liquid diffusivity and moisture dependent thermal conductivity properties of load-bearing layer

Hygrotherrmal properties of the finishing layer

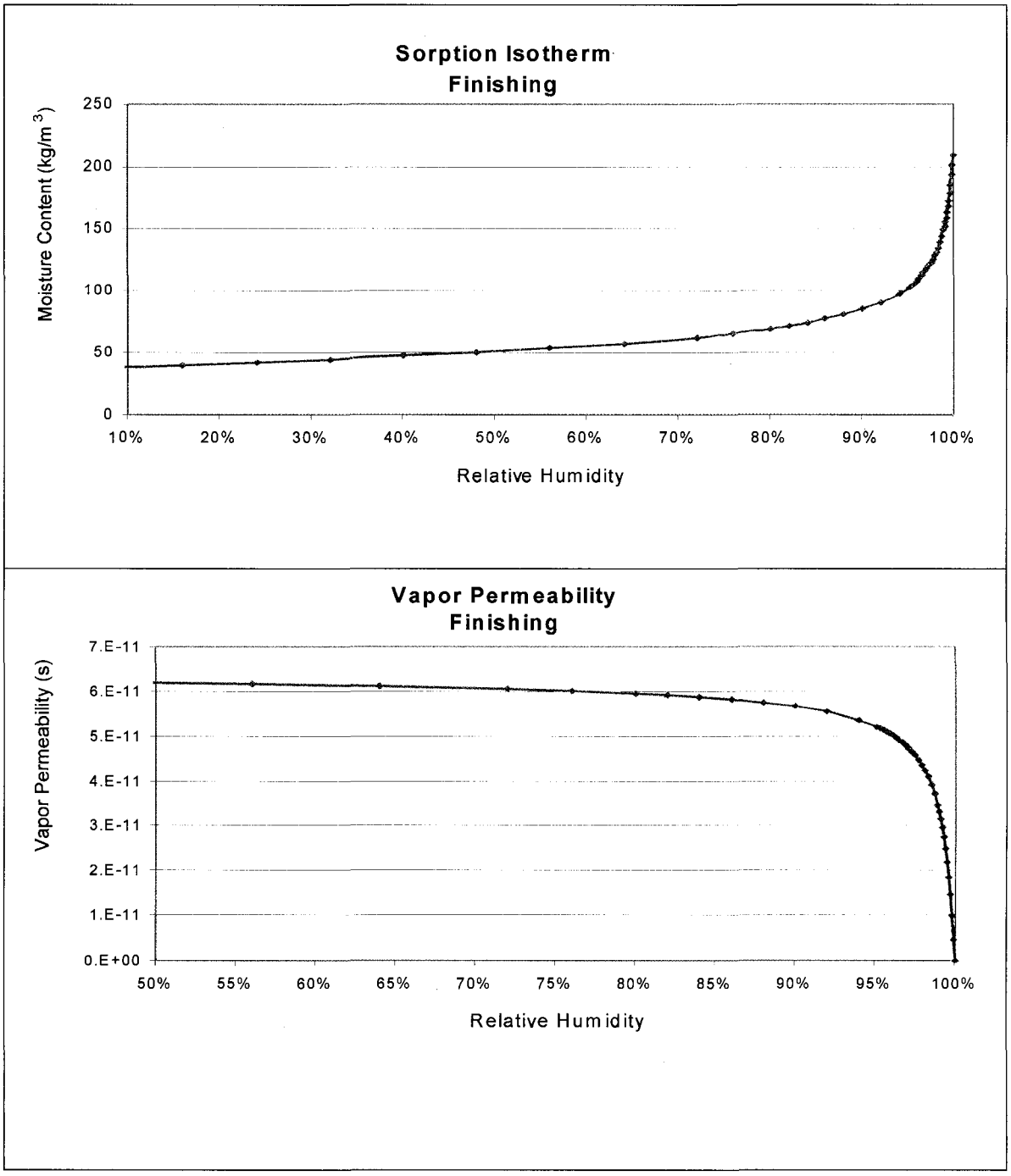

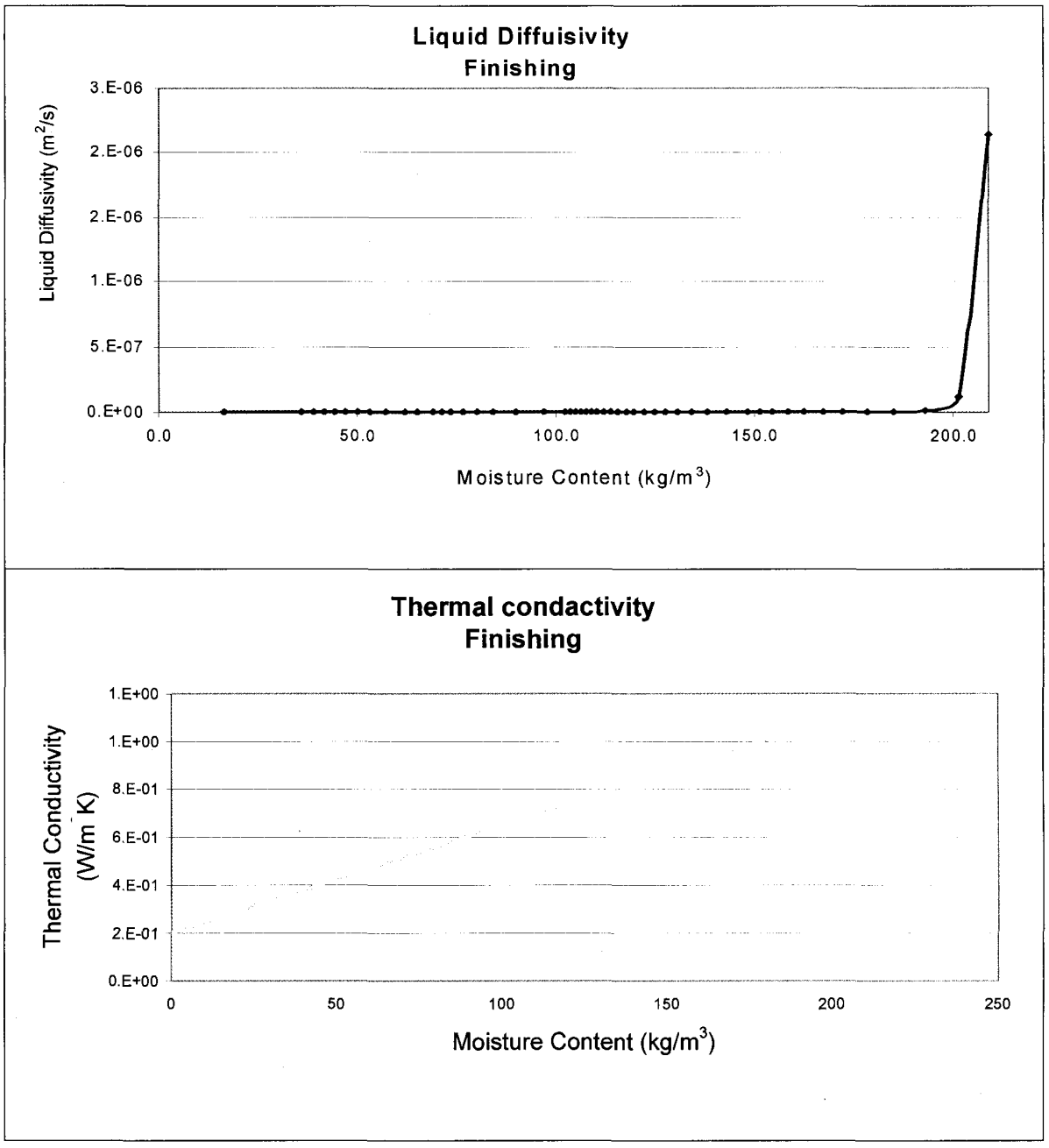

Figure B-9 Sorption-isotherm, vapor permeability, liquid diffusivity and moisture dependent thermal conductivity properties of finishing material

Surface moisture and temperature profiles

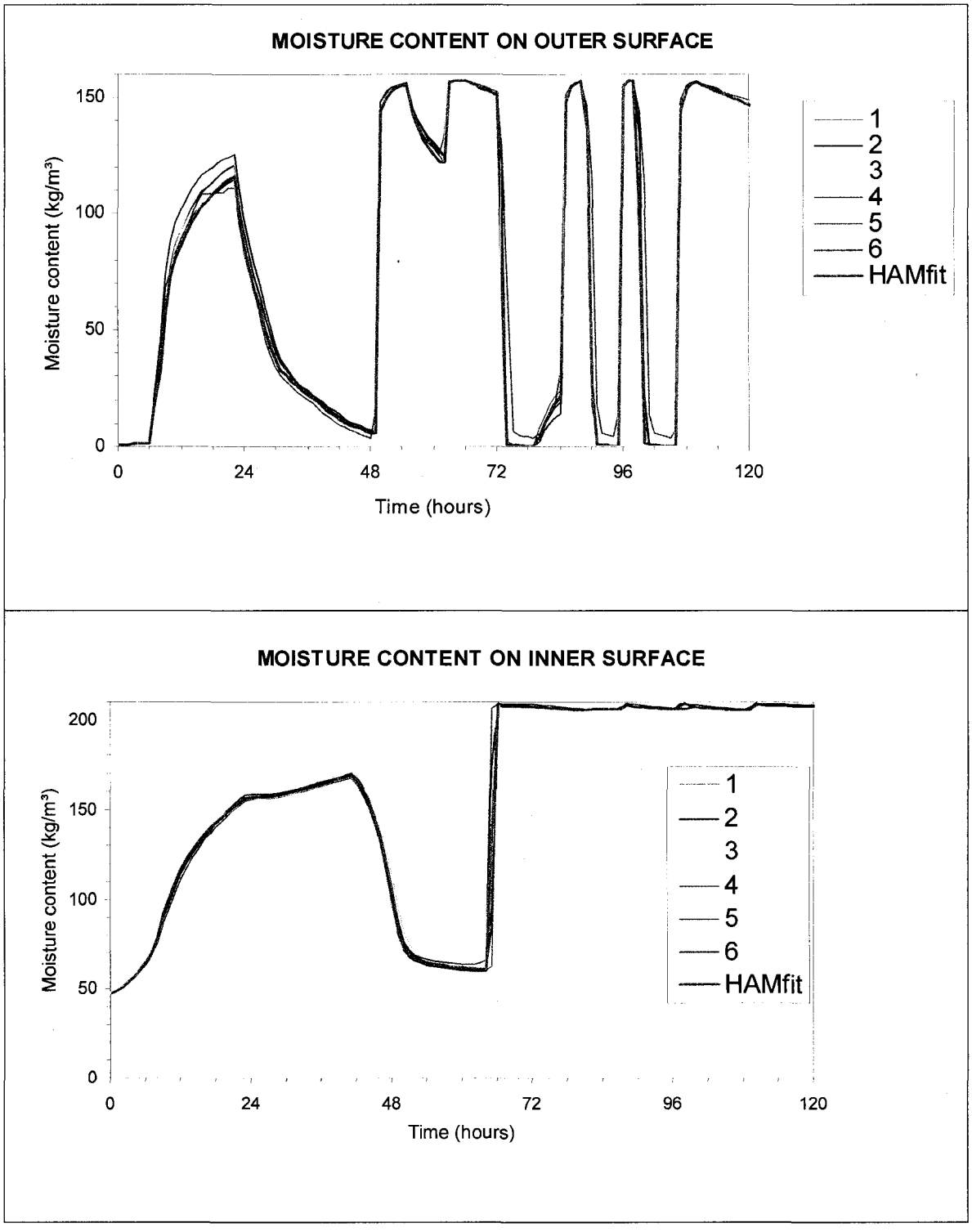

Figure B-10 Surface moisture contents of the outer and inner surfaces of the wall verses time

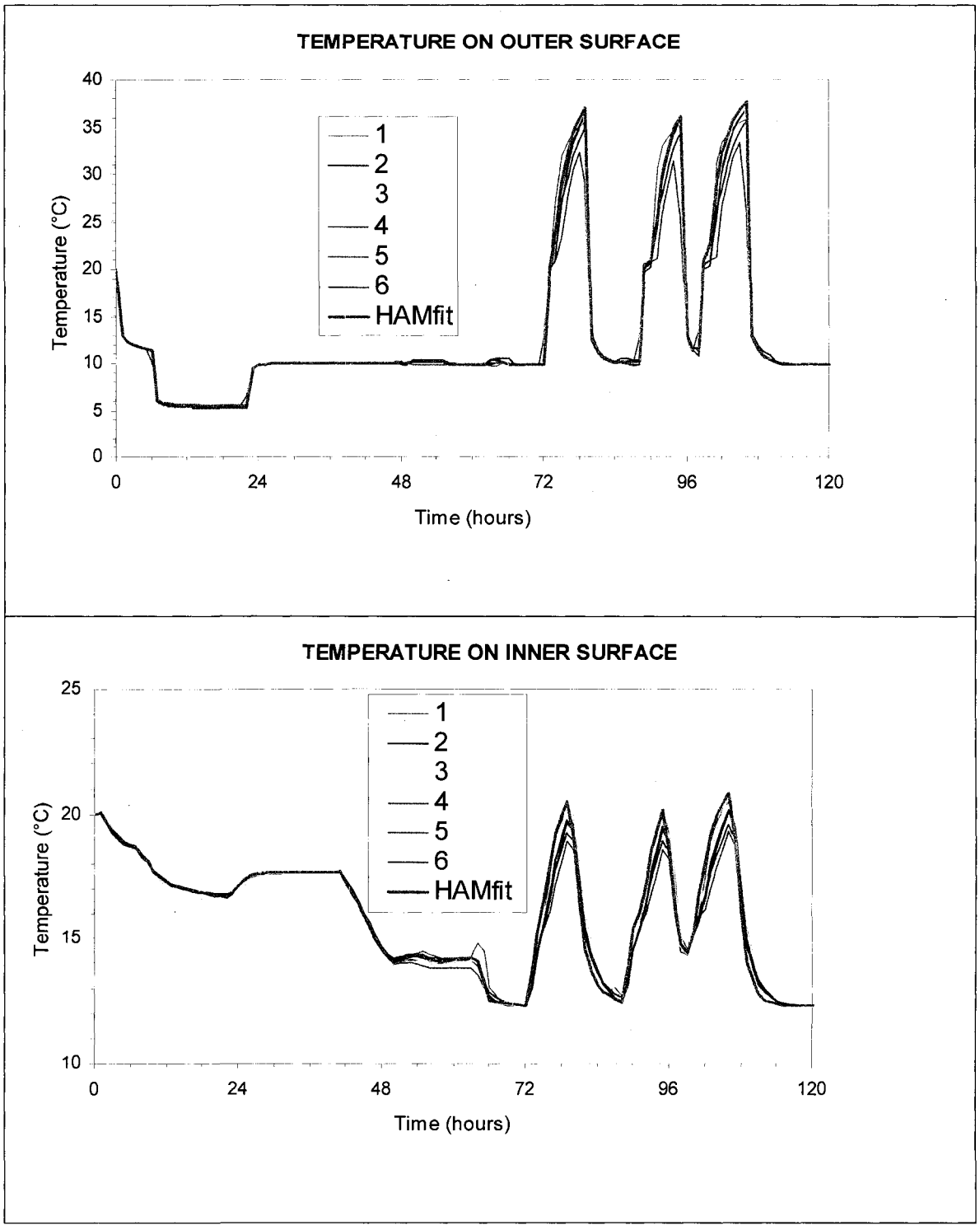

Figure B-11 Surface temperatures of the outer and inner surfaces of the wall verses time

Moisture profiles across the wall section at different times

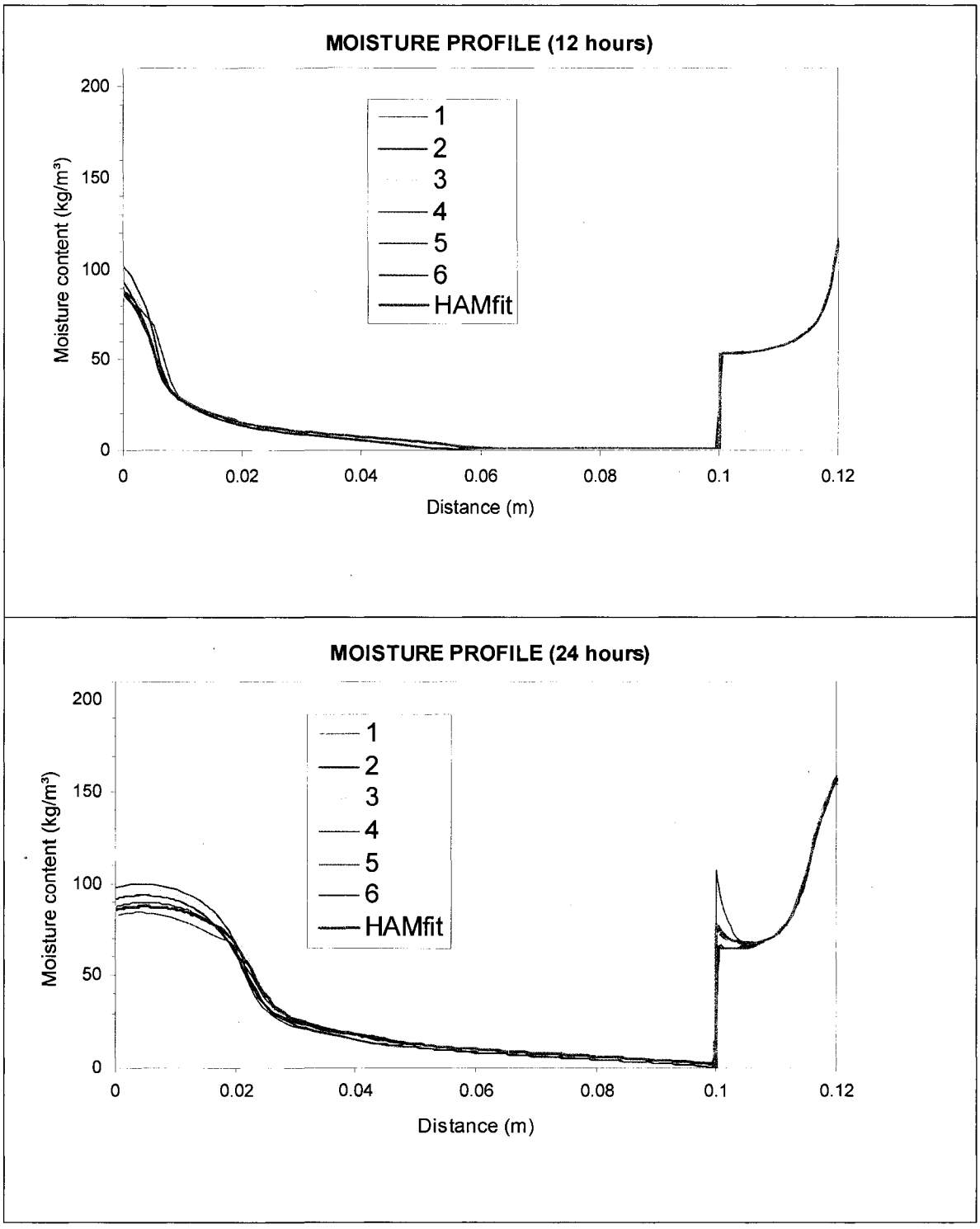

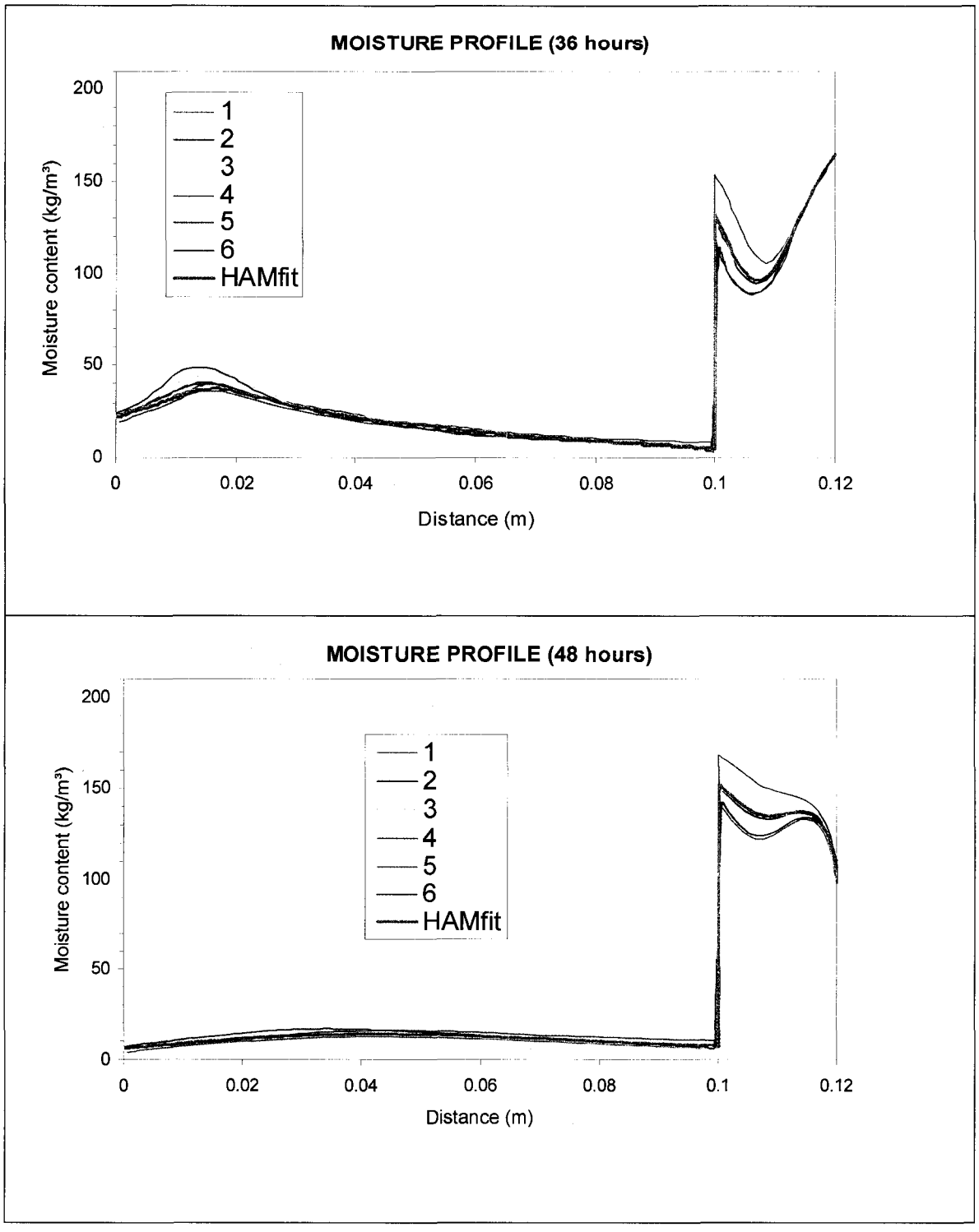
MOISTURE PROFILE (36 hours)
Moisture content (kg/m³)
200
150
100
50
0
1
2
3
4
5
6
HAMfit
0
0.02
0.04
0.06
0.08
0.1
0.12
Distance (m)
MOISTURE PROFILE (48 hours)
Moisture content (kg/m³)
200
150
100
50
0
1
2
3
4
5
6
HAMfit
0
0.02
0.04
0.06
0.08
0.1
0.12
Distance (m)

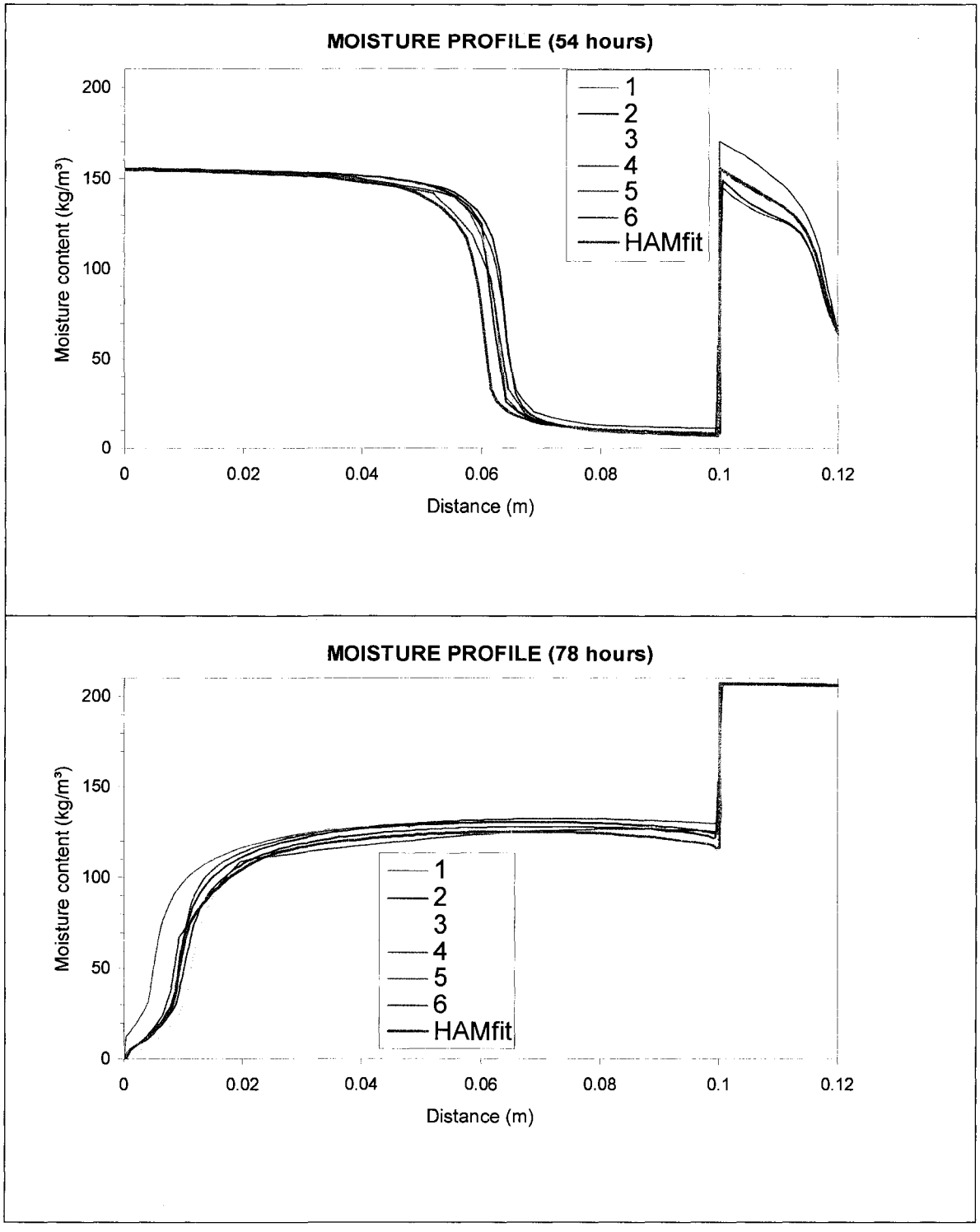
MOISTURE PROFILE (54 hours)
Moisture content (kg/m³)
200
150
100
50
0
0
0.02
0.04
0.06
0.08
0.1
0.12
Distance (m)
1
2
3
4
5
6
HAMfit
MOISTURE PROFILE (78 hours)
Moisture content (kg/m³)
200
150
100
50
0
0
0.02
0.04
0.06
0.08
0.1
0.12
Distance (m)
1
2
3
4
5
6
HAMfit

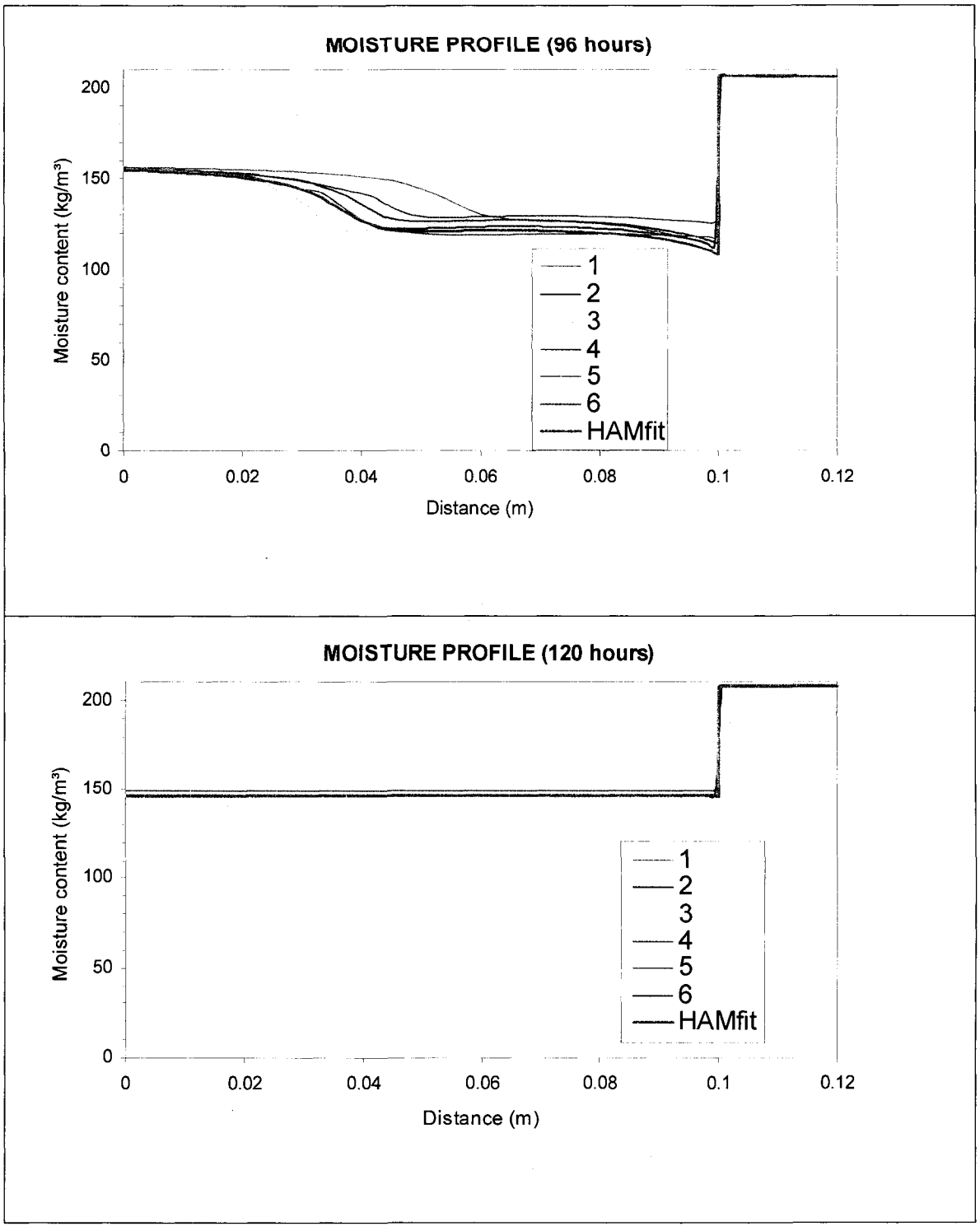

Figure B- 12 Moisture profiles across the wall section at different times

Temperature profiles across the wall section at different times

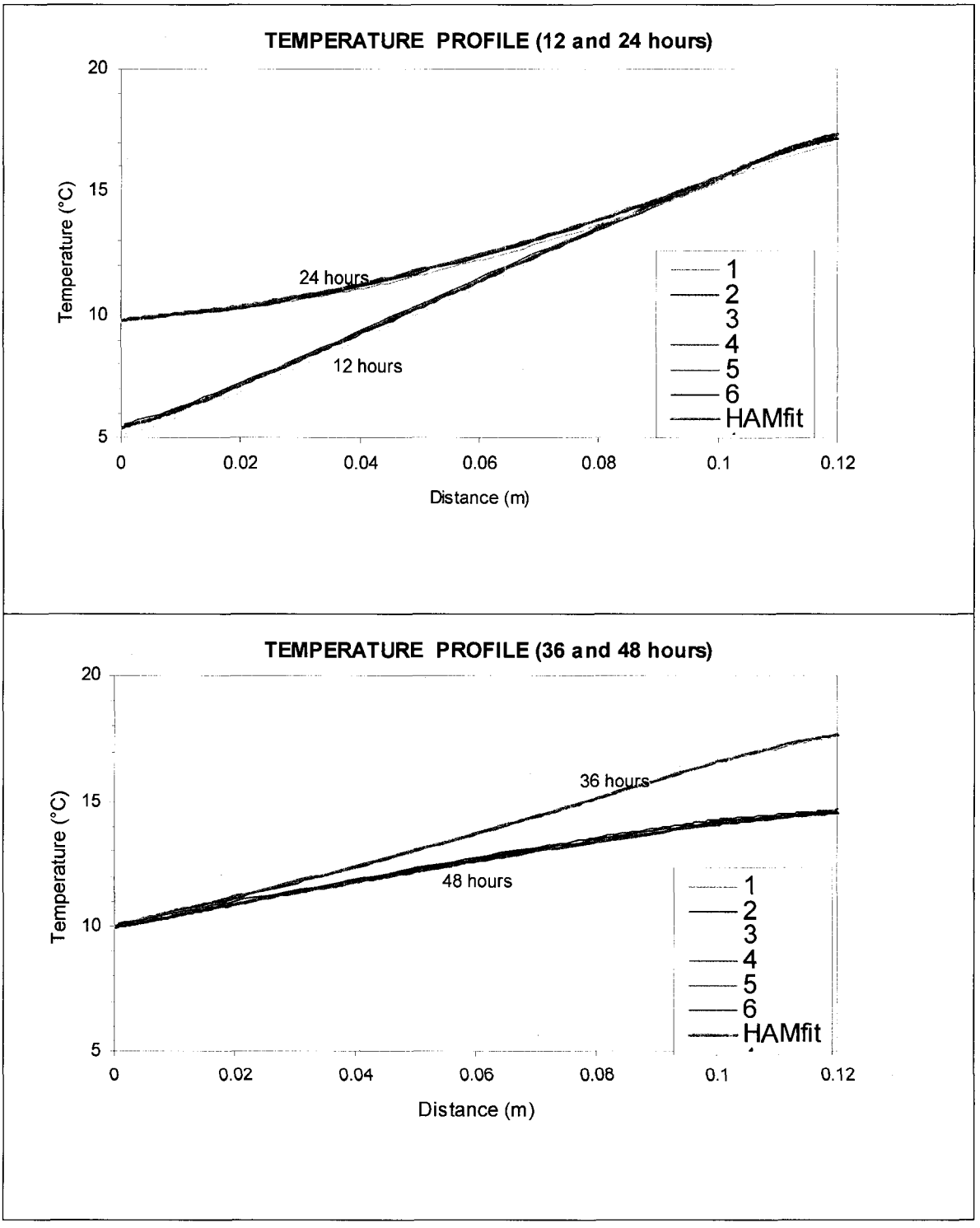

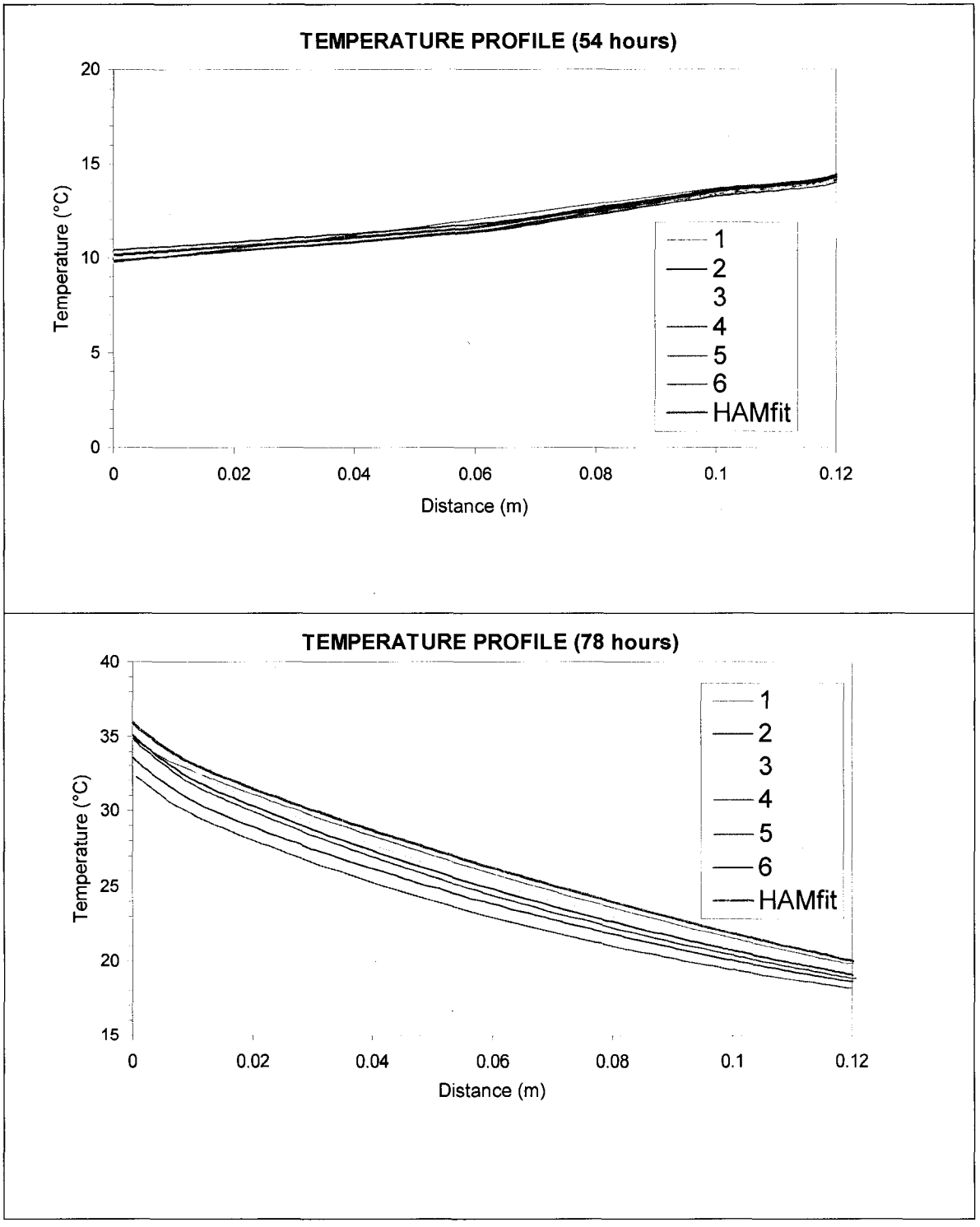
TEMPERATURE PROFILE (54 hours)
Temperature (°C)
20
15
10
5
0
0
0.02
0.04
0.06
0.08
0.1
0.12
Distance (m)
1
2
3
4
5
6
HAMfit
TEMPERATURE PROFILE (78 hours)
Temperature (°C)
40
35
30
25
20
15
0
0.02
0.04
0.06
0.08
0.1
0.12
Distance (m)
1
2
3
4
5
6
HAMfit

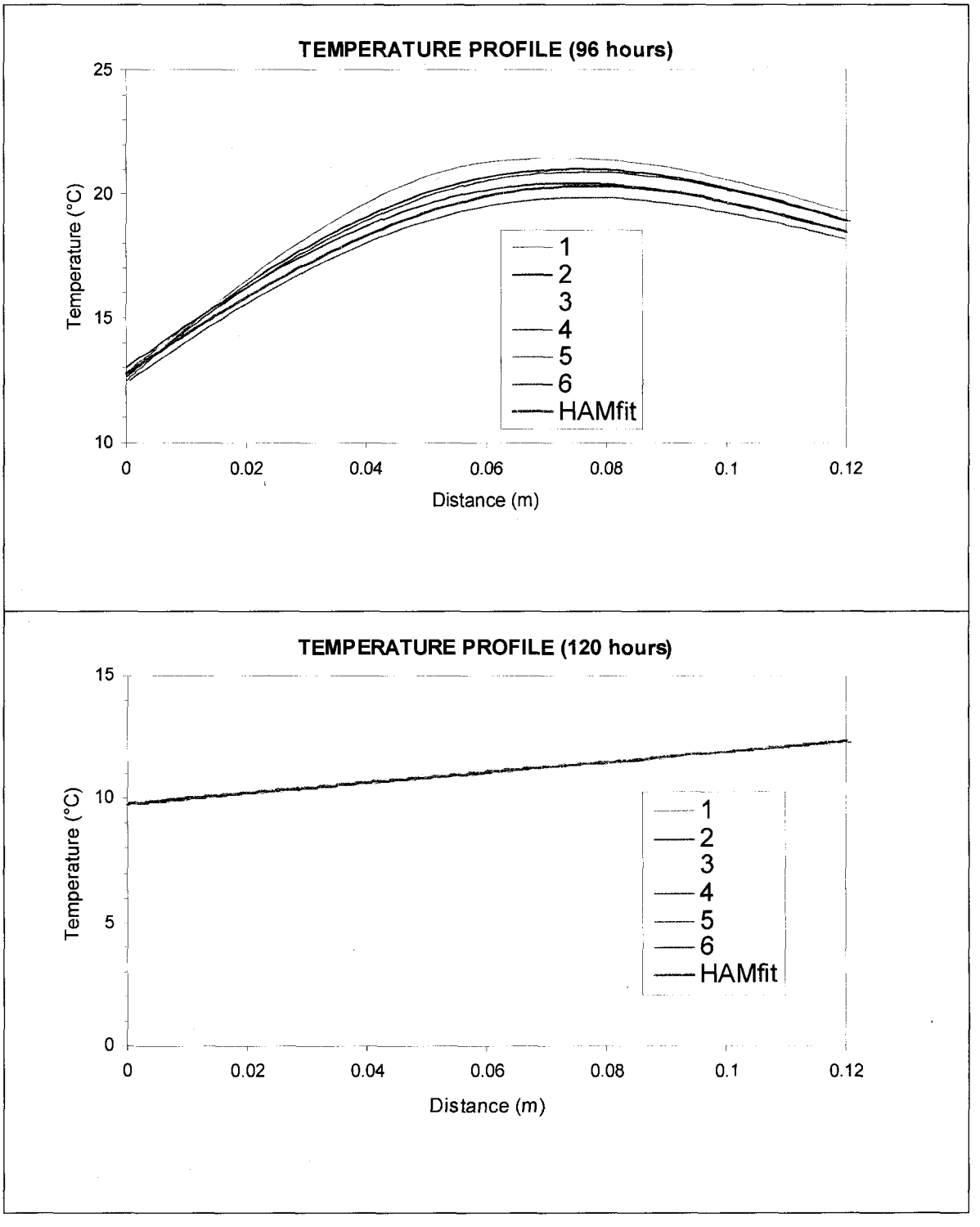

Figure B-13 Temperature profiles across the wall section at different times